

UNIVERSITAT POLITÈCNICA DE VALÈNCIA

DOCTORADO EN INGENIERÍA Y PRODUCCIÓN INDUSTRIAL



UNIVERSITAT
POLITÈCNICA
DE VALÈNCIA

IUTM

Instituto Universitario de Tecnología de Materiales



TESIS DOCTORAL

Desarrollo y caracterización de polímeros de alto rendimiento medioambiental derivados de residuos agroindustriales y aditivos de origen renovable

Autor:

Jaume Gómez Caturla

Dirigida por:

Dr. Rafael Antonio Balart Gimeno

Dr. Daniel García García

Fecha de presentación:

Febrero de 2024

UNIVERSITAT POLITÈCNICA DE VALÈNCIA

DOCTORADO EN INGENIERÍA Y PRODUCCIÓN INDUSTRIAL



**UNIVERSITAT
POLITÈCNICA
DE VALÈNCIA**

IUTM

Instituto Universitario de Tecnología de Materiales



TESIS DOCTORAL

Desarrollo y caracterización de polímeros de alto rendimiento medioambiental derivados de residuos agroindustriales y aditivos de origen renovable

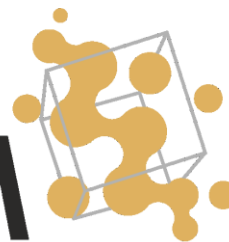
Jaume Gómez Caturla



UNIVERSITAT
POLITÈCNICA
DE VALÈNCIA

IUTM

Instituto Universitario de Tecnología de Materiales



El Dr. Rafael Antonio Balart Gimeno y el Dr. Daniel García García, Catedrático de Universidad y Titular de Universidad del Departamento de Ingeniería Mecánica y de Materiales de la Universitat Politècnica de València en calidad de directores de la Tesis Doctoral (modalidad Doctorado Internacional) presentada por D. Jaume Gómez Caturla, con el título **“Desarrollo y caracterización de polímeros de alto rendimiento medioambiental derivados de residuos agroindustriales y aditivos de origen renovable”**.

CERTIFICAN

Que la presente memoria, **“Desarrollo y caracterización de polímeros de alto rendimiento medioambiental derivados de residuos agroindustriales y aditivos de origen renovable”**, para aspirar al grado de Doctor por la Universitat Politècnica de València reúne las condiciones adecuadas para constituir la tesis doctoral de D. Jaume Gómez Caturla (modalidad Doctorado Internacional).

Asimismo, certifican que la citada tesis doctoral se ha realizado en el Instituto Universitario de Investigación de Tecnología de Materiales de la Universitat Politècnica de València, en el campus de Terni de la Universidad de Perugia (Italia) y en el Departamento de Ingeniería de Polímeros del campus de Azurém en Guimaraes (Portugal).

Y para que conste a los efectos oportunos, firman la presente en Alcoy a 13 de noviembre de 2023.

Fdo. Dr. Rafael Antonio Balart Gimeno

Fdo. Dr. Daniel García García

A todos los que me han apoyado incondicionalmente a lo largo de este camino.

“Lo que sabemos es una gota de agua, lo que ignoramos es el océano”

Isaac Newton

AGRADECIMIENTOS

En primer lugar, quiero darle las gracias al que ha sido uno de los pilares más grandes en la realización de esta tesis y aquel que hizo posible que empezara mi carrera en el mundo de la investigación, mi director Rafael Balart. Gracias Rafa por confiar en mí desde el principio y siempre demostrarme tu apoyo, por sacar tiempo para ayudarme cada vez que lo he necesitado y por compartir conmigo parte de la sabiduría que tienes (que no es poca) siempre desde la humildad y la cercanía. También me gustaría agradecer a mi codirector Daniel García, por servirme de guía durante mis primeros pasos en la investigación. Muchas gracias, Dani por todo lo que me has enseñado a lo largo de estos años y porque siempre has estado ahí para explicarme cosas nuevas y hacerme mejorar como investigador y como persona, tanto dentro como fuera del laboratorio. Muchísimas gracias a los dos por hacerme un mejor investigador y por servirme de faro tanto en lo profesional como en lo personal, ya que sin vosotros esta tesis no habría sido posible. ¡MUCHAS GRACIAS A LOS DOS!

Al ministerio de Educación, Cultura y Deporte por el apoyo financiero ofrecido a través de la ayuda otorgada (FPU20/1072).

A la Conselleria d'Educació, Cultura i Esport de la Generalitat Valenciana por el apoyo financiero a través de la ayuda otorgada (ACIF/2021/185).

Al ministerio de Ciencia e Innovación, por el apoyo financiero ofrecido a la realización de este trabajo a través de los proyectos PID2020-116496RB-C22 y TED2021-131762A-I00.

A la Generalitat Valenciana por ofrecer apoyo financiero a través de los proyectos AICO/2021/025 y CIGE/2021/094.

A la Universitat Politècnica de València por ofrecer apoyo financiero a través del proyecto PAID-06-22.

Al Instituto de Tecnología de Materiales (ITM) y al campus de Alcoy de la Universitat Politècnica de València (UPV) por ofrecerme sus instalaciones para poder llevar a cabo todo el trabajo realizado.

Quiero agradecer especialmente a la catedrática Lourdes Sánchez Nacher, por haberme guiado sobre todo en la parte docente de mi formación durante estos años. Muchas gracias Lourdes por depositar en mí tanta confianza, hacerme sentir más seguro de mí mismo y ayudar a desarrollarme como persona. Has sido como una madre para

mí y me has hecho sentir como en casa. ¡MUCHAS GRACIAS!

A los catedráticos David García Sanoguera, Teodomiro Boronat Vitoria y Juan López Martínez. Muchas gracias por toda la ayuda y consejos que me habéis dado durante la realización de esta tesis. En especial agradecer a David por su apoyo en mi formación docente.

A los profesores Octavio Fenollar, Néstor Montañés, Mado y Pelayo por compartir conmigo sus conocimientos y experiencia a pesar de disponer a veces de un tiempo limitado.

A los técnicos de laboratorio Matías, Javi y Pedro por cuidar tan bien y asegurar el mantenimiento de todos los laboratorios y equipos con los que se ha llevado a cabo esta tesis. En especial a Matías y Javi, quienes siempre me han ayudado a solucionar los problemas e imprevistos que me surgían de forma altruista.

A mis compañeros de laboratorio Diego, Harrison, Cristina, Sandra y Miguel por compartir conmigo los laboratorios, ayudarme en tantos experimentales a lo largo de la realización de la tesis e intentar resolverme siempre las dudas que me surgían.

Quiero dar un agradecimiento especial a mi compañero de laboratorio y amigo Ramón, que empezó conmigo en este camino y desde el principio siempre me ha mostrado su apoyo incondicional. Sabes que eres como un hermano para mí y te agradezco todos los buenos momentos que hemos pasado estos años, las fiestas que nos hemos pegado, las locuras que hemos hecho y la confianza que hemos tenido para lo bueno y para lo malo. Creo que durante estos tres años he mejorado mucho como persona y ha sido en gran parte gracias a ti. ¡MUCHAS GRACIAS POR TODO!

También quiero agradecer especialmente a Juan y a Luis, quienes empezaron como compañeros de laboratorio y han acabado siendo unos grandes amigos. Gracias Luis porque empezaste siendo prácticamente mi mentor, explicándome todas las técnicas que no conocía, a cómo escribir un artículo, cómo subirlo, me enseñaste a tener un espíritu más crítico y un sinfín de cosas más. Siempre te tendré como referente y ejemplo a seguir. Y gracias, Juan por inculcarme ese espíritu trabajador que te caracteriza, ayudarme siempre en todo lo que te he pedido y acompañarme a la "speedrun" de congresos y estancias que hemos hecho este año. También os agradezco a los dos esas clases de mecánica, fórmula 1, coches y motos gratuitas que me habéis dado, y como no, todos los momentos inolvidables que hemos pasado en las estancias de Italia, Portugal y dentro y fuera de los laboratorios. ¡Muchísimas gracias a los dos!

Agradecer al profesor Luigi Torre de la Universidad de Perugia, en Terni, por dejarme realizar mi estancia de investigación en las instalaciones de su campus. También agradecer a Débora, Franco, Francesca y Roberto por ayudarme en todo lo que he necesitado durante la estancia. Pero sobre todo gracias a Franco, por haber sido mi mentor, amigo y compañero durante toda la estancia y por la hospitalidad que demostró. ¡Grazie!

Al profesor José Covas de la Universidad de Minho, en Guimaraes, por aceptarme en sus instalaciones y dejarme hacer mi segunda estancia en Portugal. Gracias también a Rui y Mariana por ayudarme en todo lo que pudieron durante el experimental realizado en la estancia.

Gracias también a mis compañeros de laboratorio Antonio y Virginia, que, aunque lleven menos tiempo en el grupo de investigación siempre han estado dispuestos a ayudar en todo lo que estaba en su mano. Sobre todo, gracias a Antonio por ese humor que ha aportado dentro del laboratorio, por tratarme siempre tan bien, por esas clases de pádel y por la hospitalidad que siempre me has mostrado.

Al profesor Vicent Fombuena y a los becarios Iván Domínguez Candela y Alejandro Lerma, por las colaboraciones realizadas y por el apoyo recibido durante la realización de la tesis.

Agradecer también a mis compañeros y amigos del Departamento de Ingeniería Textil y Papelera Iván, Rubén, "Rubén el fuerte", Inés, Ainhoa y David por todos los buenos momentos pasados sobre todo fuera de los laboratorios.

A todos mis amigos, en especial a Jordi, Adri, Vice, Tomi, Jaime, Ruso, Nicole, Barea, Acha, Lidia y Marc por haberme acompañado durante todo el camino, haber estado ahí y por todos los momentos que quedarán para el recuerdo a lo largo de estos años.

A mi hermano Andreu, porque has sido más que un amigo y un apoyo no solo durante este trayecto, sino durante toda mi vida. Porque siempre has conseguido sacarme una sonrisa, por todas las tonterías que hemos hecho, taradas mentales y experiencias que hemos vivido juntos. ¡Muchas gracias hermano!

A mi padre Jorge Juan, porque, aunque últimamente ya no nos vemos con tanta frecuencia, siempre me has inculcado el espíritu del trabajo duro, me has impulsado a mejorar y me has transmitido un sinfín de conocimientos a lo largo de toda mi vida. ¡Muchas gracias por todos esos momentos y charlas que hemos tenido!

Por último, quiero agradecer a mi madre, Tina, porque independientemente de la situación siempre me ha mostrado su apoyo. Siempre has estado a mi lado para los buenos y para los malos momentos, me has animado a avanzar, aunque las cosas se pusieran difíciles, y a apreciar lo que tengo en cada momento. Gran parte de mi desarrollo personal ha sido gracias a ti y estoy orgulloso de todos los valores que me has transmitido. ¡MUCHAS GRACIAS!

RESUMEN

Desarrollo y caracterización de polímeros de alto rendimiento medioambiental derivados de residuos agroindustriales y aditivos de origen renovable

La presente tesis doctoral tiene como principal objetivo el desarrollo de materiales poliméricos que sean respetuosos con el medio ambiente y favorezcan modelos de economía circular, centrando las líneas de investigación en el reaprovechamiento de residuos de la industria del mango y en la utilización de ácido poliláctico (PLA) como principal matriz polimérica. Para ello se emplean diferentes técnicas de procesamiento como el *electrospinning*, la extrusión, la inyección o la producción de films por disolución. Además, se plantea la utilización de diferentes aditivos como plastificantes y cargas lignocelulósicas de origen renovable para mejorar las propiedades de estos materiales sin comprometer su alto potencial medioambiental.

El primer bloque de la tesis centra sus esfuerzos en el reaprovechamiento de diferentes residuos del mango (uno de los cultivos más populares del mundo), como la piel y el kernel, para desarrollar diferentes materiales con un gran contenido natural. Dentro de los estudios realizados en este bloque se incluye la extracción de almidón a partir del kernel de mango para la posterior fabricación de nanofibras por *electrospinning*, con gran aplicación en el sector médico. Otros estudios realizados proponen la combinación de matrices poliméricas como el biopolipropileno y el PLA, en combinación con harina de piel de mango y harina de hueso de mango, respectivamente, mediante procesos de extrusión, extrusión reactiva (REX) e inyección. En el caso del biopolipropileno se utilizan además agentes compatibilizantes basados en ácido itacónico para aumentar la adhesión entre las partículas lignocelulósicas de la piel del mango con la matriz polimérica, la cual es altamente apolar. Por otro lado, a las formulaciones de PLA y harina de hueso de mango se le añaden plastificantes como la triacetina y la tributirina para aumentar las propiedades dúctiles del PLA. Un cuarto estudio se enfoca en la producción de films de glicerol con harina de hueso de mango, rica en almidón, para observar cómo afecta el tamaño de partícula de la harina sobre las propiedades de los films. Por último, se propone el desarrollo de materiales termoplásticos ricos en almidón utilizando harina de kernel de mango en combinación con diferentes plastificantes como glicerol, sorbitol y urea. Estos materiales ricos en almidón son procesados por extrusión e inyección y son completamente biodegradables y de origen natural.

El segundo y último bloque de la tesis está enfocado a la utilización del ácido poliláctico obtenido de fuentes renovables en procesos de extrusión e inyección. Este poliéster es un polímero biodegradable cuya principal desventaja es su gran fragilidad. Por ello, se han empleado diferentes tipos de plastificantes naturales para incrementar las propiedades dúctiles del PLA. En un primer trabajo, se combina el PLA con α -terpinil acetato, un plastificante de origen renovable. Además, se añade piel de mandarina molida como carga natural para evaluar si este plastificante es capaz de aumentar la ductilidad de mezclas de PLA con cargas lignocelulósicas, obteniendo resultados muy positivos. Un segundo trabajo plantea la combinación de PLA con dietil-L-tartrato, un plastificante obtenido del ácido tartárico, encontrado en la uva y el tamarindo, obteniendo elongaciones de más de un 300%. Por último, dos estudios más plantean la combinación de PLA con terpenoides, más concretamente ésteres de geranilo y linalilo. En este sentido, uno de los trabajos se centra en variar la proporción de acetato de linalilo y acetato de geranilo en las composiciones, mientras que el otro trabajo evalúa como afecta la longitud de cadena de los ésteres de geranilo a la plastificación del PLA. Todos los plastificantes utilizados en este bloque ofrecieron resultados muy prometedores, con alargamientos a la rotura superiores al 200% en materiales completamente naturales y biodegradables con gran aplicación en el sector alimentario y del envase y embalaje.

RESUM

Desenvolupament i caracterització de polímers d'alt rendiment mediambiental derivats de residus agroindustrials i additius d'origen renovable

La present tesi doctoral té com a principal objectiu el desenvolupament de materials polimèrics que siguin respectuosos amb el medi ambient i afavorisquen models d'economia circular, centrant les línies d'investigació en el reaprofitament de residus de la indústria del mango i en la utilització d'àcid polilàctic (PLA) com a principal matriu polimèrica. Per a això s'empren diferents tècniques de processament com l'*electrospinning*, l'extrusió, la injecció o la producció de films per dissolució. A més, es planteja la utilització de diferents additius com a plastificants i càrregues lignocelulòsiques d'origen renovable per a millorar les propietats d'aquests materials sense comprometre el seu alt potencial mediambiental.

El primer bloc de la tesi centra els seus esforços en el reaprofitament de diferents residus del mango (un dels cultius més populars del món), com la pell i el kernel, per a desenvolupar diferents materials amb un gran contingut natural. Dins dels estudis realitzats en aquest bloc s'inclou l'extracció de midó a partir del kernel de mango per a la posterior fabricació de nanofibers per *electrospinning*, amb gran aplicació en el sector mèdic. Altres estudis realitzats proposen la combinació de matrius polimèriques com el biopolipropilè i el PLA, en combinació amb farina de pell de mango i farina d'os de mango, respectivament, mitjançant processos d'extrusió, extrusió reactiva (REX) i injecció. En el cas del biopolipropilè s'utilitzen a més agents compatibilitzants basats en àcid itacònic per a augmentar l'adhesió entre les partícules lignocelulòsiques de la pell del mango amb la matriu polimèrica, la qual és altament apolar. D'altra banda, a les formulacions de PLA i farina d'os de mango se li afigen plastificants com la triacetina i la tributirina per a augmentar les propietats dúctils del PLA. Un quart estudi s'enfoca en la producció de films de glicerol amb farina d'os de mango, rica en midó, per a observar com afecta la grandària de partícula de la farina sobre les propietats dels films. Finalment, es proposa el desenvolupament de materials termoplàstics rics en midó utilitzant farina de kernel de mango en combinació amb diferents plastificants com glicerol, sorbitol i urea. Aquests materials rics en midó són processats per extrusió i injecció i són completament biodegradables i d'origen natural.

El segon i últim bloc de la tesi està enfocat a la utilització de l'àcid polilàctic obtingut de fonts renovables en processos d'extrusió i injecció. Aquest polièster és un

polímer biodegradable el principal desavantatge del qual és la seua gran fragilitat. Per això, s'han emprat diferents tipus de plastificants naturals per a incrementar les propietats dúctils del PLA. En un primer treball, es combina el PLA amb α -terpinil acetat, un plastificant d'origen renovable. A més, s'afegia pell de mandarina molta com a càrrega natural per a avaluar si aquest plastificant és capaç d'augmentar la ductilitat de mesclures de PLA amb càrregues lignocelulòsiques, obtenint resultats molt positius. Un segon treball planteja la combinació de PLA amb dietil-L-tartrat, un plastificant obtingut de l'àcid tartàric, trobat en el raïm i el tamarinde, obtenint elongacions de més d'un 300%. Finalment, dos estudis més plantegen la combinació de PLA amb terpenoids, més concretament èsters de geranil i linalil. En aquest sentit, un dels treballs se centra en variar la proporció d'acetat de linalil i acetat de geranil en les composicions, mentre que l'altre treball avalua com afecta la longitud de cadena dels èsters de geranil a la plastificació del PLA. Tots els plastificants utilitzats en aquest bloc van oferir resultats molt prometedors, amb allargaments al trencament superiors al 200% en materials completament naturals i biodegradables amb gran aplicació en el sector alimentari i de l'envàs i embalatge.

ABSTRACT

Development and characterization of high-performance environmental polymers derived from agro-industrial wastes and renewable origin additives

The present doctoral thesis has as its main objective the development of polymeric materials that are environmentally friendly and promote circular economy models, focusing research on the reuse of waste from the mango industry and the use of polylactic acid (PLA) as the main polymer matrix. Various processing techniques such as electrospinning, extrusion, injection, or cast film are employed for this purpose. In addition, the use of different additives such as plasticizers and lignocellulosic fillers of renewable origin is proposed to improve the properties of these materials without compromising their high environmental potential.

The first part of the thesis focuses on the reuse of various mango waste products (one of the most popular crops in the world), such as peel and kernel, to develop different materials with a high natural content. Studies in this section include the extraction of starch from mango kernels for the subsequent production of nanofibers by electrospinning, which have significant applications in the medical sector. Other studies propose the combination of polymeric matrices such as biopolypropylene and PLA, in combination with mango peel flour and mango kernel flour, respectively, through extrusion, reactive extrusion (REX), and injection processes. In the case of biopolypropylene, compatibilizing agents based on itaconic acid are also used to increase the adhesion between lignocellulosic particles from mango peel and the highly apolar polymer matrix. On the other hand, PLA formulations with mango kernel flour are supplemented with plasticizers such as triacetin and tributyrin to enhance the ductile properties of PLA. A fourth study focuses on the production of glycerol films with mango kernel flour, rich in starch, to observe how the particle size of the flour affects the film properties. Finally, the development of starch-rich thermoplastic materials is proposed using mango kernel flour in combination with different plasticizers such as glycerol, sorbitol, and urea. These starch-rich materials are processed by extrusion and injection and are completely biodegradable and of natural origin.

The second and final part of the thesis is focused on the use of polylactic acid obtained from renewable sources in extrusion and injection processes. This biodegradable polyester has the main disadvantage of being very brittle. Therefore, different types of natural plasticizers have been used to increase the ductile properties

of PLA. In the first study, PLA is combined with α -terpinyl acetate, a renewable plasticizer. In addition, ground tangerine peel is added as a natural filler to evaluate if this plasticizer can increase the ductility of PLA blends with lignocellulosic fillers, yielding very positive results. A second study proposes the combination of PLA with diethyl-L-tartrate, a plasticizer obtained from tartaric acid, found in grapes and tamarind, resulting in elongations of more than 300%. Finally, two more studies propose the combination of PLA with terpenoids, specifically geranyl and linalyl esters. In this regard, one of the works focuses on varying the proportion of linalyl acetate and geranyl acetate in the compositions, while the other study evaluates how the chain length of geranyl esters affects PLA plasticization. All the plasticizers used in this section offered very promising results, with elongations at break exceeding 200% in completely natural and biodegradable materials with significant applications in the food and packaging sectors.

TABLA DE CONTENIDOS

LISTADO DE ARTÍCULOS	25
ECUACIONES.....	27
ABREVIATURAS	31
I. INTRODUCCIÓN	35
I.1. Uso de polímeros y su contexto medioambiental.....	37
I.2. Clasificación de polímeros según su origen y potencial de biodegradación... 39	
I.2.1. Polímeros no biodegradables de origen petroquímico	40
I.2.1.1. Plásticos de uso común	41
I.2.1.2. Plásticos técnicos	41
I.2.1.3. Plásticos de altas prestaciones	41
I.2.2. Polímeros no biodegradables de origen renovable	42
I.2.3. Polímeros biodegradables de origen petroquímico	43
I.2.4. Polímeros biodegradables de origen renovable.....	46
I.3. Almidón.....	49
I.3.1. Introducción.....	49
I.3.2. Obtención del almidón	52
I.3.3. Propiedades del almidón	55
I.3.3.1. Gelatinización del almidón	56
I.3.3.2. Retrogradación del almidón	57
I.3.4. Almidones modificados	59
I.3.4.1. Almidón termoplástico (plastificación)	59
I.3.4.2. Estabilización	61
I.3.4.3. Esterificación	61
I.3.4.4. Entrecruzamiento	62
I.3.5. Aplicaciones de los almidones modificados	62
I.3.5.1. Aplicaciones del almidón modificado en el sector médico y farmacéutico 63	
I.3.5.2. Aplicaciones del almidón modificado en el sector del envase y embalaje . 65	
I.4. Ácido poliláctico (PLA).....	67
I.4.1. Introducción.....	67
I.4.2. Obtención del PLA.....	67
I.4.3. Propiedades del PLA.....	69
I.4.4. Aplicaciones del PLA	73
I.4.5. Modificación del PLA.....	74
I.4.5.1. Mezcla con otros polímeros	74

I.4.5.2. Copolimerización	75
I.4.5.3. Plastificación	76
I.5. Valorización de residuos agroindustriales para su uso como aditivos en biopolímeros	82
I.5.1. Industria del mango y potencial de reaprovechamiento de sus residuos .	84
I.5.2. Industria de los cítricos y potencial de reaprovechamiento de sus residuos	88
I.5.2.1. Extracción de pectina.....	90
I.5.2.2. Extracción de carotenoides.....	90
I.5.2.3. Extracción de flavonoides	91
I.5.2.4. Extracción de terpenos.....	91
REFERENCIAS	93
II. OBJETIVOS	115
II.1. Objetivo general.....	117
II.2. Objetivos parciales	117
III. RESULTS & DISCUSSION	121
Section I: Development of environmentally friendly polymers by upgrading mango wastes	125
III.1.1. Development and evaluation of novel nanofibers based on mango kernel starch obtained by electrospinning	127
III.1.2. Biopolypropylene-based wood plastic composites reinforced with mango peel flour and compatibilized with an environmentally friendly copolymer from itaconic acid.....	159
III.1.3. Improvement of the barrier and mechanical properties of environmentally friendly mango kernel flour/ glycerol films by varying the particle size of mango kernel flour	195
III.1.4. Manufacturing and characterization of high environmentally-friendly composites with polylactide matrix and mango kernel seed flour	227
III.1.5. Development of starch-rich thermoplastic polymers based on mango kernel flour and different plasticizers	259
Section II: PLA-based environmentally friendly materials with the use of natural-derived plasticizers	287
III.2.1. Improvement of poly(lactide) ductile properties by plasticization with biobased tartaric acid ester.....	289
III.2.2. Development of biodegradable PLA composites and tangerine peel flour with improved toughness containing a natural based terpenoid	317
III.2.3. Development and characterization of new environmentally friendly polylactide formulations with terpenoid-based plasticizers with improved ductility	349

III.2.4. Effect of the chain length of geraniol esters on the plasticization efficiency with poly(lactide)	379
IV. CONCLUSIONES	409
IV.1. Conclusiones parciales	411
IV.1.1. Con relación al desarrollo de polímeros respetuosos con el medio ambiente mediante el reaprovechamiento de residuos del mango.....	411
IV.1.2. Con relación a materiales basados en ácido poliláctico aditivados con plastificantes de origen natural	412
IV.2. Conclusiones generales	414
V. APÉNDICES	415
V.1. Índice de tablas.....	417
V.2. Índice de figuras.....	422

LISTADO DE ARTÍCULOS

La presente tesis doctoral se ha estructurado teniendo en cuenta el compendio de los siguientes artículos:

- I. Development and evaluation of novel nanofibers based on mango kernel starch obtained by electrospinning.
- II. Biopolypropylene-based wood plastic composites reinforced with mango peel flour and compatibilized with an environmentally friendly copolymer from itaconic acid.
- III. Improvement of the barrier and mechanical properties of environmentally friendly mango kernel flour/glycerol films by varying the particle size of mango kernel flour.
- IV. Manufacturing and characterization of high environmentally-friendly composites with polylactide matrix and mango kernel seed flour.
- V. Development of starch-rich thermoplastic polymers based on mango kernel flour and different plasticizers.
- VI. Improvement of poly(lactide) ductile properties by plasticization with biobased tartaric acid ester.
- VII. Development of biodegradable PLA composites and tangerine peel flour with improved toughness containing a natural based terpenoid.
- VIII. Development and characterization of new environmentally friendly polylactide formulations with terpenoid-based plasticizers with improved ductility.
- IX. Effect of the chain length of geraniol esters on the plasticization efficiency with poly(lactide).

ECUACIONES

$$\text{Weight loss (\%)} = \frac{W_d - W_0}{W_0} \times 100$$

Weight loss = Pérdida de peso.

W_d = Peso de la muestra seca tras cierto tiempo de ensayo.

W_0 = Peso inicial de la muestra.

$$\chi_c(\%) = \frac{\Delta H_m - \Delta H_{cc}}{\Delta H_m^0 (1 - w)} \times 100$$

χ_c = Grado de cristalinidad.

ΔH_m = Entalpía de fusión.

ΔH_{cc} = Entalpía de recristalización en frío.

ΔH_m^0 = Entalpía de fusión del polímero si fuera 100% cristalina.

w = Fracción másica del polímero en la mezcla.

$$\delta = \sqrt{\delta_d^2 + \delta_p^2 + \delta_h^2}$$

δ = Parámetro de solubilidad.

δ_d = Contribución de las fuerzas dispersivas al parámetro de solubilidad.

δ_p = Contribución de las fuerzas polares al parámetro de solubilidad.

δ_h = Contribución de los puentes de hidrógeno al parámetro de solubilidad.

$$\delta_d = \frac{\sum F_{di}}{V_m}$$

δ_d = Contribución de las fuerzas dispersivas al parámetro de solubilidad.

F_{di} = Fuerzas dispersivas.

V_m = Volumen molar.

$$\delta_p = \frac{\sqrt{\sum F_{pi}^2}}{V_m}$$

δ_p = Contribución de las fuerzas polares al parámetro de solubilidad.

F_{pi} = Fuerzas polares.

V_m = Volumen molar.

$$\delta_h = \sqrt{\frac{\sum E_{hi}}{V_m}}$$

δ_h = Contribución de los puentes de hidrógeno al parámetro de solubilidad.

E_{hi} = Energía de los puentes de hidrógeno.

V_m = Volumen molar.

$$R_a = \sqrt{4(\delta_{d2} - \delta_{d1})^2 + (\delta_{p2} - \delta_{p1})^2 + (\delta_{h2} - \delta_{h1})^2}$$

R_a = Distancia geométrica entre los parámetros de solubilidad.

$\delta_{d2} - \delta_{d1}$ = Diferencia entre la contribución de las fuerzas dispersivas de dos materiales.

$\delta_{p2} - \delta_{p1}$ = Diferencia entre la contribución de las fuerzas polares de dos materiales.

$\delta_{h2} - \delta_{h1}$ = Diferencia entre la contribución de las fuerzas de puentes de hidrógeno de dos materiales.

$$RED = \frac{R_a}{R_0}$$

RED = Diferencia de energía relativa.

R_a = Distancia geométrica entre parámetros de solubilidad.

R_0 = Radio de la esfera de la solubilidad.

$$Grafting\ efficiency = \frac{D_\tau}{D_0} \times 100$$

D_τ = Densidad óptica relativa al espesor del film una vez que todo el ácido itacónico que no ha reaccionado se ha extraído.

D_0 = Densidad óptica relativa al espesor del film a tiempo inicial antes de la inmersión en etanol.

$$\text{Solubility (\%)} = \frac{W_i - W_f}{W_i} \times 100$$

Solubility = Solubilidad.

W_i = Peso inicial de la muestra.

W_f = Peso de la muestra tras el secado.

$$\Delta E = \sqrt{(\Delta L^*)^2 + (\Delta a^*)^2 + (\Delta b^*)^2}$$

ΔE = Diferencia total de color.

ΔL^* = Diferencia de luminancia entre la muestra y el patrón blanco.

Δa^* = Diferencia de las coordenadas de color a^* entre la muestra y el patrón blanco.

Δb^* = Diferencia de las coordenadas de color b^* entre la muestra y el patrón blanco.

$$WVTR = \frac{n \cdot l}{S}$$

WVTR = Velocidad de transmisión de vapor de agua ($\text{g } \mu\text{m}/\text{m}^2 \text{ día}$).

n = Pendiente obtenida por regresión lineal.

l = Espesor del film.

S = Área expuesta del film.

$$DPPH_{inhibition} (\%) = \frac{A_c - (A_s - A_b)}{A_c} \times 100$$

$DPPH_{inhibition}$ = Inhibición del radical DPPH de la muestra.

A_c = Absorbancia de la disolución de DPPH sin la muestra

A_s = Absorbancia de la disolución DPPH con la muestra.

A_b = Absorbancia de metanol puro sin la muestra.

Moisture content = Contenido en humedad.

$$\text{Moisture content (\%)} = \frac{W_i - W_f}{W_i} \times 100$$

W_i = Peso inicial de la muestra.

W_f = Peso de la muestra después del ensayo.

Water absorption = Absorción de agua.

$$\text{Water absorption (\%)} = \left(\frac{W_t - W_0}{W_0} \right) \times 100$$

W_t = Peso de la muestra.

W_0 = Peso inicial de la muestra seca.

ABREVIATURAS

a*	Coordenada de color <i>a*</i>
AFM	Microscopía de fuerza atómica
AH	Ácido hialurónico
AP	Policondensación azeotrópica
ATBC	Acetil tributil citrato
ATEC	Acetil trietil citrato
b*	Coordenada de color <i>b*</i>
χ_c	Cristalinidad
χ_{cmax}	Cristalinidad máxima
CF	Fibra de carbono
CL	Caprolactona
DBT	Dibutil-L-tartrato
DCP	Peróxido de dicumilo
DET	Dietil-L-tartrato
ΔH_{cc}	Entalpía de cristalización en frío
ΔH_m	Entalpía de fusión
DMTA	Análisis térmico-dinámico-mecánico
DSC	Calorimetría diferencial de barrido
E'	Módulo de almacenamiento
E	Módulo elástico
E_{hi}	Energía cohesiva de contribución de grupo
FESEM	Microscopía electrónica de barrido por emisión de campo
GA	Ácido gálico
GAc	Acetato de geraniol
GF	Fibra de vidrio
GLY	Glicerol
GMA	Glicidil metacrilato
HDPE	Polietileno de alta densidad
IA	Ácido itacónico
L*	Luminancia
LAc	Acetato de linalilo
LCA	Life cycle assesment
LDPE	Polietileno de baja densidad

MKF	Harina de kernel de mango
MKS	Almidón de kernel de mango
MKSF	Harina de semilla de kernel de mango
MPEG	Monometoxipolietilén glicol
MPF	Harina de piel de mango
MS	Almidón de mango
OLA	Oligómero de ácido láctico
OSA	Octenil succínico anhídrido
PA	Poliamida
PBAT	Poli(butilén adipato- <i>co</i> -tereftalato)
PBS	Polibutilén succinato
PBT	Polibutilén tereftalato
PC	Policarbonato
PCL	Policaprolactona
PDLA	D-ácido poliláctico
PE	Polietileno
PEEK	Poliéter éter cetona
PEI	Poliéter imida
PES	Poliéter sulfona
PET	Polietilén tereftalato
PGA	Ácido poliglicólico
PHA	Polihidroxialcanoato
PHBV	Poli(hidroxibutirato- <i>co</i> -hidroxivalerato)
PHB	Poli(hidroxibutirato)
phr	Partes por cada cien partes de mezcla
PHV	Poli(hidroxivalerato)
PLA	Ácido poliláctico
PLA-<i>co</i>-PGA	Ácido poli(láctico- <i>co</i> -glicólico)
PLLA	L-ácido poliláctico
PMMA	Polimetilmetacrilato
PO	Polietilén octeno
PP	Polipropileno
PPG	Polipropilénglicol
PS	Poliestireno
PTFE	Politetrafluoroetileno

PU	Poliuretano
PVA	Polivinil alcohol
PVC	Polivinil cloruro
PVP	Polivinil pirrolidona
RED	Diferencia de energía relativa
REX	Extrusión reactiva
RH	Humedad relativa
ROP	Polimerización por apertura de anillo
SOP	Fosfato de monosodio
SORB	Sorbitol
SSP	Polimerización en estado sólido
STMP	Trimetafosfato de sodio
STTP	Tripolifosfato de sodio
T_{5%}	Temperatura a la cual se degrada un 5% de masa
TA	Terpinil acetato
tan δ	Tangente del factor dinámico de amortiguamiento
TBC	Tributilcitrate
TBN	Tributirina
T_c	Temperatura de cristalización
T_{cc}	Temperatura de cristalización en frío
TCN	Triacetina
T_{deg}	Temperatura de degradación
TEC	Trietil citrato
T_g	Temperatura de transición vítrea
TGA	Análisis termogravimétrico
T_m	Temperatura de fusión
TPF	Harina de piel de mandarina
TPS	Almidón termoplástico
UREA	Urea
WCA	Ángulo de contacto de agua
WPC	Materiales compuestos que imitan la madera
WVTR	Velocidad de transmisión de vapor de agua
δ	Parámetro de solubilidad global
δ_d	Contribución de las fuerzas dispersivas
ΔE*_{ab}	Cambio de color total

δ_h	Contribución de las fuerzas de los puentes de hidrógeno
δ_p	Contribución de las fuerzas polares
ϵ_b	Alargamiento a la rotura
σ_{max}	Tensión máxima

I. INTRODUCCIÓN

I.1. Uso de polímeros y su contexto medioambiental

Los polímeros, son grandes moléculas formadas por la unión secuencial de varias moléculas más pequeñas (monómeros). Estos suponen actualmente la familia de materiales que más vinculada está a nuestra vida cotidiana y nuestra cultura. El primer polímero fabricado por el hombre se dio en 1850, siendo este el nitrato de celulosa o celuloide [1], aunque el primer polímero totalmente sintético fue la baquelita, una resina termoestable de fenol-formaldehído que se inventó en 1907 [2]. El primer polímero moderno desarrollado fue el cloruro de polivinilo (PVC), cuyo uso fue extendido en 1920 gracias al uso de aditivos para mejorar su plasticidad [3]. Desde su descubrimiento, estos materiales han sido objeto de numerosos estudios por parte de la comunidad científica. Esto ha hecho que este sector haya evolucionado con gran rapidez, y, actualmente, esté muy presente en nuestra cultura y en la mayoría de los productos de uso común utilizados por el ser humano. El ejemplo más claro es el sector del envase y embalaje, el cual acapara la mayor parte de la producción y uso de materiales poliméricos en la industria en forma de bolsas, botellas, cajas, todo tipo de recipientes para almacenamiento, etc. [4]. Sin embargo, los numerosos avances tecnológicos han permitido que los polímeros se extiendan a sectores mucho más técnicos y complejos, como el sector electrónico [5, 6], el sector de la construcción [7], impresión 3D [8, 9], la industria aeroespacial [10, 11], el sector automovilístico [12, 13] o en aplicaciones médicas [14-16]. El uso de los polímeros en todos estos sectores ha sido posible gracias al gran abanico de propiedades (térmicas, mecánicas, químicas, biológicas, eléctricas, barrera, etc.) que estos ofrecen dependiendo de su naturaleza, así como por su bajo coste.

A pesar de todas las ventajas que los materiales poliméricos ofrecen, en la actualidad la mayoría de ellos provienen del petróleo. Esto, junto a su producción y su consumo masivo, ha provocado varios problemas medioambientales. Entre estos destacan una enorme generación de residuos, ya que gran parte de los polímeros no son biodegradables, como es el caso del polietileno (PE), y un aumento en la huella de carbono asociada al proceso productivo de los mismos [17]. Cuantitativamente, la producción de plásticos en los últimos años supone el consumo de entre un 4 y un 6% del petróleo mundial [4].

Como respuesta a estos problemas medioambientales, unido a una disponibilidad de petróleo en el planeta cada vez menor, ha surgido una creciente concienciación por parte de la sociedad y la comunidad científica que ha derivado en la búsqueda de alternativas que generen un impacto medioambiental mucho más bajo que los polímeros petroquímicos. Cabe tener en cuenta que dentro del término polímero se

engloban tanto polímeros termoplásticos como termoestables y elastómeros. Los polímeros termoplásticos son los más relacionados con los problemas medioambientales mencionados con anterioridad, especialmente la gran generación de residuos atribuida a estos materiales. Por ello, la mayoría de los esfuerzos dirigidos al desarrollo de nuevos materiales para solucionar estos problemas se están dando dentro del ámbito de los termoplásticos.

El planteamiento de estas alternativas viene en forma de dos vertientes. La primera de ellas referente al origen de los polímeros, ya que la mayoría de ellos provienen del petróleo. En este sentido, se está intentando sustituir el petróleo por fuentes naturales renovables. Concretamente, se están utilizando residuos industriales y del sector agroforestal como materia prima para sintetizar polímeros. Esto disminuye directamente la dependencia sobre los combustibles fósiles y, además, favorece la aparición de economías circulares, las cuales permiten reaprovechar residuos de una industria para fabricar productos que se reintroduzcan en la propia industria de la que provienen [18]. La segunda vertiente se centra en la utilización de polímeros que se desintegren en condiciones de compost, es decir, polímeros biodegradables, reduciendo así la acumulación de residuos. La biodegradación es un proceso mediante el cual microorganismos presentes en el suelo son capaces de consumir un polímero y hacerlo desaparecer bajo condiciones apropiadas a nivel de pH, temperatura y oxígeno [19].

I.2. Clasificación de polímeros según su origen y potencial de biodegradación

Como se ha indicado al final del apartado anterior, existen dos aspectos a partir de los cuales pueden clasificarse los polímeros, según su origen y según el final de su ciclo de vida. Según dichas características, existen cuatro grupos dentro de los cuales pueden clasificarse todos los polímeros. Esta clasificación viene ilustrada en la **Figura I.1**, donde se ven claramente diferenciados todos los grupos de polímeros según si provienen de fuentes petroquímicas o fuentes renovables y según si son biodegradables en condiciones de compost o no lo son. Dentro de esta clasificación, todos aquellos polímeros que son biodegradables, de origen renovable o que posean ambas características son considerados biopolímeros. Hay polímeros que pueden existir en dos grupos diferentes, como el polietileno y el biopolietileno, ya que ambos polímeros poseen las mismas propiedades y estructura química, pero tienen un origen distinto. Mientras que el polietileno convencional proviene de fuentes petroquímicas, el biopolietileno puede ser obtenido a partir de bioetanol, que a su vez puede ser producido a partir de la caña de azúcar [17, 20]. Actualmente, considerando esta clasificación, se está intentando dirigir a la industria cada vez más hacia la fabricación y uso de materiales poliméricos biodegradables y con el mayor contenido natural posible.

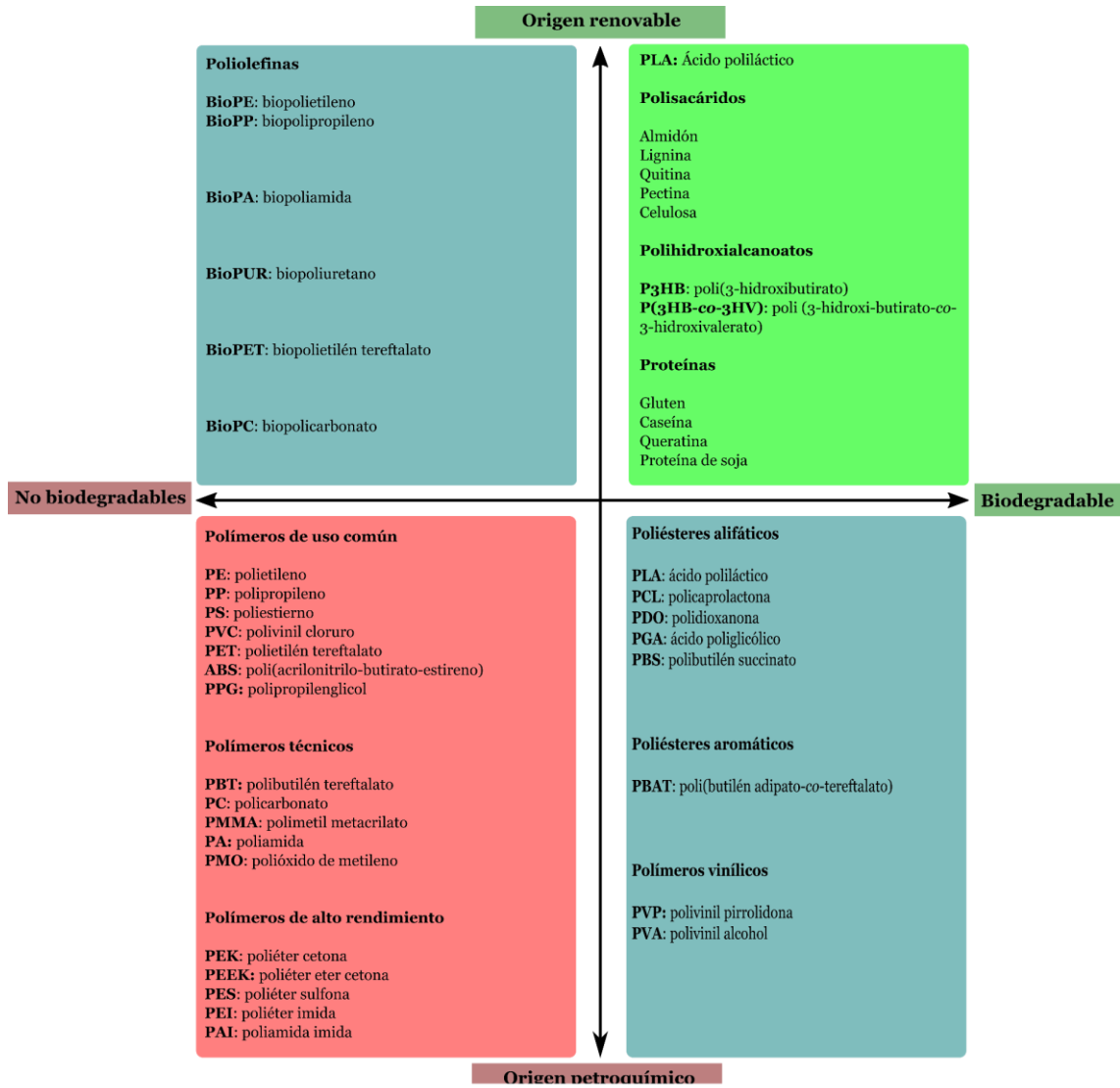


Figura I.1. Clasificación de los polímeros según su origen y su biodegradabilidad.

I.2.1. Polímeros no biodegradables de origen petroquímico

Dentro de este grupo se engloban aquellos polímeros que son responsables de la mayoría de los problemas medioambientales asociados a este tipo de material. Estos polímeros fueron los primeros en desarrollarse y debido al gran abanico de propiedades que ofrecían dependiendo de la aplicación para la que fueran destinados, además de su bajo coste, su producción se extendió muy rápidamente. Todo esto sumado al anterior desconocimiento acerca de los problemas medioambientales que el consumo de estos materiales podría provocar en un futuro, hicieron que tanto empresas como comunidades científicas no prestaran especial atención a la sostenibilidad de estos polímeros.

Dentro de este grupo de polímeros pueden diferenciarse otros subgrupos dependiendo de las aplicaciones para las que estén destinados.

I.2.1.1. Plásticos de uso común

Este tipo de polímeros, también llamados *commodities* son producidos en gran cantidad y para aplicaciones para las cuales no se requieren propiedades excelentes ni específicas. Son especialmente comunes en el sector del envase y embalaje y son los principales contribuyentes a la gran cantidad de residuos que genera este sector. Algunos ejemplos de estos polímeros son el polietileno (PE), el polipropileno (PP), el poliestireno (PS) o el policloruro de vinilo (PVC). La relación entre el coste y las propiedades ha hecho que su uso se extienda a diversos sectores además del envase y embalaje, como la automoción, la agricultura, la medicina o el juguete.

I.2.1.2. Plásticos técnicos

Este grupo de polímeros incluye todos aquellos polímeros que tienen gran importancia en el sector de la ingeniería donde las prestaciones de estos materiales son algo más exigentes que para los plásticos de uso común. Los plásticos técnicos se utilizan sobre todo en aplicaciones donde las propiedades requeridas son muy específicas, como en el sector de la automoción, donde sustituyen al vidrio. Algunos ejemplos de estos polímeros son las poliamidas (PAs), el policarbonato (PC), el polimetil metacrilato (PMMA) o el polibutilén tereftalato (PBT). El coste de estos polímeros es superior al de los plásticos comunes.

I.2.1.3. Plásticos de altas prestaciones

Estos polímeros se diseñan con propiedades muy concretas para ser utilizados en sectores de vanguardia tecnológica, como el sector aeroespacial, nuclear, eléctrico o electrónico. Son materiales de un elevado coste, con procesos de producción también muy costosos, aunque su ciclo de vida es muy prolongado en comparación con otros tipos de plásticos. Algunos ejemplos dentro de este grupo son la poliéter sulfona (PES), la poliéterimida (PEI) o la poliéter éter cetona (PEEK).

I.2.2. Polímeros no biodegradables de origen renovable

Este grupo engloba aquellos polímeros que provienen de fuentes naturales, pero no se descomponen en condiciones de compost. En los últimos años, se han realizado diversas investigaciones para desarrollar polímeros que posean la misma estructura química que los polímeros petroquímicos pero obtenidos a partir de fuentes renovables, como la biomasa. Estos polímeros poseen propiedades prácticamente idénticas a sus versiones análogas derivadas del petróleo. Además, al ser obtenidas de fuentes renovables cuentan con la ventaja de que son capaces de reducir la huella de carbono asociada a su proceso productivo y reducen también el uso de combustibles fósiles. El ejemplo más claro es el desarrollo del biopolietileno (bioPE), el cual puede ser obtenido a partir de la caña de azúcar. En este caso, el proceso se inicia con la fermentación de la caña de azúcar para obtener bioetanol, al cual se le aplica un proceso de deshidratación catalítica para convertirlo en bioetileno, siendo este el monómero del polietileno. Finalmente, mediante polimerización convencional de este etileno se obtiene el biopolietileno [21-23]. La **Figura I.2** muestra el proceso de obtención del polietileno a partir de la caña de azúcar según el procedimiento descrito anteriormente. La fabricación de biopolietileno permite eliminar la emisión de aproximadamente 2,5 toneladas de CO₂ por cada tonelada producida [20]. Esta cantidad es la que emite aproximadamente el proceso productivo del polietileno derivado del petróleo. Esto demuestra el gran aporte que hace la utilización de bioPE en cuanto a la reducción de la huella de carbono.

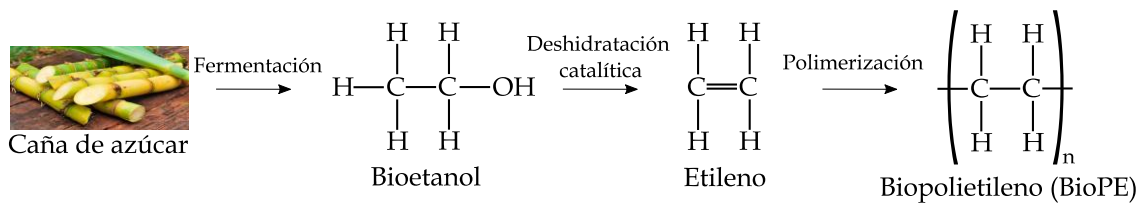


Figura I.2. Proceso de obtención del biopolietileno (bioPE).

Cabe destacar que se han realizado muchos estudios referentes al bioetileno obtenido de materiales lignocelulósicos, como la caña de azúcar antes mencionada, ya que este componente permite desarrollar varias rutas de producción de diversos polímeros. Por ejemplo, tras la deshidratación catalítica del bioetanol, el etileno puede someterse a un proceso de dimerización para obtener buteno, seguidamente se le aplica una reacción de metátesis para convertirlo en propileno y, finalmente, por polimerización se obtiene el biopolipropileno (bioPP) [20] (ver **Figura I.3**). Además de

este proceso se han propuesto otras alternativas para el desarrollo del bioPP, como es la obtención de 1,2-propanodiol (acetona) a partir de procesos de fermentación para luego convertirlo en 2-propanol y, seguidamente, obtener el monómero de propileno pasando por un proceso de deshidratación [24]. No obstante, todas estas rutas para la obtención de biopolímeros se encuentran en pleno desarrollo y aún no están plenamente extendidas en la industria.

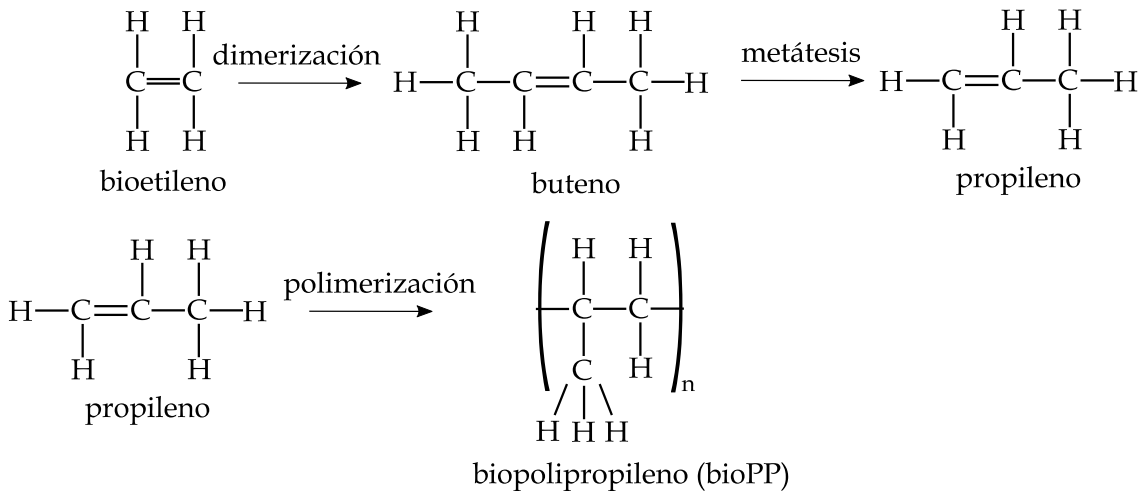


Figura I.3. Proceso de obtención del biopolipropileno (bioPP) a partir del bioetileno.

El policarbonato derivado de la isosorbida es otro de los polímeros de interés dentro de este grupo, ya que este se sintetizaba tradicionalmente a partir del bisfenol A, el cual ocasionaba problemas de toxicidad [25]. La isosorbida, al tener una estructura química parecida y una toxicidad reducida, resulta una alternativa mucho más plausible para el desarrollo de polímeros con mayor contenido renovable como el policarbonato o la polisulfona.

I.2.3. Polímeros biodegradables de origen petroquímico

En vista de la gran generación de residuos que los materiales poliméricos están provocando, en los últimos años se han ido desarrollando nuevos polímeros capaces de descomponerse en condiciones de compost, es decir, que se biodegraden. De esta forma los residuos generados al final del ciclo de vida de estos materiales se reducen considerablemente. El potencial de biodegradación de un polímero viene determinado por su capacidad para sufrir hidrólisis, la cual está definida por los grupos químicos que conforman su estructura. Algunos de los grupos más susceptibles de sufrir hidrólisis son

los grupos anhídrido [26], acetilo [27], acetato [27], amida [28] o éster [29]. Este último grupo es especialmente sensible a ser hidrolizado, por ello, los poliésteres, sobre todo los poliésteres alifáticos y algunos aromáticos, presentan una excelente biodegradabilidad. Bajo las condiciones correctas de temperatura, humedad, pH y composición del medio, el grupo éster es fácilmente hidrolizable, promoviendo la rotura de las cadenas del polímero en el que se encuentre hasta que el tamaño de estas sea lo suficientemente pequeño para poder ser atacado y descompuesto en los procesos metabólicos de ciertos microorganismos [30]. Este proceso se ve ilustrado en la **Figura I.4**.

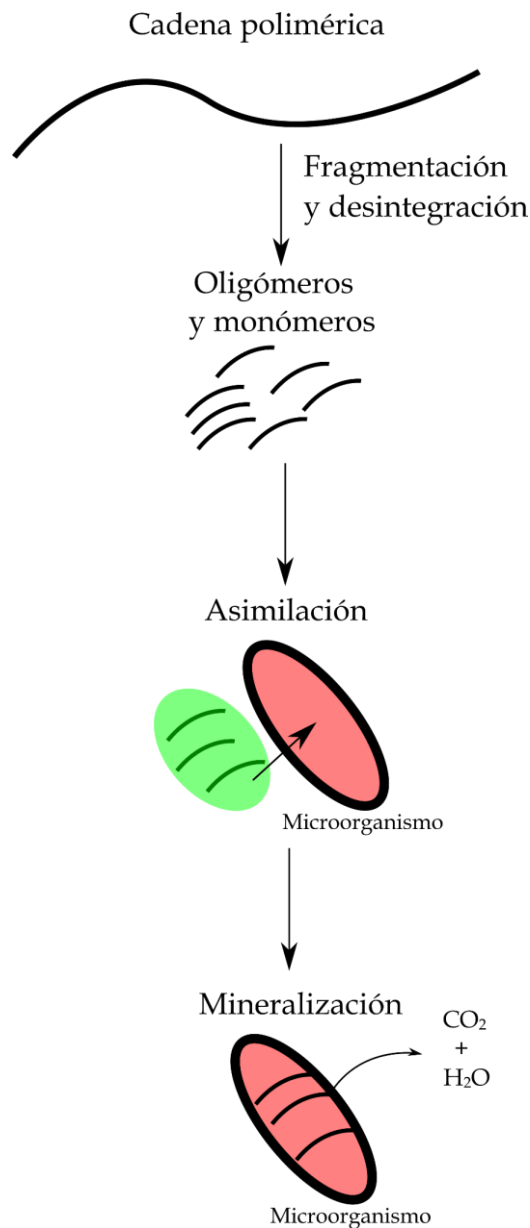


Figura I.4. Proceso de descomposición de un poliéster en condiciones de compost (biodegradación).

De entre todos los poliésteres alifáticos, los que más interés han recibido en los últimos años han sido el ácido poliláctico (PLA) [31], la policaprolactona (PCL) [32], el ácido poliglicólico (PGA) [33] o el polibutilén succinato (PBS) [34], siendo el PLA el que mayor interés presenta actualmente, tanto a nivel industrial como a nivel de investigación recibiendo especial atención en cuanto a su síntesis a partir de fuentes renovables y en cuanto a la mejora de sus propiedades. Estos polímeros poseen propiedades mecánicas y térmicas muy interesantes. Además, se caracterizan por su biodegradabilidad y por su biocompatibilidad, lo cual permite que puedan ser introducidos, absorbidos y procesados por el cuerpo humano sin consecuencias negativas para nuestro organismo. Debido a esto, estos poliésteres han encontrado gran aplicación en el sector médico y de la alimentación [35, 36]. Algunas de las aplicaciones en las que se están utilizando estos materiales actualmente son en prótesis óseas y vasculares, fabricación de tejidos, dosificación de medicamentos, placas de fijación, films biodegradables para el sector del envase en alimentación o bolsas, entre otras muchas aplicaciones [37-40].

Además de los poliésteres alifáticos mencionados, poliésteres alifáticos-aromáticos como el poli(butilén adipato-*co*-tereftalato) (PBAT) también están recibiendo especial atención debido a las buenas propiedades dúctiles que posee, además de su buena procesabilidad [41]. No obstante, este polímero presenta un coste de producción excesivo para las propiedades que ofrece y por ello suele ser empleado en forma de *blend* con otros polímeros como el PLA o el almidón.

Por otro lado, los polímeros vinílicos como la polivinilpirrolidona (PVP) o el polivinil alcohol (PVA), cuya estructura química se observa en la **Figura I.5**, se están introduciendo con gran fuerza en el sector médico y farmacéutico. Ambos polímeros han sido utilizados tanto por separado como en mezclas conjuntamente para producir hidrogeles con una constitución y unas propiedades muy parecidas a las del tejido humano (alto contenido en agua, textura gomosa y suave, elevada elasticidad y una baja tensión interfacial con el agua y fluidos biológicos). Algunas de las aplicaciones en las que se han incorporado estos materiales son la producción de cartílago artificial, sistemas vasculares, músculo artificial, tejido óseo, liberación de medicamentos o recubrimientos para heridas y quemaduras [42].

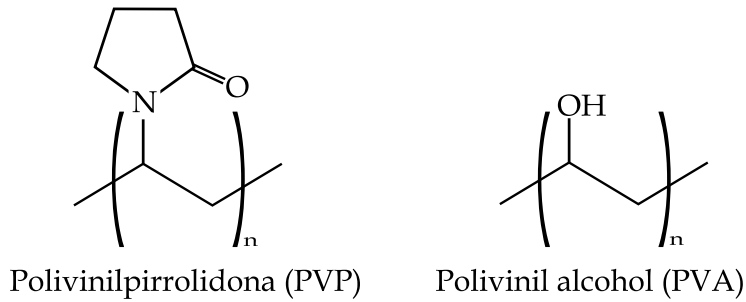


Figura I.5. Estructura química de la polivinilpirrolidona (PVP) y del polivinil alcohol (PVA).

I.2.4. Polímeros biodegradables de origen renovable

Los avances tecnológicos realizados en el campo de los polímeros han llevado al desarrollo de polímeros que sean tanto biodegradables como que provengan de fuentes naturales, siendo con diferencia el grupo de polímeros de mayor interés desde el punto de vista medioambiental. Dentro de este grupo se encuentran una gran cantidad de polímeros naturales, como son polisacáridos como el almidón, la celulosa, la quitina, el quitosano, el alginato, el ácido hialurónico (AH), entre otros [43], o los polímeros basados en proteínas [44]. Estos polímeros suelen ser utilizados en combinación con otros compuestos, ya que prácticamente carecen de cohesión por sí solos y sus propiedades, especialmente las mecánicas, son muy pobres. Un ejemplo de esto es el caso de los almidones termoplásticos, que consisten en la combinación de almidón con plastificantes como el glicerol o el sorbitol en condiciones de temperatura elevada para hacer reaccionar las cadenas del almidón con el plastificante y obtener una estructura más rígida [45]. Cabe recalcar que estos materiales tienen un fuerte componente biodegradable y su potencial desde el punto de vista de la medicina, alimentación y el envasado es enorme.

Los polímeros obtenidos por fermentación bacteriana, llamados polihidroxicanoatos (PHAs) también se encuentran en esta clasificación [46]. Los PHAs son una familia de biopoliésteres que son sintetizados por varios microorganismos. Se conocen alrededor de 150 monómeros diferentes de PHAs, diferenciados por los grupos químicos que poseen (grupos alquilo saturados, grupos alquilo insaturados, grupos alquilo ramificados y grupos alquilo sustituidos) y por la longitud en átomos de carbono de la cadena principal del PHA [47]. Debido a la gran cantidad de PHAs que existen, sus propiedades van desde polímeros que se asemejan al polipropileno hasta polímeros elastoméricos. Son característicos por su biodegradabilidad y biocompatibilidad, lo que los ha llevado a ser incluidos en el sector médico a través de aplicaciones como la

ingeniería de tejidos o en dosificación de medicamentos [48]. De entre todos los PHAs conocidos, algunos de los más utilizados son el poli(3-hidroxiбутirato) (PHB), el poli(3-hidroxiуalerato) (PHV) y algunos de sus copolímeros, como el poli(3-hidroxiбутirato-*co*-3-hidroxiуalerato) (PHBV) [49] (ver **Figura I.6**).

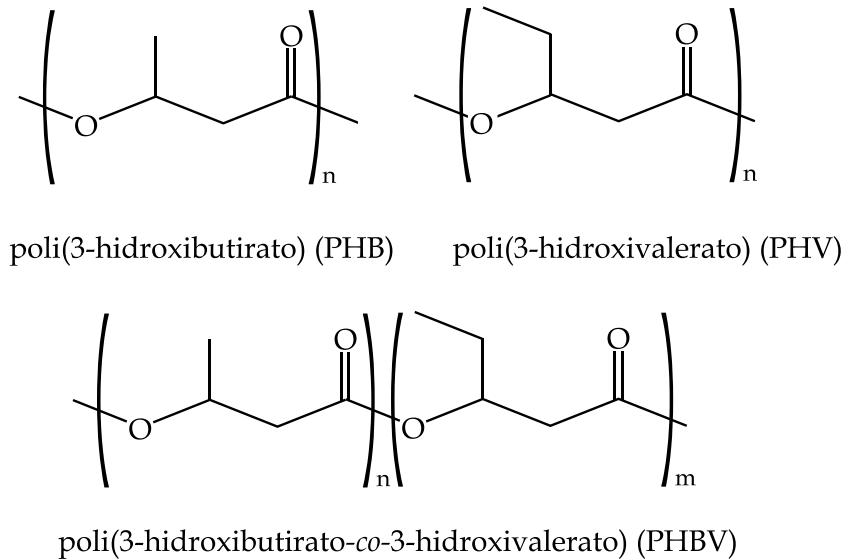
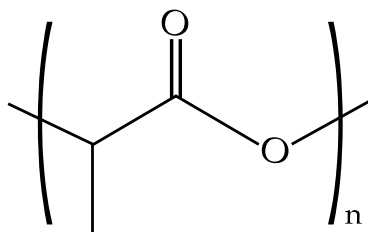


Figura I.6. Estructura química de algunos de los PHAs más utilizados: poli(3-hidroxiбутirato) (PHB), poli(3-hidroxiуalerato) (PHV) y poli(3-hidroxiбутirato-*co*-3-hidroxiуalerato) (PHBV).

Cabe destacar dentro de este grupo el PLA, pero en este caso obtenido a partir de la fermentación de polisacáridos, como el almidón, el cual a su vez puede ser obtenido de varias fuentes naturales (patata, maíz, caña de azúcar, arroz, etc.). Mediante el proceso de fermentación se obtiene ácido láctico (LA) y, posteriormente, mediante polimerización por policondensación o apertura de anillo se produce el PLA [50], cuya estructura se observa en la **Figura I.7**. El PLA se caracteriza por una elevada fragilidad, y es por eso que suele ser mezclado con otros polímeros o compuestos para reducir esta gran desventaja. Como se ha comentado en el apartado anterior, el PLA ha atraído gran atención en el sector médico, encontrándose en forma de prótesis, tornillos o suturas reabsorbibles; en el sector textil en forma de no tejido a partir de fibras; y en el sector del envase en forma de films biodegradables [51].



Ácido poliláctico (PLA)

Figura I.7. Estructura química del ácido poliláctico (PLA).

A pesar de las propiedades tan interesantes que todos estos polímeros ofrecen, especialmente su gran aporte en cuanto a sostenibilidad medioambiental, las propiedades técnicas de estos materiales (propiedades mecánicas, térmicas, reológicas, barrera, etc.) son bastante inferiores a las de los polímeros descritos en el resto de apartados de esta sección. Es por ello que el enfoque de la comunidad científica sobre estos polímeros es especialmente acusado y se están haciendo avances para intentar mejorar sus características, ya que al fin y al cabo son la alternativa más prometedora referente a la sostenibilidad del planeta.

I.3. Almidón

I.3.1. Introducción

El almidón es un polímero perteneciente a la familia de los polisacáridos que se encuentra de forma natural en plantas (tejidos vegetales, raíces, tayos, semillas, etc.), algas y algunas bacterias. Su principal función dentro de estos organismos es la de actuar como medio de almacenamiento de energía. Está considerado la segunda molécula más abundante de biomasa en la tierra, solo por detrás de la celulosa [52]. Algunas de las fuentes más comunes en las cuales se encuentra este polímero son la patata, el maíz, el trigo o el arroz. El almidón se encuentra dentro del grupo de polímeros biodegradables y de origen natural vistos en el apartado anterior. En los últimos años ha recibido especial atención debido a su gran disponibilidad, su bajo coste de obtención y su excelente rendimiento medioambiental, ya que es completamente biodegradable, no tóxico y procede de una fuente completamente renovable. Además, combinado con otros componentes, como plastificantes, mediante plastificación y gelatinización, es capaz de dar lugar a materiales con propiedades añadidas muy interesantes.

El comportamiento del almidón depende en gran medida de la naturaleza de sus componentes, ya que este está formado realmente por dos homopolisacáridos compuestos por unidades de glucosa, como es común en otros polisacáridos (celulosa, glucógeno o quitina). Estos polisacáridos son la amilosa y la amilopectina. La amilosa es un polímero de naturaleza lineal formado por entre 500 y 2000 unidades de glucosa, mientras que la amilopectina es un polímero altamente ramificado conformado por más de 1 millón de unidades de glucosa. Ambos componentes suponen aproximadamente el 98% del peso del almidón [53]. La relación entre ambos componentes dictará las propiedades del almidón, la cual viene determinada por el origen del almidón. Se estima que generalmente el almidón está formado por un 20% de amilosa y un 80% de amilopectina, aunque esto puede variar hasta almidones con un 80% de amilosa [54].

La amilosa es un polímero lineal y está formada por unidades de α -D-glucosa que están unidas por enlaces α -1,4 glicosídicos. Por otro lado, la amilopectina es un polímero ramificado formado también por unidades de α -D-glucosa, unidas en este caso por enlaces α -1,4 y α -1,6 glicosídicos. Los enlaces α -1,4 unen las moléculas de glucosa linealmente, mientras que los enlaces α -1,6 provocan la ramificación del polímero (aproximadamente un 5% de las ramas se encuentran ramificadas). La amilopectina posee un peso molecular considerablemente mayor que el de la amilosa, es por ello que la distribución de estos dos polímeros afecta de forma significativa a las propiedades

generales del almidón [55]. La **Figura I.8** ilustra la estructura anteriormente descrita de la amilosa y la amilopectina.

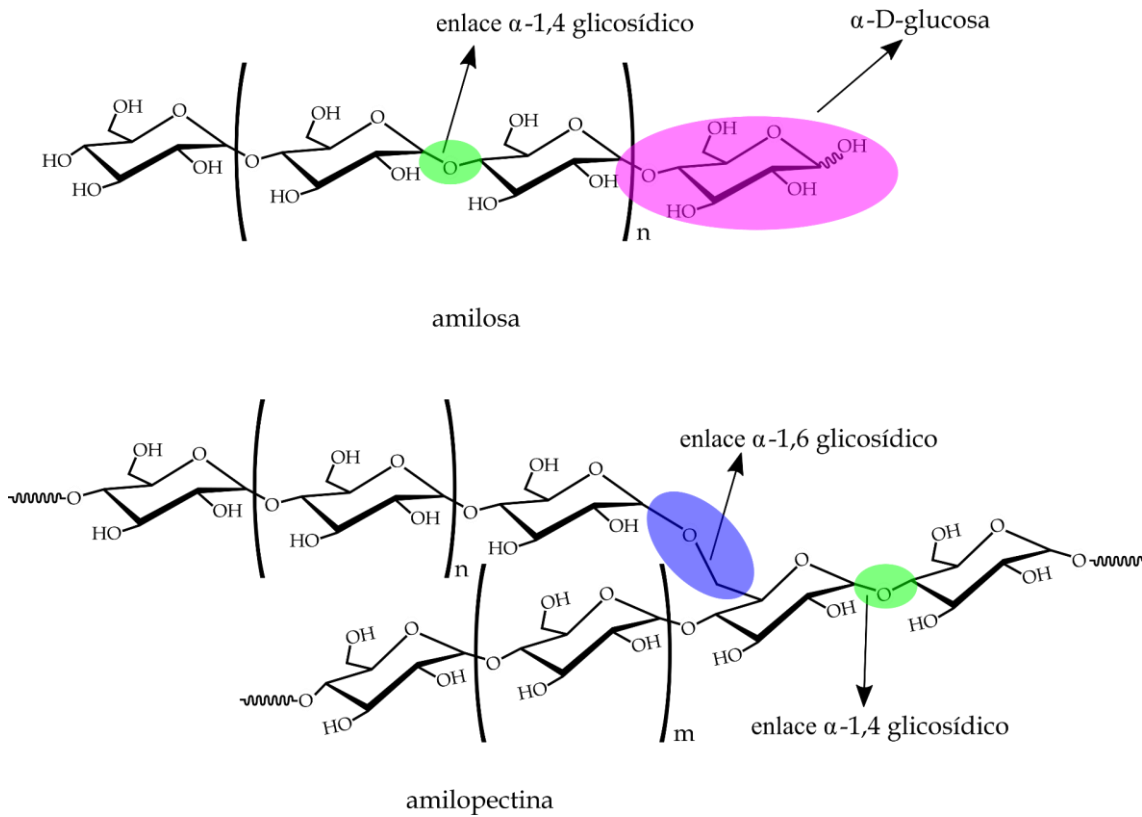


Figura I.8. Esquema de la estructura química de la amilosa y la amilopectina.

A nivel macromolecular, el almidón se acumula en forma de gránulos semicristalinos de geometrías irregulares ovaladas o esféricas. Dependiendo del origen del almidón, y por tanto también del contenido en amilosa o amilopectina, la geometría y tamaño de estos gránulos también cambia. El tamaño de los gránulos de almidón en general varía desde 1 μm hasta 100 μm , y su morfología viene determinada por las condiciones de su biosíntesis, ya que el almidón se deposita a nivel celular en diferentes partes de plantas y la presencia de otros elementos subcelulares, como la membrana amiloplasto, puede alterar la geometría de los gránulos. Muchos almidones, como el de la patata y la canna, tienen forma ovalada; el almidón de maíz, arroz y avena, es de forma poligonal; mientras que el almidón de trigo y de cebada tiene forma de disco [56]. La **Figura I.9** muestra una imagen obtenida por microscopía electrónica de barrido por emisión de campo (FESEM) de gránulos de almidón extraídos del kernel del mango, donde se observa claramente la irregularidad de la morfología del almidón.

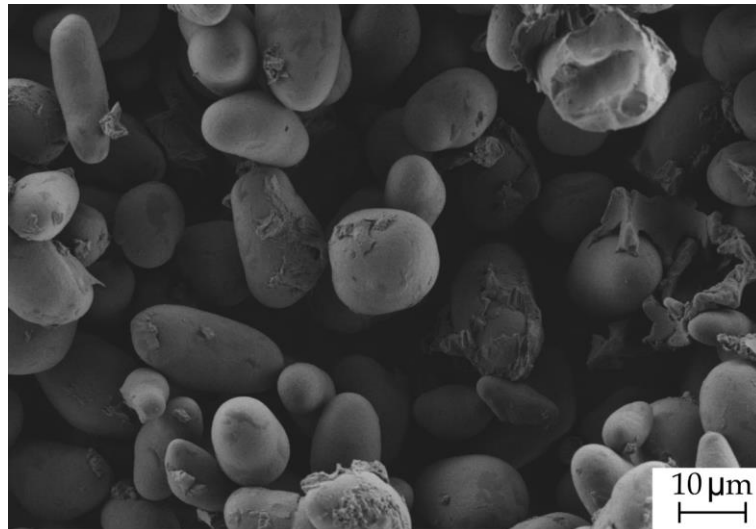


Figura I.9. Imagen FESEM de la estructura granular de almidón extraído del kernel del mango.

La presencia de los enlaces α -1,6 en la amilopectina favorece que las cadenas lineales cortas de glucosa se dispongan eficientemente de forma paralela en una estructura de doble hélice, que es la que conforma la base del gránulo semicristalino de almidón. Por otro lado, la localización precisa de la amilosa dentro de los gránulos está sujeta a debate por la comunidad científica, aunque se cree que se encuentra de forma predominante en la parte menos cristalina o amorfa de los gránulos, entre las cadenas ramificadas de amilopectina [57]. La **Figura I.10** muestra la disposición teórica de la amilosa y la amilopectina dentro del gránulo, diferenciando la parte amorfa y la parte cristalina del polímero dentro de su morfología.

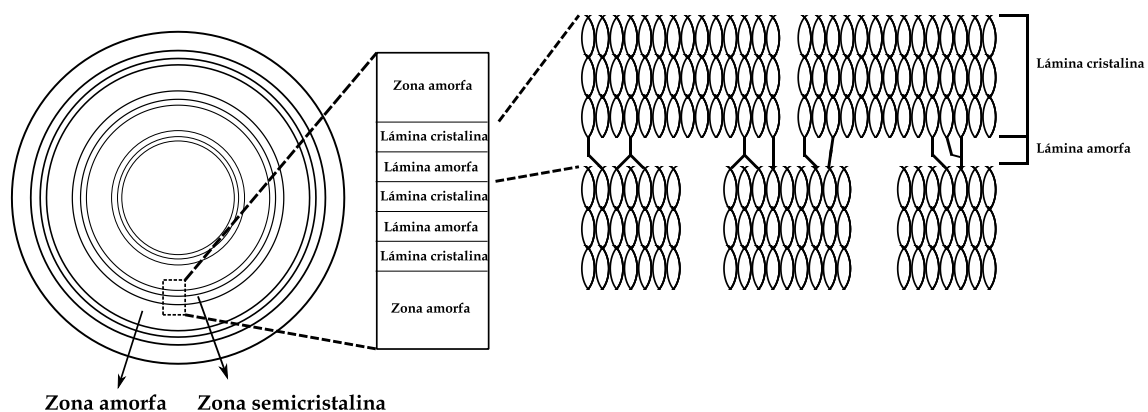


Figura I.10. Esquema de la disposición de la amilosa y la amilopectina dentro de los gránulos de almidón puro, donde se aprecia la diferenciación de la zona amorfa y la zona semicristalina.

Reproducido de [58].

I.3.2. Obtención del almidón

Como se ha comentado previamente, el almidón se encuentra en una gran cantidad de plantas, vegetales y frutas, ya que es el medio que tienen las especies vegetales de almacenar energía. Es por ello por lo que este es extraído directamente de estas fuentes o bien a partir de residuos derivados de la industria de la alimentación. Aunque la mayoría del almidón se extrae normalmente de cuatro fuentes principales, que son la patata, la yuca, el trigo y el maíz [59], hay muchas otras frutas y vegetales que tienen un gran contenido en almidón y que pueden ser aprovechadas como fuentes de este recurso. Entre estas destacan el mango [60], el melocotón [61], el plátano [62] el aguacate [63] o la piña [64]. Actualmente se está haciendo especial hincapié en la extracción del almidón a partir de los residuos de estas frutas, como la piel o el hueso, ya que de esta forma se favorece un reaprovechamiento de estos residuos y no se utiliza la parte comestible para obtener el almidón [62].

Se han desarrollado varios métodos de extracción y aislamiento de almidón dependiendo de la fuente de la que provenga el polímero. No obstante, muchos métodos son comunes para diferentes fuentes ricas en almidón. Tomando la patata como ejemplo, una de las fuentes más comunes, existen diferentes procesos de extracción:

- Extracción utilizando metabisulfito de sodio: para esta metodología, la patata se corta en trozos pequeños y se mezcla con agua destilada a una proporción de aproximadamente 1:10 (almidón:agua). Se lleva a cabo un proceso de mezclado hasta que se forma una pasta suave, a la cual se le añade metabisulfito de sodio 0,01% durante el mezclado. Una vez se tiene la pasta, esta se filtra con mallas en el rango 250-75 μm y se centrifuga la disolución filtrada durante aproximadamente 20 minutos a 5000 rpm. El almidón queda depositado en el fondo tras la centrifugación, de forma que tras un lavado con tolueno, este se seca y tritura en forma de polvo para su posterior uso [65]. La **Figura I.11** muestra este proceso de extracción de forma esquematizada.
- Extracción utilizando cloruro de sodio: en este caso, los trozos de patata se homogeneizan en una disolución 1 M de cloruro de sodio (NaCl). Seguidamente se filtra la disolución y la fracción de almidón se lava utilizando agua destilada. El almidón se deja precipitar durante 24 horas y el agua es decantada. Por último, el sedimento se centrifuga a 3000 rpm durante 10 minutos y el almidón se somete a un secado para después ser pulverizado [66].

- Extracción utilizando agua destilada: este proceso es similar a los anteriores, donde los trozos de patata se homogeneizan con agua destilada durante 1-2 minutos, formando una pasta que luego es filtrada. El filtrado se deja reposar durante 3 horas para que el almidón precipite. Este es luego lavado con agua destilada 3 veces y se deja secar durante 2 días para luego ser pulverizado y dejado listo para su uso o caracterización [67].

Como puede verse, los métodos son similares entre sí y utilizan operaciones muy parecidas, pero cambian los disolventes y sustancias químicas utilizadas para la extracción. Una extracción con agua destilada puede resultar más barata, debido a la gran disponibilidad de este disolvente, pero puede suponer un rendimiento de extracción menor que la utilización de NaCl o metabisulfito de sodio. El rendimiento de extracción de almidón puede variar entre un 30 y un 90% [68, 69]. Independientemente del método de extracción, el almidón puro es de un color blanco como el que se observa en la **Figura I.11**.

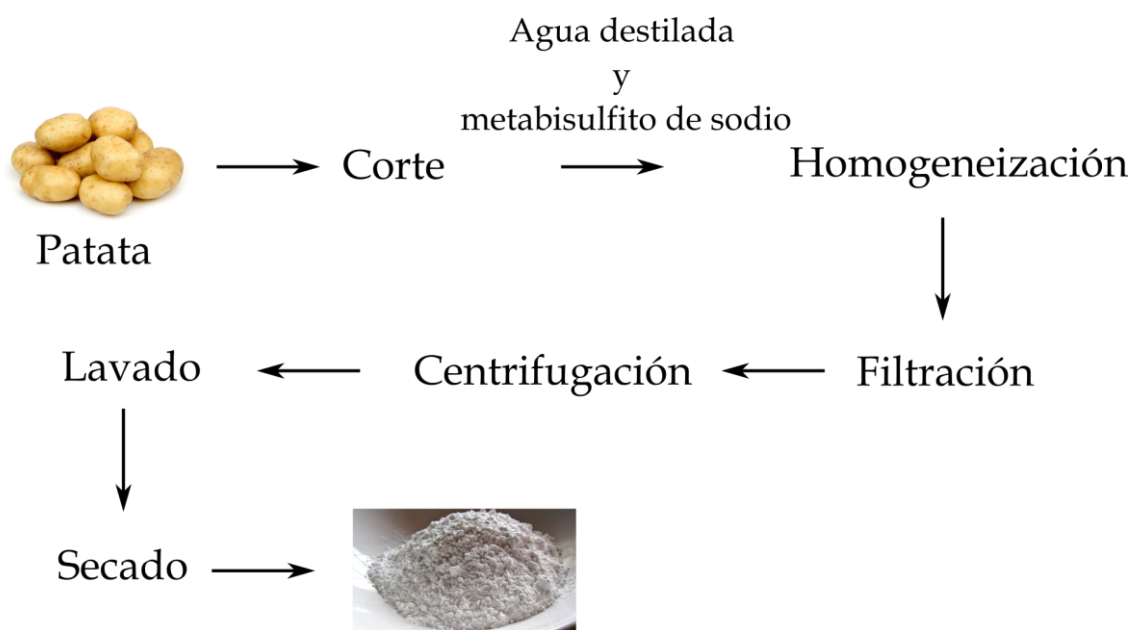


Figura I.11. Esquema del proceso de extracción de almidón de la patata utilizando metabisulfito de sodio.

En los casos expuestos anteriormente, el almidón es extraído directamente de la parte comestible del vegetal, la patata. Sin embargo, como se ha mencionado previamente, los estudios científicos se están dirigiendo cada vez más hacia un reaprovechamiento de residuos de la industria agroalimentaria para obtener el almidón.

Es el caso de la piña, cuya planta genera entre 6 y 8 kg de residuos que incluyen hojas, tallo y raíces. El tallo de la piña supone 0,6 kg de residuo que normalmente se descarta después de pelarla. Sin embargo, este posee gran potencial como fuente de extracción de almidón, ya que el 97,8% de su composición es almidón [70]. Para el proceso de extracción, los tallos de piña se cortan en trozos de aproximadamente 6 mm y se trituran en agua destilada utilizando una batidora o un homogeneizador a una relación agua:tallo de 1:1. De esta forma, similar a los procesos descritos para la patata, se obtiene una pasta con materiales fibrosos. Estas fibras se filtran y el filtrado, que contiene almidón y componentes solubles en agua, se somete a centrifugación para separar el almidón. La parte líquida se decanta y el almidón se lava con agua destilada mediante centrifugación repetidas veces hasta que la fracción de líquido adquiere una tonalidad clara, lo que indica que los elementos solubles en agua se han eliminado. Finalmente se seca el almidón y se tritura. El rendimiento de extracción en este caso se encuentra en torno a un 30% [70].

Procesos muy parecidos al descrito para el residuo de la piña pueden ser aplicados a residuos de otras frutas como el kernel del mango [71], las semillas del litchi [72], la pulpa del tamarindo [73], el kernel del níspero [74] y la semilla del longan [75], la semilla del aguacate [76] y residuos de la manzana [77], entre otros. La **Tabla I.1** muestra el contenido en almidón, el contenido en amilosa de ese almidón y el tamaño y morfología de los gránulos de almidones extraídos de diferentes residuos de una gran variedad de frutas. Puede observarse una gran variación en el contenido en almidón, desde un 11% hasta un 80%.

Tabla I.1. Fuentes de almidón de residuos de frutas, contenido en almidón, contenido en amilosa del almidón y tamaño medio de los gránulos de almidón. Adaptado de [69].

Fuente de almidón	Contenido en almidón (%)	Contenido en amilosa (%)	Tamaño de gránulo (μm)
Piel del kiwi	34,6 - 40,7	15,5 - 17,8	8,7 - 9,6
Tayo de manzana	11,0	34,0	9,7
Kernel del mango	58,9 - 64,0	9,1 - 16,3	19,3
Semilla de lichi	53,0	19,2	7,9 - 10,2
Semilla de tamarindo	20,0	14,2	2,9 - 6,1
Semilla de níspero	71,0	25,0	7,7 - 9,4
Semilla de achiote	18,0 - 20,0	24,0	0,8
Semilla de yaca	60,0 - 80,0	22,1 - 38,3	6,0 - 13,0
Semilla de aguacate	27,5 - 29,8	15,0 - 16,0	(1): 28,0 - 32,0 (2): 6,0 - 9,0
Pulpa de manzana	44,0 - 53,0	26,0 - 29,3	2,0 - 12,0
Piel de plátano	22,6	25,7	17,0

(1): Triangulares

(2): Circulares

I.3.3. Propiedades del almidón

El almidón es un polímero de naturaleza semicristalina en su estado puro (morfología granular). Posee una enorme disponibilidad a nivel industrial, ya que, como se ha visto con anterioridad, puede ser obtenido y extraído de una gran cantidad de fuentes vegetales, tanto a nivel de materia prima o productos comestibles, como a nivel de residuos de la industria agroalimentaria y agroforestal. Se trata de un polímero barato, versátil, natural y que puede ser modificado fácilmente para alterar sus propiedades fisicoquímicas por medio de tratamientos químicos, enzimáticos o físicos [58]. Además, se trata de un polímero biodegradable y biocompatible, lo cual ha extendido su uso en sectores como el de la alimentación y la medicina [78, 79]. Entre algunas de sus aplicaciones se encuentra la producción de films, su uso como agente gelificante, emulsionante, agente encapsulante para la liberación controlada de medicamentos, como adhesivo o como floculante, entre otras aplicaciones. [80]. Sin embargo, el almidón por sí solo presenta propiedades muy pobres, especialmente en el ámbito mecánico, ya que posee una estructura granular que carece de cohesión. Además, su insolubilidad en agua fría, pérdida de viscosidad, baja resistencia a cizalla y baja estabilidad térmica han creado la necesidad de combinarlo con otros elementos como plastificantes u otras matrices poliméricas que sirvan como soporte para sus propiedades químicas [81]. Así surgen los almidones modificados.

El objetivo de la modificación del almidón es estabilizar los gránulos de almidón durante su procesado y así poder aprovechar sus propiedades en combinación con las propiedades del elemento con el que se combine. En este sentido, el almidón posee una propiedad adicional que facilita el desarrollo de nuevos materiales con este polímero como base. Esta propiedad es la gelatinización.

I.3.3.1. Gelatinización del almidón

La gelatinización del almidón es una propiedad que permite una modificación fisicoquímica de las propiedades del almidón inducida térmicamente. Esta se da cuando el almidón es calentado en un medio acuoso a altas temperaturas (120-140 °C), sin llegar a su temperatura de degradación. En estas condiciones, la amilosa y la amilopectina presentes en los gránulos del polímero cambian la estructura de dichos gránulos. Estos cambios vienen determinados por las temperaturas de transición vítrea y de fusión. Dependiendo del grado de cristalinidad del almidón, la temperatura de transición vítrea exacta para dicho polímero puede variar. La transición vítrea aumenta la movilidad de la parte amorfa del almidón, facilitando la hidratación de sus moléculas y la disociación de la estructura de doble hélice en sus cristales. Esta disociación se inicia tras la transición vítrea, y es conocida como gelatinización [82]. Como es de esperar, esta transición ocurre en un rango de temperaturas diferente para cada almidón, dependiendo de su origen, y, por tanto, de la morfología y cristalinidad de sus gránulos.

La gelatinización se inicia con la absorción de agua dentro de los gránulos, llevando a una hidratación de la corteza amorfa y una ruptura de los puentes de hidrógeno allí presentes. Esto provoca una expansión de los gránulos, que termina por desestabilizar las regiones amorfas del polímero. Esta desestabilización se transmite hasta la parte cristalina de los gránulos, gobernada por las cadenas de amilopectina, provocando cambios irreversibles en la estructura que implican la fusión de los cristales de almidón. De esta forma, el almidón, que en un principio es insoluble en agua, solubiliza y se produce una lixiviación que aumenta la viscosidad de la suspensión almidón-agua. En resumen, se destruye el orden molecular de los gránulos de almidón, llevando a cambios irreversibles y a una solubilización del almidón en agua, la cual en condiciones adecuadas puede facilitar la interacción del almidón con otros componentes presentes en la disolución [83]. La **Figura I.12** ilustra el proceso de gelatinización descrito anteriormente.

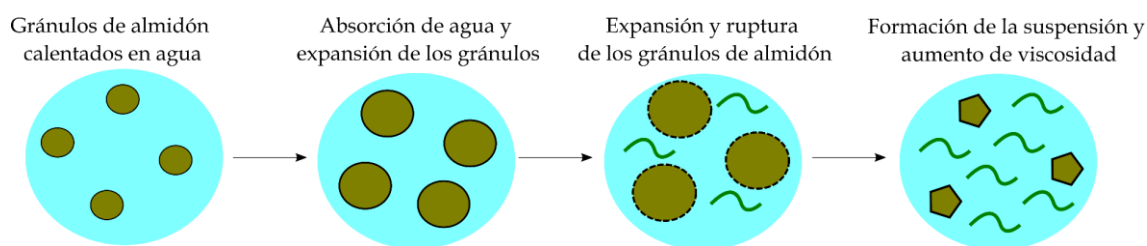


Figura I.12. Esquema del proceso de gelatinización del almidón en medio acuoso.

La suspensión que se obtiene tras la gelatinización del almidón es un medio idóneo para hacer que este interactúe con otros componentes, como pueden ser plastificantes como el glicerol, sorbitol, urea, formamida, xilitol, entre otros [84]; u otros componentes químicos que se adhieran a su estructura, como los agentes estabilizantes [85], adición de grupos lipofílicos [86] o la inducción de reacciones de esterificación o eterificación [87, 88].

Sin embargo, cuando tras el calentamiento y la consecuente gelatinización el almidón se enfría y se almacena este sufre una reacción conocida como retrogradación, la cual se debe tener en cuenta a la hora de desarrollar materiales basados en almidón.

I.3.3.2. Retrogradación del almidón

Tras la gelatinización del almidón, cuando este se enfría, las cadenas de amilosa y amilopectina que provienen de la ruptura de los gránulos de almidón pueden reasociarse paulatinamente en una estructura completamente diferente a la que tenían en un principio en un proceso conocido como retrogradación. Esta reacción implica cambios físicos, como una viscosidad aumentada, formación de geles, exudación de agua y un aumento en el grado de cristalinidad del almidón. Este aumento de cristalinidad viene definido por una reordenación de las cadenas externas más cortas de amilopectina, formando cristales polimorfos de almidón. Por otro lado, cadenas de amilosa dispersas forman estructuras de doble hélice, como las de la amilopectina, por medio de puentes de hidrógeno, incrementando así también la cristalinidad [89]. Específicamente, esta reacción tiene dos fases, una retrogradación a corto plazo provocada por la reordenación de las cadenas de amilosa y una retrogradación más lenta a largo plazo debida a la reordenación de las cadenas de amilopectina, debido a la estructura ramificada de este polisacárido. La velocidad de retrogradación general depende en gran medida, además del ratio amilosa/amilopectina, de la temperatura, del contenido en humedad y del contenido en lípidos y azúcares presentes en el almidón. La **Figura I.13** muestra de forma

esquemática el proceso de retrogradación que sufre el almidón al enfriarse y almacenarse.

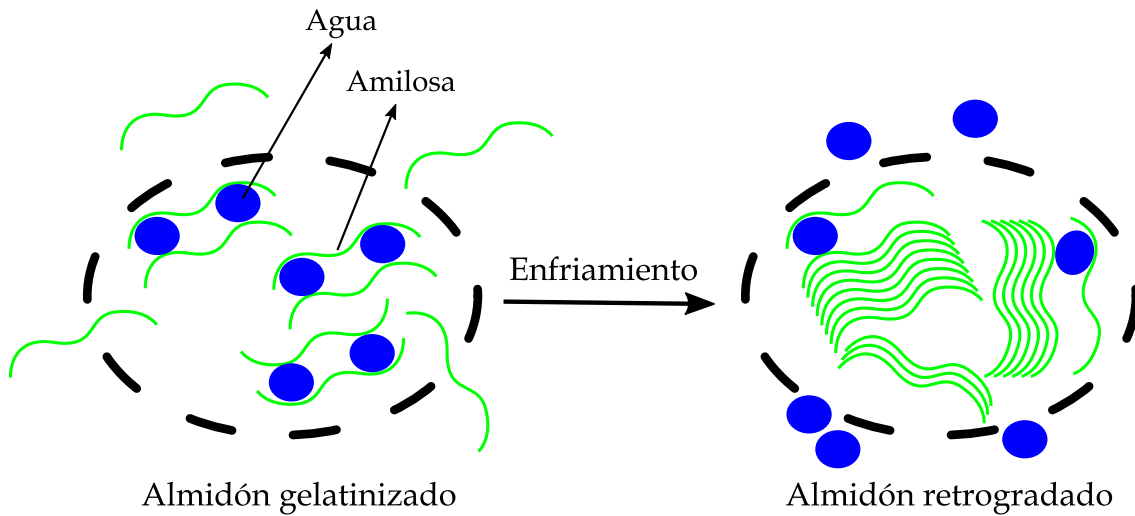


Figura I.13. Representación esquemática del proceso de retrogradación del almidón.

Una de las consecuencias de la retrogradación es un aumento en la rigidez y un endurecimiento del almidón en la forma en la que se encuentre, bien sea en forma de gel, en forma de film o en forma de material compuesto. Esto implica un aumento generalizado de las propiedades mecánicas resistentes y por consiguiente una disminución de las propiedades mecánicas dúctiles, directamente consecuencia del aumento en la cristalinidad de la estructura de los gránulos [90]. Esto puede resultar deseable en algunos casos, ya que la resistencia del almidón se ve mejorada, así como sus propiedades barrera. Además, la solubilidad del almidón también se ve modificada. No obstante, según qué aplicaciones, la retrogradación puede suponer una desventaja, ya que en el caso de la formación de films de almidón para la industria alimentaria, una retrogradación excesiva puede resultar en una estructura demasiado frágil que facilite la rotura del film y le prive de su funcionalidad en este sector [91].

Por esta razón, el almidón no suele emplearse de forma pura o solamente mezclado con agua, sino que se han desarrollado diferentes estrategias y técnicas para combinarlo con otros elementos, como plastificantes o agentes reticulantes, con el fin de evitar en parte la retrogradación o conferirle al material resultante propiedades adicionales a las del almidón, manteniendo siempre su alto potencial medioambiental (biodegradabilidad, biocompatibilidad, no toxicidad, etc.). A estas mezclas de almidón con otros componentes se les conoce como almidones modificados.

I.3.4. Almidones modificados

Los almidones modificados surgen como un tipo de materiales basados en almidón que buscan mejorar las virtudes del almidón, potenciando sus características, incorporando nuevas propiedades al material resultante e intentando suplir las desventajas que supone en algunos casos la rápida retrogradación del almidón cuando este es almacenado. Hay un gran número de técnicas empleadas para modificar almidones, dependiendo de las aplicaciones para las que se destinen. Entre estas técnicas se encuentra la combinación del almidón con otros compuestos, como plastificantes, para obtener materiales termoplásticos; la esterificación del almidón; la estabilización; el entrecruzamiento de las cadenas de amilosa y amilopectina y otras muchas posibles modificaciones, tanto físicas como químicas.

I.3.4.1. Almidón termoplástico (plastificación)

De entre todos los almidones modificados, la plastificación del almidón para obtener mezclas de almidón termoplástico (TPS) es el método más común y uno de los más efectivos para obtener materiales funcionales y respetuosos con el medio ambiente. Esta vertiente permite obtener un material con una procesabilidad y propiedades similares a las de polímeros termoplásticos comunes. Para obtener el TPS, el almidón granular se procesa de forma termomecánica, aplicando calor y esfuerzos de cizalla, mediante procesos de extrusión, inyección, moldeo por termocompresión o procesamiento de films por disolución, entre otros [92], en combinación con un exceso de agua y el uso de plastificantes.

La cantidad de plastificantes que pueden utilizarse ofrece un gran abanico de posibilidades a la hora de modificar las propiedades del almidón. Este tipo de materiales surge especialmente debido al hecho de que la temperatura de fusión del almidón está por encima de su temperatura de degradación como resultado de los fuertes puentes de hidrógeno que se forman entre las cadenas de amilosa y amilopectina, lo cual limita mucho su procesabilidad [93]. Mediante la combinación del almidón con un plastificante, como el glicerol [94], el sorbitol [95], urea [96], formamida [97], etilén glicol [98] o acetamida [99], entre otros, se consigue sustituir los fuertes puentes de hidrógeno entre moléculas de almidón por enlaces entre el plastificante y los grupos hidroxilo presentes en el almidón, flexibilizando así el material resultante.

Dos de los plastificantes más utilizados hasta ahora han sido el glicerol, un plastificante con 3 grupos hidroxilo en su estructura química, y el sorbitol, un alcohol

que posee 6 grupos hidroxilos por molécula (ver **Figura I.14**). Estos grupos químicos son esenciales desde el punto de vista de la producción de almidones termoplásticos, ya que es donde se forman los puentes de hidrógeno entre estos plastificantes y el almidón. En este sentido, generalmente un almidón termoplástico producido con sorbitol presentará propiedades mecánicas resistentes superiores a las de un almidón termoplástico producido con glicerol, sin embargo, las propiedades dúctiles serán más bajas, con una elongación y una resiliencia menor. Esto es debido a que el sorbitol posee una mayor cantidad de grupos hidroxilo en su estructura que reaccionarán con el almidón, formando una interacción mucho más fuerte que en el caso del glicerol [93]. La **Figura I.14** muestra la interacción entre el almidón y el glicerol y sorbitol ilustrando este fenómeno.

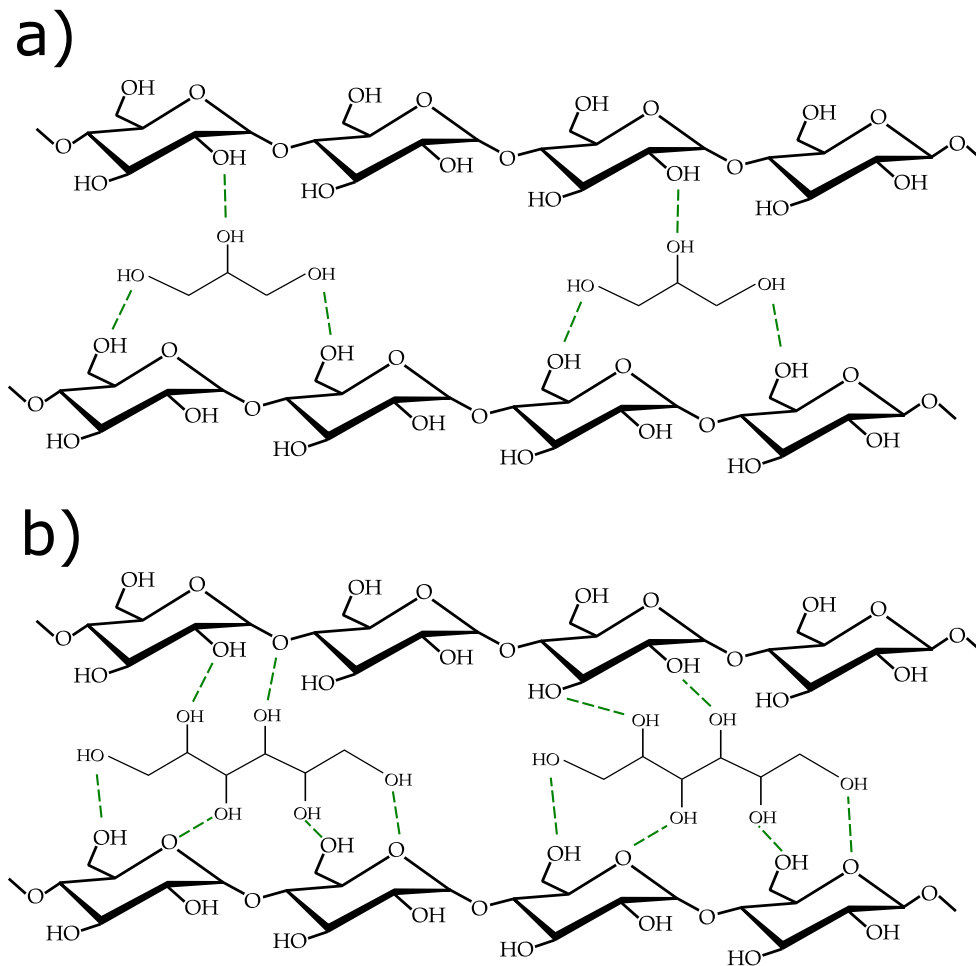


Figura I.14. Representación esquemática de la interacción por puentes de hidrógeno entre el almidón y: a) glicerol; b) sorbitol.

Sin embargo, el empleo de algunos plastificantes como el glicerol favorecen la retrogradación del almidón. Es por ello que otros plastificantes como la urea y la formamida han sido utilizados, ya que el grupo amida presente en su estructura química es capaz de prevenir, hasta cierto punto, y retrasar esta reacción química [100]. El problema de utilizar estos plastificantes es que presentan cierta toxicidad que limita su aplicación en sectores como el de la alimentación, aplicaciones biomédicas o en farmacia [93]. Por esta razón se han planteado mezclas de plastificantes para intentar ofrecer un balance entre las propiedades mecánicas resistentes y dúctiles, la toxicidad del material resultante, su acción frente a la retrogradación y su biodegradabilidad. Entre algunas de estas mezclas destacan mezclas de glicerol/sorbitol, urea/sorbitol o urea/etanolamina [101-103].

Por otro lado, el almidón termoplástico ofrece algunas desventajas, entre las que se encuentran una baja temperatura de degradación, lo cual dificulta en cierta medida su procesado; unas propiedades mecánicas reducidas y una alta sensibilidad al agua, las cuales limitan sus aplicaciones.

I.3.4.2. Estabilización

El proceso de estabilización es una modificación química de las cadenas de almidón utilizado exclusivamente para la inhibición de la reacción de retrogradación natural del almidón. En este caso, grupos inhibidores reaccionan con el almidón para evitar el alineamiento de las cadenas poliméricas y un consiguiente cambio en la estructura del polímero. Este proceso es especialmente importante en almidones que vayan a almacenarse a temperaturas bajas, ya que la retrogradación se favorece en estas condiciones. Uno de los compuestos que más se ha empleado para este fin es el octenil succínico anhídrido (OSA) [104].

I.3.4.3. Esterificación

Los ésteres de almidón son un tipo de almidones modificados donde algunos de los grupos hidroxilo presentes en el almidón son sustituidos por grupos éster. Esta reacción proporciona cierta hidrofobicidad al almidón, ya que se reduce el número de grupos hidroxilo disponibles que podrían reaccionar con moléculas de agua [105]. Por ejemplo, mediante la combinación de almidón con anhídrido acético en presencia de un catalizador alcalino se obtiene almidón acetilado con un bajo grado de succinato de dodecilo. De esta forma, primero se forma un complejo alcalino de almidón, que luego

interacciona con el anhídrido carboxílico para formar un éster de almidón [106].

Este tipo de compuestos se suelen sintetizar con anhídridos de ácidos carboxílicos, ácidos grasos, anhídrido succínico de dodecenilo o cloruros de ácidos grasos. La utilización de estos últimos tiene ciertas ventajas, como el uso de agua como disolvente (respetuoso con el medio ambiente), un tiempo de reacción más corto o la hidrofobicidad que se le otorga al almidón, que permite separarlo del agua con facilidad. Además, estos almidones tienen un carácter anfifílico que puede ser aprovechado para la preparación de nanopartículas de almidón por métodos de diálisis [107].

I.3.4.4. Entrecruzamiento

Otra de las técnicas empleadas para modificar almidones y mejorar sus propiedades es el entrecruzamiento, que se trata de un tratamiento donde se utilizan pequeñas cantidades de compuestos que son capaces de reaccionar con más de un grupo hidroxilo en el almidón. Esta modificación le otorga a los granos de almidón resistencia frente a temperatura, acidez y esfuerzos de cizalla [108]. Este tratamiento permite añadir enlaces intra e intermoleculares en los gránulos de almidón, de forma que fortalecen y estabilizan la estructura de dichos gránulos. Esto aumenta la densidad del almidón, lo cual restringe la absorción de agua del material, que es uno de sus grandes inconvenientes. Además, esta modificación dificulta la ruptura de los granos de almidón, por tanto, retrasa la gelatinización del mismo, aumentando así sus propiedades mecánicas.

Algunos de los compuestos que se utilizan para efectuar este tipo de tratamiento son el trimetafosfato de sodio (STMP), el fosfato de monosodio (SOP), el tripolifosfato de sodio (STTP) o el cloruro de fosforilo (POCl_3). Algunos estudios han demostrado que el efecto de entrecruzamiento ocurre sobre todo en las cadenas de amilopectina del almidón [109]. El entrecruzamiento se utiliza sobre todo en combinación con otros métodos de modificación como la esterificación o la hidrólisis con el objetivo de ajustar la temperatura de gelatinización, la viscosidad y propiedades relacionadas con la textura en el sector de la alimentación [110].

I.3.5. Aplicaciones de los almidones modificados

Debido a las propiedades de biodegradabilidad, biocompatibilidad, no toxicidad y la obtención del almidón a partir de fuentes naturales, este polímero tiene potencial

aplicación en el sector médico, farmacéutico y de la alimentación, tanto a nivel de productos alimenticios como de envase y embalaje.

I.3.5.1. Aplicaciones del almidón modificado en el sector médico y farmacéutico

Dentro del sector de la medicina, los almidones modificados tienen una enorme proyección en cuanto a aplicaciones se refiere. Gracias a la buena maleabilidad que poseen, los almidones plastificados están siendo muy utilizados en la producción de films con gran facilidad de desintegración, *scaffolds* o *stents* que pueden ser introducidos en el sistema digestivo humano sin peligro para el usuario [111, 112].

La posibilidad de combinar el almidón con elementos como el grafeno, que le proporcionan cierta conductividad, permite su aplicación en la fabricación de sensores reabsorbibles de gran área superficial que son capaces de estimar la cantidad de transferrina en la sangre [113].

La encapsulación y liberación controlada de medicamentos es una aplicación que se encuentra en pleno auge en este sector y en la que el almidón tiene mucho que aportar. Por ejemplo, la combinación de alginato de sodio con almidón gelatinizado por medio de enlaces de hidrógeno permite aumentar la viscosidad de la mezcla y encapsular de una forma más eficiente algunos medicamentos, como el diclofenaco sódico, para su posterior liberación, que si se empleara únicamente almidón para la encapsulación [114]. Otra aplicación dentro de este campo es el desarrollo de films comestibles de rápida desintegración (gracias a la sensibilidad del almidón al agua) para administrar dosis de vitamina C por vía oral, en este caso combinando almidón con gelatina [115].

El *electrospinning* es una técnica que ha ganado gran interés en las últimas décadas dentro del sector médico, ya que es especialmente útil para efectuar encapsulación de principios activos y compuestos de interés en la industria farmacéutica en forma de fibras a escala nanométrica. Esta estrategia es altamente compatible con el almidón y facilita la mezcla de este con una gran cantidad de compuestos. Se trata de una técnica muy versátil que se sirve de la fuerza electrostática para producir un flujo continuo de polímero desde una jeringuilla hasta un colector. La materia prima para el proceso es una disolución de polímero con disolvente, a la cual se le pueden añadir todo tipo de aditivos, como compuestos antioxidantes, que se introduce en la jeringuilla tras la homogeneización de la disolución. Aplicando una diferencia de potencial entre la punta de la jeringuilla y el colector, las partículas de polímero que salen de la jeringuilla

adquieren carga positiva y se ven atraídas por la carga negativa del colector. A su vez, el disolvente se evapora y da lugar a una fibra de polímero que se deposita sobre el colector de forma aleatoria [116]. En el caso del almidón, este puede combinarse con agua como disolvente. La **Figura I.15** muestra un esquema de este proceso.

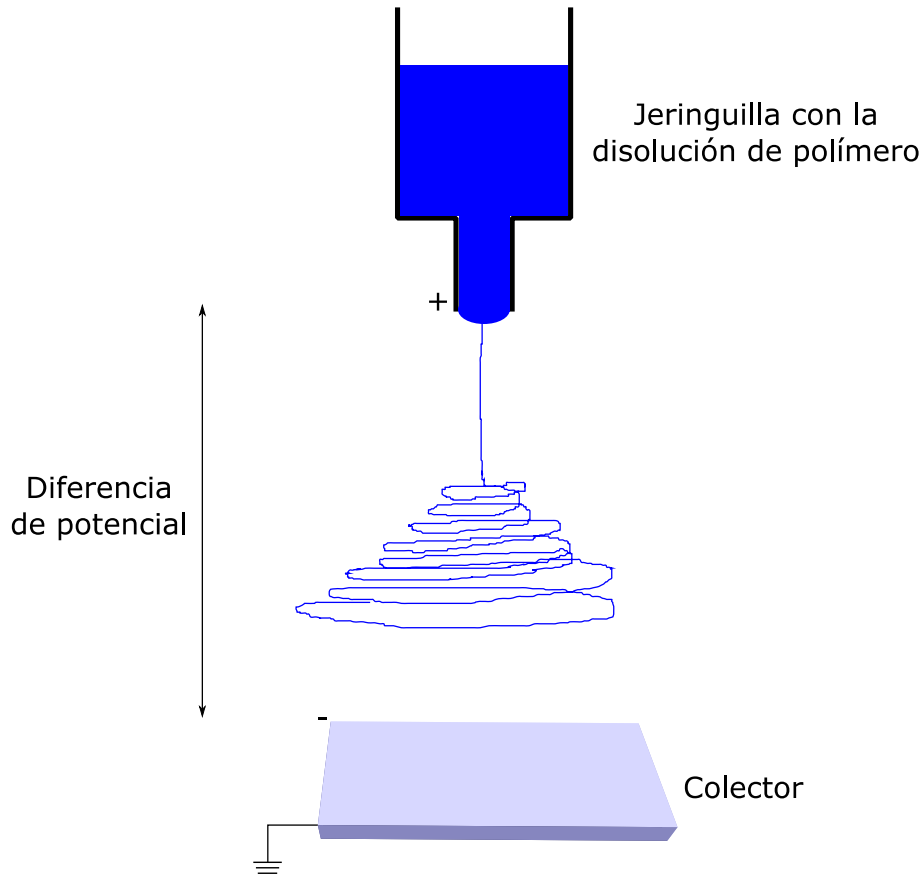


Figura I.15. Esquema del proceso de *electrospinning*.

El empleo del *electrospinning* permite obtener una capa de fibras de almidón con gran porosidad y área interfacial que puede actuar como tejido artificial o como parches para la curación de heridas [117]. El almidón por sí solo da lugar a la fabricación de fibras muy frágiles, es por ello que se puede combinar con polivinilpirrolidona (PVP) o polivinil alcohol (PVA) para mejorar su flexibilidad y obtener fibras con una mejor estabilidad dimensional [118]. Por ejemplo, fibras de almidón con PVA o con policaprolactona (PCL) se han utilizado para fabricar parches mucoadhesivos para el tratamiento de heridas. Su hidrofiliidad y gran capacidad de absorción permite que el líquido sea absorbido por las fibras y los sólidos presentes en la sangre adheridos a ellas. Si además se utilizan extractos de hierbas o componentes cicatrizantes, la curación es más rápida y la inflamación menor [119]. La gran cantidad de combinaciones en cuanto

a materiales que pueden emplearse en esta técnica y el gran abanico de parámetros que pueden modificarse de la misma da lugar a innumerables aplicaciones en ingeniería de tejidos y administración de compuestos activos, donde el almidón actúa como excelente soporte.

La **Figura I.16** muestra algunas de las aplicaciones que se están empleando con el almidón en el sector médico y farmacéutico.

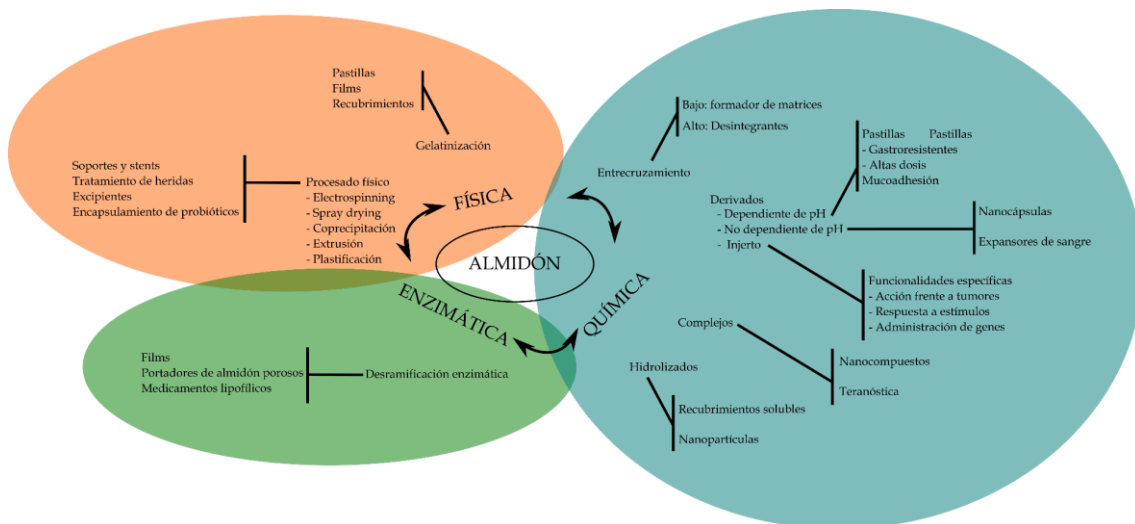


Figura I.16. Aplicaciones del almidón en farmacia y medicina.

I.3.5.2. Aplicaciones del almidón modificado en el sector del envase y embalaje

La utilización de polímeros naturales para fabricar envases a partir de recursos renovables está en el punto de mira de la comunidad científica desde hace décadas. En este contexto, el almidón ofrece grandes posibilidades para el desarrollo de productos de envasado biodegradables para el sector de la alimentación que no sean tóxicos ni supongan ningún detrimento en la conservación de alimentos. Además, el almidón puede aditivarse con compuestos antioxidantes o antibacterianos, como aceites esenciales, para mejorar aún más la preservación de los productos envasados [120].

La forma más extendida del uso del almidón para este sector es en forma de film, de forma que es capaz de aumentar la vida de productos como frutas y verduras, además de ofrecer la posibilidad de fabricar films comestibles donde este polímero actúe como el principal soporte para aditivos que hagan el envasado más efectivo. Dentro de este contexto, se han desarrollado algunos estudios referentes a la producción de films

antimicrobianos basados en almidón para la preservación de alimentos. Ali *et al.* [121] produjeron films con actividad antimicrobiana combinando almidón con harina de piel de granada. Por otro lado, Bangar *et al.* [122] mezclaron almidón con nanocristales de celulosa y aceite de clavo para fabricar films para el envasado de uvas rojas, los cuales mostraron actividad antimicrobiana frente a diferentes agentes bacteriológicos como la *E. coli*.

Otro aspecto en el desarrollo de films incluye la utilización de partículas inorgánicas para mejorar las propiedades de los films biodegradables de almidón. Francis *et al.* [123] incorporaron nanopartículas de CuO y ZnO en films biodegradables de almidón con PVA y glicerol. Los films obtenidos demostraron ser muy prometedores para el envasado de productos alimenticios, con una gran resistencia al agua, actividad antimicrobiana y excelentes propiedades térmicas y mecánicas. Los films incluso mostraron muy buenas propiedades fungicidas, con una gran capacidad para extender la vida de la comida envasada.

I.4. Ácido poliláctico (PLA)

I.4.1. Introducción

El PLA es uno de los biopolímeros más estudiados y utilizados industrialmente en la actualidad. Su producción mundial en el año 2022 fue de aproximadamente 350 mil toneladas, lo cual supone un 23% de toda la producción mundial de polímeros biodegradables (1,5 millones de toneladas). Además, se espera para el año 2035 una producción de PLA de 2 millones de toneladas, lo cual superaría a la producción actual de todos los polímeros biodegradables, incluyendo PHAs, PBAT y PBS. De toda esta producción la mayor parte está destinada al *packaging*, sector que ocupa el 48% de toda la producción global de bioplásticos.

Se trata de un poliéster alifático biodegradable que ha ganado especial interés en los últimos tiempos debido a su alto rendimiento mecánico, a su biodegradabilidad, su biocompatibilidad y al hecho de que puede ser obtenido por vías petroquímicas [124] o a partir de recursos renovables, por medio de la fermentación, como pueden ser el maíz, la caña de azúcar o la patata [125, 126]. El uso de este polímero tiene un gran potencial en cuanto a la promoción de economías circulares se refiere, ya que pueden aprovecharse residuos lignocelulósicos provenientes de la industria de la alimentación o agroforestal para sintetizarlo y producir materiales funcionales.

Uno de los principales problemas del PLA ha sido el alto coste de su síntesis. Sin embargo, los avances que se han hecho recientemente con respecto a la fermentación de glucosa han permitido una considerable mejora en el proceso productivo de este polímero.

I.4.2. Obtención del PLA

El PLA puede ser obtenido tanto de fuentes petroquímicas como renovables. En vista del contexto medioambiental en el que se encuentra la sociedad actual, es evidente que la síntesis de PLA a partir de biomasa es mucho más interesante.

Para sintetizar el PLA, como punto de partida se toman fuentes vegetales con alto contenido en hidrocarburos, a partir de las cuales se extrae D-glucosa o dextrosa. De la glucosa, mediante fermentación bacteriana, se obtienen los dos isómeros del ácido láctico (L-ácido láctico y D-ácido láctico), los cuales suponen la materia prima para la síntesis del ácido poliláctico. Una vez obtenidos los monómeros de ácido láctico, hay

varios procesos de síntesis mediante los cuales se puede obtener el polímero.

La primera línea es la polimerización por condensación (policondensación). Esta técnica une los monómeros del polímero al mismo tiempo que elimina los subproductos que se generan (agua, alcohol, etc.). En el caso del PLA, el agua es el principal subproducto, el cual es difícil de eliminar y esto provoca que el PLA obtenido por esta vía suele tener un peso molecular bajo (<50000 g/mol), lo que supone un polímero de baja calidad. Para suplir este problema se han desarrollado una serie de variantes de este método. Por un lado, se tiene la policondensación azeotrópica (AP), mediante la cual se elimina el agua del proceso utilizando disolventes azeotrópicos y donde la temperatura a aplicar es menor que la de fusión del polímero, evitando la presencia de impurezas por despolimerización. Por otro lado, está la polimerización en estado sólido (SSP), técnica que se divide en dos pasos: primero se funde el monómero para producir oligómeros a elevada temperatura y luego se pasa a estado sólido para incrementar el peso molecular entre la temperatura de transición vítrea y la temperatura de fusión. Además, se suelen utilizar extensores de cadena para aumentar el peso molecular y que así el polímero resulte funcional. El uso de estos compuestos extra aumenta el coste del proceso, hecho que ha supuesto uno de los mayores problemas de la síntesis del PLA en estos últimos años [127].

La segunda línea de síntesis de PLA se lleva a cabo mediante polimerización por apertura de anillos o *ring opening polymerization* (ROP). Este proceso permite obtener un polímero de bajo peso molecular, pero utilizando unas condiciones menos agresivas que en la polimerización por policondensación. En este caso, en lugar de utilizar extensores de cadena, se produce una despolimerización para formar lactida, un dímero cíclico intermedio que se destila posteriormente para purificarlo y obtener el PLA [128]. Esta metodología da lugar a un PLA de mayor peso molecular, además de un mayor control sobre las condiciones químicas de la síntesis, que permiten una mayor versatilidad en cuanto a la síntesis de PLA con diferentes propiedades dentro de un amplio rango. Otra gran ventaja de este método es la reducción de costes con respecto a la policondensación, ya que no se necesitan disolventes azeotrópicos ni agentes extensores de cadena. La **Figura I.17** muestra una representación esquemática simplificada de las diferentes vías de síntesis del PLA a partir de biomasa.

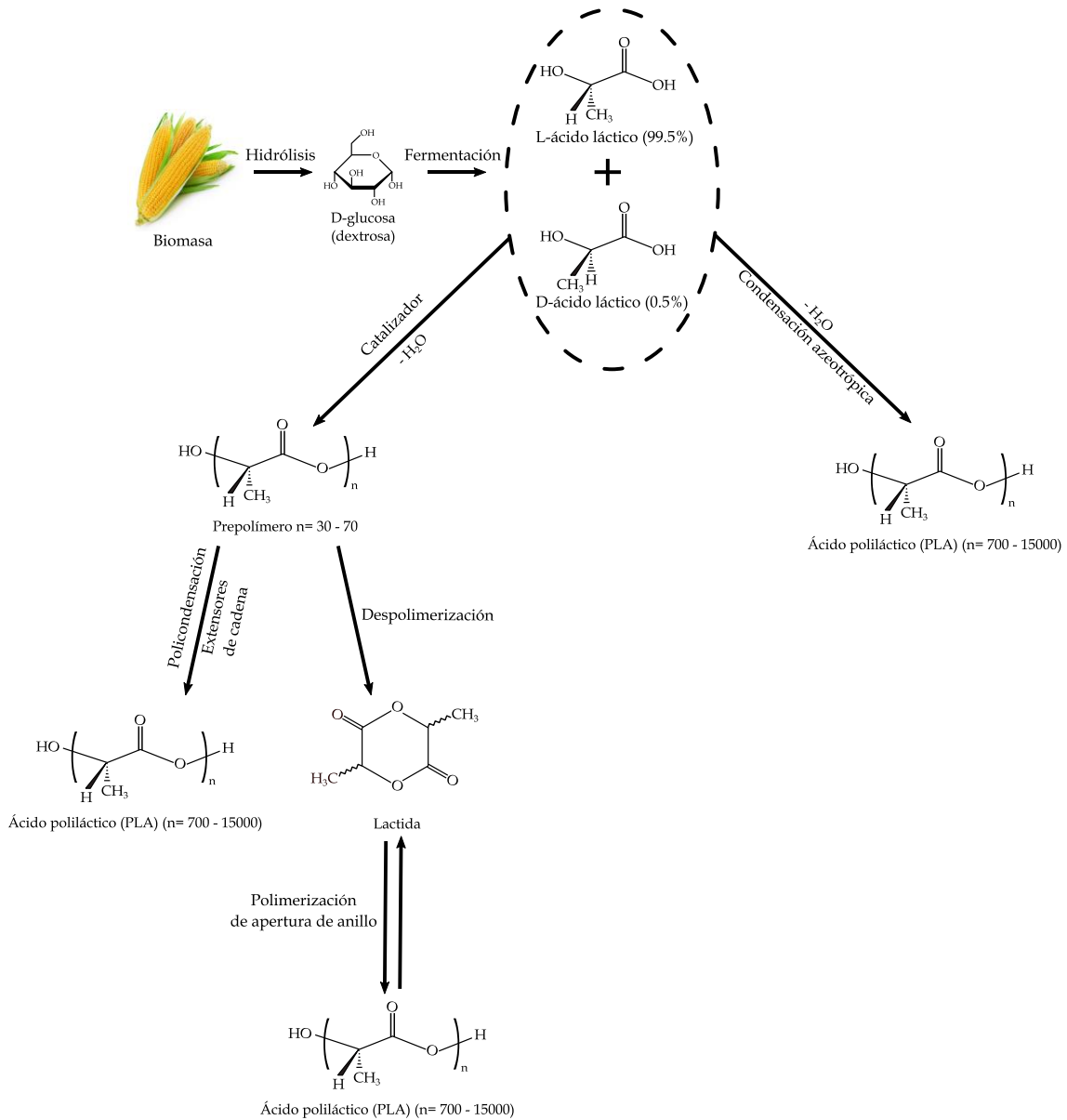


Figura I.17. Esquema de las diferentes vías de síntesis del PLA.

I.4.3. Propiedades del PLA

Dependiendo del proceso de síntesis y de la combinación que se utilice de los isómeros del PLA se pueden variar las propiedades del PLA obtenido, de forma que se puede producir un polímero amorfo o semicristalino. Esto afectará directamente a sus propiedades mecánicas, térmicas, morfológicas, etc. Comercialmente, el grado de PLA más utilizado es una mezcla de L-ácido poliláctico (PLLA) y D-ácido poliláctico (PDLA), aunque cabe destacar que el isómero L(+) es el más abundante en la naturaleza [129]. La **Figura I.18** muestra la estructura química de los dos isómeros del PLA y las dos variantes de polímero que se pueden obtener de ambos, así como el polímero que se obtiene como

combinación de los dos isómeros. Cuando se combinan ambos isómeros, el PDLLA obtenido normalmente es amorfo, aunque variando la relación entre los isómeros L- y D- y el uso de catalizadores se puede modificar la cristalinidad del polímero hasta cierto punto [130].

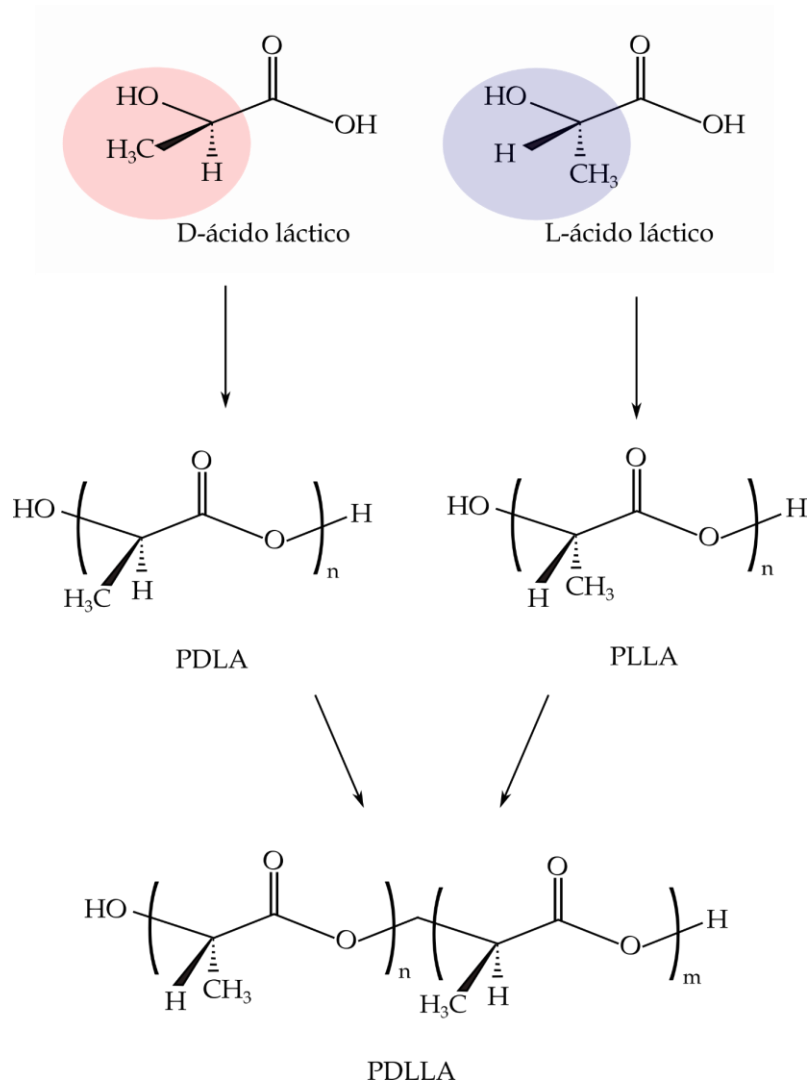


Figura I.18. Estructura química de los isómeros del PLA, los polímeros que produce cada isómero y el polímero que se obtiene como combinación de ambos isómeros.

El PLA tiene unas propiedades mecánicas muy similares a las de algunos polímeros derivados del petróleo. Su módulo elástico y tensión máxima son de aproximadamente 3500 MPa y 60 MPa, respectivamente, valores muy similares a los del PET [131]. Sin embargo, una de las principales desventajas del PLA es su excesiva fragilidad a temperatura ambiente y unas propiedades dúctiles muy pobres. Por ejemplo, su alargamiento a la rotura es de menos del 8% [132].

Las propiedades térmicas también están muy relacionadas con el ratio entre ambos isómeros. Como se ha comentado, la cristalinidad del PLA puede variar desde un grado amorfo hasta un grado semicristalino o altamente cristalino, afectando en gran medida tanto a las propiedades térmicas como mecánicas. La velocidad de cristalización, el grado de cristalinidad y por consiguiente las propiedades térmicas son altamente dependientes del proceso de síntesis del PLA. En general, el PLA es un polímero termoplástico con una temperatura de transición vítrea (T_g) entre 55 y 70 °C y una temperatura de fusión (T_m) de entre 165 y 190 °C. Esta T_g , al ser tan alta, provoca que a temperatura ambiente el polímero presente un comportamiento frágil. Por otro lado, su cristalinidad le otorga buenas propiedades barrera [133], ya que cuanto más cristalino es el polímero, sus regiones amorfas se ven reducidas y esto reduce la permeabilidad a los gases debido a que las moléculas de vapor y gas se suelen desplazar a través de estas zonas.

Una de las principales ventajas del PLA es su capacidad para biodegradarse en condiciones de compost controladas. Esta desintegración se produce por hidrólisis y viene determinada por diversos factores como el peso molecular del polímero, su pureza, la temperatura, el grado de cristalinidad, el pH, la permeabilidad al agua, la presencia de grupos reactivos como hidroxilos o carbonilos o la presencia de aditivos [134]. Bajo estas condiciones, la estructura del PLA cambia, reduciendo su peso molecular y disminuyendo el tamaño de las cadenas poliméricas. De esta forma se liberan oligómeros del PLA y ácido láctico, que son más fácilmente atacados por los microorganismos, liberando dióxido de carbono y agua en el proceso [135]. La **Figura I.19** ilustra de forma esquemática la evolución de las cadenas poliméricas durante la desintegración.

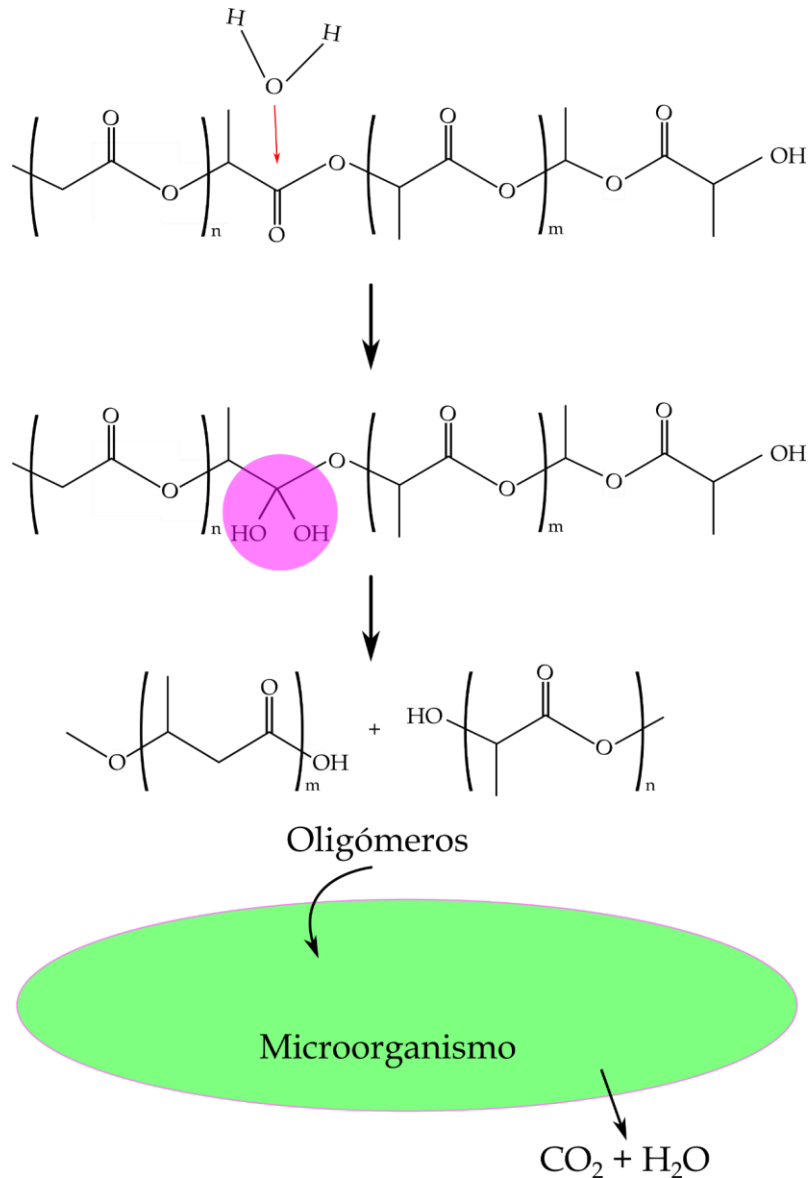


Figura I.19. Proceso de hidrólisis y desintegración bacteriana del PLA bajo condiciones controladas de compost.

El PLA también es sensible a la degradación térmica durante su procesado. Este efecto es especialmente acusado en presencia de humedad, debido a que las moléculas de agua catalizan la hidrólisis del polímero [136]. Es por ello por lo que es necesario secar bien el polímero antes de procesarlo. También es común el uso de extensores de cadena para evitar la reducción de peso molecular.

La utilización de aditivos y otras técnicas para paliar las desventajas del PLA, especialmente para aumentar su ductilidad y reducir su transición vítrea, está cobrando cada vez más importancia para incrementar la funcionalidad de este polímero, el cual posee un gran potencial medioambiental.

I.4.4. Aplicaciones del PLA

Debido a su excelente resistencia, su biocompatibilidad y su biodegradabilidad, el PLA tiene aplicación en un gran rango de sectores. Este se está utilizando en el sector de la automoción, donde la empresa Röchling Automotive ha desarrollado varios grados de PLA destinados específicamente al mundo automovilístico, con el objetivo de intentar reducir la emisión de CO₂ que tanto caracteriza a esta industria [137]. El material que proponen se sintetiza a partir de fuentes de glucosa que solo son aptas para el consumo industrial, en lugar de utilizar materia prima comestible que sea apta para el consumo humano. Se han fabricado una gran cantidad de elementos de este sector como cajas de filtrado de aire, salpicaderos, etc.

Por otro lado, el PLA en combinación con compuestos lignocelulósicos provenientes de residuos agroforestales da lugar a materiales compuestos capaces de imitar la madera, que están siendo utilizados como alternativa sostenible en aplicaciones estructurales, como la fabricación de suelos, mobiliario, decoración, etc. [138]. Dentro de estos materiales, el PLA se está combinando por un lado con serrín, paja o madera [139, 140]; y por otro lado con residuos de frutas y vegetales como fibra de cáñamo [141], piel de granada [142] o piel de mango [143].

Uno de los sectores donde encuentra más cabida el PLA es el farmacéutico y médico, principalmente gracias a su biocompatibilidad. En el caso de la industria farmacéutica, este polímero puede ser utilizado para la liberación controlada de medicamentos, ya que este se biodegrada progresivamente y, encapsulando componentes como insulina, vitaminas, inhibidores, antibióticos o agentes antiinflamatorios dentro de su estructura, estos pueden administrarse paulatinamente en el organismo a través de parches u otros dispositivos [144]. Dentro del sector médico el PLA se está utilizando para fabricar placas de fijación [145], tornillos biocompatibles [146], tejidos artificiales [147], suturas reabsorbibles [148] o prótesis de diferentes elementos corporales [149].

Una de las aplicaciones más vanguardistas del PLA es en el campo de la impresión 3D, donde tienen especial interés los materiales con memoria de forma para aplicaciones en biomedicina y tecnología celular [150]. La bioimpresión es una tecnología muy novedosa en la cual se está estudiando el desarrollo de órganos artificiales y tejidos en diferentes sistemas del organismo, como por ejemplo hígados o riñones [151]. El PLA ha sido utilizado mediante esta técnica para imprimir tejidos iniciales que luego son incubados y convertidos en órganos completos. Dentro del campo de la impresión 3D, el PLA ha sido utilizado para reparación de huesos humanos,

fabricación de sensores eléctricos, baterías, tejidos inteligentes, entre otros [152]

En general, el PLA y todos los materiales derivados de la combinación de este con otros compuestos que mantengan su potencial sostenible presentan alternativas muy prometedoras para industrias que se encuentran a la cabeza del desarrollo científico actual.

I.4.5. Modificación del PLA

Como se ha indicado anteriormente, el PLA presenta una serie de inconvenientes que limitan su funcionalidad, especialmente su extrema fragilidad, baja estabilidad térmica y el alto coste de producción. Para evitar estas desventajas y aumentar la viabilidad del PLA para su uso en la industria se han desarrollado varias estrategias, entre las que destacan la mezcla con otros polímeros con alta ductilidad, la copolimerización o el uso de plastificantes que aumenten la flexibilidad del PLA.

I.4.5.1. Mezcla con otros polímeros

La primera estrategia consiste en mezclar el PLA con otros polímeros en estado fundido, de forma que no se produzca reacción química. Esto implica una mezcla física donde los polímeros, después de fundirse, mezclarse y enfriarse, forman un nuevo material con propiedades totalmente diferentes a las de los polímeros iniciales. El objetivo en este caso es utilizar polímeros con propiedades dúctiles superiores a las del PLA. Una gran ventaja de esta estrategia es que se puede realizar mediante procesos convencionales de procesamiento de polímeros, como extrusión e inyección, lo cual hace que sea fácilmente escalable a nivel industrial y reduzca los costes generales del procesamiento [153].

Algo a tener muy en cuenta a la hora de emplear esta técnica es la miscibilidad y la compatibilidad entre los polímeros que se van a mezclar. Esto está fuertemente ligado a su estructura química. En el caso del PLA, el cual posee grupos basados en oxígeno en su estructura, este debe ser mezclado con polímeros de carácter polar que también posean grupos oxigenados en su estructura (como grupos hidroxilo o carbonilo). Por ejemplo, aunque el polietileno sea altamente dúctil, este no es adecuado para su mezclado con el PLA, ya que el PE es completamente apolar. Dependiendo de la naturaleza de la mezcla se diferencian mezclas miscibles, inmiscibles y parcialmente miscibles. Existen métodos teóricos para determinar si dos polímeros son compatibles

en base a su estructura química, como el método de van Krevelen [154]. En caso de que exista incompatibilidad entre polímeros, hay procedimientos para mejorar esta compatibilidad, como el uso de copolímeros con funcionalidades afines a los polímeros que se estén intentando combinar. Un ejemplo de copolímero es el monometoxipolietilén glicol-ácido poliláctico (MPEG-PLA) [155]. En el caso del PLA, este se ha combinado con varios polímeros biodegradables para aumentar su valor medioambiental, como el almidón termoplástico (TPS) [156], PBAT [157], PHB [158] o quitosano [159].

Algunas de las consideraciones a tener en cuenta con esta estrategia es escoger bien el polímero o polímeros a mezclar, la proporción del polímero en función de las propiedades que se deseen y el método de procesado.

I.4.5.2. Copolimerización

La copolimerización es una metodología que consiste en la reacción química de dos o más monómeros para formar cadenas poliméricas con funcionalidades adicionales a las del polímero original. Los polímeros obtenidos se denominan copolímeros y estos poseen propiedades combinadas de los monómeros a partir de los cuales se originan. Estas propiedades dependen en gran medida de la composición del copolímero en términos de los monómeros que lo forman. En este contexto, se diferencian varios tipos de copolímeros dependiendo de cómo se dispongan los monómeros en la cadena polimérica: copolímeros alternados (*-alt-*), copolímeros en bloque (*-b-*), copolímeros injertados (*-g-*) o copolímeros aleatorios (*-ran-*).

Para mejorar la miscibilidad del PLA con otros polímeros existen dos vías referentes a la copolimerización. La primera opción hace referencia a la utilización de copolímeros ya prefabricados que tengan afinidad por el PLA y el polímero con el que se va a combinar. La otra línea implica la utilización de polímeros con grupos reactivos complementarios al PLA y al polímero con el que se va a mezclar, de forma que todos los componentes se mezclan en estado fundido y se forman enlaces covalentes que aumentan la adhesión interfacial entre las fases inmiscibles [160]. Un ejemplo de esto es la utilización de polietilén octeno (PO) para mejorar las propiedades de mezclas de poliésteres o nylon [161]. Otros estudios copolimerizaron polietileno con PLA para formar PE-*b*-PLA, el cual actuó como compatibilizante para mezclas de PLA con PE [162], polímeros que en principio son incompatibles por una diferencia de polaridad.

Con respecto a la copolimerización directa del PLA con otros monómeros, cabe destacar la combinación del monómero lactida y glicólido para dar un polímero

combinado de ácido poliláctico y ácido poliglicólico (PLA-*co*-PGA), el cual se emplea para controlar la bioabsorción del PLA [163]. Otros monómeros, como la caprolactona (CL), el ácido glicólico (GA), butadieno o el etileno son utilizados para obtener copolímeros que presentan una mayor ductilidad con respecto al PLA. Los métodos más utilizados para producir estos copolímeros son la policondensación y la polimerización por apertura de anillos, métodos que se han descrito anteriormente. La **Figura I.20** muestra la estructura química de varios copolímeros de PLA.

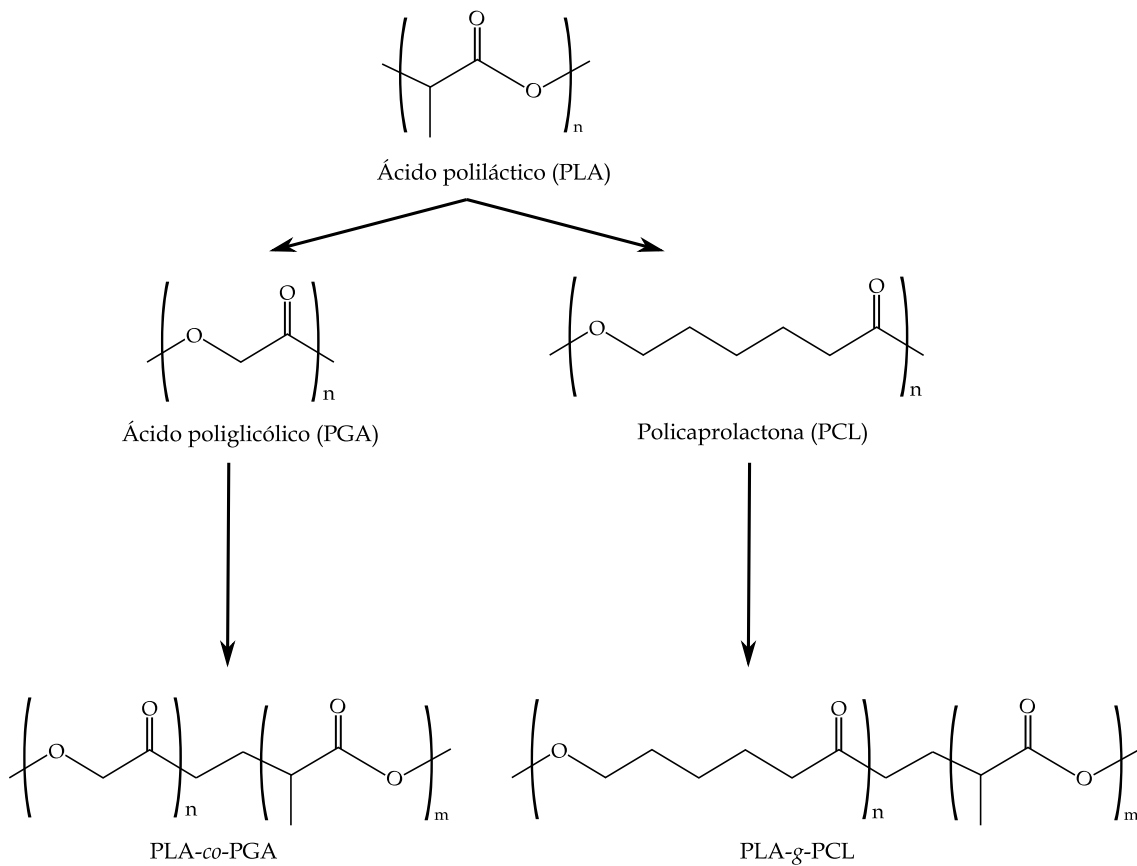


Figura I.20. Estructura química de dos copolímeros del PLA.

I.4.5.3. Plastificación

La plastificación de polímeros implica combinarlos con un compuesto, llamado plastificante, para aumentar su ductilidad, disminuir su temperatura de transición vítrea y aumentar su procesabilidad. Es una de las técnicas más interesantes, ya que presenta un menor coste que metodologías como la copolimerización o la mezcla de polímeros. En este caso, un plastificante adecuado puede suprimir las principales desventajas del PLA, que son una extrema fragilidad y una elevada temperatura de transición vítrea.

Generalmente, los agentes plastificantes deben poseer un peso molecular bajo, un alto punto de ebullición (para evitar que se evapore durante el procesado), baja volatilidad y toxicidad nula para no comprometer el potencial medioambiental del PLA [164].

Cuando un plastificante se introduce en la estructura de un polímero, por un lado aumenta sus propiedades mecánicas dúctiles, como el alargamiento a la rotura o la resiliencia, mientras que por otro reduce sus propiedades mecánicas resistentes, como la tensión máxima, el límite elástico, la dureza o el módulo elástico [165]. Además, el plastificante aumenta la movilidad de las cadenas poliméricas, disminuyendo su viscosidad y aumentando su fluidez, lo cual facilita su procesabilidad. Las propiedades térmicas también se ven afectadas por la presencia de plastificante, el cual, al aumentar la movilidad de las cadenas poliméricas, disminuye las temperaturas de transición vítrea, recristalización en frío y fusión del material. La cristalinidad, la transparencia, la conductividad eléctrica, la biodegradabilidad y el comportamiento frente al agua también se ven afectados por la presencia de plastificantes a raíz del cambio en la estructura del polímero. Por ejemplo, los plastificantes suelen aumentar la cristalinidad de los polímeros, ya que, al aumentar la movilidad de sus cadenas, facilitan que estas se reordenen y formen estructuras cristalinas [166]. Al aumentar la cristalinidad mejoran las propiedades barrera, aumenta la opacidad del material y este tarda más en degradarse.

Es importante destacar que la compatibilidad entre el plastificante y el polímero es esencial a la hora de escoger un plastificante adecuado. Esta compatibilidad está condicionada por diferentes factores como la polaridad de las moléculas, los grupos químicos que posean, la interacción entre dichos grupos químicos, la solubilidad, etc. Existen diferentes métodos para estimar la compatibilidad entre un polímero y un plastificante, aunque uno de los más efectivos es el método de van Krevelen [167], como ya se indicó en el apartado de mezclas de polímeros. Este método se basa en el cálculo de los parámetros de solubilidad de cada componente y da una idea del grado de miscibilidad entre ambos. Sin embargo, al tratarse de un estudio teórico, la compatibilidad entre polímero y plastificante no está asegurada y pueden ocurrir desviaciones respecto a la predicción.

Respecto al fundamento teórico de la plastificación, existen diferentes teorías referentes a la explicación de este fenómeno, aunque hay tres que destacan por encima de las demás [168]:

- Teoría de gel: esta teoría considera al polímero plastificado como una red tridimensional en la cual las moléculas de plastificante se unen a las cadenas

poliméricas mediante enlaces débiles. La teoría defiende que el plastificante sustituye las fuertes interacciones polímero-polímero por interacciones más débiles polímero-plastificante. Esto provoca un aumento en la movilidad de las cadenas poliméricas, aumentando su ductilidad.

- Teoría de la lubricación: la teoría de la lubricación defiende que el plastificante actúa como un agente lubricante que se inserta entre las cadenas poliméricas reduciendo así la interacción entre ellas y facilitando su movilidad y desplazamiento. Según esta teoría, las cadenas de polímero deslizan entre ellas cuando el plastificante se introduce en la estructura, de forma que la capacidad del polímero para alargarse aumenta. Esto implica que la rigidez del polímero viene definida por la fricción entre sus moléculas debido a irregularidades estructurales, de modo que cuando el plastificante está presente esta fricción se reduce considerablemente.
- Teoría del volumen libre: esta teoría se basa en el hecho de que existe un espacio libre entre las moléculas de polímero, el cual define su movimiento, de manera que cuánto mayor espacio libre, mayor es la movilidad de las moléculas y, por tanto, más flexible es el polímero. Cuando un plastificante se introduce en un polímero, este aumenta el volumen libre entre las moléculas, otorgándole mayor movilidad y, por consiguiente, aumentando su ductilidad y disminuyendo su temperatura de transición vítrea.

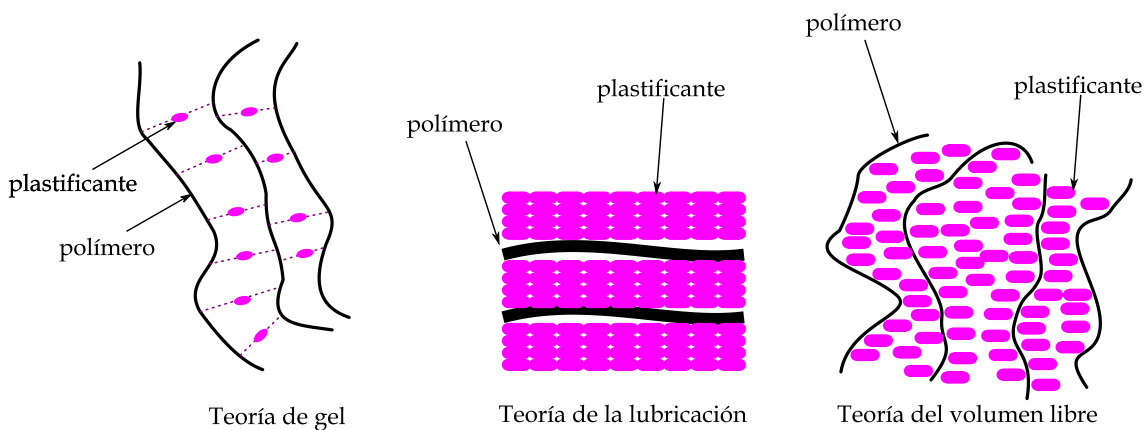


Figura I.21. Representación esquemática de las principales teorías de plastificación.

Existen plastificantes tanto monoméricos como poliméricos, dependiendo de su estructura química y peso molecular. Los plastificantes monoméricos suelen establecerse en un rango de peso molecular entre 200 y 500 g/mol, y suelen tener una volatilidad

relativamente alta. Por otro lado, los plastificantes poliméricos suelen presentar pesos moleculares entre 1000 y 10000 g/mol. Estos últimos tienen una volatilidad mucho más baja, pero su compatibilidad con el polímero a plastificar suele ser más limitada.

En el caso del PLA, el uso de plastificantes está muy extendido y ha sido objeto de muchos estudios. Se han utilizado tanto plastificantes monoméricos como poliméricos. Entre los plastificantes monoméricos destacan especialmente los citratos, como el trietil citrato (TEC), el tributil citrato (TBC), el acetil trietil citrato (ATEC) o el acetil tributil citrato (ATBC) [169-171], cuyas estructuras se pueden observar en la **Figura I.22**. Otros plastificantes monoméricos muy comunes son el glicerol [172], la triacetina [173], la tributirina [174] o los aceites vegetales epoxidados y maleinizados [175]. Con respecto a los plastificantes poliméricos, destacan sobre todo el polipropilénglicol (PPG) [176], la policaprolactona (PCL) [177], el polietilénglicol (PEG) [178] y los poliadipatos [179], entre muchos otros.

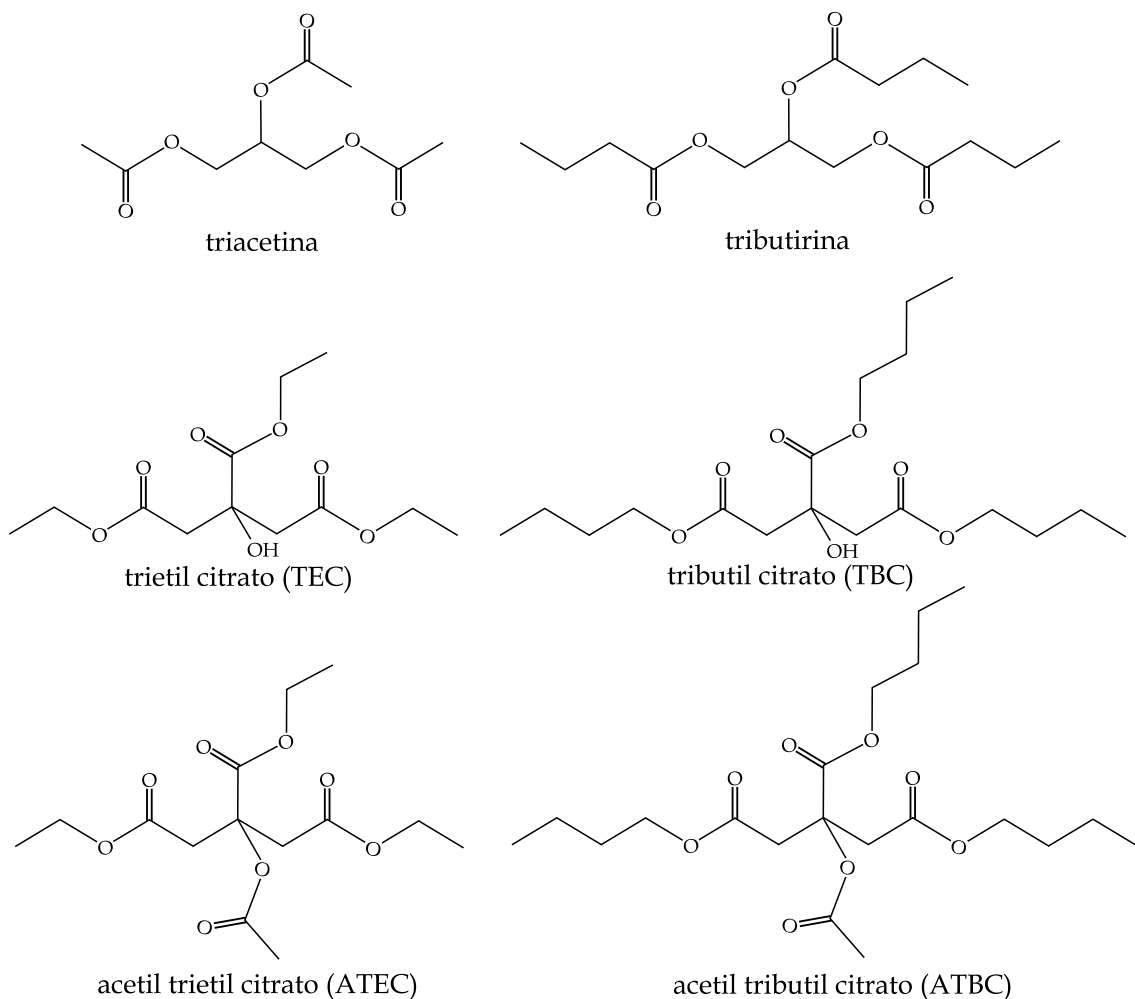


Figura I.22. Estructura química de algunos de los plastificantes más utilizados para el PLA.

Aunque el uso de plastificantes para mejorar las propiedades dúctiles del PLA está muy estudiado, están surgiendo nuevos plastificantes que son muy efectivos y además tienen un potencial medioambiental muy elevado, ya que pueden ser obtenidos de fuentes naturales. Este grupo de plastificantes son derivados de los terpenos y los terpenoides. Los terpenos son productos naturales que poseen una estructura química que consiste en la repetición de unidades de isopreno (C_5H_8). Por otro lado, los terpenoides son terpenos que poseen grupos funcionales adicionales (normalmente grupos basados en oxígeno). Los terpenoides con grupos hidroxilo en su estructura (alcoholes), como el geraniol o el linalool, en combinación con ácidos carboxílicos (ácido acético, ácido butanoico, etc.), dan lugar a ésteres de terpenoides que presentan una gran efectividad como plastificantes del PLA, además de una excelente miscibilidad con el polímero. Por ejemplo, combinando el geraniol o el linalool con ácido acético se obtiene el acetato de geranilo y el acetato de linalilo respectivamente, que pueden actuar como plastificantes para PHAs o PLA [180]. La **Figura I.23** muestra la estructura química de los alcoholes geraniol y linalool, además de sus respectivos acetatos tras combinarlos con ácido acético.

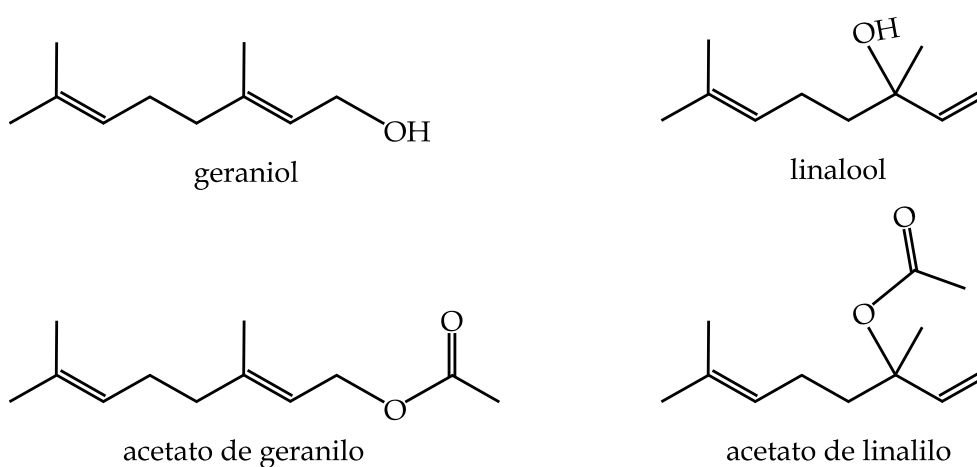


Figura I.23. Esquema químico del geraniol, del linalool, del acetato de geranilo y del acetato de linalilo.

Además de estos ésteres hay otros ésteres donde el componente principal es el ácido carboxílico y que también tienen un gran potencial de plastificación. Dentro de este grupo destaca el ácido tartárico, el cual puede ser obtenido de fuentes renovables como la uva o el tamarindo [181, 182]. La combinación del ácido tartárico con diferentes alcoholes, como el metanol, el etanol, el n-butanol o el octanol, entre otros, da lugar a ésteres (tartratos) que pueden actuar como plastificantes del PLA. Zawada *et al.* [183]

estudió el efecto plastificante de varios tartratos con PLA y concluyeron que el dietil-L-tartrato (DET) y el dibutil-L-tartrato (DBT) proveían al PLA de unas mejores propiedades dúctiles, con valores de elongación a la rotura de aproximadamente el 500%. La **Figura I.24** muestra el proceso de obtención del dietil-L-tartrato (DET), uno de los tartratos más efectivos en lo que a plastificación se refiere.

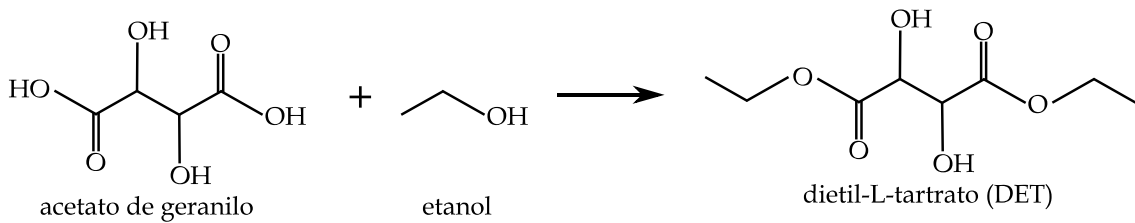


Figura I.24. Reacción de esterificación que da lugar a la obtención del dietil-L-tartrato (DET).

El uso de estos plastificantes, además de potenciar enormemente las propiedades dúctiles del PLA, aumenta también su valor medioambiental, ya que todos ellos pueden ser obtenidos de fuentes naturales y son biodegradables, por tanto no comprometen el valor que ya posee el PLA como biopolímero.

I.5. Valorización de residuos agroindustriales para su uso como aditivos en biopolímeros

Como se ha comentado en el primer apartado de esta introducción, a la vista de los problemas medioambientales actuales, la sociedad está centrando cada vez más sus esfuerzos en desarrollar soluciones o medidas que contrarresten estos problemas, entre los que destacan un aumento en la huella de carbono y una gran acumulación de residuos (sobre todo en el sector de los polímeros). Muchas de estas soluciones se centran en el aprovechamiento de la biomasa para producir nuevos materiales que no sean tan perjudiciales para el medioambiente, ya sea mediante su aprovechamiento directo realizando mezclas con otros polímeros o mediante la extracción de compuestos a partir de esta biomasa que otorguen nuevas propiedades a los polímeros, al mismo tiempo que se mantiene un enfoque de respeto con el medioambiente. Sin embargo, algunas de las propuestas que se han planteado utilizan biomasa que puede ser utilizada como alimento, como la patata. Teniendo en cuenta la fuerte crisis alimentaria mundial actual, surge la necesidad de centrar todas estas líneas de investigación en el reaprovechamiento de residuos de la industria alimentaria y agroforestal, como son pieles, huesos, semillas, tallos, hojas, cáscaras, etc. de frutas y vegetales, de tal modo, los cuales no tienen un papel directo en la alimentación humana y por tanto no implican un déficit en la disponibilidad alimentaria[184].

Dentro de este contexto surgen términos como biorrefinería y economía circular, que son vertientes que buscan aprovechar al máximo los residuos de diversas industrias, tanto del sector agrario como alimentario, para producir compuestos y materiales con un alto potencial medioambiental.

La biorrefinería incluye todos aquellos procesos que tratan de producir o extraer compuestos químicos, biocombustibles o materiales biobasados a partir de los residuos de la industria agroalimentaria. Por otro lado, la biorrefinería viene incluida en el marco de la economía circular, que implica utilizar todos estos componentes, obtenidos a partir de residuos naturales, de una forma integrada en la industria para reducir la cantidad de residuos a cero [185].

Diversos estudios se han llevado a cabo en los que se han empleado residuos de la industria alimentaria como materia prima para la obtención de diferentes compuestos, como por ejemplo la piel de naranja [186], piel de plátano [187], piel de granada [188], kernel de mango [189], cáscara de almendra [190] o cáscara de argán [191], entre muchos otros. La biorrefinería está utilizando estos residuos en procesos que pueden clasificarse

en 3 grupos principales:

- Procesos biológicos: en los cuales los residuos son convertidos en productos de valor añadido gracias a la utilización de enzimas o microorganismos. Dentro de este grupo entran procesos como la digestión anaeróbica o la fermentación.
- Procesos termoquímicos: que tratan los residuos a alta temperatura utilizando compuestos químicos como disolventes. En este grupo se incluyen la licuefacción, la pirólisis o la gasificación.
- Procesos químicos: donde compuestos químicos se utilizan como disolventes y catalizadores.

La biorrefinería permite obtener un gran abanico de compuestos y productos de valor añadido para desarrollar materiales con propiedades muy variadas. Entre estos compuestos se encuentran los polifenoles [192], la celulosa [193], la hemicelulosa [194], la lignina [195], los cristales de nanocelulosa [196], la pectina [197], diversos ésteres y alcoholes que pueden actuar como plastificantes [198, 199], almidón [200], bioetanol [201] y polímeros de origen natural [202], entre otros. Compuestos como la celulosa, la hemicelulosa o los cristales de nanocelulosa pueden actuar como refuerzo al mezclarse con polímeros, mientras que otros compuestos como los polifenoles otorgan propiedades antioxidantes a los polímeros en los que se introducen [203].

Además de extraer todos estos compuestos, también existe la posibilidad de utilizar residuos lignocelulósicos de la industria agroalimentaria de forma directa, normalmente en forma de micronizado o harina, para combinarlos con diversos polímeros y así reducir el coste del material resultante, ya que uno de los mayores inconvenientes de los biopolímeros es su elevado coste. Utilizando una parte de carga lignocelulósica (con un coste mucho menor al del polímero, puesto que se trata de un residuo), se obtienen materiales compuestos que además de reducir el coste del polímero original, le otorgan propiedades adicionales. Terroba-Delicado *et al.* [204] observaron como la adición de un 20% en masa de residuo micronizado de la industria del licor de café al PLA conseguía aumentar las propiedades dúctiles del polímero y proveerlo de cierta actividad antioxidante, dándole una mayor aplicación en el sector del envase y el embalaje. Quiles-Carrillo *et al.* [205] combinaron PLA con cáscara de almendra micronizada y aceite de linaza maleinizado, obteniendo materiales compuestos capaces de imitar la madera, con propiedades dúctiles superiores a las del PLA puro.

Todos los materiales fruto de la combinación de biopolímeros con compuestos derivados de los residuos agroalimentarios tienen un gran potencial para fomentar la sostenibilidad desde el marco de las economías circulares, ya que productos fabricados a partir de estos materiales pueden ser reinsertados en la industria de la que provienen los residuos, reduciendo así los residuos generados por la misma. Por ejemplo, se pueden desarrollar envases como cajas a partir de PLA con harina de cáscara de almendra que se destinen al almacenamiento de productos de la industria de la almendra [206]. Otro ejemplo es el desarrollo de films comestibles de almidón aditivados con compuestos fenólicos con propiedades antioxidantes que conserven mejor los productos alimenticios [207].

I.5.1. Industria del mango y potencial de reaprovechamiento de sus residuos

El mango (*Mangifera indica*) es uno de los cultivos más populares y más extendidos del planeta, el cual es predominante en países tropicales. De las más de 1500 variedades que existen de esta fruta solamente unas pocas son cultivadas y suministradas a escala comercial. India, China y Tailandia son los mayores productores del planeta, siendo India el mayor productor, con un 40% de la producción mundial [208]. Algunas de las principales variedades son la Totapuri, Chausa, Dashehari, Alphonso, Neelum, Osteen, etc.

Con respecto a la estructura del mango, este está compuesto por una piel exterior, la pulpa y la semilla, a su vez, la semilla está dividida en el kernel (parte interior) y el tegument (parte exterior). En la **Figura I.25** se puede observar la estructura del mango. En este caso, el mango se utiliza para producir una gran cantidad de productos, como pures, siropes, néctar, piezas de mango enlatadas, zumos, entre otros. La pulpa es el componente más utilizado del mango, y los residuos que quedan suelen ser la piel y las semillas.

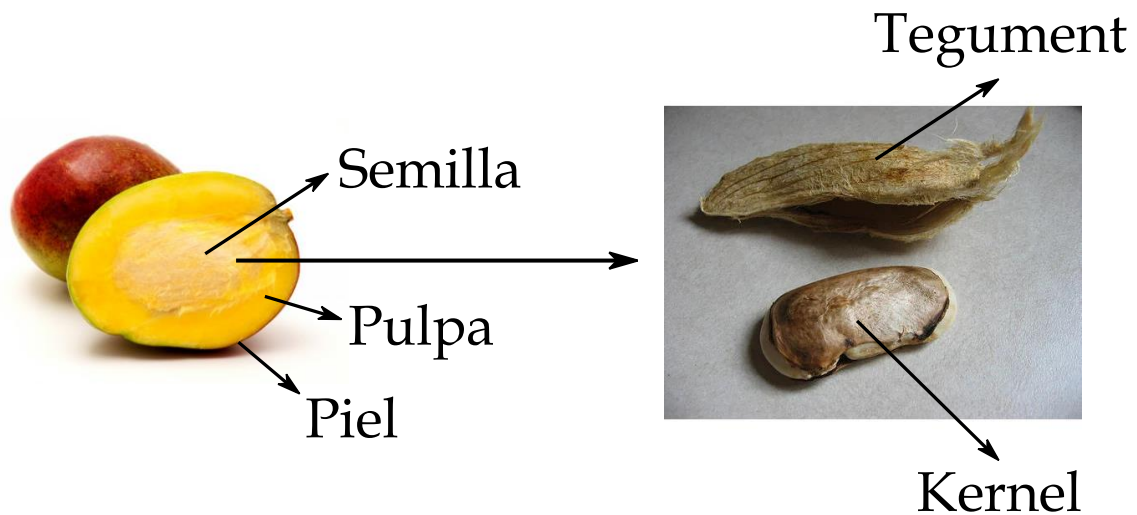


Figura I.25. Esquema de la estructura del mango.

Debido a la enorme producción de mango (46,5 millones de toneladas en 2016 [209]), la gestión de estos residuos es de vital importancia para evitar problemas medioambientales asociados y no desperdiciar una gran cantidad de materia prima con gran potencial en cuanto a valor añadido. En este aspecto, se han realizado muchos estudios referentes a los subproductos del mango, a partir de los cuales pueden obtenerse componentes de gran interés desde el punto de vista de la biorrefinería, como fibras, polifenoles, carotenoides, celulosa, almidón, etc. [208].

El mango está compuesto en un 33-85% por pulpa comestible, un 9-40% de semilla no comestible y un 7-24% de piel no comestible; estos valores varían dependiendo de la variedad del mango. La cantidad que poseen de piel y de semilla es considerable, las cuales son normalmente utilizadas como alimento para animales. Sin embargo, desde el marco de la biorrefinería son una potencial fuente de recursos de alto valor para la producción de materiales, entre los que se encuentran los siguientes:

- Polifenoles: varios estudios apuntan a la piel y el kernel del mango como fuentes ricas en compuestos fenólicos, entre los que destacan la mangiferina, el ácido gálico, el ácido clorogénico, quercetina y sus derivados, procianidinas, antocianinas o la rutina [210]. La mayoría de ellos poseen propiedades antioxidantes e incluso actividad antitumoral. Estos compuestos suelen ser extraídos por medio de maceración o extracción Soxhlet. Un aspecto muy importante es la utilización de disolventes verdes, como el etanol, etil acetato o agua.
- Carotenoides: los carotenoides son una familia de isoprenoides con cuarenta

átomos de carbono que son reconocidos como unos de los pigmentos fotosintéticos más importantes en el mundo vegetal, ya que protegen las membranas de clorofila de daño fotooxidativo. La piel del mango es rica en estos compuestos, entre los que destacan los carotenos, la violaxantina o la anteraxantina [211].

- Fibra dietética: la fibra dietética es uno de los nutrientes más importantes para los organismos vivos dada su importancia en las funciones fisiológicas de dichos organismos, como una reducción en el colesterol en sangre y una disminución de las enfermedades cardiovasculares, obesidad, diabetes, etc. La piel de mango es especialmente rica en esta fibra lignocelulósica, ya que posee un 56-66% de mezcla de celulosa, hemicelulosa, lignina, almidón y pectina [212]. Muchos estudios han revelado que estas fibras poseen actividad antioxidante y que, en combinación con polifenoles, puede otorgar efectos muy beneficiosos, especialmente en la industria de la alimentación.
- Pectina: la pectina es un polisacárido de gran importancia presente en la piel del mango que puede ser utilizada en materiales como agente reforzante o como estabilizante en la industria alimentaria. Este componente suele ser extraído por medio de hidrólisis ácida con ácido clorhídrico o sulfúrico. Sin embargo, este tratamiento puede contaminar la pectina extraída debido al uso de ácidos. Es por ello que se están implementando tratamientos hidrotérmicos libres de ácido, utilizando microondas, que ofrecen rendimientos de extracción de hasta un 11,6%. Este método incluso es capaz de extraer celulosa al mismo tiempo que la pectina [213].
- Celulosa y nanocristales de celulosa: la celulosa es el biopolímero más abundante en la naturaleza. La búsqueda de nuevas fuentes de este polímero está en constante movimiento, dada su importancia en una gran cantidad de sectores y desde el punto de vista medioambiental. Es un componente que puede actuar en mezclas de polímeros, films, etc. como agente reforzante [214]. Lo mismo se aplica a los nanocristales de celulosa, que son formaciones cristalinas nanométricas de celulosa con morfología de agujas, lo cual permite una gran dispersión en materiales poliméricos, otorgando unas propiedades mecánicas resistentes superiores en comparación con la celulosa simple [215]. La piel del mango y el tegument (piel de la semilla) han sido estudiados por poseer una gran cantidad de celulosa, siendo fuentes potenciales de este recurso [216, 217]. Estos se extraen mediante métodos con disolventes que

eliminan los compuestos no celulósicos.

- Almidón: si la celulosa es la fuente de biomasa vegetal más grande del planeta, el almidón es la segunda más importante. El kernel de mango es una gran fuente de este polímero, poseyendo hasta un 60% de contenido en peso de almidón [218]. Este tiene gran aplicación en la producción de films comestibles, nanofibras para aplicaciones médicas y textiles o para diferentes recipientes dedicados al envase y embalaje de alimentos. El almidón puede extraerse del kernel del mango utilizando métodos fisicoquímicos como la filtración, centrifugación y homogeneización. Normalmente, los kernels de mango suelen introducirse en una disolución de bisulfito de sodio para evitar la oxidación de estos durante el tratamiento [219].

La **Figura I.26** muestra un esquema de todos los residuos de la industria del mango y los subproductos que pueden obtenerse de cada uno de ellos.

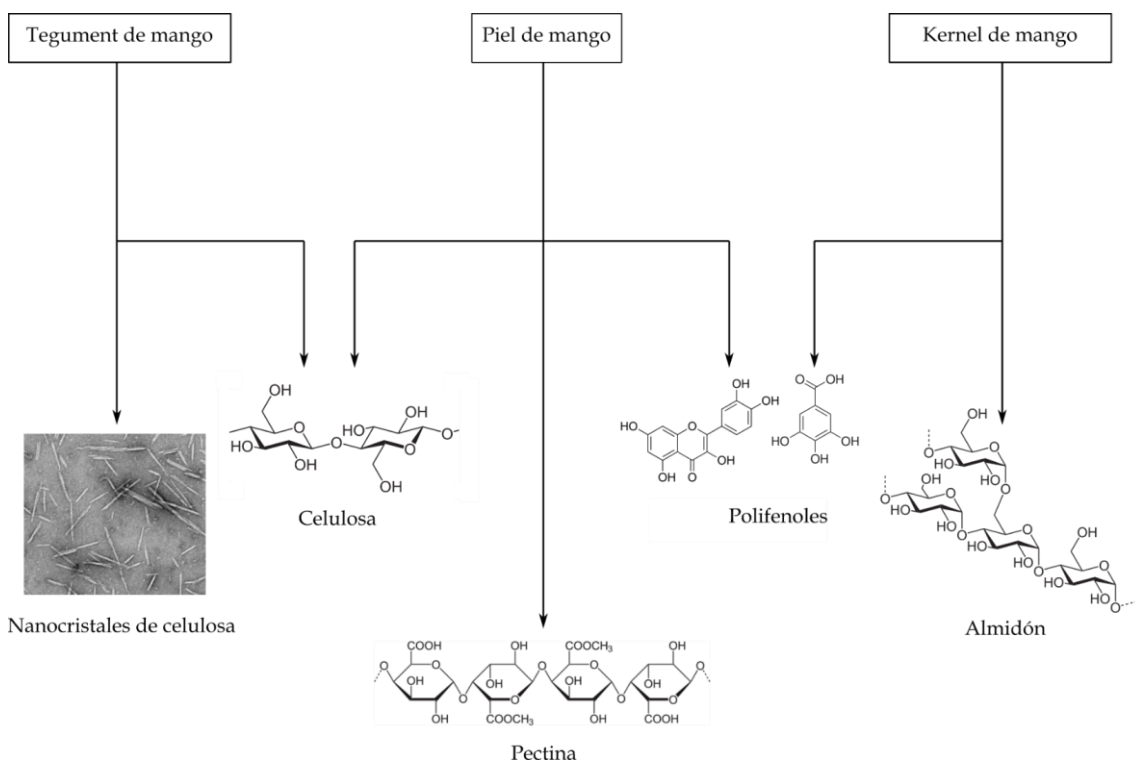


Figura I.26. Representación esquemática de los productos que pueden obtenerse de los diferentes residuos del mango.

Todos estos compuestos extraídos de los residuos del mango pueden incorporarse en materiales poliméricos como cargas o aditivos que les confieran

propiedades antioxidantes (polifenoles), incrementen sus propiedades mecánicas (celulosa, pectina o fibras) o sirvan directamente como polímero base para crear diferentes productos (almidón).

Además de estos compuestos, la piel y la semilla del mango pueden ser utilizadas directamente en forma de harina para desarrollar materiales compuestos con alto potencial medioambiental. Tras un proceso de molienda, tanto la piel del mango como el kernel han sido incorporados en diferentes polímeros, como el ácido poliláctico o el polipropileno, como cargas para reducir el coste del material resultante y darles un uso a los residuos de la industria del mango (economía circular). Además, también son capaces de otorgar propiedades antioxidantes a los polímeros en los que se introducen [209]. Haq *et al.* y Gomez-Caturla *et al.* [220, 221] estudiaron la combinación de piel de mango micronizada con biopolipropileno, trabajo que dio como resultado un material capaz de imitar a la madera con unas propiedades mecánicas muy similares a las del polipropileno puro. Por otro lado, se ha estudiado la combinación de harina de kernel de mango con ácido poliláctico en presencia de plastificantes, que permitió obtener materiales poliméricos respetuosos con el medio ambiente y con un coste reducido con respecto al ácido poliláctico puro [222].

I.5.2. Industria de los cítricos y potencial de reaprovechamiento de sus residuos

Los cítricos suponen el grupo de frutas más consumido del planeta, con una producción superior a 144 millones de toneladas en 2019 [223]. De forma similar a la industria del mango, la industria de los cítricos, donde se incluyen la naranja, la mandarina, la granada, el limón, la lima etc., también produce millones de toneladas de residuos sólidos provenientes de dichas frutas durante su procesado (por ejemplo, para producir zumos). Entre estos residuos se encuentran pieles, pulpa, semillas o aceites esenciales, teniendo la piel y la pulpa un contenido en humedad de entre el 75% y el 80% en peso. Actualmente, dichos residuos suelen ser empleados como alimento para ganado o desechados en vertederos. Además, las propiedades antimicrobianas y antioxidantes de los polifenoles presentes en la composición de estos residuos evitan la biodegradación de la materia orgánica y la acidez de estos residuos también provoca la contaminación del suelo.

La industria de los zumos produce unos 10 millones de toneladas de residuos cítricos al año [224], esto implica una gran cantidad de biomasa a partir de la cual pueden

extraerse numerosos componentes beneficiosos para la salud humana, como el limoneno, los compuestos fenólicos, azúcares libres o polisacáridos, entre otros. Comparados con otros residuos lignocelulósicos no ricos en pectina, los residuos cítricos contienen poca cantidad de lignina (la cual suele actuar como barrera física frente a la actuación de enzimas hidrolíticas), hecho que facilita la extracción de azúcares de los residuos mediante sacarificación. La **Tabla I.2** muestra algunos de los compuestos activos que se pueden extraer de una gran variedad de residuos cítricos, utilizando para ello un abanico de técnicas muy amplio.

Tabla I.2. Compuestos a extraer de varios residuos de frutos cítricos y las técnicas de extracción empleadas para ello. Adaptado de [225].

Residuo cítrico	Compuesto extraído	Técnica empleada
Piel de mandarina	Bioflavonoides, limoneno, hesperidina, ácido clorogénico	Extracción con CO ₂ y agua supercríticos
Subproductos de la naranja y la lima	Limoneno y limonina	Extracción asistida por enzimas
Epicarpo de la mandarina	Carotenoides	Extracción por ultrasonidos
Piel de mandarina híbrida	Flavonoides y ácido ascórbico	Extracción por ultrasonidos
Residuo de naranja	Ácido vanílico, ácido coumárico y hesperidina	Extracción con líquido presurizado
Residuos de lima persa	Antioxidantes y aceite palmítico, oléico y linoléico	Destilación con vapor y Soxhlet con hexano
Piel de naranja amarga	Aceites esenciales	Hidrodestilación asistida por ultrasonidos
Residuos cítricos generales	D-limoneno	Extracción asistida por ultrasonidos
Residuos de pomelo, limón, naranja y granada	Pectina	Extracción por manosonicación
Semilla de limón	Nanocristales de celulosa	Hidrólisis con ácido sulfúrico
Piel de naranja	Carotenoides	Extracción por ultrasonidos
Residuo cítrico general	Polisacáridos	Extracción por manosonicación alcalina
Semillas de limón	Nanocristales de celulosa	Oxidación TEMPO
Semillas de limón	Nanocristales de celulosa	Oxidación con persulfato de amonio
Piel cítrica	Flavonoides	Extracción dependiente de polaridad

I.5.2.1. Extracción de pectina

La capa interna de los cítricos (albedo) contiene tres tipos de polisacáridos (pectina, celulosa y hemicelulosa). A diferencia de otras fuentes de biomasa, que suelen contener una cantidad muy baja de pectina (en torno a 2,1%), los cítricos poseen hasta un 24,6% en peso de este polisacárido [226]. Otras pieles de frutas, como la manzana, tienen un 10-15% de pectina en su composición. Esto coloca a los cítricos como una de las mejores fuentes de pectina en el mundo vegetal [227]. La pectina tiene una gran variedad de usos, ya que es utilizada como agente reforzante en films y otros materiales, como modificante reológico o a modo de fibra dietética.

Dentro del mundo de los cítricos, la pectina puede extraerse a partir de la piel del pomelo, la piel de la naranja, la granada o la papaya, entre otros. El método más común de extracción es por hidrólisis ácida, utilizando ácido sulfúrico, nítrico, fosfórico o hidrocórico a temperaturas cercanas a 70 °C. Estos ácidos permiten la separación de la pectina de la matriz de celulosa/hemicelulosa, ya que, a pH menor de 3, los grupos carboxilos presentes en la pectina se ionizan, aumentando la tendencia a la formación de un gel de pectina [228]. Las condiciones de la extracción (pH, alta temperatura y tiempo extendido) provocan que el ácido galacturónico se fragmente en moléculas de pectina, obteniendo unos rendimientos de entre el 3 y el 25%.

I.5.2.2. Extracción de carotenoides

Los carotenoides, como se ha indicado anteriormente, son pigmentos isoprenoides involucrados en la fotosíntesis de muchos vegetales. Estos se dividen en dos grupos: los carotenos (hidrocarburos carotenoides) y las xantofilas (derivados oxigenados de los hidrocarburos carotenoides).

Estos pigmentos son los responsables del característico color naranja y amarillo de la pulpa y la piel de los cítricos [229]. Los carotenoides más predominantes en la composición de los cítricos son los ésteres de xantofilas, cuyo contenido depende de la especie, la madurez y la parte de la fruta. En la piel y el flavedo de la naranja dulce, por ejemplo, los carotenoides más abundantes son la violaxantina y los monoésteres y diésteres con diferentes funcionalidades como caprato, laurato, miristato, palmitato, stearato, palmitoleato u oleato de acilo. Otros de los carotenoides más abundantes son el α -caroteno y el β -caroteno. A diferencia de los compuestos fenólicos, la cantidad de carotenoides en la fruta aumenta con la madurez, de ahí ese cambio de color característico.

Estos carotenoides tienen gran aplicación en el sector del envase y embalaje como colorantes para mejorar el aspecto de los envasados. En este sentido, Stoll *et al.* [230] utilizaron extractos de carotenoides como colorantes naturales para films de PLA con el objetivo de sustituir a los colorantes sintéticos.

I.5.2.3. Extracción de flavonoides

Los flavonoides son un contribuyente importante en cuanto a compuestos antioxidantes se refiere. Se trata de compuestos polifenólicos que se encuentran ampliamente en plantas. Algunos de los flavonoides más abundantes en la composición de los cítricos son la naringina, hesperidina, eriocitrina, nariurina, quercetina, tangerina o la rutina, entre otros [231]. Estos compuestos se encuentran sobre todo en el albedo de las frutas cítricas. Un estudio sobre frutas cítricas mediterráneas reveló que los flavonoides suponían el 89,34% de la fracción de polifenoles de la fruta, siendo los principales la hesperidina y eriocitrina [232].

Estos frutos contienen la mayor parte de flavonoides durante la época de maduración, ya que a medida que la fruta madura, estos antioxidantes van desapareciendo y aumenta la concentración de carotenoides, como se ha mencionado anteriormente. Uno de los métodos más utilizados para extraer estos compuestos es la extracción Soxhlet, aunque también se utiliza la digestión o la maceración.

Paul y Das [233] realizaron un estudio en el cual incorporaron quercetina y hesperidina a materiales compuestos de CaCO_3 , observando como las propiedades mecánicas mejoraron a raíz de la incorporación de los flavonoides. Adicionalmente, también se han utilizado flavonoides como aditivos antioxidantes en polímeros. Esto tiene gran aplicación en el sector del envasado de productos alimenticios, ya que retrasa la degradación del producto [234].

I.5.2.4. Extracción de terpenos

Finalmente, una de la familia de compuestos de mayor interés que se pueden obtener a partir de los frutos cítricos son los aceites esenciales, los cuales presentan un alto contenido en terpenos. Estos compuestos se obtienen principalmente de la piel de estas frutas. Los aceites esenciales obtenidos de cítricos tienen gran cabida en el mundo farmacéutico, alimentario, de perfumería y cosmética, puesto que se trata de compuestos aromatizantes con propiedades antimicrobianas, analgésicas, ansiolíticas y

antioxidantes [235].

Los terpenos provienen de la mayoría de fracciones volátiles de los aceites esenciales de los cítricos. Estos terpenos incluyen monoterpenos hidrocarburos (limoneno, terpineno, mirceno, etc.); monoterpenos oxigenados (geranial y nonanal); terpenos alcoholes (geraniol, linalool, α -terpineol, verbenol o carveol); aldehídos (decanal) y ésteres como el etil cinamato (ver **Figura I.27**) [231]. En frutas como la mandarina, granada, naranja y el limón; el D-limoneno supone entre el 45 y el 90% de todos los terpenos que contiene la fruta [236]. En el estudio llevado a cabo por Rossi *et al.* [237] extrajeron aceites esenciales de mandarina de Montenegrin observando una presencia mayoritaria de D-limoneno y γ -terpineno, con una concentración minoritaria de citronelol y linalool. A estos dos últimos se les atribuyó una gran actividad antioxidante.

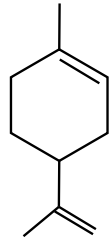
Como se ha mencionado en el apartado de plastificación, estos terpenos, como el geraniol o el linalool, se pueden utilizar para producir ésteres plastificantes de gran efectividad y valor medioambiental para polímeros como el PLA. Los ésteres como el etil cinamato, en cambio, pueden actuar directamente como plastificantes. Además, presentan la ventaja de ser compuestos de origen completamente renovable y sostenible. Cabe señalar que la mayoría de los terpenos citados no solo se extraen de los cítricos, sino que también pueden ser obtenidos de otras fuentes renovables, por ejemplo, el geraniol también puede obtenerse de las hojas de palmarosa [238].

Uno de los métodos para extraer terpenos a partir de los residuos cítricos es utilizar disolventes como el n-pentano o el dietil éter en combinación con ultrasonidos para mejorar el rendimiento de extracción [239]. Temelli *et al.* [240] utilizaron un método de extracción con dióxido de carbono supercrítico para obtener terpenos a partir de la piel de la naranja.

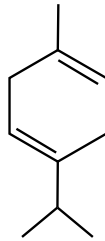
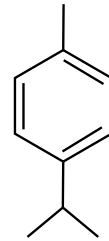
Todos los terpenos mencionados tienen un gran potencial de aplicación en el sector de la medicina a raíz de sus propiedades anticancerígenas, antiinflamatorias, antimicrobianas, antioxidantes, analgésicas, respiratorias y sedativas [241]. Además, como ya se adelantó anteriormente, estos compuestos están adquiriendo un gran interés en el campo de los polímeros para su uso como plastificantes naturales, con el objetivo de mejorar la ductilidad de polímeros frágiles, como el PLA o los PHAs, aumentando así la aplicabilidad de dichos polímeros en sectores de gran importancia como el del envase y embalaje. Mangeon *et al.* [180] combinaron linalool, geraniol y acetato de geraniol con poli(3-hidroxibutirato) (PHB), un polímero con propiedades mecánicas muy pobres, observando cómo los tres terpenos aumentaron la elongación a la rotura en más de un

200% con respecto a la del PHB puro, además de disminuir la temperatura de transición vítrea.

Monoterpenos hidrocarburos

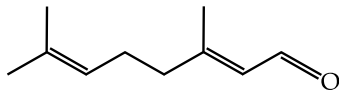


D-limoneno

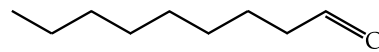
 γ -terpineno

p-cimeno

Monoterpenos oxigenados

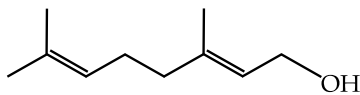


geranial

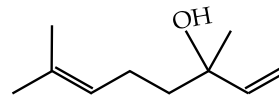


nonanal

Terpenos alcoholes

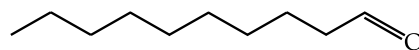


geraniol



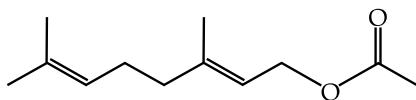
linalool

Aldehídos

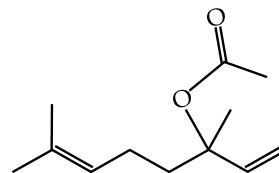


decanal

Ésteres



acetato de geranilo



acetato de linalilo

Figura I.27. Esquema de terpenos presentes en frutos cítricos.

Por tanto, los terpenos presentan un gran potencial como aditivos naturales para biopolímeros, mejorando sus propiedades sin afectar a su rendimiento medioambiental. Además, su empleo como aditivos fomenta la economía circular desde el principio de biorrefinería, ya que un material polimérico aditivado con un terpeno como el geraniol obtenido a partir de residuos de la naranja, puede ser utilizado para fabricar productos de envasado destinados a la industria de la naranja, como cajas o films de embalaje.

REFERENCIAS

- [1] Freinkel, S., *A brief history of plastic's conquest of the world*, in Sci Am. 2011.
- [2] Baekeland, A.L.H., *The Invention of Bakelite*. 2021, American Chemical Society. <https://www.acs.org/content/acs/en/education>.
- [3] Daniels, P.H., *A brief overview of theories of PVC plasticization and methods used to evaluate PVC-plasticizer interaction*. Journal of vinyl and additive technology, 2009. 15(4): 219-223.
- [4] Millet, H., et al., *The nature of plastics and their societal usage*. Issues in environmental science and technology, 2019. 2019(47): 1-20.
- [5] Zhao, Z., et al., *Designing flexible, smart and self-sustainable supercapacitors for portable/wearable electronics: from conductive polymers*. Chemical Society Reviews, 2021. 50(22): 12702-12743.
- [6] Gao, H., et al., *The research status and challenges of shape memory polymer-based flexible electronics*. Materials Horizons, 2019. 6(5): 931-944.
- [7] Shen, J., et al., *Recent progress in polymer-based building materials*. International Journal of Polymer Science, 2020. 2020(6): 1-15.
- [8] Wang, Y., et al., *Current status and prospects of polymer powder 3D printing technologies*. Materials, 2020. 13(10): 2406.
- [9] Shahbazi, M. and H. Jäger, *Current status in the utilization of biobased polymers for 3D printing process: a systematic review of the materials, processes, and challenges*. ACS Applied Bio Materials, 2020. 4(1): 325-369.
- [10] Yadav, R., et al., *Polymer composite for antistatic application in aerospace*. Defence Technology, 2020. 16(1): 107-118.
- [11] Aamir, M., et al., *Recent advances in drilling of carbon fiber-reinforced polymers for aerospace applications: A review*. The International Journal of Advanced Manufacturing Technology, 2019. 105: 2289-2308.
- [12] Ferreira, F.V., et al., *Polymer composites reinforced with natural fibers and nanocellulose in the automotive industry: A short review*. Journal of Composites Science, 2019. 3(2): 51.
- [13] Begum, S.A., A.V. Rane, and K. Kanny, *Applications of compatibilized polymer blends in automobile industry, in Compatibilization of polymer blends*. 2020, Elsevier. 563-593.

- [14] Vasile, C., *et al.*, *New developments in medical applications of hybrid hydrogels containing natural polymers*. *Molecules*, 2020. 25(7): 1539.
- [15] Saylan, Y., *et al.*, *Molecularly imprinted polymer based sensors for medical applications*. *Sensors*, 2019. 19(6): 1279.
- [16] Zhao, W., *et al.*, *Shape memory polymers and their composites in biomedical applications*. *Materials Science and Engineering: C*, 2019. 97: 864-883.
- [17] Jorda-Reolid, M., *et al.*, *Upgrading argan shell wastes in wood plastic composites with biobased polyethylene matrix and different compatibilizers*. *Polymers*, 2021. 13(6): 922.
- [18] Hong, M. and E.Y.-X. Chen, *Chemically recyclable polymers: a circular economy approach to sustainability*. *Green Chemistry*, 2017. 19(16): 3692-3706.
- [19] Arrieta, M.P., *Films de PLA y PLA-PHB plastificados para su aplicación en envases de alimentos. Caracterización y análisis de los procesos de degradación*. 2014, Universitat Politècnica de València.
- [20] Mendieta, C.M., *et al.*, *Bio-polyethylene from wood wastes*. *Journal of Polymers and the Environment*, 2020. 28: 1-16.
- [21] Kikuchi, Y., *et al.*, *Environmental performance of biomass-derived chemical production: a case study on sugarcane-derived polyethylene*. *Journal of chemical engineering of Japan*, 2013. 46(4): 319-325.
- [22] Liptow, C. and A.M. Tillman, *A comparative life cycle assessment study of polyethylene based on sugarcane and crude oil*. *Journal of Industrial Ecology*, 2012. 16(3): 420-435.
- [23] Morschbacker, A., *Bio-ethanol based ethylene*. *Journal of Macromolecular Science®, Part C: Polymer Reviews*, 2009. 49(2): 79-84.
- [24] Chen, G.-Q. and M.K. Patel, *Plastics derived from biological sources: present and future: a technical and environmental review*. *Chemical reviews*, 2012. 112(4): 2082-2099.
- [25] Tarafdar, A., *et al.*, *The hazardous threat of Bisphenol A: Toxicity, detection and remediation*. *Journal of hazardous materials*, 2022. 423: 1-15.
- [26] Drews, J., *et al.*, *Hydrolysis and stability of thin pulsed plasma polymerised maleic anhydride coatings*. *Applied surface science*, 2008. 254(15): 4720-4725.

- [27] Karim, Z., *et al.*, *Necessity of enzymatic hydrolysis for production and functionalization of nanocelluloses*. *Critical reviews in biotechnology*, 2017. 37(3): 355-370.
- [28] Pill, M.F., *et al.*, *Mechanical activation drastically accelerates amide bond hydrolysis, matching enzyme activity*. *Angewandte Chemie International Edition*, 2019. 58(29): 9787-9790.
- [29] Chiu, P.-H., *et al.*, *Deep learning for predictions of hydrolysis rates and conditional molecular design of esters*. *Journal of the Taiwan Institute of Chemical Engineers*, 2021. 126: 1-13.
- [30] Cha, Y. and C. Pitt, *The biodegradability of polyester blends*. *Biomaterials*, 1990. 11(2): 108-112.
- [31] Drumright, R.E., P.R. Gruber, and D.E. Henton, *Poly(lactic acid) technology*. *Advanced materials*, 2000. 12(23): 1841-1846.
- [32] Guarino, V., *et al.*, *Polycaprolactone: synthesis, properties, and applications*. *Encyclopedia of polymer science and technology*, 2002: 1-36.
- [33] Budak, K., O. Sogut, and U. Aydemir Sezer, *A review on synthesis and biomedical applications of polyglycolic acid*. *Journal of polymer research*, 2020. 27: 208.
- [34] Nazrin, A., *et al.*, *Nanocellulose reinforced thermoplastic starch (TPS), polylactic acid (PLA), and polybutylene succinate (PBS) for food packaging applications*. *Frontiers in chemistry*, 2020. 8: 213.
- [35] Davachi, S.M. and B. Kaffashi, *Poly(lactic acid) in medicine*. *Polymer-Plastics Technology and Engineering*, 2015. 54(9): 944-967.
- [36] Pellis, A., *et al.*, *Renewable building blocks for sustainable polyesters: new biotechnological routes for greener plastics*. *Polymer international*, 2016. 65(8): 861-871.
- [37] Jiao, Y.-P. and F.-Z. Cui, *Surface modification of polyester biomaterials for tissue engineering*. *Biomedical materials*, 2007. 2(4): R24.
- [38] Shen, H. and X. Hu, *Growth factor loading on aliphatic polyester scaffolds*. *RSC advances*, 2021. 11(12): 6735-6747.
- [39] Michalicha, A., *et al.*, *Polycatecholamine and gentamicin as modifiers for antibacterial and blood-biocompatible polyester vascular prostheses*. *Biomaterials Advances*, 2022. 133(1): 112645.

- [40] Swainson, S.M., *et al.*, *Poly (glycerol adipate) (PGA), an enzymatically synthesized functionalizable polyester and versatile drug delivery carrier: A literature update.* *Polymers*, 2019. 11(10): 1561.
- [41] Jian, J., Z. Xiangbin, and H. Xianbo, *An overview on synthesis, properties and applications of poly (butylene-adipate-co-terephthalate)-PBAT.* *Advanced Industrial and Engineering Polymer Research*, 2020. 3(1): 19-26.
- [42] Teodorescu, M., M. Bercea, and S. Morariu, *Biomaterials of PVA and PVP in medical and pharmaceutical applications: Perspectives and challenges.* *Biotechnology advances*, 2019. 37(1): 109-131.
- [43] Aravamudhan, A., *et al.*, *Natural polymers: polysaccharides and their derivatives for biomedical applications*, in *Natural and synthetic biomedical polymers*. 2014, Elsevier. 67-89.
- [44] Frandsen, J.L. and H. Ghandehari, *Recombinant protein-based polymers for advanced drug delivery.* *Chemical Society Reviews*, 2012. 41(7): 2696-2706.
- [45] Diyana, Z., *et al.*, *Physical properties of thermoplastic starch derived from natural resources and its blends: A review.* *Polymers*, 2021. 13(9): 1396.
- [46] de Castro, T.R., *et al.*, *The potential of cleaner fermentation processes for bioplastic production: a narrative review of polyhydroxyalkanoates (PHA) and polylactic acid (PLA).* *Journal of Polymers and the Environment*, 2022. 30(3): 810-832.
- [47] Tan, G.-Y.A., *et al.*, *Start a research on biopolymer polyhydroxyalkanoate (PHA): a review.* *Polymers*, 2014. 6(3): 706-754.
- [48] Elmowafy, E., *et al.*, *Polyhydroxyalkanoate (PHA): Applications in drug delivery and tissue engineering.* *Expert review of medical devices*, 2019. 16(6): 467-482.
- [49] Pederson, E.N., C.W. McChalicher, and F. Sreenc, *Bacterial synthesis of PHA block copolymers.* *Biomacromolecules*, 2006. 7(6): 1904-1911.
- [50] Xiaodong, W., G. Xuan, and S. Rakshit, *Direct fermentative production of lactic acid on cassava and other starch substrates.* *Biotechnology Letters*, 1997. 19: 841-843.
- [51] Avérous, L., *Polylactic acid: synthesis, properties and applications*, in *Monomers, polymers and composites from renewable resources*. 2008, Elsevier. 433-450.
- [52] Whistler, R.L. and J.R. Daniel, *Starch.* *Kirk-othmer encyclopedia of chemical technology*. 2000.

- [53] Durrani, C.M. and A.M. Donald, *Physical characterisation of amylopectin gels*. Polymer gels and networks, 1995. 3(1): 1-27.
- [54] Li, H.-T., et al., *Starch granular protein of high-amylose wheat gives innate resistance to amylolysis*. Food chemistry, 2020. 330: 127328.
- [55] Chang, Q., et al., *A comprehensive review of the factors influencing the formation of retrograded starch*. International Journal of Biological Macromolecules, 2021. 186: 163-173.
- [56] Buleon, A., et al., *Starch granules: structure and biosynthesis*. International journal of biological macromolecules, 1998. 23(2): 85-112.
- [57] Bertoft, E., *Understanding starch structure: Recent progress*. Agronomy, 2017. 7(3): 56.
- [58] Jobling, S., *Improving starch for food and industrial applications*. Current opinion in plant biology, 2004. 7(2): 210-218.
- [59] Waterschoot, J., et al., *Production, structure, physicochemical and functional properties of maize, cassava, wheat, potato and rice starches*. Starch-Stärke, 2015. 67(1-2): 14-29.
- [60] Tesfaye, T., et al., *Valorisation of mango seed via extraction of starch: preliminary techno-economic analysis*. Clean Technologies and Environmental Policy, 2018. 20: 81-94.
- [61] Pires, M.B., et al., *Impact of extraction methods and genotypes on the properties of starch from peach palm (Bactris gasipaes Kunth) fruits*. LWT, 2021. 150: 111983.
- [62] Hernandez-Carmona, F., et al., *Starch extraction potential from plantain peel wastes*. Journal of environmental chemical engineering, 2017. 5(5): 4980-4985.
- [63] Martins, S., et al., *Extraction and characterization of the starch present in the avocado seed (Persea americana mill) for future applications*. Journal of Agriculture and Food Research, 2022. 8: 100303.
- [64] Chu, P.H., et al., *Starch extracted from pineapple (Ananas comosus) plant stem as a source for amino acids production*. Chemical and Biological Technologies in Agriculture, 2021. 8(1): 1-15.
- [65] Vasanthan, T., et al., *Starch from Alberta potatoes: wet-isolation and some physicochemical properties*. Food Research International, 1999. 32(5): 355-365.

- [66] Kale, R., *et al.*, *Effect of isolation methods on physicochemical and functional properties of sweet potato (Ipomoea batatas L.) starch*. *Journal of Pharmacognosy and Phytochemistry*, 2017. 6(4): 223-227.
- [67] Babu, S.A. and R. Parimalavalli, *Effect of starch isolation method on properties of sweet potato starch*. *The Annals of the University Dunarea de Jos of Galati. Fascicle VI-Food Technology*, 2014. 38(1): 48-63.
- [68] Lee, H., A. Htoon, and J. Paterson, *Alkaline extraction of starch from Australian lentil cultivars Matilda and Digger optimised for starch yield and starch and protein quality*. *Food Chemistry*, 2007. 102(3): 551-559.
- [69] Kringel, D.H., *et al.*, *Fruit wastes as promising sources of starch: Extraction, properties, and applications*. *Starch-Stärke*, 2020. 72(3-4): 1900200.
- [70] Nakthong, N., R. Wongsagonsup, and T. Amornsakchai, *Characteristics and potential utilizations of starch from pineapple stem waste*. *Industrial Crops and Products*, 2017. 105: 74-82.
- [71] Gomez-Caturla, J., *et al.*, *Development and evaluation of novel nanofibers based on mango kernel starch obtained by electrospinning*. *Polymer Testing*, 2022. 106: 107462.
- [72] Bangar, S.P., *et al.*, *Litchi (Litchi chinensis) seed starch: Structure, properties, and applications-A review*. *Carbohydrate Polymer Technologies and Applications*, 2021. 2: 100080.
- [73] Onias, E.A., *et al.*, *Coating guava postharvest with the use of starch of tamarind seed and pomegranate seed oil*. *Journal of Agricultural Science*, 2018. 11(1): 313.
- [74] Tosif, M.M., *et al.*, *Loquat seed starch – Emerging source of non-conventional starch: Structure, properties, and novel applications*. *International Journal of Biological Macromolecules*, 2023. 244: 125230.
- [75] Hu, Z., *et al.*, *Hierarchical structure, gelatinization, and digestion characteristics of starch from longan (Dimocarpus longan Lour.) seeds*. *Molecules*, 2018. 23(12): 3262.
- [76] Martins, S., *et al.*, *Extraction and characterization of the starch present in the avocado seed (Persea americana mill) for future applications*. *Journal of Agriculture and Food Research*, 2022. 8: 100303.
- [77] Stevenson, D.G., P.A. Domoto, and J.-I. Jane, *Structures and functional properties of apple (Malus domestica Borkh) fruit starch*. *Carbohydrate polymers*, 2006. 63(3): 432-441.

- [78] Campelo, P.H., A.S. Sant'Ana, and M.T.P.S. Clerici, *Starch nanoparticles: production methods, structure, and properties for food applications*. *Current Opinion in Food Science*, 2020. 33: 136-140.
- [79] Ochubiojo, E.M. and A. Rodrigues, *Starch: from food to medicine*. Scientific, health and social aspects of the food industry. 2012: 355-380.
- [80] Ai, Y. and J.I. Jane, *Gelatinization and rheological properties of starch*. *Starch-Stärke*, 2015. 67(3-4): 213-224.
- [81] Regazzi, A., et al., *Microstructural and mechanical properties of biocomposites made of native starch granules and wood fibers*. *Composites Science and Technology*, 2019. 182: 107755.
- [82] Schirmer, M., M. Jekle, and T. Becker, *Starch gelatinization and its complexity for analysis*. *Starch-Stärke*, 2015. 67(1-2): 30-41.
- [83] Wang, B., et al., *An overview on plasticized biodegradable corn starch-based films: The physicochemical properties and gelatinization process*. *Critical reviews in food science and nutrition*, 2022. 62(10): 2569-2579.
- [84] Guo, S.x., et al., *Effect of Plasticizers on the Properties of Potato Flour Films*. *Starch-Stärke*, 2022. 74(1-2): 2100179.
- [85] Zainal Abiddin, N.F., *Optimisation and characterisation of octenyl succinic anhydride (OSA) modified sago starch and its capability to stabilise emulsion*. 2021, Universiti Teknologi MARA.
- [86] Egharevba, H.O., *Chemical properties of starch and its application in the food industry*. *Chemical properties of starch*. Vol. 9. 2019. 1-27.
- [87] Otache, M., et al., *Advances in the modification of starch via esterification for enhanced properties*. *Journal of Polymers and the Environment*, 2021. 29: 1365-1379.
- [88] Bakouri, H. and K. Guemra, *Etherification and cross-linking effect on physicochemical properties of Zea mays starch executed at different sequences in 1-butyl-3-methylimidazolium chloride [BMIM] Cl ionic liquid media*. *International journal of biological macromolecules*, 2019. 125: 1118-1127.
- [89] Wang, S., et al., *Starch retrogradation: A comprehensive review*. *Comprehensive Reviews in Food Science and Food Safety*, 2015. 14(5): 568-585.
- [90] Thakur, R., et al., *Starch-based films: Major factors affecting their properties*. *International journal of biological macromolecules*, 2019. 132: 1079-1089.

- [91] Rhowell Jr, N.T., A.P. Bonto, and N. Sreenivasulu, *Enhancing the functional properties of rice starch through biopolymer blending for industrial applications: A review*. International Journal of Biological Macromolecules, 2021. 192: 100-117.
- [92] Yang, J., et al., *Hydrogen bonding energy determined by molecular dynamics simulation and correlation to properties of thermoplastic starch films*. Carbohydrate Polymers, 2017. 166: 256-263.
- [93] Esmaeili, M., G. Pircheraghi, and R. Bagheri, *Optimizing the mechanical and physical properties of thermoplastic starch via tuning the molecular microstructure through co-plasticization by sorbitol and glycerol*. Polymer international, 2017. 66(6): 809-819.
- [94] Gamarano, D.d.S., et al., *Crystal structure transformations in extruded starch plasticized with glycerol and urea*. Polymer Bulletin, 2020. 77(9): 4971-4992.
- [95] Lim, W.S., et al., *Heat-sealing property of cassava starch film plasticized with glycerol and sorbitol*. Food Packaging and Shelf Life, 2020. 26: 100556.
- [96] Paluch, M., et al., *Structural and thermal properties of starch plasticized with glycerol/urea mixture*. Journal of Polymers and the Environment, 2021. 30: 728-740.
- [97] Baran, A., et al., *Effects of sorbitol and formamide plasticizers on molecular motion in corn starch studied using NMR and DMTA*. Journal of Applied Polymer Science, 2020. 137(33): 48964.
- [98] Lubis, M., et al., *The effect of ethylene glycol as plasticizer against mechanical properties of bioplastic originated from jackfruit seed starch and cocoa pod husk*. Nusantara Bioscience, 2018. 10(2): 76-80.
- [99] Montilla-Buitrago, C.E., et al., *Effect of plasticizers on properties, retrogradation, and processing of extrusion-obtained thermoplastic starch: A review*. Starch-Stärke, 2021. 73(9-10): 2100060.
- [100] Ma, X., J. Yu, and J. Wan, *Urea and ethanolamine as a mixed plasticizer for thermoplastic starch*. Carbohydrate polymers, 2006. 64(2): 267-273.
- [101] Dang, K.M. and R. Yoksan, *Thermoplastic starch blown films with improved mechanical and barrier properties*. International Journal of Biological Macromolecules, 2021. 188: 290-299.

- [102] Zdanowicz, M., *Deep eutectic solvents based on urea, polyols and sugars for starch treatment*. International Journal of Biological Macromolecules, 2021. 176: 387-393.
- [103] Montilla-Buitrago, C.E., *et al.*, *Effect of plasticizers on properties, retrogradation, and processing of extrusion-obtained thermoplastic starch: A review*. Starch-Stärke, 2021. 73(9-10): 2100060.
- [104] Abiddin, N.Z., A. Yusoff, and N. Ahmad, *Effect of octenylsuccinylation on physicochemical, thermal, morphological and stability of octenyl succinic anhydride (OSA) modified sago starch*. Food Hydrocolloids, 2018. 75: 138-146.
- [105] Otache, M., *et al.*, *Advances in the modification of starch via esterification for enhanced properties*. Journal of Polymers and the Environment, 2021. 29: 1365-1379.
- [106] Tupa, M.V., *et al.*, *Preparation and characterization of modified starches obtained in acetic anhydride/tartaric acid medium*. Starch-Stärke, 2020. 72(5-6): 1900300.
- [107] Carlos-Amaya, F., *et al.*, *Physicochemical and digestibility properties of double-modified banana (Musa paradisiaca L.) starches*. Journal of Agricultural and Food Chemistry, 2011. 59(4): 1376-1382.
- [108] Korma, S.A., *et al.*, *Chemically modified starch and utilization in food stuffs*. International Journal of Nutrition and Food Sciences, 2016. 5(4): 264-272.
- [109] Kou, T., *et al.*, *Effect of Amylose and Crystallinity Pattern on the Gelatinization Behavior of Cross-Linked Starches*. Polymers, 2022. 14(14): 2870.
- [110] Park, E.Y., *et al.*, *Effect of dual modification of HMT and crosslinking on physicochemical properties and digestibility of waxy maize starch*. Food Hydrocolloids, 2018. 75: 33-40.
- [111] Chhabra, R., *et al.*, *In vivo studies of 3D starch-gelatin scaffolds for full-thickness wound healing*. ACS Applied Bio Materials, 2020. 3(5): 2920-2929.
- [112] De Carvalho, A.J.F. and E. Trovatti, *Biomedical applications for thermoplastic starch*. Biodegradable and Biobased Polymers for Environmental and Biomedical Applications, 2016: 1-23.
- [113] Srivastava, J., *et al.*, *Glycoprotein imprinted RGO-starch nanocomposite modified EQCM sensor for sensitive and specific detection of transferrin*. Journal of Electroanalytical Chemistry, 2019. 835: 169-177.

- [114] Khlibsuwan, R., W. Tansena, and T. Pongjanyakul, *Modification of alginate beads using gelatinized and ungelatinized arrowroot (Tacca leontopetaloides L. Kuntze) starch for drug delivery*. International journal of biological macromolecules, 2018. 118: 683-692.
- [115] dos Santos Garcia, V.A., et al., *Gelatin/starch orally disintegrating films as a promising system for vitamin C delivery*. Food hydrocolloids, 2018. 79: 127-135.
- [116] Hemamalini, T. and V.R.G. Dev, *Comprehensive review on electrospinning of starch polymer for biomedical applications*. International journal of biological macromolecules, 2018. 106: 712-718.
- [117] Rahmati, M., et al., *Electrospinning for tissue engineering applications*. Progress in Materials Science, 2021. 117: 100721.
- [118] Jaiturong, P., et al., *Preparation of glutinous rice starch/polyvinyl alcohol copolymer electrospun fibers for using as a drug delivery carrier*. Asian journal of pharmaceutical sciences, 2018. 13(3): 239-247.
- [119] Waghmare, V.S., et al., *Starch based nanofibrous scaffolds for wound healing applications*. Bioactive materials, 2018. 3(3): 255-266.
- [120] Issa, A., S.A. Ibrahim, and R. Tahergorabi, *Impact of sweet potato starch-based nanocomposite films activated with thyme essential oil on the shelf-life of baby spinach leaves*. Foods, 2017. 6(6): 43.
- [121] Ali, A., et al., *Starch-based antimicrobial films functionalized by pomegranate peel*. International journal of biological macromolecules, 2019. 129: 1120-1126.
- [122] Bangar, S.P., et al., *Functionality and applicability of starch-based films: An eco-friendly approach*. Foods, 2021. 10(9): 2181.
- [123] Francis, D.V., et al., *Metallic nanoparticle integrated ternary polymer blend of PVA/starch/glycerol: a promising antimicrobial food packaging material*. Polymers, 2022. 14(7): 1379.
- [124] Jem, K.J. and B. Tan, *The development and challenges of poly (lactic acid) and poly (glycolic acid)*. Advanced Industrial and Engineering Polymer Research, 2020. 3(2): 60-70.
- [125] Kervran, M., et al., *Thermal degradation of polylactic acid (PLA)/polyhydroxybutyrate (PHB) blends: A systematic review*. Polymer Degradation and Stability, 2022. 201: 109995.

- [126] Singhvi, M., S. Zinjarde, and D. Gokhale, *Polylactic acid: Synthesis and biomedical applications*. Journal of applied microbiology, 2019. 127(6): 1612-1626.
- [127] Vink, E.T., et al., *Applications of life cycle assessment to NatureWorks™ polylactide (PLA) production*. Polymer Degradation and stability, 2003. 80(3): 403-419.
- [128] Singh, S. and S.S. Ray, *Poly lactide based nanostructured biomaterials and their applications*. Journal of Nanoscience and Nanotechnology, 2007. 7(8): 2596-2615.
- [129] Capuana, E., et al., *Poly-L-lactic acid (PLLA)-based biomaterials for regenerative medicine: A review on processing and applications*. Polymers, 2022. 14(6): 1153.
- [130] 박혜선 and 홍창국, *PLLA/PDLLA blends by controlling the crystallization of the PLLA matrix and improve the mechanical property with MgO*. 한국공업화학회 연구논문 초록집, 2022. 2022(1): 161-162.
- [131] Farah, S., D.G. Anderson, and R. Langer, *Physical and mechanical properties of PLA, and their functions in widespread applications – A comprehensive review*. Advanced drug delivery reviews, 2016. 107: 367-392.
- [132] Omar, A.A., et al., *A Best-evidence Review of Bio-based Plasticizer and the Effects on the Mechanical Properties of PLA*. Chemical Engineering Transactions, 2021. 89: 241-246.
- [133] Li, F., C. Zhang, and Y. Weng, *Improvement of the Gas Barrier Properties of PLA/OMMT Films by Regulating the Interlayer Spacing of OMMT and the Crystallinity of PLA*. ACS omega, 2020. 5(30): 18675-18684.
- [134] Park, K. and M. Xanthos, *A study on the degradation of polylactic acid in the presence of phosphonium ionic liquids*. Polymer Degradation and Stability, 2009. 94(5): 834-844.
- [135] Olewnik-Kruszkowska, E., et al., *Biodegradation of polylactide-based composites with an addition of a compatibilizing agent in different environments*. International Biodeterioration & Biodegradation, 2020. 147: 1-9.
- [136] Cairncross, R.A., et al., *Moisture sorption, transport, and hydrolytic degradation in polylactide*. in Twenty-Seventh Symposium on Biotechnology for Fuels and Chemicals. 2006. Springer.
- [137] Barillari, F. and F. Chini, *Biopolymers-sustainability for the automotive value-added chain*. ATZ worldwide, 2020. 122(11): 36-39.

- [138] Petchwattana, N., P. Naknaen, and B. Narupai, *A circular economy use of waste wood sawdust for wood plastic composite production: Effect of bio-plasticiser on the toughness*. International Journal of Sustainable Engineering, 2020. 13(5): 398-410.
- [139] Feng, J., et al., *Performance comparison of four kinds of straw/PLA/PBAT wood plastic composites*. BioResources, 2020. 15(2): 2596-2604.
- [140] Borysiuk, P., et al., *PLA Biocomposites: Evaluation of resistance to mold*. Polymers, 2021. 14(1): 157.
- [141] Mazzanti, V., et al., *Reinforcing mechanisms of natural fibers in green composites: Role of fibers morphology in a PLA/hemp model system*. Composites science and technology, 2019. 180: 51-59.
- [142] Andrade, M.A., et al., *Extending high fatty foods shelf-life protecting from lipid oxidation and microbiological contamination: an approach using active packaging with pomegranate extract*. Coatings, 2023. 13(1): 93.
- [143] Lima, E.M.B., et al., *Biocomposites of PLA and mango seed waste: Potential material for food packaging and a technological alternative to reduce environmental impact*. Starch-Stärke, 2021. 73(5-6): 2000118.
- [144] Varga, N., et al., *Vitamin E-loaded PLA-and PLGA-based core-shell nanoparticles: synthesis, structure optimization and controlled drug release*. Pharmaceutics, 2019. 11(7): 357.
- [145] Sadudeethanakul, S., et al. *Bending strength and Biological properties of PLA-HA composites for femoral canine bone fixation plate*. in IOP Conference Series: Materials Science and Engineering. 2019. IOP Publishing.
- [146] Agarwal, R., J. Singh, and V. Gupta, *Predicting the compressive strength of additively manufactured PLA-based orthopedic bone screws: A machine learning framework*. Polymer Composites, 2022. 43(8): 5663-5674.
- [147] Wang, W., et al., *3D printing of PLA/n-HA composite scaffolds with customized mechanical properties and biological functions for bone tissue engineering*. Composites Part B: Engineering, 2021. 224: 109192.
- [148] Liu, S., et al., *Enhanced surface hydrophilicity of polylactic acid sutures treated by lipase and chitosan*. Textile Research Journal, 2019. 89(16): 3291-3302.

- [149] Paz-González, J.A., *et al.*, *Structural composite based on 3D printing polylactic acid/carbon fiber laminates (PLA/CFRC) as an alternative material for femoral stem prosthesis*. *Journal of the Mechanical Behavior of Biomedical Materials*, 2023. 138(1): 105632.
- [150] Tümer, E.H. and H.Y. Erbil, *Extrusion-based 3D printing applications of PLA composites: a review*. *Coatings*, 2021. 11(4): 390.
- [151] Mirdamadi, E.S., *et al.*, *3D-printed PLA/Gel hybrid in liver tissue engineering: Effects of architecture on biological functions*. *Biotechnology and Bioengineering*, 2023. 120(3): 836-851.
- [152] Tümer, E.H. and H.Y. Erbil, *Extrusion-based 3D printing applications of PLA composites: a review*. *Coatings*, 2021. 11(4): 390.
- [153] Quiles-Carrillo, L., *et al.*, *Ductility and toughness improvement of injection-molded compostable pieces of polylactide by melt blending with poly (ϵ -caprolactone) and thermoplastic starch*. *Materials*, 2018. 11(11): 2138.
- [154] Su, S., *Prediction of the Miscibility of PBAT/PLA Blends*. *Polymers*, 2021. 13(14): 2339.
- [155] Ding, Y., *et al.*, *Compatibilization of immiscible PLA-based biodegradable polymer blends using amphiphilic di-block copolymers*. *European Polymer Journal*, 2019. 118: 45-52.
- [156] Martinez Villadiego, K., *et al.*, *Thermoplastic starch (TPS)/polylactic acid (PLA) blending methodologies: a review*. *Journal of Polymers and the Environment*, 2022. 30: 75-91.
- [157] Aversa, C., *et al.*, *Compatibilization strategies and analysis of morphological features of poly (butylene adipate-co-terephthalate)(PBAT)/poly (lactic acid) PLA blends: A state-of-art review*. *European Polymer Journal*, 2022. 173: 111304.
- [158] Arrieta, M.P., *et al.*, *On the use of PLA-PHB blends for sustainable food packaging applications*. *Materials*, 2017. 10(9): 1008.
- [159] Claro, P., *et al.*, *Biodegradable blends with potential use in packaging: A comparison of PLA/chitosan and PLA/cellulose acetate films*. *Journal of Polymers and the Environment*, 2016. 24: 363-371.
- [160] Ho, C.-H., *et al.*, *Synthesis and characterization of TPO-PLA copolymer and its behavior as compatibilizer for PLA/TPO blends*. *Polymer*, 2008. 49(18): 3902-3910.

- [161] Wang, Y., *et al.*, *Synthesis of a novel reactive compatibilizer with large surface area and the application in monomer casting nylon/polyethylene–octene elastomer blends*. *Journal of Materials Science*, 2016. 51: 9589-9601.
- [162] Wang, Y. and M.A. Hillmyer, *Polyethylene-poly (L-lactide) diblock copolymers: synthesis and compatibilization of poly (L-lactide)/polyethylene blends*. *Journal of Polymer Science Part A: Polymer Chemistry*, 2001. 39(16): 2755-2766.
- [163] Srivastava, A., S. Shukla, and R. Kumar, *Applications and characteristics properties of polymeric hydrogel*. *Journal of Chemistry and Chemical Sciences*, 2016. 6(2): 166-181.
- [164] Chieng, B.W., *et al.*, *Plasticized poly (lactic acid) with low molecular weight poly (ethylene glycol): Mechanical, thermal, and morphology properties*. *Journal of Applied Polymer Science*, 2013. 130(6): 4576-4580.
- [165] Barandiaran, A., *et al.*, *Esters of Cinnamic Acid as Green Plasticizers for Polylactide Formulations with Improved Ductility*. *Macromolecular Materials and Engineering*, 2023. 308(8): 1-12.
- [166] Ljungberg, N. and B. Wesslen, *The effects of plasticizers on the dynamic mechanical and thermal properties of poly (lactic acid)*. *Journal of Applied Polymer Science*, 2002. 86(5): 1227-1234.
- [167] Ravindra, R., K.R. Krovvidi, and A. Khan, *Solubility parameter of chitin and chitosan*. *Carbohydrate polymers*, 1998. 36(2-3): 121-127.
- [168] Xinhua, Z., *et al.*, *The newest research progresses of polyester plasticizer for PVC*. *Journal of Petrochemical Universities*, 2016. 29(4): 13.
- [169] Singh, S., M.L. Maspoch, and K. Oksman, *Crystallization of triethyl-citrate-plasticized poly (lactic acid) induced by chitin nanocrystals*. *Journal of Applied Polymer Science*, 2019. 136(36): 47936.
- [170] Ren, J., *et al.*, *Development of biomaterials based on plasticized polylactic acid and tea polyphenols for active-packaging application*. *International Journal of Biological Macromolecules*, 2022. 217: 814-823.
- [171] Carlier, E., *et al.*, *Investigation of the parameters used in fused deposition modeling of poly (lactic acid) to optimize 3D printing sessions*. *International journal of pharmaceutics*, 2019. 565: 367-377.

- [172] Li, H. and M.A. Huneault, *Comparison of sorbitol and glycerol as plasticizers for thermoplastic starch in TPS/PLA blends*. Journal of Applied Polymer Science, 2011. 119(4): 2439-2448.
- [173] Johar, M., et al., *Enhancement of mechanical, rheological and antifungal properties of polylactic acid/ethylene-vinyl-acetate blend by triacetin plasticizer*. Journal of Polymer Research, 2023. 30(7): 259.
- [174] Petchwattana, N., J. Sanetuntikul, and B. Narupai, *Plasticization of biodegradable poly (lactic acid) by different triglyceride molecular sizes: A comparative study with glycerol*. Journal of Polymers and the Environment, 2018. 26: 1160-1168.
- [175] Balart, J., et al., *Processing and characterization of high environmental efficiency composites based on PLA and hazelnut shell flour (HSF) with biobased plasticizers derived from epoxidized linseed oil (ELO)*. Composites Part B: Engineering, 2016. 86: 168-177.
- [176] Xie, D., et al., *Rheological, thermal, and degradation properties of PLA/PPG blends*. Materials, 2019. 12(21): 1-12.
- [177] Zafar, R., W. Lee, and S.-Y. Kwak, *A facile strategy for enhancing tensile toughness of poly (lactic acid)(PLA) by blending of a cellulose bio-toughener bearing a highly branched polycaprolactone*. European Polymer Journal, 2022. 175: 111376.
- [178] Ozkoc, G. and S. Kemaloglu, *Morphology, biodegradability, mechanical, and thermal properties of nanocomposite films based on PLA and plasticized PLA*. Journal of Applied Polymer Science, 2009. 114(4): 2481-2487.
- [179] Martino, V.P., A. Jiménez, and R.A. Ruseckaite, *Processing and characterization of poly (lactic acid) films plasticized with commercial adipates*. Journal of Applied Polymer Science, 2009. 112(4): 2010-2018.
- [180] Mangeon, C., et al., *Natural terpenes used as plasticizers for poly (3-hydroxybutyrate)*. ACS Sustainable Chemistry & Engineering, 2018. 6(12): 16160-16168.
- [181] Sachdev, D., et al., *Structural and optical investigation of highly fluorescent tartaric acid derived from the tamarind pulp*. Materials Chemistry and Physics, 2023. 296: 127294.
- [182] Burbidge, C.A., et al., *Biosynthesis and cellular functions of tartaric acid in grapevines*. Frontiers in plant science, 2021. 12: 309.
- [183] Zawada, K., et al., *Esters of tartaric acid, a new class of potential "double green" plasticizers*. ACS Sustainable Chemistry & Engineering, 2017. 5(7): 5999-6007.

- [184] Duque-Acevedo, M., et al., *The management of agricultural waste biomass in the framework of circular economy and bioeconomy: An opportunity for greenhouse agriculture in Southeast Spain*. *Agronomy*, 2020. 10(4): 489.
- [185] Tsegaye, B., S. Jaiswal, and A.K. Jaiswal, *Food waste biorefinery: pathway towards circular bioeconomy*. *Foods*, 2021. 10(6): 1174.
- [186] De la Torre, I., et al., *Utilisation/upgrading of orange peel waste from a biological biorefinery perspective*. *Applied microbiology and biotechnology*, 2019. 103: 5975-5991.
- [187] Pereira, B.S., et al., *Brazilian banana, guava, and orange fruit and waste production as a potential biorefinery feedstock*. *Journal of Material Cycles and Waste Management*, 2022. 24(6): 2126-2140.
- [188] Arun, K., et al., *Integrated biorefinery development for pomegranate peel: Prospects for the production of fuel, chemicals and bioactive molecules*. *Bioresource Technology*, 2022. 362: 127833.
- [189] Bello, F., *Development of multi-step biorefinery schemes for the production of nanocellulose and high value-added bioproducts from mango seed*. 2022.
- [190] Sillero, L., et al., *Life Cycle Assessment of various biorefinery approaches for the valorisation of almond shells*. *Sustainable Production and Consumption*, 2021. 28: 749-759.
- [191] Laaziz, S.A., et al., *Bio-composites based on polylactic acid and argan nut shell: Production and properties*. *International journal of biological macromolecules*, 2017. 104: 30-42.
- [192] Jovanović, A., et al., *Polyphenols extraction from plant sources*. *Lekovite sirovine*, 2017. (37): 45-49.
- [193] Ng, H.-M., et al., *Extraction of cellulose nanocrystals from plant sources for application as reinforcing agent in polymers*. *Composites Part B: Engineering*, 2015. 75: 176-200.
- [194] Huang, L.-Z., et al., *Recent developments and applications of hemicellulose from wheat straw: A review*. *Frontiers in Bioengineering and Biotechnology*, 2021. 9(1): 690773.
- [195] Ndaba, B., et al., *Influence of extraction methods on antimicrobial activities of lignin-based materials: A review*. *Sustainable Chemistry and Pharmacy*, 2020. 18: 100342.

- [196] Kassab, Z., et al., *Tomato plant residue as new renewable source for cellulose production: extraction of cellulose nanocrystals with different surface functionalities*. *Cellulose*, 2020. 27: 4287-4303.
- [197] Belkheiri, A., et al., *Extraction, characterization, and applications of pectins from plant by-products*. *Applied Sciences*, 2021. 11(14): 6596.
- [198] Roopa, G.S. and V. Kasiviswanatham, *Extraction of tartaric acid from tamarind pulp and analysis of the acid composition in leaves*. *International Journal of Students' Research in Technology*, 2013. 1(5): 478-488.
- [199] Sachdev, D., et al., *Structural and optical investigation of highly fluorescent tartaric acid derived from the tamarind pulp*. *Materials Chemistry and Physics*, 2023. 296: 127294.
- [200] Kringel, D.H., et al., *Methods for the extraction of roots, tubers, pulses, pseudocereals, and other unconventional starches sources: a review*. *Starch-Stärke*, 2020. 72(11-12): 1900234.
- [201] Fetyan, N.A., et al., *Bioethanol production from defatted biomass of *Nannochloropsis oculata* microalgae grown under mixotrophic conditions*. *Environmental Science and Pollution Research*, 2022. 29: 2588-2597.
- [202] Sergi, R., D. Bellucci, and V. Cannillo, *A review of bioactive glass/natural polymer composites: State of the art*. *Materials*, 2020. 13(23): 5560.
- [203] Brito, J., et al., *Integrating antioxidant functionality into polymer materials: fundamentals, strategies, and applications*. *ACS Applied Materials & Interfaces*, 2021. 13(35): 41372-41395.
- [204] Terroba-Delicado, E., et al., *Valorization of liquor waste derived spent coffee grains for the development of injection-molded polylactide pieces of interest as disposable food packaging and serving materials*. *Foods*, 2022. 11(8): 1162.
- [205] Quiles-Carrillo, L., et al., *Compatibilization of highly sustainable polylactide/almond shell flour composites by reactive extrusion with maleinized linseed oil*. *Industrial Crops and Products*, 2018. 111(1): 878-888.
- [206] Ivorra-Martinez, J., et al., *Development and characterization of sustainable composites from bacterial polyester poly (3-hydroxybutyrate-co-3-hydroxyhexanoate) and almond shell flour by reactive extrusion with oligomers of lactic acid*. *Polymers*, 2020. 12(5): 1097.

- [207] Pedreiro, S., *et al.*, *Bioactive edible films and coatings based in gums and starch: Phenolic enrichment and foods application*. *Coatings*, 2021. 11(11): 1393.
- [208] Kaur, B., *et al.*, *Recent trends in the management of mango by-products*. *Food Reviews International*, 2022. 39(7): 4159-4179.
- [209] Wall-Medrano, A., *et al.*, *Health benefits of mango by-products*. *Food wastes and by-products: Nutraceutical and health potential*. 2020. 159-191.
- [210] Tariq, A., *et al.*, *Extraction of dietary fiber and polyphenols from mango peel and its therapeutic potential to improve gut health*. *Food Bioscience*, 2023. 53: 102669.
- [211] Kiokias, S., C. Proestos, and T. Varzakas, *A review of the structure, biosynthesis, absorption of carotenoids-analysis and properties of their common natural extracts*. *Current Research in Nutrition and Food Science Journal*, 2016. 4(Special Issue Carotenoids March 2016): 25-37.
- [212] Kaur, B., P.S. Panesar, and A. Thakur, *Extraction and evaluation of structural and physicochemical properties of dietary fiber concentrate from mango peels by using green approach*. *Biomass Conversion and Biorefinery*, 2021: 1-10.
- [213] Matharu, A.S., *et al.*, *Acid-free microwave-assisted hydrothermal extraction of pectin and porous cellulose from mango peel waste-towards a zero waste mango biorefinery*. *Green Chemistry*, 2016. 18(19): 5280-5287.
- [214] Laxmeshwar, S.S., *et al.*, *Preparation and properties of biodegradable film composites using modified cellulose fibre-reinforced with PVA*. *International Scholarly Research Notices*, 2012. 2012(2): 154314.
- [215] Silva, A.P.M., *et al.*, *Mango kernel starch films as affected by starch nanocrystals and cellulose nanocrystals*. *Carbohydrate polymers*, 2019. 211: 209-216.
- [216] Yingkamhaeng, N. and P. Sukyai. *The potential of mango peel utilization for cellulose extraction by hydrothermal pretreatment*. in *Annual Meeting of the Thai Society for Bio-technology and International Conference*. 2014. Chiang Rai Thailand.
- [217] Henrique, M.A., *et al.*, *Valorization of an agro-industrial waste, mango seed, by the extraction and characterization of its cellulose nanocrystals*. *Journal of environmental management*, 2013. 121: 202-209.
- [218] Ferreira, S., *et al.*, *Physicochemical, morphological and antioxidant properties of spray-dried mango kernel starch*. *Journal of Agriculture and Food Research*, 2019. 1: 100012.

- [219] Patiño-Rodríguez, O., *et al.*, *Unripe mango kernel starch: Partial characterization*. *Food Hydrocolloids*, 2020. 101: 105512.
- [220] Gomez-Caturla, J., *et al.*, *Biopolypropylene-Based Wood Plastic Composites Reinforced with Mango Peel Flour and Compatibilized with an Environmentally Friendly Copolymer from Itaconic Acid*. *ACS Applied Polymer Materials*, 2022. 4(6): 4398-4410.
- [221] Haq, S. and R. Srivastava, *Wood polypropylene (PP) composites manufactured by mango wood waste with virgin or recycled PP: mechanical, morphology, melt flow index and crystalline behaviour*. *Journal of Polymers and the Environment*, 2017. 25: 640-648.
- [222] Gomez-Caturla, J., *et al.*, *Manufacturing and characterization of highly environmentally-friendly composites with polylactide matrix and mango kernel seed flour*. *Express Polymer Letters*, 2023. 17(3): 334-351.
- [223] Kim, I.J., D. Jeong, and S.R. Kim, *Upstream processes of citrus fruit waste biorefinery for complete valorization*. *Bioresource Technology*, 2022. 362: 127776.
- [224] Zema, D., *et al.*, *Valorisation of citrus processing waste: A review*. *Waste management*, 2018. 80: 252-273.
- [225] Yadav, V., *et al.*, *Integrated biorefinery approach to valorize citrus waste: A sustainable solution for resource recovery and environmental management*. *Chemosphere*, 2022. 293: 133459.
- [226] Jeong, D., *et al.*, *Recent advances in the biological valorization of citrus peel waste into fuels and chemicals*. *Bioresource Technology*, 2021. 323: 124603.
- [227] Suri, S., A. Singh, and P.K. Nema, *Recent advances in valorization of citrus fruits processing waste: A way forward towards environmental sustainability*. *Food Science and Biotechnology*, 2021. 30: 1601-1626.
- [228] Gawkowska, D., J. Cybulska, and A. Zdunek, *Structure-related gelling of pectins and linking with other natural compounds: A review*. *Polymers*, 2018. 10(7): 762.
- [229] Luan, Y., *et al.*, *Accumulation of red apocarotenoid β -citraurin in peel of a spontaneous mutant of huyou (*Citrus changshanensis*) and the effects of storage temperature and ethylene application*. *Food chemistry*, 2020. 309: 125705.
- [230] Stoll, L., *et al.*, *Carotenoids extracts as natural colorants in poly (lactic acid) films*. *Journal of Applied Polymer Science*, 2018. 135(33).

- [231] Saini, R.K., *et al.*, *Bioactive compounds of citrus fruits: A review of composition and health benefits of carotenoids, flavonoids, limonoids, and terpenes*. *Antioxidants*, 2022. 11(2): 239.
- [232] Smeriglio, A., *et al.*, *Antioxidant and cytoprotective activities of an ancient Mediterranean citrus (Citrus lumia Risso) albedo extract: Microscopic observations and polyphenol characterization*. *Food chemistry*, 2019. 279: 347-355.
- [233] Paul, D. and G. Das, *Bio-inspired synthesis of flavonoids incorporated CaCO₃: Influence on the phase, morphology and mechanical strength of the composites*. *Colloids and Surfaces A: Physicochemical and Engineering Aspects*, 2022. 642: 128720.
- [234] Nagarajan, S., *et al.*, *Antioxidant activity of synthetic polymers of phenolic compounds*. *Polymers*, 2020. 12(8): 1646.
- [235] González-Mas, M.C., *et al.*, *Volatile compounds in citrus essential oils: A comprehensive review*. *Frontiers in plant science*, 2019. 10: 12.
- [236] Raspo, M.A., *et al.*, *Antioxidant and antimicrobial activities of citrus essential oils from Argentina and the United States*. *Food bioscience*, 2020. 36: 100651.
- [237] Rossi, R.C., *et al.*, *Assessment of compounds and cytotoxicity of Citrus deliciosa Tenore essential oils: From an underexploited by-product to a rich source of high-value bioactive compounds*. *Food bioscience*, 2020. 38: 100779.
- [238] Govindarasu, R., *et al.*, *Intensified extraction of geraniol from palmarosa leaves using diverse hydrotrope-assisted extraction techniques*. *Biomass Conversion and Biorefinery*, 2023: 1-14.
- [239] Alissandrakis, E., *et al.*, *Ultrasound-assisted extraction of volatile compounds from citrus flowers and citrus honey*. *Food chemistry*, 2003. 82(4): 575-582.
- [240] Temelli, F., *et al.*, *Supercritical carbon dioxide extraction of terpenes from orange essential oil*. 1988.
- [241] Noriega, P., *Terpenes in essential oils: Bioactivity and applications*. *Terpenes and Terpenoids – Recent Advances*. 2020.

II. OBJETIVOS

II.1. Objetivo general

El objetivo general de esta tesis doctoral es el de desarrollar nuevos materiales poliméricos con un gran potencial medioambiental mediante diferentes técnicas de procesado, como son la extrusión, la inyección, la producción de films por disolución o el *electrospinning*. Al mismo tiempo, se ha centrado en el reaprovechamiento de residuos de la industria del mango para obtener tanto polímeros (almidón), como aditivos para matrices poliméricas en forma de partículas lignocelulósicas. Todo esto siguiendo los principios de la biorrefinería y la economía circular. Para obtener estos materiales se han utilizado matrices poliméricas de origen renovable, como el ácido poliláctico (PLA), el biopolipropileno (BioPP) o el almidón, polímeros que pueden ser obtenidos a partir de fuentes vegetales. Se han utilizado aditivos provenientes de residuos de la industria del mango en combinación con otros aditivos respetuosos con el medio ambiente, como agentes compatibilizantes basados en ácido itacónico para mejorar la interacción entre la matriz y la carga, o plastificantes naturales para mejorar la ductilidad de las formulaciones desarrolladas. También se han centrado esfuerzos en emplear nuevos plastificantes basados en terpenoides, que pueden ser obtenidos de fuentes renovables, para solucionar los problemas de fragilidad del PLA y de mezclas de PLA con harina de piel de mandarina. En general, el objetivo final de esta tesis ha sido desarrollar materiales que sean completamente respetuosos con el medio ambiente y que ofrezcan la posibilidad de favorecer economías circulares, sin dejar de ser competitivos dentro de sectores como el del envase y el embalaje o el médico.

II.2. Objetivos parciales

Para cumplir el objetivo general de la tesis planteado al inicio de la misma, se especificaron una serie de objetivos parciales, divididos en dos grandes bloques, para poder realizar la consecución del objetivo final. Estos objetivos parciales se especifican a continuación, divididos en dos bloques de acuerdo al tipo de materiales empleados y a los aditivos utilizados:

Bloque 1: Desarrollo de polímeros respetuosos con el medio ambiente mediante el reaprovechamiento de residuos de mango

- Extracción de almidón a partir del hueso de mango y síntesis de nanofibras biodegradables de almidón mediante la técnica de *electrospinning* con aplicación

en el sector médico.

- Estudio de la compatibilidad, propiedades mecánicas, térmicas, termomecánicas, morfológicas y de comportamiento frente al agua de formulaciones de biopolipropileno con harina de piel de mango, utilizando un copolímero de ácido itacónico como agente compatibilizante para intentar mejorar la adhesión entre la matriz polimérica y la carga lignocelulósica de mango.
- Evaluación de la variación de las propiedades barrera y propiedades mecánicas de films de harina de kernel de mango con glicerol con la variación del tamaño de partícula de la harina de kernel de mango.
- Desarrollo de materiales compuestos de PLA con harina de kernel de mango y mejora de las propiedades dúctiles de las formulaciones desarrolladas mediante el uso de plastificantes como la triacetina y la tributirina.
- Desarrollo de materiales termoplásticos ricos en almidón por medio de técnicas de extrusión e inyección utilizando harina de kernel de mango y glicerol, sorbitol y urea como plastificantes.

Bloque 2: Materiales con alto potencial medioambiental basados en PLA y plastificantes de origen renovable

- Mejora de las propiedades dúctiles del PLA mediante el uso de un éster del ácido tartárico (Dietil-L-tartrato), un plastificante de origen natural.
- Desarrollo de materiales compuestos biodegradables basados en PLA y harina de piel de mandarina y mejora de sus propiedades mecánicas, térmicas, termomecánicas y de biodegradabilidad mediante la utilización de α -terpinil acetato, un terpenoide de origen renovable.
- Evaluación de las propiedades mecánicas, térmicas, morfológicas, termomecánicas y de solubilidad de formulaciones de PLA con geranil acetato y linalil acetato, con el objetivo de mejorar ductilidad del PLA.
- Estudio del efecto de la longitud de cadena de ésteres de geraniol en las propiedades dúctiles de formulaciones plastificadas de PLA.

En la **Figura II.1** puede observarse una representación esquemática de los objetivos de la tesis.

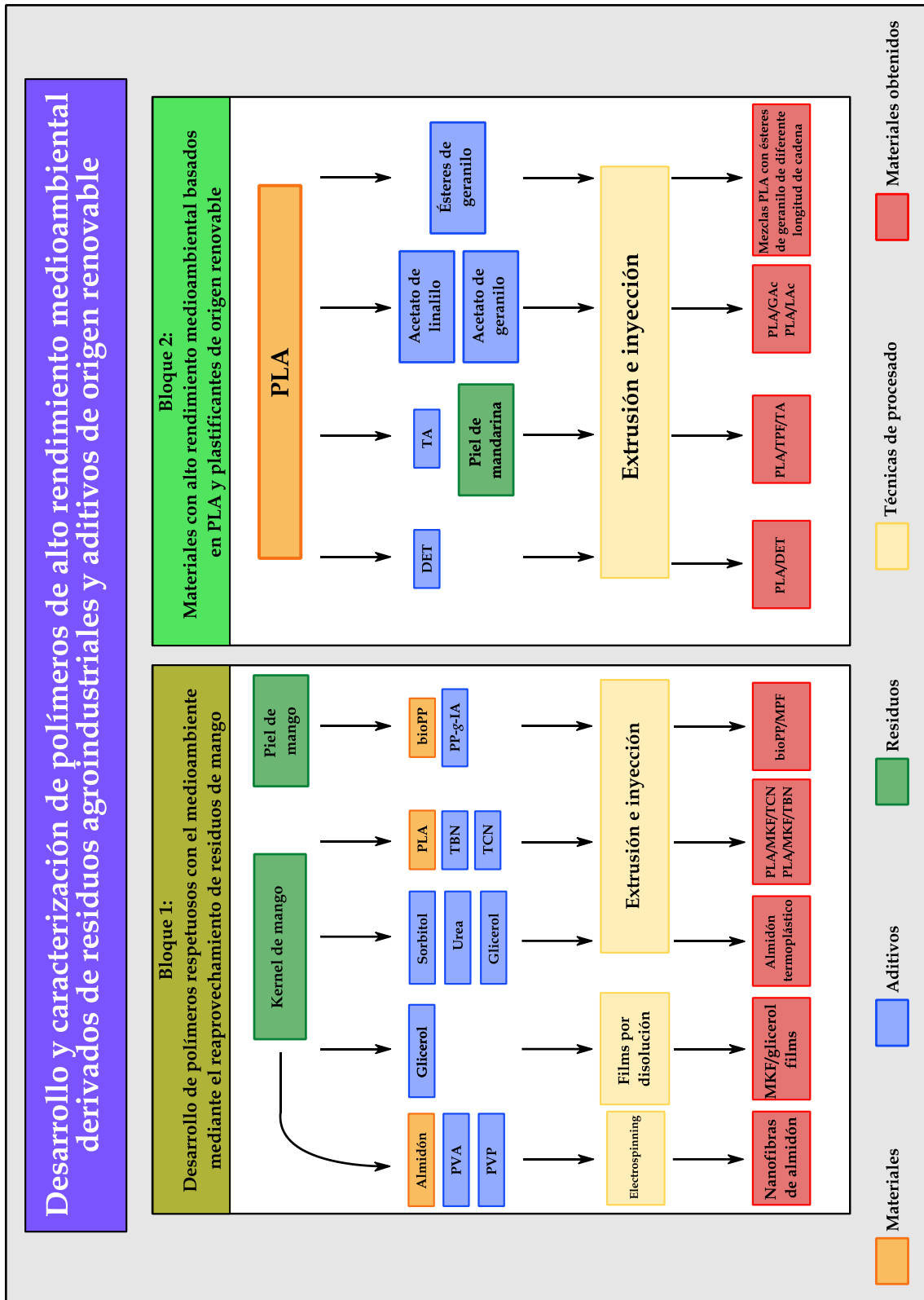


Figura II.1. Representación esquemática de los objetivos de la presente tesis.

III. RESULTS & DISCUSSION

This work reports on the development of several environmentally friendly materials especially using mango industry wastes and polylactic acid, whose aim is to promote circular economies and improve the intrinsic properties of the polymer matrices herein utilized.

All the results related to this extensive study have been organized in two well differentiated blocks related to the materials and additives used in each one of them. A total of 9 chapters are presented as a compendium of manuscripts in this thesis.

Section I: Development of environmentally friendly polymers by upgrading mango wastes.

This block is dedicated to all the studies focused on the biorefinery and reuse of mango industry wastes, such as peels and kernels, to extract and develop different polymeric materials. In this block, mango kernel starch has been used as a polymeric matrix, while mango kernel flour and mango kernel peel have been incorporated as fillers in biopolypropylene, thermoplastic starch and polylactic acid matrices. The mechanical, morphological, thermal, thermomechanical, water absorption, biodegradability and chemical properties of the formulations developed are analysed within the following chapters:

Chapter III.1.1.

Development and evaluation of novel nanofibers based on mango kernel starch obtained by electrospinning.

Chapter III.1.2.

Biopolypropylene-based wood plastic composites reinforced with mango peel flour and compatibilized with an environmentally friendly copolymer from itaconic acid.

Chapter III.1.3.

Improvement of the barrier and mechanical properties of environmentally friendly mango kernel flour/ glycerol films by varying the particle size of mango kernel flour.

Chapter III.1.4.

Manufacturing and characterization of high environmentally-friendly composites with polylactide matrix and mango kernel seed flour.

Chapter III.1.5.

Development of starch-rich thermoplastic polymers based on mango kernel flour and different plasticizers.

Section II: PLA-based environmentally friendly with the use of natural-derived plasticizers.

The second block of the thesis is centered in PLA as its main polymeric matrix. This section explores the use of new eco-friendly plasticizers, most of them terpenoids, in order to sort out the brittleness problems characteristic of PLA without compromising its environmental potential. Plasticizers such as diethyl-L-tartrate, linalyl acetate, geranyl acetate, geranyl formate or geranyl propionate, among others, have been used. Also, PLA-plasticized formulations have been combined with tangerine peel flour as a reinforcing filler in order to assess whether these terpenoids are able to improve the ductility of these mixtures.

Chapter III.2.1.

Improvement of poly(lactide) ductile properties by plasticization with biobased tartaric acid ester.

Chapter III.2.2.

Development of biodegradable PLA composites and tangerine peel flour with improved toughness containing a natural based terpenoid.

Chapter III.2.3.

Development and characterization of new environmentally friendly polylactide formulations with terpenoid-based plasticizers with improved ductility.

Chapter III.2.4.

Effect of the chain length of geraniol esters on the plasticization efficiency with poly(lactide).

Section I

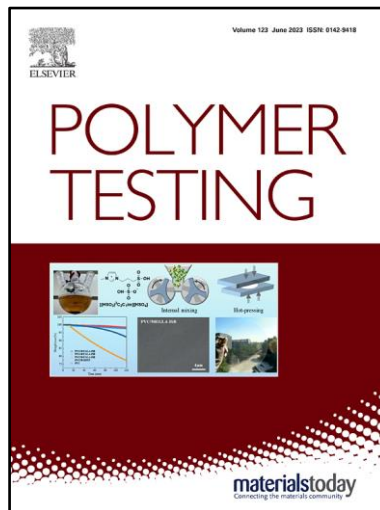
Development of environmentally friendly polymers by upgrading mango wastes

III.1.1. Development and evaluation of novel nanofibers based on mango kernel starch obtained by electrospinning

Jaume Gomez-Caturla^{1*}, Juan Ivorra-Martinez¹, Diego Lascano¹, Rafael Balart¹, Daniel Garcia-Garcia¹, Franco Dominici², Debora Puglia² and Luigi Torre²

¹ Technological Institute of Materials – ITM, Universitat Politècnica de València – UPV, Plaza Ferrándiz y Carbonell 1, 03801 Alcoy (Spain).

² Dipartimento di Ingegneria Civile ed Ambientale, University of Perugia, Udr INSTM, Strada di Pentima, 4 - 05100 Terni (TR) Italy.



Polymer Testing

2022, 106: 107462

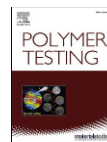
*Adapted from the original manuscript.



Contents lists available at ScienceDirect

Polymer Testing

journal homepage: www.elsevier.com/locate/polytest



Development and evaluation of novel nanofibers based on mango kernel starch obtained by electrospinning

Jaume Gomez-Caturla^{a,*}, Juan Ivorra-Martinez^a, Diego Lascano^a, Rafael Balart^a, Daniel García-García^a, Franco Dominici^b, Debora Puglia^b, Luigi Torre^b

^a *Technological Institute of Materials (ITM), Universitat Politècnica de València (UPV), Plaza Ferrnández y Carbonell 1, 03801, Alcoy, Spain*
^b *Dipartimento di Ingegneria Civile ed Ambientale, University of Perugia, UdR INSTM, Strada di Pentima, 4, 05100, Terni, TR, Italy*

ARTICLE INFO

Keywords:
 Mango kernel starch
 PVA
 PVP
 Electrospinning
 Nanofibers

ABSTRACT

This work reports on the development of fibers based on natural mango kernel starch (MKS) with diameters in the nanoscale by means of the electrospinning technique. MKS was extracted from mango kernels and two synthetic polymers, namely polyvinyl alcohol (PVA) and polyvinylpyrrolidone (PVP), were blended with MKS in order to improve its spinnability, obtaining MKS/PVA and MKS/PVP fibers with a 10 wt% of total polymer concentration. Several electrospinning conditions (voltage and flux) were tested in solutions of MKS concentrations ranging from 0 to 5 wt% for both group of fibers. The morphology of all the fibers was evaluated by field emission scanning electron microscopy (FESEM) and their topography was analysed by means of atomic force microscopy (AFM). MKS/PVA nanofibers were obtained with a diameter range from 0.146 to 0.315 μm , with a "smooth fiber concentration threshold" of 3 wt%, while MKS/PVP fibers with diameters from 0.080 to 0.339 μm were produced, but 5 wt% MKS concentration fibers were beaded fibers, as a result of an excess in starch concentration. Finally, the roughness of the optimal fibers showed quite a similar trend to that of fiber diameter, presenting roughnesses between 80 and 343 nm.

1. Introduction

In the last decade, nanomaterials have attracted great attention, as they have allowed to improve and modernize all sorts of industries, including food, medicine, pharmaceutical, cosmetics, electronics, energies, etc. [1–4]. Among all the nanostructures available in the field of nanomaterials, nanofibers are especially interesting due to their excellent mechanical performance, encapsulation efficiency, high surface area and ease of processability [5]. There are several methods to produce nanofibers, namely rotary spinning, self-assembly, electrospinning or wet spinning, which have been used to obtain fibers in the micro or nano scale [6]. In this context, electrospinning is the most common and effective methodology to fabricate nanofibers due to its simplicity and its ability to control the morphology of the fibers depending on the application they are destined for.

In this sense, the popularity of the electrospinning process has increased in recent years. The electrospinning technique makes use of electrostatic forces to produce electrically charged jets from viscoelastic

polymer solutions that upon drying, by the evaporation of the solvent [7, 8]. It is a process that allows to produce fibers in the submicron range, this feat would be rather difficult by using standard mechanical fiber-spinning techniques [9,10]. The properties of the electrospun nanofibers such as diameter and shape can be manipulated through the variation of the parameters of the electrospinning process. These fibers have great potential to be used in technological fields such as analytical chemistry, tissue engineering and drug delivery, among others [11–13]. This technique has proved to be especially useful in the fabrication of polymer scaffolds, and it has explored several avenues regarding the use of both synthetic and natural polymers. Particularly, natural polymers are of great interest as a result of their intrinsic properties in terms of biocompatibility, biodegradability, non-toxicity and efficient bioactivity responses towards several animal models [14], which makes them very attractive for biomedicine. These polymers are generally derived from animal and plant sources [15]. Polymers such as starch, xylan or cellulose [16] are plant-derived polymers, while chitin/chitosan, collagen or hyaluronan are animal-derived polymers [17]. Lately, the use of starch

* Corresponding author.

E-mail addresses: jaugoca@epsa.upv.es (J. Gomez-Caturla), juaiumar@doctor.upv.es (J. Ivorra-Martinez), dieras@epsa.upv.es (D. Lascano), rbalart@mcm.upv.es (R. Balart), dagarga4@epsa.upv.es (D. García-García), franco.dominici@unipg.it (F. Dominici), debora.puglia@unipg.it (D. Puglia), luigi.torre@unipg.it (L. Torre).

<https://doi.org/10.1016/j.polymer.2021.107462>

Received 7 November 2021; Received in revised form 23 November 2021; Accepted 26 December 2021

Available online 27 December 2021

0142-9418/© 2022 The Authors.

Published by Elsevier Ltd.

This is an open access article under the CC BY-NC-ND license

(<http://creativecommons.org/licenses/by-nc-nd/4.0/>).

Development and evaluation of novel nanofibers based on mango kernel starch obtained by electrospinning

Abstract

This work reports on the development of fibers based on natural mango kernel starch (MKS) with diameters in the nanoscale by means of the electrospinning technique. MKS was extracted from mango kernels and two synthetic polymers, namely polyvinyl alcohol (PVA) and polyvinylpyrrolidone (PVP), were blended with MKS in order to improve its spinnability, obtaining MKS/PVA and MKS/PVP fibers with a 10 wt.% of total polymer concentration. Several electrospinning conditions (voltage and flux) were tested in solutions of MKS concentrations ranging from 0 to 5 wt.% for both group of fibers. The morphology of all the fibers was evaluated by field emission scanning electron microscopy (FESEM) and their topography was analysed by means of atomic force microscopy (AFM). MKS/PVA nanofibers were obtained with a diameter range from 0.146 to 0.315 μm , with a “smooth fiber concentration threshold” of 3 wt.%, while MKS/PVP, fibers with diameters from 0.080 to 0.339 μm were produced, but 5 wt.% MKS concentration fibers were beaded fibers, as a result of an excess in starch concentration. Finally, the roughness of the optimal fibers showed quite a similar trend to that of fiber diameter, presenting roughness between 80 and 343 nm.

Keywords: Mango kernel starch, PVA, PVP, electrospinning, nanofibers.

INTRODUCTION

In the last decade, nanomaterials have attracted great attention, as they have allowed to improve and modernize all sorts of industries, including food, medicine, pharmaceutical, cosmetics, electronics, energies, etc. [1-4]. Among all the nanostructures available in the field of nanomaterials, nanofibers are especially interesting due to their excellent mechanical performance, encapsulation efficiency, high surface area and ease of processability [5]. There are several methods to produce nanofibers, namely rotary spinning, self-assembly, electrospinning or wet spinning, which have been used to obtain fibers in the micro or nano scale [6]. In this context, electrospinning is the most common and effective methodology to fabricate nanofibers due to its simplicity and its ability to control the morphology of the fibers depending on the application they are destined for.

In this sense, the popularity of the electrospinning process has increased in recent years. The electrospinning technique makes use of electrostatic forces to produce electrically charged jets from viscoelastic polymer solutions that upon drying, by the evaporation of the solvent [7, 8]. It is a process that allows to produce fibers in the submicron range, this feat would be rather difficult by using standard mechanical fiber-spinning techniques [9, 10]. The properties of the electrospun nanofibers such as diameter and shape can be manipulated through the variation of the parameters of the electrospinning process. These fibers have great potential to be used in technological fields such as analytical chemistry, tissue engineering and drug delivery, among others [11-13]. This technique has proved to be especially useful in the fabrication of polymer scaffolds, and it has explored several avenues regarding the use of both synthetic and natural polymers. Particularly, natural polymers are of great interest as a result of their intrinsic properties in terms of biocompatibility, biodegradability, non-toxicity and efficient bioactivity responses towards several animal models [14], which makes them very attractive for biomedicine. These polymers are generally derived from animal and plant sources [15]. Polymers such as starch, xylan or cellulose [16] are plant-derived polymers, while chitin/chitosan, collagen or hyaluronan are animal-derived polymers [17]. Lately, the use of starch in electrospinning has increased, especially in combination with synthetic polymers.

Starch is one of the most important natural polymers, being the second largest source of biomass just after cellulose [17]. It is a homo-polysaccharide which is compounded of glucose molecules linked by glycosidic bonds [18], whose main constituents are amylose and amylopectin. This polymer has been widely used in lots of

industries thanks to its renewability, biodegradability, biocompatibility and its low cost [19]. It can be obtained from several vegetal sources, such as potato [20], rice [21], maize [22], pea [23] and other several fruits and vegetables like cassava [24].

Among all tropical fruits, mango is one of the most popular [25]. The processing of this fruit generates 25-40% of waste [26], considering peels and kernels, which stands for a great opportunity of reutilizing them under a circular economy concept. Mango kernels from different cultivars have been reported to possess a 74-75% content in polysaccharides, being 60% starch, 9-13% fat content, 6-9% proteins and 2-3% ash [27]. This makes mango kernel the optimal source from which starch can be extracted. Mango kernel starch (MKS) has been reported to present amylose contents between 15-30 wt.% [28].

In spite of their great advantages, some of the main drawbacks of natural polymers are their poor solubility, poor tensile strength and high surface tension [29, 30], which makes starch a poor electrospun fiber forming agent, being its fibers brittle and water-sensitive [17, 31]. In order to overcome this problem, there are two main available paths. On the one hand, modifying chemically and physically native starch by reactions like crosslinking or substitutions with reporter molecules and biomolecules, which result in pre-gelatinization [32]. On the other hand, blending starch with linear-chain synthetic polymers is another approach that can improve the spinnability of the solutions [17]. Some of the polymers that have been explored in combination with starch are poly(caprolactone) [33], poly(ethylene oxide) [34], poly(lactic acid) [35], poly(lactide-co-glycolide) [36] or poly(vinyl alcohol) [37].

Polyvinyl alcohol (PVA) is a hydrophilic semi-crystalline synthetic polymer which has great application in the fabrication of fibers for food industry [23, 38] and biomedical issues such as tissue engineering or drug delivery due to its chemical and thermal stability, biocompatibility and hydrophilicity [39]. Furthermore, it presents great processability, nontoxicity and water-solubility, providing it with excellent spinnability, which is perfect for enhancing the poor spinnability of natural polymers like starch. Milasius *et al.* [40] investigated the production of composite fibers made of potato starch and PVA by electrospinning using water and ethanol as solvents. Woranuch *et al.* [41] studied the synthesis of rice starch/PVA nanofibers by electrospinning in alkaline solution conditions, obtaining very thin fibers of diameters between 36-151 nm.

Polyvinylpyrrolidone (PVP) is another synthetic polymer that has been gaining importance over the years in the production of nanofibers. PVP possesses

amphiphilicity, thanks to the polarity of its lactam group, making it hydrophilic, and the chemical nature of its non-polar methylene moiety, providing it with lipophilicity [42]. This polymer has found utility in several “biocompatible” applications, such as several drug delivery systems, as a result of its solubility in water and different organic solvents, wide availability, chemical stability, nontoxicity and biocompatibility [43]. PVP has also received great attention from the food, cosmetic and textile industries [44]. Dai *et al.* [45] blended PVP with emodin, an extract of polygonum cuspidate, a medicinal plant, to make drug carrier nanofibers by electrospinning and use them as a novel drug delivery system.

The aim of this study is to produce totally biocompatible nanofibers with great natural content, based on starch extracted from mango kernel coming from wastes of the mango industry. These fibers will be produced by electrospinning. Interestingly, there has not been any research study regarding the use of mango kernel starch (MKS) for electrospinning of nanofibers. Considering the low spinnability of MKS, two synthetic polymers will be used to produce blend solutions, namely PVA and PVP. On the one hand, different solutions of MKS/PVA, with distilled water as a solvent in order to make them as natural as possible, varying the concentration of starch from 0 to 5 wt.%, will be electrospun under several electrospinning conditions. On the other hand, another set of solutions of MKS/PVP, dissolved in methoxyethanol due to the ineffectivity of distilled water tested in preliminary studies, with concentrations of starch ranging from 0 to 5 wt.% will also be electrospun under varying electrospinning conditions. The morphology and diameter of the fibers has been characterized by field emission scanning electron microscopy (FESEM) and atomic force microscopy (AFM). This completely biocompatible nanofibers could prove to be especially useful for drug delivery applications and food packaging [46], with the possibility of reconducting mango wastes into the same industry that produced them (circular economy).

MATERIALS AND METHODS

Materials

Mangoes from the osteen variety were purchased from the local market in Alcoy, Spain. The fruits were chosen for absence of mechanical damage or any kind of infection.

Polyvinyl alcohol was provided by Sekisui Specialty Chemicals Europe, S.L. (Product Code: Selvol E325 L-0000003310), Polyvinylpyrrolidone (PVP) was also provided by Sigma-Aldrich with an average M_w of 1300000 (Product Code: 1003139835).

Finally, 2-Methoxyethanol ReagentPlus was also purchased from Sigma Aldrich (Product Code: 185469).

Mango kernel starch isolation

Mango kernel starch was extracted following the modified method of Nawab *et al.* [47]. Mango kernels were first decorticated and cut into small pieces (of about 1 cm³). The kernels were then immersed into a sodium metabisulfite 0.16 wt.% solution (kernel: solution weight ratio, 1:2) for 48 h to avoid browning of the kernels. Then the kernels were washed with distilled water using a 70 µm mesh screen until the filtrate reached neutral pH (7). After that, the kernels were ground in distilled water with an homogenizer (Daihan Scientific, model HG-15A with direct controller, Corea) for 5 minutes at 5000 rpm. The resultant slurry was then screened through a 100 µm mesh sieve followed by a 70 µm mesh sieve and was decanted for 12 h in a refrigerated environment (4 °C) to avoid enzymatic or fermentative processes. The supernatant was discarded and the starch was dried at 45 °C for 2 hours, then the brownish layer was eliminated and the white layer was dried at 45 °C for 22 hours. Thereafter, the white layer was resuspended in distilled water and centrifuged at 4500 rpm for 10 minutes, this process was repeated until the precipitate had the typical colour of starch. Finally, the extracted starch was dried at 45 °C for 24 h and then pulverized. The average starch extraction yield in relation to the weight of dried mango kernels was $8.12 \pm 2.86\%$.

The morphology of the extracted mango kernel starch was analysed by means of scanning electron microscopy (SEM). **Figure III.1.1.1** gathers the morphology of the MKS particles at 1000× magnification and a histogram of the length of the particles. MKS presents the typical morphology of starch, in form of smooth, spherical and ellipsoidal granules with lengths between 8–26 µm (average length: 15 µm) and diameters between 6 and 16 µm (average diameter: 11 µm). The morphology herein observed is very similar to most of the starches observed by Jane *et al.* [48], who studied the morphology of 54 different starches from several plant materials, namely potato, lotus root, arrow root, loly bulb, ginger, wheat and yucca, among others.

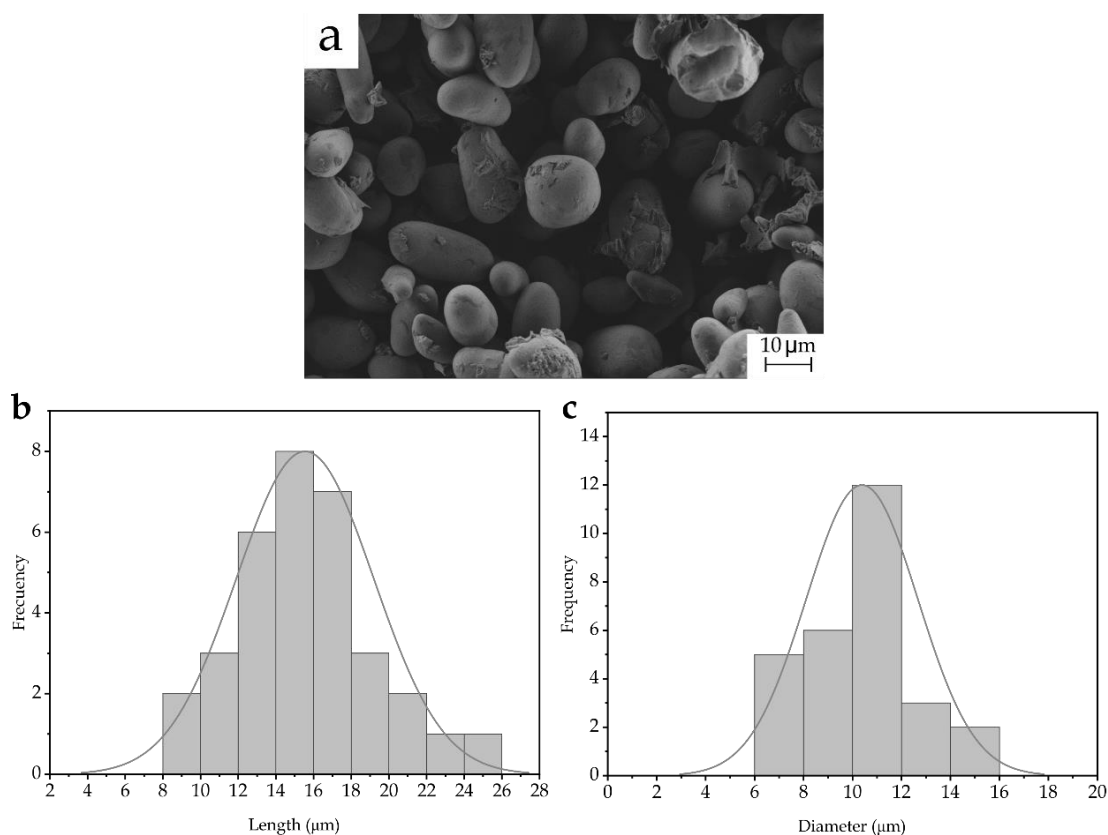


Figure III.1.1.1. Morphology of the mango kernel starch (MKS): a) FESEM image at 1000× magnification of the mango kernel starch particles; b) Histogram of the length of the MKS particles; c) Histogram of the diameter of the MKS particles.

Solution preparation method

Starch/PVA fibers

In the case of starch/PVA fibers, PVA was dissolved in hot distilled water at 95 °C and stirred for about 15 min. Then it was cooled at 65 °C and the starch was added to the solution, stirring it for about 30 more min. Once starch and PVA were correctly dissolved, the solution was cooled to room temperature and ready to use in the electrospinning process.

Starch/PVP fibers

For the starch/PVP fibers, methoxyethanol was used as the solvent [49]. PVP and starch were dissolved in methoxyethanol under constant stirring for about 40 minutes according to the established compositions. Then the solution was prepared for the electrospinning process.

Electrospinning process

The electrospinning process was carried out using a Fluidnatek LE-50 benchtop line with a variable high-voltage 0-35 kV power supply. The system was equipped with a motorized injector able to scan towards a metallic collector (20×20 cm²) that allows to obtain an homogeneous electrospun deposition. The corresponding solution (starch/PVA or starch/PVP) was first placed into a 3 mL syringe, connected by polytetrafluoroethylene (PTFE) tubes to a stainless-steel needle of 0.7 mm of diameter. The needle tip was connected to the positive terminal of the power supply, while the metal collector was connected to the negative one. A piece of aluminum foil was placed on the collector and the solution was electrospun for about 5-10 minutes under a steady flow rate in the range 0.06 - 0.2 mL/h, depending on the sample, using the motorized injector. The distance between the needle tip and the collector was 15 cm (based on preliminary tests), and the voltage was varied for each sample depending on its properties. Pure PVA and PVP solutions were also electrospun under the same conditions that have been described above. The process was conducted at 25 °C and at 40% relative humidity (RH). All the solutions prepared for electrospinning were fixed to present a 10 wt.% composition of polymer, either natural, synthetic or in combination of both of them according to the study carried out by Liu *et al.* [50].

Preliminary studies

Due to the fact that mango kernel starch had never been studied in the electrospinning field, some preliminary studies were carried out before defining the definitive experimental of this work, where different compositions, voltages, distances and solvents were tested. In order to justify the selection of the conditions in **Table III.1.1.2** and **Table III.1.1.3**, this preliminary research is presented here. **Table III.1.1.1** gathers all the electrospun nanofibers in this study, while **Figure III.1.1.2** shows their FESEM morphologies at 1000× magnification.

Samples P1, P2 and P3 showed excellent fiber formation while P4 presented very poor fiber formation, which is ascribed to an excessive distance between the collector and the needle (18 cm). This first samples demonstrate that it is possible to obtain fibers successfully at 2 wt.% starch combined with 8 wt.% PVA and water as solvent.

On the other hand, P5, P6 and P7 did not gave successful electrospinning results, obtaining particles rather than fibers (electrospraying) [51]. This was ascribed probably to an excessive proportion of starch in the samples (8 wt.%), making the blends too fluid to be electrospun. The solvent was changed to a mixture of 50% water/50% ethanol, but

it did not make any positive effect. Similarly, samples P8, P9 and P10 were tested in different conditions for 10 wt.% starch solutions (without any synthetic polymer), but the obtained results were not evaluable.

Finally, samples of 10 wt.% PVP solutions were tested (P11, P12 and P13), in order to know if it would be possible to electrospun MKS/PVP fibers with water as solvent. The morphologies obtained indicate the presence of highly beaded fibers, which are not optimal for fiber applications and are considered “defective” [52]. 2 wt.% starch and 8 wt.% PVP were tested in sample P14, obtaining the same results as with pure PVP fibers.

From this study it can be concluded that the proportion of starch in the blend must not be excessive (below 8 wt.%) to obtain smooth fibers, that 15 cm of D seems to be the optimal parameter in this experimental setup and that the optimal voltage for MKS/PVA fibers in water seems to be between 25 and 30 kV.

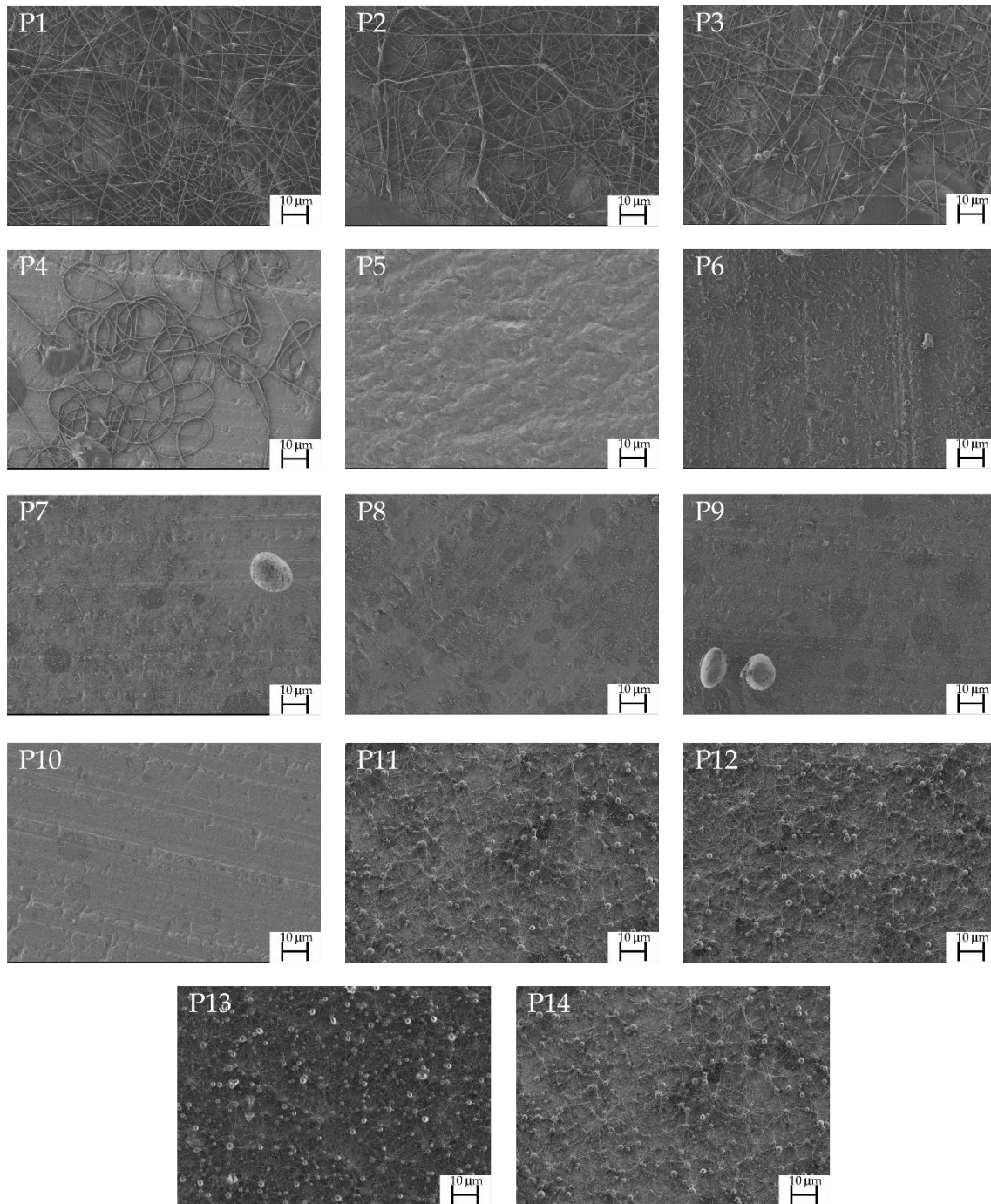


Figure III.1.1.2. FESEM images at 1000 \times magnification of all the fibers developed during preliminary studies specified in Table III.1.1.3.

Table III.1.1.1. Summary of compositions, experiment conditions and evaluation of the electrospun nanofibers preliminary studies according to the composition of the fibers, voltage (V), distance between the injector and the collector (D) and flux (F).

Sample	Starch (wt.%)	PVA (wt.%)	PVP (wt.%)	Solvent	V (kV)	D (cm)	F (mL/h)	Fiber evaluation
P1	2	8	0	Water	25	15	0.2	Smooth fibers
P2	2	8	0	Water	27	15	0.15	Smooth fibers
P3	2	8	0	Water	30	15	0.15	Smooth fibers
P4	2	8	0	Water	30	18	0.15	Poor fibers
P5	8	2	0	Water/ethanol*	20	15	0.45	-
P6	8	2	0	Water/ethanol*	20	18	0.75	Particles
P7	8	2	0	Water/ethanol*	25	15	0.35	Particles
P8	10	0	0	Water/ethanol*	18	15	0.55	Particles
P9	10	0	0	Water/ethanol*	20	18	0.75	Particles
P10	10	0	0	Water/ethanol*	23	13	0.45	-
P11	0	0	10	Water	20	15	0.15	Beaded fibers
P12	0	0	10	Water	24	15	0.15	Beaded fibers
P13	0	0	10	Water	29	15	0.15	Beaded fibers
P14	2	0	8	Water	30	15	0.05	Beaded fibers

*(50%/50%)

Final conditions

Once the preliminary studies were carried out, the final conditions were chosen. **Table III.1.1.2** gathers the compositions and the electrospinning conditions of all the MKS/PVA based nanofibers, while **Table III.1.1.3** gathers all the compositions and electrospinning conditions for the MKS/PVP based nanofibers.

Table III.1.1.2. Summary of compositions and experiment conditions of the electrospun nanofibers according to the weight content (wt.%) of mango kernel starch (MKS) and PVA (distilled water as solvent), voltage (V), distance between the injector and the collector (D) and flux (F).

Sample	Starch (wt.%)	PVA (wt.%)	V (kV)	F (mL/h)
1	0	10	25	0.15
2	0	10	27	0.15
3	0	10	29	0.15
4	2	8	25	0.15
5	2	8	27	0.15
6	2	8	30	0.15
7	3	7	25	0.15
8	3	7	27	0.15
9	3	7	29	0.15
10	4	6	32	0.06
11	4	6	34	0.06
12	4	6	36	0.06
13	5	5	30	0.1
14	5	5	32	0.07

Table III.1.1.3. Summary of compositions and experiment conditions of the electrospun nanofibers according to the weight content (wt.%) of mango kernel starch (MKS) and PVP (using metoxyethanol as solvent), voltage (V), distance between the injector and the collector (D) and flux (F).

Sample	Starch (wt.%)	PVP (wt.%)	V (kV)	F (mL/h)
15	0	10	18	0.2
16	0	10	20	0.2
17	0	10	22	0.2
18	2	8	18	0.2
19	2	8	20	0.2
20	2	8	22	0.2
21	3	7	18	0.2
22	3	7	20	0.2
23	3	7	22	0.2
24	4	6	16	0.2
25	4	6	18	0.2
26	4	6	20	0.2
27	4	6	22	0.2
28	5	5	16	0.2
29	5	5	18	0.2
30	5	5	20	0.2
31	5	5	22	0.2

Morphological characterization of nanofibers

The morphology of the electrospun nanofibers was observed by field emission scanning electron microscopy (FESEM) in a ZEISS ULTRA 55 from Oxford Instruments (Abingdon, United Kingdom). The samples were directly placed in the vacuum chamber, as they were electrospun in aluminum foil. An extra high tension (EHT) of 1.5 kV was applied to the electron beam. The average fiber diameter was determined via ImageJ Launcher v 1.41 software using, at least, 20 FESEM images.

The roughness profile of some of the obtained nanofibers was studied using an atomic force and scanning tunnel microscope (Bruker, Multimode 8, Massachusetts, EEUU). The Antimony (n) doped Si cantilever had a tip of 3 μm radius. Surface roughness was evaluated using Nanoscope Analysis software and the arithmetic mean value (R_a), which is related to the integral of the absolute value of the roughness profile height over the analysed length approximated by a trapezoidal rule, was calculated.

RESULTS AND DISCUSSION

MKS/PVA nanofibers

FESEM images for each sample of electrospun MKS/PVA nanofibers are presented in **Figure III.1.1.3**, while **Table III.1.1.4** gathers the diameter of the fibers in each sample and a short evaluation of the morphology of the fibers. They have been classified as smooth, fair of beaded fibers.

Samples 1, 2 and 3 are made of pure PVA, which exhibited an excellent fiber formation and homogeneity. These results were expected, as PVA has been widely studied in the field of electrospinning and its effectiveness has already been proven [53, 54]. The fiber diameter decreased from 0.315 μm in sample 1 to 0.276 μm and 0.280 μm in samples 2 and 3, respectively. This trend is related to an increase in the applied voltage, which results in fibers with smaller diameters due to a higher compression of the fibers exerted by higher electrostatic forces in the tip of the needle when conducting electrospinning [55]. The fiber diameters obtained for these samples are in accordance with the range observed by Koski *et al.* [54], who studied electrospun fibers of pure PVA of different molecular weights, ranging from 0.25 to 2 μm . The addition of 2 wt.% of MKS and 8 wt.% PVA leads to the formation of fibers of samples 4, 5 and 6. Sample 4 presented quite good copolymer nanofibers with some droplets, while samples 5 and 6 showed fibers not as homogeneous as sample 4 and with a higher concentration of droplets, which can be attributed to an excess of the applied electric potential, as it was observed

by Fong *et al.* [56] when they studied the formation of beaded fibers in poly(ethylene oxide) solutions. Again, a decrease in fiber diameter is observed from 0.297 μm in sample 4 to 0.233 and 0.189 μm in samples 5 and 6, respectively, which is also attributed to an increase in the applied potential (from 25 to 30 kV). It could be inferred that at this concentration, 25 kV are optimal with regard to fiber morphology. Samples 7, 8 and 9 correspond to the addition of 3 wt.% of MKS and 7 wt.% of PVA. In all three copolymer samples, smooth and uniform fibers were obtained, again experiencing a decrease in diameter (from 0.250 to 0.191 μm) with the applied voltage (from 25 kV to 29 kV), as it has been aforementioned. A similar experiment was carried out by Sukyte *et al.* [40], who developed nanofibers based on potato starch (3 wt.%) and PVA (7 wt.%), with fiber diameters of 0.275 μm approximately. Totally in contrast, the samples containing 4 wt.% of starch and 6 wt.% of PVA (samples 10, 11 and 12) show a clear detriment in the nanofibers, producing poor beaded fibers in the three cases. This beaded morphology is ascribed to a reduction in the viscosity of the solution [17], which is a direct consequence of the decrease in the PVA content and the increase in starch content. Nonetheless, the fiber diameters have been measured and they follow the same trend as before, decreasing the diameter from 0.187 μm to 0.146 μm for an increase in voltage from 32 to 36 kV. An increase in voltage in relation to the previous samples was needed in order to produce evaluable fibers, as the low viscosity of the solution required a higher electrostatic force to evaporate the solvent. Finally, samples 13 and 14 contained 5 wt.% of MKS and 5 wt.% of PVA. Similar to what has been observed for the previous samples, these are beaded fibers, as a result of the increase of starch content and decrease of PVA content, thus demonstrating that mango kernel starch is generally detrimental for the electrospinnability of polymer blends, as it has been reported in other studies [57]. In this case, the fiber diameters are practically the lowest of all MKS/PVA nanofibers, being 0.163 and 0.147 μm , respectively. Interestingly, fiber diameter seems to decrease as the content of starch increases, which could be probably ascribed to the lower viscosity of the solutions with higher content in starch, as they flow more easily from the injector to the collector. A similar phenomenon was observed by Kong *et al.* [58].

From these results it can be concluded that 3 wt.% MKS/7wt.% PVA is the optimal combination for obtaining smooth nanofibers with true applicability in fields such as biomedicine or food industry [59]. These fibers are quite similar to those of pure PVA, whose effectivity has been widely proven, and with lesser diameters, which could prove to be really useful in applications that require great interfacial area. Moreover, 3 wt.% of starch seems to be the concentration threshold in which good nanofibers are obtained in combination with PVA, as at higher concentrations of starch, the fibers turn

to beaded fibers with too many droplets in their morphology.

All in all, successful MKS/PVA starch nanofibers have been obtained, with a relatively wide range in electric voltage that allows to modify their diameter according to the function they will be destined for, maintaining the homogeneity of the fibers.

Table III.1.1.4. Diameter of the electrospun nanofibers made of MKS/PVA solution and their evaluation according to their morphology.

Sample	Diameter (μm)	Fiber Evaluation
1	0.315 ± 0.061	Smooth fibers
2	0.276 ± 0.047	Smooth fibers
3	0.280 ± 0.094	Smooth fibers
4	0.297 ± 0.048	Smooth fibers
5	0.233 ± 0.069	Fair fibers
6	0.189 ± 0.042	Fair fibers (beaded fibers)
7	0.250 ± 0.058	Smooth fibers
8	0.228 ± 0.056	Smooth fibers
9	0.191 ± 0.058	Smooth fibers
10	0.187 ± 0.038	Beaded fibers
11	0.180 ± 0.028	Beaded fibers
12	0.146 ± 0.018	Beaded fibers
13	0.163 ± 0.044	Beaded fibers
14	0.147 ± 0.053	Beaded fibers

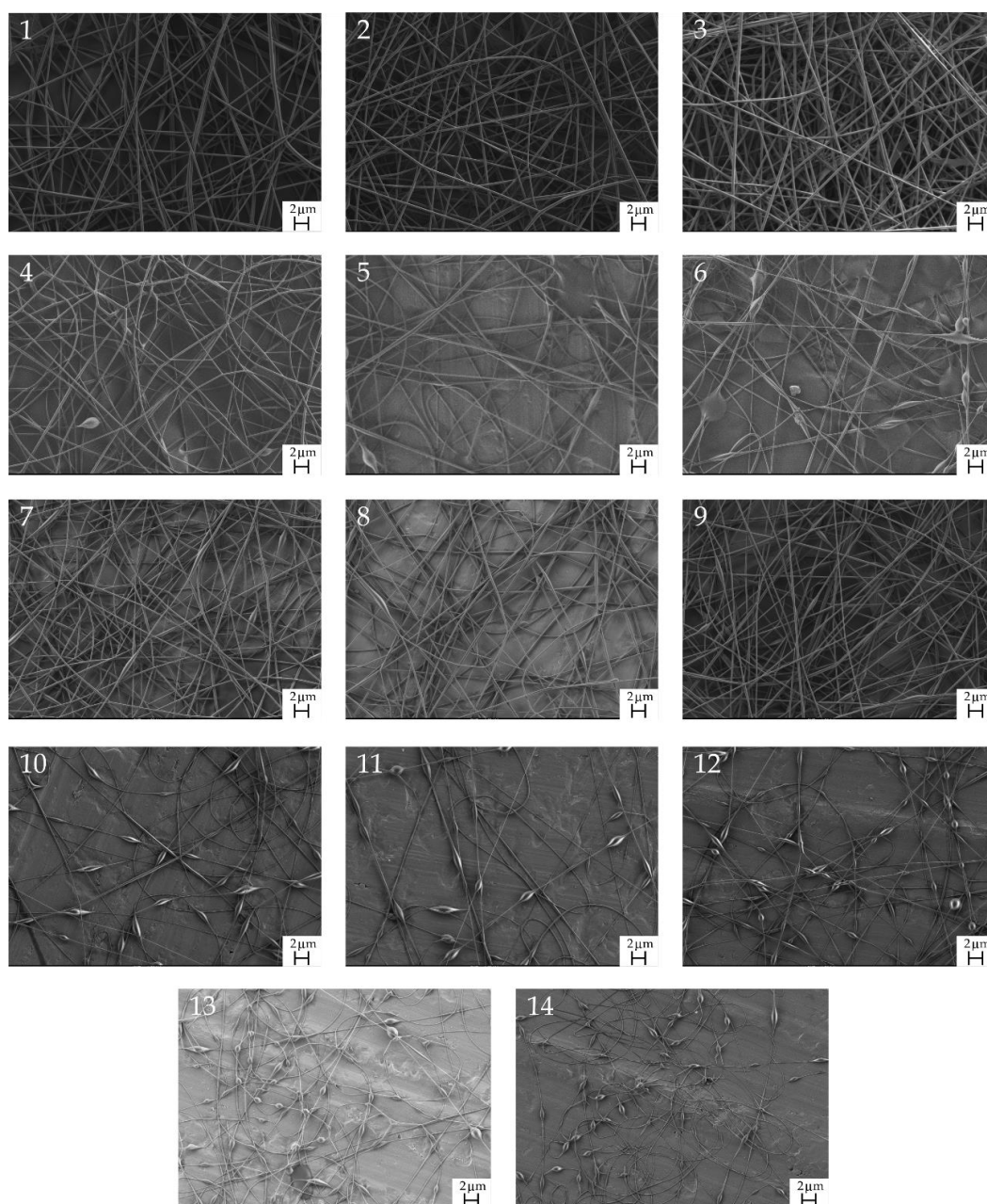


Figure III.1.1.3. FESEM images at 2500× magnification of all the MKS/PVA fibers specified in Table III.1.1.3.

MKS/PVP nanofibers

Figure III.1.1.4 shows the FESEM morphologies of all the electrospun MKS/PVP fibers, while **Table III.1.1.5** gathers the average diameter of all the samples and their corresponding evaluation according to the quality of the obtained fibers. Samples 15, 16 and 17 are related to neat PVP nanofibers using methoxyethanol as solvent at different voltages (18, 20 and 22 kV, respectively). In spite of having some droplets, quite homogeneous and smooth fibers have been obtained with diameters ranging from 0.339

to 0.241 μm , respectively. Similarly to what was observed in the case of PVA fibers, the diameter of the fibers diminishes as the voltage increases, due to an electrostatic compression phenomenon in the tip of the needle [60], which makes the fiber thinner with the increase in the electrostatic potential. Vongsetskul *et al.* [61] also observed this effect in pure PVP fibers when varying the applied electrical voltage. The diameters observed are similar to the ones obtained by Holopainen *et al.* [49], who used 10 wt.% PVP solutions to obtain nanofibers with hydroxyapatite. Next, samples 18, 19 and 20 correspond to MKS/PVP solutions with 2 wt.% of MKS and 8 wt.% of PVP. These prove to be homogeneous fibers without the presence of droplets, with diameters ranging from 0.316 to 0.260 μm , for a change in voltage from 18 to 22 kV, respectively. Interestingly, the morphology is quite similar to the morphology of pure PVP fibers, which demonstrates in this case that it is possible to successfully obtain functional starch/PVP nanofibers at this composition. Considering that there is hardly any information regarding the combination of starch with PVP to obtain fibers by electrospinning, it is an intriguing finding. In a similar manner, samples 21, 22 and 23 show nanofibers with 3 wt.% of MKS and 7 wt.% of PVP. The diameter also descends with the increase of potential in this case from 0.243 to 0.174 μm . There seems to be some concentration of droplets in sample 22, but it does not affect the homogeneity of the fibers, which are quite good in general terms. The observed diameters are lower than those of the higher concentration of PVP, which again seems to indicate that the higher the concentration of starch, the lower the diameter of the fibers. This fact is directly related to a decrease in the viscosity of the solution. The following samples, 24, 25, 26 and 27 correspond to fibers with 4 wt.% of MKS and 6 wt.% of PVP, with applied potentials of 16, 18, 20 and 22 kV, respectively. In this case, 16 kV was added because the fibers did not seem to be homogeneous and due to the change in starch concentration, another potential was considered. Samples 24, 25 and 26 presented some droplets, especially sample 26. On the other hand, sample 27 presented quite homogeneous fibers. This seems to point out to the fact that when the concentration of starch increases in the solution, a higher voltage is needed to avoid the formation of beaded fibers, which could be ascribed to the need of a higher evaporation rate of the solvent in the tip of the needle [59]. Diameters ranging from 0.079 to 0.110 μm have been obtained, which turn to be considerably smaller than the ones obtained for the previous solutions with lower concentration of starch. This reduction in diameter could be related to a marked decrease in the viscosity of the solution when going from 3 up to 4 wt.% of MKS, at the same time that PVP is decreased from 7 to 6 wt.%. Finally, samples 28, 29, 30 and 31 stand for solutions with 5 wt.% and 5 wt.% of PVP. As it was expected, beaded fibers were obtained, being the worst results

for MKS/PVP nanofibers, and again demonstrating that starch is not optimal for electrospinning at high concentrations, as it has been also reported by Hemamalini *et al.* [15]. Diameters of 0.071, 0.121, 0.073 and 0.08 μm were obtained, which are the smallest diameters obtained for nanofibers in this study, although these nanofibers are not optimal for actual applications, due to their high concentration of beads. Thus, 4 wt.% could be considered the concentration threshold from which total homogeneous nanofibers cannot be developed and beaded fibers appear.

According to these results, smooth MKS/PVP nanofibers have been successfully produced at different concentrations of starch and PVP, which is quite interesting given the fact that there are no publications of starch/PVP fibers obtained by electrospinning technique, especially referring to MKS. Moreover, smooth fibers in a wide range of diameters have been reported, even reaching less than 100 nm, which could be of special use in applications where high interfacial area may be needed. Particularly, in terms of starch fibers, fibers from 2 wt.% and 3 wt.% starch have shown very positive results, as well as sample 27, corresponding to a 4 wt.% starch solution electrospun at 22 kV, which presents very thin smooth fibers.

Table III.1.1.5. Diameter of the electrospun nanofibers made of MKS/PVP solutions.

Sample	Diameter (μm)	Fiber evaluation
15	0.339 ± 0.050	Smooth fibers
16	0.282 ± 0.076	Smooth fibers
17	0.241 ± 0.069	Smooth fibers
18	0.316 ± 0.073	Smooth fibers
19	0.299 ± 0.067	Smooth fibers
20	0.260 ± 0.069	Smooth fibers
21	0.243 ± 0.104	Smooth fibers
22	0.216 ± 0.057	Smooth fibers
23	0.174 ± 0.039	Smooth fibers
24	0.079 ± 0.036	Smooth fibers
25	0.110 ± 0.039	Smooth fibers (beaded fibers)
26	0.105 ± 0.052	Fair fibers (beaded fibers)
27	0.099 ± 0.031	Smooth fibers
28	0.071 ± 0.021	Fair fibers (beaded fibers)
29	0.121 ± 0.049	Fair fibers (beaded fibers)
30	0.073 ± 0.037	Fair fibers (beaded fibers)
31	0.080 ± 0.040	Fair fibers (beaded fibers)

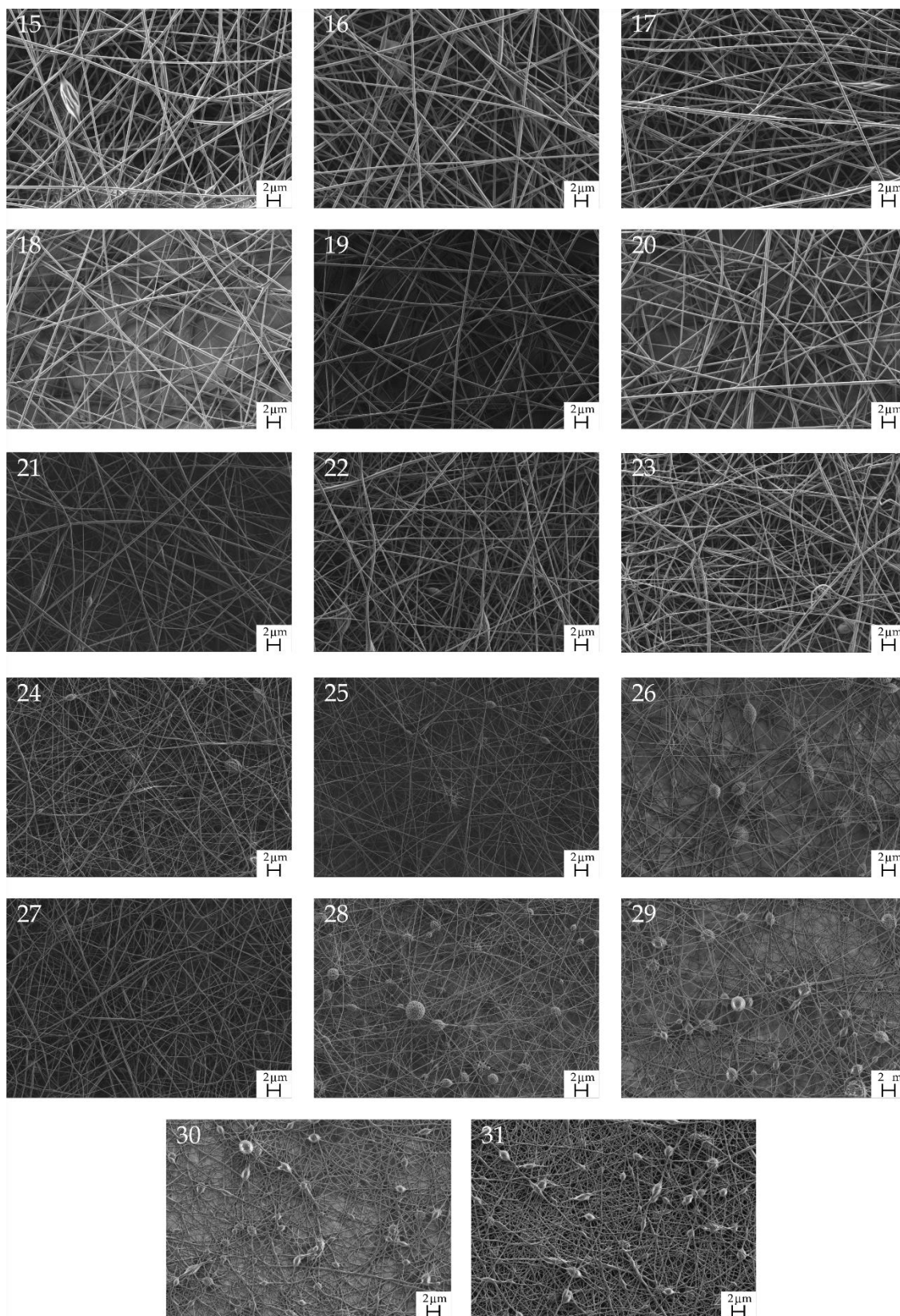


Figure III.1.14. FESEM images at 2500× magnification of all the MKS/PVP fibers specified in **Table III.1.1.5.**

AFM analysis of the MKS/PVA nanofibers and MKS/PVP nanofibers

After evaluating all fibers by field emission scanning electron microscopy (FESEM), the optimal solutions have been selected for a deeper analysis by means of atomic force microscopy (AFM). Two samples from the 3 wt.% starch 7 wt.% PVA solution have been selected (samples 7 and 9, electrospun at 25 and 29 kV, respectively). On the other hand, sample 20, electrospun at 22 kV, has been chosen from the 2 wt.% starch 8 wt.% PVP solution, sample 21, at 18 kV, from the 3 wt.% starch 7 wt.% PVP solution and sample 27, at 22 kV, from the 4 wt.% starch 6 wt.% PVP solution. **Figure III.1.1.5** shows FESEM images of these samples at 5000× magnification as well as AFM images with a scan size of 4 μm. Additionally, **Figure III.1.1.6** gathers the fiber diameter distribution of the selected nanofibers, where it can be seen how the average diameter coincides with the diameter showed in **Tables III.1.1.4** and **III.1.1.5**.

AFM is a very useful technique to study the topography of the fibers. As it can be observed, the AFM images are in good agreement with the FESEM images. First, sample 7 and 9, which correspond to MKS/PVA fibers, seem to maintain the same fiber diameter relation as in the previous section, although sample 9 presents a smaller diameter as a result of having been electrospun at 29 kV, while sample 7 was electrospun at 25 kV. Similarly, samples 20, 21 and 27 also seem to match the previously analysed results. Those samples presented fiber diameters of 260, 243 and 99 nm, respectively. It can be seen how AFM images show that sample 27 has a considerably smaller diameter than the rest of the samples, while sample 21 has also a clearly smaller diameter than fibers in sample 20. However, the diameter observed in AFM images seems to be larger than in FESEM, this is because the scan size in AFM was quite limited due to cantilever and tip sensibility. Thus, very few fibers could be observed by AFM at the same time. Nonetheless, the diameter relation is clearly observed. Additionally, the scale in the right of the AFM images is representative for the height of the image, obtained from the oscillation of the tip of the microscope. Observing these scales, it can be observed how sample 27 presents a less profound scale (from 300 nm to 500 nm approximately) in terms of depth, which is another indicative of the smaller diameter of the MKS/PVP fibers at 4 wt.% of MKS and 6 wt.% of PVP, as this scale is quite lower than that of the rest of the samples. AFM allowed to measure the roughness of the samples, measured as R_n , which is the arithmetic average of the absolute values of the roughness profile ordinates [62]. It can be observed how the roughness of MKS/PVA fibers is quite higher than that of MKS/PVP fibers, which could be ascribed to the difference in fiber diameter previously commented, as it was also reported by Adeli *et al.* [63] in a study about PVA/chitosan/starch electrospun nanofibers by AFM. Particularly in the case of sample

27, showing a roughness of 80 nm, while the rest of the samples exhibited roughnesses in the range 260–343 nm.

The results presented here suggest that MKS/PVP nanofibers present lower roughnesses than MKS/PVA nanofibers, and that increasing the concentration of MKS in MKS/PVP fibers up to 4 wt.% allows to obtain especially thin fibers. Interestingly, this fact makes the obtained fibers suitable for applications in tissue engineering for cell attachment and cell growth. The roughness range aforementioned proves to be favourable for osteoblast proliferation [64] and endothelial [65] and neuronal cells growth and proliferation [66] according to several studies.

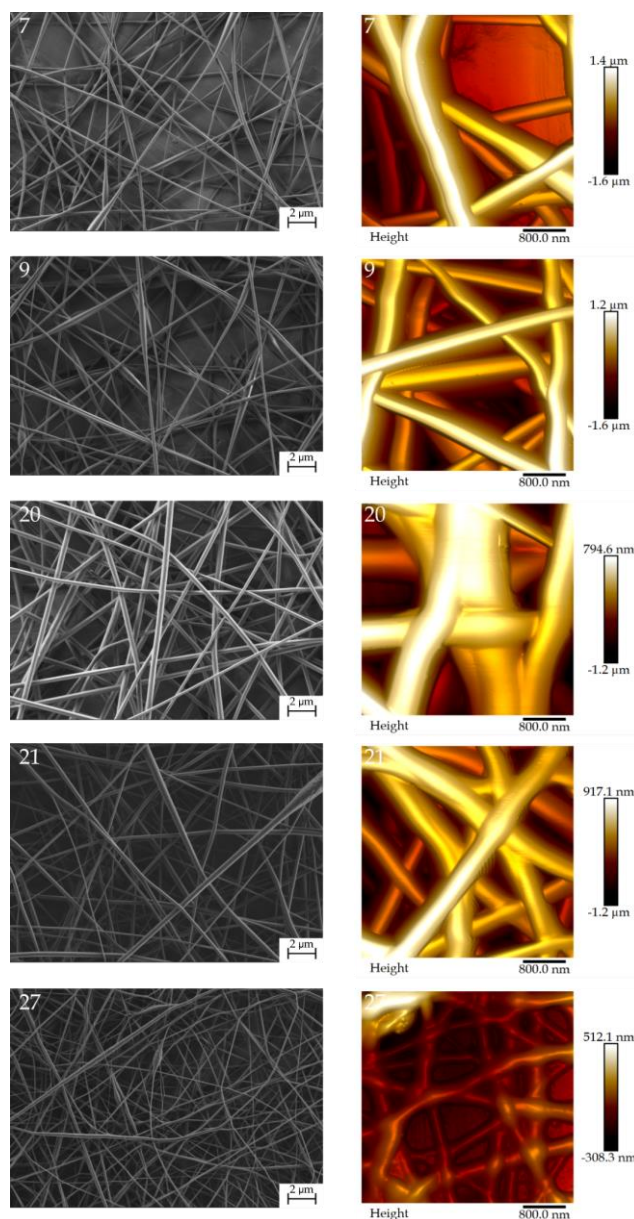


Figure III.1.1.5. FESEM images at 5000× magnification and AFM images at a scan size of 4 μm of the optimal electrospun MKS/PVA and MKS/PVP obtained fibers (samples 7, 9, 20, 21 and 27).

Table III.1.1.6. Roughness measurements of the MKS/PVA and MKS/PVP electrospun nanofibers.

Sample	Roughness R_a (nm)
7	339
9	343
20	286
21	260
27	80

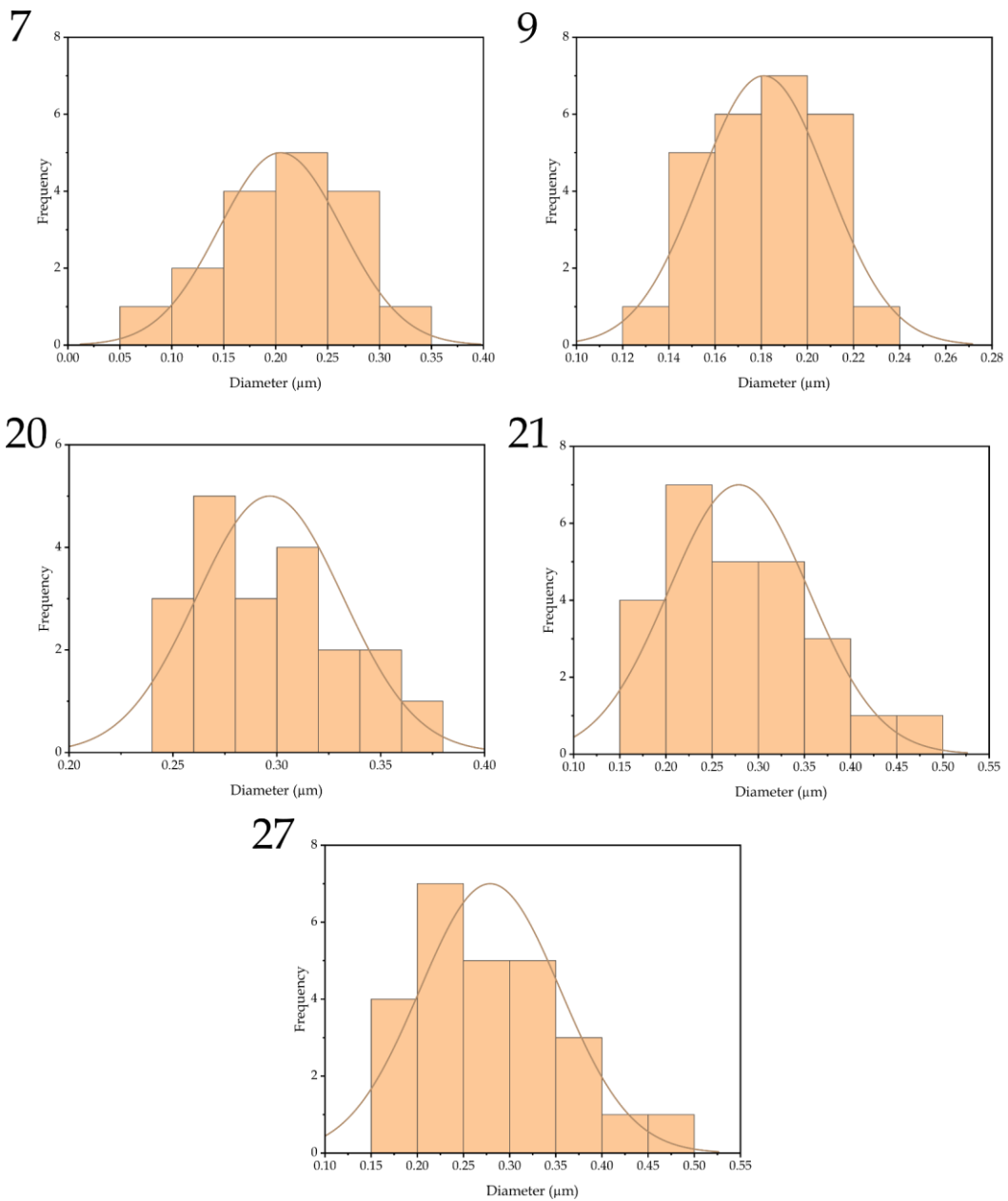


Figure III.1.1.6. Fiber diameter distributions of the optimal electrospun MKS/PVA and MKS/PVP fibers (samples 7, 9, 20, 21 and 27).

CONCLUSIONS

In this study, smooth ultrathin fibers in the nano scale based on starch extracted from mango kernel and PVA and PVP were successfully obtained by means of the electrospinning technique and evaluated by FESEM and AFM. Several experimental conditions were tested for MKS/PVA and MKS/PVP fibers. MKS/PVA nanofibers' diameter ranged from 0.146 to 0.315 μm , while MKS/PVP nanofibers' diameter ranged from 0.08 to 0.339 μm . It was observed how the diameter of the electrospun nanofibers decreased with an increase in the applied voltage, as a result of higher compression electrostatic forces in the tip of the needle. Additionally, it was demonstrated that in general, starch is detrimental for the electrospinning technique, establishing a concentration threshold for which smooth fibers are obtained in each blend. In the case of MKS/PVA fibers, starch concentrations superior to 3 wt.% provoked the appearance of droplets in their morphology, leading to beaded fibers. On the other hand, MKS/PVP fibers with starch concentrations higher than 3 wt.% also caused the appearance of beaded fibers, although there was one sample at 4 wt.% of starch that exhibited smooth and homogeneous fibers at a voltage of 22 kV. MKS/PVP nanofibers proved to be considerably thinner than MKS/PVA nanofibers when 4 wt.% or superior concentrations of starch were added. This fact could prove to be quite interesting from a scientific point of view for certain applications, where higher interfacial area is required. AFM analysis allowed to determine the topology of the optimal nanofiber samples, which were 3wt.% starch solutions electrospun at 25 and 29 kV, respectively, for MKS/PVA blends and 2, 3 and 4 wt.% starch concentration solutions electrospun at 22, 18 and 22 kV, respectively. The roughness of the samples followed a similar trend compared to fiber diameter, being the MKS/PVP sample with 4 wt.% of starch the one with the lowest roughness ($R_a=80$ nm). AFM images confirmed the results observed by FESEM.

All in all, the results obtained in this work proved that it is possible to obtain completely natural, biocompatible and biodegradable electrospun mango kernel starch nanofibers in combination with PVA and PVP with great potential in applications related to food industry or the biomedical field, such as tissue engineering. Moreover, the diameter of the fibers can be controlled within a wide range varying the conditions of the electrospinning setup, thus allowing to adjust the morphology of the fibers depending on the application they will be destined for. The high natural content of the fibers presented here makes them environmentally friendly and quite cost effective, as starch is extracted from mango, water is used as a solvent and electrospinning is a relatively simple technique. Considering that mango kernel starch has never been

previously tested in electrospinning, and that PVP has not been used in combination with starch in this technique, this work opens a whole new path towards the development of novel mango kernel starch fibers with other synthetic polymers or even with other natural polymers. The next steps of the investigation could be centered in optimizing the electrospinning conditions of MKS/PVA and MKS/PVP nanofibers and giving them an actual application, such as tissue regeneration or drug delivery systems for example, given their biocompatibility.

ACKNOWLEDGEMENTS

Authors also thank Generalitat Valenciana-GVA, grant number AICO/2021/025 for supporting this work. J. Gomez-Caturla wants to thank Generalitat Valenciana-GVA, for his FPI grant (ACIF/2021/185) and grant FPU20/01732 funded by MCIN/AEI/10.13039/501100011033 and by ESF Investing in your future. J. Ivorra-Martinez wants to thank FPU19/01759 grant funded by MCIN/AEI/10.13039/501100011033 and by ESF Investing in your future. Microscopy Services at UPV are also acknowledged by their help in collecting and analyzing images.

FUNDING

This research is a part of the grant PID2020-116496RB-C22 funded by MCIN/AEI/10.13039/501100011033.

DATA AVAILABILITY STATEMENT

The raw/processed data required to reproduce these findings cannot be shared at this time due to technical or time limitations.

REFERENCES

- [1] Thavasi, V., G. Singh, and S. Ramakrishna, *Electrospun nanofibers in energy and environmental applications*. Energy & Environmental Science, 2008. 1(2): 205-221.
- [2] Liu, W., S. Thomopoulos, and Y. Xia, *Electrospun nanofibers for regenerative medicine*. Advanced healthcare materials, 2012. 1(1): 10-25.
- [3] Chinnappan, A., et al., *An overview of electrospun nanofibers and their application in energy storage, sensors and wearable/flexible electronics*. Journal of Materials Chemistry C, 2017. 5(48): 12657-12673.
- [4] Zanin, M.H.A., N.N. Cerize, and A.M. de Oliveira, *Production of nanofibers by electrospinning technology: overview and application in cosmetics*, in Nanocosmetics and Nanomedicines. 2011. 311-332.
- [5] Rezaei, A., A. Nasirpour, and M. Fathi, *Application of cellulosic nanofibers in food science using electrospinning and its potential risk*. Comprehensive Reviews in Food Science and Food Safety, 2015. 14(3): 269-284.
- [6] Sharifi, F., et al., *Fiber based approaches as medicine delivery systems*. ACS Biomaterials Science & Engineering, 2016. 2(9): 1411-1431.
- [7] Busolo, M., et al., *Electrospraying assisted by pressurized gas as an innovative high-throughput process for the microencapsulation and stabilization of docosahexaenoic acid-enriched fish oil in zein prolamine*. Innovative Food Science & Emerging Technologies, 2019. 51: 12-19.
- [8] Quiles-Carrillo, L., et al., *Bioactive multilayer polylactide films with controlled release capacity of gallic acid accomplished by incorporating electrospun nanostructured coatings and interlayers*. Applied Sciences, 2019. 9(3): 533-550.
- [9] Sill, T.J. and H.A. Von Recum, *Electrospinning: applications in drug delivery and tissue engineering*. Biomaterials, 2008. 29(13): 1989-2006.
- [10] Ibrahim, H.M. and A. Klingner, *A review on electrospun polymeric nanofibers: Production parameters and potential applications*. Polymer Testing, 2020. 90: 106647.
- [11] Bhardwaj, N. and S.C. Kundu, *Electrospinning: a fascinating fiber fabrication technique*. Biotechnology advances, 2010. 28(3): 325-347
- [12] Hajiabbas, M., I. Alemzadeh, and M. Vossoughi, *A porous hydrogel-electrospun composite scaffold made of oxidized alginate/gelatin/silk fibroin for tissue engineering application*. Carbohydrate Polymers, 2020. 245: 116465.

-
- [13] Cesur, S., *et al.*, *Production and characterization of elastomeric cardiac tissue-like patches for Myocardial Tissue Engineering*. *Polymer Testing*, 2020. 90: 106613.
- [14] Pawar, H.A., S.R. Kamat, and P.D. Choudhary, *An overview of natural polysaccharides as biological macromolecules: their chemical modifications and pharmaceutical applications*. *Biology and Medicine*, 2015. 6(224): 2.
- [15] Hemamalini, T. and V.R.G. Dev, *Comprehensive review on electrospinning of starch polymer for biomedical applications*. *International journal of biological macromolecules*, 2018. 106: 712-718.
- [16] Petroudy, S.R.D., S.A. Kahagh, and E. Vatankhah, *Environmentally friendly superabsorbent fibers based on electrospun cellulose nanofibers extracted from wheat straw*. *Carbohydrate Polymers*, 2021. 251: 117087.
- [17] Liu, G., *et al.*, *Electrospun starch nanofibers: Recent advances, challenges, and strategies for potential pharmaceutical applications*. *Journal of Controlled Release*, 2017. 252: 95-107.
- [18] Torres, F.G., S. Commeaux, and O.P. Troncoso, *Starch-based biomaterials for wound-dressing applications*. *Starch-Stärke*, 2013. 65(7-8): 543-551.
- [19] Doi, S., *et al.*, *New materials based on renewable resources: chemically modified expanded corn starches as catalysts for liquid phase organic reactions*. *Chemical communications*, 2002. 1(22): 2632-2633.
- [20] Hoover, R. and D. Hadziyev, *Characterization of potato starch and its monoglyceride complexes*. *Starch-Stärke*, 1981. 33(9): 290-300.
- [21] Williams, V.R., *et al.*, *Rice starch, varietal differences in amylose content of rice starch*. *Journal of Agricultural and Food Chemistry*, 1958. 6(1): 47-48.
- [22] Tester, R., S. Debon, and M. Sommerville, *Annealing of maize starch*. *Carbohydrate Polymers*, 2000. 42(3): 287-299.
- [23] Min, T., *et al.*, *Electrospun pullulan/PVA nanofibers integrated with thymol-loaded porphyrin metal-organic framework for antibacterial food packaging*. *Carbohydrate Polymers*, 2021. 270: 118391.
- [24] de Morais Teixeira, E., *et al.*, *Preparation and characterisation of thermoplastic starches from cassava starch, cassava root and cassava bagasse*. in *Macromolecular symposia*. 2005. Wiley Online Library.

- [25] Makroo, H., *et al.*, *Characterization of mango puree based on total soluble solids and acid content: Effect on physico-chemical, rheological, thermal and ohmic heating behavior*. *Lwt*, 2019. 103: 316-324.
- [26] Banerjee, J., *et al.*, *A hydrocolloid based biorefinery approach to the valorisation of mango peel waste*. *Food Hydrocolloids*, 2018. 77: 142-151.
- [27] Mutua, J.K., S. Imathiu, and W. Owino, *Evaluation of the proximate composition, antioxidant potential, and antimicrobial activity of mango seed kernel extracts*. *Food science & nutrition*, 2017. 5(2): 349-357.
- [28] Nawab, A., F. Alam, and A. Hasnain, *Mango kernel starch as a novel edible coating for enhancing shelf-life of tomato (*Solanum lycopersicum*) fruit*. *International Journal of Biological Macromolecules*, 2017. 103: 581-586.
- [29] Sridhar, R., *et al.*, *Electrosprayed nanoparticles and electrospun nanofibers based on natural materials: applications in tissue regeneration, drug delivery and pharmaceuticals*. *Chemical Society Reviews*, 2015. 44(3): 790-814.
- [30] Li, W., *et al.*, *Improving the adhesion-to-fibers and film properties of corn starch by starch sulfo-itaconation for a better application in warp sizing*. *Polymer Testing*, 2021. 98: 107194.
- [31] Asl, M.A., *et al.*, *Evaluation of the effects of starch on polyhydroxybutyrate electrospun scaffolds for bone tissue engineering applications*. *International Journal of Biological Macromolecules*, 2021. 191: 500-513.
- [32] Hong, Y., G. Liu, and Z. Gu, *Recent advances of starch-based excipients used in extended-release tablets: a review*. *Drug delivery*, 2016. 23: 12-20.
- [33] Jukola, H., *et al.* *Electrospun starch-polycaprolactone nanofiber-based constructs for tissue engineering*. in *AIP conference proceedings*. 2008. American Institute of Physics.
- [34] Mahalingam, S., G. Ren, and M. Edirisinghe, *Rheology and pressurised gyration of starch and starch-loaded poly (ethylene oxide)*. *Carbohydrate polymers*, 2014. 114: 279-287.
- [35] Sunthornvarabhas, J., *et al.*, *Electrospun polylactic acid and cassava starch fiber by conjugated solvent technique*. *Materials Letters*, 2011. 65(6): 985-987.
- [36] Ulery, B.D., L.S. Nair, and C.T. Laurencin, *Biomedical applications of biodegradable polymers*. *Journal of polymer science Part B: polymer physics*, 2011. 49(12): 832-864.

- [37] Jaiturong, P., *et al.*, Preparation of glutinous rice starch/polyvinyl alcohol copolymer electrospun fibers for using as a drug delivery carrier. *Asian journal of pharmaceutical sciences*, 2018. 13(3): 239-247.
- [38] Arrieta, M., *et al.*, Electrospun PVA fibers loaded with antioxidant fillers extracted from *Durovillaea antarctica* algae and their effect on plasticized PLA bionanocomposites. *European Polymer Journal*, 2018. 103: 145-157.
- [39] Kenawy, E.-R., *et al.*, Controlled release of ketoprofen from electrospun poly (vinyl alcohol) nanofibers. *Materials Science and Engineering: A*, 2007. 459(1-2): 390-396.
- [40] Šukytė, J., E. Adomavičiūtė, and R. Milašius, Investigation of the possibility of forming nanofibres with potato starch. *Fibres & Textiles in Eastern Europe*, 2010. 82(5): 24-27.
- [41] Woranuch, S., *et al.*, Rice flour-based nanostructures via a water-based system: transformation from powder to electrospun nanofibers under hydrogen-bonding induced viscosity, crystallinity and improved mechanical property. *RSC advances*, 2017. 7(32): 19960-19966.
- [42] Koczur, K.M., *et al.*, Polyvinylpyrrolidone (PVP) in nanoparticle synthesis. *Dalton Transactions*, 2015. 44(41): 17883-17905.
- [43] Bühler, V., *Polyvinylpyrrolidone Excipients for Pharmaceuticals-povidone, crospovidone and copovidone*. Springer: Berlin Heidelberg New York, 2005.
- [44] Teodorescu, M. and M. Bercea, Poly (vinylpyrrolidone)-a versatile polymer for biomedical and beyond medical applications. *Polymer-Plastics Technology and Engineering*, 2015. 54(9): 923-943.
- [45] Dai, X.-Y., *et al.*, Electrospun emodin polyvinylpyrrolidone blended nanofibrous membrane: a novel medicated biomaterial for drug delivery and accelerated wound healing. *Journal of Materials Science: Materials in Medicine*, 2012. 23(11): 2709-2716.
- [46] Vidal, C.P., *et al.*, Antimicrobial food packaging system based on ethyl lauroyl arginate-loaded core/shell electrospun structures by using hydrophilic and hydrophobic polymers. *Polymer Testing*, 2021. 93: 106937.
- [47] Nawab, A., *et al.*, Biodegradable film from mango kernel starch: Effect of plasticizers on physical, barrier, and mechanical properties. *Starch-Stärke*, 2016. 68(9-10): 919-928.
- [48] Jane, J.L., *et al.*, Anthology of starch granule morphology by scanning electron microscopy. *Starch-Stärke*, 1994. 46(4): 121-129.

- [49] Holopainen, J., *et al.*, *Electrospinning of calcium carbonate fibers and their conversion to nanocrystalline hydroxyapatite*. *Materials Science and Engineering: C*, 2014. 45: 469-476.
- [50] Liu, Z. and J.-H. He, *Polyvinyl alcohol/starch composite nanofibers by bubble electrospinning*. *Thermal Science*, 2014. 18(5): 1473-1475.
- [51] Jaworek, A. and A.T. Sobczyk, *Electrospraying route to nanotechnology: An overview*. *Journal of electrostatics*, 2008. 66(3-4): 197-219.
- [52] Zuo, W., *et al.*, *Experimental study on relationship between jet instability and formation of beaded fibers during electrospinning*. *Polymer Engineering & Science*, 2005. 45(5): 704-709.
- [53] Tao, J. and S. Shivkumar, *Molecular weight dependent structural regimes during the electrospinning of PVA*. *Materials letters*, 2007. 61(11-12): 2325-2328.
- [54] Koski, A., K. Yim, and S. Shivkumar, *Effect of molecular weight on fibrous PVA produced by electrospinning*. *Materials Letters*, 2004. 58(3-4): 493-497.
- [55] Huan, S., *et al.*, *Effect of experimental parameters on morphological, mechanical and hydrophobic properties of electrospun polystyrene fibers*. *Materials*, 2015. 8(5): 2718-2734.
- [56] Fong, H., I. Chun, and D.H. Reneker, *Beaded nanofibers formed during electrospinning*. *Polymer*, 1999. 40(16): 4585-4592.
- [57] Kong, L. and G.R. Ziegler, *Fabrication of pure starch fibers by electrospinning*. *Food Hydrocolloids*, 2014. 36: 20-25.
- [58] Kong, L. and G.R. Ziegler, *Quantitative relationship between electrospinning parameters and starch fiber diameter*. *Carbohydrate polymers*, 2013. 92(2): 1416-1422.
- [59] Ashraf, R., *et al.*, *Recent trends in the fabrication of starch nanofibers: electrospinning and non-electrospinning routes and their applications in biotechnology*. *Applied biochemistry and biotechnology*, 2019. 187: 47-74.
- [60] Beachley, V. and X. Wen, *Effect of electrospinning parameters on the nanofiber diameter and length*. *Materials Science and Engineering: C*, 2009. 29(3): 663-668.
- [61] Vongsetskul, T., *et al.*, *Effect of solvent and processing parameters on electrospun polyvinylpyrrolidone ultra-fine fibers*. *Chiang Mai Journal of Science*, 2015. 42(2): 436-442.

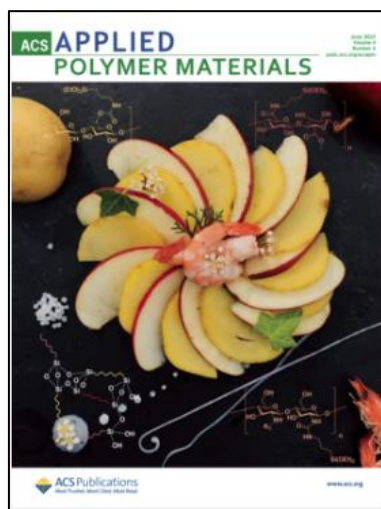
- [62] Haq, S. and R. Srivastava, *Measuring the influence of materials composition on nano scale roughness for wood plastic composites by AFM. Measurement*, 2016. 91: 541-547.
- [63] Adeli, H., M.T. Khorasani, and M. Parvazinia, *Wound dressing based on electrospun PVA/chitosan/starch nanofibrous mats: Fabrication, antibacterial and cytocompatibility evaluation and in vitro healing assay. International journal of biological macromolecules*, 2019. 122: 238-254.
- [64] Hatano, K., *et al.*, *Effect of surface roughness on proliferation and alkaline phosphatase expression of rat calvarial cells cultured on polystyrene. Bone*, 1999. 25(4): 439-445.
- [65] Chung, T.-W., *et al.*, *Enhancement of the growth of human endothelial cells by surface roughness at nanometer scale. Biomaterials*, 2003. 24(25): 4655-4661.
- [66] De Bartolo, L., *et al.*, *Influence of membrane surface properties on the growth of neuronal cells isolated from hippocampus. Journal of Membrane Science*, 2008. 325(1): 139-149.

III.1.2. Biopolypropylene-based wood plastic composites reinforced with mango peel flour and compatibilized with an environmentally friendly copolymer from itaconic acid

Jaume Gomez-Caturla^{1*}, Rafael Balart¹, Juan Ivorra-Martinez¹, Daniel Garcia-Garcia¹, Franco Dominici², Debora Puglia² and Luigi Torre²

¹ Technological Institute of Materials – ITM, Universitat Politècnica de València – UPV, Plaza Ferrándiz y Carbonell 1, 03801 Alcoy (Spain).

² Dipartimento di Ingegneria Civile ed Ambientale, University of Perugia, UdR INSTM, Strada di Pentima, 4 - 05100 Terni (TR) Italy.



ACS Applied Polymer Materials

2022, 4(6): 4047-4587

*Adapted from the original manuscript.



Biopolypropylene-Based Wood Plastic Composites Reinforced with Mango Peel Flour and Compatibilized with an Environmentally Friendly Copolymer from Itaconic Acid

Jaume Gomez-Caturla,* Rafael Balart, Juan Ivorra-Martinez, Daniel Garcia-Garcia, Franco Dominici, Debora Puglia, and Luigi Torre



Cite This: *ACS Appl. Polym. Mater.* 2022, 4, 4398–4410



Read Online

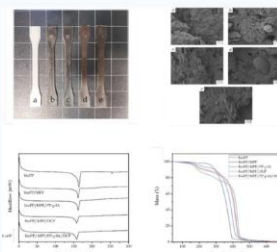
ACCESS |

Metrics & More

Article Recommendations

Supporting Information

ABSTRACT: This work reports on the successful development of biopolypropylene/mango peel flour (bioPP/MPF) composites using extrusion and injection molding processes. The compatibility between bioPP and MPF is improved through the use of PP-g-IA (3 phr) as a compatibilizer (which is prepared by reactive extrusion REX) and dicumyl peroxide (DCP) (1 phr) as a cross-linker. The mechanical, morphological, thermal, thermomechanical, chemical, colorimetric, water absorption, and flowability properties are characterized and analyzed. The results show that MPF (30 wt %) compatibilized with PP-g-IA and DCP increased the stiffness of bioPP in terms of Young's modulus values. Elongation at break also shows very promising results, with a maximum value of almost 30% for the bioPP/MPF/PP-g-IA/DCP sample. PP-g-IA and DCP seem to exert a synergetic effect. Thermal stability is also improved as a result of these additives, as well as crystallinity, which is increased due to an heterogeneous nucleation phenomenon, enhanced by a higher dispersion of MPF particles in the matrix. Moreover, the excellent mechanical results are verified in FESEM images, where a very narrow gap between the MPF particles and the bioPP matrix is appreciated.



KEYWORDS: polymer composites, biopolymers, reinforcements, mango peel flour, compatibilization

1. INTRODUCTION

In the recent years, society is becoming more concerned about the environmental issues provoked by the excessive use of petrochemical plastics, such as the increase in greenhouse gas emission related to the production process of those materials. This problem has led both industry and the scientific community to look for more environmentally friendly alternatives. One of this alternatives is the development and use of fully or partially biobased polymeric materials obtained from natural resources that could substitute conventional petrochemical polymers.^{1,2} In this field, wood plastic composites (WPCs) have become an interesting solution as these are the combination of a base polymer (or biopolymer) and a wood-like (or more generally, a lignocellulosic) reinforcement/filler.^{3,4} These fillers reduce the cost of the materials and at the same time improve some of their physical and chemical properties, leading to multifunctional materials.^{5,6} At first, only wood flour and sawdust were used as organic fillers, but lately, plant-derived lignocellulosic fillers coming from different industries have been gaining importance,⁷ such as almond shell flour,⁸ hemp fiber,⁹ or pineapple leaves,¹⁰ among others.

Among all the polymers, polypropylene (PP) has gained quite a lot of popularity, being a semicrystalline thermoplastic

with a very good balance between resistant and ductile mechanical properties and chemical resistance.¹¹ Thus, considering that biopolymers possess the same properties as that of their petrochemical counterparts,¹² biopolypropylene (bioPP) is a very promising option to be considered as a biopolymeric matrix in WPCs. The production of bioPP has not been explored as much as the production of biopolyethylene (bioPE), but it can be obtained from methanol, further processed to obtain the propylene monomer and then polymerized to obtain bioPP.¹³ However, one of the main drawbacks of using natural organic fillers with nonpolar polymers, such as polyolefins, is the polarity of the fillers, associated with the presence of lignocellulosic (lignin, cellulose, and hemicellulose) constituents in their structure (with hydroxyl groups),¹⁴ which makes them highly hydrophilic, while the biopolymer matrix is marked by high hydrophobicity. This fact directly leads to a poor mechanical

Received: March 3, 2022

Accepted: April 27, 2022

Published: May 5, 2022



Biopolypropylene-based wood plastic composites reinforced with mango peel flour and compatibilized with an environmentally friendly copolymer from itaconic acid

Abstract

This work reports on the successful development of biopolypropylene/Mango Peel Flour (bioPP/MPF) composites using extrusion and injection molding processes. The compatibility between bioPP and MPF is improved through the use of PP-g-IA (3 phr) as a compatibilizer (which is prepared by reactive extrusion REX) and dicumyl peroxide (DCP) (1 phr) as a crosslinker. The mechanical, morphologic, thermal, thermomechanical, chemical, colorimetric, water absorption and flowability properties are characterized and analysed. The results show that MPF (30 wt.%) compatibilized with PP-g-IA and DCP increased the stiffness of bioPP in terms of Young's modulus values. Elongation at break also shows very promising results, with a maximum value of almost 30% for bioPP/MPF/PP-g-IA/DCP sample. PP-g-IA and DCP seem to exert a synergetic effect. Thermal stability is also improved as a result of these additives, as well as crystallinity, which is increased due to an heterogeneous nucleation phenomenon, enhanced by a higher dispersion of MPF particles in the matrix. Moreover, the excellent mechanical results are verified in FESEM images, where a very narrow gap between MPF particles and the bioPP matrix is appreciated.

Keywords: Polymer composites, biopolymers, reinforcements, mango peel flour, compatibilization.

INTRODUCTION

In the last years, society is becoming more concerned about the environmental issues provoked by the excessive use of petrochemical plastics, such as the increase in greenhouse gas emission related to the production process of those materials. This problem has led both industry and the scientific community to look for more environmentally friendly alternatives. One of these alternatives is the development and use of fully or partially biobased polymeric materials obtained from natural resources that could substitute conventional petrochemical polymers [1, 2]. In this field, wood plastic composites (WPC) have become an interesting solution since these are the combination of a base polymer (or biopolymer) and a wood-like (or more generally, a lignocellulosic) reinforcement/filler [3, 4]. These fillers reduce the cost of the material and at the same time improve some of their physical and chemical properties, leading to multifunctional materials [5, 6]. At first, only wood flour and sawdust were used as organic fillers, but lately, plant-derived lignocellulosic fillers coming from different industries have been gaining importance [7], such as almond shell flour [8], hemp fiber [9] or pineapple leaves [10], among others.

Among all the polymers, polypropylene (PP) has gained quite the popularity, being a semicrystalline thermoplastic with a very good balance between resistant and ductile mechanical properties and chemical resistance [11]. Thus, considering that biopolymers possess the same properties that their petrochemical counterparts [12], biopolypropylene (bioPP) is a very promising option to be considered as a biopolymeric matrix in wood plastic composites. The production of bioPP has not been as explored as the production of biopolyethylene (bioPE), but it can be obtained from methanol, further processing it to obtain propylene monomer and then polymerizing it to obtain bioPP [13]. However, one of the main drawbacks of using natural organic fillers with non-polar polymers, such as polyolefins, is the polarity of the fillers, associated to the presence of lignocellulosic (lignin, cellulose, and hemicellulose) constituents in their structure (which hydroxyl groups) [14], which makes them highly hydrophilic, while the biopolymer matrix is marked by a high hydrophobicity. This fact directly leads to a poor mechanical response in these polymer/filler systems, related to a lack of interfacial adhesion and affinity between them.

In order to improve the compatibility between the filler and the surrounding matrix, several studies have been carried out based either on surface modification of the filler or on the use of a compatibilizing agent, which increase the hydrophilicity of the base polymer [15]. On the one hand, some methods such as benzylation, silanization or

acetylation involve surface modification of the lignocellulosic particles by blocking the hydroxyl groups [16]. On the other hand, a wide range of copolymers have been used to increase the affinity between the filler and the matrix. Some of the most used are polyethylene or polypropylene subjected to a grafting with maleic anhydride (PE-g-MA) or polypropylene-grafted maleic anhydride (PP-g-MA and PP-g-MA, respectively), which use the maleic anhydride group to increase the polarity of PE and PP and act as a chemical bridge between natural fillers and the polymeric chains [17]. More recently, itaconic acid, which can be obtained from renewable resources (*i.e.* from citric acid) has been proposed as an environmentally friendly grafting monomer, acting as a polar functionalization for non-polar polymers, such as PP. Pesetskii *et al.* [18] modified PP by reactive extrusion with dicumyl peroxide (DCP) in order to obtain the corresponding grafted copolymer PP-g-IA, with interesting compatibilization properties. Moncada *et al.* [19] reported the superior compatibilizing effect of PP-g-IA in a PP/Clay nanocomposite when compared to conventional PP-g-MA. Kim *et al.* [20] also reported the effectiveness of PP-g-IA as a compatibilizer in PP/EVOH blends, avoiding phase separation. These compatibilizers usually solve the compatibility problem between lignocellulosic fillers and polymer matrices, but the overall properties obtained are not so remarkable.

Reactive extrusion (REX) allows polymers to react during the extrusion process through the formation of free radicals, whose formation can be catalyzed by organic peroxides [21]. In this context, dicumyl peroxide (DCP) has been widely reported as an excellent free radical initiator, which facilitates the reaction of polymers with functional groups, which is especially useful in the case of low miscibility physical blends such as, polylactide/poly(butylene adipate-*co*-terephthalate) (PLA/PBAT) [22] and poly(3-hydroxybutyrate) and poly(ϵ -caprolactone) blends [23], among others. Not only has DCP been used in polymer blends, but also in polymer-fiber composites, as it is the case of the work reported by Ahmad *et al.* [24], which shows a clear improvement in the interactions between PE and sisal fiber for a concentration of DCP of 1 phr (parts by weight of DCP per hundred weight parts of the base polymer) during REX.

Mango (*Mangifera indica* L.) is one of the most popular fruits in the planet, as it is the fifth largest major fruit crop when it comes to world production [25]. There are several varieties that are quite marketable because of their flavour and taste. The main wastes from this fruit are the exocarp (peel), the endocarp (pit or stone) and the kernel or seed. Mango peel has been reported to be a lignocellulosic compound with high polyphenol content [26], while the mango kernel is mainly composed of starch, protein and fatty acids [27]; on the other hand, the endocarp (pit or stone) is rich in cellulose, hemicelluloses and lignin [28]. Considering the circular economy concept, this makes

mango one of the most interesting wastes to take benefit from, being one of its applications to develop wood plastic composites with additional functional properties, and at a more competitive cost. Moreover, mango wastes have not been greatly reported in literature for producing wood plastic composites.

Considering that there are hardly any investigations regarding the use of mango wastes as fillers for green composites. So, the main aim of this work is to develop wood plastic composites with partially biobased polypropylene (bioPP) as the polymer matrix and mango peel flour (MPF) as a novel reinforcing component, in order to reduce the cost of the polymer and, at the same time, improving its properties. The leading obstacle and challenge in this study is the difference in polarity and hydrophilicity between the filler and the matrix, since bioPP is a highly non-polar polymer while MPF, being a lignocellulosic filler, is a highly polar component. To overcome this issue, an environmentally friendly grafted copolymer of polypropylene and itaconic acid (PP-g-IA) is obtained by reactive extrusion (REX) with dicumyl peroxide as free radical initiator. Several formulations have been developed by extrusion (REX in the case of DCP) and injection moulding to give composites of bioPP with MPF, with improved properties by using PP-g-IA and DCP both individually and in combination. Then, the properties of these composites have been evaluated by means of mechanical, morphological, thermal, thermomechanical, colorimetric, chemical and wettability characterization.

MATERIALS AND METHODS

Materials

Bio based polypropylene was supplied by NaturePlast (Caen, France).

Mangoes from the Palmer-Kent variety were purchased from the local market in Alcoy, Spain. Mangoes were peeled and the peels were first dried at 50 °C for 48 h in a dehumidifying stove (MCP Vacuum Casting System, Lubeck, Germany) to remove any residual moisture. The peels were then crushed and milled in a ZM 200 centrifugal mill from Retsch (Düsseldorf, Germany) at a speed of 8000 rpm and finally sieved with a 250 µm mesh filter, obtaining the mango peel flour (MPF). MPF particles show a rough surface with an average length of 50 µm and an average width of 15 µm.

Dicumyl peroxide (DCP) 98% was supplied by Sigma Aldrich (Product Code: 1003031352) and itaconic acid (IA) 99+% was supplied by Acros Organics (Product Code: 122810010).

Grafting of PP-g-IA

Itaconic acid grafting process was performed following the methodology described by Pesetskii *et al.* [18], using DCP as initiator. BioPP, IA and DCP were dried at 40 °C for 48 h in a dehumidifying dryer MDEO to remove any residual moisture prior to processing. Then 1 wt.% of IA was blended with bioPP and 0.2 wt.% DCP, according to the study carried out by Pesetskii *et al.* [18]. The grafting was conducted using a twin-screw extruder from Construcciones Mecánicas Dupra, S.L. (Alicante, Spain). This extruder has a 25 mm diameter with a length-to-diameter ratio (L/D) of 24. Residence time of the compounds in the extruder was 4 minutes approximately. The temperature profile from the hopper to the extrusion die was 175-195-195-195 °C. After the extrusion, the PP-g-IA was pelletized using an air-knife unit.

Preparation of bioPP/MPF composites

BioPP, MPF, PP-g-IA and DCP were initially dried at 40 °C for 48 h in a dehumidifying dryer MDEO to remove residual moisture. Then, each formulation was mixed according to **Table III.1.2.1**. The corresponding formulations were compounded in a twin-screw extruder from Construcciones Mecánicas Dupra, S.L. (Alicante, Spain). This extruder has a 25 mm diameter with a length-to-diameter ratio (L/D) of 24. The extrusion process was carried out at a rate of 22 rpm, using the following temperature profile (from the hopper to the die): 150-155-160-165 °C. The compounded materials were pelletized using an air-knife unit. In all cases, residence time was approximately 1 min. **Table III.1.2.1** shows the compositions of the formulations developed in this work.

Table III.1.2.1. Summary of compositions according to the weight content (wt.%) of bioPP/MPF and different compatibilizers and additives.

Code	BioPP (wt.%)	MPF (wt.%)	PP-g-IA (phr)*	DCP (phr)
bioPP	100	0	0	0
bioPP/MPF	70	30	0	0
bioPP/MPF/PP-g-IA	70	30	3	0
bioPP/MPF/DCP	70	30	0	1
bioPP/MPF/PP-g-IA/DCP	70	30	3	1

*phr stands for the weight part of PP-g-IA or DCP per one hundred weight parts base bioPP/MPF composite.

To shape pellets into standard samples, a Meteor 270/75 injection moulding machine from Mateu & Solé (Barcelona, Spain) was used. The temperature profile in the injection moulding unit was 155 °C (hopper), 160 °C, 165 °C, and 170 °C (injection nozzle). A clamping force of 75 tons was applied while the cavity filling and cooling times were set to 1 and 10 s, respectively. Standard samples for mechanical and thermal characterization with an average thickness of 4 mm were obtained.

Characterization of bioPP/MPF blends

Grafting efficiency

Grafting efficiency (ratio of the grafted IA related to its total quantity added to the polymer) was measured by infrared spectroscopy according to the method used by Pesetskii *et al.* [29]. Films of 30-40 µm thickness were molded from pellets of PP-g-IA at 145 °C. Then the films were immersed in ethanol at 70 °C in order to extract the ungrafted itaconic acid. Grafting efficiency was estimated from the variation in absorbance of the films at 1720 cm⁻¹, which corresponds to carbonyl groups. The absorbance of the films was measured at different times from the immersion of the films in ethanol (0, 1, 2, 4, 6, 8, 22, 24 and 27 h). The grafting efficiency was determined using **Equation III.1.2.1**:

$$\text{Grafting efficiency (wt. \%)} = \frac{D_{\tau}}{D_0} 100 \quad (\text{III. 1.2.1})$$

where D_{τ} and D_0 stand for the optical densities related to the thickness of the film once all the ungrafted IA has been extracted and at the initial time before immersion in ethanol, respectively.

Mechanical characterization

Tensile properties of bioPP/MPF composites were obtained in an universal testing machine ELIB 50 from S.A.E. Ibertest (Madrid, Spain) as recommended by ISO 527-1:2012. A 5-kN load cell was used while the cross-head speed was set to 5 mm/min. Shore hardness was measured in a 676-D durometer from J. Bot Instruments (Barcelona, Spain), using the D-scale, on rectangular samples with dimensions 80×10×4 mm³, according to ISO 868:2003. The impact strength was also studied on injection-moulded

rectangular samples with dimensions of 80×10×4 mm³ in a Charpy pendulum (1-J) from Metrotec S.A. (San Sebastián, Spain) on notched samples (V-notch type with a radius of 0.25 mm), following the specifications of ISO 179-1:2010. All mechanical tests were performed at room temperature, and at least 6 samples of each material were tested, and the corresponding tensile parameters were averaged.

Morphology characterization

The morphology of fractured samples from Charpy tests, obtained from the impact tests, was studied by field emission scanning electron microscopy (FESEM) in a ZEISS ULTRA 55 microscope from Oxford Instruments (Abingdon, United Kingdom). Before placing the samples in the vacuum chamber, they were sputtered with a gold-palladium alloy in an EMITECH sputter coating SC7620 model from Quorum Technologies, Ltd. (East Sussex, UK). The FESEM was operated at an acceleration voltage of 2 kV.

Thermal analysis

The most relevant thermal transitions of bioPP/MPF composites were obtained by differential scanning calorimetry (DSC) in a Mettler-Toledo 821 calorimeter (Schwerzenbach, Switzerland). Samples with an average weight of 6-7 mg, were subjected to a thermal program divided into three stages: a first heating from -50 °C to 200 °C followed by a cooling to 0 °C, and a second heating to 300 °C. Both heating and cooling rates were set to 10 °C/min. All tests were run in nitrogen atmosphere with a flowrate of 66 mL/min using standard sealed aluminum crucibles with a capacity of 40 µL.

$$X_c = \left[\frac{\Delta H_m}{\Delta H_m^0 \cdot (1 - w)} \right] \cdot 100 \quad (\text{III. 1.2.2})$$

where $\Delta H_m^0 = 198 \text{ J/g}$ is the theoretical enthalpy of a 100% crystalline PP sample [30], the term $1-w$ corresponds to the PP weight fraction in the blend, and ΔH_m is the measured melting enthalpy.

The thermal degradation of the bioPP/MPF composites was assessed by thermogravimetric analysis (TGA). TGA tests were performed in a LINSEIS TGA 1000

(Selb, Germany). Samples with a weight of 15-17 mg were placed in 70 μ l alumina crucibles and subjected to a dynamic heating program from 40 °C to 700 °C at a heating rate of 10 °C/min in nitrogen atmosphere. The first derivative thermogravimetric (DTG) curves were also determined. All tests were carried out at least three times in order to obtain reliable results.

Dynamical-mechanical thermal characterization

Dynamical mechanical thermal analysis (DMTA) was carried out in a DMA1 dynamic analyzer from Mettler-Toledo (Schwerzenbach, Switzerland), working in single cantilever flexural conditions. Rectangular samples with dimensions 20×6×2.7 mm³ were subjected to a dynamic temperature sweep from -150 °C to 100 °C at a constant heating rate of 2 °C/min. The selected frequency was 1 Hz and the maximum flexural deformation or cantilever deflection was set to 10 μ m.

Water absorption test

The water absorption capacity of the bioPP/MPF composites was evaluated by the water uptake method. Rectangular samples with dimensions 80×10×4 mm³ were first weighted in a balance and then put inside a beaker filled with distilled water, all of them wrapped with tiny pieces of a metal grid so they could sink. After that, the weight of all samples was measured at intervals of several hours the first day, and then measured each week for a total period of 14 weeks in order to evaluate the amount of absorbed water. In every measurement, the moisture in the surface of the samples was removed with tissue paper.

Infrared spectroscopy

Chemical characterization of the bioPP/MPF composites was carried out by attenuated total reflection-Fourier transform infrared spectroscopy (ATR-FTIR). Spectra were recorded using a Bruker S.A Vector 22 (Madrid, Spain) coupled to a PIKE MIRacle™ single reflection diamond ATR accessory (Madison, Wisconsin, USA). Data were collected as the average of 10 scans between 4000 and 500 cm⁻¹ with a spectral resolution of 2 cm⁻¹.

Melt flow index

A melt flow indexer extrusion plastometer from Metrotec (Lezo, Spain) with a cut-off mechanism was used for melt flow index determination. The load mass was set at 2.16 kg and the temperature was established at 190 °C. Approximately, 20 g of each sample were put into the indexer, and after two minutes of heating, the load was charged, and the material started to flow. 30 seconds intervals, after which the cut-off mechanism was activated, were set to take samples of each material and calculate their mass. 5 tests were carried out for each blend.

RESULTS AND DISCUSSION

Grafting efficiency of PP-g-IA

Figure III.1.2.1 shows the variation of absorbance in the 1720 cm^{-1} band through 27 hours of extraction in ethanol solution at 70 °C for PP-g-IA. The absorbance presented is related to the thickness of the film used in the test. Absorbance drastically decreases in the first hour of extraction, and then it starts to stabilize until at 22 hours it becomes constant at a value of 1.87. This reduction in absorbance is ascribed to the removal of the ungrafted IA in the film, which is released into the ethanol solution, only remaining the true grafted IA in the PP-g-IA copolymer. A very similar extraction profile was observed by Pesetskii *et al.* [29] when studying the grafting efficiency of IA in LDPE-g-IA copolymer. Using **Equation III.2.1.1**, the grafting efficiency of PP-g-IA was calculated, giving a value of $82.12 \pm 1.83\%$. This proves that the grafting was successfully carried out, with most of the itaconic acid having reacted with bioPP in the reactive extrusion (REX) process. Pesetskii *et al.* [29] observed a very similar IA grafting efficiency of approximately 85% for a concentration of DCP of 0.2 wt.% in the reactive extrusion, which is the same proportion used in this study. Considering that reactive extrusion is a process easy to take into industrial scale, this fact in combination with the high grafting efficiency obtained makes PP-g-IA a compatibilizer that would be easy to produce not only at laboratory level, but also at industrial level. Moreover, since itaconic acid is obtained from biosourced citric acid, which is widely available at a relative low cost, grafting with itaconic acid can be a cost-effective process, compared to traditional grafting with maleic anhydride.

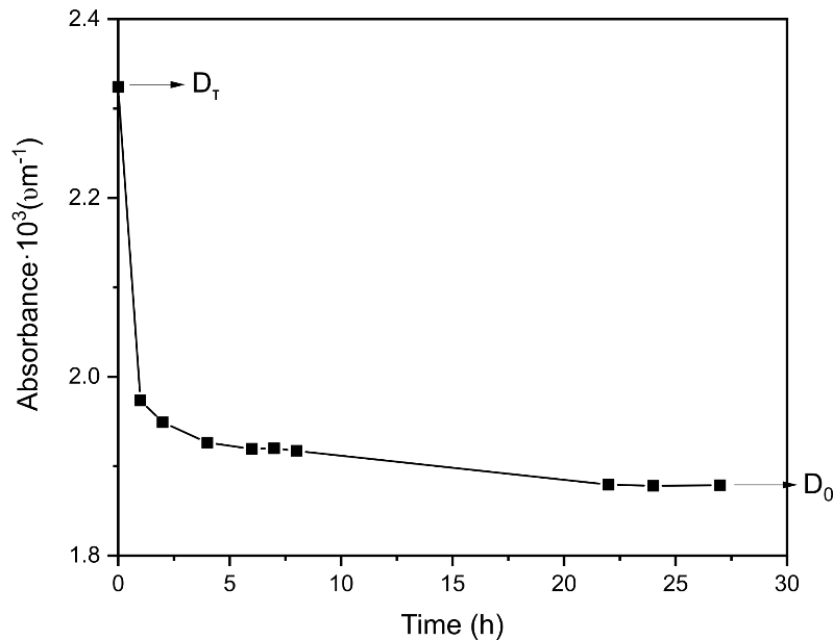


Figure III.1.2.1. Variation of the optical density of the carbonyl groups absorption bands (1720 cm^{-1}) with extraction time in ethanol.

Mechanical Properties

Table III.1.2.2 gathers the results concerning the mechanical properties of bioPP/MPF composites with DCP and PP-g-IA.

Table III.1.2.2. Summary of mechanical properties of the injection-moulded samples of bioPP/MPF composites. Tensile modulus (E), maximum tensile strength (σ_{max}), elongation at break (ϵ_b), Shore D hardness, and impact (Charpy) strength.

Code	E (MPa)	σ_{max} (MPa)	ϵ_b (%)	Shore D hardness	Impact strength (kJ/m ²)
bioPP	1936 ± 211	17.71 ± 0.77	38.96 ± 1.26	62.4 ± 0.6	9.95 ± 0.59
bioPP/MPF	1758 ± 105	11.64 ± 0.30	15.98 ± 1.63	61.7 ± 0.6	2.83 ± 0.33
bioPP/MPF/PP-g- IA	2237 ± 149	13.51 ± 0.13	18.86 ± 1.3	61.3 ± 0.4	2.80 ± 0.19
bioPP/MPF/DCP	2280 ± 191	14.17 ± 0.23	28.13 ± 1.67	63.6 ± 1.4	3.63 ± 0.43
bioPP/MPF/PP-g- IA/DCP	2349 ± 170	14.39 ± 0.25	29.69 ± 1.63	63.6 ± 0.8	3.78 ± 0.19

It can be seen how neat bioPP showed a tensile modulus (E) of 1936 MPa, a maximum tensile strength of 17.71 MPa and an elongation at break of 38.96%. These values are in accordance with the results reported by Zhou *et al.* [11], who reported a

value for E modulus of 1890 MPa. Those values show that bioPP is a ductile material, but with greater stiffness than biopolyethylene [1]. The addition of MPF in the biopolymer matrix clearly reduces all mechanical properties. The tensile modulus and strength are reduced down to 1758 MPa and 11.64 MPa, respectively, while elongation at break is reduced down to 15.98%, which is a reduction of more than 50% in relation to neat bioPP. This reduction could be ascribed to a lack of interaction between MPF and bioPP, since MPF is a lignocellulosic compound rich in polyphenols [26], and hence, with a high number of hydroxyl groups, while bioPP is a non-polar biopolymer, with no functional groups to interact with MPF [31]. This fact leads to a poor interaction of the MPF particles into the bioPP matrix, thus decreasing its mechanical cohesive properties, mainly the tensile strength and the elongation at break. A similar trend was observed by Yadav *et al.* [32] in PP composites with wood flour, which decreased its tensile strength by 15%. The addition of PP-*g*-IA in the bioPP/MPF composite increases all of its tensile properties, reaching a tensile modulus of 2237 MPa, a tensile strength of 13.51 MPa, and an elongation at break of 18.86%. These results suggest that PP-*g*-IA effectively acts as a compatibilizer, increasing the affinity and interaction of the MPF particles with the surrounding bioPP matrix, even surpassing the tensile modulus (E) of neat BioPP. A similar behaviour was observed by Poletto *et al.* [33] in PP/wood flour composites. Nevertheless, the most important thing is that addition of PP-*g*-IA, leads to an increase in both cohesive properties, the tensile strength and the elongation at break which is a clear evidence of the effectiveness of the PP-*g*-IA compatibilizer in comparison with the most commonly used PP-*g*-MA compatibilizer. Andréia *et al.* [34] studied the effect of PP-*g*-MA in PP/coir fiber composites, showing that PP-*g*-MA increased tensile strength but drastically reduced elongation at break (1.3%). This fact clearly demonstrates that PP-*g*-IA proves to be a superior compatibilizer in PP/lignocellulosic composites. The addition of DCP during REX of bioPP/MPF composites increases all the mechanical properties even more than PP-*g*-IA, leading to a tensile modulus of 2280 MPa, a tensile strength of 14.17 MPa and a clear interesting, improved elongation at break of 28.13%. This increase in the mechanical response is representative of the crosslinking effect that DCP exerts over the polymer chains with the lignocellulosic filler, thus giving support to the compatibilization between both components. DCP promotes free radical formation on both bioPP polymer chains and the different compounds in MPF, thus allowing a wide variety of reactions between them, improving the interaction between bioPP and MPF. Some studies have reported the ability of DCP to induce free radical reaction between polymers, such as low-density polyethylene (LDPE), and cellulose fibers [35]. Considering that MPF has cellulose in its chemical composition, the obtained

results are consistent with previous studies. Therefore, demonstrating the strengthening effect of DCP over the blend. Finally, the bioPP/MPF/PP-g-IA/DCP composite offers the best tensile mechanical properties of all developed composites, even besting neat bioPP in terms of tensile modulus, changing from 1936 to 2349 MPa, which is an increase of 21.33% in relation to neat bioPP. Tensile strength and elongation at break state at 14.39 MPa and 29.69%, respectively, which are not so far from neat BioPP values. These results suggest some synergetic effect between DCP and PP-g-IA, which achieve better mechanical properties than when used separately. It can be concluded that the interaction of MPF with bioPP polymer chains is enhanced by the combined effect of both DCP and PP-g-IA.

Regarding Shore D hardness, all the bioPP-based composites tested in this study showed values in the 61-64 range. Neat bioPP presented a hardness of 62.4, which is slightly lower than that reported by Caraschi *et al.* [36] for neat PP. The addition of MPF seems to slightly decrease the hardness of bioPP, although it is not a significant reduction. This agrees with the tensile properties reported previously, as a reduction in the stiffness of the material is responsible for lowered resistance to deformation. The addition of PP-g-IA did not significantly vary the hardness of the base composite. On the other hand, composites obtained by REX with DCP showed a slight increase in hardness up to 63.6 for both of them. This slight increase in hardness also remarks the improved interactions between bioPP and MPF. Compatibilization also prevents aggregate formation and improves the overall mechanical response of bioPP/MPF composites. Finally, impact strength was highly affected by the addition of MPF, PP-g-IA and DCP. Neat bioPP exhibited an impact strength of 9.95 kJ/m² on notched samples, which is indicative of a ductile material, as previously observed by elongation at break. Addition of MPF into the bioPP matrix significantly reduced the impact strength down to 2.83 kJ/m². It is important to bear in mind that the impact strength is also a mechanical property related to cohesion. This large decrease could be ascribed to an embrittlement of the material as a result of MPF aggregates that would lead to stress concentration phenomena [37]. The addition of PP-g-IA copolymer into the blend does not improve the impact strength, with values around 2.8 kJ/m². On the other hand, REX with DCP does increase the impact strength up to 3.63 and 3.78 kJ/m² for bioPP/MPF/DCP and bioPP/MPF/PP-g-IA/DCP, respectively, which also reflects some synergistic effect by using PP-g-IA and DCP during REX compounding. This increase in relation to uncompatibilized bioPP/MPF could be related to the effect of DCP, which enhances the adhesion and dispersion of MPF in the biopolymer matrix and, probably, provides a better particle-matrix interface interaction. Sari *et al.* [38] reported how the impact

strength of pandanwangi fiber reinforced polyethylene composites increased with the content of DCP during REX.

All in all, these results point out to the fact that PP-g-IA and DCP act as excellent compatibilizers for MPF and bioPP by REX, highly increasing the overall mechanical response of the bioPP/MPF blend, and even surpassing neat bioPP in terms of tensile modulus.

Morphology of bioPP/MPF composites

The mechanical properties of these composites are strongly related to their internal structure. **Figure III.1.2.2** shows the field emission scanning electron microscopy (FESEM) images at 1000x magnification of the fractured surface of impact test samples from uncompatibilized and compatibilized bioPP/MPF composites. **Figure III.1.2.2a** corresponds to neat bioPP, and it shows the typical cavernous surface with high roughness, which is ascribed to the plastic deformation of the polymer, indicating ductile behaviour [39]. When MPF was added to the polymer matrix, the lignocellulosic particles presented poor adhesion in the case of the uncompatibilized bioPP/MPF composite (**Figure III.1.2.2b**), which is clearly demonstrated by the huge gap between the MPF particles and the surrounding bioPP matrix. This is ascribed to the low interaction between these two components as a result of bioPP being non-polar, and MPF being highly polar. Nagmouchi *et al.* [40] observed the same phenomenon when studying the compatibility of olive stone flour (OSF) lignocellulosic particles with a polypropylene matrix, observing gaps between the fillers and the matrix. This corroborates the poor mechanical properties reported in the mechanical section. The addition of PP-g-IA into the bioPP/MPF composite (**Figure III.1.2.2c**) clearly improves the material cohesion between the MPF lignocellulosic particles and the bioPP matrix, which can be deduced from a reduction in the gap between both components. Toro *et al.* [41] reported the improvement in compatibility and resistant mechanical properties of PP with mineral fillers by compatibilizing with PP-g-IA. This is ascribed to the dual functionality of PP-g-IA. On the one hand PP chains can interact with the bioPP matrix while the polar IA groups can interact with the hydroxyl groups in MPF [42]. REX with DCP (**Figure III.1.2.2d**) exhibited even a better compatibility between MPF particles and the surrounding bioPP, as MPF particles are quite embedded into the polymer matrix and present a very narrow gap between them, increasing their mechanical performance. This fact is indicative of the reactive compatibilization that DCP exerts over lignocellulosic particles and the bioPP matrix during reactive extrusion, as it has been

mentioned in the mechanical properties section. Finally, **Figure III.1.2.2e** shows the FESEM image for the bioPP/MPF/PP-g-IA/DCP composite. In this case, the particle-matrix gap seems almost inexistent, which again points out to the fact that the combination of PP-g-IA and DCP during REX provides a synergistic compatibilization effect.

All in all, the observed morphologies are in total agreement with the mechanical properties above-mentioned, demonstrating that PP-g-IA and DCP act as high-performance compatibilizing system that can overcome the lack of compatibility between non-polar bioPP matrix and the dispersed polar MPF particles.

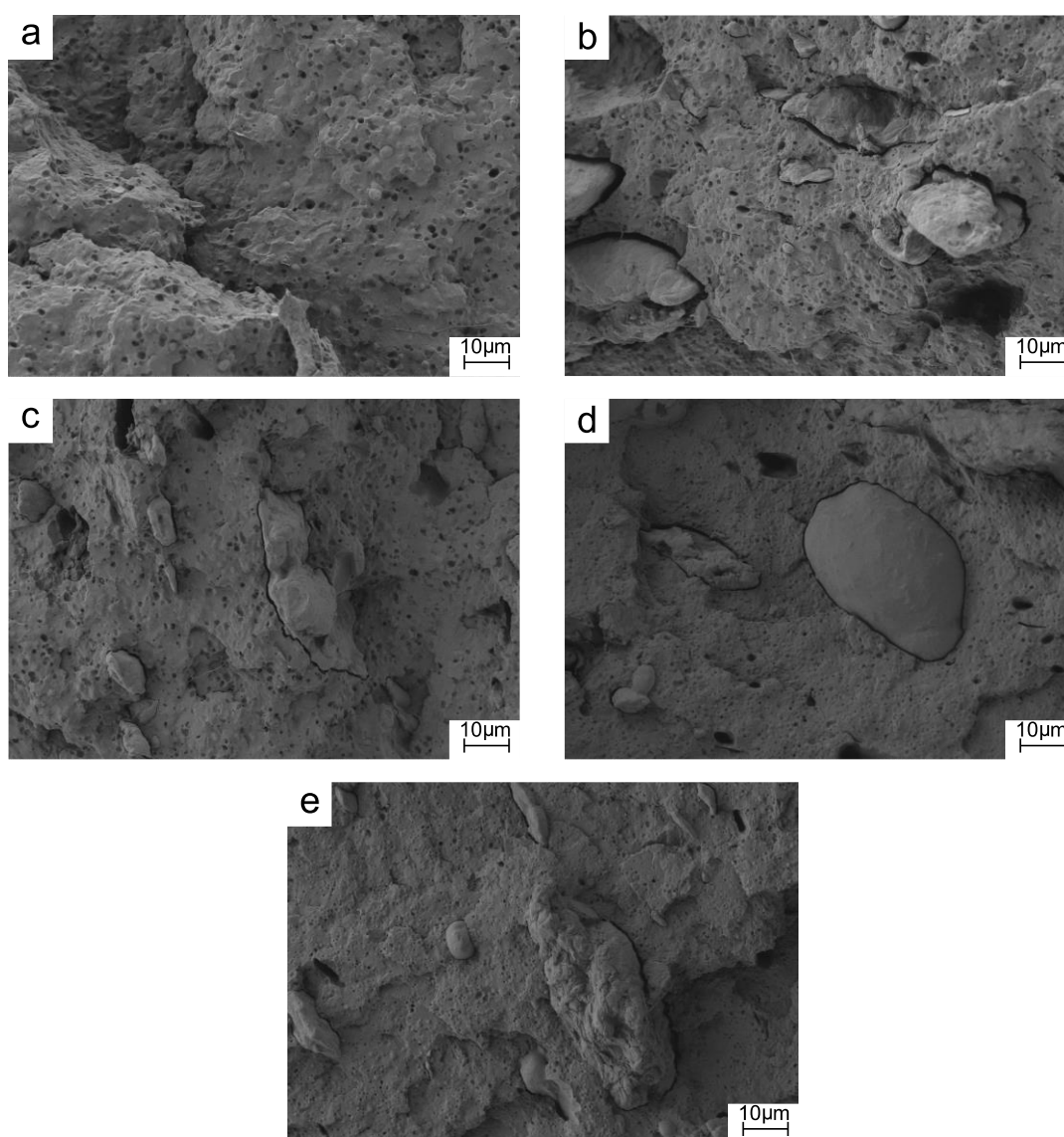


Figure III.1.2.2. Field emission scanning electron microscopy (FESEM) images at 1000 \times of the fractured surfaces of: (a) bioPP; (b) bioPP/MPF; (c) bioPP/MPF/PP-g-IA; (d) bioPP/MPF/DCP; (e) bioPP/MPF/PP-g-IA/DCP.

Thermal Properties of bioPP/MPF blends

Table III.1.2.3 gathers the main thermal parameters corresponding to the DSC second heating cycle from 0 to 300 °C of the studied samples (melting temperature T_m , melting enthalpy ΔH_m and the degree of crystallinity X_C). Only the melting temperature can be observed in the temperature range presented here, due to the glass transition temperature of bioPP being very low (-50 - 10 °C) [43]. This transition will be further studied by DMTA analysis. Neat bioPP shows a melting temperature of 164 °C and a degree of crystallinity (X_C) of 42.6%. These values are quite similar to the values reported by Shafigullin *et al.* [30] and typical of polypropylene. The incorporation of mango peel flour into the polymer matrix slightly reduces the melting point down to 161.9 °C, which is ascribed to the intrinsic low thermal stability of the lignocellulosic filler. On the other hand, crystallinity increases up to 50.0%, which is because MPF particles can induce heterogeneous nucleation and promote the crystallization process [44]. With the addition of PP-g-IA, melting temperature slightly increases related to the previous sample, which could be ascribed to a dilution effect towards MPF, as PP-g-IA, despite being less thermally stable than bioPP, is more thermally stable than the lignocellulosic particles [45]. The degree of crystallinity also increases, up to 58.0%. This could be related to a positive compatibilization of the MPF particles with bioPP thanks to PP-g-IA, which improves the particle dispersion all over the matrix, enhancing the heterogeneous nucleation phenomenon. The use of REX with DCP during compounding of bioPP/MPF composites leads to a decrease in the melting temperature down to 158.1 °C. This effect was also observed by Ahmad *et al.* [24], who attributed this phenomenon to a decrease in the size of the crystallites and thinner lamella. The degree of crystallinity remained very similar to that of bioPP/MPF, so it can be inferred that REX with DCP only affects the size and shape of the crystals, but the total amount remains almost unaltered. This phenomenon was also observed by Ahmad *et al.* [24]. Finally, the composite compatibilized with a combination of DCP and PP-g-IA by REX, presents a similar melting temperature compared to the previous sample and a degree of crystallinity of 50.2%, which is the second highest crystallinity degree of all composites developed in this work. This could be ascribed to the combined compatibilizing effect of PP-g-IA and DCP during REX.

Table III.1.2.3. Melting temperature (T_m), melting enthalpy (ΔH_m) and degree of crystallinity (X_C) of bioPP/MPF composites with different compatibilization strategies, obtained by differential scanning calorimetry (DSC). Main thermal degradation parameters of bioPP/MPF composites with different compatibilization strategies in terms of the onset degradation temperature at a mass loss of 5 wt.% ($T_{5\%}$), maximum degradation rate (peak) temperature (T_{deg}), and residual mass at 700 °C.

Samples	DSC Parameters			TGA Parameters		
	T_m (°C)	ΔH_m (J/g)	X_C (%)	$T_{5\%}$ (°C)	T_{deg} (°C)	Residual weight (%)
bioPP	164.0 ± 2.1	84.4 ± 1.1	42.6 ± 0.4	272.8 ± 0.8	382.3 ± 2.4	0.3 ± 0.1
bioPP/MPF	161.9 ± 1.9	69.4 ± 0.6	50.0 ± 0.5	182.4 ± 1.1	417.9 ± 1.3	0.1 ± 0.1
bioPP/MPF/PP-g-IA	162.1 ± 2.0	78.0 ± 0.9	58.0 ± 0.5	208.4 ± 1.4	398.9 ± 1.8	0.1 ± 0.2
bioPP/MPF/DCP	158.1 ± 1.8	67.9 ± 1.5	49.5 ± 0.3	168.4 ± 0.5	429.4 ± 2.2	0.2 ± 0.2
bioPP/MPF/PP-g-IA/DCP	157.9 ± 2.4	69.8 ± 1.3	52.4 ± 0.4	177.4 ± 1.2	417.4 ± 1.0	0.1 ± 0.1

Table III.1.2.3 also gathers the main quantitative parameters regarding the thermal degradation behavior of the bioPP/MPF composites obtained by thermogravimetric (TGA) curves and their first derivatives (DTG). First, bioPP showed the typical single stage degradation profile of a polyolefin, with an onset degradation temperature (measured at 5 wt.% mass loss, $T_{5\%}$) of 272.8 °C while the maximum degradation rate temperature (T_{deg}) is located at 382.3 °C. After the degradation process, the residual mass was 0.3 wt.%. Essabir *et al.* [46] reported a similar degradation profile for PP in a study related to the addition of nut shells of argan particles into a PP polymer matrix. Totally in contrast, the addition of MPF into the bioPP matrix provokes the degradation to occur in three main stages, ascribed to the lignocellulosic nature of the MPF. The first stage in the range 280-340 °C is related to the thermal depolymerization of hemicellulose and pectin. The second one which comprises the temperature range of 340-448 °C corresponds to the degradation of the cellulose contained in the MPF particles, and the last one, in the range 448-500 °C is associated with the progressive degradation of lignin [46]. This degradation profile is observed in all the samples with MPF. In this case the onset degradation temperature is 182.4 °C and the maximum degradation rate temperature is 417.9 °C. Interestingly, the composite with bioPP and MPF starts to degrade more rapidly than bioPP, but then presents more thermal stability than bioPP and delays the maximum degradation peak by 30 °C. This is because hemicellulose and pectin are poorer in terms of thermal stability than bioPP, while cellulose, and lignin possess higher thermal stability than the polyolefin [47]. When PP-g-IA is added into the bioPP/MPF composite, the onset degradation temperature moves

up to 208.4 °C, and the degradation temperature goes down to 398.9 °C in relation to the bioPP/MPF composite. These results suggest that PP-g-IA slightly reduced the thermal stability of the base bioPP/MPF composite in the final temperature range, which corroborates the results observed by DSC. A similar behavior was observed by Kim *et al.* [48] in PP/PP-g-IA composites with different contents of PP-g-IA from 1 to 10 wt.%. However, this composite shows greater thermal stability than neat bioPP, with a maximum degradation peak located at 398.9 °C. This result is in accordance with the increase in crystallinity observed by DSC. Comparing PP-g-IA with other studies that use PP-g-MA instead, the herein used compatibilizer improves the thermal stability at the first stages of degradation, which is the opposite to what was observed by Andréi *et al.* [34], whose study showed that PP-g-MA reduced the initial degradation temperature of PP/coir fiber composites with 30 wt.% of lignocellulosic filler. Similarly, REX with DCP reduces the thermal stability in the first stages of the degradation profile, with a $T_{5\%}$ of 168.4 °C. Nonetheless, it delays the most prominent degradation stage up to 429.4 °C. This observation perfectly matches the results obtained by DSC, where crystallinity of BioPP was increased due to REX with DCP. The combination of PP-g-IA and DCP during REX of bioPP/MPF composites gives similar results in comparison to BioPP/MPF sample. Nonetheless, they improve the overall thermal stability of the composite in almost all the temperature range.

Dynamic-Mechanical Behaviour of bioPP/MPF composites

The thermomechanical properties of bioPP/MPF composites were studied by DMTA in a temperature range from -150 to 100 °C. **Table III.1.2.4** gathers the main thermomechanical parameters extracted from the evolution of the storage modulus, E' and the dynamic damping factor $\tan \delta$. Regarding neat bioPP an initial decrease of the storage modulus can be seen until -60 °C approximately. Then, a more pronounced decrease happens until 0 °C. Both decreases will be explained in the next paragraph. BioPP exhibits a storage modulus of 2318, 1674 and 277 MPa at -100, -25 and 80 °C, respectively. This decrease in storage modulus is provoked by a softening of the polymer matrix. García-García *et al.* observed a similar thermomechanical profile for neat PP [49]. The addition of MPF increases the stiffness of the material up to 2563 and 1862 MPa at -100 and -25 °C, respectively. This is due to the presence of a rigid filler that induces mechanical restraint, which reduces the mobility of the polymer chains of bioPP [49]. The addition of PP-g-IA increases even more the stiffness of the composite, which is ascribed to the positive compatibilizing effect of the PP-g-IA copolymer, demonstrating

the improvement in mechanical properties shown in the mechanical results section. DCP increases the rigidity of the materials in almost all the temperature range, showing a value of 1774 MPa in comparison with 1674 MPa of neat bioPP at -25 °C. Mishra *et al.* [50] observed how REX with DCP increased the storage modulus of LDPE-nanosilica composites. Finally, the combination of PP-g-IA and DCP during REX, offers similar values to the bioPP/MPF/PP-g-IA sample.

With regard to the dynamic damping factor $\tan \delta$, it allows to determine the different relaxations that occur in the polymer matrix along all the temperature range. As it has been aforementioned, two main relaxation peaks are observed for neat bioPP, a less intensive β -relaxation, which appears at -44.9 °C; and α -relaxation, which is shown at 14.2 °C. The former is related to the mobility devitrification of -CH₂- groups in the main chain, while the latter is ascribed to the glass transition temperature of the polymer according to the study of Krivoguz *et al.* [51]. The addition of MPF decreases both relaxation temperatures down to -49 and 11.9 °C, respectively. This is probably due to an inefficient dispersion of the MPF particles in the polymer matrix, which does not allow a positive restriction of chain mobility [49]. On the contrary, the incorporation of PP-g-IA and REX with DCP provides a slight increase in the glass transition temperature. Addition of PP-g-IA copolymer leads to a T_g of 18.4 °C, which is mainly ascribed to the compatibilizing effect of the copolymer. Thus, it allows MPF particles to correctly disperse all over the polymer matrix, increasing the filler-matrix interface interactions, and restricting chain mobility. REX with DCP further increases the glass transition temperature up to 21.7 °C, due to the crosslinking effect DCP can provide, while the combination of PP-g-IA and DCP during REX, also delays the glass transition temperature by 15.8 °C in comparison with uncompatibilized bioPP/MPF. Thus, making the material more rigid. In general, the improvement in stiffness of all bioPP/MPF composites could be also related to the increase in crystallinity observed by DSC analysis.

Table III.1.2.4. Dynamic-mechanical properties of bioPP/MPF composites with different compatibilization strategies, at different temperatures.

Parts	E' (MPa) at -100 °C	E' (MPa) at -25 °C	E' (MPa) at 80 °C	β -relaxation T_g (°C)*	α -relaxation $(T_g)_{PP}$ (°C)*
bioPP	2318 ± 45	1674 ± 21	277 ± 7	-44.9 ± 1.3	14.2 ± 1.3
bioPP/MPF	2563 ± 33	1862 ± 27	239 ± 9	-49.0 ± 2.2	11.9 ± 2.2
bioPP/MPF/PP-g-IA	2575 ± 28	1976 ± 25	254 ± 5	-48.9 ± 2.1	18.4 ± 2.1
bioPP/MPF/DCP	2341 ± 32	1774 ± 30	210 ± 7	-49.3 ± 1.7	21.7 ± 1.7
bioPP/MPF/PP-g-IA/DCP	2544 ± 40	1939 ± 27	201 ± 8	-52.8 ± 1.5	15.8 ± 1.5

*The T_g has been measured using the $\tan \delta$ peak maximum criterion.

Wetting properties and water absorption of bioPP/MPF composites

One of the main drawbacks of wood plastic composites is their tendency to absorb water, as they contain high proportion of hydrophilic fillers. Contact angle measurements of a distilled water drop at different times (from 0 to 30 mins) have been carried out in order to evaluate the wetting properties of the developed composites. **Table III.1.2.5** gathers the water contact angle values at 0, 5, 10, 15, 20 and 30 minutes for uncompatibilized and compatibilized bioPP/MPF composites. At the initial time, all samples are quite hydrophobic, since their contact angles are around 90° and are far superior to the hydrophilic threshold according to Vogler, which is 65° [52]. These results were expected, as the base material, bioPP, is a highly non-polar polymer, being all its bonds formed by carbon and hydrogen (C-H). This non-polarity is what makes bioPP maintain a high contact angle over time, varying its contact angle from 88.4° at 0 minutes to 65.2° at 30 minutes. When adding MPF to bioPP matrix, the contact angle suffered quite a decrease at the initial time, going down to 79.4°, rapidly diminishing to 53.7° at 30 minutes. This decrease is ascribed to the polarity of the MPF particles, which have a high content in cellulose, hemicellulose, lignin and other phenolic compounds [53], all they having hydrophilic hydroxyl groups. These groups possess great affinity towards water, a polar solvent, thus increasing its absorption and decreasing the contact angle. Compatibilization with PP-g-IA copolymer seems to increase the hydrophobicity of the blend, maintaining the contact angle from 91.1° to 72.2° at 30 minutes. Although PP-g-IA should decrease the water contact angle due to the polar structure of itaconic acid (a carboxylic acid), this high hydrophobicity could be ascribed to certain esterification reaction between hydroxyl groups in MPF and itaconic acid, forming esters that somehow decrease the polarity of MPF particles [54], which is quite interesting from a practical point of view. Regarding compatibilization by REX with DCP, it does not

increase remarkably the water contact angle all over the time range in comparison to the uncompatibilized bioPP/MPF composite. This could be ascribed to the ability of DCP to increase polarity in these composites as a consequence of the reaction products obtained from the decomposition of DCP in the extruder, favoring radical formation, which could lead to crosslinking and branching, as it was observed by Rojas-Lema *et al.* [21]. Nonetheless, it gets a contact angle of 71.5 at 30 minutes, which is quite higher than that of bioPP/MPF. Finally, the bioPP/MPF/PP-g-IA/DCP composite exhibits intermediate values between the composite compatibilized with PP-g-IA copolymer and the composite obtained by REX with DCP, although the effect of PP-g-IA seems to prevail.

All in all, these results interestingly suggest that the addition of PP-g-IA and DCP during compounding by REX can solve the problem of hydrophilicity when adding natural organic particles into non-polar matrices (bioPP), even increasing its hydrophobicity up to a certain point. Therefore, this could lead to interesting applications, such as decking floors with water isolation properties, making them easier to be cleaned.

Table III.1.2.5. Contact angle (θ_w) of different bioPP/MPF composites with different compatibilization strategies at several times of exposure to distilled water: 0, 5, 10, 15, 20 and 30 minutes.

Code/time	0 min	5 min	10 min	15 min	20 min	30 min
bioPP	88.4 ± 2.3°	82.6 ± 3.1°	79.8 ± 1.5°	75.5 ± 2.2°	74.3 ± 2.0°	65.2 ± 1.6°
bioPP/MPF	79.4 ± 2.1°	75.1 ± 2.2°	69.6 ± 1.6°	65.4 ± 1.2°	62.8 ± 1.7°	53.7 ± 1.1°
bioPP/MPF/PP-g-IA	91.1 ± 2.9°	88.2 ± 2.6°	85.6 ± 3.0°	80.4 ± 2.2°	77.0 ± 1.3°	72.2 ± 1.4°
bioPP/MPF/DCP	81.2 ± 2.2°	77.9 ± 1.9°	75.5 ± 1.5°	74.2 ± 2.4°	71.9 ± 1.8°	71.5 ± 2.3°
bioPP/MPF/PP-g-IA/DCP	89.5 ± 2.3°	86.6 ± 3.2°	83.8 ± 1.8°	79.4 ± 2.8°	78.4 ± 4.1°	76.3 ± 2.9°

In addition to contact angle measurements, **Figure III.1.2.3** shows the water absorption profile of all the developed composites after a long immersion time into distilled water (14 weeks). First, it can be seen how neat bioPP did not absorb barely any water, presenting an asymptotic value of approximately 0.15 wt.% of water absorption in relation to its initial mass. This poor water absorption is ascribed to its non-polar nature, as it has been aforementioned, which makes bioPP to have low affinity for water (a polar solvent). A similar water absorption profile was observed by García-García *et al.* [49] for neat PP. The addition of MPF increases water absorption up to an asymptotic

value of 6.7 wt.%. This is mainly ascribed to hydrogen bonding formation between water molecules and hydroxyl groups present in cellulose and hemicellulose in MPF [55]. This fact makes MPF very affine towards water and thus, allows the composite to absorb great amounts of water. On the contrary, bioPP/MPF composites compatibilized with PP-g-IA reduces water absorption in the whole-time range down to approximately 3.7 wt.% after 14 weeks of immersion. This is probably due the fact that PP-g-IA can react with hydroxyl groups in MPF, reducing the total amount of free hydroxyl groups in the composite that can interact with water, thus reducing water absorption. García-García *et al.* [49] observed a very similar effect by the addition of PP-g-MA into a PP matrix with spent coffee grounds particles (SCG). On the other hand, REX with DCP does not reduce water absorption remarkably, reaching an asymptotic value of 5.7 wt.% water absorption after 14 weeks of immersion in water. This could be ascribed to the fact that the presence of DCP did not produce a great formation of free radicals during reactive extrusion, thus not impeding the contact between water molecules and cellulose based compounds in MPF [56]. Finally, the bioPP/MPF composite compatibilized by REX with both DCP and PP-g-IA presents a water absorption curve very similar to that of the previous sample, exhibiting an asymptotic value of 6.1 wt.% of water absorption at 14 weeks of water immersion. This implies that somehow, DCP inhibits the ability of PP-g-IA to reduce water absorption in a great extent, which could be ascribed to the fact that PP-g-IA reacts in a higher degree with bioPP rather than with MPF in this case, as a result of the crosslinking effect of DCP.

These results show that bioPP/MPF composites have great water absorption capabilities. Nonetheless, PP-g-IA is able to reduce water absorption down to half the water absorption of bioPP/MPF composite, which is an interesting property that could prove to be useful in applications where low interaction with water is needed, such as the production of floors, roofs or windows.

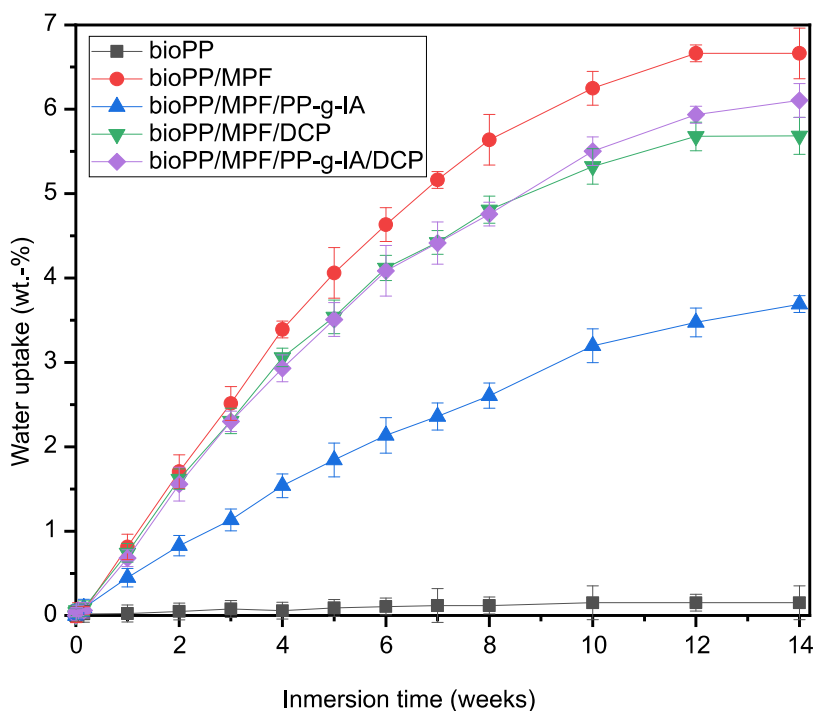


Figure III.1.2.3. Water uptake of uncompatibilized and compatibilized bioPP/MPF composites.

Infrared spectroscopy

FTIR technique is very useful to analyse the chemical interactions on composites developed in this study. **Figure III.1.2.4.a** shows the infrared spectra of MPF, PP-g-IA and DCP, while **Figure III.1.2.4.b** shows the spectra of uncompatibilized and compatibilized bioPP/MPF composites from 4000 to 500 cm^{-1} .

First, MPF presents a very typical spectrum of a lignocellulosic filler, with a very characteristic band at 3340 cm^{-1} , ascribed to the O-H stretching vibration and hydrogen bonding of hydroxyl groups, present in cellulose, hemicellulose, pectin and lignin. Then, another little peak at 2920 cm^{-1} , which is related to the C-H stretching vibration in CH and CH₂ in cellulose and hemicellulose [57]. The peak at 1730 cm^{-1} is attributed to the carbonyl C=O stretching vibration of carboxylic acid in lignin or ester groups in hemicellulose. The absorption band at 1450 cm^{-1} is related to the CH₂ symmetric bending in cellulose. An additional peak at 1230 cm^{-1} , attributed to the C-O stretching vibration of the acetyl group in lignin and hemicellulose could be observed [46]. The most intense band is located at 1030 cm^{-1} , ascribed to the CO and O-H stretching vibration in polysaccharides present in cellulose [58]. Next, the FTIR spectrum of PP-g-IA is very similar to that of neat bioPP, which will be commented in the next paragraph. The most remarkable band is located at 1720 cm^{-1} , which corresponds to the stretching vibration of the carbonyl groups of IA [45]. With regard to DCP, it exhibits several bands

characteristic of a peroxide: C-O-O and C-C-O antisymmetric stretching vibrations at 1265 cm^{-1} and 1250 cm^{-1} , respectively; symmetric stretching vibration of C-O-O at 1151 cm^{-1} ; deformation and rocking of CH_3 in isopropyl $-\text{C}(\text{CH}_3)_2-$ group at 1377, 1358 and 857 cm^{-1} ; and the presence of monosubstituted benzene rings at 1496, 1445 and 766 cm^{-1} [59].

Referring to the spectra of the bioPP/MPF composites, neat bioPP presents several representative bands. Absorption peaks at 972, 997 and 1165 cm^{-1} are indicative of $-\text{CH}_3$ rocking vibration. At 1375 cm^{-1} the symmetric bending vibration mode of $-\text{CH}_3$ is detected [60]. The peak at 2952 cm^{-1} is also ascribed to the methyl group, particularly to its asymmetric stretching vibration [60]. The bands at 1455, 2838 and 2917 cm^{-1} are related to the $-\text{CH}_2-$ symmetric bending, $-\text{CH}_2-$ symmetric stretching and $-\text{CH}_2-$ asymmetric stretching, respectively [61]. These peaks can be observed in all the composites, because bioPP is the base polymer of all the materials developed in this study. The addition of the lignocellulosic MPF filler alters the FTIR spectra, making some additional peaks that have been commented in the individual spectra of MPF to appear. The absorption peak at 3340 cm^{-1} , ascribed to the characteristic O-H stretching vibration and hydrogen bonding in hydroxyl groups, which are present in MPF compounds (cellulose, hemicellulose, pectin and lignin) [62]. The band at 1720 cm^{-1} , indicative of the carbonyl $\text{C}=\text{O}$ stretching vibration of linkage of carboxylic acid in lignin or in the ester group in hemicellulose [63]. The little shoulder that is located at 1600 cm^{-1} could be associated with water present in the particles [64], as they are highly hydrophilic. These bands commented for MPF are also present in all composites containing MPF. The FTIR spectra of the bioPP/MPF/PP-g-IA composite does not present hardly any differences in comparison with the uncompatibilized composite. The presence of dicumyl peroxide during extrusion and injection-molding processes did modify the FTIR spectra of the corresponding composites. First of all, at 1263 cm^{-1} an individual peak can be observed ascribed to the asymmetrical stretching of the C-C-O and C-O-O groups present in DCP. Next, another band at 1151 cm^{-1} is seen, related to the symmetric stretching of the C-C-O and C-O-O functionalizations, and the stretching of C-O. Finally, an intense peak at 761 cm^{-1} is ascribed to the presence of a monosubstituted benzene ring, which is characteristic of dicumyl peroxide [59]. All these bands have been also observed in the individual FTIR absorption spectrum of DCP. The composite compatibilized by REX with PP-g-IA and DCP (bioPP/MPF/PP-g-IA/DCP) presents practically all the peaks and bands aforementioned, although the peaks related to the radical free production of DCP are not so intense in this composite, probably due to certain interaction between PP-g-IA and DCP.

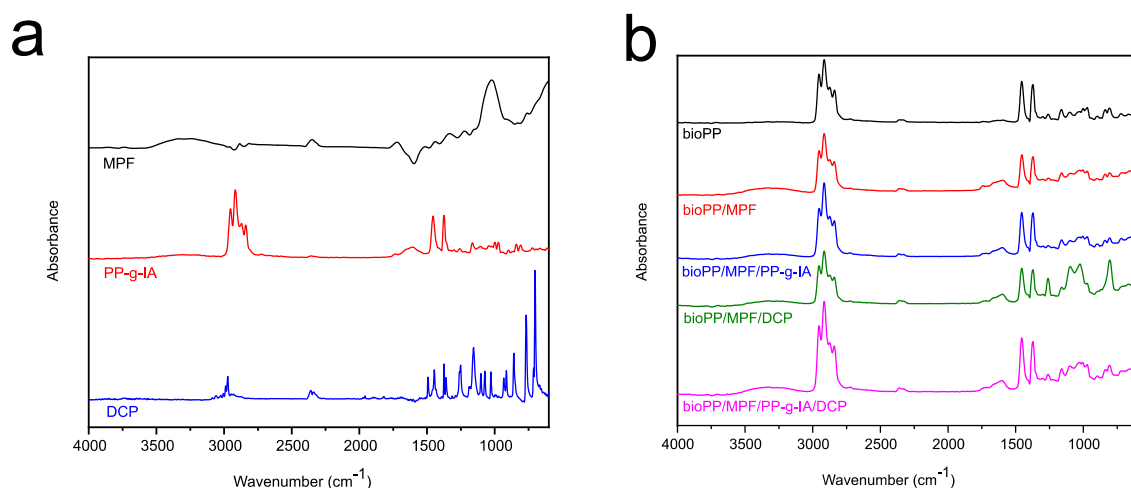


Figure III.1.2.4. Fourier Transformed Infrared Spectroscopy (FTIR) spectra of MPF, PP-g-IA, DCP and uncompatibilized and compatibilized bioPP/MPF composites in the wavenumber range 4000–500 cm⁻¹.

Effect of the compatibilization strategy on melt flow index of bioPP/MPF composites

Figure III.1.2.5 shows the melt flow index (MFI) for the different bioPP/MPF composites, measured at 190 °C and a load mass of 2.16 kg. It can be seen how bioPP showed the highest melt flow index, with a value of 23.25 g/10 min. This value is highly related to a poor entangled polymer, and presents a melt flow index slightly higher than that reported by Sarabi *et al.* [65]. MPF diminishes MFI down to 19.8 g/10 min. This is due to the filler proportion in the blend, which influences the rheology of the polymer, substituting the flexible polymer matrix for a more ridged filler, which affects the way polymer chains entangle during the flowing process [66]. Compatibilization with PP-g-IA also reduces MFI, which was expected since this compatibilizer improves the interactions between bioPP and MPF, making the entanglement between both compounds and between polymeric chains stronger [19]. As expected, composites obtained by REX with DCP show a drastic reduction of the melt flow index down to 10.2 g/10 min, which is clearly related to the crosslinking effect of DCP, which improves the bonding between polymeric chains, thus increasing the entanglement of the polymer and making it more rigid and more difficult to flow. Finally, the MFI results of the composite obtained by REX with PP-g-IA and DCP, again shows the synergistic effect exerted by combination of PP-g-IA copolymer and REX with and DCP, which, combined, improve the entanglement of the polymeric chains, obtaining a more rigid material and thus, with lower melt flow index.

All in all, the results presented here agree with the results observed in the mechanical, thermal and morphological characterizations, corroborating the compatibilizing efficiency of both PP-g-IA and DCP.

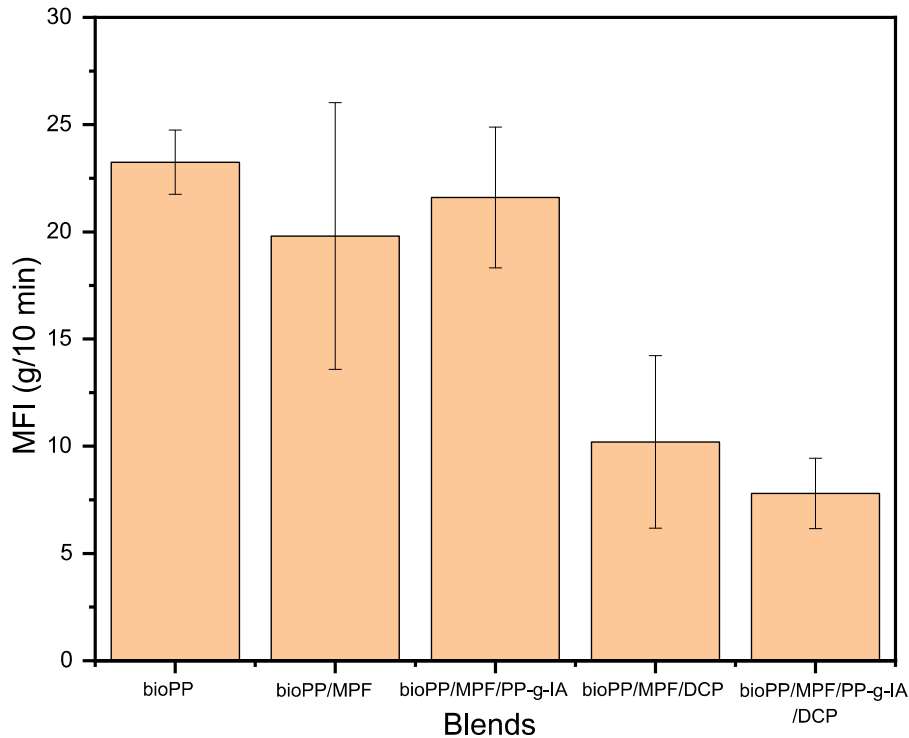


Figure III.1.2.5. Melt flow index (MFI) of the bioPP/MPF blends at 190 °C/2.16 kg.

CONCLUSIONS

This work shows the positive effect of the incorporation of mango peel flour in wood plastic composites based on a biopolypropylene matrix with PP-g-IA and DCP as compatibilizers. The correct grafting of PP-g-IA has also been shown in this study. The addition of this specific load has great potential to be used as a new reinforcement in thermoplastic matrices to make parts by industrial processes, such as injection molding. Regarding mechanical properties, the incorporation of MPF (30 wt.%) with PP-g-IA exhibited a Young's modulus of 2237 MPa, far superior to the modulus of neat bioPP and bioPP/MPF samples. The addition of DCP to the bioPP/MPF blend further increased this value up to 2280 MPa; and the combined effect of PP-g-IA and DCP even increased it further beyond 2349 MPa. This was ascribed to an improvement of the interaction between bioPP and MPF, directly related to the compatibilizing and crosslinking effect of PP-g-IA and DCP, respectively. The elongation at break results were quite promising too, going from 15.98% for bioPP/MPF to 29.69% for

bioPP/MPF/PP-g-IA/DCP. These excellent mechanical properties were corroborated by FESEM images, which showed a very close gap between the lignocellulosic particles and the polymeric matrix. With regard to thermal properties, the introduction of MPF with compatibilizers lead to an increase in thermal stability and crystallinity reaching a crystallinity degree of 58% for the sample with PP-g-IA, which is another proof of the improvement in mechanical resistance. DMTA results also verified an increase in stiffness of the materials due to an increase in the storage modulus of the compatibilized samples, confirming the results commented in mechanical properties, associated with a correct dispersion of the MPF particles in the matrix. Generally, the incorporation of MPF provided the blends with dark brown colours that would allow their use in the manufacturing of wood-based products, such as floors, doors, furniture and so on. Water absorption of the composites also increased as a result of the lignocellulosic nature of the filler. Nonetheless, it was observed how the incorporation of PP-g-IA reduced water absorption in a certain degree, which is quite interesting and useful for applications where water absorption is not desirable. Finally, it was also reported on how the compatibilizing and crosslinking effects of PP-g-IA and DCP lead to a reduction in the melt flow index of the composites, directly related to an increase in the adhesion between polymeric chains.

The results obtained in this work indicate the possibility of obtaining bio-based wood plastic composites with a considerable natural content in mango peel flour, reducing the cost of the material in relation to the neat bioPP. Moreover, obtaining composites with very interesting properties in terms of excellent mechanical properties, on parallel with neat bioPP; enhanced thermal stability and delay in degradation processes; and attractive dark brown colours. All those characteristics make them perfect candidates for substituting wood-based products and give them great application in several fields. All in all, this work opens a new research route in terms of using MPF as reinforcing agent and PP-g-IA and DCP as successful compatibilizing agents in other composites.

AUTHOR INFORMATION

Corresponding Author

*J. Gomez-Caturla. E-mail: jaugoca@epsa.upv.es tlf. number: +34 693779697

Author Contributions

The manuscript was written through contributions of all authors. All authors have given approval to the final version of the manuscript. All authors contributed equally.

FUNDING

J. Gomez-Caturla, R. Balart, J. Ivorra-Martinez, D. Garcia-Garcia, F. Dominici, D. Puglia and L. Torre received funding from the grant PID2020-116496RB-C22 funded by MCIN/AEI/10.13039/501100011033 (Agencia estatal de Investigación). J. Gomez-Caturla, R. Balart, J. Ivorra-Martinez, D. Garcia-Garcia, F. Dominici, D. Puglia and L. Torre also received funding from Generalitat Valenciana-GVA with grant number AICO/2021/025.

ACKNOWLEDGEMENTS

J. Gomez-Caturla wants to thank grant FPU20/01732 funded by MCIN/AEI/10.13039/501100011033 and by ESF Investing in your future. J. Ivorra-Martinez wants to thank FPU19/01759 grant funded by MCIN/AEI/10.13039/501100011033 and by ESF Investing in your future. Microscopy Services at UPV are also acknowledged by their help in collecting and analyzing images.

REFERENCES

- [1] Jorda-Reolid, M., *et al.*, *Upgrading Argan Shell Wastes in Wood Plastic Composites with Biobased Polyethylene Matrix and Different Compatibilizers*. *Polymers*, 2021. 13(6): 922.
- [2] Xie, S., *et al.*, *Synthesis of Fully Biobased Semi-aromatic Furan Polyamides with High Performance through Facile Green Synthesis Process*. *European Polymer Journal*, 2021. 162: 110932.
- [3] Torres, F., S. Rodriguez, and A. Saavedra, *Green composite materials from biopolymers reinforced with agroforestry waste*. *Journal of Polymers and the Environment*, 2019. 27: 2651-2673.
- [4] Sakakibara, K., Y. Moriki, and Y. Tsujii, *Preparation of high-performance polyethylene composite materials reinforced with cellulose nanofiber: simultaneous nanofibrillation of wood pulp fibers during melt-compounding using urea and diblock copolymer dispersant*. *ACS Applied Polymer Materials*, 2018. 1(2): 178-187.
- [5] Kalusulingam, R., *et al.*, *Biomass-derived humin-like furanic polymers as an effective UV-shielding agent for optically transparent thin-film composites*. *ACS Applied Polymer Materials*, 2021. 3(4): 1932-1942.
- [6] Heredia-Guerrero, J.A., *et al.*, *Plant-inspired polyaleuritate–nanocellulose composite photonic films*. *ACS Applied Polymer Materials*, 2020. 2(4): 1528-1534.
- [7] Singha, S., V. Gowda, and M.S. Hedenqvist, *Plant Cuticle-Inspired Polyesters as Promising Green and Sustainable Polymer Materials*. *ACS Applied Polymer Materials*, 2021. 3(8): 4088-4100.
- [8] Quiles-Carrillo, L., *et al.*, *Effect of different compatibilizers on injection-molded green composite pieces based on polylactide filled with almond shell flour*. *Composites Part B: Engineering*, 2018. 147: 76-85.
- [9] Schirp, A. and J. Stender, *Properties of extruded wood-plastic composites based on refiner wood fibres (TMP fibres) and hemp fibres*. *Eur. J. Wood Prod*, 2010. 68(2): 219-231.
- [10] Kengkhetkit, N. and T. Amornsakchai, *A new approach to “Greening” plastic composites using pineapple leaf waste for performance and cost effectiveness*. *Materials & Design*, 2014. 55: 292-299.

-
- [11] Zhou, Y., *et al.*, *Experimental study on thermal and mechanical behavior of polypropylene, talc/polypropylene and polypropylene/clay nanocomposites*. *Materials Science and Engineering: A*, 2005. 402(1-2): 109-117.
- [12] Bahcegul, E.G., E. Bahcegul, and N. Ozkan, *3D printing of hemicellulosic biopolymers extracted from lignocellulosic agricultural wastes*. *ACS Applied Polymer Materials*, 2020. 2(7): 2622-2632.
- [13] Siracusa, V. and I. Blanco, *Bio-Polyethylene (Bio-PE), Bio-Polypropylene (Bio-PP) and Bio-Poly (ethylene terephthalate)(Bio-PET): recent developments in bio-based polymers analogous to petroleum-derived ones for packaging and engineering applications*. *Polymers*, 2020. 12(8): 1641.
- [14] Avérous, L. and F. Le Digabel, *Properties of biocomposites based on lignocellulosic fillers*. *Carbohydrate polymers*, 2006. 66(4): 480-493.
- [15] Ouyang, Y., *et al.*, *Recyclable polyethylene insulation via reactive compounding with a maleic anhydride-grafted polypropylene*. *ACS Applied Polymer Materials*, 2020. 2(6): 2389-2396.
- [16] Arrakhiz, F., *et al.*, *Mechanical properties of high density polyethylene reinforced with chemically modified coir fibers: Impact of chemical treatments*. *Materials & Design*, 2012. 37: 379-383.
- [17] Zhang, Y., J. Chen, and H. Li, *Functionalization of polyolefins with maleic anhydride in melt state through ultrasonic initiation*. *Polymer*, 2006. 47(13): 4750-4759.
- [18] Pesetskii, S., B. Jurkowski, and O. Makarenko, *Free radical grafting of itaconic acid and glycidyl methacrylate onto PP initiated by organic peroxides*. *Journal of applied polymer science*, 2002. 86(1): 64-72.
- [19] Moncada, E., *et al.*, *Use of PP grafted with itaconic acid as a new compatibilizer for PP/clay nanocomposites*. *Macromolecular Chemistry and Physics*, 2006. 207(15): 1376-1386.
- [20] Kim, J.S., *et al.*, *Preparation of PP-g-IA and its Compatibilizing Effects in PP/EVOH Blends*. *Elastomers and Composites*, 2014. 49(3): 225-231.
- [21] Rojas-Lema, S., *et al.*, *Improved Performance of Environmentally Friendly Blends of Biobased Polyethylene and Kraft Lignin Compatibilized by Reactive Extrusion with Dicumyl Peroxide*. *Macromolecular Materials and Engineering*, 2021. 306(9): 2100196.

- [22] Ma, P., *et al.*, *In-situ compatibilization of poly (lactic acid) and poly (butylene adipate-co-terephthalate) blends by using dicumyl peroxide as a free-radical initiator*. *Polymer degradation and stability*, 2014. 102: 145-151.
- [23] Garcia-Garcia, D., *et al.*, *Improvement of the compatibility between poly (3-hydroxybutyrate) and poly (ϵ -caprolactone) by reactive extrusion with dicumyl peroxide*. *European Polymer Journal*, 2017. 86: 41-57.
- [24] Ahmad, E. and A. Luyt, *Effects of organic peroxide and polymer chain structure on morphology and thermal properties of sisal fibre reinforced polyethylene composites*. *Composites Part A: Applied Science and Manufacturing*, 2012. 43(4): 703-710.
- [25] Abdul Aziz, N.A., *et al.*, *Evaluation of processed green and ripe mango peel and pulp flours (*Mangifera indica* var. Chokanan) in terms of chemical composition, antioxidant compounds and functional properties*. *Journal of the Science of Food and Agriculture*, 2012. 92(3): 557-563.
- [26] Safdar, M.N., T. Kausar, and M. Nadeem, *Comparison of ultrasound and maceration techniques for the extraction of polyphenols from the mango peel*. *Journal of Food Processing and Preservation*, 2017. 41(4): e13028.
- [27] Ferreira, S., *et al.*, *Physicochemical, morphological and antioxidant properties of spray-dried mango Kernel starch*. *Journal of Agriculture and Food Research*, 2019. 1: 100012.
- [28] Henrique, M.A., *et al.*, *Valorization of an agro-industrial waste, mango seed, by the extraction and characterization of its cellulose nanocrystals*. *Journal of environmental management*, 2013. 121: 202-209.
- [29] Pesetskii, S., *et al.*, *Itaconic acid grafting on LDPE blended in molten state*. *Journal of applied polymer science*, 1997. 65(8): 1493-1502.
- [30] Shafigullin, L., *et al.*, *Thermal properties of polypropylene and polyethylene blends (PP/LDPE)*. in *IOP Conference Series. Materials Science and Engineering*. 2018. IOP Publishing.
- [31] Novák, I. and Š. Florián, *Study of the change in polarity of polypropylene modified in bulk by polar copolymers*. *Journal of materials science*, 2001. 36(20): 4863-4867.
- [32] Yadav, S.M. and K.B. Yusoh, *Mechanical and physical properties of wood-plastic composites made of polypropylene, wood flour and nanoclay*. *International Journal of Agriculture, Forestry and Plantation*, 2015. 1: 52-58.

- [33] Poletto, M., *Polypropylene-based wood-plastic composites: Effect of using a coupling agent derived from a renewable resource*. Maderas. Ciencia y tecnología, 2017. 19(3): 265-272.
- [34] Morandim-Giannetti, A.A., et al., *Lignin as additive in polypropylene/coir composites: Thermal, mechanical and morphological properties*. Carbohydrate Polymers, 2012. 87(4): 2563-2568.
- [35] Joseph, K., S. Thomas, and C. Pavithran, *Effect of chemical treatment on the tensile properties of short sisal fibre-reinforced polyethylene composites*. Polymer, 1996. 37(23): 5139-5149.
- [36] Caraschi, J.C. and A.L. Leão, *Woodflour as reinforcement of polypropylene*. Materials research, 2002. 5: 405-409.
- [37] Torres-Giner, S., et al., *Preparation and characterization of compression-molded green composite sheets made of poly (3-hydroxybutyrate) reinforced with long pita fibers*. Advances in Polymer Technology, 2018. 37(5): 1305-1315.
- [38] Sari, N.H., et al., *Synthesis and properties of pandanwangi fiber reinforced polyethylene composites: evaluation of dicumyl peroxide (DCP) effect*. Composites Communications, 2019. 15: 53-57.
- [39] Burgada, F., et al., *Upgrading Recycled Polypropylene from Textile Wastes in Wood Plastic Composites with Short Hemp Fiber*. Polymers, 2021. 13(8): 1248-1270.
- [40] Naghmouchi, I., et al., *Polypropylene composites based on lignocellulosic fillers: how the filler morphology affects the composite properties*. Materials & Design (1980-2015), 2015. 65: 454-461.
- [41] Toro, P., et al., *Influence of grafted polypropylene on the mechanical properties of mineral-filled polypropylene composites*. Journal of applied polymer science, 2007. 103(4): 2343-2350.
- [42] Yazdani-Pedram, M., et al., *Mechanical and thermal properties of multiwalled carbon nanotube/polypropylene composites using itaconic acid as compatibilizer and coupling agent*. Macromolecular Research, 2013. 21(2): 153-160.
- [43] Grebowicz, J., S.F. Lau, and B. Wunderlich, *The thermal properties of polypropylene*. in Journal of Polymer Science: Polymer Symposia. 1984. Wiley Online Library.
- [44] Essabir, H., et al., *Biocomposites based on Argan nut shell and a polymer matrix: effect of filler content and coupling agent*. Carbohydrate Polymers, 2016. 143: 70-83.

- [45] Kim, J.S., *et al.*, *Morphological, thermal, rheological, and mechanical properties of PP/EVOH blends compatibilized with PP-g-IA*. *Polymer Engineering & Science*, 2016. 56(11): 1240-1247.
- [46] Essabir, H., *et al.*, *Mechanical and thermal properties of bio-composites based on polypropylene reinforced with Nut-shells of Argan particles*. *Materials & Design*, 2013. 49: 442-448.
- [47] Albano, C., *et al.*, *Thermal stability of blends of polyolefins and sisal fiber*. *Polymer Degradation and Stability*, 1999. 66(2): 179-190.
- [48] Kim, J.H., *et al.*, *Compatibilizing effects of polypropylene-g-itaconic acid on the polypropylene composites*. *Fibers and Polymers*, 2016. 17(5): 671-677.
- [49] García-García, D., *et al.*, *Green composites based on polypropylene matrix and hydrophobized spend coffee ground (SCG) powder*. *Composites part B: engineering*, 2015. 78: 256-265.
- [50] Mishra, A. and A. Luyt, *Effect of sol-gel derived nano-silica and organic peroxide on the thermal and mechanical properties of low-density polyethylene/wood flour composites*. *Polymer Degradation and Stability*, 2008. 93(1): 1-8.
- [51] Krivoguz, Y., *et al.*, *Structure and properties of polypropylene/low-density polyethylene blends grafted with itaconic acid in the course of reactive extrusion*. *Journal of applied polymer science*, 2006. 102(2): 1746-1754.
- [52] Vogler, E.A., *Structure and reactivity of water at biomaterial surfaces*. *Advances in colloid and interface science*, 1998. 74(1-3): 69-117.
- [53] Noor, S.A.A., N.M. Siti, and N.J. Mahmad, *Chemical composition, antioxidant activity and functional properties of mango (*Mangifera indica* l. var *Perlis Sunshine*) peel flour (MPF)*. in *Applied Mechanics and Materials*. 2015. Trans Tech Publ.
- [54] Alonso, D.M., *et al.*, *Polarity of the acid chain of esters and transesterification activity of acid catalysts*. *Journal of Catalysis*, 2009. 262(1): 18-26.
- [55] Ichazo, M., *et al.*, *Polypropylene/wood flour composites: treatments and properties*. *Composite structures*, 2001. 54(2-3): 207-214.
- [56] George, J., S. Bhagawan, and S. Thomas, *Effects of environment on the properties of low-density polyethylene composites reinforced with pineapple-leaf fibre*. *Composites Science and Technology*, 1998. 58(9): 1471-1485.

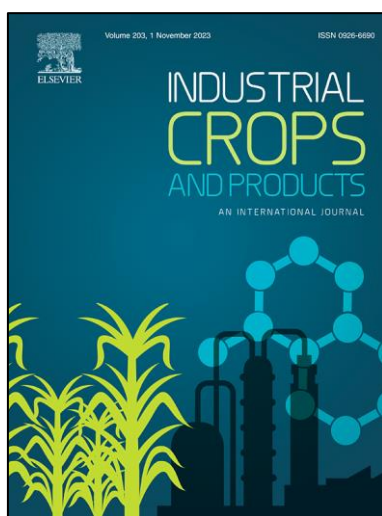
- [57] Arrakhiz, F., *et al.*, *Mechanical and thermal properties of natural fibers reinforced polymer composites: Doum/low density polyethylene*. *Materials & Design*, 2013. 43: 200-205.
- [58] Liu, D., *et al.*, *Composition and structure study of natural Nelumbo nucifera fiber*. *Carbohydrate polymers*, 2009. 75(1): 39-43.
- [59] Uhniat, M., M. Sudoł, and S. Kudła, *Stabilisation of LDPE cross-linked in the presence of peroxidesII. FTIR study of chemical changes taking place in the LDPE–dicumyl peroxide–Irganox 1081 system*. *Polymer degradation and stability*, 2000. 71(1): 75-82.
- [60] Gopanna, A., *et al.*, *Fourier transform infrared spectroscopy (FTIR), Raman spectroscopy and wide-angle X-ray scattering (WAXS) of polypropylene (PP)/cyclic olefin copolymer (COC) blends for qualitative and quantitative analysis*. *Polymer Bulletin*, 2019. 76(8): 4259-4274.
- [61] Larkin, P., *Infrared and Raman spectroscopy: principles and spectral interpretation*. 2017: Elsevier.
- [62] Spinace, M.A., *et al.*, *Characterization of lignocellulosic curaua fibres*. *Carbohydrate Polymers*, 2009. 77(1): 47-53.
- [63] Olsson, A.-M. and L. Salmén, *The association of water to cellulose and hemicellulose in paper examined by FTIR spectroscopy*. *Carbohydrate research*, 2004. 339(4): 813-818.
- [64] Paiva, M., *et al.*, *Alfa fibres: Mechanical, morphological and interfacial characterization*. *Composites Science and Technology*, 2007. 67(6): 1132-1138.
- [65] Sarabi, M.T., *et al.*, *Effect of polymeric matrix melt flow index in reprocessing extruded wood–plastic composites*. *Journal of Thermoplastic Composite Materials*, 2014. 27(7): 881-894.
- [66] Ariff, Z.M., *et al.*, *Rheological behaviour of polypropylene through extrusion and capillary rheometry*. *Polypropylene*, 2012: 29-49.

III.1.3. Improvement of the barrier and mechanical properties of environmentally friendly mango kernel flour/glycerol films by varying the particle size of mango kernel flour

Jaume Gomez-Caturla^{1*}, Juan Ivorra-Martinez¹, Luis Quiles-Carrillo¹, Rafael Balart¹, Daniel Garcia-Garcia¹, Franco Dominici², Debora Puglia² and Luigi Torre²

¹Technological Institute of Materials – ITM, Universitat Politècnica de València – UPV, Plaza Ferrándiz y Carbonell 1, 03801 Alcoy (Spain).

²Dipartimento di Ingegneria Civile ed Ambientale, University of Perugia, UdR INSTM, Strada di Pentima, 4 - 05100 Terni (TR) Italy.



Industrial Crops and Products

2022, 188: 115668

*Adapted from the original manuscript.



Improvement of the barrier and mechanical properties of environmentally friendly mango kernel flour/glycerol films by varying the particle size of mango kernel flour

Jaume Gomez-Caturla ^{a,*}, Juan Ivorra-Martinez ^a, Luis Quiles-Carrillo ^a, Rafael Balart ^a, Daniel Garcia-Garcia ^a, Franco Dominici ^b, Debora Puglia ^b, Luigi Torre ^b

^a Instituto de Tecnología de Materiales (ITM), Universitat Politècnica de València (UPV), Plaza Ferrándiz y Carbonell 1, 03801 Alcoy, Alicante, Spain

^b Dipartimento di Ingegneria Civile ed Ambientale, University of Perugia, Udr INSTM, Strada di Pentima, 4, 05100 Terni, TR, Italy

ARTICLE INFO

Keywords:
Mango kernel flour
Biodegradability
Antioxidant
Glycerol
Film

ABSTRACT

The development of environmentally friendly films based on glycerol and different sizes of mango kernel flour particles (MKF), ranging from 100 to 600 μm , is reported. The casting solution method was used to produce the films, using distilled water as the solvent. The mechanical, morphological, barrier, surface, optical, wettability and biodegradability properties of the films were assessed. The mechanical analysis revealed that smaller particles lead to superior mechanical performance in terms of tensile strength, elastic modulus and elongation at break, achieving an elongation at break of 18.1 % for the films with the smallest particle size (100 μm). These results were confirmed by field emission scanning electron microscopy (FESEM) images of the films, where the gap between the mango kernel particles and the glycerol matrix is practically non-existent in films with the smallest particle size (100 μm). On the other hand, it was observed that as the particle size decreased, the barrier properties improved, showing a decrease in water vapor permeability rate (WVPR). With respect to antioxidant properties, it was observed that the films showed strong antioxidant activity, as assessed by 2,2-diphenyl-1-picrylhydrazyl (DPPH) inhibition above 90 % for all films after 1 week. Finally, MKF films proved to be completely biodegradable, with a 100 % of disintegration after 4 weeks of incubation time in compost soil, with the smallest MKF particle size films exhibiting the highest disintegration rate.

1. Introduction

In the last few decades, the production of plastics all over the globe has risen up considerably. Most of those plastics are based on fossil resources, which provoke several environmental problems, such as large amount of wastes or greenhouse gas emissions (Shen et al., 2020). In addition, the petroleum used to produce these plastics has suffered a noticeable depletion since the 20th century. Among all the industries, the packaging industry stands out as the main consumer, which accounts for the 36 % of the total plastic production (approximately 400 million ton per year) (Jang et al., 2020). This fact has led society to concern about environmentally friendly alternatives as substitutes for traditional synthetic plastics (Liminana et al., 2018). Among all the environmentally friendly materials that are being developed in search for better alternatives in food packaging, edible films and coatings obtained from biopolymers, especially polysaccharides and proteins, have attracted

great interest (Ghiasi et al., 2020). Biopolymeric films find important applications in the food industry thanks to their ability to provide protection to food products against mechanical damage and adverse effects of microbiological, chemical, and physical origin (Giosafatto et al., 2018). Additionally, these films are characterized by their low cost, wide availability and biodegradability (Kocabaş et al., 2021; Zhang et al., 2016).

Proteins, polysaccharides and lipids are the most common used biopolymers for biodegradable films preparation. Some examples are protein films, which possess good barrier properties against lipids, aromas and oxygen under low relative humidity environments (Bamdad et al., 2006), but they are poor water vapor barriers because of their hydrophilicity (Mokrejs et al., 2009). There are also starch films, which have balanced tensile strength and good oxygen barrier properties, but they are also very sensitive to moisture and become very brittle in low humidity atmospheres (Li et al., 2018; Wang et al., 2021b). To overcome

* Corresponding author.

E-mail address: jaugoca@epsa.upv.es (J. Gomez-Caturla).

<https://doi.org/10.1016/j.indcrop.2022.115668>

Received 5 April 2022; Received in revised form 24 August 2022; Accepted 13 September 2022

Available online 20 September 2022

0926-6690/© 2022 The Author(s). Published by Elsevier B.V. This is an open access article under the CC BY-NC-ND license (<http://creativecommons.org/licenses/by-nc-nd/4.0/>).

<http://creativecommons.org/licenses/by-nc-nd/4.0/>

Improvement of the barrier and mechanical properties of environmentally friendly mango kernel flour/glycerol films by varying the particle size of mango kernel flour

Abstract

The development of environmentally friendly films based on glycerol and different sizes of mango kernel flour particles (MKF), ranging from 100 to 600 μm , is reported. The casting solution method was used to produce the films, using distilled water as the solvent. The mechanical, morphological, barrier, surface, optical, wettability and biodegradability properties of the films were assessed. The mechanical analysis revealed that smaller particles lead to superior mechanical performance in terms of tensile strength, elastic modulus and elongation at break, achieving an elongation at break of 18.1% for the films with the smallest particle size (100 μm). These results were confirmed by field emission scanning electron microscopy (FESEM) images of the films, where the gap between the mango kernel particles and the glycerol matrix is practically non-existent in films with the smallest particle size (100 μm). On the other hand, it was observed that as the particle size decreased, the barrier properties improved, showing a decrease in water vapour permeability rate (WVPR). With respect to antioxidant properties, it was observed that the films showed strong antioxidant activity, as assessed by 2,2-diphenyl-1-picrylhydrazyl (DPPH) inhibition above 90% for all films after 1 week. Finally, MKF films proved to be completely biodegradable, with a 100% of disintegration after 4 weeks of incubation time in compost soil, with the smallest MKF particle size films exhibiting the highest disintegration rate.

Keywords: mango kernel flour, biodegradability, antioxidant, glycerol, film.

INTRODUCTION

In the last few decades, the production of plastics all over the globe has risen up considerably. Most of those plastics are based on fossil-resources, which provoke several environmental problems, such as large amount of wastes or greenhouse gas emissions [1]. In addition, the petroleum used to produce these plastics has suffered a noticeable depletion since the 20th century. Among all the industries, the packaging industry stands out as the main consumer, which accounts for the 36% of the total plastic production (approximately 400 million ton per year) [2]. This fact has led society to concern about environmentally friendly alternatives as substitutes for traditional synthetic plastics [3]. Among all the environmentally friendly materials that are being developed in search for better alternatives in food packaging, edible films and coatings obtained from biopolymers, especially polysaccharides and proteins, have attracted great interest [4]. Biopolymeric films find important applications in the food industry thanks to their ability to provide protection to food products against mechanical damage and adverse effects of microbiological, chemical, and physical origin [5]. Additionally, these films are characterized by their low cost, wide availability and biodegradability [6, 7].

Proteins, polysaccharides and lipids are the most common used biopolymers for biodegradable films preparation. Some examples are protein films, which possess good barrier properties against lipids, aromas and oxygen under low relative humidity environments [8], but they are poor water vapour barriers because of their hydrophilicity [9]. There are also starch films, which have balanced tensile strength and good oxygen barrier properties, but they are also very sensitive to moisture and become very brittle in low humidity atmospheres [10, 11]. To overcome these weaknesses, some studies have focused on developing blends of commercial starch and protein to make films [12]. In some cases, lipids have been added in order to reduce the hydrophilicity of the blends and increase the water vapour barrier properties of the obtained films [13]. However, results are not always optimal, due to possible incompatibility between the biopolymers during blending, which could provoke phase separation [14]. Nonetheless, in order to sort out this problem, composite films are also an interesting solution, where flours or micronizates from raw materials coming from plants such as cereals, fruits or other vegetables can act as “natural mixtures” of starch, lipids and proteins [15]. Several flour-based materials have been studied as film-forming agents. Tapia-Blácido *et al.* [16], reported the good film forming ability of amaranth flour in films with glycerol as plasticizer. Other researches have developed films based on eggplant flour, corn starch [17] or chia seeds [18]. However, those films gave poor results, lacking homogeneity and

showing low mechanical properties. Mikus *et al.* [19], developed and tested several oilseed flours (flax, evening primrose, pumpkin, hemp, sunflower and sesame), as film forming agents, also analysing the effect of the size of the particles of the different flours. The study showed that the films with highest amount of protein, namely sesame and pumpkin, had the best barrier properties in terms of water vapour permeability. Additionally, Wang *et al.* [20] made a considerable contribution to the cellulose-based packaging investigation route by developing a lignocellulose-derived strategy through the deposition of oxalic acid modified microfibrillated cellulose (OMFC) and infiltration of nanosized alkali lignin (NAL) in paper packaging. They achieved a great increase in barrier properties (reduction of WVTR of 93%). Quiles-Carrillo *et al.* [21] reported on the development of bioactive multilayer polylactide films with enhanced barrier properties against the diffusion of gallic acid.

Mango (*Mangifera indica*) is one of the most popular tropical crops worldwide. Its production reached 46.5 million metric tons in 2016 [22], and India is its main exporter, which represents more than 40% share of the global market [23]. Several studies have demonstrated that mango by-products, like mango peel or mango stone, are potential feedstocks for biorefineries, due to their content in several interesting components, such as starch, cellulose, proteins, polyphenols, and so on [24]. The mango seed is divided into two main components, the kernel (interior) and the tegument (exterior). Mango kernel represents about the 13 wt.% of Tommy Atkins mangoes variety, which is the predominant one [25], and it can be utilized as a supplement to wheat flour or for extracting edible oil [26]. The main component of mango kernels is starch. According to previous studies, mango kernel has around 74-75 wt.% of polysaccharides with starch accounting for 60 wt.%. Other components of the mango kernel are 9-13 wt.% fats, 6-9 wt.% proteins, and 2-3 wt.% ashes as shown by Augustin *et al.* [27]. It even has phenolic compounds, as it was demonstrated by Adilah *et al.* [28]. All these compounds make mango kernel an excellent option to be considered for producing edible films.

When producing edible coatings and films, barrier properties and mechanical properties are essential. In this sense, the particle size of the flour plays a key role in those properties. However, little research has been done with regard to the different behaviour of edible films based on the particle size of the film-forming agent flour. Pérez-Gago *et al.* [29], conducted a study on how the lipid particle size affected the water vapour permeability (WVP) of films based on whey protein/Beeswax emulsion, and observed that smaller particles lead to better barrier and mechanical properties. This fact suggests that it would be of interest to study how particle size of starch-based flours would affect the properties of films. Another important characteristic considering films

focused on food packaging applications is their antioxidant activity. Lipid oxidation consists on a radical chain reaction that affects food with high concentration of unsaturated lipids, which results in the release of free radicals and volatiles that produce oxidative rancidity [22]. Antioxidants respond to this reaction by scavenging those free radicals and donating hydrogen atoms to free radicals, thus delaying or even stopping the chain reaction. Melo *et al.* [22], reported the positive radical scavenging activity of mango kernel flour and phenolic extracts from mango kernel flour in edible antioxidant films.

The main aim of this study is to obtain environmentally friendly films based on mango kernel flour (MKF) with several particle sizes and glycerol as plasticizer. Thus, the objective is to assess how the particle size affects the properties of the films and which is the size threshold at which films with balanced properties for use in the packaging sector are obtained. To meet this end, five different particle size ranges have been studied (600-500 μm , 500-400 μm , 400-300 μm , 300-200 μm and 200-100 μm). The mechanical, morphological, barrier, colorimetric, biodegradability, moisture and water solubility, contact angle and antioxidant properties have been characterized and evaluated in order to compare the effect of the particle size. Considering that a similar analysis has not been reported before in literature with regard to starch-based flours, the authors deem that this study could be of considerable usefulness for the packaging industry to improve the quality and performance of starch-based films.

MATERIALS AND METHODS

Materials

Osteen variety mangoes were obtained from the local market in Alcoy, Spain. The fruits were selected according to their appearance, so they had no apparent infection. Glycerol was provided by Sigma-Aldrich, and it was ReagentPlus >99.0% (Product Code: G7757-1GA). 2,2-diphenyl-1-picrylhydrazyl radical (DPPH) was supplied by Sigma Aldrich (Madrid, Spain). DPPH is a stable organic radical that presents a strong hydrogen acceptor capacity towards antioxidants. In the presence of antioxidants, the characteristic violet colour of DPPH solution in methanol changes into yellow. Methanol ($\geq 99.8\%$) of HPLC grade was supplied by Panreac Química (Barcelona, Spain).

Mango kernel particles preparation

Mango kernels were first dried at 50 °C during 168 h in a dehumidifying dryer MDEO (Barcelona, Spain). They were then decorticated and cut into small pieces using an air knife unit. Afterwards, they were milled in a ZM 200 centrifugal mill from Retsch (Düsseldorf, Germany) at a speed of 12,000 rpm and sieved with a 500- μm mesh filter. Finally, in order to evaluate the behavior of the films with different particle size, the mango kernel flour (MKF) was sieved using a vibratory sieve shaker model RP09 from CISA (Barcelona, Spain) through several mesh sizes: 600, 500, 400, 300, 200 and 100 μm . This allowed to separate the flour in different particle size sets. **Figure III.1.3.1** illustrates the proportion of each particle size in the milled MKF. It can be observed how the most abundant range is 500-400 μm , which was expected as the initial mesh size was 500 μm . According to Adjei-Fremah *et al.* [30], the particle size distribution is a decisive factor regarding the functional properties of the films, particularly the hydration properties, which are greatly influenced by porosity.

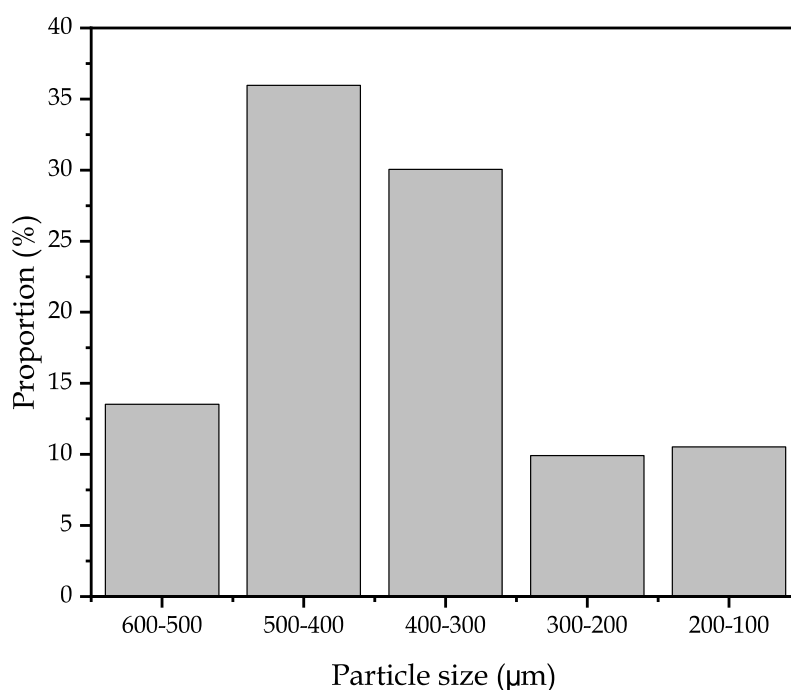


Figure III.1.3.1. Particle size distribution of milled mango kernel flour (MKF) after sieving at different size ranges.

Preparation of reinforced MKF/glycerol films

The MKF/glycerol films were prepared by solution casting process using MKF, glycerol and distilled water. For this purpose, MKF (5% w/w) of each particle size set

was mixed with distilled water. After stirring for 10 minutes, the mixture was heated up to 90 °C and stirred for 30 min. Afterwards, glycerol was added to the mixture (50% w/w in relation to the MKF mass) as a plasticizer, and the solution was stirred for 30 min once more. Then the solutions were ultrasonicated with an ultrasonicator model MH-010S from Valens (Palma de Mallorca, Spain) for 10 min with the objective of removing bubbles. The solutions were thereafter casted onto Petri plates (8.5 cm diameter) and allowed to dry in a dehumidifying dryer MDEO for 48 h at 40 °C. Finally, the dried films were extracted from the Petri plates and stored at 52% relative humidity (RH) at 25 °C for 48 h before characterization. Three films from each formulation were prepared. The nomenclature for the prepared films is shown in **Table III.1.3.1**.

Table III.1.3.1. Code for the developed films with different MKF particle size.

Code	Composition
MKF-600/500	Film with MKF particles with a size between 600 and 500 μm
MKF-500/400	Film with MKF particles with a size between 500 and 400 μm
MKF-400/300	Film with MKF particles with a size between 400 and 300 μm
MKF-300/200	Film with MKF particles with a size between 300 and 200 μm
MKF-200/100	Film with MKF particles with a size between 200 and 100 μm

Characterization of MKF/glycerol films

Film thickness

Film thickness was determined using a micrometer Mitutoyo No. 2109S-10 (Tokyo, Japan) with a sensitivity of 0.001 mm. Ten measurements were made all along the surface of each film sample.

Mechanical properties

The mechanical tensile properties, namely tensile strength, tensile modulus and elongation at break of MKF/glycerol films were determined following ASTM D882-02, using a tensile machine model DUOTRAC-10/1200 from ibertest (Madrid, Spain). Rectangular strips (30×4 mm²) were cut from preconditioned MKF/glycerol films and placed between the tensile grips with a distance of 15 mm. The crosshead speed during the test was 5 mm/min. Five samples from each film were used for the tensile test in order to obtain the average results.

Moisture content

The moisture of MKF/glycerol films was determined gravimetrically. 10×10 mm² film pieces were cut and weighted, then they were dried in an oven for 24 h at 105 °C and weighted again until reaching a constant weight [31]. Three pieces from each film were used to calculate the moisture content and the results were averaged. The moisture content for each sample was obtained through **Equation III.1.3.1**:

$$\text{Moisture content (\%)} = \frac{W_i - W_f}{W_i} 100 \quad (\text{III. 1.3.1})$$

where W_i and W_f are the initial and dried weight of the samples, respectively.

Morphology

Nitrogen cryofractured cross-sections of MKF/glycerol films were used to study their morphology by means of field emission scanning electron microscopy (FESEM). A ZEISS model ULTRA55 (Eindhoven, The Netherlands) was used. The acceleration voltage was 2 kV. The film samples were sputtered with a platinum coating in a high vacuum sputter coater EM MED20 from Leica Microsystems (Milton Keynes, United Kingdom).

Solubility

The solubility of MKF/glycerol film samples in distilled water was calculated following the methodology of K. Masamba *et al.* [32]. Rectangular pieces of the films (10×10 mm²) were dried in an oven for 24 h at 105 °C. They were then weighted and the film pieces were placed into test tubes with approximately 10 mL of distilled water. The tubes were submitted to periodical agitation for 24 h at room temperature. Then, the non-solubilized fraction was dried in an oven 24 h at 105 °C with the aim of determining the weight of undissolved dry matter in distilled water. Solubility was calculated according to **Equation III.1.3.2**:

$$\text{Solubility (\%)} = \frac{W_i - W_f}{W_i} 100 \quad (\text{III. 1.3.2})$$

where W_i is the initial weight of the sample, and W_f is the weight of the sample after drying. Three measurements were made for each film.

Dynamic contact angle measurements

Dynamic water contact angles (θ) of preconditioned films were measured using an optical goniometer model FM140 (110/220 V, 50/60 Hz) from KRÜSS GmbH (Hamburg, Germany) at room temperature. Five distilled water drops were placed in the surface of the films and their contact angle was measured. Ten measurements for each water droplet were taken and averaged. The contact angle was measured at different times from the deposition of the water drop onto the film surface (0, 5, 10, 20, 30 seconds), thus obtaining the dynamic water contact angle.

Colour characterization

The change in colour produced by MKF in the glycerol films was assessed using a colorimeter model KONICA CM-3600d COLORFLEX-DIFF2 from Hunter Associates Laboratory (Virginia, EEUU). A white standard was used to calibrate the equipment. Colour analysis of each film was carried out through the study of the Ciel^{*}a^{*}b^{*} colour space, whose coordinates are L^* (lightness), a^* (red-green) and b^* (yellow-blue). The results were obtained by averaging five measurements at ten random points of each film. The total difference in colour (ΔE) was obtained using **Equation III.1.3.3**:

$$\Delta E = \sqrt{(\Delta L^*)^2 + (\Delta a^*)^2 + (\Delta b^*)^2} \quad (\text{III. 1.3.3})$$

where ΔL^* , Δa^* and Δb^* are the differences between the corresponding colour parameter of the samples and the colour parameter values of the white standard plate ($L^* = 95.17$, $a^* = -0.93$, $b^* = 0.53$).

Water vapour transmission rate (WVTR)

MKF/glycerol films' water vapour transmission rate (WVTR) was measured gravimetrically according to ISO 2525. First, permeability cups were filled with 2 g of dry silica gel; then they were sealed with film samples and placed in a desiccator at 90% relative humidity (RH) and 23 °C. The cups were weighted each hour for 7 h. The changes in the weight of the cup were plotted as a function of time and their slope was

obtained through linear regression. WVTR was calculated using **Equation III.1.3.4** [33]:

$$WVTR = \frac{n \cdot l}{S} \quad (\text{III. 1.3.4})$$

where n is the slope obtained by linear regression, l is the thickness of the film and S is the exposed area of the film.

Antioxidant activity

The antioxidant activity of MKF/glycerol films was assessed using 2,2-diphenyl-1-picrylhydrazyl radical (DPPH) inhibition test. DPPH is a stable organic radical that presents a strong hydrogen acceptor capacity towards antioxidants. In the presence of antioxidants, the characteristic violet colour of DPPH solution in methanol changes into yellow. This colour change was measured by means of UV spectrophotometry. A standard DPPH solution with a concentration of 0.025 g/L in methanol was prepared and placed in dark glass vials. ≈ 100 mg samples from each film were prepared and immersed in 4 mL of the standard solution. Vials containing all the samples and a control were closed and kept away from light for one week.

An Agilent Technologies (Barcelona, Spain) Cary series UV-Vis-NIR spectrophotometer was used to measure the absorbance of the samples at 517 nm, at 1, 24, 72, and 168 h after the start of the test, in triplicate. The percentage inhibition of DPPH was calculated according to **Equation III.1.3.5**:

$$DPPH_{inhibition} (\%) = \frac{A_c - (A_s - A_b)}{A_c} 100 \quad (\text{III. 1.3.5})$$

where A_c is the absorbance of the DPPH solution without the sample, A_s is the absorbance of the DPPH solution with the sample, and A_b is the absorbance value of pure methanol with the sample. Tests were done by triplicate to obtain reliable results.

Disintegration test

The biodegradation rate under controlled compost soil conditions of MKF/glycerol films with different particle sizes of MKF was studied following ISO

20200. Pieces of 2.5×2.5 cm² were cut from the obtained films and dried for 24 h at 40 °C. Then they were weighted and buried in a bioreactor of dimensions 30×20×10 cm³ in a solid synthetic wet soil prepared with 40 wt% sawdust, 10 wt% corn starch, 30 wt% rabbit-feed, 10 wt% compost, 5 wt% sugar, 4 wt% of corn oil, and 1 wt% of urea. This mixture was mixed with distilled water in a 45:55 ratio. In these conditions, the samples were aerobically degraded at a constant temperature of 58 °C in an air circulating oven during 4 weeks. Measurements were taken by extracting samples from the reactor, washing them with distilled water, drying them for 24 h at 40 °C and finally weighting them. The samples were individually placed inside a textile mesh that allows a direct contact with the compost soil during the disintegration period and, at the same time, since the textile mesh does not disintegrate, it facilitates the removal of the degraded film or films pieces to carry out weight measurements as indicated before. Once the weight measurement was done, the film or remaining film pieces were placed again into the textile mesh to continue with the disintegration test. Several measurements were taken during the 4 weeks to observe the biodegradation profile of the samples over time.

Roughness

The surface roughness of the MKF/glycerol films was characterized using a roughness meter Mitutoyo model SJ301. A linear path with a length of 4 mm was studied in each film following ISO1997. The mean surface roughness (R_a) was measured in triplicate for each MKF/glycerol film.

RESULTS AND DISCUSSION

Mechanical properties

The mechanical properties of the MKF/glycerol films allow to determine how the films behave under tensile stress depending on the difference in particle size. In this sense, **Table III.1.3.2** gathers the main tensile parameters of the films as well as the film thickness. It can be observed how the thickness of the films varies between 420 μm for the smallest MKF particle film, and 528 μm for the largest MKF particle film. This reduction in thickness could be closely ascribed to the particle size. In the case of the 600/500 μm particles film, the particles almost comprise the entirety of the film thickness. The tensile modulus (E) obtained for the film with 600-500 μm MKF particle size was 9.85 MPa, while tensile strength and elongation at break were 0.75 MPa and 11.4%, respectively. Those values are within the range reported by other studies such as

the work by Mikus *et al.* [19], who studied several films with different lignocellulosic fillers. They reported elastic modulus values ranging from 1 to 19 MPa, tensile strengths comprised in the 0.6 to 3.1 MPa range, and elongation at breaks varying from 4 to 25%.

It can be clearly seen how a decrease in the particle size promotes a direct improvement in the overall tensile properties of the MKF/glycerol films. The tensile modulus increases up to 22.1 MPa for the film with 200-100 μm MKF particles, which means an increase of 124% in relation to the 600-500 μm MKF particle size film. A similar trend occurs when analyzing tensile strength and elongation at break. Those parameters boost up to 1.08 MPa and 18.1% for the MKF-200/100 film, respectively. This means an improvement of 44% and 58.8%, respectively, in comparison with the MKF-600/500 film. This increase is mainly ascribed to two factors. First, smaller MKF particles make the films more homogeneous and decrease the number of stress concentration points in the films in comparison with the samples with the highest MKF particles. This is ascribed to a greater concentration of agglomerates due to the higher size of the lignocellulosic particles. Moreover, the size of some of the highest MKF particles (MKF-600/500) can even surpass the thickness of the film. The formation of agglomerates leads to a detriment in the cohesion of the films, thus, increasing the brittleness of the film [19]. This also leads to the appearance of considerably large areas where only glycerol is present, as it would be demonstrated by FESEM characterization. Additionally, smaller particle size allows a better particle dispersion over the film surface, making a higher amount of particles to be present in the film, with a higher overall surface area. This directly leads to a superior interaction of the oxygen based molecules present in the particles (mainly starch and protein) with the plasticizer (glycerol), as they have more hydrogen bonding capacity to interact with the plasticizer, which enhances both the tensile strength of the material and its ability to elongate [34].

Table III.1.3.2. Average thickness and mechanical properties of the MKF/glycerol films from tensile test: tensile modulus (E), tensile strength (σ_{max}) and elongation at break (ε_b).

Film	Thickness (μm)	E (MPa)	σ_{max} (MPa)	ε_b (%)
MKF-600/500	528.3 \pm 58.4 ^a	9.85 \pm 1.66 ^a	0.75 \pm 0.06 ^a	11.4 \pm 2.1 ^a
MKF-500/400	511.1 \pm 30.2 ^a	14.42 \pm 1.21 ^b	0.90 \pm 0.17 ^b	11.4 \pm 0.9 ^a
MKF-400/300	520.9 \pm 74.8 ^a	22.40 \pm 7.78 ^c	0.90 \pm 0.07 ^b	11.8 \pm 0.3 ^a
MKF-300/200	474.5 \pm 13.8 ^b	20.07 \pm 3.24 ^d	0.93 \pm 0.06 ^b	15.3 \pm 1.0 ^b
MKF-200/100	420.9 \pm 22.8 ^c	22.10 \pm 3.73 ^e	1.08 \pm 0.08 ^c	18.1 \pm 1.2 ^c

a-e Different letters in the same column indicate a significant difference ($p < 0.05$).

Water susceptibility

Table III.1.3.3 shows the moisture content and water solubility, while **Table III.1.3.4** gathers the dynamic contact angle results for each one of the films developed in this study. The solubility of all the MKF/glycerol films is quite similar, as it is indicated by the statistical analysis. The MKF-600/500 film shows values of 26.7 and 31.2% for moisture and water solubility, respectively; while the MKF-300/200 film exhibits values of 31.0 and 34.7%, respectively, which is the only film that exhibited a little higher water solubility. Starch-based MKF particles possess great affinity towards water due to their content in starch (60 wt.%) and other highly hydrophilic compounds, such as proteins and carbohydrates [26, 35]. Both proteins and carbohydrates possess hydroxyl groups which can readily interact with hydroxyl groups in glycerol. This increase in moisture and water solubility could be ascribed to the fact that smaller lignocellulosic particles possess higher surface contact area, which leads to a superior interaction with water and thus, a higher concentration of -OH groups can interact with H₂O molecules [36, 37]. Additionally, part of this ability to absorb water is also due to the presence of glycerol, which is considered a water-holding agent that contributes to hydrophilicity, as observed by Tapia-Blácido *et al.* [16].

Contact angle measurements of the films over time also show remarkable differences in terms of water affinity. The herein developed films are highly hydrophilic, as the water contact angle is quite inferior to 65°, which is the hydrophilicity threshold according to Vogler [38]. At the initial time, all the contact angles are already quite low, being the highest value 50.7° for the higher particle size film and the lowest 31.4° for the MKF-400/300 film. Moreover, the water contact angle rapidly decreases to even lower values after 30 s. The value for MKF-600/500 decreases down to 39.5°, while the contact angle for MKF-400/300 goes down to 13.0°, which is another proof of the extreme

hydrophilicity of these films. There seems to be a trend of reduction of contact angle with smaller particle sizes. This could be ascribed to a higher surface area in films with the smaller particle size, as it has been aforementioned. Furthermore, it could be directly related to roughness, as higher particle size films are considerably rougher than lower particle size films, which are more homogeneous. This homogeneity could provoke a decrease in the water contact angle [39]. **Figure III.1.3.2** perfectly illustrates this effect, which shows the evolution of the shape of the distilled water drop onto the surface of the film MKF-500/400 over time. It can be seen how the drop drastically flattens with time.

Table III.1.3.3. Moisture content and water solubility for MKF/glycerol films.

Code	Moisture content (%)	Water solubility (%)
MKF-600/500	26.7 ± 0.1 ^a	31.2 ± 0.2 ^a
MKF-500/400	27.2 ± 1.1 ^a	31.4 ± 0.4 ^a
MKF-400/300	29.9 ± 0.7 ^b	32.8 ± 0.6 ^a
MKF-300/200	31.0 ± 0.2 ^b	34.7 ± 0.1 ^b
MKF-200/100	28.4 ± 0.1 ^c	31.3 ± 0.3 ^c

a-c Different letters in the same column indicate a significant difference ($p < 0.05$).

Table III.1.3.4. Water contact angle at different times (0, 5, 10, 20 and 30 seconds) for MKF/glycerol films.

Code\Time	Water contact angle (°)				
	0 s	5 s	10 s	20 s	30 s
MKF-600/500	50.7 ± 0.5 ^a	45.9 ± 0.9 ^a	43.0 ± 0.6 ^a	41.0 ± 0.1 ^a	39.5 ± 0.3 ^a
MKF-500/400	36.9 ± 0.4 ^b	26.6 ± 0.7 ^b	25.8 ± 0.5 ^b	25.5 ± 0.6 ^b	25.3 ± 0.8 ^b
MKF-400/300	31.4 ± 0.5 ^c	24.1 ± 0.8 ^c	13.1 ± 0.6 ^c	13.1 ± 0.3 ^c	13.0 ± 0.6 ^c
MKF-300/200	31.7 ± 0.8 ^c	25.1 ± 0.6 ^c	23.6 ± 0.6 ^d	23.5 ± 1.1 ^d	22.0 ± 0.8 ^d
MKF-200/100	35.3 ± 0.7 ^d	34.6 ± 1.2 ^d	26.2 ± 1.1 ^e	25.8 ± 0.4 ^e	24.7 ± 0.8 ^e

a-e Different letters in the same column indicate a significant difference ($p < 0.05$).

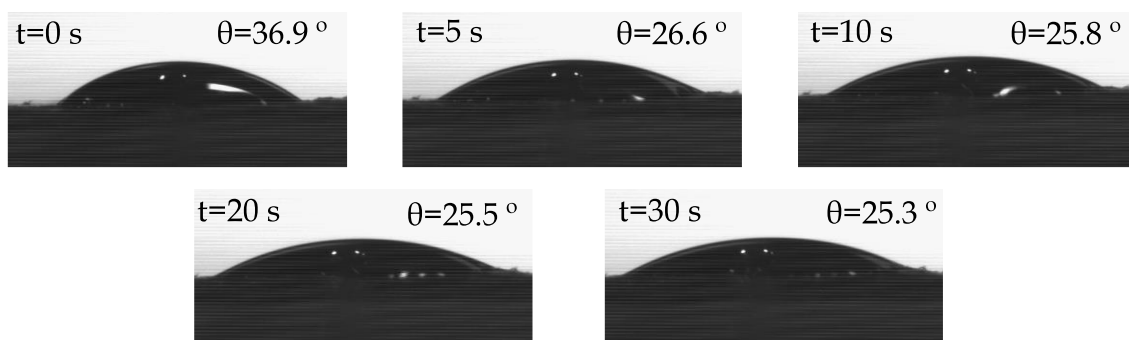


Figure III.1.3.2. Evolution of the water contact angle of a distilled water drop onto the surface of MKF-500/400 film over time.

In accordance with these results, the films are clearly water soluble. This feat still makes them suitable for packaging applications, especially in the oil packaging field [40]. Romero-Bastida *et al.* [41], reported that films obtained from banana, okenia and mango starches plasticized with glycerol (starch-to-glycerol weight ratio of 2:1), showed high water solubility values, above 50%. They used a different film formation procedure based on thermal and cold gelatinization. They concluded that these films could find interesting applications as edible films and candy wrap edible films, as other carboxymethylated starch films. Therefore, the films obtained in this work could also find use in these applications due to the high water solubility values.

Morphological properties

The morphology of the cross-section of cryofractured samples of the MKF/glycerol films was studied by FESEM. **Figure III.1.3.3** shows the FESEM images of the films at 1000× magnification. It can be seen in **Figure III.1.3.3a**, the presence of MKF particles, which before processing were initially between 600 and 500 μm large, embedded in the glycerol matrix with quite a large gap between the particles and the matrix. This is ascribed to a certain lack of adhesion of MKF particles in the film, which could be due to the large size of the starch-based particles leading to inhomogeneity within the film structure. A similar morphology was observed by Melo *et al.* [22], in mango kernel starch (MKS) films with MKF, which presented a great concentration of discontinuities. The black spots found in the films could be ascribed to the presence of lipid globules. These discontinuities are responsible for the low mechanical response observed in the mechanical properties section. It can be appreciated how a decrease in the particle size leads to smaller gaps between the MKF particles and the glycerol matrix. This can be clearly observed in **Figures III.1.3.3d** and **III.1.3.3e**, where the particles are

strongly embedded in the glycerol matrix, especially in the case of the film with 200-100 μm particle size, which presents an almost inexistent gap. Additionally, a superior homogeneity in the surface of the cryofractured films is also seen, which directly relates to the higher mechanical performance of MKF-300/200 and MKF-200/100 films, respectively. This homogeneity and the absence of voids in the film matrix also results in increased barrier properties as can be observed and will be discussed.

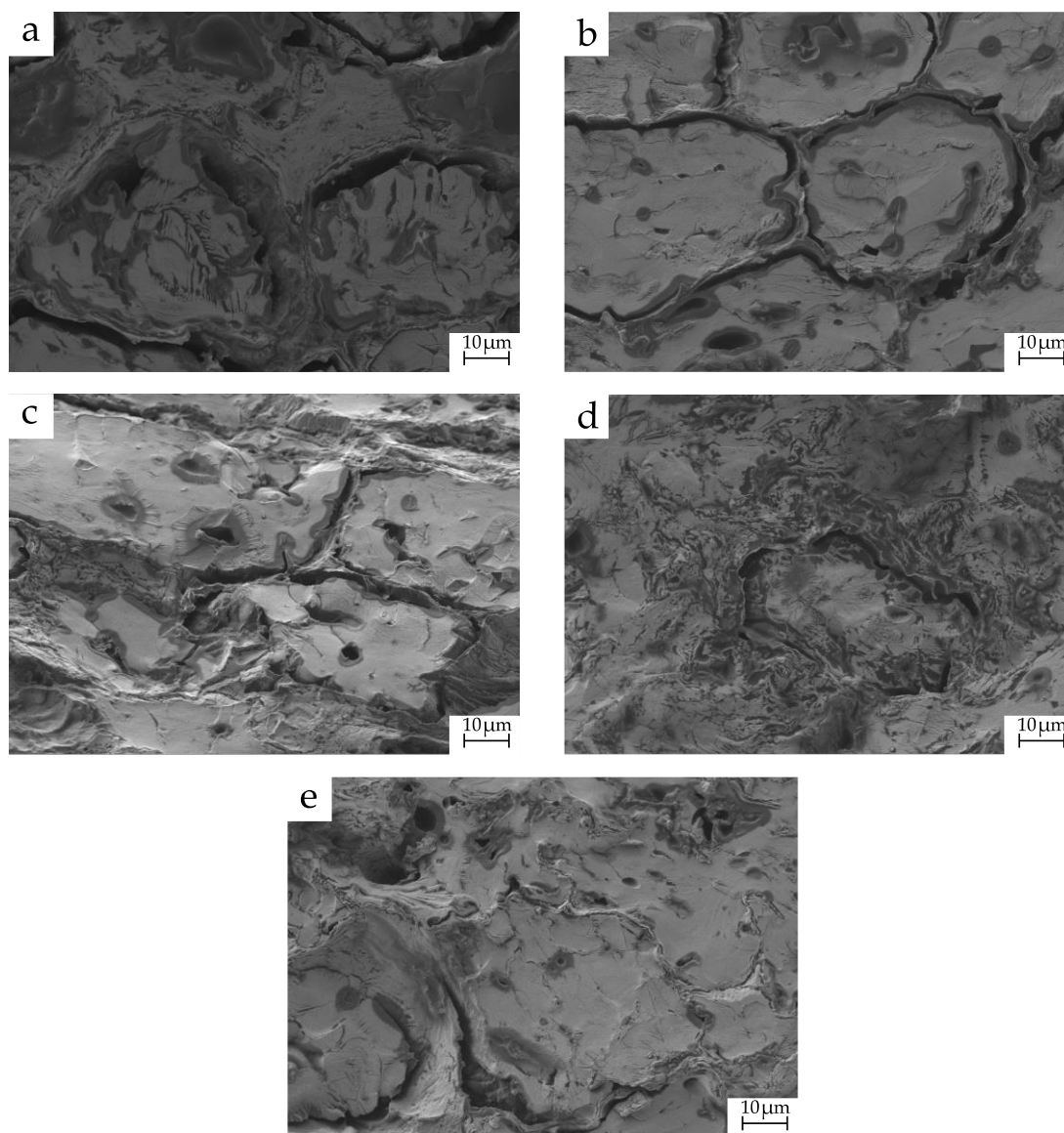


Figure III.1.3.3. FESEM images at 1000 \times magnification of the MKF/glycerol films: a) MKF-600/500; b) MKF-500/400; c) MKF-400/300; d) MKF-300/200 and e) MKF-200/100.

It is important to note that, after processing, the MKF particles decrease their size, as it can be observed in the FESEM images. This is due to a partial solubility of the

lignocellulosic MKF particles in water, thus, reducing their size [42]. In order to expose this phenomenon, **Figure III.1.3.4** shows the distribution of particle sizes in each one of the films. As it was expected, for smaller initial particle sizes, smaller final particle sizes were obtained. The film with particles between 600 and 500 μm presented an average final particle size of 42.5 μm , while the film with initial particles between 200 and 100 μm exhibited an average particle size of 15 μm . Therefore, it can be said that there is a certain correlation between the initial size of the particles and the final size of the particles in the film.

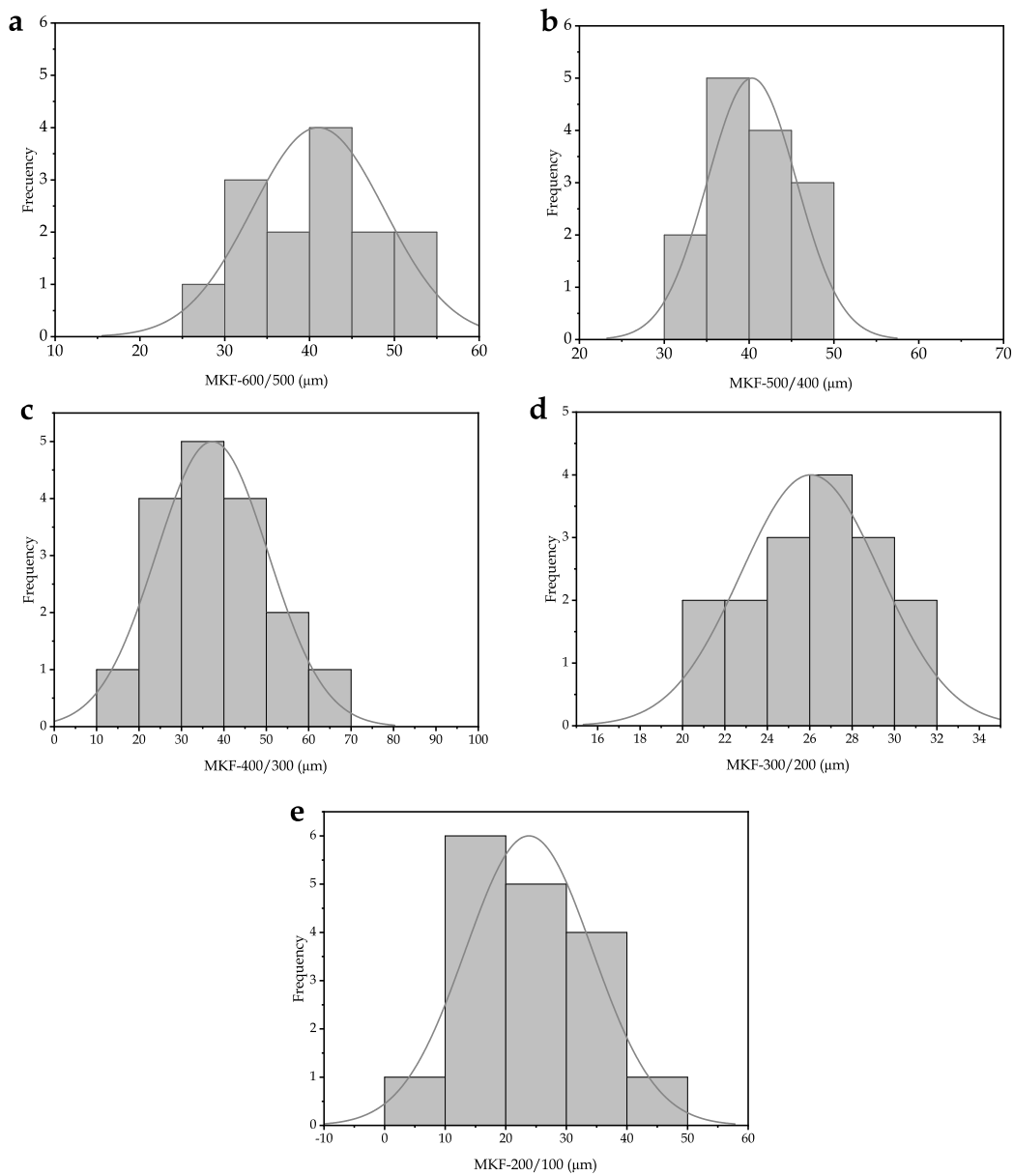


Figure III.1.3.4. Histograms of the MKF particles in the films after processing: a) MKF-600/500; b) MKF-500/400; c) MKF-400/300; d) MKF-300/200; e) MKF-200/100.

Barrier properties

Figure III.1.3.5 shows the WVTR value of MKF/glycerol films. It can be observed how the WVTR of the films decreases as the MKP particle size decreases. The WVTR value for MKF-600/500 is $6.9 \cdot 10^5$ g $\mu\text{m}/\text{cm}^2$ day; while the WVTR value for MKF-200/100 is $3.7 \cdot 10^5$ g $\mu\text{m}/\text{cm}^2$ day. This represents a reduction of 46% in terms of WVTR, which is a remarkable improvement. Smaller particle size leads to higher water affinity in the films as a result of an enhanced starch-based surface area, which should increase WVTR. However, in this case the prevailing phenomenon seems to be an increase in the density of the structure of the films, as a result of a more homogeneous distribution of the particles due to their smaller size. Consequently, WVTR decreases with the size of the particles, as the tortuosity of the diffusion path of water molecules through the film becomes higher [43]. Melo *et al.* [22], observed how MKF was capable of reducing the water vapour permeability of MKF/glycerol films, ascribing this effect to the hydrophobic fat content in the particles. These results perfectly match the findings observed in FESEM images, where the homogeneity was observed to increase as the particle size was reduced. It has been also shown that water vapour permeability can be controlled and drastically reduced by reducing the particle size of MKF, which can prove to be an advantage for food packaging and coatings [22].

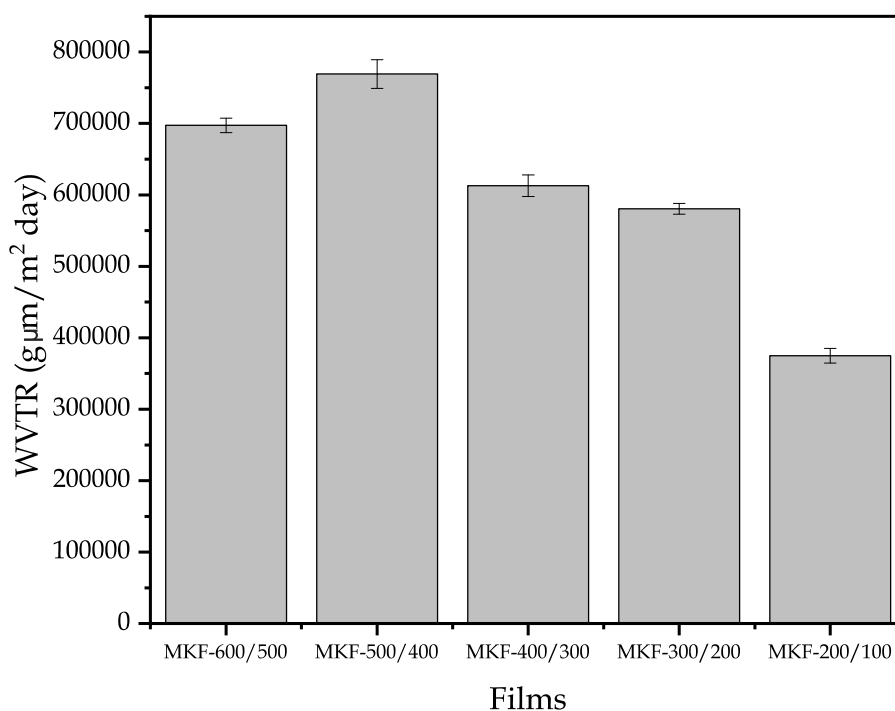


Figure III.1.3.5. Water vapour transmission rate (WVTR) of MKF/glycerol films with different particle size.

Visual aspect and colour properties

Table III.1.3.5 shows the main colorimetric parameters and the colour coordinates of the $CieL^*a^*b^*$ chromatic space for all the films herein developed. Additionally, **Figure III.1.3.6** shows the visual aspect of all the MKF/glycerol films. At first sight, it can be seen how all the films present very similar colours between them, with very similar ΔE values. Additionally, they lack any sign of transparency, due to the intrinsic dark colour of the MKF particles. On the other hand, it can be observed that luminance (L^*), which is related to the lightness of the samples, decreases with the particle size, which was expected, as smaller particles lead to more homogeneous films and thus, darker colours. This can be confirmed in **Figure III.1.3.6**, where MKF-200/100 exhibits a unique dark brown colour, while samples MKF-600/500, MKF-500/400 and MKF-400/300 show signs of heterogeneity, with clearer tonalities in certain areas.

With regard to colour coordinate a^* , it stands for green (negative) and red (positive) colours [44]. The a^* coordinate seems to decrease with the particle size, which could be ascribed to the fact that larger particle samples lead to more heterogeneous films, and show signs of reddish like spots, as it can be seen in **Figure III.1.3.6**, thus leading the a^* value towards more positive values. On the other hand, the b^* coordinate is related to blue (negative) and yellow (positive) colours [45]. In this case, there is a clear difference between the MKF/glycerol films with the three largest particle samples, with values very similar and close to 3.0; and the other two samples, with lower values, close to 2.0. This is mainly ascribed to the fact that the first samples have reddish-yellow like areas (rich in glycerol) as a result of their heterogeneity, while the other two samples lack these areas due to being more homogeneous and thus, decreasing the b^* coordinate value.

Table III.1.3.5. Luminance (L^*), colour coordinates (a^*b^*) and total colour difference (ΔE) of MKF/glycerol films with different MKF particle size.

Code	L^*	a^*	b^*	ΔE
MKF-600/500	26.2 ± 0.1^a	3.41 ± 0.10^a	3.01 ± 0.08^a	69.2 ± 0.2^a
MKF-500/400	25.8 ± 0.2^a	3.26 ± 0.38^a	3.03 ± 0.16^a	69.5 ± 0.5^a
MKF-400/300	25.7 ± 0.1^a	3.03 ± 0.37^b	3.02 ± 0.15^a	69.6 ± 0.4^a
MKF-300/200	25.2 ± 0.1^a	2.47 ± 0.06^c	2.15 ± 0.15^b	70.1 ± 0.2^a
MKF-200/100	25.2 ± 0.1^a	2.72 ± 0.12^d	2.22 ± 0.14^b	70.0 ± 0.2^a

a-d Different letters in the same column indicate a significant difference ($p < 0.05$).

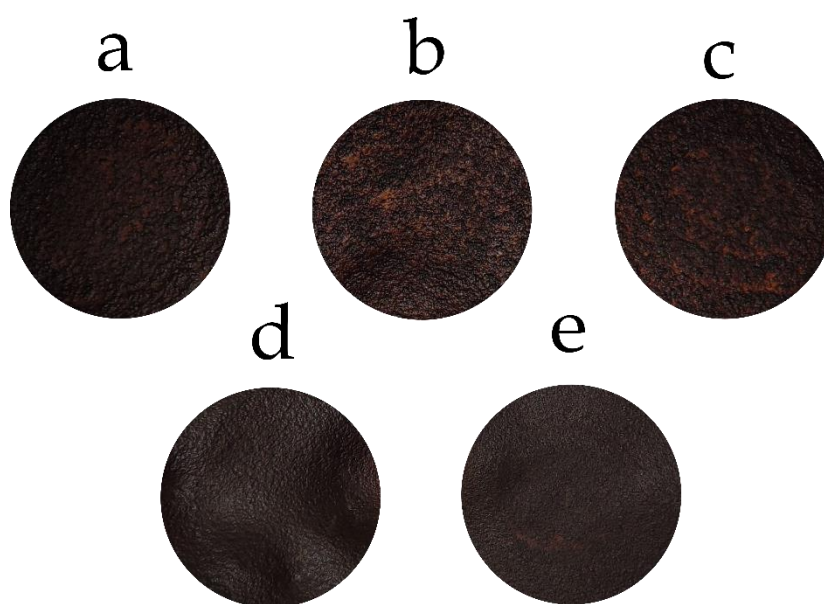


Figure III.1.3.6. Visual aspect of MKF/glycerol films: a) MKF-600/500; b) MKF-500/400; c) MKF-400/300; d) MKF-300/200 and e) MKF-200/100.

Antioxidant activity

DPPH free radical method was used in this study to evaluate the antioxidant activity of the MKF/glycerol films. In this technique, solutions present an initial purple colour, that changes into yellow when antioxidant substances are present in the sample. This change in colour is based on antioxidants donating hydrogens from their phenolic hydroxyl groups to scavenge free radicals of DPPH and form more stable compounds [46]. **Figure III.1.3.7** shows the DPPH inhibition (%) profile for all the developed films at different times, from 1 h to 168 h of exposure of the samples to the DPPH solution. It can be seen how all the samples present a very high antioxidant activity (between 85 and 95%), compared to other antioxidant films with active compounds such as

epigallocatechin gallate nanocapsules [47], tea extracts [48, 49], licorice waste extract [50] and even mango peel extracts [51]. Melo *et al.* [22], reported a similar antioxidant activity, superior to 90% for films with mango kernel phenolic extracts and mango kernel flour. It can be observed how the radical scavenging activity increases with a decrease in the particle size, being the MKF-200/100 film the one with the highest DPPH inhibition in all the time range, achieving almost 95% at 168 h. This could be ascribed to the fact that lower particle size leads to a major interface area of the MKF particles with the DPPH solution, thus presenting higher disponibility of hydroxyl groups to donate hydrogens into the DPPH solution [52]. Additionally, it should be noted the rate with which these films achieve their maximum DPPH inhibition, as at only 1 h of the test, this parameter is almost at its maximum, with small variations along the following week until 168 h. Adilah *et al.* [28], also observed a DPPH inhibition of almost 90% for samples with 5 wt% of mango kernel extract. Nonetheless the results presented here show exceptional radical scavenging activity.

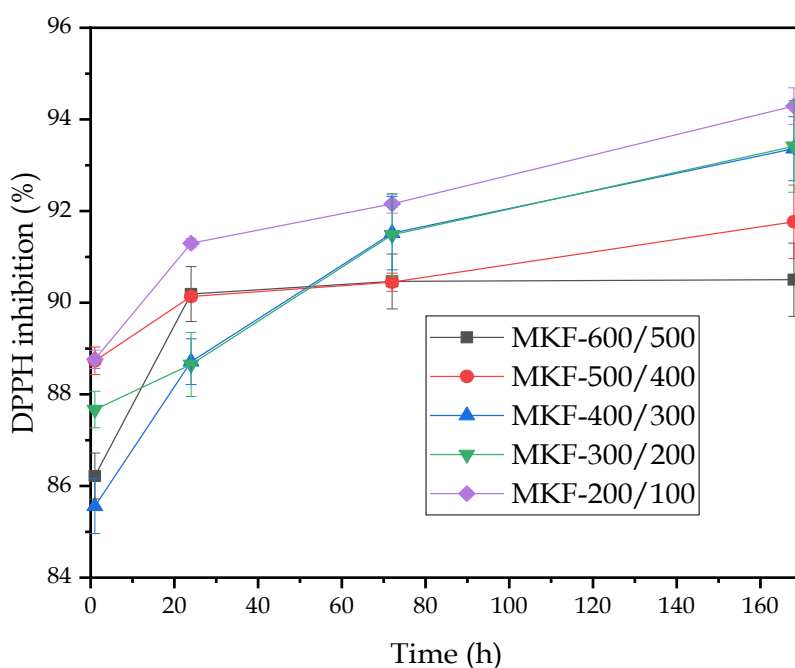


Figure III.1.3.7. Percentage of 2,2-diphenyl-1-picrylhydrazyl radical (DPPH) inhibition of MKF/glycerol films with different particle sizes of MKF.

Disintegration test

The biodegradability of the films was studied by means of the disintegration test. **Figure III.1.3.8** shows the quantitative evolution of the weight of the samples over time through the disintegration process during 28 days (the red line indicates 90%, which is the disintegration goal), while **Figure III.1.3.9** shows the visual appearance of the film samples all over this process. It can be seen how the disintegration profile of all the samples is quite similar in terms of the weight loss rate. All the films strongly disintegrate at the first day of the test, losing more than 20% of their mass just after that short period of time. This is a sign of the high biodegradability of these films. Moreover, all the samples completely disintegrate after 28 days of incubation in compost soil, which is another indicator of their degradability under these conditions. The disintegration profile is similar to the one observed by Seligra *et al.* [53], in starch/glycerol films, which were disintegrated in 30 days. This behavior is mainly ascribed to the high hydrophilicity that those films possess, as water diffuses into the polymeric film sample causing swelling and increasing microbial growth. In spite of the fact that all the films have a similar disintegration profile, the samples with smaller MKF particle size present a slightly higher biodegradation rate, as they achieve 90% of disintegration (which is the weight loss goal for considering a material biodegradable according to the standard mentioned in the experimental section) faster than the rest of the samples. This could be ascribed to a higher hydrophilic surface of these samples, as shown in wettability and contact angle measurements. This disintegration profile can be confirmed by its visual appearance, which clearly shows how at day 7, the films become very brittle and start to decompose. It can also be seen that at day 21, all the films have suffered strong disintegration, especially samples MKF-300/200 and MKF-200/100, which are almost completely gone.

These results confirm the total biodegradability of these films, as well as their high biodegradation rate in comparison with other biodegradable polymers such as PHB or TPS [54, 55], whose disintegration time is superior to 40 days. This fact gives MKF/glycerol films of great applicability in environmentally friendly packaging.

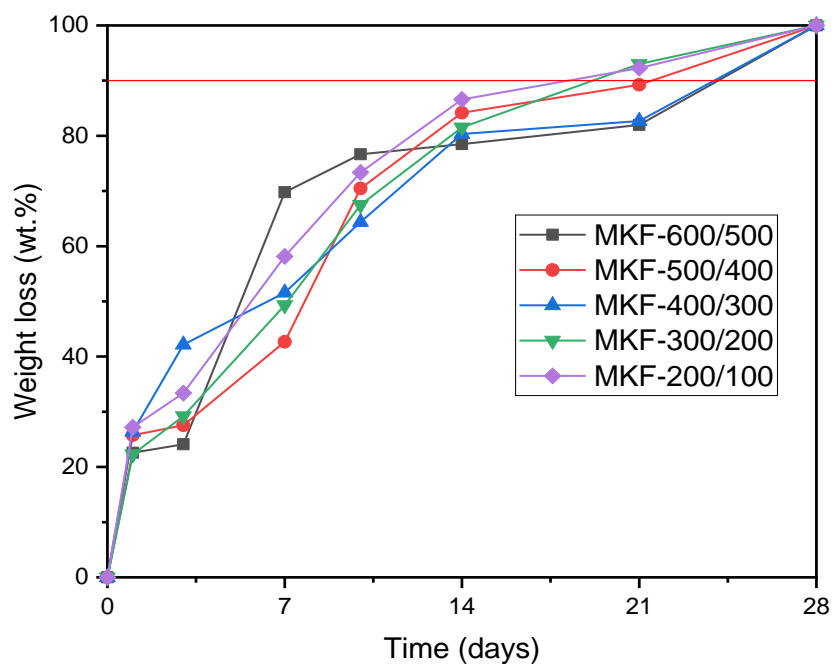


Figure III.1.3.8. Biodegradation profile under controlled compost soil in terms of the incubation time of all the MKF/glycerol films with different MKF particle size.

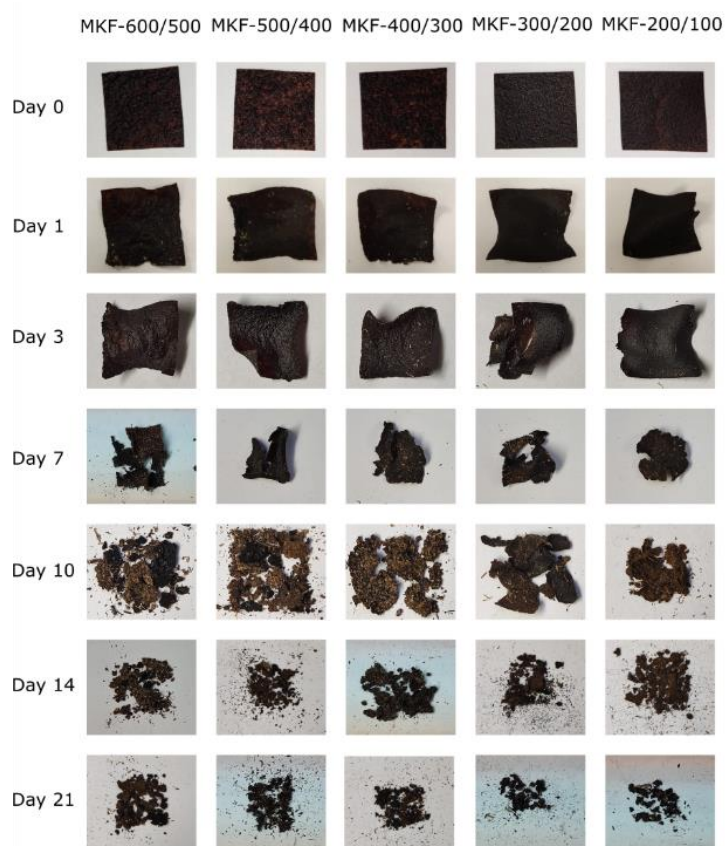


Figure III.1.3.9. Visual appearance of the disintegration process of MKF/glycerol films over time with different MKF particle size.

Roughness measurements

The surface topography of the films was studied and evaluated through roughness measurements. **Table III.1.3.6** gathers the mean roughness values (R_a) of all the films. The roughness of the MKF-600/500 film was 17.38 μm , which represents a considerable rough surface in comparison with glycerol and starch films, which show values of 3.0 nm [56]. This is clearly due to the large size of MKF compared to neat starch films. Observing the mean roughness values of all MKF/glycerol films, there is a clear decreasing trend of R_a with a decrease in the size of the MKF particles. Particularly, MKF-300/200 and MKF-200/100 show the lowest roughness, with values of 7.52 and 6.42 μm , respectively. This decreasing tendency is ascribed to an increase in the homogeneity of the surface of the films as a result of the presence of smaller particles, which make an efficient dispersion easier and avoid the formation of MKF aggregates that alter the smoothness of the film surface. These results are in accordance with what was observed in **Figure III.1.3.6**, where the heterogeneity of samples with higher particle size was observed.

Table III.1.3.6. Arithmetic Roughness (R_a) of the MKF/glycerol films with different MKF particle size.

Film	Roughness R_a (μm)
MKF-600/500	17.38 \pm 0.08 ^a
MKF-500/400	16.10 \pm 1.10 ^b
MKF-400/300	13.10 \pm 0.76 ^c
MKF-300/200	7.52 \pm 0.22 ^d
MKF-200/100	6.42 \pm 0.53 ^e

a-e Different letters in the same column indicate a significant difference ($p < 0.05$).

CONCLUSIONS

Totally natural, biodegradable and environmentally friendly glycerol films with mango kernel flour (MKF) of different sizes, ranging from 600 to 100 μm , were successfully obtained by the casting solution method. The obtained films showed an increasing trend in their mechanical properties as the particle size diminished, with a tensile strength and elongation at break of 1.08 MPa and 18.1%, respectively, for the MKF-200/100 sample. These results were in accordance with FESEM images, which showed that smaller particles lead to more homogeneous structures within the film. Additionally, narrower gaps between the starch-based particles and the glycerol matrix

were observed, positively affecting the cohesion of the films and, thus, the mechanical performance as well. The decrease in the particle size of the MKF also improved the barrier properties of the films due to a more homogeneous surface, which increases the density of the film and difficults water vapour to pass through its pores. The MKF-200/100 sample exhibited a WVTR of $3.7 \cdot 10^5$ g $\mu\text{m}/\text{cm}^2$ day, which is 46% smaller than the WVTR of the MKF-600/500 film. The developed films showed very dark brown colours, which were due to the intrinsic natural colour of mango kernel, and they proved to possess a remarkable DPPH radical scavenging capability. Interestingly, just after 1 hour of the DPPH test, the films had almost achieved their maximum DPPH inhibition (over 90% DPPH radical scavenging), which demonstrates their strong antioxidant nature, which is a favourable characteristic in the field of food packaging. The films were also subjected to the disintegration test in controlled compost soil, where they proved to be completely biodegradable, achieving 100% of weight loss just after 28 days of incubation time. The samples with smaller particles presented a superior biodegradation rate, which may be an interesting feature for food packaging and coating applications. Finally, the roughness of the samples demonstrated that the homogeneity of their surfaces increases as the particle size decreases. The MKF-200/100 film showed the lowest roughness of them all, with a R_a of 6.42 μm .

All in all, the presented results show that the overall properties of the MKF/glycerol films improve when the particle size of MKF decreases, as the structure of the film becomes more homogeneous. This also demonstrates that some properties, such as water vapour permeability, can be controlled through the particle size. Moreover, this fact could be applicable to other films with different starch-based fillers. The herein developed films have proved to be suitable for applications where completely biodegradable, antioxidant and natural films are required.

ACKNOWLEDGEMENTS

This research is a part of the grant PID2020-116496RB-C22 funded by MCIN/AEI/10.13039/501100011033. Authors also thank Generalitat Valenciana-GVA, grant number AICO/2021/025 for supporting this work. J. Gomez-Caturla wants to thank Generalitat Valenciana-GVA, for his FPI grant (ACIF/2021/185) and grant FPU20/01732 funded by MCIN/AEI/ 10.13039/501100011033 and by ESF Investing in your future. J. Ivorra-Martinez wants to thank FPU19/01759 grant funded by MCIN/AEI/ 10.13039/501100011033 and by ESF Investing in your future. Microscopy Services at UPV are also acknowledged by their help in collecting and analyzing images.

REFERENCES

- [1] Shen, M., et al., *(Micro) plastic crisis: Un-ignorable contribution to global greenhouse gas emissions and climate change*. *Journal of Cleaner Production*, 2020. 254: 120138.
- [2] Jang, Y.-C., et al., *Recycling and management practices of plastic packaging waste towards a circular economy in South Korea*. *Resources, Conservation and Recycling*, 2020. 158: 104798.
- [3] Liminana, P., et al., *Development and characterization of environmentally friendly composites from poly (butylene succinate)(PBS) and almond shell flour with different compatibilizers*. *Composites Part B: Engineering*, 2018. 144: 153-162.
- [4] Ghiasi, F., et al., *A new approach in the hydrophobic modification of polysaccharide-based edible films using structured oil nanoparticles*. *Industrial Crops and Products*, 2020. 154: 112679.
- [5] Giosafatto, C.V.L., et al., *Preparation and characterization of bioplastics from grass pea flour cast in the presence of microbial transglutaminase*. *Coatings*, 2018. 8(12): 435.
- [6] Zhang, S., et al., *Soy protein isolate-based films reinforced by surface modified cellulose nanocrystal*. *Industrial Crops and Products*, 2016. 80: 207-213.
- [7] Kocabaş, D.S., et al., *Bulgur bran as a biopolymer source: Production and characterization of nanocellulose-reinforced hemicellulose-based biodegradable films with decreased water solubility*. *Industrial Crops and Products*, 2021. 171: 113847.
- [8] Bamdad, F., A.H. Goli, and M. Kadivar, *Preparation and characterization of proteinous film from lentil (*Lens culinaris*): Edible film from lentil (*Lens culinaris*)*. *Food research international*, 2006. 39(1): 106-111.
- [9] Mokrejs, P., et al., *Thermal study and solubility tests of films based on amaranth flour starch–protein hydrolysate*. *Journal of thermal analysis and calorimetry*, 2009. 98(1): 299-307.
- [10] Li, W., et al., *One-step quaternization/hydroxypropylsulfonation to improve paste stability, adhesion, and film properties of oxidized starch*. *Polymers*, 2018. 10(10): 1110.
- [11] Wang, Y., et al., *Bioinspired colored degradable starch-based films with excellent tensile strength*. *Industrial Crops and Products*, 2021. 167: 113525.
- [12] Huntrakul, K., et al., *Effects of pea protein on properties of cassava starch edible films produced by blown-film extrusion for oil packaging*. *Food Packaging and Shelf Life*, 2020. 24: 100480.

- [13] Colla, E., P.J. do Amaral Sobral, and F.C. Menegalli, *Amaranthus cruentus flour edible films: influence of stearic acid addition, plasticizer concentration, and emulsion stirring speed on water vapor permeability and mechanical properties*. Journal of agricultural and Food Chemistry, 2006. 54(18): 6645-6653.
- [14] Grinberg, V.Y. and V. Tolstoguzov, *Thermodynamic incompatibility of proteins and polysaccharides in solutions*. Food Hydrocolloids, 1997. 11(2): 145-158.
- [15] Hassan, B., et al., *Recent advances on polysaccharides, lipids and protein based edible films and coatings: A review*. International journal of biological macromolecules, 2018. 109: 1095-1107.
- [16] Tapia-Blácido, D., P. do Amaral Sobral, and F. Menegalli, *Optimization of amaranth flour films plasticized with glycerol and sorbitol by multi-response analysis*. LWT-Food Science and Technology, 2011. 44(8): 1731-1738.
- [17] Nouraddini, M., M. Esmaili, and F. Mohtarami, *Development and characterization of edible films based on eggplant flour and corn starch*. International journal of biological macromolecules, 2018. 120: 1639-1645.
- [18] Dick, M., et al., *Edible films based on chia flour: Development and characterization*. Journal of Applied Polymer Science, 2016. 133(2): 42455.
- [19] Mikus, M., et al., *Development and Characterization of Novel Composite Films Based on Soy Protein Isolate and Oilseed Flours*. Molecules, 2021. 26(12): 3738.
- [20] Wang, W., et al., *Multilayer surface construction for enhancing barrier properties of cellulose-based packaging*. Carbohydrate Polymers, 2021. 255: 117431.
- [21] Quiles-Carrillo, L., et al., *Bioactive multilayer polylactide films with controlled release capacity of gallic acid accomplished by incorporating electrospun nanostructured coatings and interlayers*. Applied Sciences, 2019. 9(3): 533.
- [22] Melo, P.E., et al., *Antioxidant films from mango kernel components*. Food Hydrocolloids, 2019. 95: 487-495.
- [23] Thakor, N., *Indian Mango–Production and Export Scenario*. Peach, 2019. 18(107): 0-12.
- [24] Silva, A.P.M., et al., *Mango kernel starch films as affected by starch nanocrystals and cellulose nanocrystals*. Carbohydrate polymers, 2019. 211: 209-216.
- [25] Bally, I.S., et al., *The ‘Tommy Atkins’ mango genome reveals candidate genes for fruit quality*. BMC plant biology, 2021. 21: 1-18.

-
- [26] Yatnatti, S., D. Vijayalakshmi, and R. Chandru, *Processing and nutritive value of mango seed kernel flour*. *Current Research in Nutrition and Food Science Journal*, 2014. 2(3): 170-175.
- [27] Augustin, M. and E. Ling, *Composition of mango seed kernel*. *Pertanika (Malaysia)*, 1987. 10(1).
- [28] Adilah, Z.M., B. Jamilah, and Z.N. Hanani, *Functional and antioxidant properties of protein-based films incorporated with mango kernel extract for active packaging*. *Food Hydrocolloids*, 2018. 74: 207-218.
- [29] Pérez-Gago, M.B. and J.M. Krochta, *Lipid particle size effect on water vapor permeability and mechanical properties of whey protein/beeswax emulsion films*. *Journal of agricultural and food chemistry*, 2001. 49(2): 996-1002.
- [30] Adjei-Fremah, S., et al., *Effect of microfluidization on microstructure, protein profile and physicochemical properties of whole cowpea flours*. *Innovative Food Science & Emerging Technologies*, 2019. 57: 102207.
- [31] Tonyali, B., S. Cikrikci, and M.H. Oztop, *Physicochemical and microstructural characterization of gum tragacanth added whey protein based films*. *Food Research International*, 2018. 105: 1-9.
- [32] Masamba, K., et al., *Effect of Gallic acid on mechanical and water barrier properties of zein-oleic acid composite films*. *Journal of food science and technology*, 2016. 53(5): 2227-2235.
- [33] Trifol, J., et al., *Hybrid poly (lactic acid)/nanocellulose/nanoclay composites with synergistically enhanced barrier properties and improved thermomechanical resistance*. *Polymer International*, 2016. 65(8): 988-995.
- [34] Basiak, E., A. Lenart, and F. Debeaufort, *How glycerol and water contents affect the structural and functional properties of starch-based edible films*. *Polymers*, 2018. 10(4): 412.
- [35] Nawab, A., F. Alam, and A. Hasnain, *Mango kernel starch as a novel edible coating for enhancing shelf-life of tomato (*Solanum lycopersicum*) fruit*. *International Journal of Biological Macromolecules*, 2017. 103: 581-586.
- [36] Cheng, L.H., A.A. Karim, and C.C. Seow, *Effects of water-glycerol and water-sorbitol interactions on the physical properties of konjac glucomannan films*. *Journal of Food Science*, 2006. 71(2): 62-67.

- [37] Godbillot, L., *et al.*, *Analysis of water binding in starch plasticized films*. Food Chemistry, 2006. 96(3): 380-386.
- [38] Vogler, E.A., *Structure and reactivity of water at biomaterial surfaces*. Advances in colloid and interface science, 1998. 74(1-3): 69-117.
- [39] Ryan, B.J. and K.M. Poduska, *Roughness effects on contact angle measurements*. American Journal of Physics, 2008. 76(11): 1074-1077.
- [40] Rosenbloom, R.A. and Y. Zhao, *Hydroxypropyl methylcellulose or soy protein isolate-based edible, water-soluble, and antioxidant films for safflower oil packaging*. Journal of Food Science, 2021. 86(1): 129-139.
- [41] Romero-Bastida, C.A., *et al.*, *Physicochemical and microstructural characterization of films prepared by thermal and cold gelatinization from non-conventional sources of starches*. Carbohydrate Polymers, 2005. 60(2): 235-244.
- [42] Källdström, M., *et al.*, *Fractionation of 'water-soluble lignocellulose' into C 5/C 6 sugars and sulfur-free lignins*. Green Chemistry, 2014. 16(5): 2454-2462.
- [43] Rojas-Lema, S., *et al.*, *Faba bean protein films reinforced with cellulose nanocrystals as edible food packaging material*. Food Hydrocolloids, 2021. 121: 107019.
- [44] Jorda-Reolid, M., *et al.*, *Upgrading Argan Shell Wastes in Wood Plastic Composites with Biobased Polyethylene Matrix and Different Compatibilizers*. Polymers, 2021. 13(6): 922.
- [45] Kaur, A. and B. Kranthi, *Comparison between YCbCr color space and CIELab color space for skin color segmentation*. International Journal of Applied Information Systems, 2012. 3(4): 30-33.
- [46] Pimpley, V.A. and P.S. Murthy, *Influence of green extraction techniques on green coffee: Nutraceutical compositions, antioxidant potential and in vitro bio-accessibility of phenolics*. Food Bioscience, 2021. 43: 101284.
- [47] Liang, J., *et al.*, *Preparation and characterization of antioxidant edible chitosan films incorporated with epigallocatechin gallate nanocapsules*. Carbohydrate polymers, 2017. 171: 300-306.
- [48] Lei, Y., *et al.*, *Investigation of the structural and physical properties, antioxidant and antimicrobial activity of pectin-konjac glucomannan composite edible films incorporated with tea polyphenol*. Food Hydrocolloids, 2019. 94: 128-135.

- [49] Wu, H., *et al.*, *Preparation and characterization of bioactive edible packaging films based on pomelo peel flours incorporating tea polyphenol*. *Food Hydrocolloids*, 2019. 90: 41-49.
- [50] Han, Y., M. Yu, and L. Wang, *Preparation and characterization of antioxidant soy protein isolate films incorporating licorice residue extract*. *Food Hydrocolloids*, 2018. 75: 13-21.
- [51] Adilah, A.N., *et al.*, *Utilization of mango peel extracts on the biodegradable films for active packaging*. *Food packaging and shelf life*, 2018. 16: 1-7.
- [52] Prasedya, E., *et al.*, *Effect of particle size on phytochemical composition and antioxidant properties of Sargassum cristaefolium ethanol extract*. *Scientific Reports*, 2021. 11(1): 17876.
- [53] Seligra, P.G., *et al.*, *Biodegradable and non-retrogradable eco-films based on starch-glycerol with citric acid as crosslinking agent*. *Carbohydrate Polymers*, 2016. 138: 66-74.
- [54] Garcia-Garcia, D., *et al.*, *Reinforcing capability of cellulose nanocrystals obtained from pine cones in a biodegradable poly (3-hydroxybutyrate)/poly (ϵ -caprolactone)(PHB/PCL) thermoplastic blend*. *European Polymer Journal*, 2018. 104: 10-18.
- [55] Pavon, C., *et al.*, *Films based on thermoplastic starch blended with pine resin derivatives for food packaging*. *Foods*, 2021. 10(6): 1171.
- [56] Villacrés, R.A.E., S.K. Flores, and L.N. Gerschenson, *Biopolymeric antimicrobial films: Study of the influence of hydroxypropyl methylcellulose, tapioca starch and glycerol contents on physical properties*. *Materials Science and Engineering: C*, 2014. 36: 108-117.

III.1.4. Manufacturing and characterization of high environmentally-friendly composites with polylactide matrix and mango kernel seed flour

Jaume Gomez-Caturla^{1*}, Diego Lascano¹, Luis Montanes¹, Rafael Balart¹, Franco Dominici², Debora Puglia² and Luigi Torre²

¹Technological Institute of Materials – ITM, Universitat Politècnica de València – UPV, Plaza Ferrándiz y Carbonell 1, 03801 Alcoy (Spain).

²Dipartimento di Ingegneria Civile ed Ambientale, University of Perugia, UdR INSTM, Strada di Pentima, 4 - 05100 Terni (TR) Italy.



Express Polymer Letters

2023, 17(3): 334-351

*Adapted from the original manuscript.

Express Polymer Letters Vol.17, No.3 (2023) 334–351
 Available online at www.expresspolymlett.com
<https://doi.org/10.3144/expresspolymlett.2023.24>

express
polymer letters

Research article

Manufacturing and characterization of highly environmentally-friendly composites with polylactide matrix and mango kernel seed flour

Jaume Gomez-Caturla^{1*}, Diego Lascano¹, Nestor Montanes¹, Rafael Balart¹,
 Franco Dominici², Debora Puglia², Luigi Torre²

¹Technological Institute of Materials (ITM), Universitat Politècnica de València (UPV), Plaza Ferrándiz y Carbonell 1, 03801 Alcoy, Spain

²Dipartimento di Ingegneria Civile ed Ambientale, University of Perugia, Udr INSTM, Strada di Pentima 4, 05100 Terni (TR) Italy

Received 7 July 2022; accepted in revised form 5 October 2022

Abstract. This work reports on the development of polylactide (PLA)/mango kernel seed flour (MKSF) composites combined with tributyrin (TBN) and triacetin (TCN) as plasticizers. Thus, wood plastic composites (WPC) are obtained by extrusion and injection-molding processes. The solubility, mechanical, morphological, thermal, colorimetric, water absorbance, flowability, and disintegrability properties are evaluated. The ductility of the PLA+MKSF composite is improved by the plasticizing effect of TBN and TCN (10 phr (parts per hundred resin) each). Elongation at break is increased from 4.4 up to 9.5 and 8.3%, respectively. The theoretical solubility analysis supports the good miscibility between PLA with TBN and TCN (relative energy difference (RED) values of 0.86 and 0.73, respectively) deduced from the mechanical performance. Field emission scanning electron microscopy (FESEM) images also corroborate the mechanical findings, where a decrease in the presence of voids in the PLA matrix suggests certain compatibility between MKSF and TBN, and TCN. Differential scanning calorimetry (DSC) and dynamic-mechanical-thermal analysis (DMTA) results show that the plasticizers decrease the glass transition temperature and the melting temperature of PLA, thus improving its ductility. Thermogravimetric analysis (TGA) results indicate that the thermal stability of the composite is slightly decreased due to the relatively high volatility of the plasticizers, while MKSF does not affect this matter. The composites exhibit excellent biodegradability, presenting more than 90% of disintegration in compost soil conditions in 12 weeks. Finally, MKSF provided the composites with a wood-like dark brown color and with high water absorbance.

Keywords: polymer composites, biodegradable polymers, mechanical properties, thermal properties, plasticizer

1. Introduction

Wood-plastic composites (WPC) have risen as an alternative for products made of wood. Those materials have a visual appearance similar to that of wood. The main difference is that they are composed of a thermoplastic polymeric matrix (such as polyethylene and polypropylene, among others), which is loaded with fillers from the wood industry (sawdust, fibres, flour) [1, 2]. In the first approach, the manufacturing

of WPC implies the incorporation of wood-based elements. However, in the last years, other fillers have been proposed as alternatives for wood-derived fillers, either lignocellulosic fillers or mineral fillers (talc, calcium carbonate, among others), or agroforestry waste flours [3, 4]. The latter have gained quite a popularity due to the significant amount of generated waste (skin, calyx, seeds) [5–7]. As a result of their low cost and abundance, the incorporation

*Corresponding author, e-mail: jaugoca@epsa.upv.es
 © BME-PT

Manufacturing and characterization of high environmentally-friendly composites with polylactide matrix and mango kernel seed flour

Abstract

This work reports on the development of polylactide (PLA)/mango kernel seed flour (MKSF) composites, combined with tributyrin (TBN) and triacetin (TCN) as plasticizers. Thus, wood plastic composites (WPC) are obtained by extrusion and injection-molding processes. The solubility, mechanical, morphological, thermal, colorimetric, water absorbance, flowability and disintegrability properties are evaluated. The ductility of the PLA+MKSF composite is improved by the plasticizing effect of TBN and TCN (10 phr (parts per hundred resin) each). Elongation at break is increased from 4.4% up to 9.5 and 8.3%, respectively. The theoretical solubility analysis supports the good miscibility between PLA with TBN and TCN (relative energy difference (RED) values of 0.86 and 0.73, respectively) deduced from the mechanical performance. Field emission scanning electron microscopy (FESEM) images also corroborate the mechanical findings, where a decrease in the presence of voids in the PLA matrix suggests certain compatibility between MKSF and TBN and TCN. Differential scanning calorimetry (DSC) and dynamic-mechanical-thermal analysis (DMTA) results show that the plasticizers decrease the glass transition temperature and the melting temperature of PLA, thus improving its ductility. Thermogravimetric analysis (TGA) results indicate that the thermal stability of the composite is slightly decreased due to the relatively high volatility of the plasticizers, while MKSF does not affect in this matter. The composites exhibit excellent biodegradability, presenting more than 90% of disintegration in compost soil conditions in 12 weeks. Finally, MKSF provided the composites with a wood-like dark brown colour and with high water absorbance.

Keywords: Polymer composites, biodegradable polymers, mechanical properties, thermal properties, plasticizer.

INTRODUCTION

Wood-plastic composites (WPC) have risen as an alternative for products made of wood. Those materials have a visual appearance similar to that of wood. The main difference is that they are composed of a thermoplastic polymeric matrix (such as polyethylene, and polypropylene, among others), which is loaded with fillers from the wood industry (sawdust, fibers, flour) [1, 2]. In the first approach, the manufacturing of WPC implies the incorporation of wood-based elements. However, in the last years, other fillers have been proposed as alternatives for wood-derived fillers, either lignocellulosic fillers or mineral fillers (talc, calcium carbonate, among others) or agroforestry waste flours [3, 4]. The latter have gained quite popularity due to the significant amount of generated waste (skin, calyx, seeds) [5-7]. As a result of their low cost and abundance, the incorporation of fillers from food byproducts and agroforestry wastes has become a technical and viable solution in the plastics industry. Moreover, the materials obtained from them possess balanced properties and an advantageous environmental efficiency [8]. The use of biofillers presents several advantages, such as facilitating or accelerating the disintegration of material; reducing the amount of used polymer, and the revalorization of a lignocellulosic waste, all these promoting the transition from a traditional linear economy to a circular economy and thus, remarkably reducing the carbon footprint [9, 10]. Rojas Lema *et al.* [11] used wastes from persimmon peel to manufacture composite materials with a biopolyethylene matrix. Moreover, they studied the effect of silanization treatments and esterification with palmitic acid to enhance compatibilization between the filler and the polymer matrix. They reported interesting results compared to the conventional use of a maleic anhydride-grafted copolymer of polyethylene as a reference compatibilizer. It was also proved that this waste provided additional features to composites with polyethylene. In particular, it was observed that the persimmon peel wastes gave a tremendous antioxidant activity to the polyethylene matrix. The compatibility between the polymeric matrix and the filler was also increased. The esterification with palmitic chloride treatment improved the hydrophobic behaviour of the materials, diminishing their water absorption capacity.

Tropical crops like mango have become one of the preferred products for consumers in the European market. This is because this fruit is considered exotic, has attractive colours, delicious flavour and a comfortable odour [12]. Moreover, it presents a high nutritional value as it contains a large number of macronutrients (carbohydrates, proteins, lipids) and micronutrients (vitamins A, B, C, folic acid and minerals), which help to prevent degenerative diseases [13]. The greatest producers in 2019 were Asia, accounting for the 71.5% of the global market, followed by Africa (16%), America (12.3%)

and finally Oceania, with a 0.1% of the global production, according to the Food and Agriculture Organization of the United Nations. Even though the composition of mango fruit varies depending on its species, the flesh includes typically between 33-85 wt.% of the total mass, resulting in a waste of 7-24 wt.% of mango peel and 9-40 wt.% of the kernel. The kernel contains 6-16 wt.% of mango oil [14]. It has been reported that the kernel possesses a large amount of carbohydrates and proteins (58-80 wt.% and 6-13 wt.%, respectively), apart from containing oleic and stearic acids [15] and polyphenols [16].

The search to reduce the use of petrochemical polymers in the composite fabrication sector has made the development and use of renewable and biodegradable materials to gain popularity in the last years [17]. Polylactic acid (PLA) is one of the most widely used polymer matrices in environmentally friendly materials. This is because PLA monomers are obtained from the fermentation of starch-rich compounds, so the products are biodegradable in controlled compost soil conditions [18, 19].

PLA-based composites present several limitations provoked by PLA's low impact strength and toughness and, subsequently, high fragility [20]. One of the most common techniques to overcome this inconvenience is mixing PLA with more flexible polymers and/or incorporating additives (plasticizers) [21, 22]. Lascano *et al.* [21] developed a binary blend using PLA and poly (butylene succinate-co-adipate) (PBSA). It was observed that the ductile behaviour of the blend improved, increasing the elongation at break and impact strength from 9.23% and 2.48 kJ/m² for neat PLA, respectively, to 56% and 5.75 kJ/m² for the blend with 30 wt.% of PBSA. Several natural-origin plasticizers are being utilized due to their low toxicity. Among those plasticizers are lactic acid, lactic acid oligomers (OLA), vegetal oils (VO), citrate esters, tributyrin, triacetin and so on. Montes *et al.* [23] developed a blend made of poly(lactic acid)/poly(3-hydroxybutyrate) utilizing tributyrin as a plasticizer to produce completely natural films for food packaging applications. They observed that the incorporation of 15 wt.% tributyrin increased the ductile properties of the material apart from presenting good water vapour barrier properties and certain transparency. Crystallinity was also increased. Coltelli *et al.* [24] studied the behavior of composites based on PLA and polyhydroxybutyrate plasticized with triacetin. They observed that PLA biodegradability improved thanks to the disintegration of the amorphous phase.

This work aims to develop a completely natural composite based on a polylactic acid (PLA) matrix and mango kernel seed flour (MKSF) as a biobased filler. To overcome the low intrinsic toughness of the PLA matrix, two bio-derived plasticizers were used,

namely glycerol tributyrate (tributylin) and glycerol triacetate (triacetin). There is little literature regarding the use of mango kernel flour as a filler for polylactide. Additionally, TBN and TCN have not been widely used for plasticizing PLA wood plastic composites, and never have been used in a PLA/MKSF composite. The effects of both plasticizers and the MKSF filler were evaluated through standard mechanical, thermal, and thermomechanical tests, morphology characterization, water absorption and disintegrability under controlled compost soil characterization.

MATERIALS AND METHODS

Materials

Bio-based PLA Purapol L130 grade (min. 99% of L-isomer) was supplied by Corbion Purac (The Netherlands, Amsterdam), with a density of 1.24 g/cm³, a melt flow index of 16 g/10 min (measured at a temperature of 210 °C and a load of 2.16 kg) and a melting temperature of 175 °C.

Flour extracted from mango kernel from *Mangifera indica* L. species was used as a filler. The mango seed was dried at 65 °C for a week. The mango kernel was extracted and submitted to a milling process in a Retsch GmbH model ZM 1000 ultracentrifugal mill (Haan, Germany) with a sieve size of 25 µm and a rotation speed of 12,000 rpm. **Figure III.1.4.1** shows the morphology and histogram (size distribution) of the mango kernel seed flour particles (MKSF), which present an average particle diameter size of 18-20 µm.

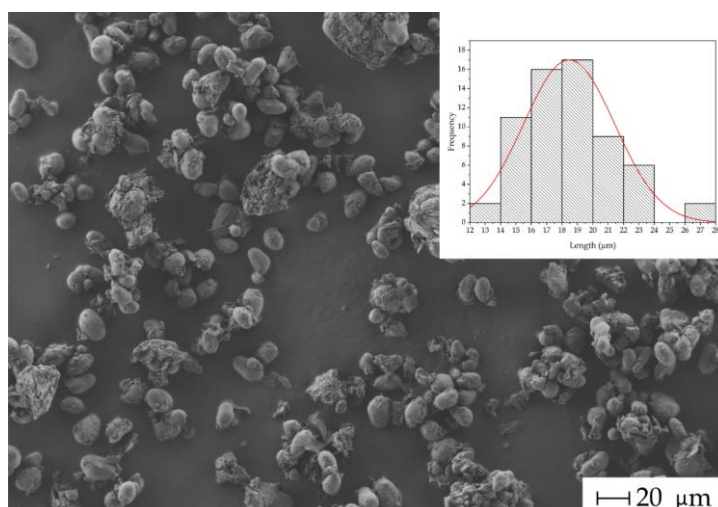


Figure III.1.4.1. FESEM image of mango kernel seed flour (MKSF) particles at 150× with a marker scale of 20 µm.

Glycerol tributyrate (tributylin) from ACROS Organics™ and distributed by Thermo Fisher Scientific (Geel, Belgium) (Product Code: A11830.0B) and glycerol triacetate (triacetin) from Sigma Aldrich (Madrid, Spain) (Product Code: 90240) were used as plasticizers. Tributyrin is 97% pure, with a density of 1.0335 g/mL and a melting point of -75 °C. Triacetin presents a purity of 99%, a density of 1.16 g/mL and a melting point of 3 °C.

Manufacturing of PLA-MKSF composites

Prior to processing, PLA pellets and MKSF particles were dried in an air circulating oven at 65 °C for 12 hours to eliminate humidity. The compounds were formulated with a constant MKSF weight percentage of 30 wt%. Plasticizers (tributylin and triacetin) were added directly in the extrusion process, always maintaining 10 phr (parts by weight of plasticizer per one hundred parts by weight of the PLA/MKSF base composition taking the work of Pawlak *et al.* as reference [25]). The compounds were named using the code PLA-MKSF/XX, where XX refers to the used plasticizer, TBN for tributyrin and TCN for triacetin. These formulations were placed in a ziplock bag for the initial mixing. Then, they were submitted to an extrusion process in a co-rotating twin-screw extruder from Dupra S.L. (Alicante, Spain). The extrusion temperature profile was 160-170-180-190 °C with a rotating speed of 20 rpm. Then, the extruded filaments were pelletized in an air-knife unit. Finally, an injection-moulding process was carried out using a Meteor 270/75 from Mateu & Solé (Barcelona, Spain). Standardized tensile test and impact strength test specimens were obtained. The injection-moulding temperature profile was 170-175-180-190 °C from the hopper to the injection nozzle, with an injection time of 5 s and a cooling time of 60 s.

Characterization of PLA-MKSF composites

Theoretical miscibility between PLA and the plasticizers

When studying the interaction between a polymer and a plasticizer, the solubility of both components is a very useful information to consider before initiating all the experimental setup. The general solubility parameter (δ) for each component can be calculated, according to the method of Van Krevelen and Hoftyzer [26], following **Equation III.1.4.1**, which takes into account the contributions of the dispersion forces (δ_d), polar forces (δ_p), and hydrogen bonding (δ_h):

$$\delta = \delta_d^2 + \delta_p^2 + \delta_h^2 \quad (\text{III.1.4.1})$$

Each one of the contributions can be calculated following **Equations III.1.4.2, III.1.4.3 and III.1.4.4:**

$$\delta_d = \frac{\sum F_{di}}{V} \quad (\text{III.1.4.2})$$

$$\delta_p = \frac{\sqrt{\sum F_{pi}^2}}{V} \quad (\text{III.1.4.3})$$

$$\delta_h = \frac{\sqrt{\sum E_{hi}}}{V} \quad (\text{III.1.4.4})$$

where F_{di} is the dispersive force contribution of the chemical groups present in the molecule, F_{pi} is the polar force contribution of the chemical groups present in the molecule, E_{hi} is the hydrogen cohesive energy contribution of the chemical groups in the molecule and V is the molar volume of the molecule.

Considering the chemical structure and the group contribution of neat PLA and both plasticizers (tributyrin and triacetin), **Table III.1.4.1** gathers all the solubility components and the solubility parameter. Moreover, the parameter R_a was also calculated, which indicates the distance that exists between the solubility coordinates of the plasticizers and the ones of PLA. If R_a is zero, it is indicative of a good miscibility between the polymer and the plasticizer. So, the solubility between both materials becomes poorer as the parameter R_a (the distance) increases, until it surpasses a certain threshold, from which both polymer and plasticizer become incompatible. This distance relates to the polymer radius, R_0 , which defines a spherical solubility region of a polymer. The center of this sphere is determined by the three solubility contributions δ_d , δ_p and δ_h . R_a is calculated following **Equation III.1.4.5**.

$$R_a = \sqrt{4 \cdot (\delta_{d_{plast}} - \delta_{d_{PLA}})^2 + (\delta_{p_{plast}} - \delta_{p_{PLA}})^2 + (\delta_{h_{plast}} - \delta_{h_{PLA}})^2} \quad (\text{III.1.4.5})$$

Additionally, the relative energy difference (RED) was also calculated. This parameter indicates the ratio between R_a and the solubility sphere radius of neat PLA, R_0 , which is $10.7 \text{ MPa}^{1/2}$ (Equation III.1.4.6) [27]. The lower the RED parameter is, the better the affinity between the polymer and the plasticizer. When the RED value is close to 1, it means that both elements are in the threshold of good miscibility, while values superior to 1 are indicative of a poor miscibility between both elements.

$$RED = \frac{R_a}{R_0} \quad (\text{III.1.4.6})$$

As it can be observed in Table III.1.4.1, both tributyrin and triacetin have good miscibility for PLA, as their RED value is smaller than the unity, both plasticizers exhibiting RED values of 0.86 and 0.73, respectively.

Table III.1.4.1. Theoretical solubility parameters of PLA with tributyrin and triacetin plasticizers.

Material	δ_d (MPa ^{1/2})	δ_p (MPa ^{1/2})	δ_h (MPa ^{1/2})	δ (MPa ^{1/2})	R_a (MPa ^{1/2})	RED
PLA	15.33	8.44	10.98	20.66	-	
Tributyrin (TBN)	15.96	1.67	4.89	16.78	9.19	0.86
Triacetin (TCN)	16.21	2.6	6.1	17.51	7.81	0.73

Mechanical characterization

The mechanical characterization of neat PLA and PLA-MKSF composites was carried out through tensile, impact strength, and hardness (Shore D) tests. Tensile tests were done following the ISO 527 using a universal testing machine ELIB 30 from Ibertest (Madrid, Spain), equipped with a cell load of 5 kN and a crosshead speed of 5 mm/min. Young's modulus, tensile strength and elongation at break were obtained with this test. Five specimens were tested, and their results were averaged.

The impact strength was determined through the Charpy test, using a Charpy pendulum with an energy of 6 J, from Metrotec S.A. (San Sebastian, Spain) on injection moulded rectangular unnotched samples with dimensions $80 \times 10 \times 4 \text{ mm}^3$ following ISO 179. Finally, Shore D hardness was measured using a durometer model 673-D from J. Bot S.A. (Barcelona Spain), according to ISO 868. At least five samples were tested for

each composite, and their corresponding parameters were averaged.

Morphology characterization

Morphology of fractured Charpy test samples was studied by field emission scanning electron microscopy (FESEM) using a ZEISS ULTRA 55 microscope from Oxford Instruments (Abingdon, United Kingdom). The samples were sputtered with a gold-palladium alloy in an EMITECH sputter coating SC7620 from Quorum Technologies, Ltd. (East Sussex, UK). The microscope was operated with an acceleration voltage of 1.5 kV.

Thermal characterization

The main thermal transitions of the PLA-MKSF composites were evaluated through differential scanning calorimetry (DSC) in a DSC 821 from Mettler-Toledo Inc. (Schwerzenbach, Switzerland). Samples weighed about 5–8 mg and were placed in 40 μL aluminium crucibles. The samples were subjected to a thermal cycle divided into three steps: a first heating cycle from 30 $^{\circ}\text{C}$ to 180 $^{\circ}\text{C}$ was followed by a cooling cycle down to -50 $^{\circ}\text{C}$ and, finally, a second heating stage from -50 $^{\circ}\text{C}$ up to 220 $^{\circ}\text{C}$ was scheduled. The heating and cooling stages were run at a rate of 10 $^{\circ}\text{C}/\text{min}$ in a nitrogen atmosphere (66 mL/min). Parameters such as the glass transition temperature (T_g), the cold crystallization peak temperature (T_{cc}) and enthalpy (ΔH_{cc}), the melt peak temperature (T_m) and enthalpy (ΔH_m) were obtained from the second heating stage. Moreover, the degree of crystallinity ($\chi_c\%$) was calculated following **Equation III.1.4.7**.

$$\chi_c (\%) = \left[\frac{|\Delta H_m| - |\Delta H_{cc}|}{|\Delta H_m^0| \cdot (1 - w)} \right] \cdot 100 \quad (\text{III.1.4.7})$$

where ΔH_m^0 is a theoretical value representing the theoretical melt enthalpy of a fully crystalline PLA polymer, *i.e.* 93.7 J/g as reported in the literature [28], and $1-w$ is weight fraction of PLA.

To evaluate the thermal stability and thermal degradation of the PLA-MKSF composites and MKSF at high temperatures, thermogravimetric analysis (TGA) was carried out on a TGA1000 thermobalance from Linseis (Selb, Germany). Samples of 15–20 mg were used, which were placed in standard alumina crucibles (70 μL). The heating

cycle was established from 30 °C to 700 °C with a heating rate of 10 °C/min, with a nitrogen atmosphere (66 mL/min). The onset degradation temperature was estimated at a mass loss of 5% ($T_{5\%}$) in the corresponding TGA curve, while the maximum degradation rate temperature (T_{max}) was obtained from the first derivative thermogravimetric (DTG) curve.

Thermomechanical characterization

Dynamical mechanical thermal analysis (DMTA) was carried out in a DMA1 dynamic analyzer from Mettler-Toledo (Schwerzenbach, Switzerland), working in single cantilever flexural conditions. Rectangular samples with dimensions 20×6×2.7 mm³ were subjected to a dynamic temperature sweep from -50 °C to 140 °C at a constant heating rate of 2 °C/min. The selected frequency was 1 Hz, and the maximum flexural deformation or cantilever deflection was set to 10 μm.

Water uptake characterization

Water uptake of neat PLA and PLA-MKSF composites was characterized following ISO 62:2008. Rectangular samples of dimensions 80×10×4 mm³ were sunk in distilled water at room temperature for nine weeks up to saturation. The samples were extracted from the distilled water, dried with absorbent paper and weighed; the specimens were then again immersed in the distilled water. The weighting process was made on an analytical balance model AG245 provided by Mettler-Toledo (Schwerzenbach, Switzerland) with an accuracy of 0.001 g. This process was repeated every week under the same conditions; measurements were taken in triplicate to ensure reliable results. The percentage of water absorption was calculated using **Equation III.1.4.8**:

$$\text{Water absorption (\%)} = \left(\frac{W_t - W_0}{W_0} \right) \cdot 100 \quad (\text{III.1.4.8})$$

where W_t (g) is the weight of the dry sample at any time, and W_0 (g) is the weight of the initial dry sample.

Disintegration in controlled compost soil

The degree of disintegration under composting conditions of PLA samples and PLA-MKFS composites was studied at a temperature of 58 °C and a relative humidity of 55% according to ISO 20200. Samples of dimensions 25×2×1 mm³ were placed inside a textile mesh to facilitate their removal. Then they were buried in a controlled compost soil made of organic solids 45%, vegetable solids 40%, 30% water content, and pH between 6 and 7. Samples were periodically extracted from the compost and cleaned with distilled water. Then they were dried and weighted with an analytical balance model AG245 from Mettler-Toledo (Schwerzenbach, Switzerland) with an accuracy of 0.001 g. The percentage of weight loss was calculated using **Equation III.1.4.9**:

$$\text{Weight loss (\%)} = \left(\frac{W_0 - W_t}{W_0} \right) \cdot 100 \quad (\text{III.1.4.9})$$

where W_0 is the initial dry weight of the sample and W_t is the weight of the sample after t burial time. All assays were carried out in triplicate to ensure accuracy and reliability.

Melt flow index

The melt flow index of neat PLA and PLA-MKSF composites was determined using an MFI equipment from Metrotec S.A. (San Sebastian, Spain), equipped with a 1-mm diameter nozzle. Measurements were taken using a temperature of 190 °C and an applied load of 2.16 kg, following ISO 1133. MFI measurements were done in triplicate for each composition.

Surface wettability and colour measurement

The wettability of the PLA and the PLA-MKSF composites was estimated by water contact angle (WCA) measurements. To this, an Easy drop FM140 goniometer supplied by Krüss equipments (Hamburg, Germany) was used. The test was carried out at room temperature with water droplets of approximately ~ 15 µL randomly deposited on the sample surface. The WCA was measured eight times for each droplet for each formulation and the average values were provided.

The effect of MKSF on the colour of the PLA matrix was analysed with a

colourimeter model KONICA CM-3600d Colorflex-DIFF2 from Hunter Associates Laboratory (Reston, Virginia, USA). The instrument was calibrated considering the standard white tile and a mirror unit for black. The Ciel^{*}a^{*}b^{*} colour scale (coordinates L^* , a^* and b^*) was recorded. L^* refers to lightness, a^* stands for the colour coordinate between red and green, and b^* represents the colour coordinate between yellow and blue. The total colour difference (ΔE_{ab}^*) was calculated by **Equation III.1.4.10**:

$$\Delta E_{ab}^* = \sqrt{(\Delta L^*)^2 + (\Delta a^*)^2 + (\Delta b^*)^2} \quad (\text{III.1.4.10})$$

where ΔL^* , Δa^* , and Δb^* are the differences between the Ciel^{*}a^{*}b^{*} colour coordinates of the samples and the reference colour.

RESULTS AND DISCUSSION

Mechanical characterization

Table III.1.4.2 summarises the main values of the tensile test parameters, impact strength and Shore D hardness of neat PLA and PLA-MKSF composites. In the case of neat PLA, high values of elastic modulus (E_t) and tensile strength (σ_t) are obtained (3848.5 MPa and 40.1 MPa, respectively), while a low percentage of elongation at break (ε_b) is obtained (4.7%). These properties are typical of PLA, being a rigid and brittle material [21]. The incorporation of MKSF leads to an increase in the stiffness and brittleness of the material. This is demonstrated by the high elastic modulus values reported, which are 35% higher than the values of neat PLA. It is also verified by a decrease in tensile strength and elongation at break of 40 and 35%, respectively, related to neat PLA. This provokes a highly brittle behavior in PLA-MKSF composites. This behaviour can be related to the low interaction between the MKSF and the surrounding PLA matrix, which generates a stress concentration effect, provoking a detriment of mechanical properties [29].

Table III.1.4.2. Mechanical properties of PLA, PLA-MKSF composites obtained from tensile tests (elastic modulus – E_t , tensile strength – σ_t , elongation at break – % ϵ_b), shore D, impact strength.

Code	Tensile			Shore D Hardness	Impact strength (kJ/m ²)
	Elastic Modulus, E_t (MPa)	Strength, σ_t (MPa)	Elongation at break, ϵ_b (%)		
PLA	3848 ± 245	40.1 ± 3.7	4.7 ± 0.5	63.8 ± 1.3	33.6 ± 3.6
PLA-MKSF	5219 ± 27	23.9 ± 0.9	4.4 ± 0.6	60.8 ± 1.3	21.7 ± 1.5
PLA-MKSF/TBN	2424 ± 193	16.9 ± 0.5	9.5 ± 0.6	61.0 ± 1.3	27.7 ± 1.6
PLA- MKSF/TCN	2995 ± 199	18.7 ± 0.6	8.3 ± 0.7	61.7 ± 1.2	33.1 ± 3.1

As expected, the incorporation of tributyrin (TBN) and triacetin (TCN) improves the ductile behaviour of PLA-MKSF composites. In the case of PLA-MKSF/TBN, a decrease in the tensile modulus and tensile strength of 37% and 58% can be observed, respectively. An increase in elongation at break can also be observed up to 9.5%, thus, demonstrating the plasticizing effect of tributyrin. Even though impact strength is lower than neat PLA, the PLA-MKSF composite plasticized with tributyrin has a higher impact strength than the unplasticized PLA-MKSF composite. This effect was also reported by other studies [30], with tributyrin as a plasticizer in a PLA/PHB blend. In general, it was observed how the incorporation of tributyrin provoked a reduction of the tensile strength and elastic modulus in all formulations. However, no significant changes were observed in the elongation at break.

As it occurs with the composites with TBN, the incorporation of triacetin is quite notorious regarding ductile properties. On the one hand, a decrease in the elastic modulus and tensile strength of 22 and 33% with respect to neat PLA is observed. Additionally, an increase of 77% in elongation at break is observed. In spite of this, the impact strength of the material remains quite high, with a value of 33.1 kJ/m², comparable to the impact strength of neat PLA but with a noticeable difference since ductile properties have been improved. This effect can be related to the excellent miscibility that TCN has with the PLA matrix, as it was stated in the theoretical solubility section. This phenomenon, together with the compatibility of TCN with MKSF (composed mainly of polysaccharides and protein), enhances the general plasticization effect [31]. Some studies have reported that the plasticizer embeds the surface of lignocellulosic particles, thus making the particles slide all over the matrix [32].

Regarding Shore D hardness, it can be observed that the incorporation of MKSF provokes a slight decrease in hardness from 63.8 down to 60.8. Different plasticizers

(TBN and TCN) do not significantly affect the hardness, despite a little increase. These results are similar to those reported by Gonzalez *et al.* [33], who observed that the use of maleinized linseed oil (MLO) plasticizer did not alter the hardness of the matrix.

These results are in accordance with the estimated miscibility between neat PLA and tributyrin and triacetin. As the theoretical study showed good compatibility between the plasticizers and the polymer, which has been demonstrated by the good mechanical response in both cases.

Morphological characterization

Figure III.1.4.2 shows the morphology of the fracture surface of impact test samples of each one of the developed composites observed by FESEM at 1000× magnification. **Figure III.1.4.2a** corresponds to neat PLA, which shows the typical morphology of a brittle polymer. This behaviour is detected by a smooth and flat surface, with the presence of little microcracks [21]. This perfectly matches the mechanical results observed in the previous section, where PLA exhibited an extremely low ductility (low elongation at break). In the case of **Figure III.1.4.2b**, the morphology of PLA with the incorporation of MKSF is shown. The presence of MKSF particles is clearly seen all over the matrix, where the adhesion of the particles is undoubtedly poor, as evidenced by the presence of voids (white arrows) in the matrix surface. Pulled-out MKSF particles generate those voids during impact fracture due to the poor compatibility between PLA and MKSF [34]. **Figures III.1.4.2c** and **III.1.4.2d** show the FESEM morphology of the composites with tributyrin and triacetin, respectively. The concentration of voids in the PLA matrix has been observed to be reduced with respect to the unplasticized PLA/MKSF composite. This indicates an increase in the affinity between PLA and MKSF microparticles, thanks to the addition of both plasticizers, which possess ester groups that enhance interaction with MKSF through hydrogen bonds [20]. Additionally, the gap (yellow arrows) between the MKSF particles and the surrounding PLA matrix is smaller than in the unplasticized composite. This fact corroborates the increased ductile properties observed in the mechanical characterization section, especially by using triacetin, which provided an elongation at break of 9.5%.

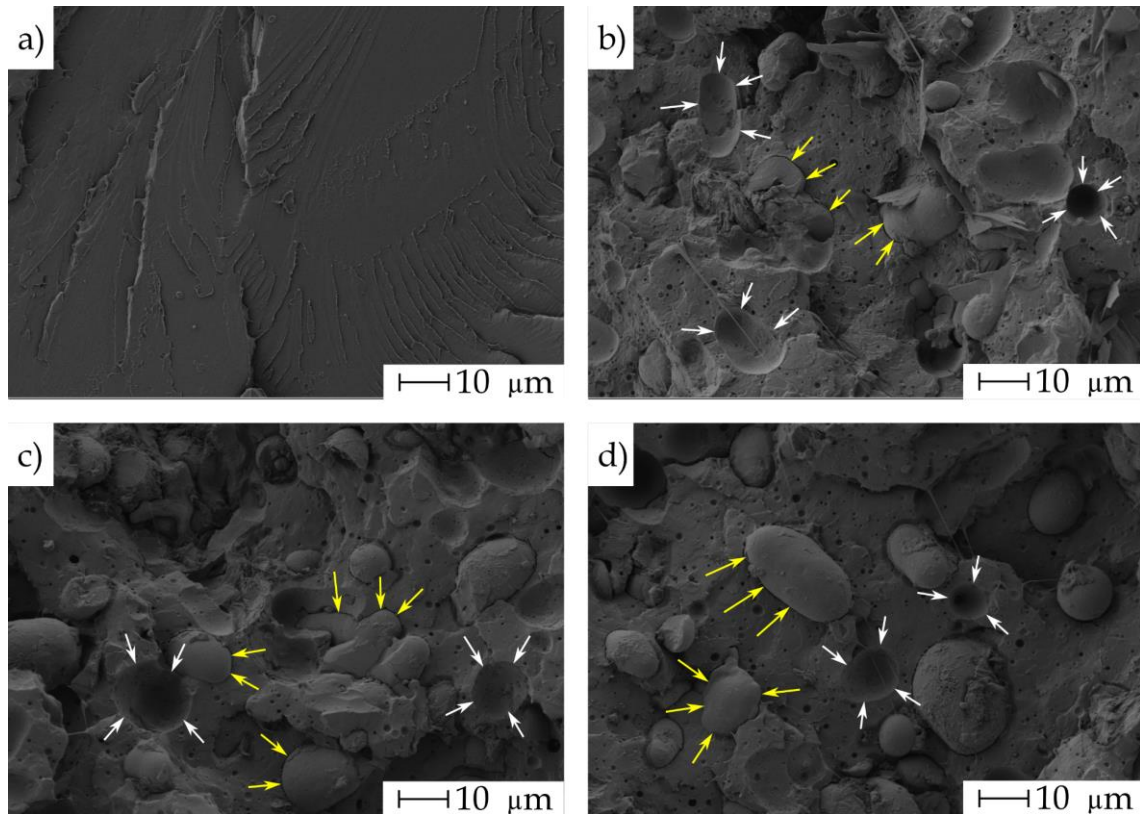


Figure III.1.4.2. FESEM image of mango kernel seed flour (MKSF) particles at 1000 \times with a marker scale of 10 μm . a) PLA, b) PLA-MKSF, c) PLA-MKSF/TBN, d) PLA-MKSF/TCN.

Thermal properties of PLA-MKSF composites

Differential scanning calorimetry (DSC) was used in order to study the thermal properties of the PLA-MKSF composites. **Figure III.1.4.3** gathers the thermograms that correspond to the second heating cycle of neat PLA and each one of the PLA-MKSF composites. At the same time, **Table III.1.4.3** summarizes the main thermal parameters extracted from these thermograms. Neat PLA shows a glass transition temperature at about 62 $^{\circ}\text{C}$, which is a typical value for this polymer as observed by Petchwattana *et al.* [20]. Addition of MKSF into the polymer matrix decreases this value by approximately 1 $^{\circ}\text{C}$, indicating almost negligible plasticization.

On the other hand, adding tributyrin and triacetin decreases this temperature down to 40.6 and 46.4 $^{\circ}\text{C}$, respectively. This remarkable decrease is ascribed to increased chain mobility of the amorphous phase of PLA induced by both plasticizers [20]. The addition of triacetin and tributyrin also plays a key role in the cold crystallization process. The cold crystallization peak temperature of neat PLA is located at 115.3 $^{\circ}\text{C}$. In contrast, the addition of MKSF decreases it down to 109 $^{\circ}\text{C}$, but, once again, the incorporation of tributyrin and triacetin plasticizers moves the cold crystallization peak

temperature down to such low values of 89 °C and 98 °C, respectively. This decrease in cold crystallization is also ascribed to the increase in PLA chain mobility, which provokes polymer chains to rearrange more quickly to a packed structure in the presence of plasticizers. Pure PLA exhibits a melting temperature of 167 °C approximately, which is increased by the presence of MKSF up to 169 °C. This effect is typical in rigid lignocellulosic fillers, as they are more thermally stable than neat PLA, thus delaying the melting phenomenon.

Similarly, addition of the plasticizers follows an analogous trend to the glass transition and cold crystallization temperatures. Tributyrin and triacetin decrease T_m to 164 °C and 165 °C, respectively, due to higher segmental mobility [20]. Finally, the crystallinity of PLA did not suffer significant changes, presenting a value of around 10%, except for the sample with tributyrin, which showed a crystallinity of 17.3%. This increase is related to the aforementioned enhanced chain mobility, which accelerates the crystallization rate of PLA, allowing it to crystallize at a lower T_{cc} and then present a higher crystalline region.

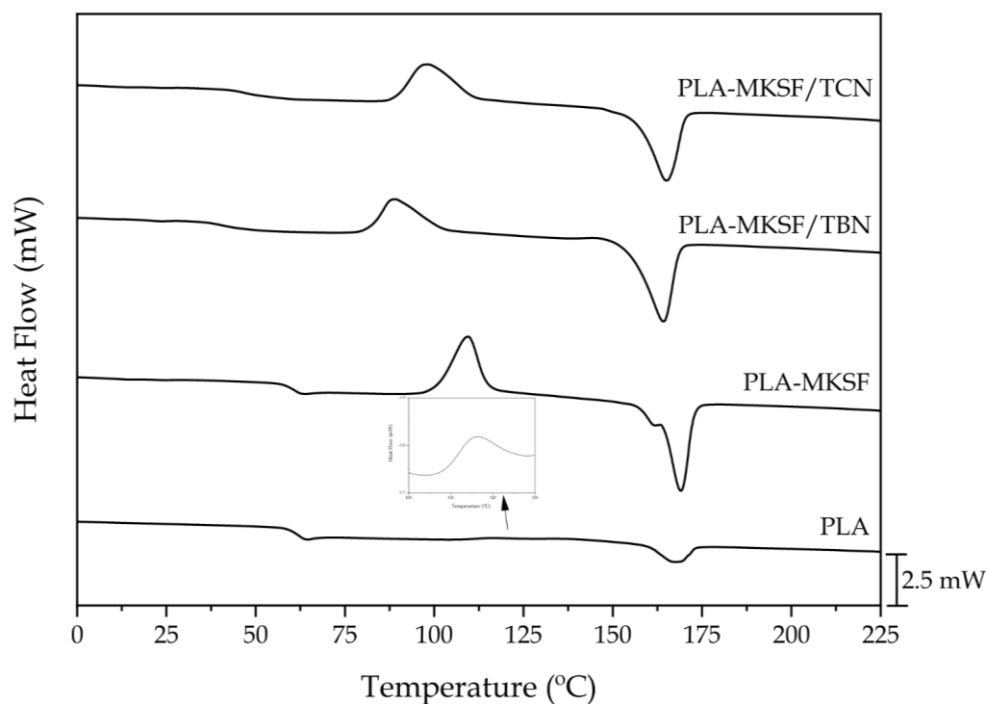


Figure III.1.4.3. Differential scanning calorimetry (DSC) thermograms of neat PLA and plasticized and unplasticized PLA-MKSF composites.

Table III.1.4.3. Glass transition temperature (T_g), cold crystallization peak temperature (T_{cc}), cold crystallization enthalpy (ΔH_{cc}), melting temperature (T_m), melting enthalpy (ΔH_m) and crystallinity X_c of the PLA-MKSF composites, obtained by differential scanning calorimetry (DSC).

Code	T_g (°C)	T_{cc} (°C)	ΔH_{cc} (J/g)	T_m (°C)	ΔH_m (J/g)	X_c (%)
PLA	62.4 ± 1.2	115.3 ± 3.5	0.7 ± 0.1	167.1 ± 0.2	10.1 ± 0.1	10.1 ± 0.5
PLA-MKSF	61.3 ± 1.5	109.5 ± 4.1	24.6 ± 0.4	169.1 ± 0.4	30.3 ± 1.2	8.7 ± 0.2
PLA-MKSF/TBN	40.6 ± 2.1	88.9 ± 3.6	19.1 ± 1.1	164.1 ± 1.0	30.4 ± 1.7	17.3 ± 0.1
PLA-MKSF/TCN	46.4 ± 1.7	98.2 ± 2.7	24.7 ± 0.5	165.0 ± 1.2	29.3 ± 1.2	7.1 ± 0.3

In order to assess the thermal degradation behaviour of the composites, a thermogravimetric (TGA) analysis was carried out. **Figure III.1.4.4** shows the thermogravimetric (TGA) and first derivative (DTG) curves of the studied composites, whereas **Table III.1.4.4** gathers the main thermal parameters related to this analysis. Neat PLA exhibits a single-step degradation curve, typical of this polyester. Its onset degradation temperature ($T_{5\%}$) is drastically reduced from 365 °C down to 273 °C due to the incorporation of MKSF. This is due to the earlier decomposition of low molecular weight hemicellulose in the mango kernel seed flour [20]. A similar trend occurs with the maximum degradation rate temperature extracted from the first derivative diagram; as it decreases from 404.5 °C down to 322.6 °C for PLA-MKSF. This is ascribed to the inherent lower thermal degradation stability of the lignocellulosic particles of MKSF, namely hemicellulose, cellulose, lignin and pectin [35]. This phenomenon is clearly observed in the TGA diagrams, where the PLA mass decreases far later than in the rest of the samples. The TGA curves of the samples with tributyrin and triacetin show a two-step degradation process, which is ascribed to the initial degradation (plasticizer removal) of both plasticizers, which are more volatile than the PLA matrix [36]. In this case, the onset degradation temperature is further decreased to 218 °C and 203 °C for tributyrin and triacetin, respectively. This demonstrates the results observed in DSC, as both plasticizers reduce the interaction between polymer chains and increase their mobility, thus diminishing thermal stability. The maximum degradation rate temperature is also reduced to 325 °C and 322 °C, respectively, a decrease of approximately 20% relative to neat PLA. The residual mass of PLA-MKSF composites increases due to a higher tendency of MKSF for char formation than PLA.

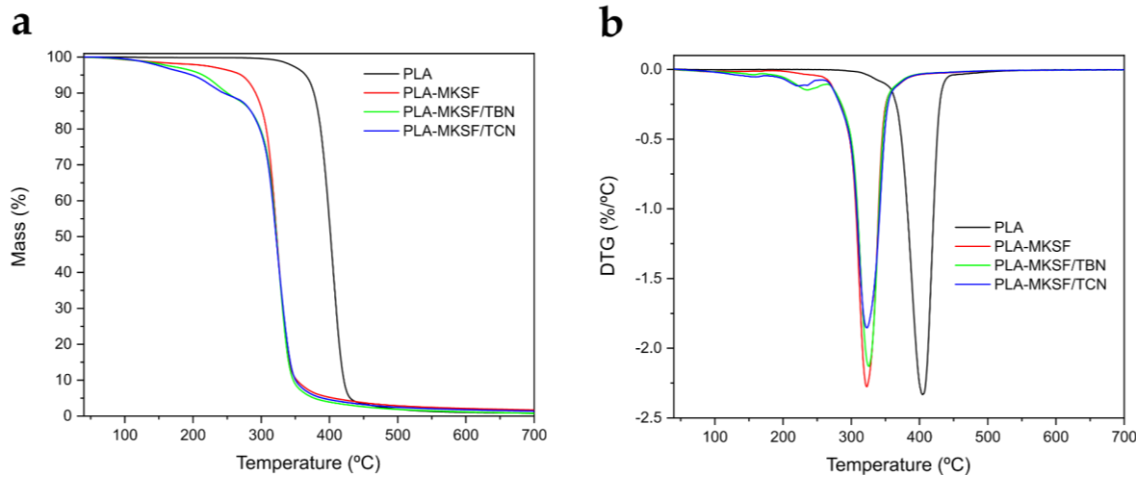


Figure III.1.4.4. Thermal degradation of PLA-MKSF composites, a) thermogravimetric (TGA), and b) first derivative (DTG) of neat PLA, plasticized and unplasticized PLA-MKSF composites.

Table III.1.4.4. Main thermal degradation parameters of the PLA-MKSF composites: onset degradation temperature at a mass loss of 5 wt.% ($T_{5\%}$), maximum degradation rate temperature (T_{deg}) and the residual mass at 700 °C.

Code	$T_{5\%}$ (°C)	T_{deg} (°C)	Residual mass (%)
PLA	365.2 ± 2.5	404.5 ± 3.1	0.2 ± 0.1
PLA-MKSF	272.7 ± 1.2	321.1 ± 1.3	0.2 ± 0.2
PLA-MKSF/TBN	216.4 ± 2.0	324.7 ± 3.3	0.1 ± 0.2
PLA-MKSF/TCN	204.1 ± 1.1	321.2 ± 1.1	0.1 ± 0.2

Thermomechanical characterization

To assess the mechanical properties of the composites in dynamic thermal conditions, DMTA was carried out. This analysis also allows a more detailed evaluation of the glass transitions of polymers. **Figure III.1.4.5** shows the dynamic-mechanical thermal analysis (DMTA) curves for all the PLA-MKSF composites, namely the evolution of the storage modulus (E') and the dynamic damping factor ($\tan \delta$). At the same time, **Table III.1.4.5** gathers the main thermomechanical parameters to be analyzed. **Figure III.1.4.5a** shows the variation of the storage modulus, which slowly decreases in the whole temperature range until a sudden drop is detected. This drop occurs between 60 °C and 70 °C for neat PLA and PLA-MKSF, and between 40 °C and 50 °C for the plasticized PLA-MKSF composites. Those drops are related to the α -relaxation of PLA chains once the glass transition region is surpassed [37]. This is due to the plasticizing effect of TBN and TCN, which increases the mobility of PLA chains, thus

reducing their stiffness in comparison with neat PLA. These changes in rigidity are registered in **Table III.1.4.5**, where there is a significant difference between the storage modulus at 5 °C and 70 °C, which goes down from 1500-1700 MPa to values of 8-50 MPa, respectively. **Figure III.1.4.5b** allows observing more precisely the glass transition temperature of the materials, which is indicated by a peak in the evolution of the dynamic damping factor ($\tan \delta$) with temperature. The glass transition temperature of neat PLA is located at approximately 65 °C, as already observed in DSC. Adding MKSF does not provoke significant changes in its T_g , with an average value of 63 °C. On the other hand, adding the TBN and TCN plasticizers reduces the glass transition temperature to 43 °C and 44 °C, respectively. This is again due to the chain mobility enhancement phenomenon that both plasticizers provide. This result proves the successful plasticization of PLA and demonstrates the increase in elongation at break reported in the mechanical properties section. After the glass transition process, there is a slight rise of E' in the plasticized samples and the PLA+MKSF composite, which can also be observed in the $\tan \delta$ graph, around 80 °C. This rise is due to crystallization, as an increase in chain mobility favors the formation of crystals after the T_g [38]. This crystal formation slightly increases the stiffness of the composites, which is why E' increases a little bit at high temperatures (75 to 100 °C). This is in accordance with the DSC results, where a cold crystallization peak was recorded for the PLA+MKSF and the TBN and TCN plasticized samples in the 75-100 °C temperature range.

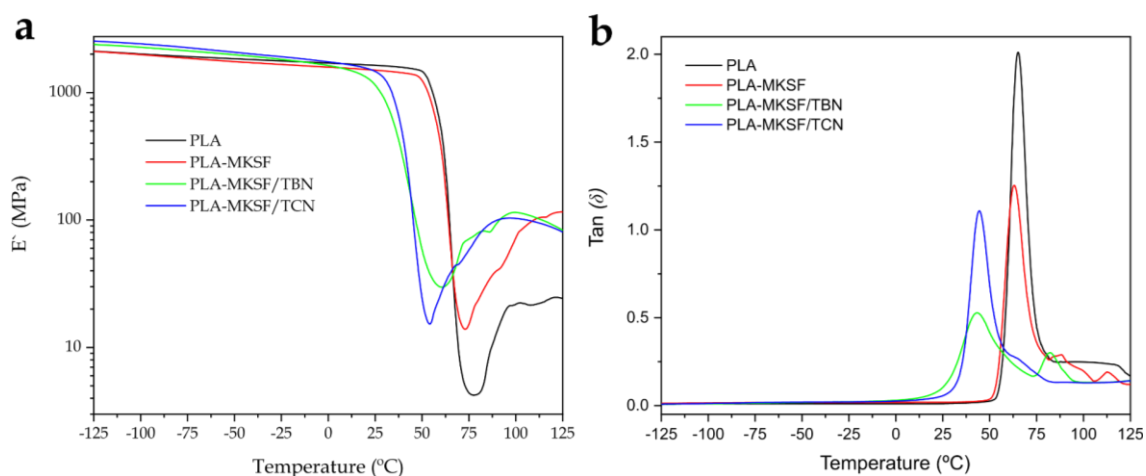


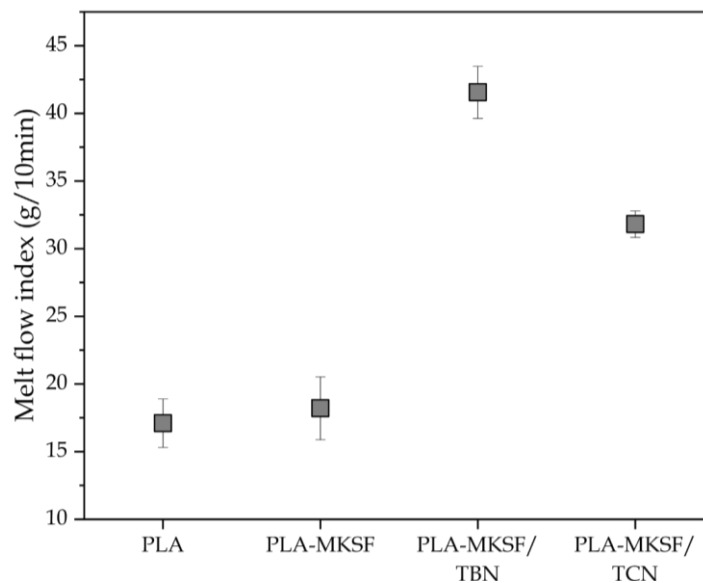
Figure III.1.4.5. Plot evolution of (a) the storage modulus (E') and (b) the dynamic damping factor ($\tan \delta$) of the PLA-MKSF composites.

Table III.1.4.5. Main dynamic-mechanical parameters of the PLA MKSF composites.

Code	E' at 5 °C (MPa)	E' at 70 °C (MPa)	T_g (°C)
PLA	1690.6 ± 33.8	8.4 ± 0.1	65.26 ± 0.97
PLA-MKSF	1569.4 ± 29.8	16.9 ± 0.3	63.13 ± 1.39
PLA-MKSF/TBN	1579.0 ± 27.01	54.1 ± 1.1	43.36 ± 0.65
PLA-MKSF/TCN	1704.9 ± 30.7	45.9 ± 0.9	44.43 ± 0.71

Melt flow index (MFI)

Figure III.1.4.6 gathers the melt flow index (MFI) for neat PLA and the PLA-MKSF composites developed in this work, measured at 190 °C with a load mass of 2.16 kg. Neat PLA presents an MFI of approximately 17 g/10 min, similar to that provided in the technical data sheet. Once the MKSF is incorporated into the PLA matrix, the melt flow index increases up to about 18 g/10 min. A similar effect was observed by Pantyukhov *et al.* [39] in polyethylene composites with lignocellulosic fibers as fillers. As expected, the addition of tributyrin and triacetin drastically increased the MFI of the composites. This is ascribed to the enhanced chain mobility that both plasticizers provide to PLA-MKSF composites. Thus, the PLA polymer chain entanglement becomes poorer, positively affecting the composite's flowability. The measured MFI values for PLA-MKSF/TBN and PLA-MKSF/TCN are 42.5 g/10 min and 32.5 g/10 min, respectively. This indicates that the plasticizing effect of tributyrin is stronger than that of triacetin, as it has also been demonstrated in the mechanical and thermal properties.

**Figure III.1.4.6.** Melt flow index (MFI) of neat PLA and PLA-MKSF composites.

Visual appearance and water contact angle characterization

Visual appearance is an essential factor regarding the product's perception by the consumer. **Figure III.1.4.7** shows the visual appearance of PLA-MKSF composites. At first sight, it can be seen that only the neat PLA sample shows certain transparency due to the semicrystalline nature of the polyester [40]. The incorporation of MKSF leads the samples to turn completely opaque with characteristic dark brown colours, which are especially attractive from the point of view of wood-plastic composites. Meanwhile, **Table III.1.4.6** gathers the $L^*a^*b^*$ colour coordinates. Neat PLA exhibited a luminance of 36.8, which is reduced to values close to 26 for all the rest of the samples as a result of the incorporation of MKSF, which turns the samples into darker colours.

Regarding colour coordinates a^* and b^* , neat PLA displays very low values (-0.2 and 0.9, respectively) due to its characteristic white colour. Adding MKSF increases those values to 3.1 and 3.5, respectively. This was expected, as the observed dark brown colour is composed of red and yellow components. With the addition of tributyrin and triacetin, both values increase even more, as they provide a clearer tonality to the dark brown colour of the PLA-MKSF composite, as seen in **Figure III.1.4.7**. The values of a^* and b^* for TBN and TCN are very close to 4 and 5, respectively, in both cases. Finally, the colour difference ΔE^*_{ab} is very similar for all three PLA-MKSF composites, giving values of approximately 12. That was expected, as the three samples presented very similar colours. A similar tonality was reported in previous work for a polypropylene matrix with mango peel wastes [37].

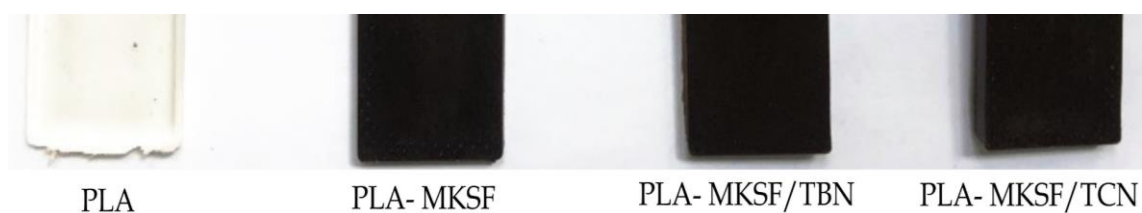


Figure III.1.4.7. The visual appearance of the PLA-MKSF composites.

Table III.1.4.6. Main colour parameters of the PLA-MKSF composites in terms of the Ciel^{*}a^{*}b^{*} colour space (L^{*}a^{*}b^{*}) and the colour difference ΔE_{ab}^* .

Code	L [*]	a [*]	b [*]	ΔE_{ab}^*
PLA	36.8 ± 0.3	-0.2 ± 0.1	0.9 ± 0.1	-
PLA-MKSF	25.8 ± 0.3	3.1 ± 0.1	3.5 ± 0.1	11.7 ± 0.3
PLA-MKSF/TBN	26.0 ± 0.1	4.2 ± 0.2	5.3 ± 0.1	12.4 ± 0.1
PLA-MKSF/TCN	26.9 ± 0.3	4.0 ± 0.1	5.4 ± 0.2	11.6 ± 0.3

The water contact angle analysis gives information regarding the affinity and interaction of the studied materials with water. **Figure III.1.4.8** shows the contact angle of distilled water with the surface of each one of the PLA-MKSF composites developed in this study. As it can be observed, neat PLA presents a contact angle of 85°, which is characteristic of a hydrophobic polymer according to Vogler, who established the hydrophilic threshold at 65° [41]. Once MKSF is added to the polymer matrix, the contact angle considerably decreases down to 75°, increasing the hydrophilicity of the polymer. This behaviour is ascribed to the polar groups contained in MKSF, mainly from polysaccharides and proteins. Those molecules have a great capacity to form hydrogen bonds, thus increasing affinity towards water and then enhancing hydrophilicity [42]. The addition of plasticizers into the PLA-MKSF composite reduces the affinity towards water, exhibiting contact angles of 78.5° and 82° for tributyrin and triacetin, respectively. Both plasticizers reduce the contact angle of neat PLA, as tributyrin and triacetin are certainly hydrophilic [43]. However, they increase the contact angle in relation to the PLA-MKSF sample. This could be due to the interaction of ester groups contained in both plasticizers with the hydroxyl groups in MKSF, thus reducing the availability of -OH functionalities in MKSF that can hydrogen-bond with water molecules.

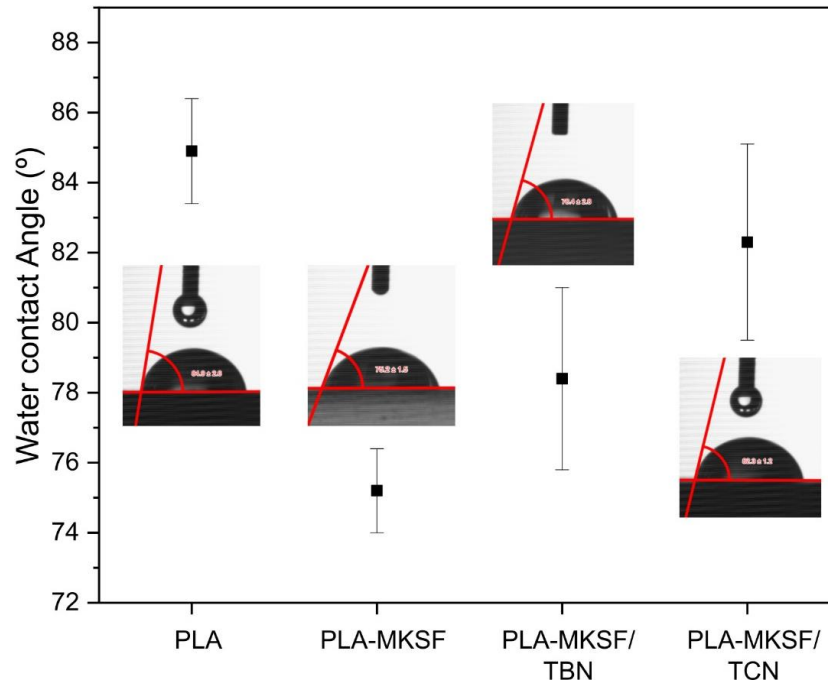


Figure III.1.4.8. Water contact angle measurements of plasticized and unplasticized PLA-MKSF composites.

Water uptake

The water uptake test evaluated the water absorption capacity of neat PLA and PLA-MKSF composites over 11 weeks. **Figure III.1.4.9** shows the evolution of the water absorption of the samples over 11 weeks in terms of the percentage of water mass absorbed in relation to the initial weight of the specimens. As expected, neat PLA presents the lowest water absorption profile, with a maximum absorption of less than 1 wt.%. This is the typical behaviour of a hydrophobic polymer; a similar profile was observed in previous works [37] for neat PLA. When MKSF is added into the PLA matrix, the water uptake of the composite drastically increases up to almost 12 wt.% at 11 weeks of immersion in distilled water. This effect is ascribed to the presence of polar groups in the composite coming from starch, proteins and lignin. Their characteristic functionalities provide the material with a great affinity for water, as observed in the contact angle measurements. Finally, adding tributyrin and triacetin also increases the water absorption compared with neat PLA up to 6.5 and 5 wt.%, respectively. However, they decrease the water absorption capacity with respect to the PLA-MKSF composite. This decrease could be related to the interaction between carbonyl groups in both plasticizers and hydroxyl groups in MKSF, reducing the possible reaction with distilled water [44]. The sample with tributyrin seems to slightly decrease its mass over time from 4 weeks of immersion. This could be ascribed to certain water solubility of the plasticizer

in distilled water. The results presented here are in total accordance with the contact angle measurements, where tributyrin also presented a slightly higher affinity for water than triacetin.

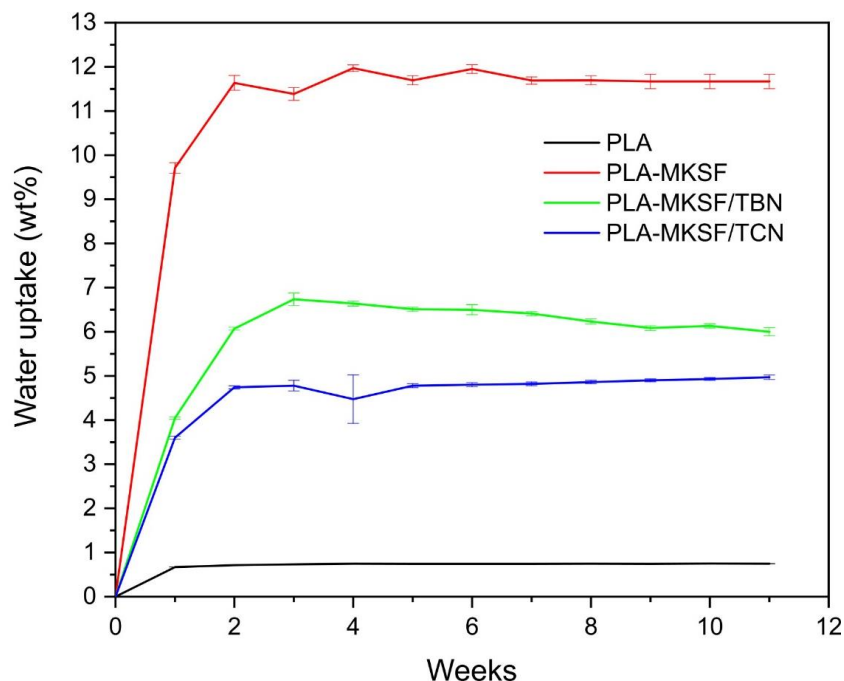


Figure III.1.4.9. Water uptake evolution of the PLA-MKSF composites over 11 weeks.

Disintegration test

The disintegrability of the PLA-MKSF composites was assessed through the disintegration test. **Figure III.1.4.10** shows the disintegration profile of all the studied PLA-based samples in terms of the mass loss. As it can be observed, only neat PLA disintegrated at 100% (at 9 weeks). Nonetheless, the remaining specimens disintegrated up to 90% at 12 weeks, which is the objective for considering a material biocompostable [45]. Neat PLA exhibited the typical behaviour of a biodegradable polymer, fully disintegration at 9 weeks due to a hydrolytic degradation process. Once MKSF is added to the polymer matrix, the disintegration capacity decreases to 90% at 12 weeks of incubation time in compost soil.

Moreover, the addition of plasticizers does not significantly vary the disintegration process. This decrease in biodegradability could be ascribed to an increase in the crystallinity of the polymer, especially in the PLA-MKSF/TBN composite. The hydrolytic degradation process occurs more easily in the amorphous regions of the polymer. Thus, the higher the crystallinity, the lower the proportion of amorphous phase

in the polymer, providing more resistance against biodegradation [37]. Nonetheless, both plasticizers do increase the disintegrability rate during the first 8 weeks. This phenomenon could be ascribed to the hydrophilic nature of TBN and TCN, which makes water absorption and diffusion through the polymer bulk in the initial phase of disintegration to be faster. Thus, resulting in higher hydrolysis in the polymer chains, leading to smaller molecules (monomers and short-chain oligomers) to be available for microorganisms to attack [46]. In the last weeks, the samples with MKSF seem to have a disintegrability threshold, which could correspond to the MKSF fraction left in the samples, which does not fully disintegrate.

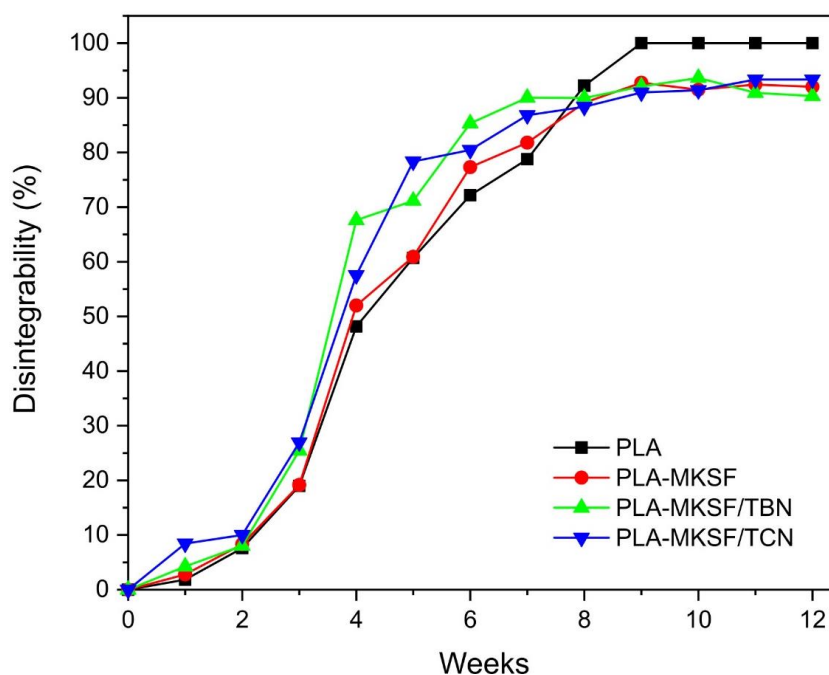


Figure III.1.4.10. Disintegration profile of the PLA-MKSF specimens over 12 weeks.

Figure III.1.4.11 gathers images that record the visual aspect of the samples all over the test. As it has been aforementioned, it is observed that neat PLA is entirely disintegrated after 9 weeks, while the rest of the specimens continue to degrade until week 12, when just little remnants are left (90% of biodegradation). Moreover, neat PLA started to decompose at week 2, as demonstrated by the macrocracks that appear in the square sample in Figure III.1.4.11. In contrast, the MKSF samples start their decomposition at week 4. Thus, the results herein presented are in total accordance with the disintegration profile shown in Figure III.1.4.10.




















Week	PLA	PLA-MKSF	PLA-MKSF /TBN	PLA-MKSF /TCN
0				
1				
2				
3				
4				
5				
6				
7				
8				
9				
10				
11				
12				

Figure III.1.4.11. Evolution of the visual appearance of the samples during the disintegration test. Size (25×2×1 mm³)

CONCLUSIONS

This work shows the successful development of wood plastic composites based on a polyester PLA matrix with mango kernel seed flour (MKSF) as a reinforcing agent and tributyrin (TBN) and triacetin (TCN) as plasticizers. The addition of MKSF gave the composites a characteristic dark brown colour, which could prove to be interesting to replace wood-based materials for these wood plastic composites. Regarding their mechanical response, tributyrin and triacetin improved the ductility of the polymer matrix, increasing the elongation at break from 4.4% for the PLA+MKSF sample to 9.5 and 8.3% for PLA+MKSF/TBN and PLA+MKSF/TCN, respectively. These results matched the theoretical solubility parameters of neat PLA and the plasticizers, which were also studied, showing good compatibility between PLA, TBN and TCN (RED values of 0.86 and 0.73, respectively). FESEM results also supported the mechanical properties of the composites, as well as certain compatibility effect exerted by the plasticizers over the polymer matrix and the MKSF particles. The plasticizing effect was further verified by thermal analysis, where the glass transition temperature and melting temperatures were reduced in relation to neat PLA as a result of the increased chain mobility provided by both TBN and TCN. MKSF made the affinity for water of the composite to drastically increase, as it was observed by means of contact angle measurements and water uptake. Both plasticizers reduced this considerably large water absorption of PLA+MKSF thanks to their bonding with MKSF particles. The thermal degradation of the composites became faster as a result of the presence of both plasticizers, again attributed to the increased chain mobility of the polymer chains ascribed to the plasticizing effect. Finally, all the composites showed a positive response towards disintegration under compost soil conditions. Disintegrating over 90% of the total mass of the samples.

All in all, these results prove that environmentally friendly wood plastic composites can be obtained from the combination of PLA, MKSF, TBN and TCN, with enhanced ductility, good thermal stability and excellent biodegradability. Thus, they could be used in applications substituting wood-based products, as they present quite attractive dark brown colours.

REFERENCES

- [1] Azeez, A.T., *A review of wood plastic composites effect on the environment*. Journal of University of Babylon, 2017. 25(2): 360-367.
- [2] Siakeng, R., et al., *Alkali treated coir/pineapple leaf fibres reinforced PLA hybrid composites: Evaluation of mechanical, morphological, thermal and physical properties*. Express Polymer Letters, 2020. 14(8): 717-730.
- [3] Mokhena, T., et al., *Mechanical properties of fire retardant wood-plastic composites: A review*. Express Polymer Letters, 2021. 15(8): 744-780.
- [4] Akintayo, O., et al., *Poly (lactic acid)-silkworm silk fibre/fibroin bio-composites: A review of their processing, properties, and nascent applications*. Express Polymer Letters, 2020. 14(10): 924-951.
- [5] Persic, M., et al., *Chemical composition of apple fruit, juice and pomace and the correlation between phenolic content, enzymatic activity and browning*. LWT-Food Science and Technology, 2017. 82: 23-31.
- [6] Mala, T., M.B. Sadiq, and A.K. Anal, *Optimization of thermosonication processing of pineapple juice to improve the quality attributes during storage*. Journal of Food Measurement and Characterization, 2021. 15(5): 4325-4335.
- [7] Kringel, D.H., et al., *Fruit wastes as promising sources of starch: Extraction, properties, and applications*. Starch-Stärke, 2020. 72(3-4): 1900200.
- [8] Haeldermans, T., et al., *Poly (lactic acid) biocomposites containing biochar particles: effects of fillers and plasticizers on crystallization and thermal properties*. Express Polymer Letters, 2021. 15(4): 343-360.
- [9] Kalita, N.K., et al., *Biodegradation of biopolymeric composites and blends under different environmental conditions: Approach towards end-of-life panacea for crop sustainability*. Bioresource Technology Reports, 2021. 15: 100705.
- [10] Rojas-Lema, S., et al., *Improved performance of environmentally friendly blends of biobased polyethylene and kraft lignin compatibilized by reactive extrusion with dicumyl peroxide*. Macromolecular Materials and Engineering, 2021. 306(9): 2100196.
- [11] Rojas-Lema, S., et al., *Manufacturing and Characterization of High-Density Polyethylene Composites with Active Fillers from Persimmon Peel Flour with Improved Antioxidant Activity and Hydrophobicity*. Macromolecular Materials and Engineering, 2021. 306(11): 2100430.

- [12] Tharanathan, R., H. Yashoda, and T. Prabha, *Mango (Mangifera indica L.), "The king of fruits" – An overview*. Food Reviews International, 2006. 22(2): 95-123.
- [13] Maldonado-Celis, M.E., et al., *Chemical composition of mango (Mangifera indica L.) fruit: Nutritional and phytochemical compounds*. Frontiers in plant science, 2019. 10: 1073.
- [14] Wadhwa, M. and M. Bakshi, *Utilization of fruit and vegetable wastes as livestock feed and as substrates for generation of other value-added products*. Rap Publication, 2013. 4: 67.
- [15] Das, P., et al., *Rehydration kinetics of flour from dehydrated mango kernel*. Food Res, 2018. 2(5): 474-480.
- [16] Ribeiro, S., et al., *Phenolic compounds and antioxidant capacity of Brazilian mango (Mangifera indica L.) varieties*. Food chemistry, 2008. 110(3): 620-626.
- [17] Gao, C., et al., *Synthesis of bio-based waterborne polyesters as environmentally benign biodegradable material through regulation of unsaturated acid structure*. European Polymer Journal, 2021. 156: 110632.
- [18] Garcia-Garcia, D., et al., *Improvement of PLA film ductility by plasticization with epoxidized karanja oil*. Polymer Degradation and Stability, 2020. 179: 109259.
- [19] Gürler, N., et al., *The fabrication of bilayer polylactic acid films from cross-linked starch as eco-friendly biodegradable materials: synthesis, characterization, mechanical and physical properties*. European Polymer Journal, 2020. 127: 109588.
- [20] Petchwattana, N., P. Naknaen, and B. Narupai, *A circular economy use of waste wood sawdust for wood plastic composite production: effect of bio-plasticiser on the toughness*. International Journal of Sustainable Engineering, 2020. 13(5): 398-410.
- [21] Lascano, D., et al., *Development of injection-molded polylactide pieces with high toughness by the addition of lactic acid oligomer and characterization of their shape memory behavior*. Polymers, 2019. 11(12): 2099.
- [22] Tejada-Oliveros, R., et al., *Improved Toughness of Polylactide by Binary Blends with Polycarbonate with Glycidyl and Maleic Anhydride-Based Compatibilizers*. Macromolecular Materials and Engineering, 2021. 306(12): 2100480.
- [23] Montes, M.I., et al., *Effect of natural glyceryl tributyrates as plasticizer and compatibilizer on the performance of bio-based polylactic acid/poly (3-hydroxybutyrate) blends*. Journal of Polymers and the Environment, 2019. 27(7): 1429-1438.

- [24] Coltelli, M.-B., *et al.*, *Compatibilization of Poly (Lactic Acid)(PLA)/Plasticized Cellulose Acetate Extruded Blends through the Addition of Reactively Extruded Comb Copolymers*. *Molecules*, 2021. 26(7): 2006.
- [25] Pawlak, F., *et al.*, *Silane-functionalized sheep wool fibers from dairy industry waste for the development of plasticized PLA composites with maleinized linseed oil for injection-molded parts*. *Polymers*, 2020. 12(11): 2523.
- [26] Van Krevelen, D.W. and K. Te Nijenhuis, *Properties of polymers: their correlation with chemical structure; their numerical estimation and prediction from additive group contributions*. 2009: Elsevier.
- [27] Auras, R.A., *et al.*, *Poly (lactic acid): synthesis, structures, properties, processing, and applications*. 2011: John Wiley & Sons.
- [28] Kangalli, E. and E. Bayraktar, *Preparation and characterization of poly (lactic acid)/boron oxide nanocomposites: Thermal, mechanical, crystallization, and flammability properties*. *Journal of Applied Polymer Science*, 2022. 139(28): e52521.
- [29] Quiles-Carrillo, L., *et al.*, *Compatibilization of highly sustainable polylactide/almond shell flour composites by reactive extrusion with maleinized linseed oil*. *Industrial Crops and Products*, 2018. 111: 878-888.
- [30] D'amico, D.A., *et al.*, *Fully bio-based and biodegradable polylactic acid/poly (3-hydroxybutyrate) blends: Use of a common plasticizer as performance improvement strategy*. *Polymer Testing*, 2016. 49: 22-28.
- [31] Murariu, M., *et al.*, *Polylactide (PLA)-CaSO₄ composites toughened with low molecular weight and polymeric ester-like plasticizers and related performances*. *European Polymer Journal*, 2008. 44(11): 3842-3852.
- [32] Herrera, N., A.P. Mathew, and K. Oksman, *Plasticized polylactic acid/cellulose nanocomposites prepared using melt-extrusion and liquid feeding: Mechanical, thermal and optical properties*. *Composites Science and Technology*, 2015. 106: 149-155.
- [33] Gonzalez, L., *et al.*, *Optimization of the loading of an environmentally friendly compatibilizer derived from linseed oil in poly (lactic acid)/diatomaceous earth composites*. *Materials*, 2019. 12(10): 1627.
- [34] Liminana, P., *et al.*, *Optimization of maleinized linseed oil loading as a biobased compatibilizer in poly (butylene succinate) composites with almond shell flour*. *Materials*, 2019. 12(5): 685.

- [35] Mwaurah, P.W., *et al.*, *Physicochemical characteristics, bioactive compounds and industrial applications of mango kernel and its products: A review*. *Comprehensive Reviews in Food Science and Food Safety*, 2020. 19(5): 2421-2446.
- [36] Avolio, R., *et al.*, *PLA-based plasticized nanocomposites: Effect of polymer/plasticizer/filler interactions on the time evolution of properties*. *Composites Part B: Engineering*, 2018. 152: 267-274.
- [37] Terroba-Delicado, E., *et al.*, *Valorization of Liquor Waste Derived Spent Coffee Grains for the Development of Injection-Molded Polylactide Pieces of Interest as Disposable Food Packaging and Serving Materials*. *Foods*, 2022. 11(8): 1162.
- [38] Martin, O. and L. Avérous, *Poly (lactic acid): plasticization and properties of biodegradable multiphase systems*. *Polymer*, 2001. 42(14): 6209-6219.
- [39] Pantyukhov, P., N. Kolesnikova, and A. Popov, *Preparation, structure, and properties of biocomposites based on low-density polyethylene and lignocellulosic fillers*. *Polymer Composites*, 2016. 37(5): 1461-1472.
- [40] Nguyen, T.L., *et al.*, *Mechanical investigation of confined amorphous phase in semicrystalline polymers: Case of PET and PLA*. *Polymer Engineering & Science*, 2015. 55(2): 397-405.
- [41] Vogler, E.A., *Structure and reactivity of water at biomaterial surfaces*. *Advances in colloid and interface science*, 1998. 74(1-3): 69-117.
- [42] Jorda-Reolid, M., *et al.*, *Upgrading Argan Shell Wastes in Wood Plastic Composites with Biobased Polyethylene Matrix and Different Compatibilizers*. *Polymers*, 2021. 13(6): 922.
- [43] Zięba, A., *et al.*, *Transesterification of triacetin with methanol on various solid acid catalysts: A role of catalyst properties*. *Applied Catalysis A: General*, 2010. 387(1-2): 13-25.
- [44] Meskens, F.A., *Methods for the preparation of acetals from alcohols or oxiranes and carbonyl compounds*. *Synthesis*, 1981. 1981(07): 501-522.
- [45] Rojas-Lema, S., *et al.*, *Faba bean protein films reinforced with cellulose nanocrystals as edible food packaging material*. *Food Hydrocolloids*, 2021. 121: 107019.
- [46] Arrieta, M.P., *et al.*, *Disintegrability under composting conditions of plasticized PLA-PHB blends*. *Polymer Degradation and Stability*, 2014. 108: 307-318.

III.1.5. Development of starch-rich thermoplastic polymers based on mango kernel flour and different plasticizers

Jaume Gomez-Caturla^{1*}, Juan Ivorra-Martinez¹, Octavio Fenollar¹, Daniel Garcia-Garcia¹, Franco Dominici², Debora Puglia² and Luigi Torre²

¹ Technological Institute of Materials – ITM, Universitat Politècnica de València – UPV, Plaza Ferrándiz y Carbonell 1, 03801 Alcoy (Spain).

² Dipartimento di Ingegneria Civile ed Ambientale, University of Perugia, UdR INSTM, Strada di Pentima, 4 - 05100 Terni (TR) Italy.

*Sent to the journal.

Development of starch-rich thermoplastic polymers based on mango kernel flour and different plasticizers

Abstract

This work reports on the development of starch-rich thermoplastic based formulations produced by using mango kernel flour (MKF). Glycerol, sorbitol and urea at 15 wt.% are used as plasticizers to obtain thermoplastic starch (TPS) formulations by extrusion and injection-moulding processes. Mechanical results show that sorbitol and urea provided the samples with tensile strength and elongation at break higher than the glycerol-plasticized sample, achieving values of 2.9 MPa of tensile strength and 42% of elongation at break at 53% RH. These results are supported by field emission scanning electron microscopy (FESEM) micrographs, where a limited concentration of voids was observed in the samples with sorbitol and urea, indicating a better interaction between starch and the plasticizers. Lignocellulosic particles act as reinforcing agents. Thermogravimetric analysis (TGA) shows that urea and sorbitol increase the thermal stability of TPS in comparison to the glycerol-plasticized sample. Differential scanning calorimetry (DSC) and dynamic-mechanical-thermal analysis (DMTA) verify the increase in stiffness of the sorbitol and urea plasticized TPS and also illustrate an increase in the glass transition temperature of both samples in comparison to the glycerol-plasticized sample. Glass transition temperatures of 45 °C were achieved for the sample with sorbitol.

Keywords: Thermoplastic starch, mango kernel flour, plasticizer, mechanical properties, mango kernel starch.

INTRODUCTION

In the last decades, the production of products based on plastics has undergone a great increase in terms of popularity and volume. The majority of those plastics are based on polymers derived from petroleum or from other fossil-resources. The extensive use of these plastics provokes a series of environmental problems, such as an increase in greenhouse gas emissions or a massive amount of generated wastes. The global plastic production increased by almost 10 million metric tons from 2008 to 2019, seeing a slight decline in 2020 due to Covid 19 [1].

As a response to these petroleum-based, non-degradable, non-renewable plastics, society and the scientific community have focused research on environmentally friendly biodegradable polymers, which pose a significant role in replacing them. One of the most interesting approaches is the use of natural polymers, which are inherently biodegradable [2].

Among natural polymers, starch is of great interest [3]. Starch is the second largest source of biomass in the planet, it is found in plants and vegetables and has been used due to its great availability, biodegradability, renewability, biocompatibility and low cost [4, 5]. It is conformed by amylose, a linear polysaccharide based on D-glucose units linked by α -1,4 glycosidic bonds, and amylopectin, a branched polysaccharide composed of D-glucose units bonded by α -1,4 and α -1,6 glycosidic bonds [6, 7]. This biopolymer allows to produce thermoplastic starch (TPS), a biodegradable material which is composed of native starch and a plasticizer and represents an alternative to some petroleum-derived plastics. Starch is not truly thermoplastic, but when it is combined with plasticizers (glycerol, polyols, polyesters or water) at high temperatures and shearing stresses, it undergoes gelatinization. Under these conditions, it melts and flows, thus allowing it to be used for extrusion or injection processes, acquiring similar properties to those of commodity thermoplastics [8, 9]. Moreover, films can also be produced through the solving casting methodology [10]. During this process, the plasticizers form hydrogen bonds with the hydroxyl groups present in starch [11].

Normally, starch is used in its native form for producing TPS. However, the extraction of starch from plants or vegetables implies energetic and economic costs [12]. Additionally, starch-based materials present some drawbacks, which include limited long-term stability due to water absorption, bad processability and poor mechanical properties [13]. Moreover, starch undergoes retrogradation over time, which is a natural chemical reaction that produces a recrystallization of the starch granules provoked by a rearrangement of amylose and amylopectin molecules [14]. This modification in the

starch structure embrittles it and reduces its ductile mechanical properties [15]. Thus, the production of bioplastics directly from lignocellulosic flours could prove to be a very interesting and economical approach. Some studies have been made using starch-rich wheat flour where the properties of flour-derived TPS were not so different from TPS obtained from native starch, except for a lower strain-to-break behavior [16, 17].

This fact opens a new research line centered on developing TPS from flours derived from starch-rich wastes coming from different crops, such as wheat flour [18], date palm flour [19] or mango kernel flour [2]. This new approach allows to directly reuse organic wastes from the agroforestry and food industries, at the same time the extraction process of starch is avoided, thus making the thermoplastic material obtained more cost effective.

Mango (*Mangifera indica*) is a very popular tropical crop that has attracted great interest in the last years. It is harvested at a physiologically mature green stage, and it is the third most exported tropical fruit, with a worldwide production of more than 100 million metric tons in 2018 [20]. Mango possesses a great deal of by-products that are considered of notable interest from the point of view of biorefinery [21]. These by-products include mango peel, mango kernel and mango tegument or shell. The mango kernel or mango stone is comprised mainly of starch, which makes for about 60% of the mango kernel [22]; lipids, which stand at 11% of the total weight of mango kernel; and proteins, with a composition of 6% in weight of the mango kernel. This makes mango kernel a very promising raw material to be used in the production of thermoplastic polymers due to its high starch content.

In the production of TPS, thermoplastification occurs between starch and the plasticizers, if hydrogen bonding is promoted between both components. To meet that end, plasticizers capable of forming those bonds need to be used. Some of the most common plasticizers used for the production of TPS are polyols, such as glycerol, sorbitol, xylitol or glycols [23-25]. Other small molecules based on the -CO-NH functionalization have also been used as plasticizers in TPS, such as urea [26], or formamide [27]. Formamide has been reported to produce TPS with water resistance better than glycerol-plasticized thermoplastic starch, but on the other hand, the tensile behavior was rather worse. Additionally, the amide group in these plasticizers has been reported to prevent retrogradation of starch up to some point [28].

The main aim of this study is to produce starch-rich thermoplastic materials using mango kernel flour (MKF) as the main starch source. Mango kernel flour will be combined with three different plasticizers, namely, glycerol, sorbitol and urea in order

to compare the properties of the obtained TPS in relation to the used plasticizer. This is of special interest since MKF has never been reported to be combined directly with glycerol, sorbitol and urea to process TPS-based materials. Prior to processing the different formulations, a preliminary study is carried out in order to determine the optimal amount of plasticizer that would be suitable for proper plasticization of the starch present in MKF, taking glycerol as the base for this study. Finally, processability, mechanical, morphological and thermal properties of the different developed mango kernel flour-based TPS are characterized and evaluated.

MATERIALS AND METHODS

Materials

The mango endocarps were kindly supplied by a local marmalade company, “El Rincón de las Mermeladas” (Alicante, Spain). The seed coat was removed, and the mango kernel was micronized in a Retsch GmbH model ZM 1000 ultracentrifugal mill (Haan, Germany) with a sieve size of 25 μm and a rotation speed of 12,000 rpm. **Figure III.1.5.1** shows the morphology of the mango kernel flour particles through field emission scanning electron microscopy (FESEM) at 500 \times magnification and their dimensional distribution; it can be seen that the average particle size is about 16 μm . Glycerol (GLY) was supplied by Sigma-Aldrich (ReagentPlus >99.0%; Product Code: G7757-1GA). D-Sorbitol (SORB) (99.0%; Product Code: 240850), Urea (UREA) (ReagentPlus >99.5%; Product Code: U1250), Formamide (FORM) (ReagentPlus >99.0%; Product Code: F7503) and Magnesium Stearate (MS) (technical grade; Product Code: 415057) were also provided by Sigma-Aldrich.

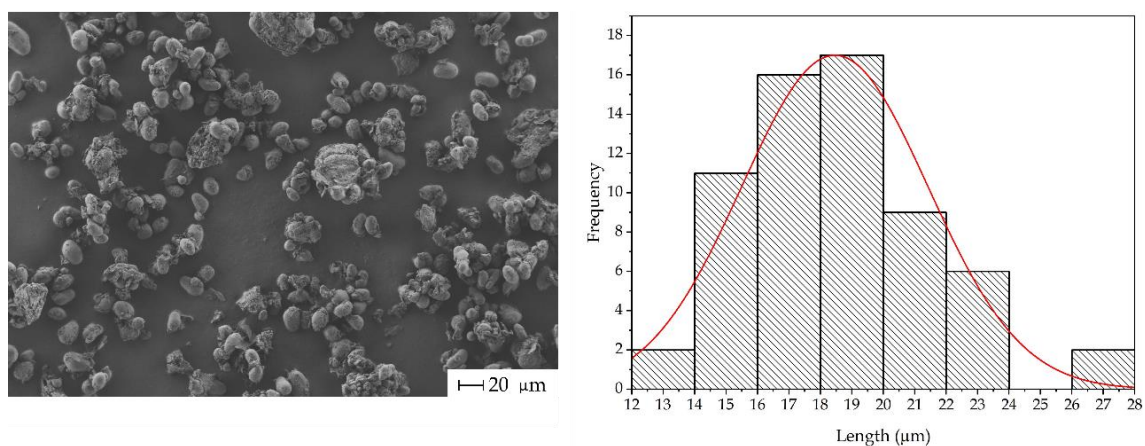


Figure III.1.5.1. FESEM morphology of mango kernel flour particles and their size distribution.

Extraction and morphological characterization of mango kernel starch (MKS)

In addition to the morphology of mango kernel flour, starch was extracted from mango kernel in order to also observe its morphology, as well as determining the content in starch of mango kernel.

Starch was extracted using the methodology of Nawab *et al.* [29] with some modifications. Mango kernels were decorticated and cut into pieces of about 1 cm³. Then, the kernels were soaked in a sodium metabisulfite solution (0.16 wt.%) with a kernel:solution ratio of 1:2. The kernels were maintained in the solution for 48 hours in order to avoid their oxidation and browning. They were then washed with distilled water utilizing a 70 µm mesh screen until the filtrate had pH 7. Afterwards, they were ground in distilled water using an homogenizer (Daihan Scientific, model HG-15A with direct controller, Corea) for 5 minutes at 5,000 rpm. A slurry was obtained, which was screened through a 100 µm mesh screen sieve and consequently through a 70 µm mesh screen. Then it was left for about 12 h at 4 °C (to avoid fermentative or enzymatic processes) in order to precipitate the starch. The resulting supernatant was discarded, and the starch was dried at 45 °C for 2 h. The brownish layer was then eliminated with a small spoon and then the white layer was dried at 45 °C for 24 h. Next, the white layer was resuspended with distilled water and it was then washed by several centrifugation cycles at 4500 rpm and 10 minutes until the precipitate had the typical white colour of starch. The last step was to dry the starch and pulverize it. The extraction yield of starch was approximately 10.2 ± 1.2% in relation to the weight of dry mango kernels.

Figure III.1.5.2 shows the morphology of the extracted starch, as well as the distribution of its geometry in terms of diameter and length, as the granules have a typical spheroidal structure. As it can be observed, mango kernel starch (MKS) presents the typical granulometric structure with an average diameter of 10 µm and an average length of 15 µm. This morphology is very similar to the one observed in other studies [2].

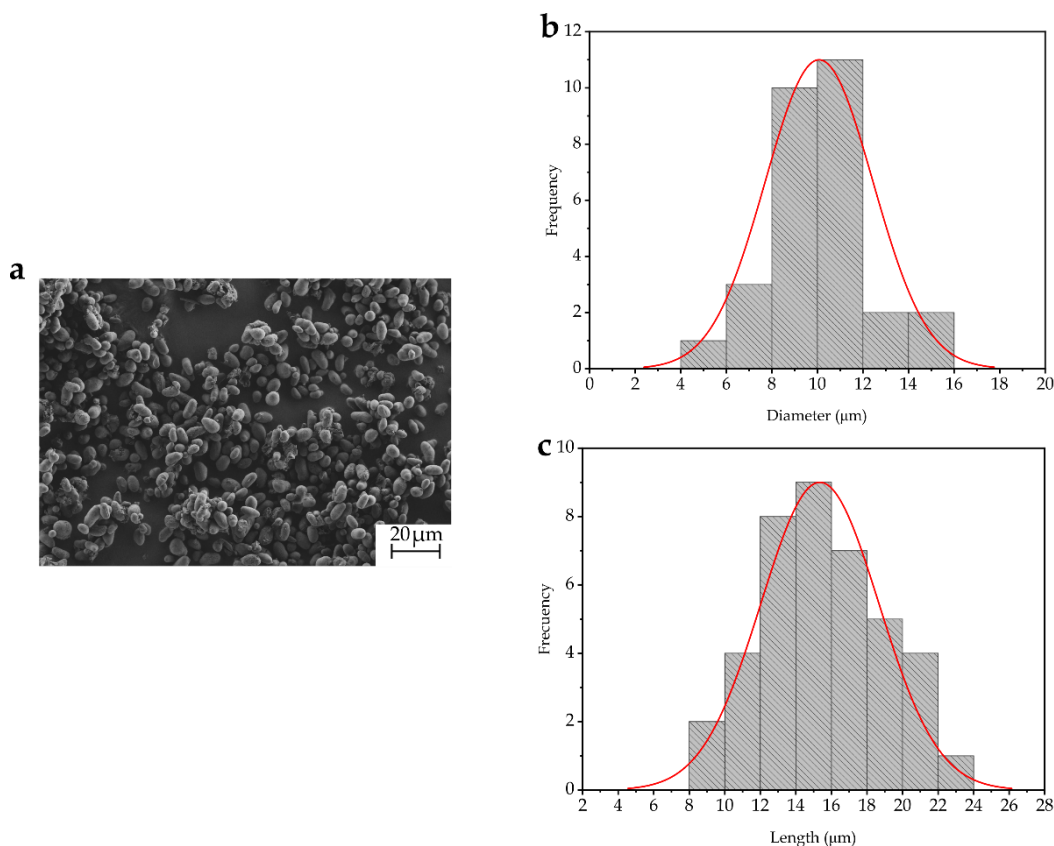


Figure III.1.5.2. FESEM morphology of the extracted starch from mango kernel and the diameter and length distributions of the starch granules.

Preliminary study for determination of MKF proportion and plasticizers' amount

The objective of this work was to plasticize the starch present in MKF so that TPS with optimal properties were obtained. To meet this end, a preliminary study was made for determining the appropriate amount of plasticizer required to plasticize starch without exceeding the amount of plasticizer needed for optimum plasticization. This study was based on the mixture MKF/glycerol and a recipe used in previous works [16, 18], for plasticizing different starch-rich flours. This recipe uses 68 wt.% of the flour, 23 wt.% of the plasticizer, 5.2 wt.% of D-sorbitol, 1.8 wt.% of magnesium stearate and 2 wt.% of a solution 1:20 PVA:distilled water. In our case, PVA solution was substituted by pure distilled water (40 phr), as distilled water can also act as a plasticizer for starch and an excess in water is essential for the gelatinization reaction. The amount of water was selected according to the study of Zuraida *et al.* [30].

The study was based on varying the proportion of MKF and the plasticizer, while maintaining the same composition for the rest of the components. The iterative process started by preparing the aforementioned recipe with 20 wt.% of glycerol and 73 wt.% of

MKF (MKF-20GLY) and another mixture with 15 wt.% glycerol and 78 wt.% MKF (MKF-15GLY). The TPS processing is detailed in the processing section and the samples were stored at 53% RH for a week. The tensile mechanical properties of both samples were measured and compared according with the methodology previously described.

Figure III.1.5.3 shows the stress-strain curves of both samples. It is obvious that the mechanical behavior of MKF-15GLY is considerably better than that of MKF-20GLY, both in terms of strength and toughness. The sample with 15 wt.% of glycerol shows a maximum mean tensile strength of 1.7 MPa, while the sample with 20 wt.% roughly reaches 0.5 MPa. In a similar manner, elongation at break of MKF-15GLY is located at 38%, while the elongation at break of MKF-20GLY is less than 30%. Additionally, the stiffness of the sample with 15 wt.% glycerol is far greater than the sample with 20 wt.% glycerol, which is indicated by a much higher slope in the first stage of the stress-strain curve. This behavior could be ascribed to an excessive amount of plasticizer used in the sample with 20 wt.% glycerol, thus obstructing the normal molecular combination and reducing the efficiency of weakening intermolecular hydrogen bonds between starch molecules [31]. So, taking this study as base, 15 wt.% of glycerol seems to be the appropriate content of plasticizer in MKF-based thermoplastic polymers.

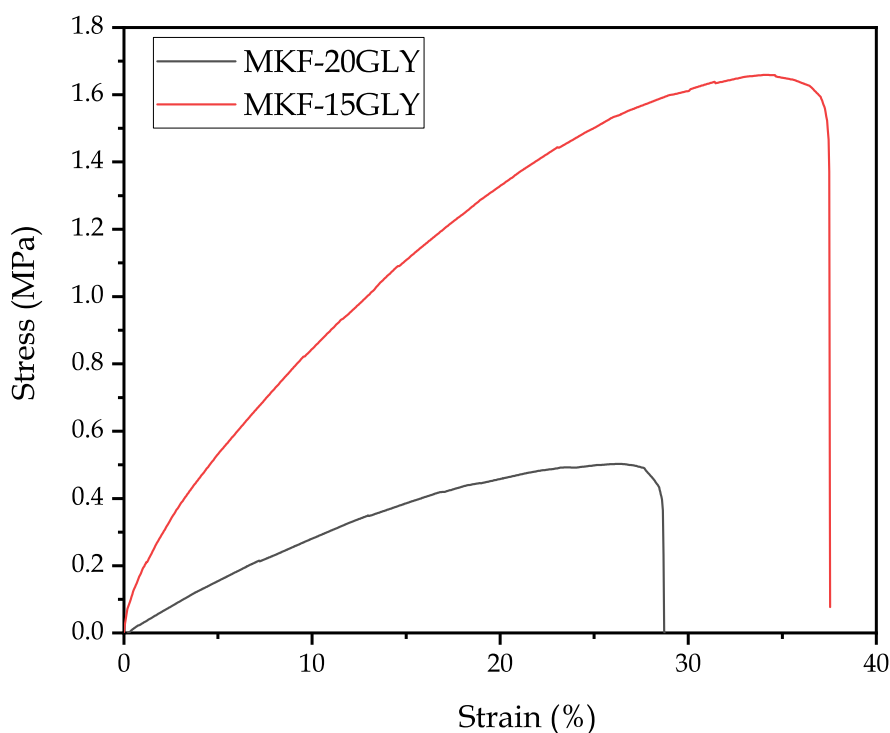


Figure III.1.5.3. Stress-strain curves of the MKF-based TPS developed in the preliminary study to assess the optimum plasticizer content.

The optimal amount of glycerol was taken as reference for the amount of plasticizer to be introduced into the blends to produce the starch-rich thermoplastics. It should be noted that all formulations possess sorbitol in its composition, which was taken as reference from the work of Puglia *et al.* [16]. Studies with very good results in terms of combination of glycerol with sorbitol has been made [28, 32]. Also, other studies reported the effectiveness of using sorbitol in combination with urea, such as the study of Zdanowicz *et al.* [33]. In this sense, both glycerol and urea are compatible plasticizers with sorbitol, which is another reason why it was used in all compositions.

Processing of MKF TPF

The different MKF TPS formulations were processed according to the compositions described in **Table III.1.5.1**, which were obtained from the preliminary study presented in the previous section and other studies present in literature [34]. Glycerol, sorbitol and urea act as plasticizers in synergy with water, while magnesium stearate is normally used as a lubricant in plastic processing. Tensile test samples were obtained by means of a twin-screw microextruder (DSM Explorer 5&15 CC Micro Compounder) provided with an injection unit DSM Xplore of 10 mL capacity. All the ingredients were mixed at low speed in a laboratory mixer (planetary mixer, 60 rpm, for 3 min), then the mixture was introduced into the extruder, and it was further mixed at 30 rpm at different times depending on the plasticizer, as it would be discussed in the results and discussion section.

Table III.1.5.1. Composition of the different TPS developed formulations based on MKF.

Code	MKF (wt.%)	GLY (wt.%)	SORB (wt.%)	UREA (wt.%)	MS (wt.%)	Water (phr)
MKF-GLY	78	15	5.2	0	1.8	40
MKF-SORB	78	0	20.2	0	1.8	40
MKF-UREA	78	0	5.2	15	1.8	40

A temperature profile of 135-140-145 °C was used in the three sections of the extruder (feeding, metering and die), in accordance with Puglia *et al.* [16]. The injection unit operated at a pressure of 16 bars. Tensile test samples were obtained and stored at 53 and 11% RH.

Characterization of MKF TPS blends

Mechanical characterization

The tensile properties of the MKF TPS blends were assessed using a universal testing machine ELIB 50 from S.A.E. Ibertest (Madrid, Spain) as recommended by ISO 527-1:2012. A 5 kN load cell was used, the cross-head speed was set at 5 mm/min. The Shore D hardness was measured in a 676-D durometer from J. Bot Instruments (Barcelona, Spain), on 80×10×4 mm³ rectangular samples according to ISO 868:2003. All samples were tested 5 times in order to obtain average results.

Field emission scanning electron microscopy (FESEM)

The surface morphology of samples broken by the tensile test was evaluated by field emission scanning electron microscopy (FESEM) by means of a ZEISS ULTRA 55 microscope from Oxford Instruments (Abingdon, United Kingdom). The MKF TPS samples were sputtered with a gold-palladium alloy in an EMITECH sputter coating SC7620 model from Quorum Technologies, Ltd. (East Sussex, UK). The microscope operated with an acceleration voltage of 2 kV.

Thermal characterization

Differential scanning calorimetry (DSC) was used to measure the thermal parameters of the MKF TPS samples with different plasticizers, as well as the DSC thermograms of the developed samples. A DSC 821 from Mettler-Toledo Inc. (Schwerzenbach, Switzerland) was used for this analysis. Samples weighted about 5–8 mg were placed in 40 µl aluminum crucibles. For the non-plasticized samples, a DSC heating scan from 30 to 180 °C was performed to observe the plasticizing peak. In the case of plasticized samples, three thermal steps were considered: an initial heating cycle from 30 °C to 170 °C, then a cooling cycle down to 0 °C and, finally, a second heating stage from 0 °C up to 180 °C. The heating rate was set at 10 °C/min and the tests were carried out in a nitrogen atmosphere. The main thermal parameters were calculated according to the aforementioned thermograms.

The thermal degradation of the MKF TPS samples was studied by thermogravimetric analysis (TGA). These analyses were done in a LINSEIS TGA 1000 (Selb, Germany). The samples weighting between 15 and 17 mg were placed in 70 µl alumina crucibles and submitted to a dynamic heating program from 30 °C to 700 °C at a heating rate of 10 °C/min in nitrogen atmosphere. The weight (%) - temperature (°C)

curves for each material were obtained. Additionally, the first derivative of the TGA curves (DTG) were also analyzed. Each material was analyzed three times in order to obtain average results.

Dynamical mechanical thermal characterization

Dynamic mechanical thermal analysis (DMTA) was carried out in a DMA1 dynamic analyzer from Mettler-Toledo (Schwerzenbach, Switzerland), working in single cantilever flexural conditions. Rectangular samples with dimensions 20×6×2.7 mm³ were subjected to a dynamic temperature sweep from -150 °C to 100 °C at a constant heating rate of 2 °C/min. The selected maximum flexural deformation or cantilever deflection was set to 10 μm and the frequency was 1 Hz.

Visual appearance analysis

The colour of the MKF TPS samples was analysed with a colorimeter model KONICA CM-3600d Colorflex-DIFF2 from Hunter Associates Laboratory (Reston, Virginia, USA). The instrument was calibrated considering the standard white tile and a mirror unit for black. The Ciel^{*}a^{*}b^{*} colour scale (coordinates L^{*}, a^{*} and b^{*}) were recorded. L^{*} refers brightness, a^{*} denotes the range between red and green colours, and b^{*} denotes the range between yellow and blue colours. The total colour difference (ΔE_{ab}^*) was calculated by **Equation III.1.5.1**:

$$\Delta E_{ab}^* = \sqrt{(\Delta L^*)^2 + (\Delta a^*)^2 + (\Delta b^*)^2} \quad (\text{III.1.5.1})$$

where ΔL^* , Δa^* , and Δb^* are the differences between the colour of the samples and the reference colour.

RESULTS AND DISCUSSION

Study of the plasticization during processing

Figure III.1.5.4 shows the variation of the shearing force (N) applied during the extrusion processing of the different MKF TPS samples. These curves allow to observe how the force varies during plasticization of the starch, as well as the time it takes to plasticize. All the curves show a typical increasing tendency, which is related to the

reaction between the oxygen-based functionalities of starch with the active functionalities of the corresponding plasticizer by hydrogen bonding. At some point, this increasing tendency stops and starts a plateau zone, which indicates the end of the plasticization. This is indicative of an almost total reaction of the starch available in MKF with the corresponding plasticizer. It is at this plateau zone that the extrusion is stopped, and the sample is injected. It can be seen that the sample with glycerol shows a maximum force of approximately 1750 N and a plasticizing time of 190 s (approximately 3 minutes), which is the typical plasticizing time for TPS of flours with glycerol [18]. A drastic increase in the maximum force is observed for the sample with sorbitol, which achieves a value of 4600 N and a plasticizing time of 650 s (11 min). This fact is ascribed to the superior molecular mass of sorbitol compared with glycerol, as well as its higher number of functionalities in the plasticizer chemical structure. This originates a more rigid thermoplastic starch that requires longer times to plasticize [35], this observation is also corroborated by results of mechanical characterization that will be shown in the following section 3.2. Finally, the sample plasticized with urea shows a maximum compounding force of 4000 N and a plasticizing time of 11 minutes. This could mean a very effective interaction between urea and starch, obtaining a rigid TPS. **Figure III.1.5.5** presents a scheme of the possible interactions between each plasticizer and the glucose units in starch. As it is observed, sorbitol and urea allow to produce more hydrogen bond interactions with starch, which accounts for a stronger linkage and therefore a more resistant material.

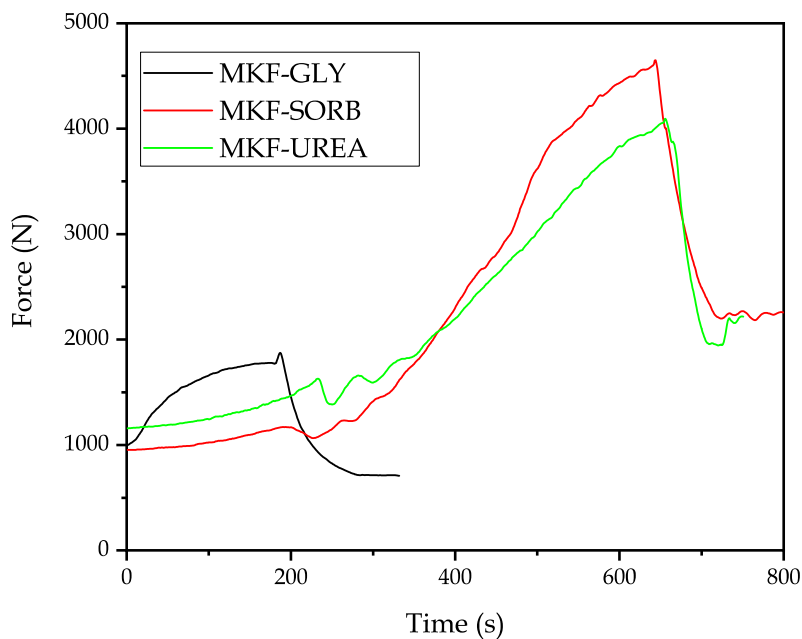


Figure III.1.5.4. Evolution of the force during processing for all the MKF TPS samples.

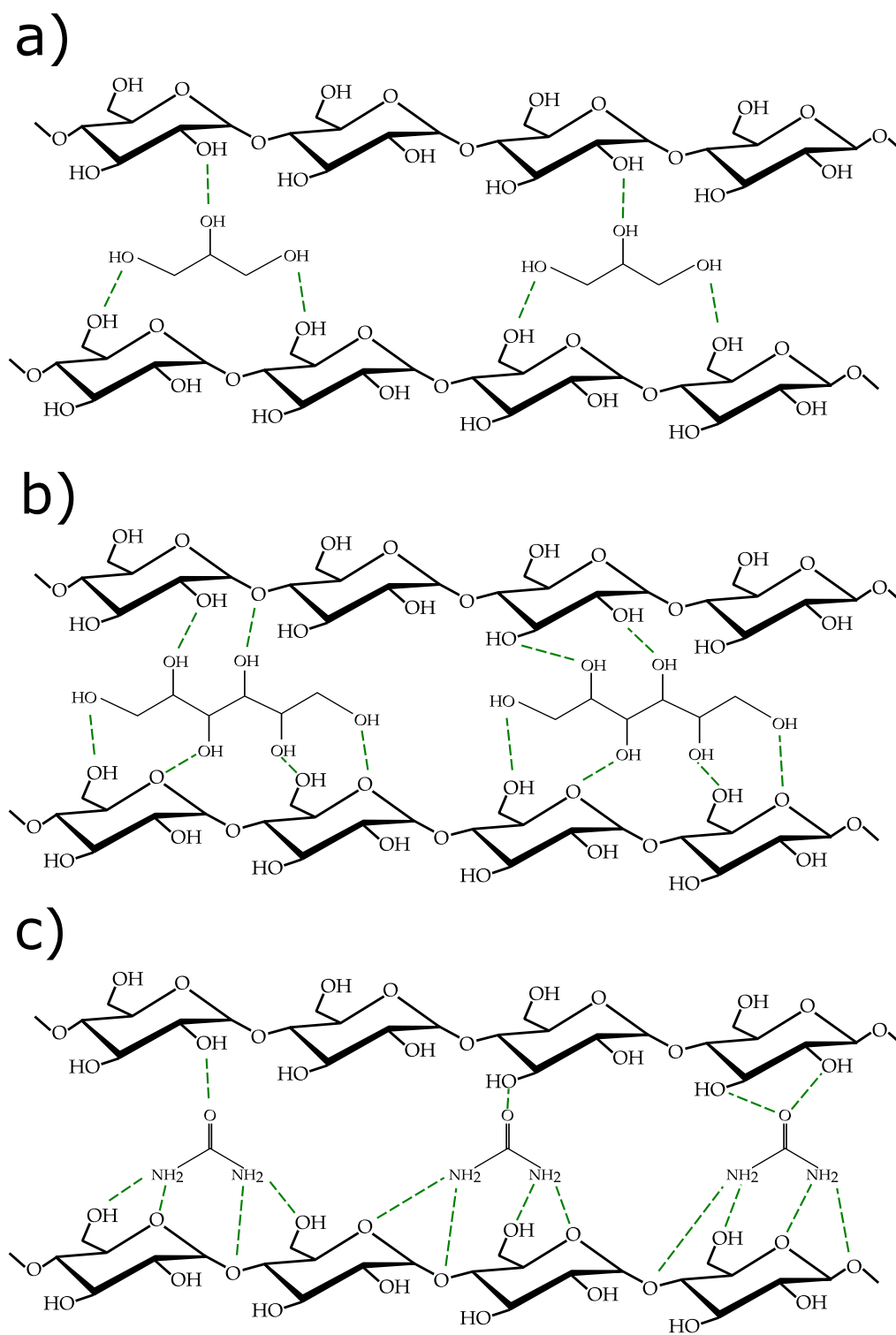


Figure III.1.5.5. Schematic representation of the hydrogen bonding interaction between starch and: a) glycerol; b) sorbitol; c) urea.

Mechanical properties

The mechanical properties of the MKF TPS samples were studied, by means of tensile tests, by considering two different storage conditions (53 and 11% RH), in order

to see how humidity affects the mechanical performance of these starch rich materials. Also, Shore D hardness measured at 53% RH was obtained. **Table III.1.5.2** gathers the main mechanical parameters extracted from both tests for all the samples, which were stored at 53% RH, whereas **Table III.1.5.3** gathers the same parameters for samples stored at 11% RH. The sample with 15 wt.% glycerol presents a mean value for tensile modulus of 15 MPa, a maximum tensile strength of 1.5 MPa and an elongation at break of 29%. These values are very similar to those obtained by Benincasa *et al.* [18] for samples of TPS made with wheat flour with a similar proportion of glycerol. The sample with sorbitol reaches better results in all the mechanical parameters, reaching 26 MPa of tensile modulus, 2.6 MPa of tensile strength and an elongation at break of 35.8%. This could be ascribed to the fact that sorbitol possesses a higher molecular weight than glycerol and a higher amount of active functionalities, which makes for stronger plasticizer-TPS bonds and therefore, more rigid materials. These properties corroborate the results observed in the processing section. The study of Li *et al.* [35] about blends of PLA and TPS plasticized with glycerol and sorbitol showed a very similar trend. The TPS with urea exhibited slightly lower resistant mechanical properties compared with sorbitol, with a tensile modulus of 16 MPa and a tensile strength of 2.1 MPa, nonetheless it presented the higher elongation at break of all the TPS samples (42.2%). This indicates that the amount of urea used for plasticizing the starch in MKF was very close to the optimal amount required, as an excess in urea would have extremely embrittled the material, as it was stated by Ma *et al.* [36]. Thus, this material has very well balanced resistant and ductile mechanical properties. Moreover, the amide functionalization in urea has been reported to prevent retrogradation of starch, which would explain the superior ductile mechanical properties observed [28].

The analysis of Shore D hardness showed a very similar trend to that of the elastic modulus, as both parameters are closely related. MKF-15GLY sample shows a hardness of 21.3, while the samples with sorbitol and urea present hardness values of 44.7 and 44.3, respectively. This is ascribed to a more rigid and resistant polymeric structure. Summarizing, the mechanical properties reported here perfectly match the results obtained in the processing section, where it was shown how sorbitol and urea produced a TPS that required higher shearing forces to be processed.

Table III.1.5.2. Mechanical properties of the MKF TPS samples stored at 53% RH.

Code	E (MPa)	σ_{max} (MPa)	ϵ_b (%)	Shore D hardness
MKF-GLY	15 ± 5	1.5 ± 0.2	29.0 ± 6.2	21.3 ± 1.1
MKF-SORB	26 ± 8	2.6 ± 0.4	35.8 ± 2.2	44.7 ± 1.3
MKF-UREA	16 ± 2	2.1 ± 0.1	42.2 ± 3.4	44.3 ± 1.2

Comparatively, the tensile modulus and tensile strength values observed in **Table III.1.5.3**, which correspond to a 11% relative humidity storage conditions, are much higher than the previous values, while elongation at break undergoes a considerable decrease. These results were expected, as lower relative humidity provokes an embrittlement of TPS, thus increasing its resistant mechanical properties and reducing its ductile properties [23, 36]. For example, glycerol plasticized samples present a tensile modulus and a tensile strength of 97 and 3.5 MPa, respectively, while at 53% RH those values were 15 and 1.5 MPa, respectively. Sorbitol plasticized MKF exhibits the highest resistant mechanical performance of all the samples (165 MPa tensile modulus and 4.8 MPa tensile strength). However, elongation at break value decreases in comparison with glycerol, which suggests that sorbitol-plasticized TPS are more sensitive to low-humidity embrittlement. Urea plasticized TPS shows balanced mechanical properties, although its elongation at break suffers a considerable decrease in comparison with the sample at 53% RH. This extreme embrittlement was also observed by Ma *et al.* [36], who observed that the unbound urea reduces the ductile properties in a great extent when the moisture is at low levels.

Table III.1.5.3. Mechanical properties of the MKF TPS samples stored at 11% RH.

Code	E (MPa)	σ_{max} (MPa)	E_b (%)
MKF-GLY	97 ± 25	3.5 ± 0.5	13.4 ± 3.1
MKF-SORB	165 ± 7	4.8 ± 0.1	6.1 ± 0.6
MKF-UREA	146 ± 3	3.7 ± 0.5	7.7 ± 0.6

Morphological properties

Figure III.1.5.6 shows the morphology of the cross-sectional fractured surfaces of tensile tested specimens stored at 53% RH. **Figure III.1.5.6a** corresponds to the MKF-15GLY sample, which shows a continuous phase of glycerol with the starch of MKF. This

is a very similar micrograph to those observed by Huand *et al.* [37] and Curvelo *et al.* [38], who made TPS with native starch and glycerol. Some particles can be observed in the micrographs, which could be ascribed to other lignocellulosic compounds present in MKF, such as cellulose, hemicellulose, lignin or pectin. Those compounds could even act as reinforcing agents due to the good adhesion observed between them and the polymeric matrix. The sample with sorbitol presents quite a similar micrograph to the previous one (**Figure III.1.5.6b**). Nonetheless, its continuous phase seems to present a lower concentration of voids in the matrix, which would be responsible for worse mechanical properties in the sample with glycerol. MKF-UREA sample seems to show a denser structure, with MKF particles embedded in the plasticized matrix (excellent adhesion) and a very low presence of voids (**Figure III.1.5.6c**). [2]. The results herein presented totally corroborate the findings observed in the mechanical properties section.

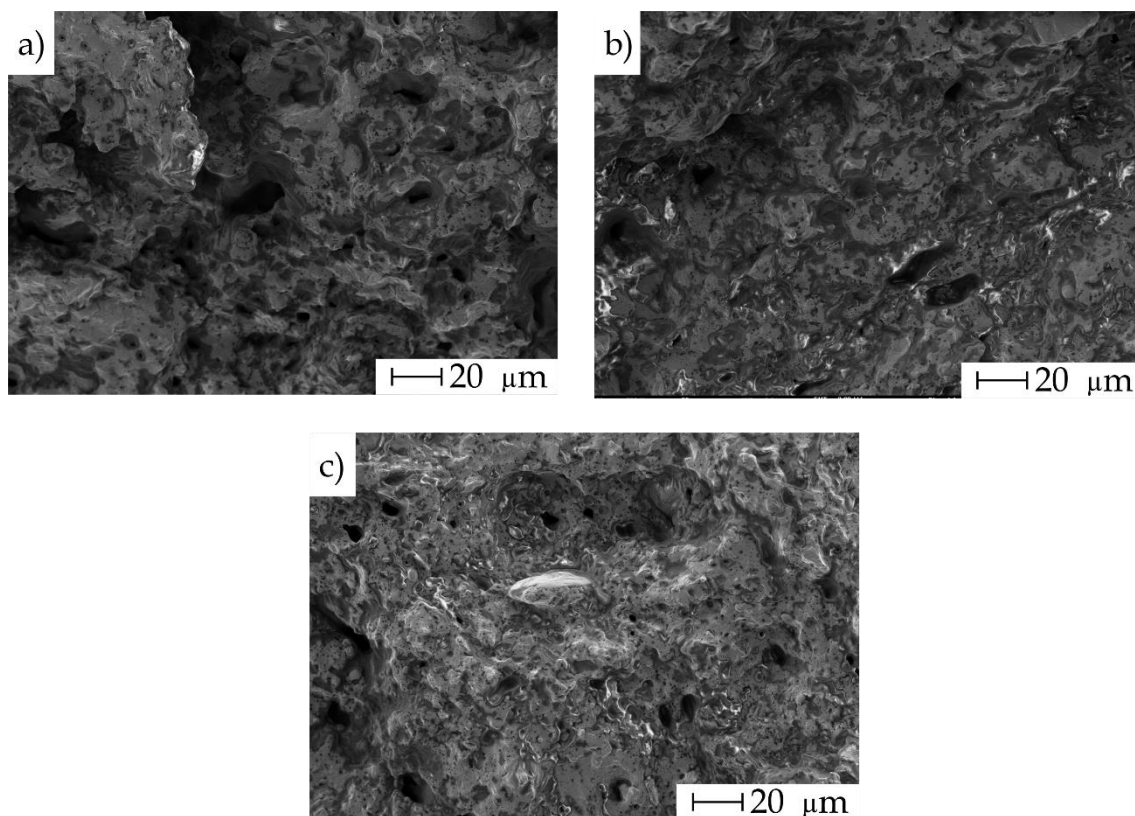


Figure III.1.5.6. FESEM morphological images at 500× of each one of the developed TPS stored at 53% RH: a) MKF-GLY; b) MKF-SORB; c) MKF-UREA.

Differential scanning calorimetry (DSC)

Figure III.1.5.7 shows the different thermograms for all the MKF TPS developed formulations. As it can be observed, the only thermal transition present in the

thermograms is the glass transition temperature of starch. The sample with glycerol presents a glass transition temperature of approximately 38.5 °C. This value is within the typical glass transition range of thermoplastic starch. Forssell *et al.* [39] observed a glass transition of about 20 °C for starch-glycerol-water mixtures. Sorbitol and urea plasticized starch present glass transitions of about 49 and 45 °C, respectively. This indicates a higher thermal stability than that of glycerol TPS. Sorbitol has been reported to form denser thermoplastic structures and preventing free water from entering the plasticized starch structure, which in turn would decrease both its mechanical and thermal stability due to increased chain mobility [40]. This effect is partly enhanced by its high molecular weight. Additionally, these results again point out to the fact that urea and sorbitol form a stronger linkage with starch than glycerol. This would directly decrease the mobility of the polymeric chains of the material, thus leading to more thermally and mechanically resistant materials. In addition, no retrogradation of starch is observed in this temperature range, as there is no sign of recrystallization of starch, thus, these materials are certainly resistant to starch retrogradation, which would negatively affect their ductile properties.

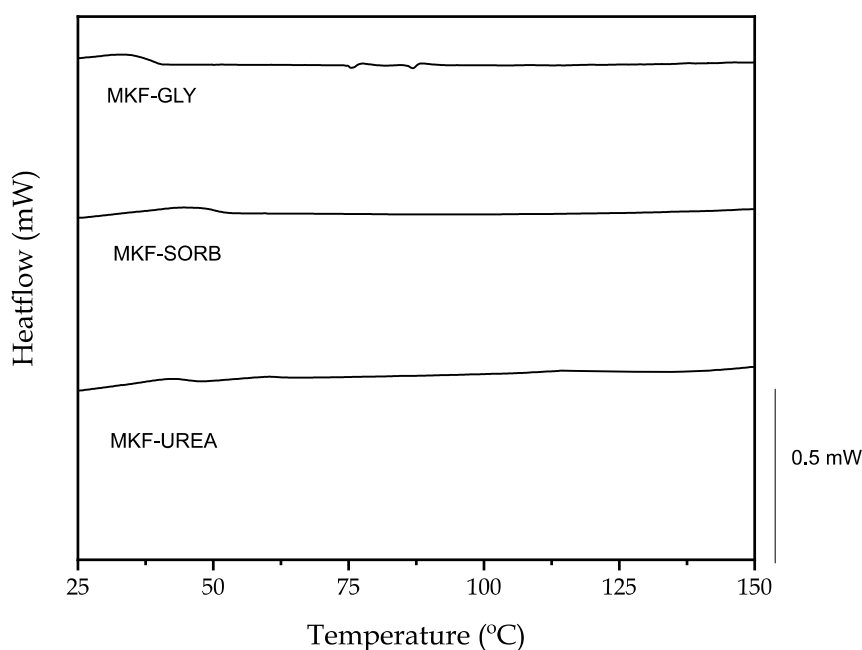


Figure III.1.5.7. DSC thermograms of all the MKF TPS samples.

Thermogravimetric analysis (TGA)

Figure III.1.5.8 shows the thermogravimetric analysis (TGA) thermograms of the MKF TPS developed samples as well as its first derivative, which is indicative of the rate

of thermodegradation, while **Table III.1.5.4** gathers the main thermal parameters related to this analysis. As it can be observed, the thermal degradation of all the samples occurs in several steps. The first little step corresponds to the evaporation of the free plasticizer, which is the least thermally stable component in the blends, this degradation starts at approximately 150 °C for all the samples. This is indicative of the plasticizer fraction that has not bonded with starch, and it is especially acute in the glycerol and urea samples, probably because of the lower molecular weight of both plasticizers [28]. Moreover, the thermal degradation profiles of the sorbitol and urea-plasticized TPS prove to be more thermally stable than the sample with glycerol. This fact is related to the higher molecular weight of sorbitol and the ability of urea to better interact with starch, making them more thermally stable. The next step occurs at approximately 300 °C, which is related to starch and the hydrogen-bonded plasticizer, as it was observed by Mano *et al.* [41]. In this sense, sorbitol slightly delayed the maximum degradation peak of starch up to 331 °C due to its strong interaction with starch (6 hydrogen bonds per sorbitol molecule). Finally, another step can be observed between 450 and 480 °C. This final step could be the product of the degradation of lignocellulosic components, such as lignin [42], as the thermoplastic starches were developed from mango kernel flour rather than native starch. **Figure III.1.5.8b** better displays the maximum degradation peaks of the plasticizer evaporation and the decomposition of starch and the lignocellulosic particles, where the superior thermal stability of urea-starch and sorbitol-starch is depicted. In general, the TPS with sorbitol and urea have presented greater thermal stability than the other samples, which perfectly matches the findings reported in the mechanical and morphological sections.

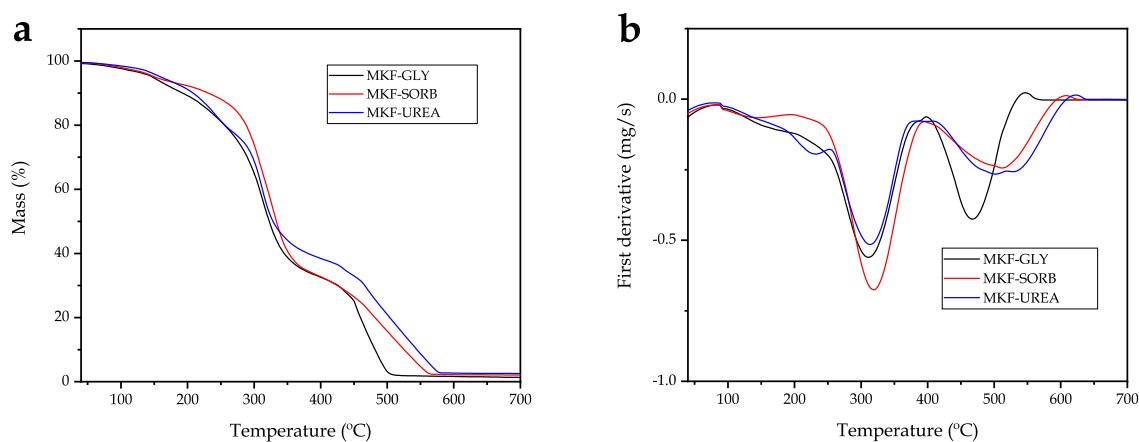


Figure III.1.5.8. Thermogravimetric analysis (TGA) and the first derivative (DTG) of the plasticized MKF TPS samples.

Table III.1.5.4. Main thermal degradation parameters of the MKF TPS formulations with different plasticizers in terms of the onset degradation temperature at a mass loss of 5 wt.% ($T_{5\%}$), maximum degradation rate (peak) temperature (T_{deg}), and residual mass at 700 °C.

Code	$T_{5\%}$ (°C)	T_{deg1} (°C)	T_{deg2} (°C)	Residual weight (%)
MKF-GLY	146.7 ± 0.6	312.3 ± 0.5	454.7 ± 0.3	1.3 ± 0.1
MKF-SORB	151.3 ± 0.4	331.0 ± 0.3	471.0 ± 0.5	2.1 ± 0.1
MKF-UREA	160.7 ± 0.7	312.3 ± 0.8	471.0 ± 0.4	2.5 ± 0.1

Thermomechanical analysis

The dynamic mechanical thermal analysis (DMTA) thermograms of the samples are shown in **Figure III.1.5.9**, where the evolution of the storage modulus with temperature is presented, as well as the evolution of the dynamic damping factor $\tan \delta$ with temperature. The glass transition temperature has been determined as the temperature of the peak in the $\tan \delta$ graph. As it can be seen, the storage modulus of the MKF TPS plasticized with sorbitol and urea are greater in all the temperature range in comparison with the glycerol plasticized TPS, especially the sorbitol-plasticized sample. The sample with glycerol exhibits a storage modulus of 2054 MPa at -40 °C, while the sorbitol and urea samples present 3807 and 2449 MPa, respectively, at the same temperature. These results were expected, as it was commented in the mechanical properties section, due to a higher stiffness provided by urea and sorbitol to the formulation. This is probably ascribed to the higher molecular weight that sorbitol possesses, as well as a higher concentration of functionalities in sorbitol and urea, which allows them to form stronger bonds with the starch in MKF, thus increasing the rigidity of the materials [35]. The curves present a sudden decrease, which is ascribed to an increase in the mobility of the amorphous region of the polymeric chains, related to the glass transition of the polymer. The storage modulus value of the glycerol sample at 50 °C is 0.4 MPa, whereas for the sorbitol and urea samples it is 0.6 MPa for both of them, again showing higher stiffness at higher temperatures, although this value is almost 0. Additionally, the glass transition temperature has been calculated as the inflection point in each one of the curves, represented by the peak observed in the $\tan \delta$ graph. It can be clearly seen that the glass transition of the MKF-GLY sample is shifted towards lower temperatures (20 °C) in comparison with sorbitol and urea (45.8 and 41.5 °C, respectively). This fact is directly related to a substitution of the intermolecular and intramolecular bonds of starch for hydrogen bonds with the plasticizer, which in turn decrease the glass transition of starch [43]. Due to these bonds being stronger with urea

and sorbitol, the glass transition in those formulations is moved towards higher temperatures, which also accounts for materials with greater stiffness. In spite of the fact that these glass transition temperatures are not similar to the ones observed in DSC analysis, the glass transitions presented here could be considered more precise, as DMTA analysis allows to study the samples at lower temperatures.

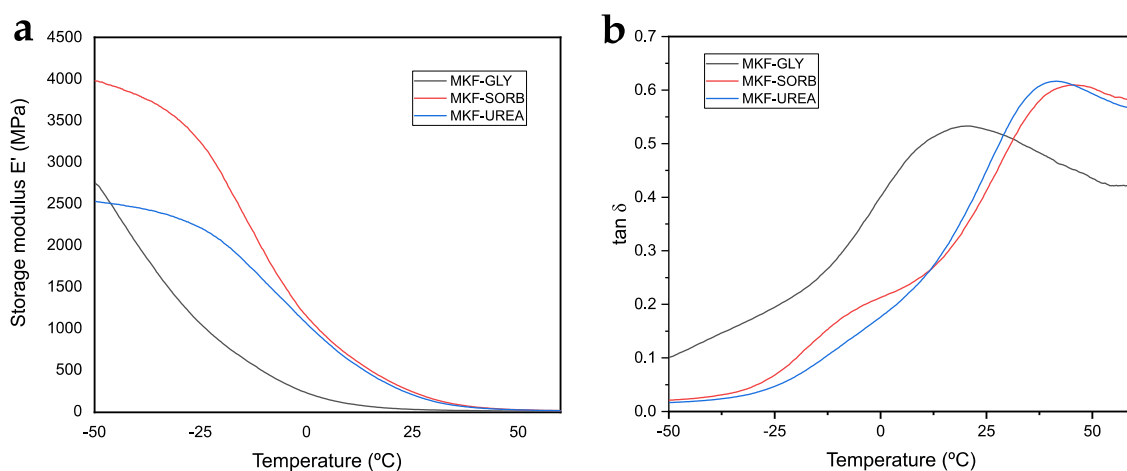


Figure III.1.5.9. Storage modulus (E') evolution with temperature of the plasticized MKF TPS samples.

Visual appearance analysis

The visual aspect of the samples herein developed was evaluated through colorimetry. This is an interesting property to be observed due to the characteristic brown colour of the samples, which could affect its possible applications. **Figure III.1.5.10** shows the visual appearance of the three materials presented in this study, while **Table III.1.5.5** gathers the main colorimetric parameters. It can be clearly seen that the three materials present very similar characteristic brown colours. This is ascribed to the intrinsic brownish tonality of mango kernel [44]. The parameter L^* refers to the lightness of the sample, in other words, how close to white is the sample. The L^* values for the three samples is quite close to 25, which is a low value compared with values of approximately 40 for polymers such as PLA [44], which are mostly white. This is reasonable considering the dark colour presented by these samples. The a^* colour coordinate is indicative for green (negative) and red (positive) tonalities. In this case, the three samples present positive values between 1.8 and 2.4. This is due to the red contribution to the brown colour herein observed. On the other hand, the b^* coordinate stands for blue (negative) and yellow (positive) shades. As expected, all the MKF TPS

samples present positive values (between 2 and 4) due to the yellow contribution to the brownish tonality of the materials. Additionally, the difference in colour is presented taking the MKF-GLY sample as the reference. It is clearly seen that this values for MKF-SORB and MKF-UREA are very low (1.7 and 1.5, respectively) as a result of the very similar colour between the samples. All in all, the colour observed in this study suggests that these materials could be used for applications suitable for wood plastic composites as alternatives to wood-based products, due to the characteristic brown colour they present.

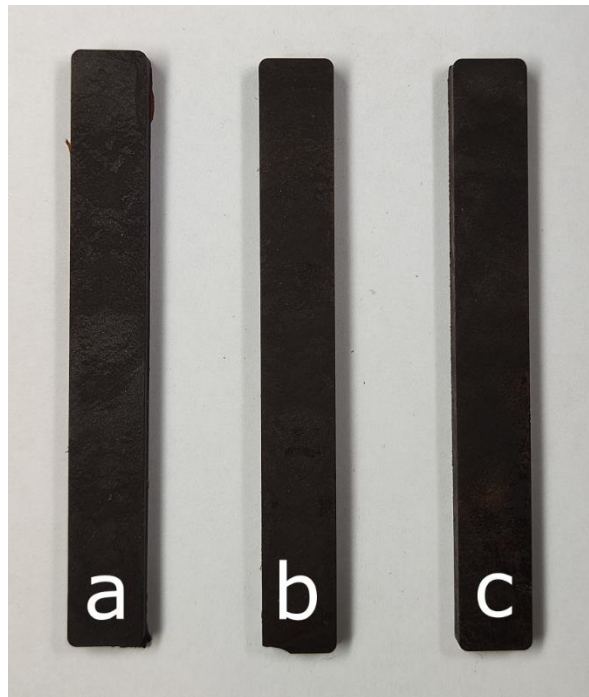


Figure III.1.5.10. Visual aspect of the MKF TPS samples: a) MKF-GLY; b) MKF-SORB; c) MKF-UREA.

Table III.1.5.5. Colorimetric parameters related to the starch rich thermoplastic samples: L^* (lightness), colour coordinates a^* and b^* and the difference in colour ΔE^*_{ab} taking the MKF-GLY sample as the reference.

Code	L^*	a^*	b^*	ΔE^*_{ab}
MKF-GLY	24.3 ± 0.1	1.8 ± 0.1	2.2 ± 0.1	-
MKF-SORB	25.9 ± 0.2	1.8 ± 0.1	2.9 ± 0.1	1.7 ± 0.1
MKF-UREA	24.7 ± 0.5	2.4 ± 0.2	3.5 ± 0.1	1.5 ± 0.1

CONCLUSIONS

This work has proved that it is possible to obtain environmentally friendly thermoplastic materials using starch-rich lignocellulosic mango kernel flour instead of native starch. Moreover, several plasticizers were tested and TPS were obtained with properties very similar to those of native starch TPS. The processing and mechanical analysis showed that sorbitol and urea allowed to produce TPS with general superior mechanical properties, both in terms of strength and ductility. A maximum tensile strength of 4.8 MPa for the MKF-SORB sample at 11% RH and a maximum elongation at break of 42.2% for the MKF-UREA sample at 53% RH conditions were obtained, which are quite remarkable values for TPS. Those results were verified by FESEM morphological analysis, which showed that all TPS presented quite homogeneous structures. Moreover, it was observed that some lignocellulosic particles were embedded in the polymer matrix, which could have acted as reinforcing agents. The thermal characterization showed an increase in the glass transition temperature both in DSC and DMTA results for the urea and sorbitol plasticized samples, proving the formation of more rigid and thermally stable materials. This was ascribed to the formation of stronger hydrogen bonds sorbitol-starch and urea-starch than glycerol-starch. Moreover, the thermal degradation profile showed an improvement for the samples with sorbitol and urea, proving that those plasticizers gave enhanced thermal stability to the blends. This work opens a new research line in which thermoplastic starches can be produced directly from untreated mango kernel flour, with several plasticizers to be tested that could provide these formulations with a wide range of different properties depending on the used plasticizer. It can be said that the hypotheses stated at the end of the work were confirmed. This opens up new hypotheses referring to future studies, such as the hydrogen bonding between sorbitol and mango kernel starch is stronger than the hydrogen bonding with urea; another hypothesis could be that a plasticizer like xylitol should bring properties in some point between the properties provided by glycerol and sorbitol, as it possesses 5 hydroxyl functionalizations. Future works could focus on studying the strength of the hydrogen bonding between the starch and the studied plasticizers, or even trying to use new plasticizers and mixtures of plasticizers in order to find a more effective plasticization of starch with even greater mechanical and thermal performances. Films could also been produced in order to evaluate the barrier properties of those materials.

ACKNOWLEDGEMENTS

This research is a part of the grant PID2020-116496RB-C22, funded by MCIN/AEI/10.13039/501100011033 and the grant TED2021-131762A-I00, funded by MCIN/AEI/10.13039/501100011033 and by the European Union “NextGenerationEU”/PRTR. Authors also thank Generalitat Valenciana-GVA for funding this research through the grant numbers AICO/2021/025 and CIGE/2021/094. Funded with Aid for First Research Projects (PAID-06-22), Vice-rectorate for Research of the Universitat Politècnica de València (UPV). J. I.-M. wants to thank FPU19/01759 grant funded by MCIN/AEI/10.13039/501100011033 and by ESF Investing in your future. J. G.-C. wants to thank FPU20/01732 grant funded by MCIN/AEI/10.13039/501100011033 and by ESF Investing in your future. Microscopy Services at UPV are also acknowledged by their help in collecting and analyzing images.

DATA AVAILABILITY STATEMENT

The raw/processed data required to reproduce these findings cannot be shared at this time due to technical or time limitations.

REFERENCES

- [1] Mensah, R.A., *et al.*, *A review of sustainable and environment-friendly flame retardants used in plastics*. *Polymer Testing*, 2022. 108: 107511.
- [2] Gomez-Caturla, J., *et al.*, *Development and evaluation of novel nanofibers based on mango kernel starch obtained by electrospinning*. *Polymer Testing*, 2022. 106: 107462.
- [3] Chen, J., *et al.*, *Oxidized microcrystalline cellulose improve thermoplastic starch-based composite films: Thermal, mechanical and water-solubility properties*. *Polymer*, 2019. 168: 228-235.
- [4] Agarwal, S., *Major factors affecting the characteristics of starch based biopolymer films*. *European Polymer Journal*, 2021. 160: 110788.
- [5] Majdzadeh-Ardakani, K. and B. Nazari, *Improving the mechanical properties of thermoplastic starch/poly (vinyl alcohol)/clay nanocomposites*. *Composites Science and Technology*, 2010. 70(10): 1557-1563.
- [6] Yu, L., *et al.*, *Two 1, 4- α -glucan branching enzymes successively rearrange glycosidic bonds: A novel synergistic approach for reducing starch digestibility*. *Carbohydrate Polymers*, 2021. 262: 117968.
- [7] Wang, J., *et al.*, *Thermoplastic starch plasticized by polymeric ionic liquid*. *European Polymer Journal*, 2021. 148: 110367.
- [8] Bai, J., *et al.*, *Reactive compatibilization and properties of low-cost and high-performance PBAT/thermoplastic starch blends*. *European Polymer Journal*, 2021. 143: 110198.
- [9] Gironès, J., *et al.*, *Natural fiber-reinforced thermoplastic starch composites obtained by melt processing*. *Composites Science and Technology*, 2012. 72(7): 858-863.
- [10] Kargarzadeh, H., N. Johar, and I. Ahmad, *Starch biocomposite film reinforced by multiscale rice husk fiber*. *Composites Science and Technology*, 2017. 151: 147-155.
- [11] Peidayesh, H., *et al.*, *In situ dual crosslinking strategy to improve the physico-chemical properties of thermoplastic starch*. *Carbohydrate Polymers*, 2021. 269: 118250.
- [12] Leblanc, N., *et al.*, *Structural investigation and thermal stability of new extruded wheat flour based polymeric materials*. *Carbohydrate polymers*, 2008. 73(4): 548-557.
- [13] Gaspar, M., *et al.*, *Reducing water absorption in compostable starch-based plastics*. *Polymer Degradation and Stability*, 2005. 90(3): 563-569.

- [14] Ogunsona, E., E. Ojogbo, and T. Mekonnen, *Advanced material applications of starch and its derivatives*. European Polymer Journal, 2018. 108: 570-581.
- [15] Adewale, P., M.S. Yancheshmeh, and E. Lam, *Starch modification for non-food, industrial applications: Market intelligence and critical review*. Carbohydrate Polymers, 2022. 291: 119590.
- [16] Puglia, D., et al., *Tensile behavior of thermoplastic films from wheat flours as function of raw material baking properties*. Journal of Polymers and the Environment, 2016. 24: 37-47.
- [17] Ayadi, F., C. Bliard, and P. Dole, *Materials based on maize biopolymers: Effect of flour components on mechanical and thermal behavior*. Starch-Stärke, 2011. 63(10): 604-615.
- [18] Benincasa, P., et al., *Relationships between wheat flour baking properties and tensile characteristics of derived thermoplastic films*. Industrial Crops and Products, 2017. 100: 138-145.
- [19] Toumi, N., M. Guessoum, and S. Nekkaa, *Biocomposites based on date palm flour reinforced (70/30) polypropylene/thermoplastic starch blend: Effects of flour treatment and selective dispersion*. Journal of Adhesion Science and Technology, 2019. 33(19): 2071-2092.
- [20] Yadav, S.P.S. and P. Paudel, *The process standarizing of mango (Mangifera indica) seed kernel for its value addition: A review*. Reviews In Food And Agriculture, 2022. 3(1): 6-12.
- [21] Ferraz, C.A., et al., *Extraction, modification, and chemical, thermal and morphological characterization of starch from the agro-industrial residue of mango (Mangifera indica L) var. Ubá*. Starch-Stärke, 2019. 71(1-2): 1800023.
- [22] Melo, P.E., et al., *Antioxidant films from mango kernel components*. Food Hydrocolloids, 2019. 95: 487-495.
- [23] Dang, K.M. and R. Yoksan, *Thermoplastic starch blown films with improved mechanical and barrier properties*. International Journal of Biological Macromolecules, 2021. 188: 290-299.
- [24] Ozeren, H.s.D., et al., *Ranking plasticizers for polymers with atomistic simulations: Pot, mechanical properties, and the role of hydrogen bonding in thermoplastic starch*. ACS Applied Polymer Materials, 2020. 2(5): 2016-2026.
- [25] Martins, I.M., et al., *New biocomposites based on thermoplastic starch and bacterial cellulose*. Composites Science and Technology, 2009. 69(13): 2163-2168.

- [26] Ivanič, F., M. Kováčová, and I. Chodak, *The effect of plasticizer selection on properties of blends poly (butylene adipate-co-terephthalate) with thermoplastic starch*. *European Polymer Journal*, 2019. 116: 99-105.
- [27] Martinez Villadiego, K., *et al.*, *Thermoplastic starch (TPS)/polylactic acid (PLA) blending methodologies: a review*. *Journal of Polymers and the Environment*, 2022. 30: 75-91.
- [28] Esmaeili, M., G. Pircheraghi, and R. Bagheri, *Optimizing the mechanical and physical properties of thermoplastic starch via tuning the molecular microstructure through co-plasticization by sorbitol and glycerol*. *Polymer International*, 2017. 66(6): 809-819.
- [29] Nawab, A., *et al.*, *Biodegradable film from mango kernel starch: Effect of plasticizers on physical, barrier, and mechanical properties*. *Starch-Stärke*, 2016. 68(9-10): 919-928.
- [30] Zuraida, A., *et al.*, *The effect of water and citric acid on sago starch bio-plastics*. *International Food Research Journal*, 2012. 19(2): 715-719.
- [31] Wang, C.-z., *et al.*, *Research on thermoplastic starch and different fiber reinforced biomass composites*. *RSC Advances*, 2015. 5(62): 49824-49830.
- [32] Gao, C., E. Pollet, and L. Avérous, *Innovative plasticized alginate obtained by thermo-mechanical mixing: Effect of different biobased polyols systems*. *Carbohydrate polymers*, 2017. 157: 669-676.
- [33] Zdanowicz, M. and K. Sałasińska, *Characterization of Thermoplastic Starch Plasticized with Ternary Urea-Polyols Deep Eutectic Solvent with Two Selected Fillers: Microcrystalline Cellulose and Montmorillonite*. *Polymers*, 2023. 15(4): 972.
- [34] Saiter, J.M., L. Dobircau, and N. Leblanc, *Are 100% green composites and green thermoplastics the new materials for the future?* *International Journal of Polymer Science*, 2012.
- [35] Li, H. and M.A. Huneault, *Comparison of sorbitol and glycerol as plasticizers for thermoplastic starch in TPS/PLA blends*. *Journal of Applied Polymer Science*, 2011. 119(4): 2439-2448.
- [36] Ma, X., J. Yu, and Y. Ma, *Urea and formamide as a mixed plasticizer for thermoplastic wheat flour*. *Carbohydrate Polymers*, 2005. 60: 111-116.
- [37] Huang, M.-F., J.-G. Yu, and X.-F. Ma, *Studies on the properties of montmorillonite-reinforced thermoplastic starch composites*. *Polymer*, 2004. 45(20): 7017-7023.

- [38] Curvelo, A.A.d.S., A. De Carvalho, and J. Agnelli, *Thermoplastic starch–cellulosic fibers composites: preliminary results*. Carbohydrate polymers, 2001. 45(2): 183-188.
- [39] Forssell, P.M., *et al.*, *Phase and glass transition behaviour of concentrated barley starch-glycerol-water mixtures, a model for thermoplastic starch*. Carbohydrate Polymers, 1997. 34(4): 275-282.
- [40] Baran, A., *et al.*, *Effects of sorbitol and formamide plasticizers on molecular motion in corn starch studied using NMR and DMTA*. Journal of Applied Polymer Science, 2020. 137(33): 48964.
- [41] Mano, J.F., D. Koniarova, and R. Reis, *Thermal properties of thermoplastic starch/synthetic polymer blends with potential biomedical applicability*. Journal of materials science: Materials in medicine, 2003. 14(2): 127-135.
- [42] Jorda-Reolid, M., *et al.*, *Upgrading argan shell wastes in wood plastic composites with biobased polyethylene matrix and different compatibilizers*. Polymers, 2021. 13(6): 922.
- [43] Yang, J.h., J.g. Yu, and X.f. Ma, *Preparation of a novel thermoplastic starch (TPS) material using ethylenebisformamide as the plasticizer*. Starch-Stärke, 2006. 58(7): 330-337.
- [44] Gomez-Caturla, J., *et al.*, *Manufacturing and characterization of highly environmentally-friendly composites with polylactide matrix and mango kernel seed flour*. Express Polymer Letters, 2023. 17(3): 334-351.

Section II

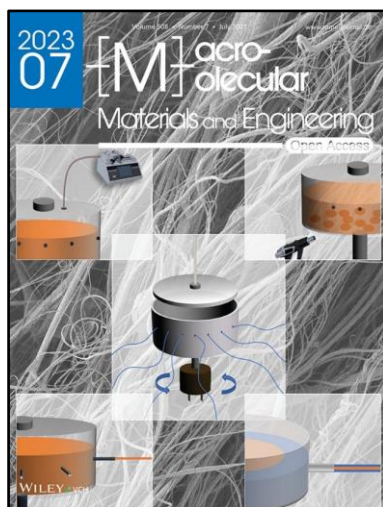
**PLA-based environmentally friendly
materials with the use of natural-derived
plasticizers**

III.2.1. Improvement of poly(lactide) ductile properties by plasticization with biobased tartaric acid ester

Jaume Gomez-Caturla^{1*}, Ivan Dominguez-Candela², Marta Patricia Medina-Casas¹,
Juan Ivorra-Martinez¹, Rafael Balart¹, Daniel Garcia-Garcia¹

¹ Technological Institute of Materials – ITM, Universitat Politècnica de València – UPV,
Plaza Ferrándiz y Carbonell 1, 03801 Alcoy (Spain).

² Instituto de Seguridad Industrial, Radiofísica y Medioambiental (ISIRYM) Universitat
Politécnica de València (UPV), Plaza Ferrándiz y Carbonell s/n, 03801 Alcoy, (Spain).



Macromolecular Materials and Engineering

2023, 308(7): 2200694

*Adapted from the original manuscript.

RESEARCH ARTICLE

Improvement of Poly(lactide) Ductile Properties by Plasticization with Biobased Tartaric Acid Ester

Jaume Gomez-Caturla,* Ivan Dominguez-Candela, Martha Patricia Medina-Casas, Juan Ivorra-Martinez, Virginia Moreno, Rafael Balart, and Daniel Garcia-Garcia

Diethyl L-tartrate (DET) is used as a biobased plasticizer for poly(lactide) (PLA) formulations with improved ductile properties without compromising biodegradation. Different weight percentages (wt.%) of DET in the 0–50 wt.% range are added to PLA by melt compounding and subsequently processed by injection molding. The effect of wt.% DET on mechanical, thermal, thermo-mechanical, morphology, biodegradation, and crystallinity is studied. Addition of 20 wt.% DET leads to a noticeable increase in elongation at break up to values of 567%, which is quite an interesting result considering the extreme brittleness of PLA. These results are verified by field emission scanning electron microscopy (FESEM) images, where filament-like structures are observed, indicative of an effective plasticization. Differential scanning calorimetry (DSC) and dynamic mechanical thermal analysis (DMTA) show that the glass transition temperature of PLA is drastically decreased down to values of 23 °C for the sample with the highest amount of DET (50 wt.%), thus increasing its ductility and processability. Fourier-transformed infrared spectroscopy (FTIR) spectra show that there exists chemical interactions between PLA and DET. Finally, the biodegradability analysis proves that the developed blends are fully biodegradable, achieving complete disintegration after 49 days. It is observed that DET enhanced the disintegration rate of PLA.

1. Introduction

Poly(lactide) (PLA) is an aliphatic polyester that can be obtained from fermentation of starch-rich materials.^[1] It has been raised as one of the most promising biopolymers since it combines balanced properties and processability, it is mostly obtained from natural resources, it can undergo biodegradation and, in addition, it is biocompatible and bioabsorbable. All these features, together with the potential of additives to tune its behavior, have contributed to a widespread use of PLA in a variety of applications such as the packaging industry,^[2] textile, electronics,^[3,4] automotive industry,^[5] and medical applications,^[6] among others. It is also a standard material in 3D printing^[7] and, due to its shape-memory behavior it has been proposed for several biomedical applications.^[8]

Despite all these interesting features, PLA shows some drawbacks such as poor gas-barrier properties, relatively low thermal stability, and a high inherent brittleness. PLA is a low-toughness polymer with very low elongation at break (less than 10%).^[9–11] Therefore, numerous research works have been focused on improving its flexibility.^[12,13] Plasticization is a quite common procedure to overcome its brittleness. A wide range of plasticizers have been proposed for PLA plasticization, including adipates,^[14,15] sebacates,^[16] oligomers of lactic acid (OLA),^[17] epoxidized vegetable oils,^[18,19] glycerol triesters,^[20] citrates,^[21] among others. Nonetheless, there exist some other methods to improve the ductility of PLA, such as the work of Kuang et al.^[22] who modified the crystalline structure of PLA through a pressure-driven flow treatment without additives, modifying its structure; other method includes the nanofibrillation of PLA using polytetrafluoroethylene as a nucleating agent by means of a loop oscillatory push-pull molding method.^[23]

In general, the effect of a plasticizer on PLA is an increase in the elongation at break. This is a consequence of a dramatic decrease in the glass transition temperature (T_g), even below room temperature as reported by Maiza et al.^[21] for plasticized PLA formulations with 10–20 wt.% triethyl citrate (TEC), and acetyl tributyl citrate (ATBC). In general, a plasticizer content between 10–20 wt.% is needed to promote a significant decrease in T_g while over 20–30 wt.% plasticizer, phase separation usually occurs.^[21,24]

J. Gomez-Caturla, M. P. Medina-Casas, J. Ivorra-Martinez, V. Moreno, R. Balart, D. Garcia-Garcia
 Institute of Materials Technology (ITM)
 Technical University of Valencia (UPV)
 Plaza Ferrándiz y Carbonell 1, Alcoy, Alicante 03801, Spain
 E-mail: jaugoca@epsa.upv.es
 I. Dominguez-Candela
 Research Institute for Industrial, Radiophysical and Environmental Safety (ISIRYM)
 Technical University of Valencia (UPV)
 Plaza Ferrándiz y Carbonell s/n, Alcoy 03801, Spain

 The ORCID identification number(s) for the author(s) of this article can be found under <https://doi.org/10.1002/mame.202200694>

© 2023 The Authors. Macromolecular Materials and Engineering published by Wiley-VCH GmbH. This is an open access article under the terms of the Creative Commons Attribution License, which permits use, distribution and reproduction in any medium, provided the original work is properly cited.

DOI: 10.1002/mame.202200694

Improvement of poly(lactide) ductile properties by plasticization with biobased tartaric acid ester

Abstract

Diethyl L-tartrate (DET) was used as biobased plasticizer for poly(lactide) (PLA) formulations with improved ductile properties without compromising biodegradation. Different weight percentages (wt.%) of DET in the 0–50 wt.% were added to PLA by melt compounding and subsequently processed by injection moulding. The effect of the wt.% DET on mechanical, thermal, thermo-mechanical, morphology, biodegradation and crystallinity was studied. Addition of 20 wt.% DET led to a noticeable increase in elongation at break up to values of 567%, which is quite an interesting result considering the extreme brittleness of PLA. These results were verified by field emission scanning electron microscopy (FESEM) images, where filament-like structures were observed, indicative of an effective plasticization. Differential scanning calorimetry (DSC) and dynamic mechanical thermal analysis (DMTA) showed that the glass transition temperature of PLA was drastically decreased down to values of 23 °C for the sample with the highest amount of DET (50 wt.%), thus increasing its ductility and processability. Fourier transformed infrared spectroscopy (FTIR) spectra showed that there existed chemical interactions between PLA and DET. Finally, the biodegradability analysis proved that the developed blends were fully biodegradable, achieving complete disintegration after 49 days. It was observed that DET enhanced the disintegration rate of PLA, promoting hydrolysis of the polymeric chains.

Keywords: Poly(lactide), diethyl L-tartrate, plasticizer, biodegradable, mechanical properties.

INTRODUCTION

Poly(lactide) (PLA) is an aliphatic polyester that can be obtained from fermentation of starch-rich materials [1]. It has raised as one of the most promising biopolymers since it combines balanced properties and processability, it is mostly obtained from natural resources, it can undergo biodegradation and, in addition, it is biocompatible and bioabsorbable. All these features, together with the potential of additives to tune its behaviour, have contributed to a widespread use of PLA in a variety of applications such as packaging industry [2], textile, electronics [3, 4], automotive industry [5], and medical applications [6], among others. It is also a standard material in 3D printing [7] and, due to its shape-memory behaviour it has been proposed for several biomedical applications [8].

Despite all these interesting features, PLA shows some drawbacks such as poor gas-barrier properties, relatively low thermal stability, and a high inherent brittleness. PLA is a low toughness polymer with very low elongation at break (less than 10%) [9-11]. Therefore, numerous research works have been focused on improving its flexibility [12, 13]. Plasticization is a quite common procedure to overcome its brittleness. A wide range of plasticizers have been proposed for PLA plasticization, including adipates [14, 15], sebacates [16], oligomers of lactic acid (OLA) [17], epoxidized vegetable oils [18, 19], glycerol triesters [20], citrates [21], among others. Nonetheless, there exist some other methods to improve the ductility of PLA, such as the work of Kuang *et al.* [22], who modified the crystalline structure of PLA through a pressure-driven flow treatment without additives, modifying its structure; other method includes the nanofibrillation of PLA using polytetrafluoroethylene as a nucleating agent by means of a loop oscillatory push-pull molding method [23].

In general, the effect of a plasticizer on PLA is an increase in the elongation at break. This is a consequence of a dramatic decrease in the glass transition temperature (T_g), even below room temperature as reported by Maiza *et al.* [21], for plasticized PLA formulations with 10-20 wt.% triethyl citrate (TEC), and acetyl tributyl citrate (ATBC). In general, a plasticizer content between 10-20 wt.% is needed to promote a significant decrease in T_g while over 20-30 wt.% plasticizer, phase separation usually occurs [21, 24]. This phase separation phenomenon has also been observed in plasticized PLA formulations containing polymeric plasticizers such as polyethylene glycol (PEG) [25].

With the aim of developing environmentally friendly PLA formulations, new plasticizers are continuously being developed. Tartrates or diesters of tartaric acid, have been proposed as “double green” plasticizers in PLA formulations since they can be

bioderived and can undergo biodegradation. Zawada *et al.* [26] have reported the synthesis of different tartrate esters, and methylated tartrate esters by reacting tartaric acid with different chain length alcohols such as methanol, ethanol, n-butanol, 2-ethylhexanol, octanol, among others. They evaluated the efficiency of the synthesized tartrates as plasticizers for PLA and concluded that diethyl-L-tartrate (DET) and dibutyl-L-tartrate (DBT) gave the best plasticization properties to PLA according to the highest decrease in T_g provided by both tartrates. They also reported an exceptional increase in elongation at break from less than 10% up to values of around 500% with a DET content of 30 wt.%. They used a mixing time of 30 min prior to mechanical characterization. As they indicate, the actual residence time of PLA formulations under real manufacturing conditions is remarkably shorter. Despite tartrates have shown their plasticization efficiency, the processing conditions play a key role, especially when industrial conditions are used instead of laboratory conditions. The main aim of this work is to assess the effect of the real processing conditions by extrusion/injection moulding on mechanical, thermal, thermomechanical and biodegradation properties of plasticized PLA formulations with varying the content of diethyl-L-tartrate (DET) in the 0-50 wt.% range.

MATERIALS AND METHODS

Materials

Bio-based PLA Purapol L130 grade was supplied by Corbion purac (The Netherlands, Amsterdam), with a melt flow index (MFI) of 16 g/10 min (at 210 °C/2.16 kg), a density of 1.24 g/cm³ and a melt peak temperature of 175 °C. Diethyl L-tartrate was purchased from Sigma Aldrich (Product Code: W237809) with a molar mass of 206.19 g/mol.

Preparation of PLA/DET formulations

PLA was initially dried at 40 °C for 48 h in a dehumidifying dryer before processing in order to remove any residual moisture. Afterwards, according to **Table III.2.1.1**, the corresponding amount of plasticizer (wt%. DET) was mixed with PLA and compounded in a twin-screw extruder from Construcciones Mecánicas Dupra, S.L. (Alicante, Spain). This extruder has a screw diameter of 25 mm and length-to-diameter ratio (L/D) of 24. The extrusion process was carried out at a rate of 22 rpm, using the following temperature profile (from the hopper to the die): 170-175-180-185 °C. The

compounded materials were pelletized using an air-knife unit. Residence time was approximately 1 minute. **Table III.2.1.1** shows the compositions of the formulations developed in this work.

Table III.2.1.1. Composition of the developed formulations of plasticized poly(lactide) (PLA) with diethyl L-tartrate (DET).

Code	PLA (wt.%)	DET (wt.%)
PLA	100	0
PLA90DET10	90	10
PLA80DET20	80	20
PLA70DET30	70	30
PLA60DET40	60	40
PLA50DET50	50	50

The compounded pellets were injection moulded in an injection moulding unit from Mateu & Solé (Barcelona, Spain) Meteor 270/75. The temperature profile used was 155 °C (hopper), 160 °C, 165 °C, and 170 °C (injection nozzle). A clamping force of 75 tons was applied while the cavity filling and cooling times were set to 1 and 10 s, respectively. Standard samples for mechanical and thermal characterization with an average thickness of 4 mm were obtained.

Characterization of PLA/DET blends

Theoretical approach to solubility of PLA and DET

The miscibility between a polymer and a plasticizer is essential when they are to be combined in a blend. The group contribution method proposed by Van Krevelen and Hoftyzer [27] is very useful to calculate the solubility parameters (δ) of both components. **Equation III.2.1.1** shows the contribution of the dispersion forces (δ_d), polar forces (δ_p), and hydrogen bonding (δ_h), to the overall solubility parameter:

$$\delta = \delta_d^2 + \delta_p^2 + \delta_h^2 \quad \text{(III.2.1.1)}$$

At the same time, each contribution can be calculated according to **Equation III.2.1.2 to III.2.1.4**:

$$\delta_d = \frac{\sum F_{di}}{V} \quad (\text{III.2.1.2})$$

$$\delta_p = \frac{\sqrt{\sum F_{pi}^2}}{V} \quad (\text{III.2.1.3})$$

$$\delta_h = \frac{\sqrt{\sum E_{hi}}}{V} \quad (\text{III.2.1.4})$$

where V [$\text{cm}^3 \text{ mol}^{-1}$] stands for the molar volume, F_{di} [$(\text{MJ}/\text{m}^3)^{1/2} \text{ mol}^{-1}$] corresponds to the group contributions of the molar attraction constant with regard to the dispersion component, F_{pi} [$(\text{MJ}/\text{m}^3)^{1/2} \text{ mol}^{-1}$] stands for the characteristic molar attraction constants related to the polar component, while E_{hi} [J mol^{-1}] values are representative for the hydrogen bonding energy which are almost constant per structural group.

Table III.2.1.2 gathers all the solubility contributions and the solubility parameter. Additionally, the parameter R_a has been calculated. The latter is indicative of the distance between the solubility coordinates of the plasticizer and the solubility coordinates of PLA. The lower R_a is, the higher the miscibility between PLA and the plasticizer, so that if R_a is zero, both components are totally miscible. There exists a R_a threshold from which the solubility between polymer and plasticizer becomes poor, this value is R_0 , which is intrinsic for each polymer and defines a spherical solubility region for a specific polymer. The center of this sphere is determined by the three solubility contributions aforementioned. R_a is calculated according to **Equation III.2.1.5**:

$$R_a = \sqrt{4 \cdot (\delta_{d_{plast}} - \delta_{d_{PLA}})^2 + (\delta_{p_{plast}} - \delta_{p_{PLA}})^2 + (\delta_{h_{plast}} - \delta_{h_{PLA}})^2} \quad (\text{III.2.1.5})$$

Moreover, the relative energy difference (RED) can also be calculated. This parameter is defined as the ratio between R_a and R_0 , which in the case of PLA is $10.7 \text{ MPa}^{1/2}$ (**Equation III.2.1.6**) [28]. The lower the RED value becomes, the higher the solubility between polymer and plasticizer is. If RED is equal to 1, this means that both elements are in the borderline of good miscibility, while values above 1 are indicative

for poor solubility.

$$RED = \frac{R_a}{R_0} \quad (III.2.1.6)$$

As it can be observed in **Table III.2.1.2**, diethyl L-tartrate presents good miscibility with PLA, as its RED value is lower than 1 (0.69). Nonetheless, this result is just a theoretical approach, and it will be corroborated by experimental results.

Table III.2.1.2. Theoretical solubility parameters of PLA with diethyl L-tartrate.

Material	δ_d (MPa ^{1/2})	δ_p (MPa ^{1/2})	δ_h (MPa ^{1/2})	δ (MPa ^{1/2})	R_a (MPa ^{1/2})	RED
Poly(lactide) (PLA)	15.33	8.44	10.98	20.66	-	
Diethyl L-tartrate (DET)	16.00	5.78	17.76	24.59	7.40	0.69

Mechanical characterization

The tensile behavior of PLA/DET blends were obtained in a universal testing machine ELIB 50 from S.A.E. Ibertest (Madrid, Spain) according to ISO 527-1:2012. Cross-head speed was set to 5 mm/min and a 5-kN load cell was used. Shore D hardness was measured in a 676-D durometer from J. Bot Instruments (Barcelona, Spain) on rectangular samples with dimensions 80×10×4 mm³, according to ISO 868:2003. All mechanical tests were performed at room temperature, and at least 6 samples of each material were tested and the corresponding mechanical parameters were averaged.

Morphological characterization

The surface of fractured samples from Charpy test was studied to see the morphology of the plasticized blends. The morphology was studied by field emission scanning electron microscopy (FESEM) in a ZEISS ULTRA 55 microscope from Oxford Instruments (Abingdon, United Kingdom). The samples were sputtered with a gold-palladium alloy in an EMITECH sputter coating SC7620 model from Quorum Technologies, Ltd. (East Sussex, UK). The microscope was worked at an acceleration voltage of 2 kV.

Thermal analysis

Differential scanning calorimetry (DSC) was used to study the most relevant thermal transitions of the samples in a Mettler-Toledo 821 calorimeter (Schwerzenbach, Switzerland). Samples with an average weight of 5-10 mg were subjected to a thermal program divided into three stages: a first heating from -50 °C to 200 °C followed by a cooling to 0 °C, and a second heating step up to 300 °C. Both heating and cooling rates were set to 10 °C/min. All tests were run in a nitrogen atmosphere with a flowrate of 66 mL/min using 40 µL standard sealed aluminum crucibles. Crystallinity was calculated according to **Equation III.2.1.7**:

$$X_c = \left[\frac{\Delta H_m}{\Delta H_m^0 \cdot (1 - w)} \right] \cdot 100 \quad (\text{III. 2.1.7})$$

where $\Delta H_m^0 = 93 \text{ J/g}$ is the theoretical enthalpy of a 100% crystalline PLA polymer [48], the term $1-w$ corresponds to the PLA weight fraction in the blend, and ΔH_m is the measured melting enthalpy.

Thermal decomposition of the PLA/DET blends was assessed by thermogravimetric analysis (TGA) in a LINSEIS TGA 1000 (Selb, Germany) thermobalance. Samples with a weight of 15-25 mg were placed into 70 µL alumina crucibles and subjected to a dynamic heating program from 35 °C to 700 °C at a heating rate of 10 °C/min in nitrogen atmosphere.

Dynamical-mechanical thermal characterization

Dynamical mechanical thermal analysis (DMTA) was carried out in a DMA1 dynamic analyzer from Mettler-Toledo (Schwerzenbach, Switzerland), working in single cantilever flexural conditions. The selected frequency was 1 Hz and the maximum flexural deformation or cantilever deflection was set to 10 µm. Rectangular samples with dimensions 20×6×2.7 mm³ were subjected to a dynamic temperature sweep from -150 °C to 100 °C at a constant heating rate of 2 °C/min.

Fourier transform infrared spectroscopy

The interactions of PLA and DET in the PLA/DET blends was analysed by means of attenuated total reflection-Fourier transform infrared spectroscopy (ATR-FTIR)

spectroscopy. Spectra were collected using a Bruker S.A Vector 22 (Madrid, Spain) coupled to a PIKE MIRacle™ single reflection diamond ATR accessory (Madison, Wisconsin, USA). Data were collected as the average of 20 scans between 4000 and 500 cm^{-1} with a spectral resolution of 2 cm^{-1} .

Biodegradability

The biodegradability of the plasticized PLA/DET blends under controlled compost soil was assessed through the disintegration test following ISO 20200. Samples sizing 2.5×2.5 cm^2 were dried for 24 h at 40 °C. They were then weighted and buried in a bioreactor of dimensions 30×20×10 cm^3 in a solid synthetic wet soil prepared with 40 wt.% sawdust, 10 wt.% corn starch, 30 wt.% rabbit-feed, 10 wt.% compost, 5 wt.% sugar, 4 wt.% of corn oil, and 1 wt.% of urea. This mixture was combined with distilled water in a 45:55 ratio (wt./wt.). In these conditions, the samples were aerobically degraded at a constant temperature of 58 °C in an air circulating oven during 4 weeks. Measurements were taken by extracting samples from the reactor, washing them with distilled water, drying them for 24 h at 40 °C and finally weighting them. Several measurements were taken during the 4 weeks to observe the biodegradation profile of the samples over time.

RESULTS AND DISCUSSION

Mechanical characterization

Table III.2.1.3 gathers the results concerning the mechanical performance of plasticized PLA/DET blends in terms of elastic modulus, tensile strength, elongation at break and Shore D hardness; while **Figure III.2.1.1** shows the stress - strain curves of all the samples. Neat PLA presents the typical behavior of a hard, brittle polymer with low toughness [29]. This is indicated by its low elongation at break (11.26%) and by its high tensile strength (68.34 MPa). When 10 wt.% DET is added into the polymer matrix, the elastic modulus decreases from 926 down to 837 MPa. The tensile strength decreases from 68.3 down to 53.3 MPa, and elongation at break also decreases down to 8.2%. This implies that 10 wt.% of plasticizer is not sufficient to effectively plasticize PLA, with a general worsening of the mechanical performance. This effect is known as anti-plasticization and it occurs when little amount of plasticizer is added to some polymers [30]. Nonetheless, when the amount of plasticizer is increased to 20 wt.% the ductility of the blend impressively increases, presenting an elongation at break of 567.6%, maintaining a tensile strength of 26 MPa. This behavior is ascribed to the plasticizing

effect of DET, which promotes a reduction in the attraction forces between PLA polymer chains, so their movement requires less energy, making it possible to obtain more elongation capacity [31]. Once 20 wt.% of DET is surpassed, the plasticizing effect is still surprising, with elongation at break values of 463% for 30wt.% of DET or 399% for 50 wt.% of DET, although it is worse in comparison with 20 wt.% of DET. This could be related to PLA reaching saturation related to the plasticizer, a very similar phenomenon to the one observed by Ivorra-Martinez *et al.* [31] when plasticizing PLA with dibutyl itaconate (DBI). Therefore, 20 wt.% DET can be considered the optimal plasticizer concentration in order to achieve the best mechanical properties. As expected, tensile strength decreases as the amount of plasticizer increases, reaching a minimum value of 15.2 MPa for the sample with 50 wt.% DET. This is ascribed to the softening effect previously described, which gives more mobility to the polymer chains. Anyway, the tensile strength in plasticized formulations containing 20-30 wt.% DET, are close to that of polyethylene (around 20 MPa). Therefore, despite a decrease in tensile strength is observed, the obtained values allow using PLA in many applications that do not require high tensile strength such as the food packaging, thus broadening its potential applications.

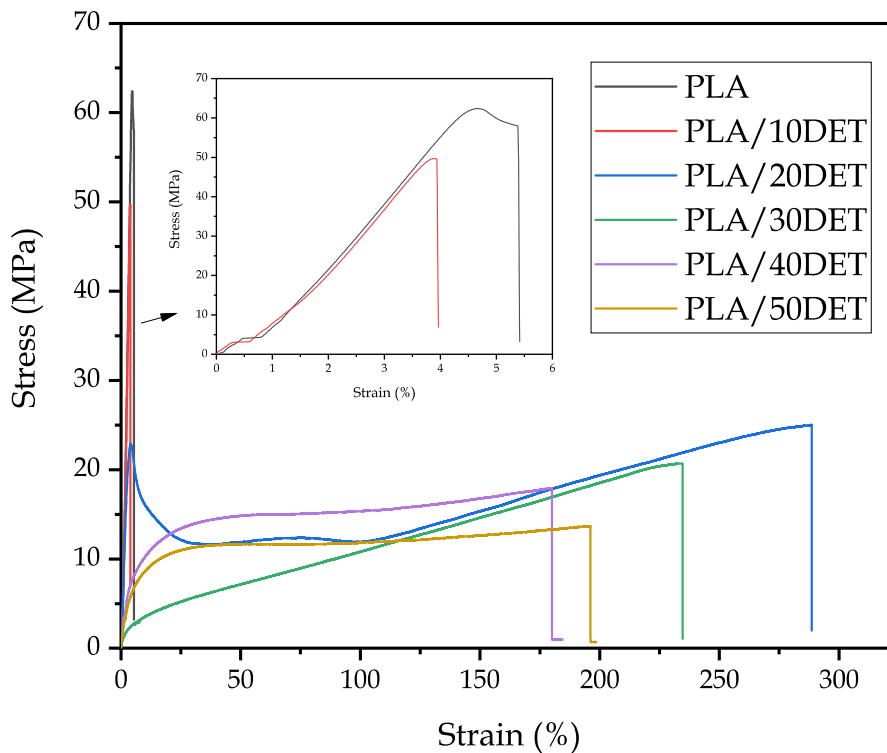


Figure III.2.1.1. Stress - Strain curves of PLA and the plasticized PLA/DET samples.

Table III.2.1.3. Mechanical properties of the plasticized poly(lactide) (PLA) blends with diethyl L-tartrate (DET).

Material	Elastic modulus, E (MPa)	Tensile strength, σ_{max} (MPa)	Elongation at break, ϵ_b (%)	Shore D hardness
PLA	926 ± 15	68.3 ± 2.2	11.3 ± 0.8	82.4 ± 1.1
PLA/10DET	837 ± 39	53.3 ± 3.5	8.2 ± 0.5	82.0 ± 1.0
PLA/20DET	315 ± 29	26.0 ± 1.0	567.6 ± 8.3	78.2 ± 3.1
PLA/30DET	57 ± 8	21.7 ± 1.2	463.0 ± 41.5	57.2 ± 1.9
PLA/40DET	121 ± 11	18.6 ± 1.1	362.3 ± 22.8	62.2 ± 0.8
PLA/50DET	120 ± 1	15.2 ± 0.6	399.7 ± 39.9	57.6 ± 0.9

Regarding Shore D hardness, it follows a very similar trend to that of elastic modulus and tensile strength. Neat PLA presents a hardness of 82.4, and it can be seen how as the amount of plasticizer increases, this value is diminished. PLA/10DET presents a value of 82, while PLA/50DET presents a value of 57.6, which is a considerable decrease. This phenomenon is obviously related to the plasticizing effect exerted by DET, which makes the polymer chains more easily deformable as a result of an increase in their mobility. The results presented here seem to corroborate the good miscibility between PLA and DET calculated in the theoretical solubility section.

Morphological characterization

Figure III.2.1.2 shows the FESEM morphology of PLA/DET blends at 500×. **Figure III.2.1.2a** illustrates the morphology of neat PLA. The observed flat surface shows the typical brittle behavior of this polymer, which is indicative of a low ductility, and a fracture process with very low plastic deformation. Fracture in neat PLA occurs without plastic deformation which could be identified as wavy surface. As only a flat surface with different microcrack can be observed, it can be assessed that fracture of PLA occurs with almost negligible plastic deformation which is responsible for the low toughness [31]. **Figure III.2.1.2b** (10 wt.% DET) also shows a surface with very little roughness, which is also indicative of a hard and brittle behavior, as it was also observed in the mechanical properties section. Interestingly, the rest of the samples (from 20 wt.% to 50 wt.% of DET) show clear signs of plasticization. This is noted by a rough surface with filament-like formations and a cavernous morphology, especially in **Figure III.2.1.2c**. This perfectly matches the mechanical results reported before, as the sample with 20 wt.% DET was the optimal one in terms of plasticization, with an elongation at break of more than 500%. Nonetheless, the rest of the samples also showed great elongation at

break, which is also reflected in the morphologies herein presented. In spite of the fact that PLA reached its saturation point related to diethyl L-tartrate, no phase separation was observed in the FESEM images, which is in accordance with the calculated solubility parameters that showed good miscibility between PLA and DET. A very similar result was observed by Ivorra-Martinez *et al.* [31] in plasticized PLA blends with dibutyl itaconate (DBI).

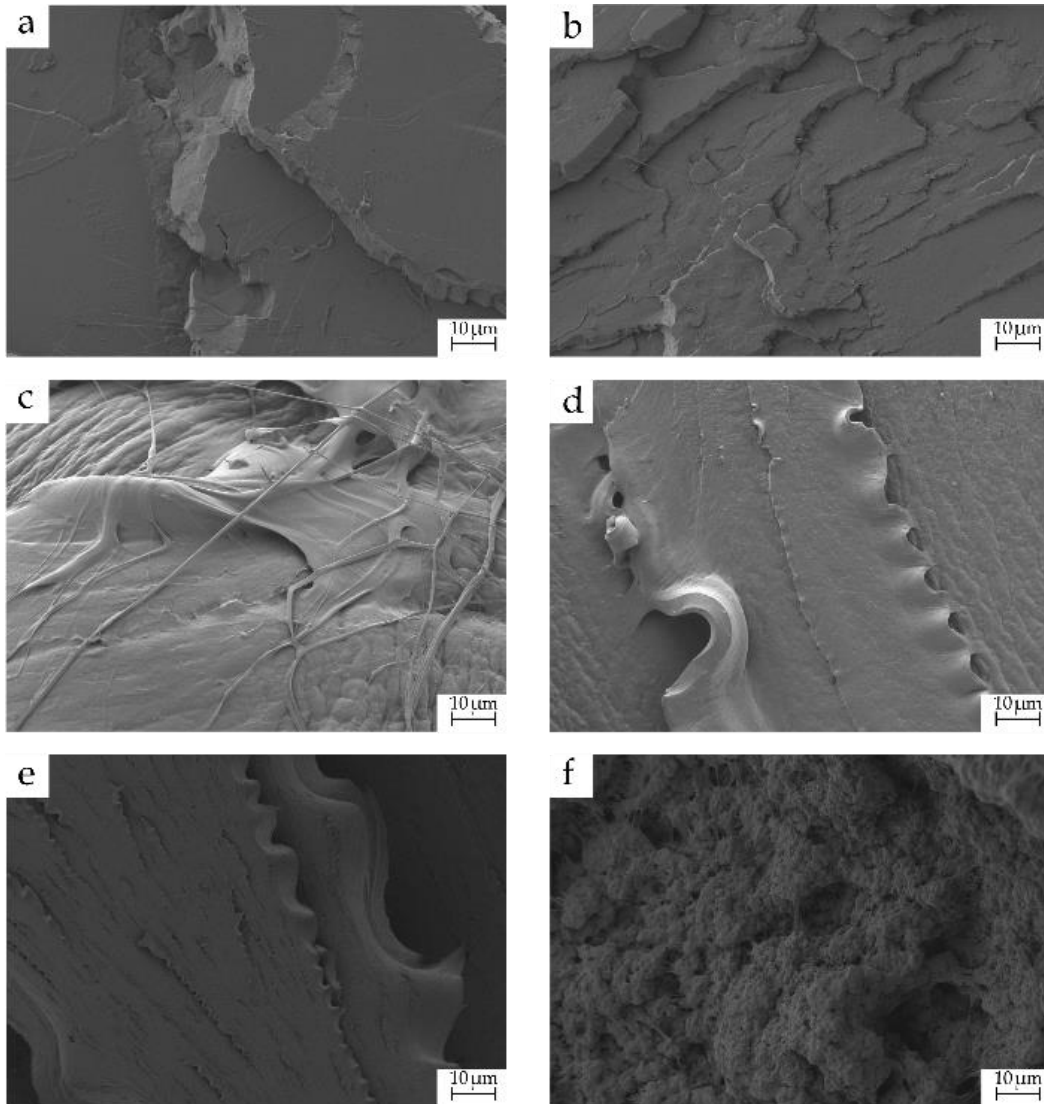


Figure III.2.1.2. Field emission scanning electron microscopy (FESEM) images at 500× of the fractured surfaces of: a) neat PLA; b) PLA/10DET; c) PLA/20DET; d) PLA/30DET; e) PLA/40DET; f) PLA/50DET.

Thermal characterization

Figure III.2.1.3 and **Figure III.2.1.4** show the DSC thermograms for the first heating cycle and the cooling cycle of the PLA/DET samples, respectively, while **Table III.2.1.4** gathers the most important thermal parameters regarding those thermograms. It can be seen that the glass transition temperature of PLA in the first heating cycle is 64.2 °C, which is a typical value for this rigid polymer [32]. When 10 wt.% DET is added to PLA, the glass transition is reduced down to 47.9 °C, which is ascribed to an enhanced chain mobility exerted by the plasticizer [32]. The glass transition cannot be observed in the rest of the samples because the test was done from 30 °C to 200 °C, and higher proportion of plasticizer lead to glass transition temperatures very close to 40 °C, which disables its proper analysis in these thermograms. The cold crystallization temperature (T_{cc}) of PLA is about 98 °C, which is decreased down to values of 81 °C when 10 wt.% DET is added to it. This peak appears due to a rapid cooling after the injection process, which disables the crystalline phase of PLA to properly crystallize. The rest of the samples do not present this peak because they were analyzed from pelletized blends after the extrusion process, which implies a slow cooling, that allows the crystalline phase to form adequately [33]. This thermal transition will be better discussed in the second heating cycle, as the first cycle is made with the objective of removing all the thermal memory of the material. On the other hand, the melting temperature of PLA is located at 175 °C, and it can be observed how the plasticizer progressively decreases it down to a value of 150 °C for the sample with 50 wt.% of DET. This phenomenon was also observed by Ivorra-Martinez *et al.* [31] in PLA plasticized with dibutyl itaconate. The crystallinity degree is also increased from a value of 33% for neat PLA to values of 57 and 67% for the samples with 40 and 50 wt.% of DET, respectively. This fact is ascribed to a promotion of crystallization induced by the presence of the plasticizer, altogether to the thermal cycle, as the samples herein presented are not analyzed under the same conditions, while the first two samples have suffered a rapid cooling, the other four have undergone a slow cooling rate. Finally, the crystallization temperature (T_c) during cooling is a thermal transition that occurs very slowly, as it is demonstrated by the very wide temperature range of the peak of this transition. This allows to study all the samples in the same conditions in the second heating cycle, as all of the materials pass through the same cooling rate. The crystallization temperature of PLA is about 62 °C, which is quite lower than the melting temperature. Nonetheless this is ascribed to the phenomenon previously mentioned, which makes this transition to occur between 100 and 50 °C, approximately. A similar phenomenon happens in the plasticized samples.

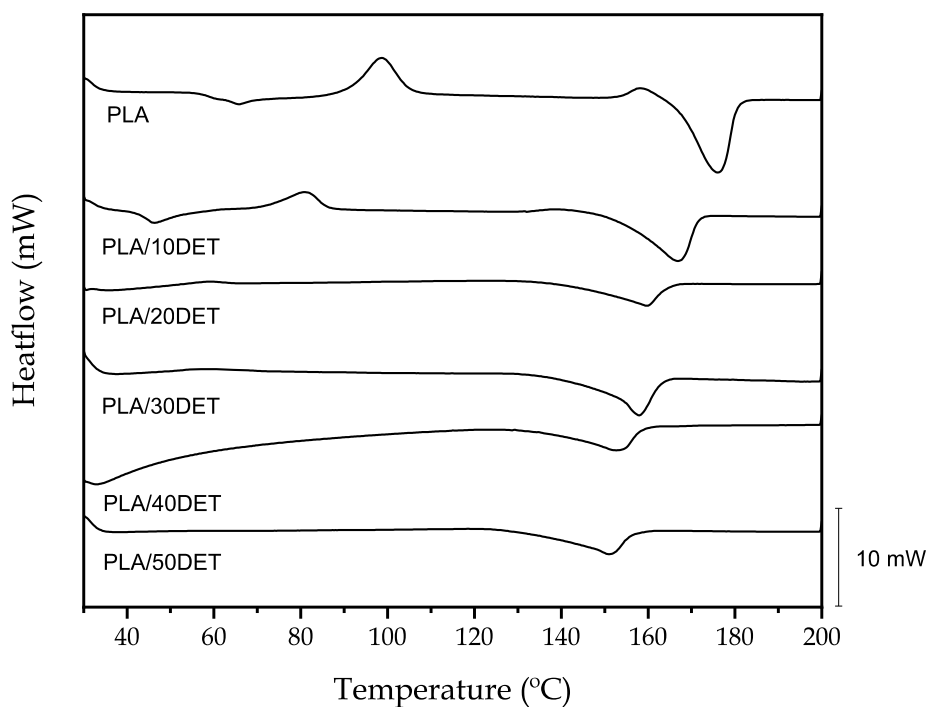


Figure III.2.1.3. Differential scanning calorimetry (DSC) thermograms of the first heating cycle of the plasticized PLA/DET blends.

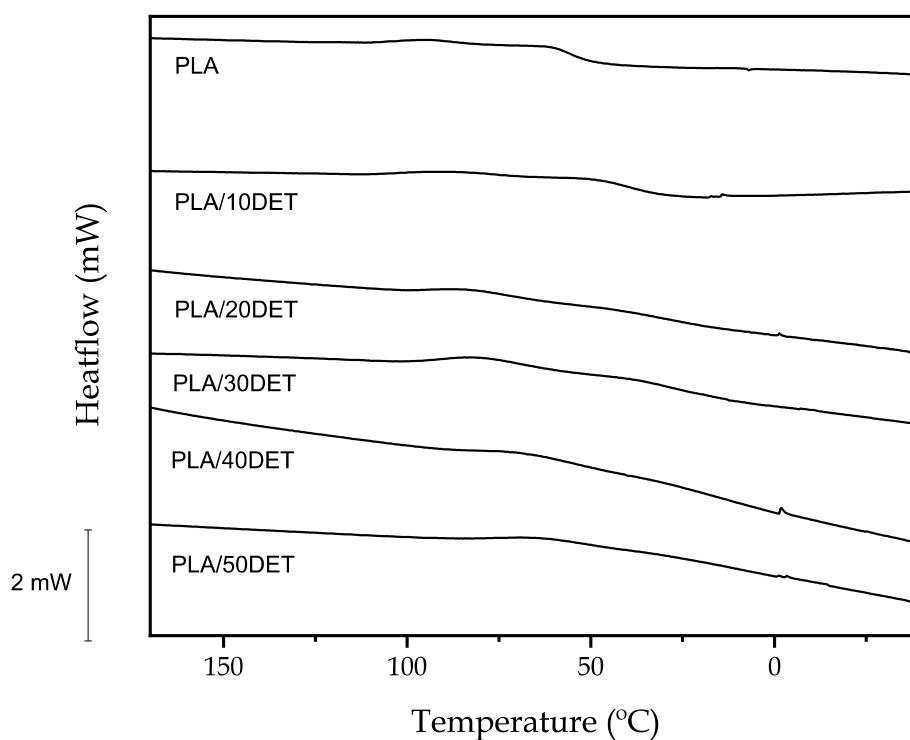


Figure III.2.1.4. Differential scanning calorimetry (DSC) thermograms of the cooling cycle of the plasticized PLA/DET blends.

Table III.2.1.4. Main thermal parameters extracted from the DSC thermograms of the first heating cycle and the cooling cycle of the poly(lactide) (PLA) – diethyl L-tartrate (DET) blends.

Code	T_g (°C)	T_{cc} (°C)	ΔH_{cc} (J/g)	T_m (°C)	ΔH_m (J/g)	χ_c (%)	T_c (°C)
PLA	64.2 ± 0.8	98.7 ± 3.1	25.5 ± 0.3	175.5 ± 2.1	56.7 ± 0.3	33.5 ± 0.2	62.1 ± 0.9*
PLA/10DET	47.9 ± 1.1	81.0 ± 3.2	11.1 ± 0.2	166.5 ± 3.4	44.9 ± 1.6	40.4 ± 1.1	51.2 ± 2.3*
PLA/20DET	-	-	-	159.5 ± 1.6	21.4 ± 0.9	23.0 ± 1.6	81.9 ± 2.1*
PLA/30DET	-	-	-	157.5 ± 2.3	35.1 ± 0.7	37.7 ± 1.5	80.1 ± 1.9*
PLA/40DET	-	-	-	152.7 ± 3.2	32.0 ± 1.2	57.3 ± 2.7	67.9 ± 4.7*
PLA/50DET	-	-	-	150.8 ± 2.9	31.5 ± 0.2	67.7 ± 3.4	61.1 ± 2.5*

*The crystallization temperature occurs in quite a wide range, the value shown in the table is the peak value of the crystallization band.

Figure III.2.1.5 shows the DSC thermograms of the second heating cycle of PLA/DET blends, while **Table III.2.1.5** gathers the main thermal parameters related to the aforementioned thermograms. Neat PLA presents a glass transition temperature of 61.4 °C, which is a typical value for this polymer [34], being indicative of quite a brittle material at room temperature. As it was expected, the incorporation of the plasticizer drastically decreased the glass transition temperature. The higher the DET proportion in the blend, the lower the glass transition temperature. This is ascribed to the plasticization effect of DET, which increases the mobility of the PLA polymeric chains [31]. Considering that the glass transition is related to the mobility of the amorphous phase of the polymer, this result was predictable, achieving a value of 23 °C for the sample with 50 wt.% of DET. The PLA used in this study is a semicrystalline polymer, as it can be deduced from the cold crystallization temperature peak, which appears at 103.6 °C. The incorporation of DET also favors crystallization, as it can be observed by the cold crystallization peaks in the PLA/DET samples. Addition of DET moves the cold crystallization peak down to values around 85 °C. This fact is also related to the enhanced chain mobility exerted by DET, which favors the rearrangement, promoting crystal formation. Choin *et al.* [35] observed a similar effect in PLA plasticized with polyethylene glycol monoacrylate (PEGA), reporting a cold crystallization peak of 85.2 °C, which is indeed very similar to the one observed in this study. Regarding the melting temperature, a notable decrease in this thermal transition is also observed for the plasticized blends. Neat PLA presents a melting temperature of 173.7 °C, whereas the sample plasticized with 50 wt.% of DET exhibits the lowest value, which is 152 °C. Finally, it can be observed that the crystallinity proportion of PLA increases with the content of DET, going from a crystallinity degree of 45.4% for neat PLA to 60.6% for

PLA/50DET. These results are in accordance with those observed by Ivorra-Martinez *et al.* [31], who reported an increase in the crystallinity of PLA after introducing dibutyl itaconate (DBI) plasticizer on its structure. This is ascribed to the fact that DET promotes the formation of crystal growth nuclei from where the crystallization process is catalyzed.

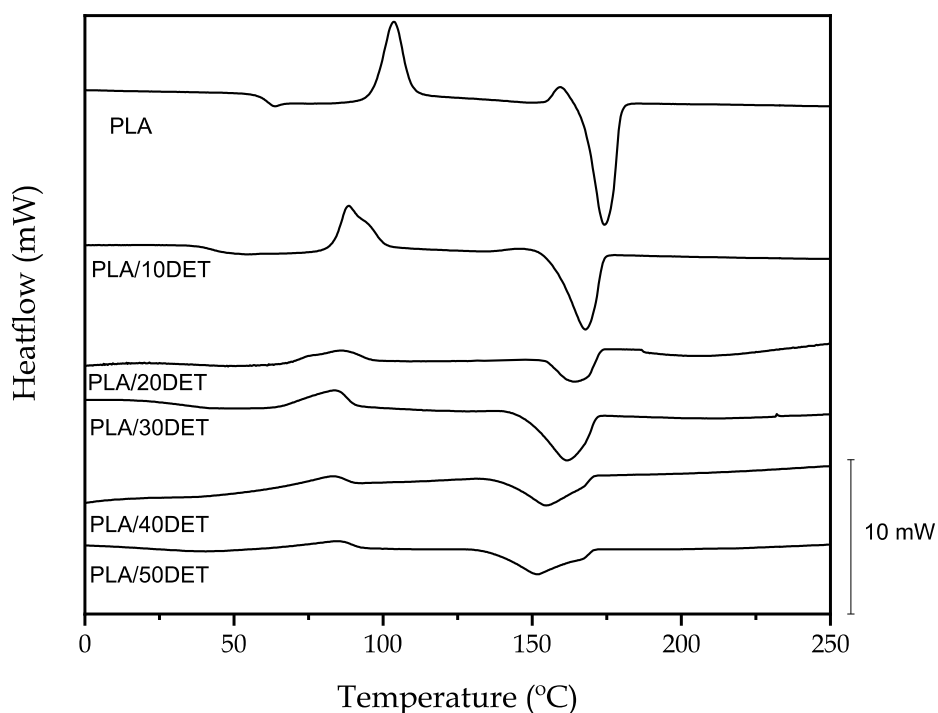


Figure III.2.1.5. Differential scanning calorimetry (DSC) thermograms of the second heating cycle of the plasticized PLA/DET blends.

Table III.2.1.5. Main thermal parameters extracted from the DSC thermograms of the poly(lactide) (PLA) - diethyl L-tartrate (DET) blends.

Code	T_g (°C)	T_{cc} (°C)	ΔH_{cc} (J/g)	T_m (°C)	ΔH_m (J/g)	χ_c (%)
PLA	61.4 ± 1.2	103.6 ± 3.5	29.2 ± 0.1	173.7 ± 3.5	42.6 ± 0.1	45.5 ± 0.5
PLA/10DET	42.6 ± 1.5	88.5 ± 4.1	22.9 ± 0.4	167.5 ± 4.1	36.8 ± 1.2	43.6 ± 0.2
PLA/20DET	39.4 ± 2.1	87.0 ± 3.6	17.6 ± 1.1	166.0 ± 3.6	34.3 ± 1.7	45.9 ± 0.1
PLA/30DET	37.1 ± 1.7	83.6 ± 2.7	13.4 ± 0.5	161.2 ± 2.7	33.3 ± 1.2	50.9 ± 0.3
PLA/40DET	38.2 ± 1.7	85.2 ± 1.7	13.0 ± 0.5	163.1 ± 1.7	29.7 ± 0.5	52.9 ± 0.5
PLA/50DET	23.0 ± 1.7	85.3 ± 1.7	12.0 ± 0.5	152.0 ± 1.7	28.4 ± 0.5	60.6 ± 0.5

The thermal degradation of PLA/DET blends was also analyzed by means of thermogravimetric analysis (TGA). **Figure III.2.1.6** shows the evolution of the mass of all samples with the temperature and the first derivative (DTG), while **Table III.2.1.6** gathers the main thermal parameters that can be extracted from both thermograms. First, neat PLA shows the typical single-stage degradation profile of this polymer, as it is also observed in other studies [36].

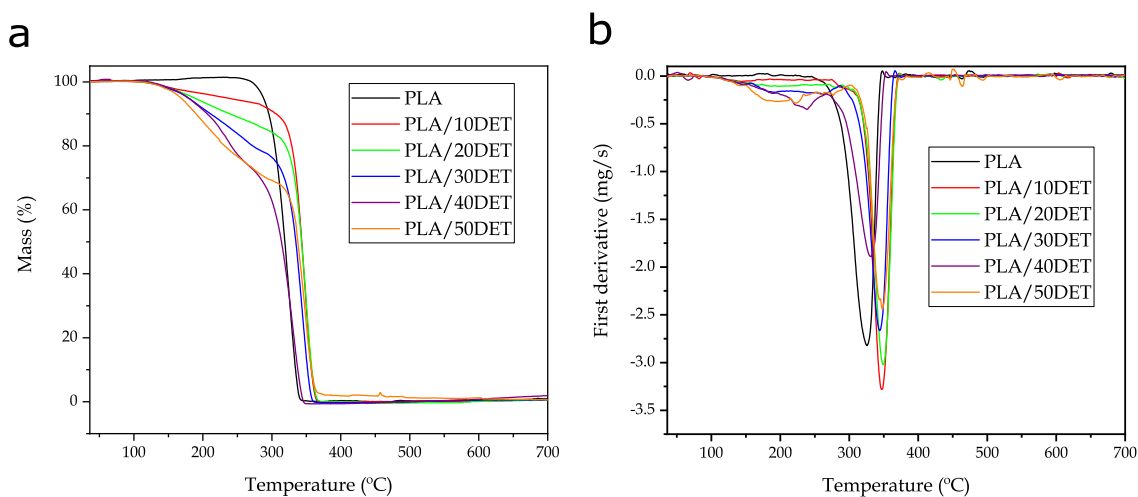


Figure III.2.1.6. Thermal decomposition of poly(lactide) (PLA)-diethyl L-tartrate (DET) blends
a) Thermogravimetric (TG); b) First derivative (DTG).

The onset degradation temperature (temperature at which the polymer has lost 5% of its mass) of PLA stands at 287.6 °C and its maximum degradation rate temperature is 324.6 °C. The incorporation of the plasticizer into the polymer matrix clearly decreases the thermal stability of the blend in the temperature range between 200 °C and 300 °C. This fact is clearly demonstrated by the low onset degradation temperatures for the PLA/DET samples. As expected, the higher the DET proportion in the blend, the lower the onset degradation temperature and the faster the blend degrades, reaching values of 166.1 °C for the PLA/50DET blend. Diethyl L-tartrate has a boiling point of 280 °C, but its low molecular weight allows plasticizer removal at lower temperatures than PLA. This high boiling point of DET prevents from plasticizer removal during processing. On the other hand, the maximum degradation rate temperature for the plasticized samples does not vary a lot from neat PLA, showing values between 335 and 350 °C. This is probably due to the fact that the plasticizer has already been volatilized in this temperature range due to its low molecular weight. Finally, the residual mass in all the samples is practically zero, with no ash formation.

Table III.2.1.6. Thermal parameters related to the thermal degradation of poly(lactide) (PLA)-diethyl L-tartrate (DET) blends extracted from the TGA analysis.

Code	$T_{5\%}$ (%)	T_{deg} (°C)	Residual mass (%)
PLA	287.6 ± 2.5	324.6 ± 3.1	0.2 ± 0.1
PLA/10DET	229.1 ± 1.8	349.1 ± 1.3	0.1 ± 0.1
PLA/20DET	184.6 ± 2.1	349.1 ± 2.9	0.2 ± 0.1
PLA/30DET	177.6 ± 1.9	345.6 ± 1.2	0.1 ± 0.1
PLA/40DET	178.3 ± 1.9	331.8 ± 1.2	0.1 ± 0.1
PLA/50DET	166.1 ± 1.9	335.6 ± 1.2	0.2 ± 0.1

Dynamic-mechanical thermal analysis.

Figure III.2.1.7 shows the storage modulus (E') and the dynamic damping factor ($\tan \delta$) variation with temperature for the PLA/DET blends, while Table III.2.1.7 gathers the main thermal parameters related to this characterization.

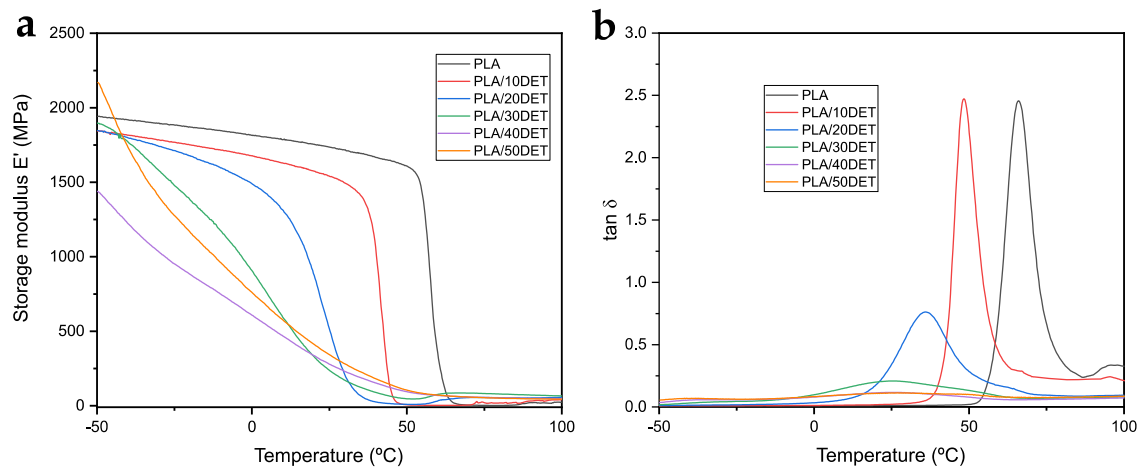


Figure III.2.1.7. Dynamic mechanical thermal analysis of poly(lactide) (PLA)-diethyl L-tartrate (DET) blends: a) storage modulus *vs* temperature; b) dynamic damping factor *vs* temperature.

Neat PLA shows its typical storage modulus decrease, which comes as a result of an α -relaxation process, attributed to the glass transition temperature. The glass transition is located in the sudden decrease of the storage modulus from values around 1940 MPa at -50 °C, to values around 3 MPa at 75 °C. The dynamic damping factor better indicates the position of the glass transition temperature, indicated by a peak maximum. In this case, the glass transition temperature of neat PLA is about 67 °C, which is a similar value to the one observed in DSC and very similar to the one observed by Ivorra-

Martinez *et al.* [31]. The incorporation of DET drastically decreases the glass transition temperature down to values of 24 °C and 26 °C for the samples with the highest DET content. The plot of the storage modulus also shows a drastic decrease in E' , which occurs long before the sudden decrease in neat PLA. This is another indicative of a highly lower glass transition temperature. This fact is related to an increased mobility of the polymeric chains as a result of the plasticizing effect. Interestingly, the higher the composition of the plasticizer, the wider the $\tan \delta$ peak. This effect is especially noticeable in samples with 30 wt.% DET and above. This phenomenon implies that the polymer can show ductile properties even at temperatures below the glass transition, due to this transition occurring at a broader temperature range. This interesting phenomenon was also observed by Quiles-Carrillo *et al.* [37] in PLA formulations plasticized with acrylated epoxidized soybean oil (AESO).

Table III.2.1.7. Thermal parameters related to the thermal degradation of the PLA/DET blends extracted from the DMTA analysis.

Code	E' at -50 °C (MPa)	E' at 75 °C (MPa)	T_g (°C)
PLA	1942.0 ± 33.8	2.6 ± 0.9	67.0 ± 0.2
PLA/10DET	1842.4 ± 29.8	20.7 ± 1.2	48.1 ± 0.1
PLA/20DET	1848.1 ± 27.0	55.4 ± 3.8	36.3 ± 0.9
PLA/30DET	1897.5 ± 30.7	82.1 ± 2.4	24.6 ± 0.7
PLA/40DET	1439.6 ± 28.0	56.0 ± 1.2	24.1 ± 0.1
PLA/50DET	2170.0 ± 36.1	54.3 ± 1.2	26.0 ± 0.2

Chemical interactions in poly(lactide) (PLA)-diethyl L-tartrate (DET) blends

Figure III.2.1.8 shows the FTIR spectra of PLA and all the PLA/DET blends. Neat PLA presents the typical spectra of this polymer. The main absorption bands of PLA are observed at 1750 and 1180 cm^{-1} , which are ascribed to C=O stretching bonds and the C-O-C stretching of PLA, respectively [38]. The band at 1452 cm^{-1} is related to C-H bonding in lactic acid fractions, while the low intensity peak located at 3000 cm^{-1} is due to the antisymmetric and symmetric stretching vibrations of CH_2 [39]. These peaks are present in all the samples, as PLA is the main component of all the blends. The incorporation of diethyl L-tartrate into the poly(lactide) polymeric matrix does not change the spectra of PLA in a great measure. Nonetheless, some slight changes can be appreciated. A low intensity band appears at 3450 cm^{-1} , especially in the sample with 50 wt.% of DET, which is ascribed to the presence of hydrogen bonding between PLA and DET [40]. Additionally, the peak at 1180 cm^{-1} seems to decrease in intensity when DET is added

into the blend. Considering that this peak is ascribed to the ester group, it could be related to certain chemical interaction between PLA and DET that reduces the availability of ester groups in the blends, as a result of their good miscibility, as it was predicted in the theoretical solubility analysis.

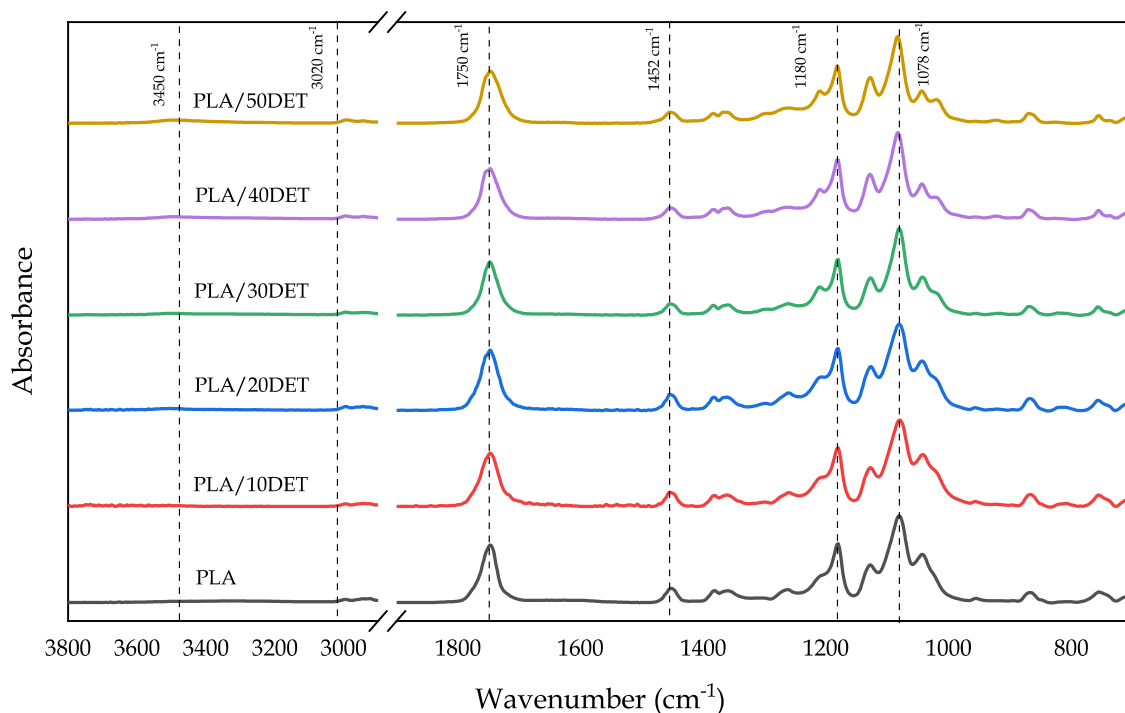


Figure III.2.1.8. FTIR spectra of the poly(lactide) (PLA)-diethyl L-tartrate (DET) blends.

Biodegradability of poly(lactide) (PLA)-diethyl L-tartrate (DET) blends

Figure III.2.1.9 shows the evolution of the weight loss of PLA/DET samples under controlled compost soil over time, while **Figure III.2.1.10** gathers the visual appearance of the disintegration process of the materials. 90% of disintegration is considered as the disintegration goal for considering the samples as biodegradable. It can clearly be seen that all samples are completely biodegradable, as they lose the 100% of their mass after 49 days.

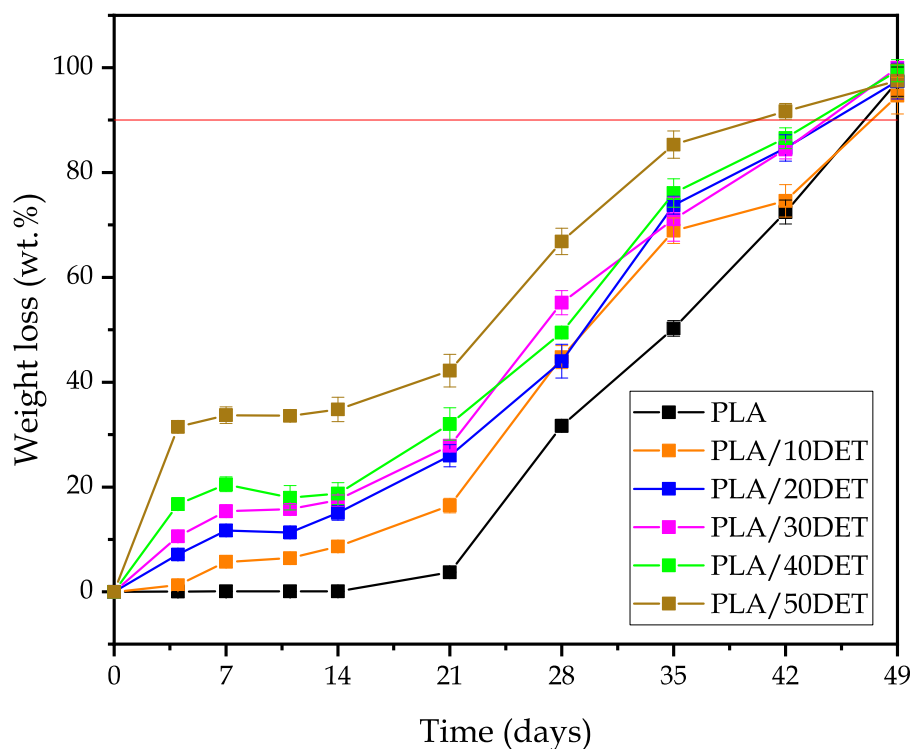


Figure III.2.1.9. Disintegration process of poly(lactide) (PLA)-diethyl L-tartrate (DET) blends under controlled compost soil conditions.

However, the disintegration rate changes with the plasticizer amount in the blend. The greater the amount of plasticizer in the blend, the faster the disintegration rate is. This fact is clearly reflected in **Figure III.2.1.9**, where the sample with 50 wt.% of DET achieves 90% of disintegration between 35 and 42 days, while the rest of the samples achieve 90% of disintegration between 42 and 49 days. Nonetheless, plasticized samples disintegrate faster than neat PLA, as it is indicated by the graphs. This fact is ascribed to the hydrophilic nature of the plasticizer, which promotes hydrolysis in the polymer chains, resulting in the formation of small molecules that are easier for the microorganisms to attack, thus accelerating the disintegrating rate [41]. This can be corroborated in **Figure III.2.1.10**, where it can be seen that at day 49 all samples are drastically disintegrated. Additionally, from day 14 to day 21 there is a drastic increase in weight loss, which is both seen in **Figure III.2.1.9**, indicated by a sudden increase of weight loss in the graph, and in **Figure III.2.1.10**, where day 28 is the first measurement in which the disintegration of the samples is clearly visible.

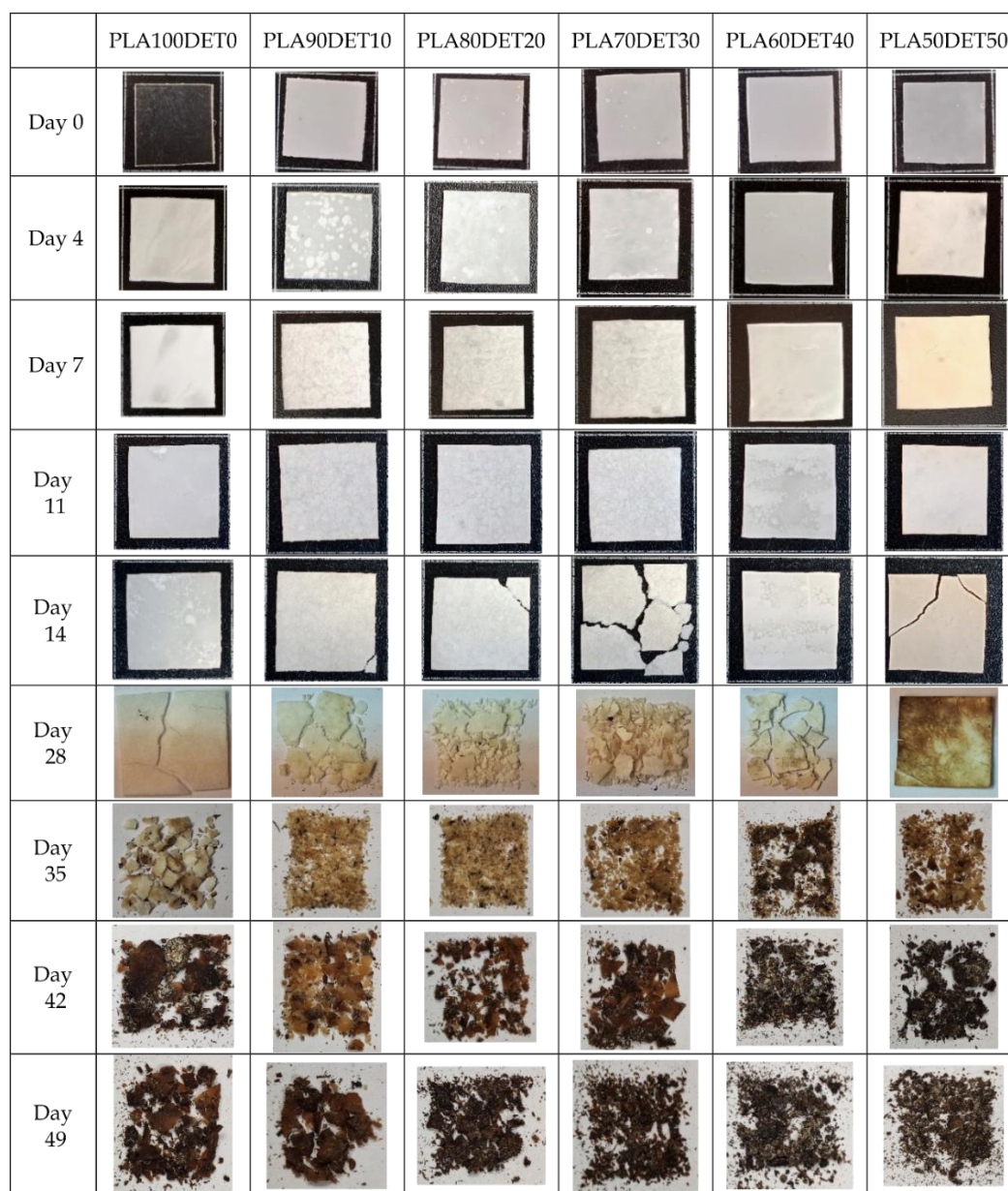


Figure III.2.1.10. Visual evolution of the biodegradation process of poly(lactide) (PLA)-diethyl L-tartrate (DET) blends.

CONCLUSIONS

The work herein presented reports on the effective development of environmentally friendly plasticized poly(lactide) (PLA) blends with different contents of diethyl L-tartrate (DET). The developed blends have proved to possess an excellent ductility as a result of the plasticizing effect exerted by DET, reporting elongation at break values of nearly 600% for the sample with 20 wt.% of DET, which was the optimal PLA/DET composition. These results are quite impressive considering the extreme brittleness of PLA. FESEM images supported the mechanical findings, as typical

plasticized morphologies were observed for all the plasticized samples. Furthermore, a theoretical solubility study demonstrated that PLA and DET show good miscibility and possess good compatibility. Regarding thermal properties, the glass transition temperature of PLA was drastically decreased from values of 63 °C down to values close to 40 °C, which implies a great enhancement in processability. Additionally, the melting temperature was also reduced down to 152 °C for the sample with 50 wt.% of DET as a result of its plasticizing effect, which increases the mobility of polymeric PLA chains. The thermogravimetric analysis of the samples illustrated the high volatility of DET, which made the PLA/DET blends less thermally stable than neat PLA, as the plasticizer starts to volatilize in the above 200-220 °C. FTIR spectra suggested that there were certain chemical interactions between PLA and DET, as the characteristic band for the ester group decreased in intensity. Finally, the herein presented blends proved to be completely biodegradable, as it was demonstrated by disintegration test under controlled compost soil conditions. All blends achieved a 90% of disintegration, which is the disintegration goal, at 49 days of incubation time. Moreover, it was observed that DET accelerated the disintegration rate of PLA. This makes for an enhancement in the environmentally friendly potential of these composites.

ACKNOWLEDGEMENTS

This research is a part of the grant PID2020-116496RB-C22 funded by MCIN/AEI/10.13039/501100011033. Authors also thank Generalitat Valenciana-GVA, grant number AICO/2021/025 and CIGE/2021/094 for supporting this work. J. Gomez-Caturla wants to thank Generalitat Valenciana-GVA, for his FPI grant (ACIF/2021/185) and grant FPU20/01732 funded by MCIN/AEI/ 10.13039/501100011033 and by ESF Investing in your future. J. Ivorra-Martinez wants to thank FPU19/01759 grant funded by MCIN/AEI/ 10.13039/501100011033 and by ESF Investing in your future. V. Moreno wants to thank Generalitat Valenciana - GVA for funding a postdoc position through the APOSTD program co-funded by ESF Investing in your future, grant number CIAPOS/2021/67. Microscopy Services at UPV are also acknowledged by their help in collecting and analyzing images.

DATA AVAILABILITY STATEMENT

The raw/processed data required to reproduce these findings cannot be shared at this time due to technical or time limitations.

REFERENCES

- [1] Singhvi, M., S. Zinjarde, and D. Gokhale, *Poly(lactic acid): synthesis and biomedical applications*. Journal of applied microbiology, 2019. 127(6): 1612-1626.
- [2] Auras, R., B. Harte, and S. Selke, *An overview of polylactides as packaging materials*. Macromolecular bioscience, 2004. 4(9): 835-864.
- [3] Hufenus, R., et al., *Melt-spun fibers for textile applications*. Materials, 2020. 13(19): 4298.
- [4] Atreya, M., et al., *Poly (lactic acid)-based ink for biodegradable printed electronics with conductivity enhanced through solvent aging*. ACS applied materials & interfaces, 2020. 12(20): 23494-23501.
- [5] Notta-Cuvier, D., et al., *Tailoring polylactide (PLA) properties for automotive applications: Effect of addition of designed additives on main mechanical properties*. Polymer Testing, 2014. 36: 1-9.
- [6] Bergström, J.S. and D. Hayman, *An overview of mechanical properties and material modeling of polylactide (PLA) for medical applications*. Annals of biomedical engineering, 2016. 44(2): 330-340.
- [7] Liu, Z., et al., *A critical review of fused deposition modeling 3D printing technology in manufacturing polylactic acid parts*. The International Journal of Advanced Manufacturing Technology, 2019. 102(9): 2877-2889.
- [8] Mehrpouya, M., et al., *4D printing of shape memory polylactic acid (PLA)*. Polymer, 2021. 230: 124080.
- [9] Zafar, R., W. Lee, and S.-Y. Kwak, *A facile strategy for enhancing tensile toughness of poly (lactic acid)(PLA) by blending of a cellulose bio-toughener bearing a highly branched polycaprolactone*. European Polymer Journal, 2022. 175: 111376.
- [10] Niaounakis, M., *Recycling of biopolymers—the patent perspective*. European Polymer Journal, 2019. 114: 464-475.
- [11] Aversa, C., et al., *Compatibilization strategies and analysis of morphological features of Poly (Butylene Adipate-Co-Terephthalate)(PBAT)/Poly (Lactic Acid) PLA blends: a state-of-art review*. European Polymer Journal, 2022. 173: 111304.
- [12] Wang, Y., et al., *Improved fracture toughness and ductility of PLA composites by incorporating a small amount of surface-modified helical carbon nanotubes*. Composites Part B: Engineering, 2019. 162: 54-61.

- [13] Dominguez-Candela, I., *et al.*, *Novel compatibilizers and plasticizers developed from epoxidized and maleinized chia oil in composites based on PLA and chia seed flour*. *European Polymer Journal*, 2022. 173: 111289.
- [14] Shirai, M.A., *et al.*, *Adipate and citrate esters as plasticizers for poly (lactic acid)/thermoplastic starch sheets*. *Journal of Polymers and the Environment*, 2015. 23: 54-61.
- [15] Tsou, C.-H., *et al.*, *Preparation and characterization of poly (lactic acid) with adipate ester added as a plasticizer*. *Polymers and Polymer Composites*, 2018. 26(8-9): 446-453.
- [16] Gzyra-Jagiela, K., *et al.*, *Modification of Poly (lactic acid) by the Plasticization for Application in the Packaging Industry*. *Polymers*, 2021. 13(21): 3651.
- [17] Burgos, N., V.P. Martino, and A. Jiménez, *Characterization and ageing study of poly (lactic acid) films plasticized with oligomeric lactic acid*. *Polymer degradation and stability*, 2013. 98(2): 651-658.
- [18] Zych, A., *et al.*, *Super tough polylactic acid plasticized with epoxidized soybean oil methyl ester for flexible food packaging*. *ACS Applied Polymer Materials*, 2021. 3(10): 5087-5095.
- [19] Carbonell-Verdu, A., *et al.*, *Plasticization effect of epoxidized cottonseed oil (ECSO) on poly (lactic acid)*. *Industrial Crops and Products*, 2017. 104: 278-286.
- [20] Kladnickova, I., T. Klein, and M. Dittrich, *Effect of plasticizers of the triester glycerol type on the release of albumin from biodegradable polymer matrices*. *CESKA A SLOVENSKA FARMACIE*, 2004. 53(1): 27-30.
- [21] Maiza, M., M.T. Benaniba, and V. Massardier-Nageotte, *Plasticizing effects of citrate esters on properties of poly (lactic acid)*. *Journal of Polymer Engineering*, 2016. 36(4): 371-380.
- [22] Kuang, T., *et al.*, *A Simple, Low-Cost, and Green Method for Preparing Strong, Tough, and Ductile Poly (lactic acid) Materials with Good Transparency and Heat Resistance*. *ACS Sustainable Chemistry & Engineering*, 2022. 10(49): 16389-16398.
- [23] Kuang, T., *et al.*, *External flow-induced highly oriented and dense nanohybrid shish-kebabs: A strategy for achieving high performance in poly (lactic acid) composites*. *Composites Communications*, 2022. 29: 101042.
- [24] Ljungberg, N. and B. Wesslén, *Preparation and properties of plasticized poly (lactic acid) films*. *Biomacromolecules*, 2005. 6(3): 1789-1796.

- [25] Courgneau, C., *et al.*, *Analysis of the structure-properties relationships of different multiphase systems based on plasticized poly (lactic acid)*. *Journal of Polymers and the Environment*, 2011. 19(2): 362-371.
- [26] Zawada, K., *et al.*, *Esters of tartaric acid, a new class of potential "double green" plasticizers*. *ACS Sustainable Chemistry & Engineering*, 2017. 5(7): 5999-6007.
- [27] Van Krevelen, D.W. and K. Te Nijenhuis, *Properties of polymers: their correlation with chemical structure; their numerical estimation and prediction from additive group contributions*. 2009: Elsevier.
- [28] Auras, R.A., *et al.*, *Poly (lactic acid): synthesis, structures, properties, processing, and applications*. 2011: John Wiley & Sons.
- [29] Cailloux, J., *et al.*, *Effect of the viscosity ratio on the PLA/PA10. 10 bioblends morphology and mechanical properties*. *Express polymer letters*, 2018. 12(6): 569-582.
- [30] Mascia, L., *et al.*, *Antiplasticization of polymer materials: Structural aspects and effects on mechanical and diffusion-controlled properties*. *Polymers*, 2020. 12(4): 769.
- [31] Ivorra-Martinez, J., *et al.*, *The Potential of an Itaconic Acid Diester as Environmentally Friendly Plasticizer for Injection-Moulded Polylactide Parts*. *Macromolecular Materials and Engineering*, 2022. 307(12): 2200360.
- [32] Armentano, I., *et al.*, *Processing and characterization of plasticized PLA/PHB blends for biodegradable multiphase systems*. 2015. 9(7): 583-596.
- [33] Wunderlich, B., *Theory of cold crystallization of high polymers*. *The Journal of Chemical Physics*, 1958. 29(6): 1395-1404.
- [34] da Silva, J.M.F. and B.G. Soares, *Epoxidized cardanol-based prepolymer as promising biobased compatibilizing agent for PLA/PBAT blends*. *Polymer Testing*, 2021. 93: 106889.
- [35] Choi, K.-M., *et al.*, *Properties of poly (ethylene glycol)-grafted poly (lactic acid) plasticized with poly (ethylene glycol)*. *Macromolecular Research*, 2014. 22(12): 1312-1319.
- [36] Xiang, S., *et al.*, *Evaluation of PLA content in PLA/PBAT blends using TGA*. *Polymer Testing*, 2020. 81: 106211.
- [37] Quiles-Carrillo, L., *et al.*, *On the use of acrylated epoxidized soybean oil as a reactive compatibilizer in injection-molded compostable pieces consisting of polylactide filled with orange peel flour*. *Polymer International*, 2018. 67(10): 1341-1351.

- [38] Yang, S.-l., *et al.*, *Thermal and mechanical properties of chemical crosslinked polylactide (PLA)*. *Polymer Testing*, 2008. 27(8): 957-963.
- [39] Quiles-Carrillo, L., *et al.*, *Compatibilization of highly sustainable polylactide/almond shell flour composites by reactive extrusion with maleinized linseed oil*. *Industrial Crops and Products*, 2018. 111: 878-888.
- [40] Debabhuti, N., *et al.*, *Development of QCM sensor to detect α -terpinyl acetate in cardamom*. *Sensors and Actuators A: Physical*, 2021. 319: 112521.
- [41] Arrieta, M.P., *et al.*, *Disintegrability under composting conditions of plasticized PLA-PHB blends*. *Polymer Degradation and Stability*, 2014. 108: 307-318.

III.2.2. Development of biodegradable PLA composites and tangerine peel flour with improved toughness containing a natural based terpenoid

Jaume Gomez-Caturla^{1*}, Nestor Montanes², Luis Quiles-Carrillo¹, Rafael Balart¹, Franco Dominici², Debora Puglia², Luigi Torre²

¹ Technological Institute of Materials – ITM, Universitat Politècnica de València – UPV, Plaza Ferrándiz y Carbonell 1, 03801 Alcoy (Spain).

² Dipartimento di Ingegneria Civile ed Ambientale, University of Perugia, UdR INSTM, Strada di Pentima, 4 - 05100 Terni (TR) Italy.



Express Polymer Letters

2023, 17(8): 789-805

*Adapted from the original manuscript.

Express Polymer Letters Vol.17, No.8 (2023) 789–805
Available online at www.expresspolymlett.com
<https://doi.org/10.3144/expresspolymlett.2023.59>

express
polymer letters

Research article

Development of biodegradable PLA composites and tangerine peel flour with improved toughness containing a natural-based terpenoid

Jaume Gomez-Caturla^{1*}, Nestor Montanes¹, Luis Quiles-Carrillo¹, Rafael Balart¹, Daniel Garcia-Garcia¹, Franco Dominici², Debora Puglia², Luigi Torre²

¹Technological Institute of Materials (ITM), Universitat Politècnica de València (UPV), Plaza Ferrándiz y Carbonell 1, 03801 Alcoy, Spain

²Dipartimento di Ingegneria Civile ed Ambientale, University of Perugia, UdR INSTM, Strada di Pentima, 4-05100 Terni (TR) Italy

Received 11 February 2023; accepted in revised form 20 April 2023

Abstract. The present work reports on the development of environmentally friendly, completely biodegradable wood plastic composites based on polylactide (PLA) and tangerine peel flour (TPF), plasticized by α -terpinyl acetate (TA). The TPF varied in the 10–30 wt% while the PLA to TA (wt%/wt%) was set to 4 (i.e., 25 wt% TA plasticizer was added with regard to the PLA wt%). The developed composites were processed by extrusion and injection molding. The composites presented excellent elongation at break, achieving values of 300% for the PLA+TA sample. Elongation at break values of 200% for the PLA composite with 10 wt% TPF and plasticized with TA were obtained. Those results were confirmed by the appearance of filament-like structures observed in field emission scanning electron microscopy images. Differential scanning calorimetry and dynamic mechanical thermal analysis revealed a remarkable decrease in the glass transition temperature of PLA as a result of the plasticizing effect of TA. Glass transition was reduced from 63 °C down to 41 °C approximately. This implied an increase in the ductility of the material. The samples with TPF exhibited a dark brown color, making them perfect for wood plastic composite applications. Water contact angle results show that TA and TPF change the wetting properties of the obtained composites. A general decrease in the water contact angle was observed with the addition of TPF and TA. Finally, disintegration tests proved that the developed composites are fully biodegradable. All the samples except for neat PLA achieved 100% disintegration in controlled compost soil conditions after 5 weeks, while neat PLA reached complete disintegration in 6 weeks.

Keywords: polylactide, tangerine peel flour, α -terpinyl acetate, plasticization, wood plastic composites, biodegradable

1. Introduction

In the last decades, the environmental issues provoked by the extended use of petrochemical polymers, such as an increase in the carbon footprint and a great amount of generated waste, have risen social and scientific awareness related to the use of these polymers. Therefore, more environmentally friendly polymers and materials have attracted great attention in this field. One of the most popular examples is the development of wood plastic composites (WPC),

which arise as an alternative to wood-based products [1]. These kinds of materials are based on a thermoplastic polymer matrix, such as polypropylene (PP), polylactide (PLA), or polyethylene (PE), among others, and fillers obtained from the food and agroforestry industry. At first, the most popular fillers were sawdust and wood fibers [2]. However, other alternative fillers have been proposed in the last years, such as lignocellulosic fillers from the food industry, including fruit peels, seeds, and other wastes

*Corresponding author, e-mail: jaugoca@epsa.upv.es
© BME-PT

Development of biodegradable PLA composites and tangerine peel flour with improved toughness containing a natural based terpenoid

Abstract

The present work reports on the development of environmentally friendly, completely biodegradable wood plastic composites based on polylactide (PLA) and tangerine peel flour (TPF), plasticized by α -terpinyl acetate (TA). The TPF varied in the 10-30 wt.% while the PLA to TA (wt.%/wt.%) was set to 4 (*i.e.* 25 wt.% TA plasticizer was added with regard to the PLA wt.%). The developed composites were processed by extrusion and injection moulding. The composites presented excellent elongation at break, achieving values of 300% for the PLA+TA sample. Elongation at break values of 200% for the PLA composite with 10 wt.% TPF and plasticized with TA were obtained. Those results were confirmed by the appearance of filament-like structures observed in field emission scanning electron microscopy (FESEM) images. Differential scanning calorimetry (DSC) and dynamic mechanical thermal analysis (DMTA) revealed a remarkable decrease in the glass transition temperature of PLA as a result of the plasticizing effect of TA. Glass transition was reduced from 63 °C down to 41 °C approximately. This implied an increase in the ductility of the material. The samples with TPF exhibited a dark brown colour, making them perfect for wood plastic composite applications. Water contact angle results shown that TA and TPF change the wetting properties of the obtained composites. A general decrease in the water contact angle was observed by the addition of TPF and TA. Finally, disintegration tests proved that the developed composites are fully biodegradable. All the samples except for neat PLA achieved 100% disintegration in controlled compost soil conditions after 5 weeks, while neat PLA reached complete disintegration in 6 weeks.

Keywords: Polylactide, tangerine peel flour, α -terpinyl acetate, plasticization, wood plastic composites, biodegradable.

INTRODUCTION

In the last decades, the environmental issues provoked by the extended use of petrochemical polymers, such as an increase in the carbon footprint and a great amount of generated wastes, have risen social and scientific awareness related to the use of these polymers. Therefore, more environmentally friendly polymers and materials have attracted great attention in this field. One of the most popular examples is the development of wood plastic composites (WPC), which arise as an alternative for wood-based products [1]. This kind of materials are based on a thermoplastic polymer matrix such as polypropylene (PP), polylactide (PLA) or polyethylene (PE) among others; and fillers obtained from the food and agroforestry industry. At first, the most popular fillers were sawdust and wood fibers [2]. However, other alternative fillers have been proposed in the last years, such as lignocellulosic fillers from the food industry, including fruit peels, seeds and other wastes [3, 4]. These fillers allow to reduce the cost of the material, as they are obtained from wastes and are far cheaper than the neat polymer itself. Depending on the fruit, the amount of by-products ranges from 10 to 60 wt.%, so using those by-products as fillers in polymer technology helps to upgrade them and even provide polymers with additional properties, such as enhanced mechanical resistance, biodegradability, antioxidant activity, antimicrobial properties, or even different colours [5, 6].

Polylactide (PLA) is a biobased biodegradable linear aliphatic polyester. Lactic acid is its main monomer, which is obtained from the fermentation of starch-rich sources (rice, sugarcane, potato, corn, and so on) [7]. This thermoplastic polymer is considered one of the most promising materials in the bioplastics market, with an annual production of 140000 tons [8]. Its most attractive properties being its biodegradability and its renewable origin. However, composites based on this polymer matrix present some limitations in terms of ductility, as PLA itself is a brittle polymer and this brittleness is more pronounced in PLA-lignocellulosic fillers, characterized by a low impact strength and toughness [9]. Despite there are several technical solutions to this drawback, a widely and cost-effective technical solution is the use of plasticizers that increase its ductility. Another methodology is blending PLA with other flexible polymers [10, 11]. The use of biobased plasticizers is becoming especially important and interesting these days, as they are very cost-effective, efficient and help to preserve the environmentally friendly nature of PLA. These plasticizers mainly help to increase the chain mobility of the polymer matrix by increasing the free volume in PLA. Low molecular weight natural plasticizers such as cardanol are preferred due to their high plasticizing effectiveness [12, 13]. Plasticizers are preferred instead of copolymer synthesis due to their ability to

reduce the glass transition temperature of PLA, increasing its toughness and overall ductile properties [14, 15].

Tangerine (*Citrus reticulata*) is one of the most by-product generating crops, being its peel the main waste produced in the tangerine industry. This waste possesses great amounts of cellulose, lignin and hemicellulose, which are essential components for defining a lignocellulosic filler, similar to wood flour fillers [16, 17]. Tangerine peel has a composition of around 4 wt.% essential oils [18, 19], which possess several interesting chemical compounds. These compounds include terpenes and terpenoids, such as D-limonene, β -myrcene, α -pinene, γ -terpinene and linalool [20]. These compounds generally present great antioxidant, antimicrobial and antifungal activities, and have proved to provide some plasticization to PLA.

Some research works have studied the possibility of combining citric waste fillers, such as orange peel flour, into thermoplastic polymers, such as poly(vinyl alcohol) (PVA) [21], or low density polyethylene (LDPE) [22]. Nonetheless, hardly any study has been carried out related to the use of tangerine peel flour as a filler for thermoplastic composites, especially with polylactide. Hejna *et al.* [20] developed wood plastic composites based on high density polyethylene (HDPE) with tangerine peel flour, which gave the polymer enhanced thermal stability, mechanical strength and flowability.

In this study, tangerine peel flour (TPF) is used as a lignocellulosic filler for developing environmentally friendly wood plastic composites based on polylactide (PLA). Considering that tangerine peel has not been extendedly studied in the field of composites, several amounts of tangerine peel flour, ranging from 10 to 30 wt.% (with regard to PLA) have been used in the study. Additionally, α -terpinyl acetate (TA), which is a natural plasticizer originated from citric acid, is utilized in order to reduce the brittleness of PLA and its composites with TPF. TA and tangerine peel are expected to have certain synergy, as TA is derived from citric fruits and it is a monoterpenoid [23]. This fact makes TA to possess great affinity for TPF, as it has terpenes and terpenoids in its composition, as stated before. Therefore, plasticized and unplasticized wood plastic composites have been produced and their properties have been evaluated according to theoretical solubility parameters, tensile tests and fracture surface morphology observation by field emission scanning electron microscopy (FESEM). The main thermal properties of the developed PLA composites were obtained by differential scanning calorimetry (DSC), thermogravimetric analysis (TGA), and dynamic-mechanic-thermal analysis (DMTA). Moreover, the surface appearance and wettability were measured by

colorimetry and water drop goniometry.

MATERIALS AND METHODS

Materials

Bio-based PLA Purapol L130 grade was supplied by Corbion purac (The Netherlands, Amsterdam), with a density of 1.24 g/cm^3 , a melt flow index of 16 g/10 min (at $210 \text{ }^\circ\text{C}/2.16 \text{ kg}$) and a melting temperature of $175 \text{ }^\circ\text{C}$.

Tangerines from the Clemenvilla variety were purchased from the local market in Alcoy, Spain. α -terpinyl acetate (TA) (Product Code: 1003313906) was supplied by Sigma Aldrich. Tangerines were peeled and the peels were first dried at $45 \text{ }^\circ\text{C}$ for 48 h in a dehumidifying stove (MCP Vacuum Casting System, Lubeck, Germany) to remove residual moisture. Then, the peels were milled in a ZM 200 centrifugal mill from Retsch (Düsseldorf, Germany) at a speed of 8,000 rpm and finally sieved with a $300 \text{ }\mu\text{m}$ mesh filter. Thus, tangerine peel flour was obtained (TPF). **Figure III.2.2.1** illustrates the field emission scanning electron microscopy (FESEM) image of TPF, as well as the distribution of the particle size. The average diameter of the particles was $25 \text{ }\mu\text{m}$, approximately, as obtained from FESEM study.

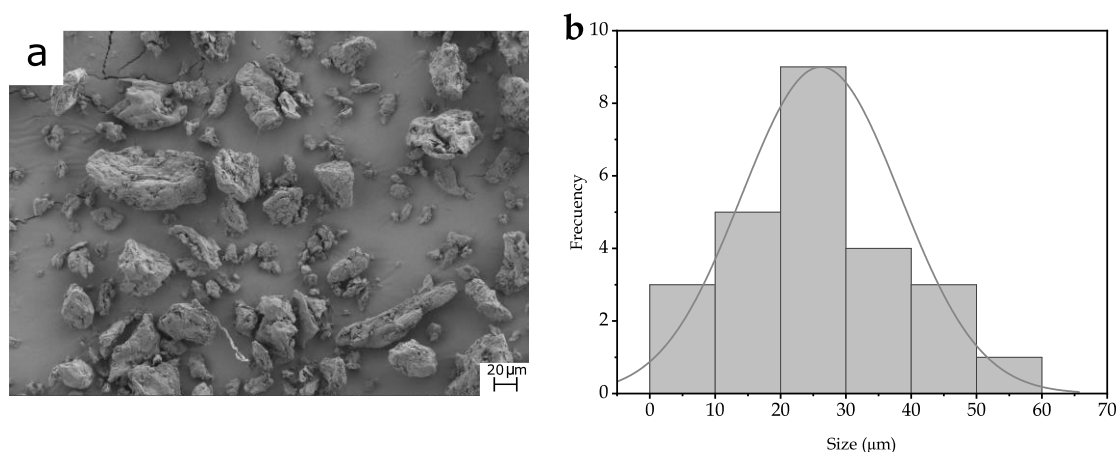


Figure III.2.2.1. Tangerine peel flour morphology (TPF) (a) FESEM image at $250\times$ magnification of TPF (b) Histogram of the particle size of TPF.

Processing of PLA/TPF composites

PLA and TPF were initially dried at $40 \text{ }^\circ\text{C}$ for 48 h in a dehumidifying dryer MDEO to remove any residual moisture prior to processing. Thereafter, corresponding

proportion of each component, including the α -terpinyl acetate plasticizer, were mixed and homogenized. **Table III.2.2.1** shows the composition of each developed formulation, the plasticizer content was kept constant with regard to PLA wt.%. In particular, the wt.% PLA to wt.% plasticizer ratio was 4 for all compositions (*i.e.* 25 wt.% plasticizer was added with regard to the wt.% PLA). The formulations were compounded by an extrusion process in a twin-screw extruder from Construcciones Mecánicas Dupra, S.L. (Alicante, Spain). This extruder has a 25 mm diameter with a length-to-diameter ratio (L/D) of 24. The extrusion process was carried out at a rate of 22 rpm, with a temperature profile from the hopper to the die of 170-175-180-185 °C. The compounded materials were pelletized using an air-knife unit. In all cases, residence time was approximately 1 min.

Table III.2.2.1. Compositions of the developed formulations of PLA/TPF with TA plasticizer.

Code	PLA (wt.%)	TPF (wt.%)	TA (phr)
PLA	100	0	0
PLA+10TPF	90	10	0
PLA+10TPF+22.5TA	90	10	22.5
PLA+20TPF+20TA	80	20	20
PLA+30TPF+17.5TA	70	30	17.5
PLA+20TA	80	0	20*

*This composition means 20 wt.% instead of 20 phr.

Pellets were shaped into standard samples using a Meteor 270/75 injection moulding machine from Mateu & Solé (Barcelona, Spain). The temperature profile in the injection moulding unit was 175 °C (hopper), 180 °C, 185 °C, and 190 °C (injection nozzle). This injection unit was operated with a clamping force of 75 tons. Other processing parameters such as the filling and cooling times were set to 1 and 10 s, respectively. Standard samples for mechanical and thermal characterization with an average thickness of 4 mm were obtained.

Characterization of PLA/TPF composites

Theoretical analysis of the PLA/plasticizer interaction

In the process of plasticization, the solubility of the selected plasticizer into the chosen polymer plays a very important role. In this work, the group-contribution

method developed by Van Krevelen and Hoftyzer was used to calculate the solubility parameter (δ). Its main contributions were also calculated, which are related to the dispersion forces (δ_d), polar forces (δ_p), and hydrogen bonding (δ_h) (see **Equation III.2.2.1**).

$$\delta = \delta_d^2 + \delta_p^2 + \delta_h^2 \quad (\text{III.2.2.1})$$

As proposed by Van Krevelen and Hoftyzer, the three solubility components can be estimated from group contributions as indicated by **Equations III.2.2.2 to III.2.2.4**:

$$\delta_d = \frac{\sum F_{di}}{V} \quad (\text{III.2.2.2})$$

$$\delta_p = \frac{\sqrt{\sum F_{pi}^2}}{V} \quad (\text{III.2.2.3})$$

$$\delta_h = \frac{\sqrt{\sum E_{hi}}}{V} \quad (\text{III.2.2.4})$$

The F-method, based on the molar attraction constants, is quite accurate for predicting the dispersive and polar contributions (δ_d , and δ_p , respectively) as indicated in equation 2 and 3, respectively. However, the F-method cannot be applied to the hydrogen bonding component (δ_h). Hansen concluded that the hydrogen bonding energy (E_{hi}) per structural group can be considered almost constant. Considering the structure and the group contribution proposed by Van Krevelen and Hoftyzer [24], the solubility components are gathered in **Table III.2.2.2** Additionally, **Table III.2.2.2** includes the R_a parameter, which is indicative of the distance existing between the solubility coordinates of the plasticizer in relation to neat PLA. R_a has been calculated according to **Equation III.2.2.5**, where the constant 4 in the first term was obtained from plots of experimental data to define spherical solubility regions rather than spheroidal regions. If R_a (the distance) equals zero, it means that both plasticizer and polymer are thermodynamically similar, which leads to great affinity and a good solubility. As expected, the greater the distance, the lower the solubility. When a certain distance threshold is surpassed, the solubility becomes negligible. This distance is related to the polymer radius (or sphere radius), R_0 , which defines a spherical solubility region of a

polymer. The center of the sphere is defined by the three solubility parameters δ_d , δ_p and δ_h .

$$R_a = \sqrt{4 \cdot (\delta_{d_{plast}} - \delta_{d_{PLA}})^2 + (\delta_{p_{plast}} - \delta_{p_{PLA}})^2 + (\delta_{h_{plast}} - \delta_{h_{PLA}})^2} \quad (\text{III.2.2.5})$$

The relative energy difference (RED) is also calculated, and it is defined as the relation between R_a and the solubility sphere radius of neat PLA, R_0 , which is $10.7 \text{ MPa}^{1/2}$ (Equation III.2.2.6) [25]. The closer the RED value is to zero, the better the miscibility between PLA and the chosen plasticizer. When the RED parameter is close to 1, it means the plasticizer and the polymer are in the threshold of good affinity, whereas RED values greater than 1 indicate a poor affinity between them. Brüster *et al.* [26] reported RED values of 0.93 and 0.99 for limonene and myrcene in PLA-plasticized formulations. Despite the RED values are close to 1, they observed that limonene, with a lower RED value, gave PLA more efficient plasticization than myrcene, which RED value was very close to the solubility borderline.

$$RED = \frac{R_a}{R_0} \quad (\text{III.2.2.6})$$

As it is denoted by the values in **Table III.2.2.2**, α -terpinyl acetate possesses great affinity for PLA, as its RED value is far below 1, thus proving their potential miscibility. This theoretical result will be verified by the results obtained in the experimental section.

Table III.2.2.2. Theoretical approach for the solubility of polylactide (PLA) formulations with α -terpinyl acetate.

Material	δ_d (MPa ^{1/2})	δ_p (MPa ^{1/2})	δ_h (MPa ^{1/2})	δ (MPa ^{1/2})	R_a (MPa ^{1/2})	RED
PLA	15.33	8.44	10.98	20.66	-	
α -terpinyl acetate (TA)	15.34	2.38	5.83	16.58	6.57	0.61

Mechanical characterization

The tensile properties of the PLA/TPF composites were evaluated using a universal testing machine ELIB 50 from S.A.E. Ibertest (Madrid, Spain). The test was conducted following the instructions of ISO 527-1:2012. A 5-kN load cell was used while the cross-head speed was set to 5 mm/min. Tensile test specimens of dimensions 150×10×4 mm³. The Shore D hardness was measured in a 676-D durometer from J. Bot Instruments (Barcelona, Spain), on 80×10×4 mm³ rectangular samples according to ISO 868:2003. Impact strength was studied on 80×10×4 mm³ rectangular samples in a Charpy pendulum (1-J) from Metrotec S.A. (San Sebastián, Spain) on notched samples (V-notch type with a radius of 0.25 mm), following ISO 179-1:2010. A minimum of 5 samples were tested for each material.

Field emission scanning electron microscopy (FESEM)

The surface morphology of the cross section of fractured impact test samples was evaluated by field emission scanning electron microscopy (FESEM) using a ZEISS ULTRA 55 microscope from Oxford Instruments (Abingdon, United Kingdom). The samples were sputtered with a gold-palladium alloy in an EMITECH sputter coating SC7620 model from Quorum Technologies, Ltd. (East Sussex, UK). The microscope was operated with an acceleration voltage of 1.5 kV.

Thermal characterization

The main thermal properties of the PLA/TPF composites were obtained by means of differential scanning calorimetry (DSC) in a DSC 821 from Mettler-Toledo Inc. (Schwerzenbach, Switzerland). Samples weighted about 5–8 mg and they were placed in 40 µl aluminum crucibles. Three thermal steps were applied to the samples: first a heating cycle from 30 °C to 200 °C, then a cooling cycle down to 0 °C and, finally, a second heating stage from 0 °C up to 250 °C. The heating/cooling rate was 10 °C/min and the tests were carried out in a nitrogen atmosphere with a flow rate of 66 mL/min. The glass transition temperature (T_g), the cold crystallization temperature (T_{cc}) and enthalpy (ΔH_{cc}), the melting temperature (T_m) and enthalpy (ΔH_m) were obtained from the second heating stage. Additionally, crystallinity ($\chi_c\%$) was calculated according to **Equation III.2.2.7**:

$$\chi_c (\%) = \left[\frac{|\Delta H_m| - |\Delta H_{cc}|}{|\Delta H_m^0| \cdot (1 - w)} \right] \cdot 100 \quad (\text{III.2.2.7})$$

where ΔH_m^0 is a theoretical value that represents the estimated melt enthalpy of a 100% crystalline PLA polymer, *i.e.* 93.7 J g⁻¹, where 1-w is the PLA weight fraction.

Dynamical mechanical thermal characterization

Dynamical mechanical thermal analysis (DMTA) was carried out in a DMA1 dynamic analyzer from Mettler-Toledo (Schwerzenbach, Switzerland), working in single cantilever flexural conditions. Rectangular samples with dimensions 20×6×2.7 mm³ were subjected to a dynamic temperature sweep from -150 °C to 100 °C at a constant heating rate of 2 °C/min. The selected frequency was 1 Hz, and the amplitude of the cantilever flexural deformation was set to 10 μm.

Visual appearance characterization

The visual appearance of the PLA/TPF composites was assessed by colorimetric analysis, using a colorimeter model KONICA CM-3600d Colorflex-DIFF2 from Hunter Associates Laboratory (Reston, Virginia, USA). Prior to measurements, the instrument was calibrated using a standard white tile and a light trap. Ciel*a*b* colour coordinates were measured and recorded. Measurements were taken in triplicate and averaged.

Water contact angle measurements

The distilled water contact angle in PLA/TPF composites was evaluated in order to assess their hydrophilicity. An Easy drop FM140 goniometer supplied by Krüss equipments (Hamburg, Germany) was used. Distilled water drops were deposited at random in the surface of impact test samples. At least 10 measurements were taken for each material.

Fourier transformed infrared spectroscopy (FTIR)

The chemical interactions present in the PLA/TPF composites were studied through the use of attenuated total reflection-Fourier transformed infrared spectroscopy (ATR-FTIR). Three spectra of each material were recorded by using a Bruker S.A Vector 22 (Madrid, Spain) coupled to a PIKE MIRacle™ single reflection diamond ATR

accessory (Madison, Wisconsin, USA). 20 scans were taken and averaged for each measurement, between 4000 and 500 cm^{-1} with a resolution of 2 cm^{-1} .

Biodegradability

The biodegradability of PLA/TPF composites was evaluated in compost soil conditions at a temperature of 58 °C and a relative humidity of 55% according to ISO 20200. 25×25×1 mm^3 samples were placed in a textile mesh. Then they were buried in a solid synthetic wet soil prepared with 40 wt.% sawdust, 30 wt.% rabbit-feed, 10 wt.% corn starch, 10 wt.% compost, 5 wt.% sugar, 4 wt.% of corn oil, and 1 wt.% of urea. Samples were periodically extracted from the compost and cleaned with distilled water, then they were dried and weighted with an analytical balance model AG245 provided by Mettler-Toledo (Schwerzenbach, Switzerland) with an accuracy of 0.001 g. The percentage of weight loss was calculated using **Equation III.2.2.8**.

$$\text{Weight loss (\%)} = \left(\frac{w_0 - w_t}{w_0} \right) \cdot 100 \quad (\text{III.2.2.8})$$

where w_0 is the initial dry weight of the sample and w_t is the weight of the sample after t burial time. All assays were carried out in triplicate to ensure more accuracy and reliability.

RESULTS AND DISCUSSION

Mechanical properties

Table III.2.2.3 gathers the main mechanical parameters for PLA/TPF composites regarding the tensile test, the shore D hardness test and the Charpy impact test. As it can be seen, neat PLA shows an elastic modulus of 3761 MPa, a tensile strength of 56 MPa and a very low elongation at break of 5.6%. These are typical values of a strong and brittle polymer. Very similar results were reported by Lascano *et al.* [27]. The incorporation of 10 wt.% of TPF provokes a decrease of all tensile parameters, especially reducing the elongation at break of the composite (from 5.6 down to 3.3%). It is possible that TPF is provoking a stress concentration effect as a result of the formation of aggregates that act as stress concentrators [7]. Interestingly, the addition of TA into the PLA+10TPF composite drastically enhances its ductile properties, exhibiting an

elongation at break of 194%, which is an impressive feat considering the extreme brittleness of the PLA+10TPF composite (3.3% elongation at break). On the other hand, a decrease in elastic modulus and tensile strength from 3420 and 37.4 down to 1804 and 11.1 MPa is observed. This proves the plasticizing effect that TA exerts over the composite, which is also a direct indicative of the good miscibility between PLA and TA, as predicted in the theoretical solubility parameter section. It is observed that when the proportion of TPF is increased, elongation at break is clearly decreased, so that for the samples with 20 and 30 wt.% of TPF elongation at break is 156% and 104%, respectively. This is ascribed to the great amount of lignocellulosic particles, which make the formation of stress concentrator aggregates more likely to happen [28]. Nevertheless, the reported values are still very impressive, considering the great amount of lignocellulosic filler contained in the PLA-based composites (30 wt.%). In fact, tensile strength and the elastic modulus decrease with the increase in TPF, probably due to an excessive load of hard organic particles. This effect was also observed by Jorda-Reolid *et al.* [28] in biopolypropylene composites with 30 wt.% of argan shell particles, who observed the formation of argan shell particles aggregates in the composites, which acted as stress concentrators. Finally, the plasticized PLA (PLA+20TA) shows the highest elongation at break registered within these composites (327.6%). This definitely proves the excellent plasticizing effect that TA provides to the PLA matrix, considering that PLA is extremely fragile (5.6% elongation at break), which increases the mobility of the polymer chains and makes them more flexible.

Table III.2.2.3. Summary of the mechanical parameters of the PLA/TPF composites regarding tensile test: tensile modulus (E), tensile strength (σ_{max}) and elongation at break (ϵ_b); Shore D hardness and impact strength.

Code	E (MPa)	σ_{max} (MPa)	ϵ_b (%)	Shore D hardness	Impact strength (kJ/m ²)
PLA	3761 ± 787	56.0 ± 1.9	5.6 ± 0.5	79.8 ± 3.3	1.8 ± 0.2
PLA+10TPF	3420 ± 470	37.4 ± 3.6	3.3 ± 0.5	82.0 ± 1.4	1.8 ± 0.5
PLA+10TPF+22.5TA	1804 ± 328	11.1 ± 1.5	194.4 ± 12.0	71.6 ± 3.8	3.1 ± 0.3
PLA+20TPF+20TA	2159 ± 251	8.4 ± 1.6	156.6 ± 13.6	74.6 ± 2.3	4.3 ± 0.9
PLA+30TPF+17.5TA	1976 ± 375	6.8 ± 0.5	104.0 ± 17.7	70.8 ± 1.3	4.2 ± 1.1
PLA+20TA	1861 ± 170	15.9 ± 1.3	327.6 ± 0.1	71.4 ± 3.0	5.1 ± 2.0

Regarding Shore D hardness, neat PLA shows a hardness of 79.8, which is very similar to the value reported by Lascano *et al.* [27]. The incorporation of TPF to the PLA matrix increases the hardness up to 82.0. This was expected, as TPF is a hard lignocellulosic filler, thus enhancing the hardness of the composite. Quiles-Carrillo *et al.* [29] also reported an increase in the Shore D hardness of PLA composites with orange peel flour. This increase in hardness is due to the intrinsic hardness of the filler, which is a lignocellulosic element with considerable crystallinity. The addition of the plasticizer to PLA and PLA/TPF composites clearly reduces their hardness down to values in the range 70-75, which is due to the plasticizing effect of TA and the enhancement of the mobility of PLA chains.

Finally, the impact strength results show that neat PLA presents an impact strength of 1.8 kJ/m², indicative of quite a fragile polymer. The addition of TPF to PLA does not vary this value, while the presence of the plasticizer in the polymer matrix clearly improves its absorption of impact energy up to values in the range 3 to 5 kJ/m². Specifically, the sample with 20TA is the one that presents the highest impact strength (5.1 kJ/m²). This is a direct consequence of the plasticizing effect, that improves the ductile properties of PLA.

Morphological properties

Figure III.2.2.2 gathers the morphology of plasticized and unplasticized PLA/TPF cross section samples by means of field emission scanning electron microscopy (FESEM) at a 500× magnification. **Figure III.2.2.2a** shows the typical flat and uniform morphology of a resistant and brittle polymer such as PLA [30]. **Figure III.2.2.2b** shows the addition of TPF into the PLA matrix, in which the presence of the lignocellulosic particles (black arrows) is clearly seen. The adhesion between the particles and the matrix seems to be good, as the gap between them is very narrow, thus indicating certain affinity between both components. Nonetheless, as it was reported in the mechanical properties section, it seems that TPF particles have formed aggregates that act as stress concentrators, increasing the brittleness of PLA. On the other hand, as observed in **Figures III.2.2.2c, III.2.2.2d and III.2.2.2e**, the presence of the plasticizer in the matrix with TPF leads to a rougher surface with filament-like formations (indicative of a ductile fracture) (black circles) and even a better interaction between TPF and PLA. This could be ascribed to a compatibilizing effect exerted by the plasticizer between TPF and PLA, as α -terpinyl acetate can act as a chemical bridge between lignocellulosic particles and the PLA matrix, considering that both plasticizer and PLA possess good

miscibility, as studied in the theoretical solubility parameter section by means of the Van Krevelen-Hoftyzer method. This improvement in adhesion is denoted by a very narrow and practically inexistent particle-matrix gap. Additionally, the increase in particle concentration from **Figure III.2.2.2c** (10 wt.%) to **Figure III.2.2.2e** (30 wt.%) is clearly observed, especially in the sample with 30 wt.% TPF, where a higher number of particles is present in the matrix. Finally, **Figure III.2.2.2f** shows the morphology of PLA/TA, where some filament-like structures can be observed. These structures are related to the ductile behavior observed in the mechanical characterization [31]. All in all, the results presented here match the mechanical properties exhibited in the previous section, concluding in a high ductility provided by the plasticizer and a higher strength provided by the TPF.

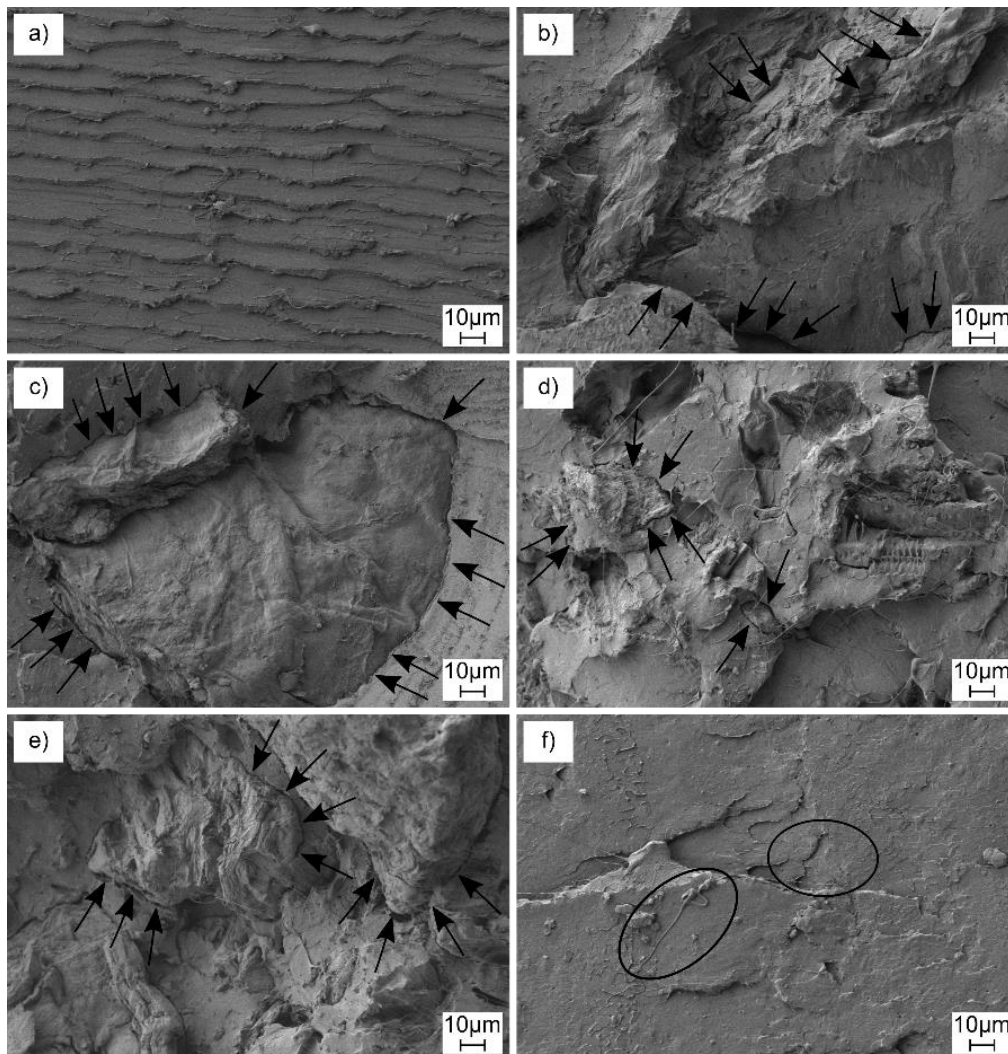


Figure III.2.2.2. FESEM images at 500 \times magnification of the PLA/TPF composites: a) PLA; b) PLA+10TPF; c) PLA+10TPF+22.5TA; d) PLA+20TPF+20TA; e) PLA+30TPF+17.5TA and f) PLA+20TA.

Thermal properties

Figure III.2.2.3 shows all the DSC thermograms obtained for the PLA/TPF composites, while **Table III.2.2.4** gathers all the main thermal parameters extracted from those thermograms. The first thermal transition observed in the thermograms is the glass transition temperature (T_g). Neat PLA shows a typically high T_g value of 62.6 °C, which is indicative of a certain rigid material at room temperature [32]. The addition of TPF does not significantly vary the glass transition temperature of PLA. On the other hand, the addition of the plasticizer drastically decreases the T_g of the polymer matrix, especially the PLA+20TPF+20TA and PLA+20TA samples, which exhibit values of 44.0 and 41.6 °C, respectively. This is ascribed to the enhanced chain mobility that the plasticizer provides the PLA matrix, as T_g is a thermal parameter that depends on the mobility of the amorphous phase of the polymer [33]. Interestingly, the incorporation of TPF and TA led to the appearance of a cold crystallization peak in all the samples containing those components. This is ascribed to an heterogeneous nucleating effect, which provokes the appearance of several points from where crystallites start to grow [34]. The plasticized sample exhibits a considerable decrease in this peak, this fact is related to the enhanced mobility of PLA chains, which can arrange more easily (at a lower temperature). Regarding the melting point of the materials, neat PLA shows a melting temperature of 173.2 °C, which is a very typical value for this rigid polymer [35]. This value is slightly affected by the incorporation of the plasticizer, which reduces it down to 168, 171 and 169 °C, for the PLA+20TPF+20TA, PLA+30TPF+17.5TA and PLA+20TA samples, respectively. This effect is ascribed to an increase in the chain mobility of the polymer exerted by the plasticizer. Finally, the crystallinity of PLA was increased as a result of the addition of TPF and TA from a value of 5.2% for neat PLA up to 27.7 for the sample with 20 wt.% TPF and 20 phr TA, which can also be responsible for the observed mechanical performance. This effect is due to the aforementioned increase in chain mobility, which increases the crystallization rate of the amorphous phase of PLA, allowing it to crystallize at a lower cold crystallization temperature, as it was observed in the PLA+20TPF+20TA and PLA+20TA samples. On the other hand, TPF also promotes the crystallization of PLA due to an heterogeneous nucleating effect. This effect promotes the distribution of TPF particles all along the polymer matrix, forming different points from which crystals start to grow [28].

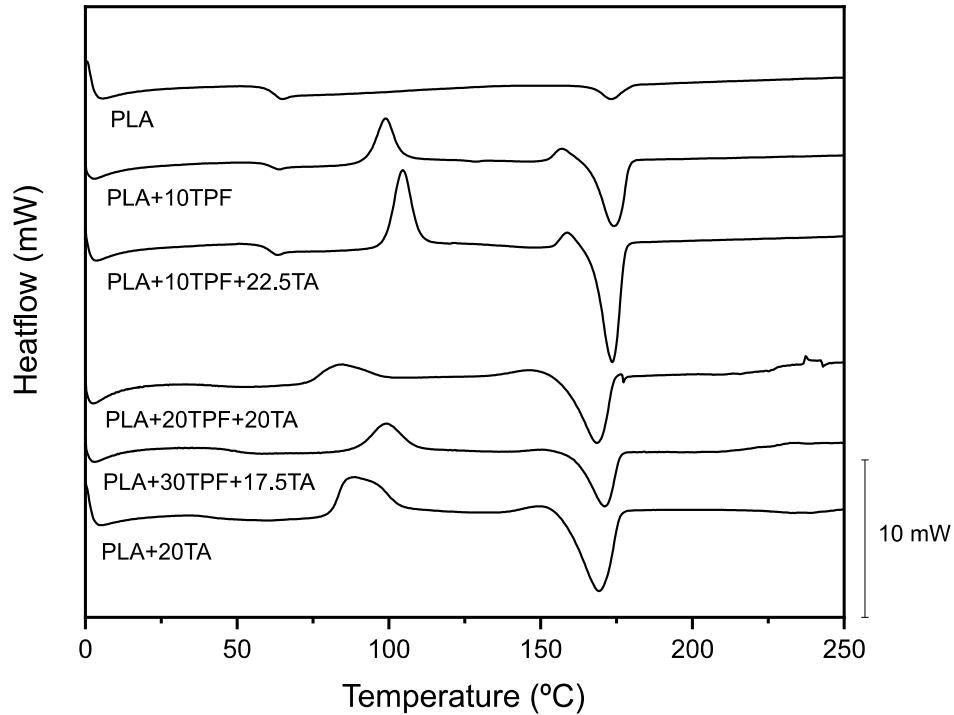


Figure III.2.2.3. DSC thermograms of all the PLA/TPF samples.

Table III.2.2.4. Glass transition temperature (T_g), Cold crystallization temperature (T_{cc}), Cold crystallization enthalpy (ΔH_{cc}) Melting temperature (T_m), melting enthalpy (ΔH_m) and degree of crystallinity (χ_c) of PLA/TPF plasticized and unplasticized composites obtained by differential scanning calorimetry (DSC).

Code	T_g (°C)	T_{cc} (°C)	ΔH_{cc} (J/g)	T_m (°C)	ΔH_m (J/g)	χ_c (%)
PLA	62.6 ± 1.1	-	-	173.2 ± 3.0	4.8 ± 0.1	5.2 ± 0.1
PLA+10TPF	61.6 ± 0.9	99.1 ± 2.0	27.1 ± 0.5	173.9 ± 2.2	50.2 ± 0.6	27.6 ± 0.3
PLA+10TPF+22.5TA	61.1 ± 1.2	104.8 ± 1.5	24.2 ± 0.3	173.3 ± 1.2	40.5 ± 0.8	19.5 ± 0.1
PLA+20TPF+20TA	44.0 ± 0.8	83.7 ± 1.3	10.7 ± 1.0	168.3 ± 1.0	31.3 ± 0.6	27.7 ± 0.2
PLA+30TPF+17.5TA	47.5 ± 0.7	99.5 ± 1.6	21.3 ± 0.7	170.9 ± 1.5	27.9 ± 0.4	10.1 ± 0.1
PLA+20TA	41.6 ± 1.1	88.5 ± 1.0	25.6 ± 0.1	168.9 ± 2.0	38.5 ± 0.2	17.3 ± 0.3

The thermal degradation of the developed composites was studied by thermogravimetric analysis (TGA) and its first derivative (DTG). **Figure III.2.2.4** shows the TGA thermal degradation profiles and their first derivatives while **Table III.2.2.5** gathers the main thermal parameters related to this analysis. First of all, the onset degradation temperature (temperature at which 5% of the mass is lost) of neat PLA stays at 305 °C, which is a very similar value that the one observed by Quiles Carrillo *et al.* [7]. The addition of TPF clearly decreases this value down to 290 °C. This is ascribed to the

relatively low thermal stability of the lignocellulosic filler, which, in turn, reduces the overall thermal stability of the composite. This fact occurs due to the thermal degradation of cellulose and lignin between 250 and 350 °C, as well as hemicellulose which degrades even at lower temperatures than cellulose [7]. With the introduction of the plasticizer into the polymer matrix, the thermal stability of the composites considerably decreases, showing values of the onset degradation temperature from 154 to 232 °C, far below the values reported for neat PLA and PLA/TPF. This phenomenon is clearly related to the volatility of the plasticizer (*i.e.* α -terpinyl acetate is a typical component of some essential oils), which possess a boiling point of approximately 220 °C. The volatility of the plasticizer is clearly detectable on the TGA thermograms, noted by a first mass loss step in the thermal degradation in all the plasticized composites, which occurs approximately at 220 °C, coinciding with the boiling point of the plasticizer. This decrease in the thermal stability is also ascribed to an enhanced chain mobility in PLA. A similar trend is observed for the maximum degradation peak temperature, although in this case, the decrease in thermal stability is not so acute, as the plasticizer has already been almost completely gone, reporting values in the range 321-356 °C. In the case of residual weight, it is very close to zero in all cases. This was expected as all the samples are organic and at 700 °C they are completely disintegrated.

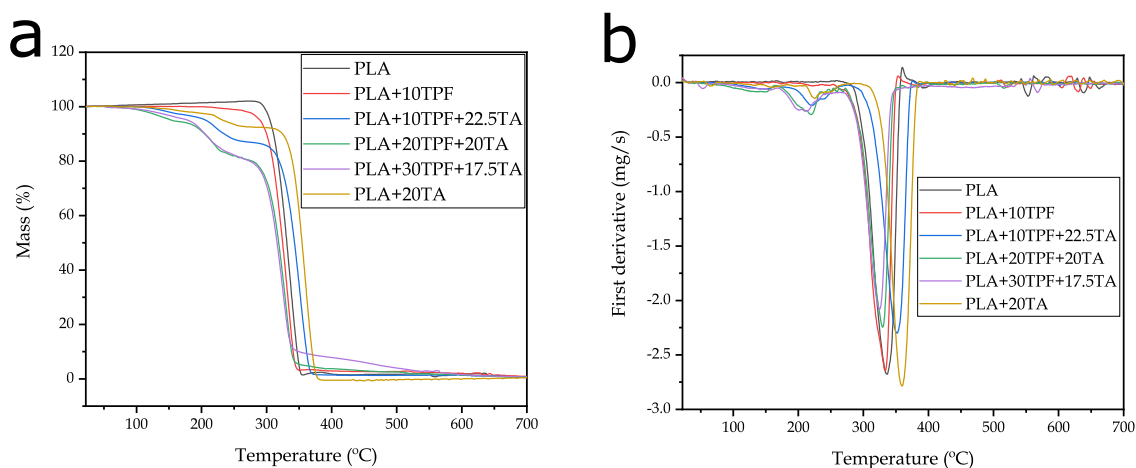


Figure III.2.2.4. Thermogravimetric analysis (TGA) and its first derivative of the plasticized and unplasticized PLA/TPF composites.

Table III.2.2.5. Main thermal degradation parameters of PLA/TPF composites plasticized with TA in terms of the onset degradation temperature at a mass loss of 5 wt.% ($T_{5\%}$), maximum degradation rate (peak) temperature (T_{deg}), and residual mass at 700 °C.

Code	$T_{5\%}$ (°C)	T_{deg} (°C)	Residual weight (%)
PLA	305.0 ± 0.6	337.5 ± 0.5	0.5 ± 0.1
PLA+10TPF	290.0 ± 0.4	332.0 ± 0.3	0.9 ± 0.1
PLA+10TPF+22.5TA	206.5 ± 0.7	349.0 ± 0.8	0.7 ± 0.1
PLA+20TPF+20TA	154.0 ± 0.6	330.5 ± 1.2	0.5 ± 0.1
PLA+30TPF+17.5TA	179.0 ± 1.0	321.0 ± 0.5	0.7 ± 0.1
PLA+20TA	232.5 ± 1.3	356.0 ± 1.1	0.5 ± 0.1

Dynamic mechanical thermal properties

Figure III.2.2.5a shows the storage modulus (E') variation of the different PLA-based composites with TPF, **Figure III.2.2.5b** shows the dynamic damping factor ($\tan \delta$) diagram of these composites, whereas **Table III.2.2.6** gathers the main thermomechanical parameters of the composites, in which the glass transition temperature was calculated utilizing the $\tan \delta$ criterion (peak maximum). The DMTA curve of PLA shows a glassy region comprised between -150 and 50 °C approximately. This region is characterized by a rigid behavior with a storage modulus or around 1500 MPa. Between 50–70 °C, a dramatic decrease (of at least two-three orders of magnitude) in the storage modulus can be seen, which is related to the glass transition region. Above 70 °C, the DMTA shows a rubbery plateau region characterized by a very low storage modulus. The glass transition temperature (T_g) can be assessed by several criteria such as the onset of the storage modulus decrease, or what is more common, as the peak maximum of the dynamic damping factor as seen in **Figure III.2.2.5b**, resulting in a T_g for neat PLA of 63.9 °C. the addition of TPF lignocellulosic filler provides the expected behavior. In general, lignocellulosic fillers lead to more rigid polymers which is reflected in DMTA by a shift of the characteristic DMTA curve of neat PLA to higher E' values as observed in **Figure III.2.2.5a**. As it can be seen, the glass transition region is similar to that of neat PLA, but a slight decrease can be observed in the peak maximum of the dynamic damping factor (**Figure III.2.2.5b**), with a T_g value of 60.4 °C. As the TPF increases, the corresponding DMTA curves are shifted to higher E' values, thus indicating more rigid materials are obtained (this is clearly observed at low temperatures, below -10 °C). Nevertheless, at room temperature, the plasticization effects are evident, since the characteristic DMTA curves are shifted to lower E' values,

thus indicating more flexible materials at room temperature. The combination of TPF with the terpene-based plasticizer leads to some synergistic effect since higher E' values are obtained, but a decrease in the T_g can be seen too with values comprised between 40-45 °C approximately.

PLA shows the lowest initial storage modulus, with a value of 1464 MPa at -100 °C. A very similar thermomechanical profile was observed by Lascano *et al.* [27]. The incorporation of TPF increases this value up to 1965 MPa, which coincides with what was observed in mechanical properties, as the hard lignocellulosic filler increases the rigidity of the polymer. Surprisingly, the addition of the plasticizer also increases the storage modulus in the temperature range between -150 and -10 °C, with values higher to 2000 MPa, probably due to some interaction between the plasticizer and the lignocellulosic filler below their characteristic T_g values. Nonetheless, as temperature rises, the plasticized samples clearly decrease their storage modulus more rapidly, as a result of the increased polymer chain mobility. Thus, it can be seen that at room temperature (20 °C approximately), the storage modulus of the plasticized samples is far lower than that of neat PLA and PLA/TPF (PLA presents a value of 1245 MPa, while the plasticized samples have values in the range 756–982 MPa). A sudden decrease in the storage modulus can be appreciated for all samples, which is indicative of their glass transition temperature, related to the mobility of the amorphous region of the polymer [36]. This thermal transition is more accurately observed in the $\tan \delta$ plot, where it is indicated by a peak. As it was expected, the glass transition of neat PLA (peak maximum of the $\tan \delta$ peak) and PLA/TPF occurs at higher temperatures than the plasticized samples. The glass transition of neat PLA is located at 63.9 °C, which is very close to the value reported in DSC analysis. The glass transition of the unplasticized PLA/TPF composite is 60.4 °C. On the other hand, the plasticized samples exhibit values in the range 40-46 °C, being the samples with 20TA the ones with the lowest T_g . This fact is ascribed to the enhanced mobility of the amorphous region of the polymer as a result of the presence of α -terpinyl acetate molecules, which diminish the activation energy barrier for segmental relaxations of the surrounding polymer molecules to occur [37]. These results perfectly match the findings reported in DSC, where the effect of the plasticizer was reflected in the glass transition values. It is also worthy to note the cold crystallization process which can be observed by DMTA by an increase in the storage modulus at temperatures above 60-70 °C as seen in **Figure III.2.2.5a**. Neat PLA does not show this process, which is consistent with the previous DSC results on thermal properties. On the other hand, both the TPF and the terpene-based plasticizer promote the cold crystallization since TPF has a nucleant effect, and the plasticizer increases the

chain mobility, both phenomena having a positive effect on increasing crystallinity, which confirm the previously reported results by DSC.

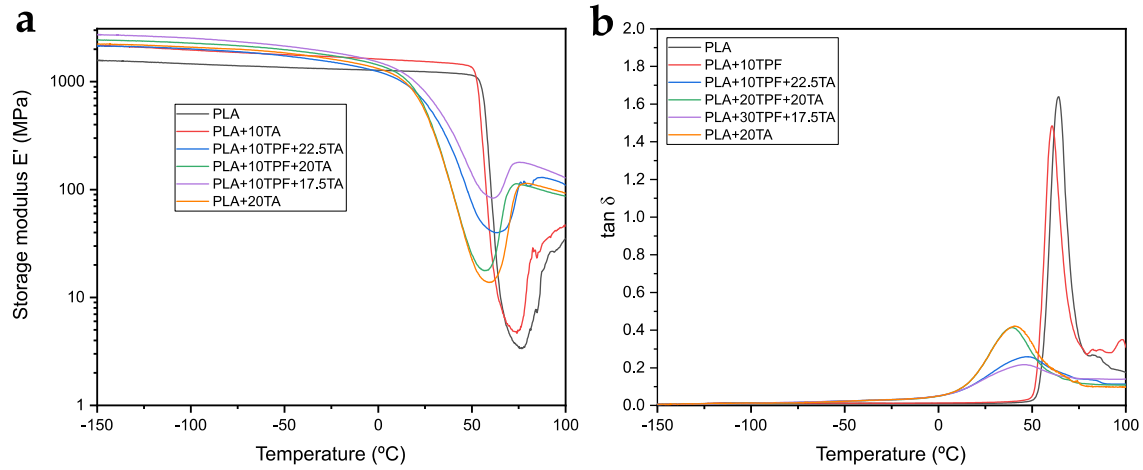


Figure III.2.2.5. Thermomechanical diagrams of the plasticized and unplasticized PLA/TPF composites: a) Storage Modulus (E'); b) Dynamic damping factor ($\tan \delta$).

Table III.2.2.6. Dynamic-mechanical-thermal properties of PLA/TPF plasticized with α -terpinyl acetate (TA), at different temperatures.

Code	E' (MPa) at -100 °C	E' (MPa) at 20 °C	E' (MPa) at 80 °C	T_g (°C)
PLA	1464 ± 45	1245 ± 21	4 ± 7	63.9 ± 1.3
PLA+10TPF	1965 ± 33	1551 ± 27	16 ± 9	60.4 ± 2.2
PLA+10TPF+22.5TA	2013 ± 28	798 ± 25	108 ± 5	46.2 ± 2.1
PLA+20TPF+20TA	2280 ± 32	811 ± 30	108 ± 7	39.9 ± 1.7
PLA+30TPF+17.5TA	2534 ± 40	982 ± 27	174 ± 8	46.5 ± 1.5
PLA+20TA	2081 ± 40	756 ± 40	114 ± 40	40.6 ± 1.5

*The T_g has been measured using the $\tan \delta$ peak maximum criterion.

Visual aspect and colour properties

Colour and luminance are essential parameters when it comes to wood plastic composites, as these parameters determine the visual appearance of the composites and the degree of similarity with several woods. **Figure III.2.2.6** shows the visual aspect of all the developed composites, while **Table III.2.2.7** gathers the main colour parameters regarding the $CieL^*a^*b^*$ colour space. As it can be inferred for the appearance of the samples, both the samples of neat PLA and PLA with the plasticizer show clear colours, being the plasticized PLA composite more opaque than neat PLA. This is also seen in

luminance values, where these two samples present higher values of luminance than the samples with TPF, going from values of approximately 45 down to values of 22-25, respectively. This is because luminance stands for white (higher values) and black (lower values). As expected, TPF samples possess darker brownish colours that resemble that of certain woods, which give them great application as plastic materials that can substitute wood-based materials [3].



Figure III.2.2.6. Visual appeal of the samples: a) PLA; b) PLA+20TA; c) PLA+10TPF d) PLA+10TPF+22.5TA; e) PLA+20TPF+20TA and f) PLA+30TPF+17.5TA.

Regarding colour coordinates a^* (green for negative values and red for positive values) and b^* (blue for negative values and yellow for positive values), the samples that have TPF in its composition present higher positive a^* values than neat PLA and plasticized PLA. This is ascribed to a characteristic brown colour that approaches the red colour, which is located in the positive region of a^* . On the other hand, with regard to b^* colour coordinate, all samples except for neat PLA possess positive values superior to 1. This is related to an approach of the samples to the yellow colour, located in the positive side of the chromatic space. These values can be verified by **Figure III.2.2.6**, where the plasticized sample presents a more yellow-like colour than neat PLA; while the TPF samples present dark brown colours, which are closer to yellow than the colour of neat PLA.

Table III.2.2.7. Luminance and colour coordinates ($L^*a^*b^*$) of the PLA/TPF composites plasticized with α -terpinyl acetate.

Code	L^*	a^*	b^*
PLA	46.16 ± 0.87	0.08 ± 0.04	0.72 ± 0.15
PLA+10TPF	25.05 ± 0.21	1.55 ± 0.12	1.78 ± 0.05
PLA+10TPF+22.5TA	22.25 ± 0.19	0.74 ± 0.35	1.72 ± 0.18
PLA+20TPF+20TA	23.57 ± 0.24	1.14 ± 0.14	1.13 ± 0.10
PLA+30TPF+17.5TA	23.61 ± 0.13	1.15 ± 0.14	1.29 ± 0.37
PLA+20TA	44.22 ± 0.01	-0.41 ± 0.06	1.59 ± 0.07

Wettability

Wood plastic composites present a great trend to absorb water, due to the presence of highly hydrophilic components in their composition (*i.e.* cellulose, hemicellulose, pectin and lignin) [38]. This is considered as one of the main drawbacks of this kind of materials. **Figure III.2.2.7** gathers the contact angle measurements carried out in each one of the samples, with the objective of studying the wettability of the developed composites. Neat PLA presents a contact angle of 87.3° [39], which is a typical value for this polymer and it is indicative of a hydrophobic behavior, considering the hydrophilic threshold of Vogler located at 65° [40]. The addition of 10 wt.% TPF decreased the water contact angle of PLA down to 83° . This is ascribed to the presence of the aforementioned lignocellulosic components, which are highly polar molecules and possess a great concentration of hydroxyl groups (-OH). These functionalities give TPF great affinity for water, as they make possible to create hydrogen bonds. The addition of α -terpinyl acetate slightly decreases the contact angle in relation to the PLA/10TPF sample as a result of the free volume it provides to PLA. As expected, the contact angle decreases as the proportion of TPF is superior. This is corroborated by a contact angle of 63.4° for the sample with 30 wt.% of TPF, which makes more -OH functionalities to be readily available to interact with water. Finally, the sample of PLA/TA also demonstrates the increased free volume provided by the plasticizer, as the contact angle decreases from 87 down to 81.4° in relation to neat PLA.

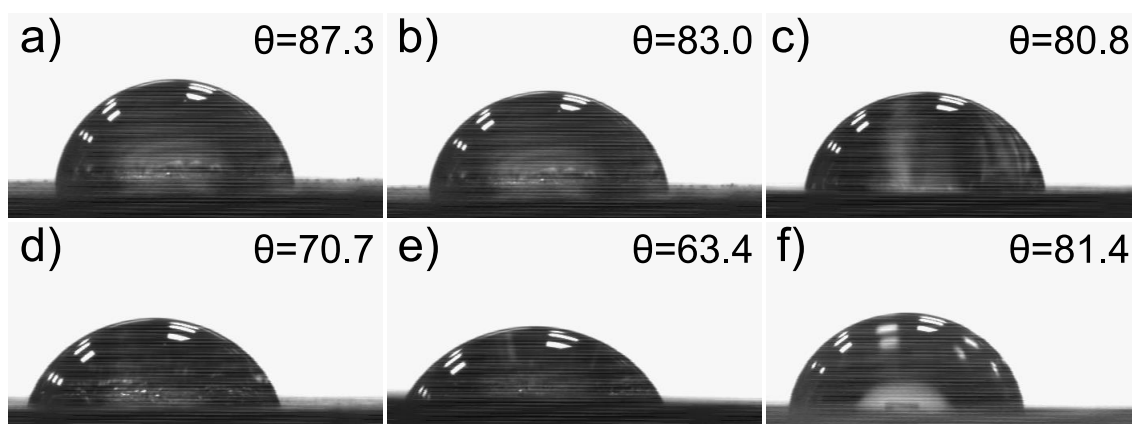


Figure III.2.2.7. Contact angle measurements of the PLA/TPF composites: a) PLA; b) PLA+10TPF; c) PLA+10TPF+22.5TA; d) PLA+20TPF+20TA; e) PLA+30TPF+17.5TA and f) PLA+20TA.

Chemical characterization

Figure III.2.2.8 shows the FTIR spectra of neat PLA, PLA with TPF and the plasticized and unplasticized PLA/TPF composites. First of all, neat PLA presents a common spectrum for this polymer. One of the main representative bands is located at 1751 cm^{-1} and it is ascribed to the C=O stretching. The bands between 1250 and 1000 cm^{-1} are also significative and are related to the ester C-O and C-O-C stretching vibrations. The bands in the range 1500 - 1300 cm^{-1} are indicative of symmetric and antisymmetric deformational vibrations of the C-H bond in methyl groups [29]. The incorporation of TPF into the polymer matrix did not significantly change the spectra of PLA. On the other hand, the incorporation of α -terpinyl acetate induced some interesting changes in the spectra. In the region of 3400 cm^{-1} a small band can be observed for all the plasticized samples, which could be related to the presence of hydrogen bonding between TA and PLA or TA with lignocellulosic compounds in TPF [41]. Then, another peak appears at approximately 1450 cm^{-1} , which is ascribed to C=O stretching in the ester group present in TA, this peak becomes more intense in the PLA/TA sample, as the concentration of plasticizer is higher in this composite. Finally, a small peak at around 1200 cm^{-1} appears due to the rocking vibration of the C-H bond.

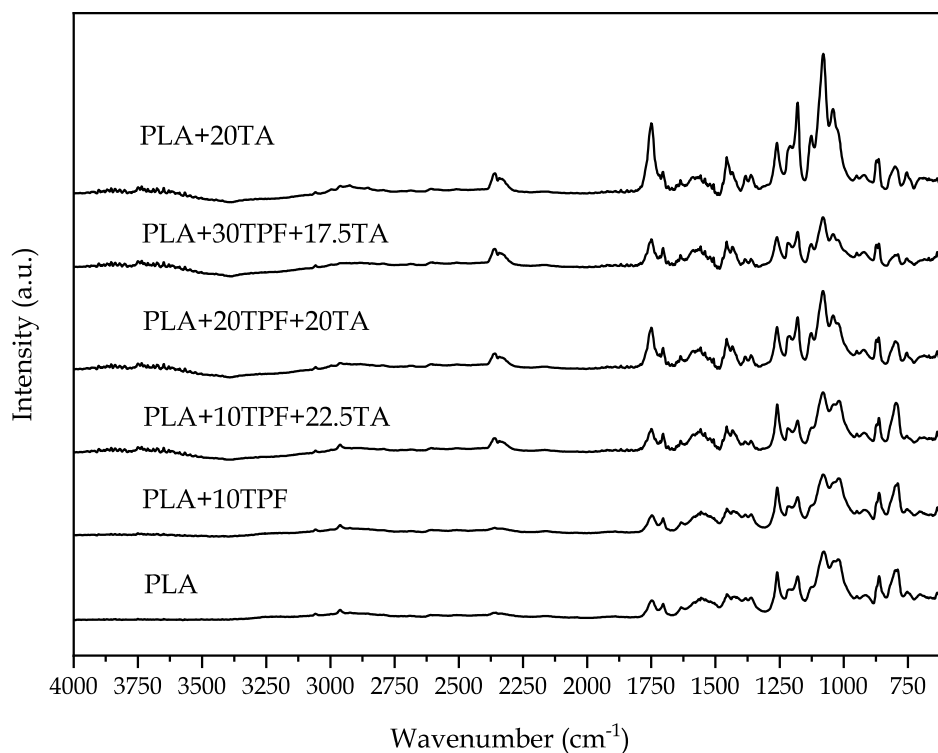


Figure III.2.2.8. FTIR diagrams of neat PLA and the plasticized and unplasticized PLA/TPF composites.

Disintegration test

The biodegradability of the samples was assessed through the disintegration test in controlled compost soil. **Figure III.2.2.9** shows the disintegration evolution (mass loss) all over 6 weeks in which the samples were buried in controlled compost soil (the black line at 90% is indicative of the disintegration goal). On the other hand, **Figure III.2.2.10** illustrates the visual appearance of the samples throughout the disintegration process. It can be seen that after an incubation time of 5 weeks, all samples except for neat PLA have achieved complete disintegration, while PLA completely disintegrates after 6 weeks. This fact demonstrates the biodegradability of all the herein presented composites. The disintegration profile of neat PLA is very similar to the one observed by Quiles-Carrillo *et al.* [29], who also observed complete disintegration of neat PLA and PLA/orange peel flour samples. This suggests that both the lignocellulosic filler (TPF) and the plasticizer enhance the biodegradability of PLA. Interestingly, in spite of the fact that all samples except PLA fully disintegrate in 5 weeks, the plasticized samples present a higher disintegration rate in the first weeks. This is probably ascribed to the low thermal stability of the α -terpinyl acetate, which provokes a higher weight loss rate [42]. Moreover, the plasticizer seems to catalyze the hydrolysis of PLA, making it easier for

bacteria to decompose the polymer. The visual appearance of the samples supports these results, where it can be seen how in the second week all materials have undergone severe weight loss. A colour change in neat PLA and PLA+20TA can be observed from a white clear colour to a darker tonality as a result of the disintegration process. Therefore, it can be concluded that all samples are effectively biodegradable and that TPF and the plasticizer contribute to reduce the amount of time necessary to achieve 100% disintegration. Probably due to the hydrophilic behavior of both components, as demonstrated in the contact angle analysis.

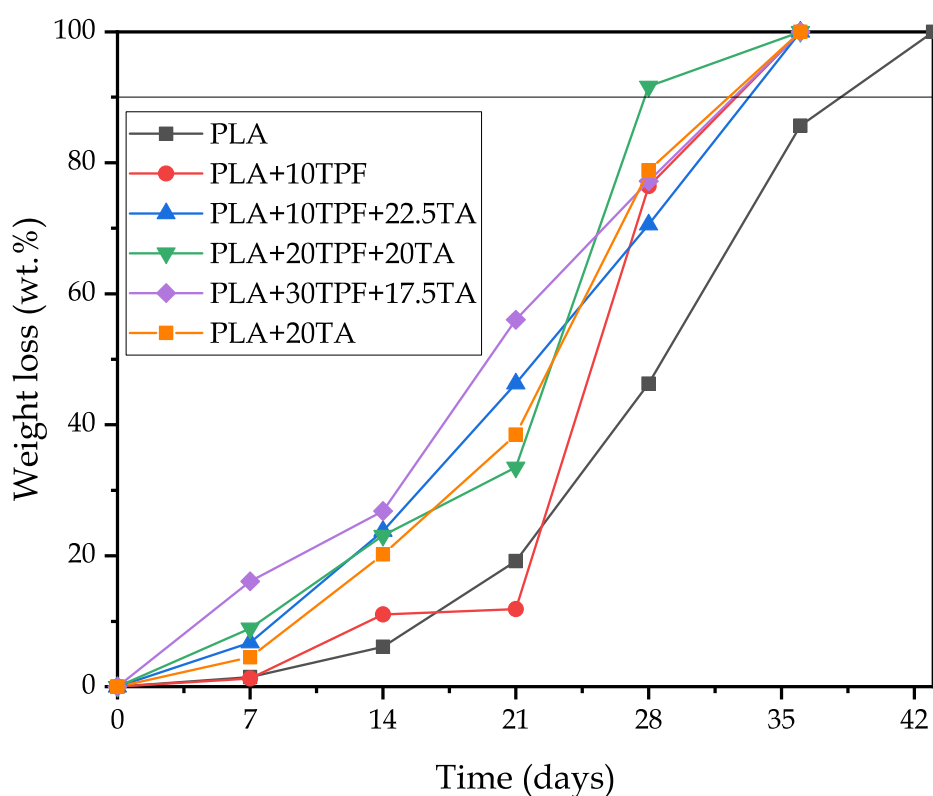


Figure III.2.2.9. Disintegration profile of the plasticized and unplasticized PLA/TPF composites over time.

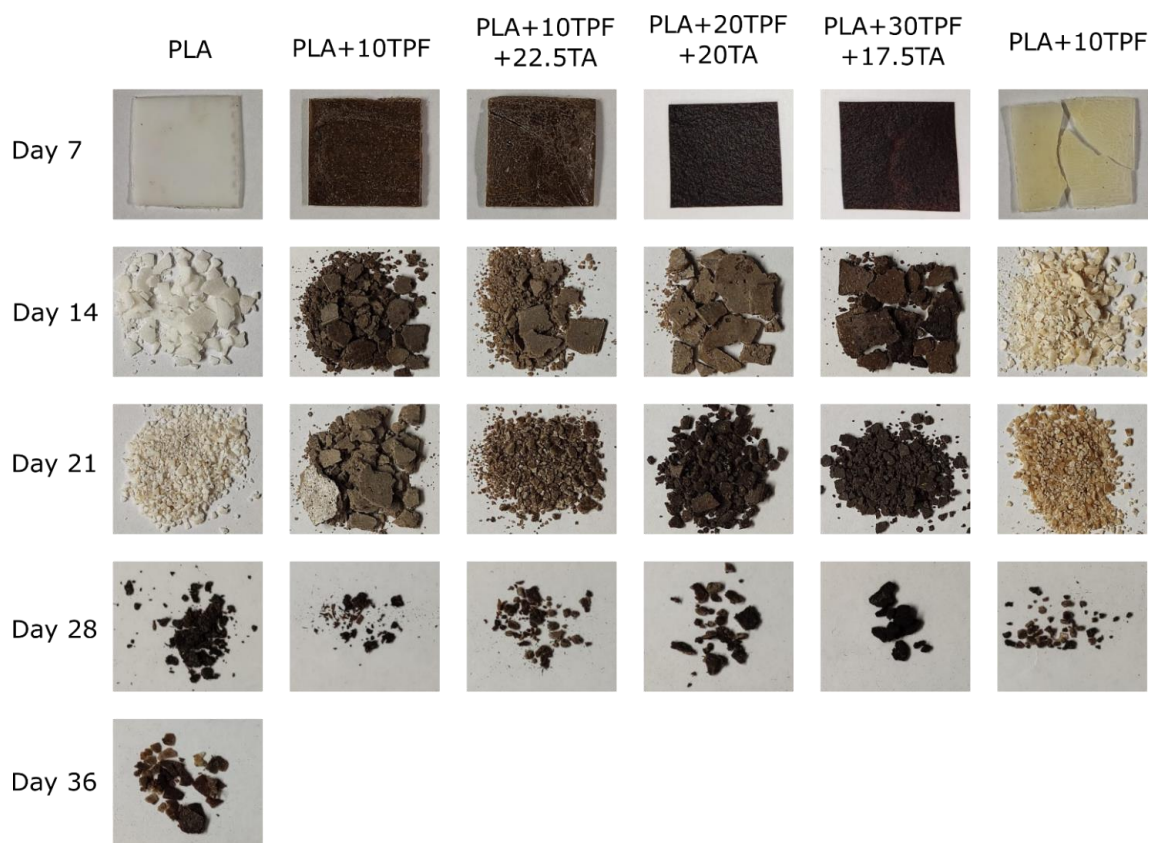


Figure III.2.2.10. Visual appearance of the disintegration process of PLA/TPF composites over time.

CONCLUSIONS

In this work, environmentally friendly and fully biodegradable composites have been obtained combining a PLA polymer matrix, tangerine peel flour (TPF) as a reinforcing filler and α -terpinyl acetate as a natural origin plasticizer to improve toughness. The herein presented materials have proved to possess an excellent mechanical performance in terms of ductility. Especially thanks to the plasticizing effect of α -terpinyl acetate, which allowed to achieve elongations at break superior to 300% in the case of the PLA+20TA sample, and elongations at break close to 200% in the case of PLA+10TPF+22.5TA. The performance of PLA+10TPF+22.5TA is quite an interesting result considering that TPF is a hard and rigid filler that would normally increase the brittleness of PLA. This good interaction between PLA and the plasticizer was confirmed by theoretical solubility parameter determination, which concluded that indeed both elements were highly compatible. The mechanical characterization was verified by FESEM, where filament-like structures were observed, which were indicative of effective plasticization. In terms of thermal characterization, α -terpinyl acetate drastically

reduced the glass transition temperature of PLA, which gave the composites greater ductility and better processability, reaching glass transition temperatures around 40 °C, which is a noticeable reduction considering that neat PLA presents a glass transition temperature of 63 °C. Additionally, it was observed how the plasticizer increased the thermal disintegration rate of the composites due to its volatility, decreasing the thermal stability of the materials in the temperature range 200-300 °C. The composites presented characteristic dark brown colours, similar to that of wood, making them perfect for substituting wood-based products. Moreover, the presence of TPF and the acetate increased the affinity of PLA for water, according to contact angle measurements, reaching contact angle values of 60°. Finally, the disintegration test proved that all the developed samples were completely biodegradable after 5 weeks under controlled compost soil conditions, surpassing the biodegradability of neat PLA (100% disintegration after 6 weeks), which greatly enhances the environmentally friendly nature of these materials, altogether with the natural origin of all of their components. All in all, this work opens up a new research line centered in the use of tangerine wastes as lignocellulosic fillers for polymers. The great effectiveness of TA as a plasticizer has also been demonstrated, which could be tried in other brittle polymers such as poly(3-hydroxybutyrate-co-3-hydroxyhexanoate) (PHBH) in order to evaluate if it is capable of increasing its ductility.

ACKNOWLEDGEMENTS

This research is a part of the grant PID2020-116496RB-C22 funded by MCIN/AEI/10.13039/501100011033. Authors also thank Generalitat Valenciana-GVA, grant number AICO/2021/025 and CIGE/2021/094 for supporting this work. J. Gomez-Caturla wants to thank Generalitat Valenciana-GVA, for his FPI grant (ACIF/2021/185) and grant FPU20/01732 funded by MCIN/AEI/ 10.13039/501100011033 and by ESF Investing in your future. J. Ivorra-Martinez wants to thank FPU19/01759 grant funded by MCIN/AEI/ 10.13039/501100011033 and by ESF Investing in your future. Microscopy Services at UPV are also acknowledged by their help in collecting and analyzing images.

REFERENCES

- [1] Khan, M.Z., S.K. Srivastava, and M. Gupta, *A state-of-the-art review on particulate wood polymer composites: Processing, properties and applications*. Polymer Testing, 2020. 89: 106721.
- [2] Petchwattana, N., P. Naknaen, and B. Narupai, *A circular economy use of waste wood sawdust for wood plastic composite production: Effect of bio-plasticiser on the toughness*. International Journal of Sustainable Engineering, 2020. 13(5): 398-410.
- [3] Gomez-Caturla, J., et al., *Biopolypropylene-Based Wood Plastic Composites Reinforced with Mango Peel Flour and Compatibilized with an Environmentally Friendly Copolymer from Itaconic Acid*. ACS Applied Polymer Materials, 2022. 4(6): 4398-4410.
- [4] Botta, L., et al., *PBAT based composites reinforced with microcrystalline cellulose obtained from softwood almond shells*. Polymers, 2021. 13(16): 2643.
- [5] Bashar, D.-a., *Long term thermo-mechanical prediction of banana stem particulate reinforced PVC composite as piping material*. Pakistan Journal of Engineering and Applied Sciences, 2018.
- [6] Banerjee, J., et al., *Bioactives from fruit processing wastes: Green approaches to valuable chemicals*. Food chemistry, 2017. 225: 10-22.
- [7] Quiles-Carrillo, L., et al., *Compatibilization of highly sustainable polylactide/almond shell flour composites by reactive extrusion with maleinized linseed oil*. Industrial Crops and Products, 2018. 111: 878-888.
- [8] Nampoothiri, K.M., N.R. Nair, and R.P. John, *An overview of the recent developments in polylactide (PLA) research*. Bioresource technology, 2010. 101(22): 8493-8501.
- [9] Luna, C.B., et al., *Annealing efficacy on PLA. Insights on mechanical, thermomechanical and crystallinity characters*. Momento, 2021. (62): 1-17.
- [10] Martinez Villadiego, K., et al., *Thermoplastic starch (TPS)/polylactic acid (PLA) blending methodologies: a review*. Journal of Polymers and the Environment, 2021. 30: 75-91.
- [11] Patil, S.S. and H.M. Jena, *Performance assessment of polyvinyl chloride films plasticized with Citrullus lanatus seed oil based novel plasticizer*. Polymer Testing, 2021. 101: 107271.

- [12] Martin, O. and L. Avérous, *Poly (lactic acid): plasticization and properties of biodegradable multiphase systems*. *Polymer*, 2001. 42(14): 6209-6219.
- [13] da Silva, J.M.F. and B.G. Soares, *Epoxidized cardanol-based prepolymer as promising biobased compatibilizing agent for PLA/PBAT blends*. *Polymer Testing*, 2021. 93: 106889.
- [14] Yu, R.-l., et al., *Improvement in toughness of polylactide by melt blending with bio-based poly (ester) urethane*. *Chinese Journal of Polymer Science*, 2014. 32(8): 1099-1110.
- [15] Wypych, G., *Handbook of plasticizers*. 2004: ChemTec Publishing.
- [16] Ojha, P. and S. Thapa, *Quality evaluation of biscuit incorporated with mandarin peel powder*. Scientific Study & Research. Chemistry & Chemical Engineering, Biotechnology, Food Industry, 2017. 18(1): 19.
- [17] Ordóñez-Santos, L.E., J. Esparza-Estrada, and P. Vanegas-Mahecha, *Ultrasound-assisted extraction of total carotenoids from mandarin epicarp and application as natural colorant in bakery products*. *Lwt*, 2021. 139: 110598.
- [18] Mackenzie, L.S., et al., *Valorization of waste orange peel to produce shear-thinning gels*. *Journal of Chemical Education*, 2019. 96(12): 3025-3029.
- [19] Farahmandfar, R., et al., *Comparison of different drying methods on bitter orange (Citrus aurantium L.) peel waste: Changes in physical (density and color) and essential oil (yield, composition, antioxidant and antibacterial) properties of powders*. *Journal of Food Measurement and Characterization*, 2020. 14(2): 862-875.
- [20] Hejna, A., et al., *Mandarin peel as an auspicious functional filler for polymer composites*. *Macedonian Journal of Chemistry and Chemical Engineering*, 2021. 1: 1-18.
- [21] Rathinavel, S. and S. Saravanakumar, *Development and Analysis of Poly Vinyl Alcohol/Orange peel powder biocomposite films*. *Journal of Natural Fibers*, 2021. 18(12): 2045-2054.
- [22] Fehlberg, J., et al., *Orange peel waste from juicing as raw material for plastic composites intended for use in food packaging*. *Journal of Applied Polymer Science*, 2020. 137(26): 48841.
- [23] Chowdhury, S. and S. Kumar, *Alpha-terpinyl acetate: A natural monoterpenoid from Elettaria cardamomum as multi-target directed ligand in Alzheimer's disease*. *Journal of Functional Foods*, 2020. 68: 103892.

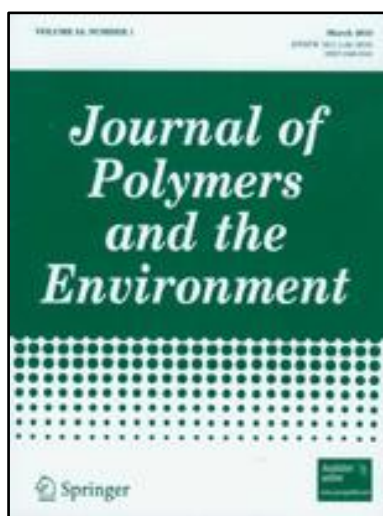
- [24] Van Krevelen, D.W. and K. Te Nijenhuis, *Properties of polymers: their correlation with chemical structure; their numerical estimation and prediction from additive group contributions*. 2009: Elsevier.
- [25] Auras, R.A., *et al.*, *Poly (lactic acid): synthesis, structures, properties, processing, and applications*. 2011: John Wiley & Sons.
- [26] Brüster, B., *et al.*, *Plasticization of polylactide with myrcene and limonene as bio-based plasticizers: Conventional vs. reactive extrusion*. *Polymers*, 2019. 11(8): 1363.
- [27] Lascano, D., *et al.*, *Development of injection-molded polylactide pieces with high toughness by the addition of lactic acid oligomer and characterization of their shape memory behavior*. *Polymers*, 2019. 11(12): 2099.
- [28] Jorda-Reolid, M., *et al.*, *Upgrading argan shell wastes in wood plastic composites with biobased polyethylene matrix and different compatibilizers*. *Polymers*, 2021. 13(6): 922.
- [29] Quiles-Carrillo, L., *et al.*, *On the use of acrylated epoxidized soybean oil as a reactive compatibilizer in injection-molded compostable pieces consisting of polylactide filled with orange peel flour*. *Polymer International*, 2018. 67(10): 1341-1351.
- [30] Barczewski, M., *et al.*, *Synergistic effect of different basalt fillers and annealing on the structure and properties of polylactide composites*. *Polymer Testing*, 2020. 89: 106628.
- [31] Ivorra-Martinez, J., *et al.*, *The Potential of an Itaconic Acid Diester as Environmentally Friendly Plasticizer for Injection-Moulded Polylactide Parts*. *Macromolecular Materials and Engineering*, 2022. 307(12): 2200360.
- [32] Zhorina, L.A., *et al.*, *Thermal characterization and sorption of FeIII ion by ternary polylactide–poly-3-hydroxybutyrate–chitosan compositions*. *Mendeleev Communications*, 2021. 31(1): 104-106.
- [33] Xuan, W., K. Odelius, and M. Hakkarainen, *Tunable polylactide plasticizer design: Rigid stereoisomers*. *European Polymer Journal*, 2021. 157: 110649.
- [34] Gao, X., *et al.*, *Synergistic effect of plasticizer and nucleating agent on crystallization behavior of polylactide during fused filament fabrication*. *Polymer*, 2021. 215: 123426.
- [35] Demchenko, V., *et al.*, *Nanocomposites based on polylactide and silver nanoparticles and their antimicrobial and antiviral applications*. *Reactive and Functional Polymers*, 2022. 170: 105096.
- [36] Mathew, A.P., K. Oksman, and M. Sain, *Mechanical properties of biodegradable composites from poly lactic acid (PLA) and microcrystalline cellulose (MCC)*. *Journal of applied polymer science*, 2005. 97(5): 2014-2025.

- [37] DeFelice, J. and J.E. Lipson, *The influence of additives on polymer matrix mobility and the glass transition*. *Soft Matter*, 2021. 17(2): 376-387.
- [38] Hiasa, S., *et al.*, *Isolation of cellulose nanofibrils from mandarin (Citrus unshiu) peel waste*. *Industrial Crops and Products*, 2014. 62: 280-285.
- [39] Prus-Walendziak, W. and J. Kozłowska, *Design of sodium alginate/gelatin-based emulsion film fused with polylactide microparticles charged with plant extract*. *Materials*, 2021. 14(4): 745.
- [40] Vogler, E.A., *Water and the acute biological response to surfaces*. *Journal of Biomaterials Science, Polymer Edition*, 1999. 10(10): 1015-1045.
- [41] Debabhuti, N., *et al.*, *Development of QCM sensor to detect α -terpinyl acetate in cardamom*. *Sensors and Actuators A: Physical*, 2021. 319: 112521.
- [42] Arrieta, M.P., *et al.*, *Disintegrability under composting conditions of plasticized PLA-PHB blends*. *Polymer Degradation and Stability*, 2014. 108: 307-318.

III.2.3. Development and characterization of new environmentally friendly polylactide formulations with terpenoid-based plasticizers with improved ductility

Jaume Gomez-Caturla^{1*}, Ramon Tejada-Oliveros², Juan Ivorra-Martinez¹, David Garcia-Sanoguera¹, Rafael Balart¹, Daniel Garcia-Garcia¹

¹ Technological Institute of Materials – ITM, Universitat Politècnica de València – UPV, Plaza Ferrándiz y Carbonell 1, 03801 Alcoy (Spain).



Journal of Polymers and the Environment

2023, 1(1): 1-14

*Adapted from the original manuscript.



Development and Characterization of New Environmentally Friendly Polylactide Formulations with Terpenoid-Based Plasticizers with Improved Ductility

J. Gomez-Caturla¹ · R. Tejada-Oliveros¹ · J. Ivorra-Martinez¹ · D. Garcia-Sanoguera¹ · R. Balart¹ · D. Garcia-Garcia¹Accepted: 15 July 2023
© The Author(s) 2023

Abstract

This work addresses the potential of two biobased terpenoids, linalyl acetate and geranyl acetate, as environmentally friendly monomeric plasticizers for polylactide (PLA). Plasticized formulations of PLA containing 10 wt.% and 20 wt.% terpenoids were melt-compounded in a twin-screw co-rotating extruder and, subsequently, processed by injection moulding for further characterization. In addition, a reactive extrusion process (REX) was carried out on plasticized formulations containing 20 wt.% terpenoids with dicumyl peroxide to anchor the plasticizer molecules into the PLA backbone. Both terpenoids led to a remarkable plasticization effect on PLA, with a noticeable increase in ductile properties. In particular, the elongation at break of PLA, around 4.7%, was improved to values above 230% for all the plasticized formulations, even for low terpenoid concentration of 10 wt.%. Terpenoids also provide increased crystallinity because polymer chains have more mobility and are more readily arranged. This was observed by shifting the cold crystallization process to lower temperatures. As with other monomeric plasticizers, a clear decrease in the glass transition temperature from 61.5 °C (neat PLA), to values of around 40 °C for the plasticized formulations with 20 wt.% terpenoid was obtained. The obtained formulations show high potential since the plasticization efficiency of these terpenoids is very high, thus leading to new toughened-PLA formulations with improved ductility.

Keywords Poly(lactide) (PLA) · Plasticizer · Terpenoids · Reactive extrusion · Ductility

Introduction

Environmental issues such as petroleum depletion, the increase in the carbon footprint, global warming, greenhouse emissions, and life cycle assessment (LCA) are leading to important changes in how we conceive, produce, use, and remove materials. Petroleum-derived polymers and additives have been widely used over the past decades due to their low cost, enhanced durability, easy processing, and a wide range of properties [1], but with a high environmental impact due to the huge amount of generated wastes. To provide a more sustainable polymer industry, research has focused on two main topics related to their synthesis and/or disposal [2].

In the last years, the commercialization of polymers and/or additives from natural resources has risen. These include fully or partially biobased polymers such as polyethylene-PE, polypropylene-PP, polyamide-PA, polycarbonate-PC, polyethylene terephthalate-PET, polyurethane-PU, and so on [3–7]. These polymers offer similar properties to their corresponding petroleum-derived counterparts, including non-biodegradation. On the other hand, a promising group of biobased and biodegradable polymers has risen in the last years. This group includes natural polymers such as polysaccharides, *i.e.* starch, cellulose, chitin (and its derivative, chitosan), pectin [8–10], as well as protein-based polymers such as gluten, casein, ovalbumin, bean proteins (soy, faba, alubia) [11–15], among others. Moreover, bacterial polyesters or polyhydroxyalkanoates-PHAs offer promising applications [16, 17], as well as some other petroleum-based polyesters that are susceptible to disintegration in controlled compost soil, such as polybutylene succinate-PBS, polyglycolide-PGA, poly- ϵ -caprolactone-PCL, polybutylene succinate-*co*-adipate-PBSA and so on [18–21]. Polylactide

✉ R. Tejada-Oliveros
rateol@epsa.upv.es

¹ Institute of Materials Technology (ITM), Universitat Politècnica de València (UPV), Plaza Ferrándiz Y Carbonell 1, 03801 Alcoy, Alicante, Spain

Development and characterization of new environmentally friendly polylactide formulations with terpenoid-based plasticizers with improved ductility

Abstract

This work addresses the potential of two biobased terpenoids, linalyl acetate and geranyl acetate, as environmentally friendly monomeric plasticizers for polylactide (PLA). Plasticized formulations of PLA containing 10 wt.% and 20 wt.% terpenoids were melt-compounded in a twin-screw co-rotating extruder and, subsequently, processed by injection moulding for further characterization. In addition, a reactive extrusion process (REX) was carried out on plasticized formulations containing 20 wt.% terpenoids with dicumyl peroxide to anchor the plasticizer molecules into the PLA backbone. Both terpenoids led to a remarkable plasticization effect on PLA, with a noticeable increase in ductile properties. In particular, the elongation at break of PLA, around 4.7%, was improved to values above 230% for all the plasticized formulations, even for low terpenoid concentration of 10 wt.%. Terpenoids also provide increased crystallinity because polymers chains have more mobility and are more readily arranged. This was observed by shifting the cold crystallization process to lower temperatures. As with other monomeric plasticizers, a clear decrease in the glass transition temperature from 61.5 °C (neat PLA), to values of around 40 °C for the plasticized formulations with 20 wt.% terpenoid was obtained. The obtained formulations show high potential since the plasticization efficiency of these terpenoids is very high, thus leading to new toughened-PLA formulations with improved ductility.

Keywords: Poly(lactide), plasticizer, terpenoids, reactive extrusion; ductility.

INTRODUCTION

Environmental issues such as petroleum depletion, the increase in the carbon footprint, global warming, greenhouse emissions, and life cycle assessment (LCA) are leading to important changes in how we conceive, produce, use, and remove materials. Petroleum-derived polymers and additives have been widely used over the past decades due to their low cost, enhanced durability, easy processing, and a wide range of properties [1], but with a high environmental impact due to the huge amount of generated wastes. To provide a more sustainable polymer industry, research has focused on two main topics related to their synthesis and/or disposal [2]. In the last years, the commercialization of polymers and/or additives from natural resources has risen. These include fully or partially biobased polymers such as polyethylene-PE, polypropylene-PP, polyamide-PA, polycarbonate-PC, polyethylene terephthalate-PET, polyurethane-PU, and so on [3-7]. These polymers offer similar properties to their corresponding petroleum-derived counterparts, including non-biodegradation. On the other hand, a promising group of biobased and biodegradable polymers has risen in the last years. This group includes natural polymers such as polysaccharides, *i.e.* starch, cellulose, chitin (and its derivative, chitosan), pectin [8-10], as well as protein-based polymers such as gluten, casein, ovalbumin, bean proteins (soy, faba, alubia) [11-15], among others. Moreover, bacterial polyesters or polyhydroxyalkanoates-PHAs offer promising applications [16, 17], as well as some other petroleum-based polyesters that are susceptible to disintegration in controlled compost soil, such as polybutylene succinate-PBS, polyglycolide-PGA, poly- ϵ -caprolactone-PCL, polybutylene succinate-*co*-adipate-PBSA and so on [18-21]. Polylactide (PLA) is the most promising commercially available aliphatic polyester [1]. PLA can be obtained by direct polycondensation of lactic acid or, more commonly, by ring-opening polymerization (ROP) of lactide, obtained after fermentation of starch-rich compounds [22]. Despite it offers good processability and rather balanced properties, its mechanical, chemical, and physical properties are inferior to traditional petroleum-derived polymers. One of the main drawbacks of PLA is its low ductility, with an elongation at break typically lower than 10%, leading to low toughness [23]. To overcome this, different strategies have been proposed. Blending is one of the most interesting alternatives. A wide range of flexible polymers have been blended with PLA with and without compatibilizers, *i.e.* polyurethanes (PUs), polyethylene-*co*-glycidyl methacrylate (PE-*co*-GMA), polyethylene (PE), polypropylene (PP), poly- ϵ -caprolactone (PCL) and polybutylene adipate-*co*-terephthalate (PBAT) [24-27].

A second approach is plasticization. Plasticizers also provide PLA with improved biodegradation properties, as reported by Arrieta *et al.* [28]. Polyethylene glycol (PEG) with different molecular weights has been extensively used as a plasticizer for PLA, as it shows exceptional miscibility [29, 30]. Citrate esters such as triethyl citrate (TEC) and acetyl tributyl citrate (ATBC) have been widely used as plasticizers in PLA formulations, exhibiting excellent ductile properties. Maiza *et al.* [31] reported plasticized PLA formulations with up to 30 wt.% TEC or ATBC with a noticeable decrease in the glass transition temperature (T_g). Adipate esters have also been widely used in PLA plasticization [32].

Recently, new biobased plasticizers for aliphatic polyesters have been proposed, such as those derived from terpenes. Terpenes include a group of natural products that consist of repeated isoprene (C_5H_8) units, while terpenoids are terpenes with additional functional groups (usually oxygen-containing groups). Esterifying alcohol-based terpenoids with carboxylic acids leads to terpenoid esters with increased interest in polyester plasticization. Terpenes and terpenoids are commonly employed as fragrance chemicals in scented products with additional antibacterial and wound-healing properties [33, 34]. Aside from camphor ($C_{10}H_{16}O$), a naturally-occurring terpenoid, which was the first industrial plasticizer, there is little recent literature regarding the potential of terpene-based compounds as environmentally friendly plasticizers. Arrieta *et al.* [35] reported the potential of limonene, a natural terpene, as a biobased plasticizer for PLA, showing great plasticization efficiency.

Moreover, terpenes contain one or more unsaturated carbon-carbon bonds that an organic peroxide can activate. Brüster *et al.* [36] reported the potential of limonene and myrcene as plasticizers for PLA processed by conventional and reactive extrusion (REX), followed by injection moulding. They also concluded that REX is an interesting strategy to obtain balanced plasticization properties without compromising other mechanical properties. Mangeon *et al.* [37] have reported the potential of several terpenoids, namely geraniol (G), linalool (L) and geranyl acetate (GAc), as plasticizers for PHB with an interesting but limited increase in elongation at break. Although terpenes have proved to be suitable plasticizers for PLA, the chemical structure of terpenoids and their derivatives (mainly their esters from different carboxylic acids) suggest they could provide improved plasticization properties to PLA. In this work, for the first time, the high plasticization efficiency of two terpenoid esters, namely linalyl acetate (LAc) and geranyl acetate (GAc), on polylactide (PLA) formulations with improved ductility is reported. Moreover, this research assesses the potential of reactive extrusion (REX) with the terpenoid esters mentioned above to attach the plasticizers

molecules onto the polylactide backbone. Mechanical, thermal, thermomechanical, crystallinity and morphological properties are studied as a function of the plasticizer content and reactive extrusion process. These plasticized-PLA materials could prove to be effective in applications within the packaging sector, for example in the food industry, helping to preserve safety, quality and extending the shelf life of packaged foods during storage and consumption. The plasticizers would increase the ductility of PLA, improving its mechanical properties to produce a more suitable biodegradable packaging product, as those kind of products need sufficient flexibility and resilience [38].

MATERIALS AND METHODS

Materials

PLA from Total Corbion (Gorinchem, The Netherlands) grade PURAPOL L130 with a melt flow index of 16 g/10 min (ISO 1133-A 210 °C/2.16 kg) was employed. Linalyl acetate and geranyl acetate were purchased from Sigma-Aldrich (Steinheim am Albuch, Germany) with CAS numbers 115-95-7 and 105-87-3. Finally, dicumyl peroxide (DCP) was purchased from Sigma-Aldrich (Lyon, France) with a CAS number 80-43-3. The chemical structure of the employed materials is represented in **Figure III.2.3.1**, and the formulations employed in the experiments are summarized in **Table III.2.3.1**.

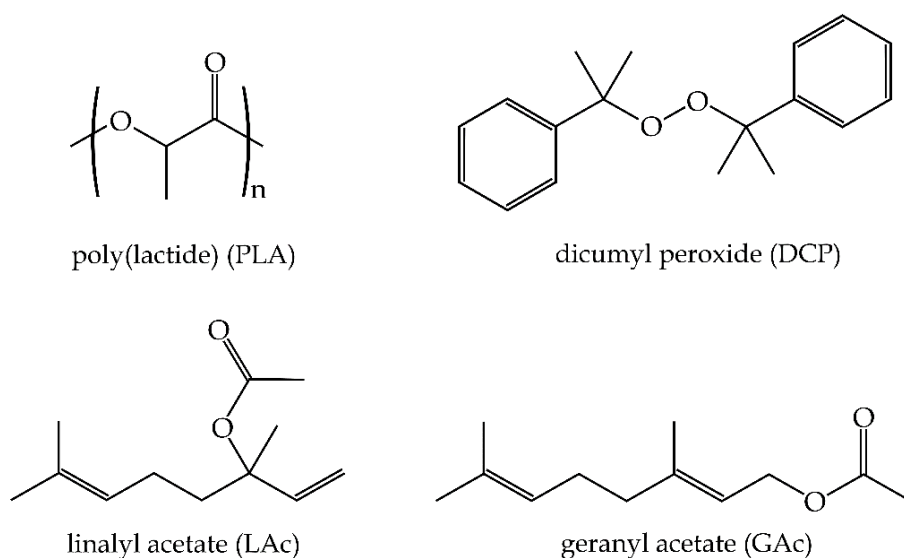


Figure III.2.3.1. Scheme of the chemical structures of polylactide (PLA), terpenoid-based plasticizers, *i.e.* linalyl acetate (LAc) and geranyl acetate (GAc), and free radical initiator, dicumyl peroxide (DCP) for reactive extrusion (REX).

Table III.2.3.1. Composition of plasticized poly(lactide) formulations with terpenoid-based plasticizers processed by conventional and reactive (REX) extrusion.

Code	PLA (wt.%)	Linalyl acetate (Lac) (wt.%)	Geranyl acetate (Gac) (wt.%)	DCP (phr)*
PLA	100			
PLA-10LAc	90	10		
PLA-20LAc	80	20		
PLA-20LAc-DCP	80	20		1
PLA-10GAc	90		10	
PLA-20GAc	80		20	
PLA-20GAc-DCP	80		20	1

*phr stands for parts per hundred resin in the blend

Theoretical framework of PLA/plasticizer solubility

An essential issue in plasticization is the solubility of the selected plasticizer into the polymer matrix. To this end, the group contribution method proposed by Van Krevelen and Hoftyzer was used to calculate the solubility parameter (δ) and its main contributions related to the dispersion and polar forces, represented by δ_d and δ_p , respectively, and the contribution of hydrogen bonding (δ_h). These parameters are related through **Equation III.2.3.1**:

$$\delta = \delta_d^2 + \delta_p^2 + \delta_h^2 \quad (\text{III.2.3.1})$$

As proposed by Van Krevelen and Hoftyzer, the different components of the solubility parameter may be predicted from group contributions as indicated by **Equations III.2.3.2 to III.2.3.4**:

$$\delta_d = \frac{\sum F_{di}}{V} \quad (\text{III.2.3.2})$$

$$\delta_p = \frac{\sqrt{\sum F_{pi}^2}}{V} \quad (\text{III.2.3.3})$$

$$\delta_h = \frac{\sqrt{\sum E_{hi}}}{V} \quad (\text{III.2.3.4})$$

Based on the molar attraction constants, the F-method is rather accurate for predicting the dispersive and polar contributions (δ_d , and δ_p , respectively) as mentioned above. Nevertheless, it does not apply to the hydrogen bonding contribution (δ_h). To this, Hansen indicated that the hydrogen bonding energy (E_{hi}) per structural group is almost constant. By taking into account the structure and the group contribution defined by Van Krevelen and Hoftyzer [39], the solubility parameters and their corresponding components are summarized in **Table III.2.3.2**. **Table III.2.3.2** also includes the R_a values, which stand for the distance between the solubility coordinates of the plasticizer with regard to PLA and have been calculated using **Equation III.2.3.5**.

$$R_a = \sqrt{4 \cdot (\delta_{d_{plast}} - \delta_{d_{PLA}})^2 + (\delta_{p_{plast}} - \delta_{p_{PLA}})^2 + (\delta_{h_{plast}} - \delta_{h_{PLA}})^2} \quad (\text{III.2.3.5})$$

In this equation, the constant $\times 4$ in the first term (meaning doubled values of the dispersion parameter in a 3D plot) was obtained from plots of experimental data to define spherical solubility regions instead of spheroidal. When the distance, R_a , equals zero, the plasticizer and the polymer are thermodynamically very similar, leading to an excellent solubility. As expected, the solubility is reduced as the distance becomes more remarkable. It is widely recognized that above a certain distance, the solubility can be considered negligible. This distance corresponds to the polymer radius (or sphere radius), R_0 , and defines a spherical solubility region of a polymer. The sphere centre corresponds to the polymer's three solubility parameter coordinates, δ_d , δ_p , and δ_h .

The relative energy difference (RED) was calculated by the ratio between the R_a values and the solubility sphere radius for PLA, R_0 , which is $10.7 \text{ MPa}^{1/2}$ (see **Equation III.2.3.6**) [40]. As suggested by **Equation III.2.3.6**, the closer the RED value to zero, the better miscibility between PLA and the considered plasticizer. RED values close to 1 are on the borderline, while RED values above 1 suggest poor miscibility. Brüster *et al.* have reported RED values of 0.93 and 0.99 for limonene and myrcene in PLA-plasticized formulations [36]. Even though the RED values are close to 1, they observed that limonene, with a lower RED value, gave PLA more efficient plasticization than myrcene, which RED value is very close to the solubility borderline.

$$RED = \frac{R_a}{R_0} \quad (\text{III.2.3.6})$$

Table III.2.3.2. Main parameters related to the theoretical approach for the solubility between poly(lactide) and terpenoid-based plasticizers.

Material	δ_d (MPa ^{1/2})	δ_p (MPa ^{1/2})	δ_t (MPa ^{1/2})	δ (MPa ^{1/2})	Ra (MPa ^{1/2})	RED
PLA	15.32	8.44	10.98	20.66	-	
Linallyl acetate (LAc)	15.65	2.25	5.67	16.80	8.18	0.764
Geranyl acetate (GAc)	15.96	2.29	5.72	17.11	8.19	0.765

Processing of plasticized PLA formulations.

PLA pellets were dried at 60 °C for 48 h in a dehumidifying dryer MDEO from Industrial Marsé (Barcelona, Spain). Materials were weighted and premixed before the extrusion process in a co-rotating twin-screw extruder from Construcciones Mecánicas Dupra S.L. (Alicante, Spain) with a 25 mm diameter and a length/diameter ratio of 24. The temperature profile in the four heated zones was 185 °C–180 °C–175 °C–170 °C from the die to the hopper. The residence time was 2 min. Pelletized materials were introduced in an injection moulding machine 270/70 from Mateu&Solé (Barcelona, Spain) with a temperature profile of 190 °C (injection nozzle)–185 °C–180 °C–175 °C (hopper) and a filling time of 1 s. Tensile test samples of 150×40×10 mm³ obtained, as well as impact test samples with dimensions of 80×40×10 mm³.

Mechanical properties of plasticized PLA formulations

Universal testing machine ELIB 50 from S.A.E. Ibertest (Madrid, Spain) was employed to obtain the main tensile properties (ISO 527-2:2012), namely tensile modulus (E), maximum tensile strength (σ_{max}), and the elongation at break (ϵ_b). A 5-kN load cell was used for all tests, and the cross-head speed was set to 20 mm/min. The Shore-D hardness was measured in a 676-D durometer from J. Bot Instruments (Barcelona, Spain) on injection-moulded samples with 4 mm thickness, according to ISO 868:2003. The impact behaviour was measured on injection-moulded rectangular (80×10×4 mm³) subjected to a prior notching type “V-notched” with a radius of 0.25 mm according to ISO 179:2010. A 6-J Charpy pendulum from Metrotec S.A. (San Sebastián, Spain) es used to obtain the impact strength. At least 5 specimens of each plasticized PLA formulations were tested to obtain the main mechanical properties at room temperature; results were averaged, and the standard deviation was calculated.

Morphological properties of plasticized PLA formulations

Morphology of the fractured cross-section of the test samples was analyzed in a field emission scanning electron microscope (FESEM) ZEISS ULTRA 55 from Oxford Instruments (Abingdon, UK), working at an acceleration voltage of 2.5 kV. Before the analysis, a sputtering stage was carried out with gold-palladium alloy under an argon atmosphere in a SC7620 sputter coater from Quorum Technologies Ltd. (East Sussex, UK).

Thermal properties of plasticized PLA formulations

The main thermal properties of the PLA and plasticized PLA formulations were obtained by differential scanning calorimetry (DSC) and thermogravimetry (TGA). The DSC runs allowed obtaining the main thermal transitions (melting peak temperature - T_m , cold crystallization peak temperature - T_{cc}) and the corresponding enthalpies (ΔH_m and ΔH_{cc} , respectively). The maximum degree of crystallinity, χ_{cmax} , was obtained by **Equation III.2.3.7**, where w represents the weight fraction of PLA in the considered formulation, ΔH_m stands for the melting enthalpy, ΔH_{cc} stands for the enthalpy of the cold crystallization transition and ΔH_m^0 stands for the melting enthalpy of a theoretically fully crystalline PLA, which was assumed to have a value of 93 J/g as reported in the literature [41]. The crystallinity related to the cold crystallization process was also calculated by **Equation III.2.3.7** by taking ΔH as the cold crystallization enthalpy (ΔH_{cc}).

$$\chi_c(\%) = \frac{\Delta H_m - \Delta H_{cc}}{\Delta H_m^0 \cdot w} \cdot 100 \quad (\text{III.2.3.7})$$

DSC runs were conducted in a Q2000 DSC from TA Instruments (New Castle, DE, USA) under a nitrogen atmosphere (66 mL/min), and an average sample weight in the 5 - 7.5 mg was used. The thermal cycle consisted of three steps. First, a heating cycle was programmed to remove the thermal history from 30 °C to 200 °C at 10 °C/min. Afterwards, a controlled cooling down to -40 °C at -10 °C/min was scheduled. Finally, a second heating cycle was programmed up to 300 °C at 10 °C/min. The thermal stability of the samples was studied by thermogravimetry (TGA). The onset degradation temperature - $T_{5\%}$ (temperature to reach a mass loss of 5%), the maximum degradation rate temperature - T_{deg} , and the residual weight, were collected from the characteristic TGA thermograms. A TG-DSC2 thermobalance from Mettler-Toledo (Columbus, OH,

USA) was used. Around 6 mg of each formulation were placed into alumina crucibles and subjected to a heating program from 30 °C to 700 °C at 10 °C/min under an air atmosphere. All thermal tests were carried out in triplicate to obtain reliable results.

Thermo-mechanical properties of plasticized PLA formulations

Dynamic mechanical thermal analysis (DMTA) tests were carried out in a Mettler-Toledo DMA1 (Columbus, OH, USA) in a single cantilever mode. Samples with dimensions 20×6×3 mm³ were subjected to a dynamic deformation with an amplitude of 10 μm, while the frequency for the sinusoidal cycles was 1 Hz. Regarding the heating cycle, tests started at -100 °C and samples were heated up to 100 °C with a heating rate of 2 °C/min. Measurements were performed in triplicate.

X-ray diffraction characterization of plasticized PLA formulations

X-ray diffraction patterns were collected at room temperature using a KRISTALLOFLEX K 760-80F x-ray generator at 40 kV and a 40 mA. The radiation from the Cu K α target was nickel filtered ($\lambda = 0.154$ nm). The scattering angles (2θ) ranged from 5° to 70° with a step size of 0.05° and a speed rate of 1°/min. The d -spacing in the crystalline domains of PLA was calculated with Bragg's equation (**Equation III.2.3.8**), where λ is the wavelength of the applied radiation, and θ stands for the peak angle measured.

$$d = \frac{\lambda}{2 \cdot \sin(\theta)} \quad (\text{III.2.3.8})$$

XRD analysis was done on 10×10×10 mm³ samples.

RESULTS AND DISCUSSION

Mechanical properties of plasticized PLA formulations

The incorporation of terpenoids as plasticizers into the PLA polymer matrix has a noticeable effect on the mechanical properties, as observed in **Table III.2.3.3**. Regarding stiffness, the introduction of geranyl acetate (GAc) and linalyl acetate (LAc) promotes a dramatic decrease in the tensile moduli (E), thus suggesting the typical

plasticization phenomenon. While neat PLA shows a relatively high tensile modulus of 3984 MPa, typical of a brittle polymer, this is dramatically reduced to 104 MPa for the plasticized formulation containing 20 wt.% LAc. The addition of plasticizers promotes the enhancement of chain motion. As a result, a decrease in the intensity of Van der Waals forces occurs, and the polymer-polymer interactions are considerably reduced. Typically, this effect gives rise to a decrease in the tensile modulus (E) and the tensile strength (σ_{\max}) [42, 43]. In this work, the tensile strength of neat PLA was reduced from 57.0 MPa to 15-16 MPa for all the plasticized PLA formulations. This reduced interaction between the polymer chains also promotes the enhancement of the elongation at break ($\varepsilon_b\%$) with such high values of 298.4% for the plasticized PLA formulation with 10 wt.% LAc. Neat PLA shows the typical brittle behaviour with very low elongation at break (4.7%). Both terpenoids significantly plasticize PLA, with an increase in elongation at break comparable or even superior to other widely used PLA plasticizers such as PEG, TEC, ATBC, and adipates, among others. Another interesting finding is that $\varepsilon_b\%$ is not improved for plasticized PLA formulations with 20 wt.% plasticizer. This means that plasticizer saturation occurs, as reported by Liu *et al.* [44]. As can be seen in **Table III.2.3.3**, the $\varepsilon_b\%$ for the plasticized PLA formulation with 10 wt.% LAc reaches a value of 298.4%, while an increase to 20 wt.% LAc does not improve $\varepsilon_b\%$ and, on the contrary, is decreased down to 236.0%. In terms of the plasticizing effect obtained by both terpenoid-based plasticizers in this work, LAc provides PLA with higher elongation at break than GAc. Using plasticizers with similar chemical structures at the same concentrations can lead to remarkable changes in plasticized PLA formulations, as reported by Burgos *et al.* [45], in PLA formulations plasticized with three different oligomers of lactic acid (OLAs). In addition to the observed plasticization properties, both terpenoids contain several carbon-carbon double bonds, which could be used to graft the terpenoid-based plasticizer onto the PLA backbone. This can be obtained by reactive extrusion (REX) with an organic peroxide, as reported by Bruester *et al.* [36] in plasticized PLA formulations with limonene and myrcene. Due to the REX process, they obtained increased tensile strength and modulus. At the same time, the elongation at break was reduced, thus suggesting plasticizer anchorage onto PLA polymeric chains after REX with 2,5-bis(*tert*-butylperoxy)-2,5-dimethylhexane. In the present work, dicumyl peroxide (DCP) was used as a free radical initiator during REX in plasticized PLA formulations containing 20 wt.% LAc and GAc. During the reactive extrusion, the dicumyl peroxide decomposes into cumyloxy radicals that tend to abstract protons from the polymer backbone and plasticizers, as reported by Liao *et al.* [46]. They proposed a mechanism for the covalent bonding between tannin acetate (with different acetylation

degrees) and PLA during REX with low amounts of DCP. This consisted in a first stage in which DCP was decomposed by β -scission to the respective free radical. The formed free radicals then could abstract hydrogen from both PLA polymer chains and tannin acetate (from hydroxyl groups and from benzene rings). After this, the recombination of free radicals led to grafting tannin molecules into the PLA backbone, with a subsequent increase in tensile strength and Young's modulus. Similar effects were obtained through REX of PLA-LAc and PLA-GAc in the presence of DCP. It is worthy to note that all tensile properties are increased by REX with DCP in PLA-LAc and PLA-GAc formulations, thus suggesting that REX is an efficient method to improve both resistant and ductile properties on plasticized PLA formulations. **Figure III.2.3.2** shows a schematic representation of the grafting process of terpenoids onto the PLA backbone. In the first stage, the organic peroxide is decomposed by β -scission into free radicals. These free radicals promote hydrogen abstraction from PLA and terpenoid in the second stage. Finally, recombination of the free radicals on PLA and terpenoid, lead to chemical grafting of the terpenoid molecule into the main PLA backbone.

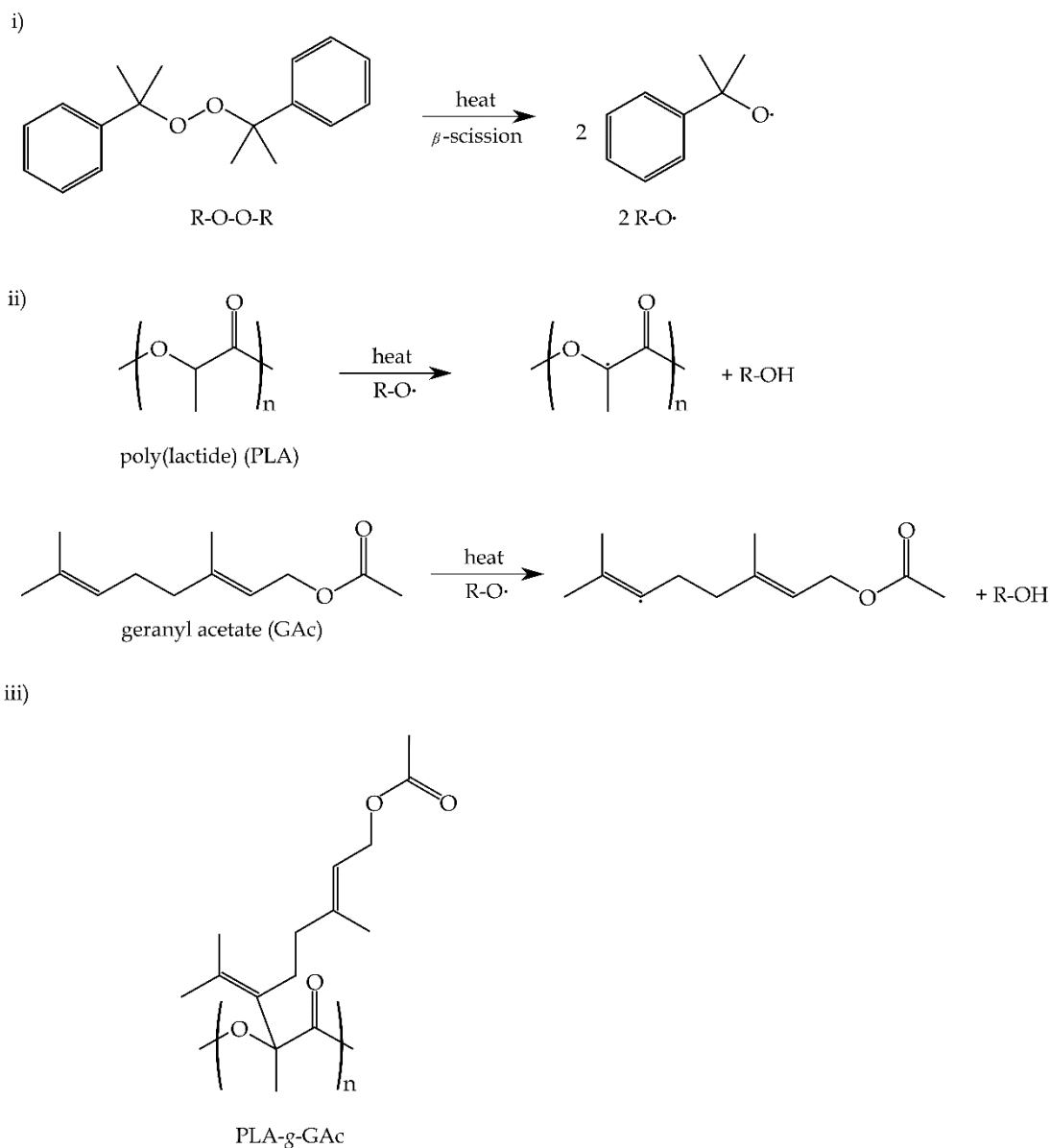


Figure III.2.3.2. Schematic representation of the plausible reactions occurring during REX of PLA and terpenoids in presence of dicumyl peroxide (DCP).

This behaviour was also observed in Shore D hardness values. The incorporation of LAc and GAc remarkably reduces the initial Shore D hardness of PLA (80.2) to such low values of 65. A clear decreasing tendency can be detected with increasing LAc and GAc content in plasticized PLA formulations. As expected, REX with DCP provided slightly higher Shore D hardness values for both terpenoids used in this research, thus supporting the hypothesis of somewhat anchorage of LAc and GAc molecules onto the PLA backbone by grafting.

Table III.2.3.3. Mechanical properties of PLA and plasticized PLA formulations with terpenoids in terms of tensile modulus (E), maximum tensile strength (σ_{max}), elongation at break (ϵ_b), Shore D hardness.

Code	E (MPa)	σ_{max} (MPa)	ϵ_b (%)	Shore D
PLA	3984 ± 56	57.0 ± 1.0	4.7 ± 0.4	80.2 ± 1.6
PLA-10LAc	1347 ± 42	15.9 ± 1.3	298.4 ± 4.6	70.5 ± 2.1
PLA-20LAc	104 ± 7	14.2 ± 0.6	236.0 ± 7.7	65.2 ± 0.9
PLA-20LAc-DCP	362 ± 13	16.2 ± 0.5	253.4 ± 6.5	68.6 ± 1.5
PLA-10GAc	1579 ± 55	16.2 ± 0.3	239.8 ± 6.7	70.1 ± 1.2
PLA-20GAc	193 ± 12	14.5 ± 0.4	215.0 ± 9.4	65.4 ± 1.4
PLA-20GAc-DCP	404 ± 24	16.6 ± 0.4	230.7 ± 7.0	67.8 ± 0.8

Morphological properties of plasticized PLA formulations with terpenoids

The surface morphology obtained after the fracture of the samples in the tensile test was analyzed by field-emission scanning electron microscopy (FESEM). The results are shown in **Figure III.2.3.3**. The obtained structure changed from a flat surface observed for neat PLA (**Figure III.2.3.3a**), representative of a typical brittle fracture, to a rough surface resulting from plastic deformation, representative of a ductile fracture. As observed in **Table III.2.3.3**, the highest value of elongation at break observed in the tensile test was obtained for the PLA-10LAc formulation. This effect was reflected in the surface morphology with the highest roughness with the formation of filament-like structures during fracture (**Figure III.2.3.3c**), as reported by Arrieta *et al.* in plasticized PLA formulations with limonene [35]. Although the elongation at break is not improved for plasticized formulations containing 20 wt.% of LAc or GAc, which could suggest plasticizer saturation, this phenomenon was not observed by FESEM since phase separation was not detected. As mentioned above, the solubility parameters of PLA, LAc and GAc suggest good solubility between them, which was confirmed by relative energy difference (RED) values lower than 1. Lundberg *et al.*, have reported phase separation phenomena in plasticized PLA films with oligomers of tributyl citrate (TBC). They observed that as the molecular weight of oligomers increased, the saturation threshold was reduced to values of 10-15 wt.%. They did not observe phase separation with TBC.

In contrast, a clear phase separation phenomenon was detected in plasticized PLA formulations containing TBC oligomers (TBC-3 and TBC-7 with molecular weights of 980 and 2240 g/mol, respectively). So, although the elongation at break of PLA-20LAc and PLA-20GAc does not increase with respect to lower plasticizer content formulations,

phase separation does not occur due to good miscibility and low molecular weight. As reported by Rojas-Lema *et al.* [47], phase separation is more common in polymer blends due to the high molecular weight of polymers.

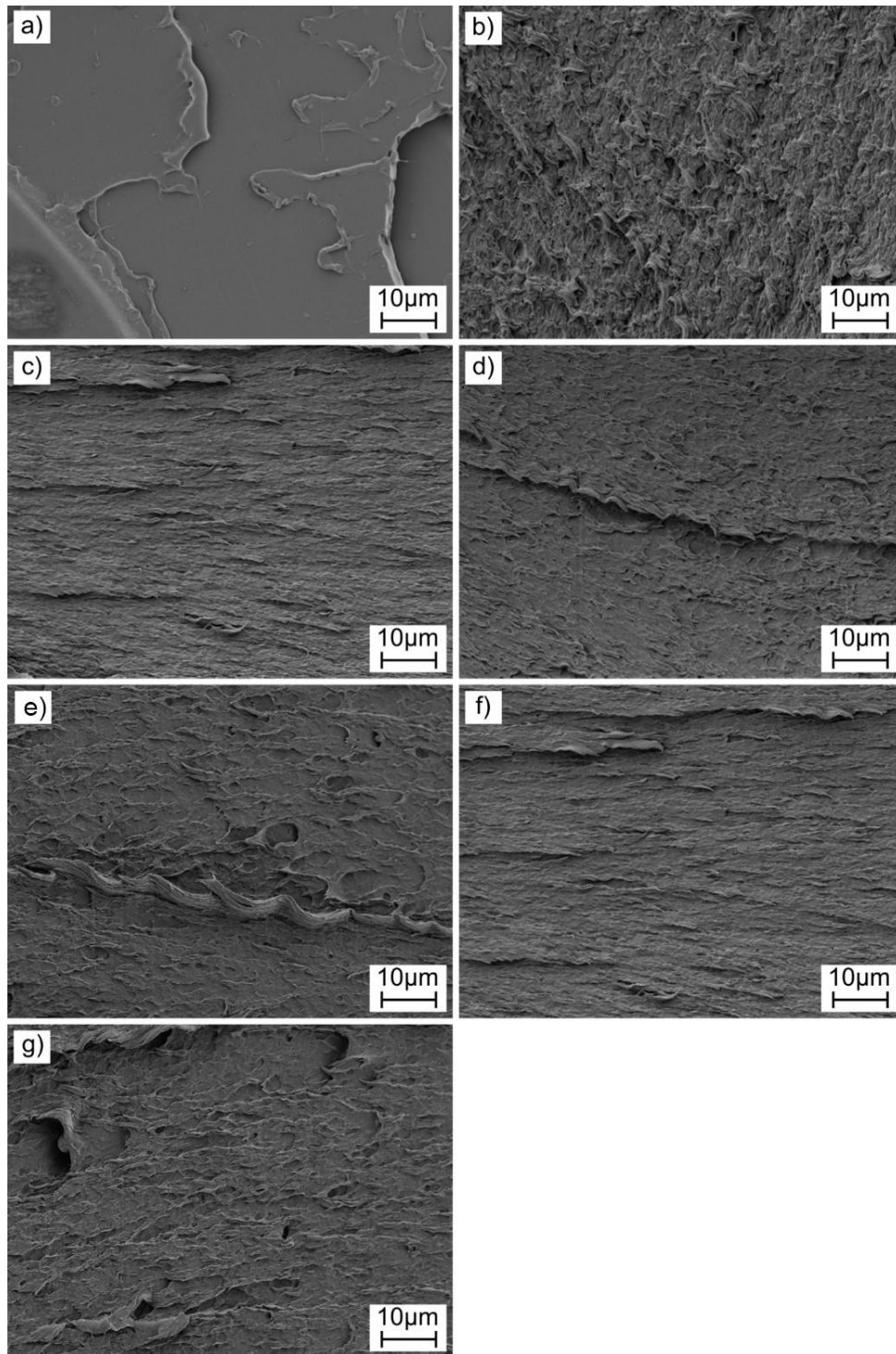


Figure III.2.3.3. Field-emission scanning electron microscopy (FESEM) images of the fractured samples from the tensile tests at 1000 \times . a) PLA; b) PLA-10LAc; c) PLA-20LAc; d) PLA-20LAc-DCP; e) PLA-10GAc; f) PLA-20GAc and g) PLA-20GAc-DCP. Scale bar 10 μ m.

Thermal properties of plasticized PLA formulations with terpenoids

The main thermal transitions of the PLA and plasticized PLA formulations with LAc and GAc were measured by differential scanning calorimetry (DSC). **Figure III.2.3.4** shows the corresponding thermograms, while **Table III.2.3.4** summarizes the main thermal parameters. After removing the thermal history in the first heating cycle, **Figure III.2.3.4** gathers the DSC thermograms corresponding to the second heating cycle. The glass transition temperature of neat PLA is 61.5 °C. This is moved down to values of 50.4 °C and 39.5 °C with 10 wt.% and 20 wt.% LAc, respectively, thus showing excellent plasticization efficiency. A similar tendency can be observed for plasticized PLA with GAc, despite the characteristic T_g values being slightly higher than those obtained with LAc. These values are similar to those reported by Maiza *et al.* [32], in plasticized PLA formulations with citrate esters, which indicates the exceptional plasticization effects of LAc and GAc compared to the widely used PLA plasticizers based on citrate esters such as TEC and ATBC. As it can be seen in **Table III.2.3.4**, the lowest T_g values are obtained with 20 wt.% LAc. These results are very interesting because they suggest a clear decreasing tendency of T_g , even though they are not reflected in increased elongation at break in plasticized formulations with 20 wt.% LAc or GAc. The T_g values obtained by REX with DCP are slightly higher than those obtained by conventional extrusion. This confirms the grafting of terpenoids onto the PLA backbone, which hinders chain motion and, subsequently, an increase in T_g . Similar behaviour can be observed for the cold crystallization temperature (T_{cc}). Both plasticizers provide increased chain mobility due to the internal lubricity effect; consequently, the cold crystallization is moved to lower temperatures. Neat PLA shows a cold crystallization peak temperature, T_{cc} , of 139.9 °C, and this is remarkably shifted down to values of 90 °C in formulations with 20 wt.% LAc and GAc. These results are in agreement with those reported by Chieng *et al.* [52] in plasticized PLA formulations with 10 wt.% PEG with a decrease in T_{cc} by 50 °C regarding neat PLA. In this study, a remarkable decrease of almost 40 °C is obtained with 10 wt.% LAc. As mentioned above, the plasticizer enhances reduced interactions between polymer chains, thus leading to increase chain mobility. Accordingly, the cold crystallization peak temperature is moved to lower values. Moreover, as the chain mobility increases, the tendency of PLA polymeric chains are more readily to pack [43], and this is reflected by a noticeable increase in the cold crystallization enthalpy (ΔH_{cc}) that changes from 3.0 J/g for neat PLA up to values of 29.1 J/g for the PLA formulation containing 10 wt.% LAc. A similar increase in ΔH_{cc} has been reported by Xiao *et al.* [53], in plasticized PLA formulations with triphenyl phosphate (TPP) as plasticizer. The degree of crystallinity (χ_{cmax}) was calculated by **Equation III.2.3.7**. This parameter is

higher than PLA for all compositions. This is ascribed to improved segmental molecular mobility, as suggested by Clarkson *et al.* [48], in plasticized PLA formulations with PEG with the aid of nucleants derived from nanocelluloses. Another interesting finding is that much of this value corresponds to the cold crystallization process. Similar results have been reported by Xiao *et al.* [53] in plasticized PLA formulations with TPP plasticizer. The effect of the REX with DCP is also evident in T_{cc} . As expected, terpenoid grafting hinders chain mobility, and, subsequently, a noticeable increase in T_{cc} is also observed.

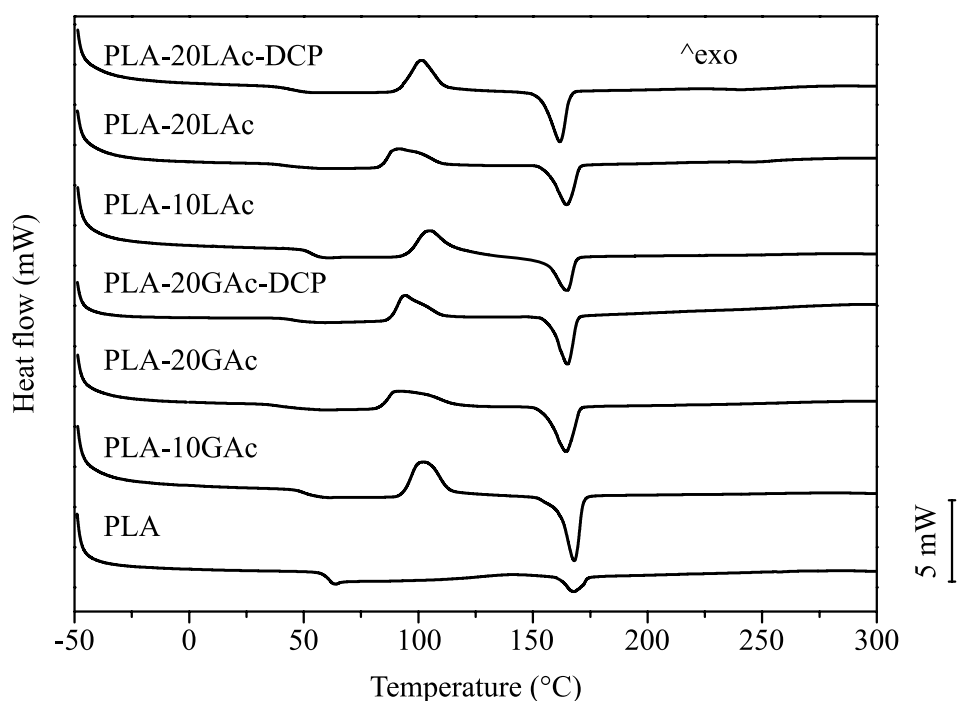


Figure III.2.3.4. Differential scanning calorimetry (DSC) thermograms of neat PLA and plasticized PLA formulations with terpenes by conventional and reactive extrusion, corresponding to the second heating cycle after removing thermal history.

Table III.2.3.4. Summary of the DSC results for the PLA/terpene formulations: glass transition temperature (T_g), cold crystallization temperature (T_{cc}), melting temperature (T_m), cold crystallization enthalpy (ΔH_{cc}), melting enthalpy (ΔH_m) and degree of crystallinity (χ_c).

Code	T_g (°C)	T_{cc} (°C)	T_m (°C)	ΔH_{cc} (J/g)	ΔH_m (J/g)	χ_c (%)
PLA	61.5 ± 0.5	139.9 ± 1.1	160.1 ± 1.2	3.0 ± 0.2	5.5 ± 0.3	2.7 ± 0.1
PLA-10LAc	50.4 ± 0.4	101.2 ± 1.3	161.0 ± 1.5	29.1 ± 0.8	34.3 ± 0.9	6.2 ± 0.2
PLA-20LAc	39.5 ± 0.3	90.4 ± 1.1	160.8 ± 1.4	27.7 ± 0.7	36.1 ± 0.8	11.3 ± 0.5
PLA-20LAc-DCP	45.3 ± 0.4	93.3 ± 1.0	163.1 ± 1.2	23.4 ± 0.7	29.7 ± 0.8	8.5 ± 0.1
PLA-10GAc	53.3 ± 0.3	103.6 ± 1.5	164.1 ± 1.0	15.2 ± 0.6	22.5 ± 0.7	8.7 ± 0.1
PLA-20GAc	42.2 ± 0.5	90.7 ± 1.4	163.5 ± 1.2	21.0 ± 0.5	28.5 ± 0.6	10.1 ± 0.1
PLA-20GAc-DCP	43.9 ± 0.5	101.1 ± 1.3	161.7 ± 0.8	27.1 ± 1.2	30.9 ± 0.9	5.1 ± 0.1

Additionally, the samples' thermal stability was measured by thermogravimetric analysis (TGA); the results are represented in **Figure III.2.3.5** and **Table III.2.3.5**. The thermal degradation of PLA occurred in a single step due to the chain scission with a maximum degradation rate temperature located at 373.8 °C [49]. The introduction of the plasticizer reduced the thermal stability of the plasticized PLA formulations due to the lower molecular weight of the terpenoid-based plasticizer. The temperature at which a mass loss of 5 wt.% occurs ($T_{5\%}$), changes from 333.2 °C to approximately 292 °C and 232 °C for the plasticized formulations with 10 wt.% and 20 wt.%, respectively of both LAc and GAc. Chieng *et al.* [52] observed a similar tendency in plasticized PLA formulations with low molecular weight PEG (200 g/mol). They reported a decrease in $T_{5\%}$ from 274.26 °C to 194.50 °C for a PEG-200 content of 10 wt.%. As the PEG-200 content increased, $T_{5\%}$ was proportionally reduced. In this study, LAc and GAc have the same molecular weight of 196.29 g/mol, and they provide an excellent plasticization effect on PLA, as demonstrated by tensile properties. Nevertheless, $T_{5\%}$ is reduced by 41 °C and 100 °C for LAc and GAc contents of 10 wt.% and 20 wt.%, respectively. From these results, the plasticized PLA formulations with 10 wt.% of either LAc or GAc seem to offer the best-balanced performance since the plasticization properties are exceptional and the degradation temperature is not remarkably reduced. This same behaviour has been reported by Maiza *et al.* [32] in plasticized PLA with TEC and ATBC, which are widely used as environmentally friendly plasticizers for PLA. For a 10 wt.% of TEC ($M_w=276.283$ g/mol) and ATBC ($M_w=402.484$ g/mol), the $T_{5\%}$ was reduced from 348.94 °C (neat PLA) down to 303.54 °C and 313.63 °C, respectively. Therefore, the degradation temperatures obtained with LAc and GAc are comparable to those obtained with TEC and ATBC, thus suggesting similar performance. The maximum degradation rate of the

formulations was similar to that of neat PLA. This was ascribed to independent degradation processes. Arrieta *et al.* [35] reported excellent plasticization properties in limonene-PLA films, but the onset degradation temperature (at a mass loss of 1%) was dramatically reduced from 322 °C to 109 °C for a plasticized formulation with 15 wt.% limonene, which is much volatile than the terpenoids used in this work due to its lower molecular weight.

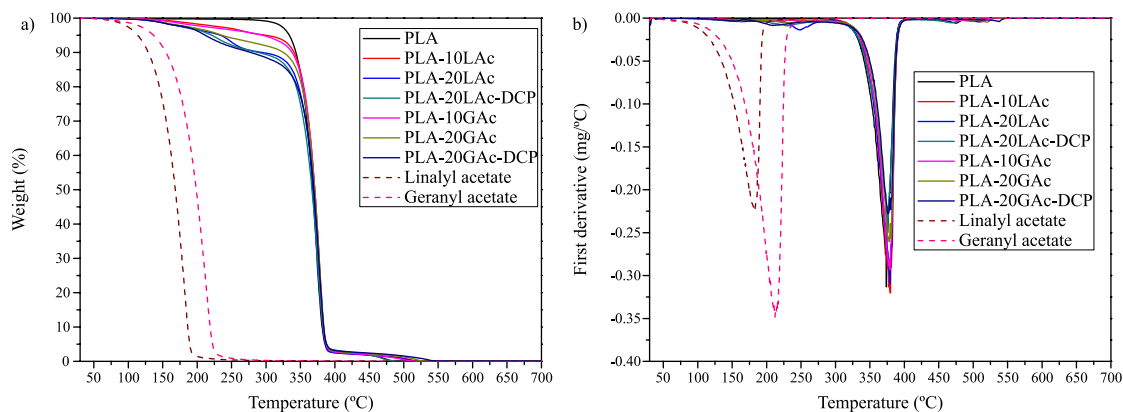


Figure III.2.3.5. Thermogravimetric (TGA) behaviour for the PLA/terpene formulations in terms of a) mass loss and b) first derivative of neat PLA and plasticized PLA formulations with terpenes by conventional and reactive extrusion.

Table III.2.3.5. Summary of the TGA results for the PLA/terpene formulations: initial temperature degradation at 5 wt.% loss ($T_{5\%}$), maximum rate degradation temperature (T_{deg}) and residual weight.

Code	$T_{5\%}$ (°C)	T_{deg} (°C)
PLA	333.2 ± 1.2	373.8 ± 1.0
PLA-10LAc	292.2 ± 1.2	379.2 ± 1.2
PLA-20LAc	232.5 ± 1.1	378.7 ± 1.3
PLA-20LAc-DCP	218.1 ± 1.3	376.4 ± 1.1
PLA-10GAc	292.5 ± 1.0	378.3 ± 1.4
PLA-20GAc	232.4 ± 0.9	377.8 ± 1.2
PLA-20GAc-DCP	209.7 ± 0.8	377.2 ± 1.0

Thermo-mechanical properties of plasticized PLA formulations with terpenoids

The thermomechanical properties of the terpenoid-plasticized PLA formulations were measured through dynamic-mechanical thermal analysis (DMTA). In **Figure**

III.2.3.6a, the storage modulus of the samples with increasing temperature is shown, while **Figure III.2.3.6b** gathers the evolution of the dynamic damping factor ($\tan \delta$) as a function of temperature of all developed formulations. The storage modulus, E' , for neat PLA shows three different regions. Below 50 °C the storage modulus is almost constant. In the temperature range comprised between 55–75 °C, a dramatic decrease in E' (three-fold) occurs. This is associated with the glass transition region. After this, a plateau region with low E' values is observed and, finally, an increase in E' is observed in the temperature range of 80–90 °C, which is attributable to the cold crystallization process since this increase in crystallinity involves an increase in stiffness. As expected from DSC results, as the LAc and GAc content increases, the glass transition region and the cold crystallization process remarkably shift to lower temperatures due to increased segment chain motions. Another interesting finding is that the glass transition in neat PLA takes a very narrow temperature range, while this temperature range is broader for all plasticized formulations, as it can be seen in **Figure III.2.3.6b**. **Table III.2.3.6** summarizes some interesting parameters obtained by DMTA characterization. By taking the T_g as the peak temperature of the dynamic damping factor, a clear decreasing tendency is observed from 63 °C to 46.3 °C and 39.9 °C for the plasticized formulation with 10 wt.% and 20 wt.% LAc, respectively, thus corroborating the DSC results mentioned above. Similar T_g values are obtained for the plasticized system with GAc. As expected, REX with DCP provides a slight increase in T_g due to the grafting of terpenoids onto the PLA backbone, which restricts chain motion. Concerning the dynamic damping factor, the peak height is reduced, as observed in **Figure III.2.3.6b**. Moreover, it can also be observed that the $\tan \delta$ peak is broader with increasing plasticizer content. This phenomenon was attributed to the fact that plasticized formulations have a wide range of relaxation times. Plasticizers have been reported to change the microheterogeneity of the plasticized PLA formulations with different compositions and interactions. In particular, hydrogen bonding and interactions with oxygen atoms in plasticizer esters are responsible for this peak broadening. Shi *et al.* [50] also reported this peak broadening by adding different amounts of PEG into PLA formulations.

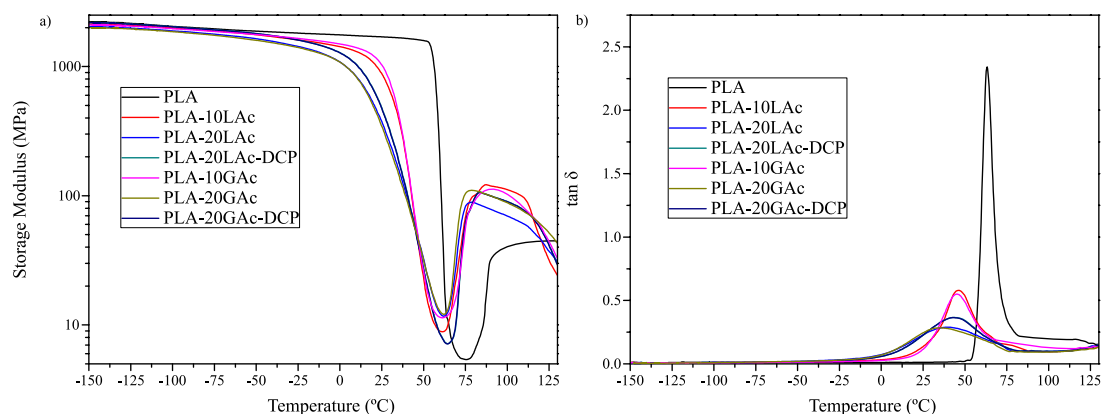


Figure III.2.3.6. Dynamic-mechanical thermal analysis (DMTA) behaviour of neat PLA and plasticized PLA formulations with terpenes by conventional and reactive extrusion. a) storage modulus *vs* temperature and b) dynamic damping factor ($\tan \delta$) *vs* temperature.

Table III.2.3.6. Summary of the DMTA properties for the PLA/terpene formulations in terms of: storage modulus (E') and glass transition temperature (T_g).

Code	E' at -20°C (MPa)	E' at 25°C (MPa)	T_g ($^\circ\text{C}$)
PLA	1814 ± 20	1698 ± 24	63.0 ± 0.5
PLA-10LAc	1605 ± 15	887 ± 10	46.3 ± 0.4
PLA-20LAc	1432 ± 11	376 ± 8	39.9 ± 0.4
PLA-20LAc-DCP	1605 ± 17	478 ± 6	43.5 ± 0.6
PLA-10GAc	1647 ± 18	1011 ± 17	45.8 ± 0.5
PLA-20GAc	1402 ± 25	345 ± 15	39.4 ± 0.5
PLA-20GAc-DCP	1610 ± 20	466 ± 9	43.1 ± 0.4

X-ray diffraction properties of plasticized PLA formulations with terpenoids

The measured X-Ray diffraction pattern of the plasticized PLA formulations are presented in **Figure III.2.3.7**, and the main parameters obtained from XRD are gathered in **Table III.2.3.7**. The main diffraction peak of the semicrystalline PLA is located at $2\theta=16.35^\circ$. This peak corresponds to diffraction planes (110)/(200) and α -type crystals [51, 52]. According to Bragg's equation, the distances between planes (d -spacing) were obtained. Very small changes in diffraction angles could be detectable, as seen in **Table III.2.3.7**. The introduction of plasticizers, as mentioned above, enhanced the crystallization ability of PLA chains. As a result of the rearrangement of the polymer chains, the structure packs into a more compact structure that reduces the d -spacing between the crystalline planes [53]. Another phenomenon after plasticization with LAc

and GAc is the increase of the d -spacing due to the placement of plasticizer molecules between the crystalline planes [54]. In this work, both phenomena occur, but they are overlapped, so the differences in the crystalline structure between neat PLA and the plasticized formulations with LAc and GAc are very small. The peak height is directly related to the degree of crystallinity. Therefore, as previously observed by DSC, neat PLA shows the lowest XRD peak height while this peak height is increased with increasing plasticizer content [55]. The introduction of terpenoid-based plasticizers resulted in an enhanced degree of crystallization.

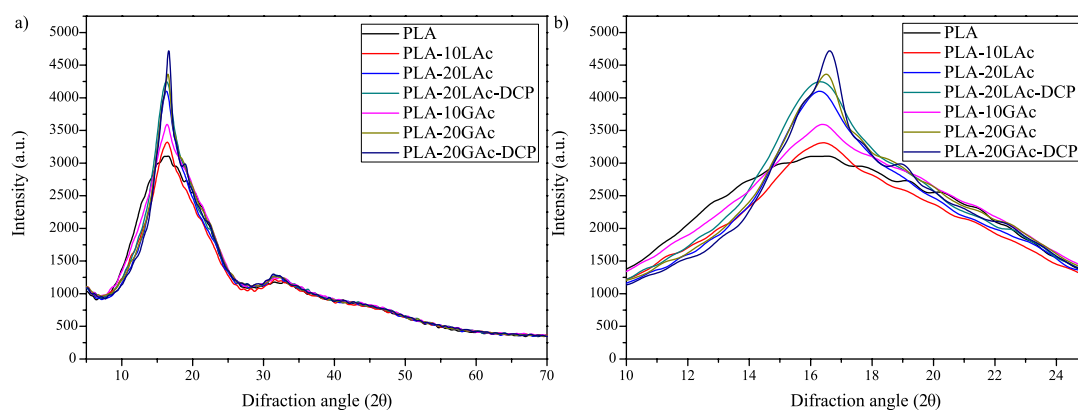


Figure III.2.3.7. X-ray patterns of neat PLA and plasticized PLA formulations with terpenes by conventional and reactive extrusion.

Table III.2.3.7. Summary of X-ray diffraction patterns (XRD) of neat PLA and plasticized PLA formulations with terpenes by conventional and reactive extrusion, in terms of the diffraction angle peak and d -spacing.

Code	2θ ($^{\circ}$)	d -spacing (nm)
PLA	16.35	0.542
PLA-10LAc	16.40	0.540
PLA-20LAc	16.30	0.543
PLA-20LAc-DCP	16.35	0.542
PLA-10GAc	16.40	0.540
PLA-20GAc	16.50	0.537
PLA-20GAc-DCP	16.60	0.533

CONCLUSIONS

Two terpenoids, namely linalyl acetate (LAc) and geranyl acetate (GAc), have proved to provide exceptional plasticization properties to poly(lactide) (PLA). In terms

of mechanical properties, plasticized PLA formulations with 10 wt.% LAc offered the most remarkable improvement in elongation at break from 4.7% to 298.4%, which is 62.5 times much higher. The performance of these terpenoids is comparable, or even superior, to other conventional plasticizers for PLA, such as citrate esters, adipates and poly(ethylene glycol). These terpenoids have a solubility parameter close to that of PLA, which was reflected in low (<1) relative energy dispersion (RED) values which suggested good miscibility. Thermal characterization by differential scanning calorimetry (DSC) revealed a remarkable decrease in the glass transition temperature from 61.5 °C to such low values of 39.5 °C for the plasticized formulation containing 10 wt.% LAc. Moreover, due to the particular structure of both terpenoids with several carbon-carbon double bonds, reactive extrusion (REX) with an organic peroxide, namely dicumyl peroxide (DCP), provides some grafting of the terpenoid molecules onto the PLA backbone. This phenomenon was confirmed by an increase in tensile strength (from values close to 14 MPa up to 16 MPa) and Young's modulus (from values around 200 MPa up to values near 400 MPa) and a slight increase in T_g compared to the respective formulation processed by conventional extrusion. Additionally, TGA results showed a clear decrease in $T_{5\%}$ for the plasticized samples, especially in the case with higher proportion of plasticizer (20 wt.%). This value decreased from a value of 300 °C for neat PLA down to approximately 210 °C for the plasticized samples. All in all, this research offers alternative plasticizers for environmentally friendly PLA formulations.

ACKNOWLEDGEMENTS

J. Gomez-Caturla wants to thank grant FPU20/01732 funded by MCIN/AEI/10.13039/501100011033 and by ESF Investing in your future. J. Ivorra-Martinez wants to thank FPU19/01759 grant funded by MCIN/AEI/10.13039/501100011033 and by ESF Investing in your future. R. Tejada-Oliveros wants to thank Universitat Politècnica de València for the grant received through the PAID-01-20 program. Microscopy Services at UPV are also acknowledged for their help in collecting and analyzing images.

FUNDING

This research is a part of the grant PID2020-116496RB-C22 funded by MCIN/AEI/10.13039/501100011033 and the project AICO/2021/025 funded by Generalitat Valenciana-GVA.

REFERENCES

- [1] Jem, K.J. and B. Tan, *The development and challenges of poly (lactic acid) and poly (glycolic acid)*. *Advanced Industrial and Engineering Polymer Research*, 2020. 3(2): 60-70.
- [2] Ramesh, P. and S. Vinodh, *State of art review on Life Cycle Assessment of polymers*. *International Journal of Sustainable Engineering*, 2020. 13(6): 411-422.
- [3] Winnacker, M. and B. Rieger, *Biobased Polyamides: Recent Advances in Basic and Applied Research*. *Macromolecular Rapid Communications*, 2016. 37(17): 1391-1413.
- [4] Zhang, C., S.A. Madbouly, and M.R. Kessler, *Biobased Polyurethanes Prepared from Different Vegetable Oils*. *Acs Applied Materials & Interfaces*, 2015. 7(2): 1226-1233.
- [5] Siracusa, V. and I. Blanco, *Bio-Polyethylene (Bio-PE), Bio-Polypropylene (Bio-PP) and Bio-Poly(ethylene terephthalate) (Bio-PET): Recent Developments in Bio-Based Polymers Analogous to Petroleum-Derived Ones for Packaging and Engineering Applications*. *Polymers*, 2020. 12(8): 1641.
- [6] Yang, Z., et al., *Cost-Effective Synthesis of High Molecular Weight Biobased Polycarbonate via Melt Polymerization of Isosorbide and Dimethyl Carbonate*. *Acs Sustainable Chemistry & Engineering*, 2020. 8(27): 9968-9979.
- [7] Tsiropoulos, I., et al., *Life cycle impact assessment of bio-based plastics from sugarcane ethanol*. *Journal of Cleaner Production*, 2015. 90: 114-127.
- [8] Shen, L. and M.K. Patel, *Life Cycle Assessment of Polysaccharide Materials: A Review*. *Journal of Polymers and the Environment*, 2008. 16(2): 154-167.
- [9] Valdes, A., et al., *Natural Pectin Polysaccharides as Edible Coatings*. *Coatings*, 2015. 5(4): 865-886.
- [10] Abedini, F., et al., *Overview on natural hydrophilic polysaccharide polymers in drug delivery*. *Polymers for Advanced Technologies*, 2018. 29(10): 2564-2573.
- [11] Song, F., et al., *Biodegradable Soy Protein Isolate-Based Materials: A Review*. *Biomacromolecules*, 2011. 12(10): 3369-3380.
- [12] Kowalczyk, T., et al., *Elastin-like polypeptides as a promising family of genetically-engineered protein based polymers*. *World Journal of Microbiology & Biotechnology*, 2014. 30(8): 2141-2152.

- [13] Rojas-Lema, S., *et al.*, "Faba bean protein films reinforced with cellulose nanocrystals as edible food packaging material". *Food Hydrocolloids*, 2021. 121: 107019.
- [14] Montalvo-Paquini, C., *et al.*, *Preparation and Characterization of Proteinaceous Films from Seven Mexican Common Beans (Phaseolus vulgaris L.)*. *Journal of Food Quality*, 2018. 2018.
- [15] Pallos, F.M., *et al.*, *Thermoformed wheat gluten biopolymers*. *Journal of Agricultural and Food Chemistry*, 2006. 54(2): 349-352.
- [16] Mozejko-Ciesielska, J. and R. Kiewisz, *Bacterial polyhydroxyalkanoates: Still fabulous?* *Microbiological Research*, 2016. 192: 271-282.
- [17] Rehm, B.H.A., *Bacterial polymers: biosynthesis, modifications and applications*. *Nature Reviews Microbiology*, 2010. 8(8): 578-592.
- [18] Seyednejad, H., *et al.*, *Functional aliphatic polyesters for biomedical and pharmaceutical applications*. *Journal of Controlled Release*, 2011. 152(1): 168-176.
- [19] Xu, J. and B.-H. Guo, *Poly(butylene succinate) and its copolymers: Research, development and industrialization*. *Biotechnology Journal*, 2010. 5(11): 1149-1163.
- [20] Woodruff, M.A. and D.W. Hutmacher, *The return of a forgotten polymer- Polycaprolactone in the 21st century*. *Progress in Polymer Science*, 2010. 35(10): 1217-1256.
- [21] Budak, K., O. Sogut, and U.A. Sezer, *A review on synthesis and biomedical applications of polyglycolic acid*. *Journal of Polymer Research*, 2020. 27: 1-19.
- [22] Robert, J.L. and K.B. Aubrecht, *Ring-opening polymerization of lactide to form a biodegradable polymer*. *Journal of Chemical Education*, 2008. 85(2): 258-260.
- [23] Razavi, M. and S.-Q. Wang, *Why Is Crystalline Poly(lactic acid) Brittle at Room Temperature?* *Macromolecules*, 2019. 52(14): 5429-5441.
- [24] Zhao, X., *et al.*, *Super tough poly(lactic acid) blends: a comprehensive review*. *Rsc Advances*, 2020. 10(22): 13316-13368.
- [25] Fortelny, I., *et al.*, *Phase Structure, Compatibility, and Toughness of PLA/PCL Blends: A Review*. *Frontiers in Materials*, 2019. 6: 206.
- [26] Moradi, S. and J.K. Yeganeh, *Highly toughened poly(lactic acid) (PLA) prepared through melt blending with ethylene-co-vinyl acetate (EVA) copolymer and simultaneous addition of hydrophilic silica nanoparticles and block copolymer compatibilizer*. *Polymer Testing*, 2020. 91: 106735.

- [27] Quiles-Carrillo, L., *et al.*, *Ductility and Toughness Improvement of Injection-Molded Compostable Pieces of Polylactide by Melt Blending with Poly(epsilon-caprolactone) and Thermoplastic Starch*. *Materials*, 2018. 11(11): 2138.
- [28] Arrieta, M.P., *Influence of plasticizers on the compostability of polylactic acid*. *Journal of Applied Research in Technology & Engineering*, 2021. 2(1): 1-9.
- [29] Li, D., *et al.*, *Preparation of plasticized poly (lactic acid) and its influence on the properties of composite materials*. *Plos One*, 2018. 13(3): e0193520.
- [30] Athanasoulia, I.-G. and P.A. Tarantili, *Preparation and characterization of polyethylene glycol/poly(L-lactic acid) blends*. *Pure and Applied Chemistry*, 2017. 89(1): 141-152.
- [31] Maiza, M., M.T. Benaniba, and V. Massardier-Nageotte, *Plasticizing effects of citrate esters on properties of poly(lactic acid)*. *Journal of Polymer Engineering*, 2016. 36(4): 371-380.
- [32] Tsou, C.-H., *et al.*, *Preparation and characterization of poly(lactic acid) with adipate ester added as a plasticizer*. *Polymers & Polymer Composites*, 2018. 26(8-9): 446-453.
- [33] Guimaraes, A.C., *et al.*, *Antibacterial Activity of Terpenes and Terpenoids Present in Essential Oils*. *Molecules*, 2019. 24(13): 2471.
- [34] Barreto, R.S.S., *et al.*, *A Systematic Review of the Wound-Healing Effects of Monoterpenes and Iridoid Derivatives*. *Molecules*, 2014. 19(1): 846-862.
- [35] Arrieta, M.P., *et al.*, *Characterization of PLA-limonene blends for food packaging applications*. *Polymer Testing*, 2013. 32(4): 760-768.
- [36] Bruester, B., *et al.*, *Plasticization of Polylactide with Myrcene and Limonene as Bio-Based Plasticizers: Conventional vs. Reactive Extrusion*. *Polymers*, 2019. 11(8): 1363.
- [37] Mangeon, C., *et al.*, *Natural Terpenes Used as Plasticizers for Poly(3-hydroxybutyrate)*. *Acs Sustainable Chemistry & Engineering*, 2018. 6(12): 16160-16168.
- [38] Farah, S., D.G. Anderson, and R. Langer, *Physical and mechanical properties of PLA, and their functions in widespread applications – A comprehensive review*. *Advanced drug delivery reviews*, 2016. 107: 367-392.
- [39] Van Krevelen, D.W. and K. Te Nijenhuis, *Properties of polymers: their correlation with chemical structure; their numerical estimation and prediction from additive group contributions*. 2009: Elsevier.

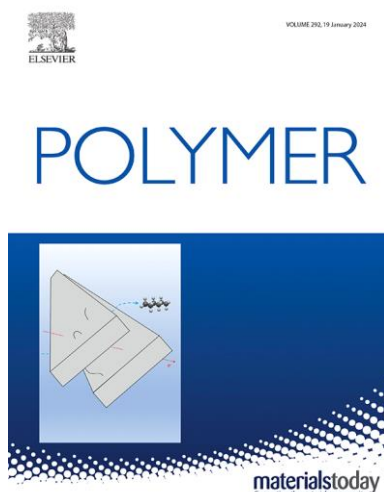
- [40] Abbott, S., *Chemical compatibility of poly (lactic acid): A practical framework using Hansen solubility parameters*. Poly (Lactic Acid) Synthesis, Structures, Properties, Processing, and Applications, 2010: 83-95.
- [41] Gomez-Caturla, J., et al., *Improvement of Poly (lactide) Ductile Properties by Plasticization with Biobased Tartaric Acid Ester*. Macromolecular Materials and Engineering, 2023. 308(7): 2200694.
- [42] Llanes, L.C., et al., *Mechanical and thermal properties of poly(lactic acid) plasticized with dibutyl maleate and fumarate isomers: Promising alternatives as biodegradable plasticizers*. European Polymer Journal, 2021. 142: 110112.
- [43] Ge, H., et al., *Thermal, mechanical, and rheological properties of plasticized poly(L-lactic acid)*. Journal of Applied Polymer Science, 2013. 127(4): 2832-2839.
- [44] Liu, H. and J. Zhang, *Research progress in toughening modification of poly(lactic acid)*. Journal of Polymer Science, Part B: Polymer Physics, 2011. 49(15): 1051-1083.
- [45] Burgos, N., et al., *Synthesis and Characterization of Lactic Acid Oligomers: Evaluation of Performance as Poly(Lactic Acid) Plasticizers*. Journal of Polymers and the Environment, 2014. 22(2): 227-235.
- [46] Liao, J., et al., *Interfacial improvement of poly (lactic acid)/tannin acetate composites via radical initiated polymerization*. Industrial Crops and Products, 2021. 159: 113068.
- [47] Rojas-Lema, S., et al., *Manufacturing and compatibilization of binary blends of polyethylene and poly (butylene succinate) by injection molding*. Journal of Applied Research in Technology & Engineering, 2021. 2(2): 71-81.
- [48] Clarkson, C.M., et al., *Crystallization kinetics and morphology of small concentrations of cellulose nanofibrils (CNFs) and cellulose nanocrystals (CNCs) melt-compounded into poly(lactic acid) (PLA) with plasticizer*. Polymer, 2020. 187: 122101.
- [49] Oliveira, M., et al., *The role of shear and stabilizer on PLA degradation*. Polymer Testing, 2016. 51: 109-116.
- [50] Shi, X., et al., *Synergistic effects of nucleating agents and plasticizers on the crystallization behavior of poly (lactic acid)*. Molecules, 2015. 20(1): 1579-1593.
- [51] Li, F., C. Zhang, and Y. Weng, *Improvement of the Gas Barrier Properties of PLA/OMMT Films by Regulating the Interlayer Spacing of OMMT and the Crystallinity of PLA*. ACS Omega, 2020. 5(30): 18675-18684.

- [52] Singh, S., M.L. Maspoch, and K. Oksman, *Crystallization of triethyl-citrate-plasticized poly(lactic acid) induced by chitin nanocrystals*. *Journal of Applied Polymer Science*, 2019. 136(36): 47936.
- [53] Yu, L., et al., *Effect of annealing and orientation on microstructures and mechanical properties of polylactic acid*. *Polymer Engineering and Science*, 2008. 48(4): 634-641.
- [54] Meng, Q., M.C. Heuzey, and P.J. Carreau, *Hierarchical structure and physicochemical properties of plasticized chitosan*. *Biomacromolecules*, 2014. 15(4): 1216-1224.
- [55] Ghasemlou, M., F. Khodaiyan, and A. Oromiehie, *Rheological and structural characterisation of film-forming solutions and biodegradable edible film made from kefiran as affected by various plasticizer types*. *International Journal of Biological Macromolecules*, 2011. 49(4): 814-21.

III.2.4. Effect of the chain length of geraniol esters on the plasticization efficiency with poly(lactide)

Jaume Gomez-Caturla^{1*}, Juan Ivorra-Martinez¹, Ramon Tejada-Oliveros¹, Virginia Moreno¹, Daniel Garcia-Garcia¹, Rafael Balart¹

¹Technological Institute of Materials – ITM, Universitat Politècnica de València – UPV, Plaza Ferrándiz y Carbonell 1, 03801 Alcoy (Spain).



Polymer

2024, 290: 126522

*Adapted from the original manuscript.



Effect of the chain length of geraniol esters on the plasticization efficiency with poly(lactide)

J. Gomez-Caturla^{a,*}, J. Ivorra-Martinez^a, R. Tejada-Oliveros^a, V. Moreno^a, D. Garcia-Garcia^a, R. Balart^a

^a Institute of Materials Technology (ITM), Universitat Politècnica de València (UPV), Plaza Ferrándiz y Carbonell 1, 03801, Alcoy, Alicante, Spain

ARTICLE INFO

Keywords:
Poly(lactic acid)
Plasticizer
Geraniol ester
Ductility
Mechanical properties

ABSTRACT

This work reports on the development of environmentally friendly PLA formulations utilizing different esters derived from geraniol as plasticizers. Geranyl formate, acetate, propionate, butyrate, isovalerate and caproate at 10 wt% were combined with PLA in formulations that were produced through extrusion and injection moulding processes. Theoretical solubility parameter studies predicted good miscibility between PLA and all the plasticizers. This was confirmed by tensile test, which showed elongation at break values between 200 and 300 %, totally in contrast with the 8 % value of neat PLA. Geranyl acetate and geranyl formate exhibited the highest elongation at break behavior. These values of elongation at break were supported by FESEM images, which showed clear signs of plasticization. The plasticization effect was further corroborated by DSC and DMTA analysis, where a clear decrease in the glass transition temperature was observed from a typical value of 60 °C for neat PLA down to 40–50 °C for the plasticized blends. This was related to an enhanced chain mobility of the amorphous regions of PLA. Moreover, the plasticizers slightly increased the water absorption capabilities of PLA, as demonstrated by an increase in the water contact angle and water uptake for 11 weeks.

1. Introduction

Poly(lactide) (PLA) is, with difference, one of the most widely used biobased and biodegradable polymers obtained from renewable resources. It has gained significant attention in recent years due to its eco-friendly nature, and currently it can be found in a wide variety of sectors such as packaging, automotive, medical, electronics, construction and building, 3D-printing technology, among others [1–4]. However, PLA is also known for its intrinsic brittleness, which can be a limiting factor in many applications. To overcome or minimize this drawback, several strategies have been proposed.

One of those strategies is blending, which implies the combination of PLA with more ductile polymers in order to increase the ductility of the brittle polymer. To meet this end, several polymers such as poly(ethylene) (PE), poly(propylene) (PP), polyurethanes (PUs), poly(ϵ -caprolactone) (PCL), poly(butylene adipate-co-terephthalate) (PBAT) or poly(ethylene-co-glycidyl methacrylate) (PE-co-GMA) have been used in blends with PLA to improve its ductile properties [5,6].

Another very interesting option is copolymerization. For example, Mulchandani et al. [7] studied the copolymerization of PLA with

polycaprolactone (PCL) in a triblock copolymer, achieving elongation at breaks superior to 500 %. Stefaniak et al. and Coudane et al. [8,9] showed studies where PLA was copolymerized with PCL, maleic anhydride (MA), natural rubber, polyethylene glycol (PEG), glycolic acid (GA) or polyhedral oligomeric silsesquioxane (POSS). All those copolymers show improved toughness in comparison with neat PLA.

Fibers have also been used to enhance the mechanical properties of PLA. Glass fibers (GF) and carbon fibers (CF) are some of the most popular ones. Natural fibers are also being studied, such as jute, abaca, hemp or flax fibers [10,11]. In spite of the fact that some of these fibers are quite rigid, they are capable of improving the toughness and general mechanical properties of PLA.

Incorporation of plasticizers is an effective technical solution to provide improved ductility to PLA. In general, plasticizers increase flexibility and toughness. A wide range of plasticizers have been proposed, including monomeric plasticizers such as citrates, malonates, glycerol esters, oligomers of lactic acid, adipates, among others. Polymeric plasticizers have also given interesting properties to PLA. It is worthy to highlight the use of poly(butylene succinate) (PBS), poly(ϵ -caprolactone) (PCL), poly(butylene succinate-co-adipate) (PBSA),

* Corresponding author.

E-mail address: jaugoca@epsa.upv.es (J. Gomez-Caturla).

<https://doi.org/10.1016/j.polymer.2023.126522>

Received 8 September 2023; Received in revised form 15 November 2023; Accepted 18 November 2023

Available online 22 November 2023

0032-3861/© 2023 The Authors. Published by Elsevier Ltd. This is an open access article under the CC BY-NC-ND license (<http://creativecommons.org/licenses/by-nc-nd/4.0/>).

Effect of the chain length of geraniol esters on the plasticization efficiency with poly(lactide)

Abstract

This work reports on the development of environmentally friendly PLA formulations utilizing different esters derived from geraniol as plasticizers. Geranyl formate, acetate, propionate, butyrate, isovalerate and caproate at 10 wt.% were combined with PLA in formulations that were produced through extrusion and injection moulding processes. Theoretical solubility parameter studies predicted good miscibility between PLA and all the plasticizers. This was confirmed by tensile test, which showed elongation at break values between 200 and 300%, totally in contrast with the 8% value of neat PLA. Geranyl acetate and geranyl formate exhibited the highest elongation at break behavior. These values of elongation at break were supported by FESEM images, which showed clear signs of plasticization. The plasticization effect was further corroborated by DSC and DMTA analysis, where a clear decrease in the glass transition temperature was observed from a typical value of 60 °C for neat PLA down to 40-50 °C for the plasticized blends. This was related to an enhanced chain mobility of the amorphous regions of PLA. Moreover, the plasticizers slightly increased the water absorption capabilities of PLA, as demonstrated by an increase in the water contact angle and water uptake for 11 weeks.

Keywords: Poly(lactic acid), plasticizer, geraniol ester, ductility, mechanical properties.

INTRODUCTION

Poly(lactide) (PLA) is, with difference, one of the most widely used biobased and biodegradable polymers obtained from renewable resources. It has gained significant attention in recent years due to its eco-friendly nature, and currently it can be found in a wide variety of sectors such as packaging, automotive, medical, electronics, construction and building, 3D-printing technology, among others [1-4]. However, PLA is also known for its intrinsic brittleness, which can be a limiting factor in many applications. To overcome or minimize this drawback, several strategies have been proposed.

One of those strategies is blending, which implies the combination of PLA with more ductile polymers in order to increase the ductility of the brittle polymer. To meet this end, several polymers such as poly(ethylene) (PE), poly(propylene) (PP), polyurethanes (PUs), poly(ϵ -caprolactone) (PCL), poly(butylene adipate-*co*-terephthalate) (PBAT) or poly(ethylene-*co*-glycidyl methacrylate) (PE-*co*-GMA) have been used in blends with PLA to improve its ductile properties [5, 6].

Another very interesting option is copolymerization. For example, Mulchandani *et al.* [7] studied the copolymerization of PLA with polycaprolactone (PCL) in a triblock copolymer, achieving elongation at breaks superior to 500%. Stefaniak *et al.* and Coudane *et al.* [8, 9] showed studies where PLA was copolymered with PCL, maleic anhydride (MA), natural rubber, polyethylene glycol (PEG), glycolic acid (GA) or polyhedral oligomeric silsesquioxane (POSS). All those copolymers show improved toughness in comparison with neat PLA.

Fibers have also been used to enhance the mechanical properties of PLA. Glass fibers (GF) and carbon fibers (CF) are some of the most popular ones. Natural fibers are also being studied, such as jute, abaca, hemp or flax fibers [10, 11]. In spite of the fact that some of these fibers are quite rigid, they are capable of improving the toughness and general mechanical properties of PLA.

Incorporation of plasticizers is an effective technical solution to provide improved ductility to PLA. In general, plasticizers increase flexibility and toughness. A wide range of plasticizers have been proposed, including monomeric plasticizers such as citrates, malonates, glycerol esters, oligomers of lactic acid, adipates, among others. Polymeric plasticizers have also given interesting properties to PLA. It is worthy to highlight the use of poly(butylene succinate) (PBS), poly(ϵ -caprolactone) (PCL), poly(butylene succinate-*co*-adipate) (PBSA), poly(butylene adipate-*co*-terephthalate) (PBAT), poly(ethylene glycol) (PEG), among others, as polymeric plasticizers for PLA,

thus leading to binary/ternary blends with full or partial miscibility, depending on the polymeric plasticizer [12-14]. In general, monomeric plasticizers offer exceptional plasticization performance, but the migration is higher than plasticized PLA formulations containing polymeric plasticizers due to a lower molecule size.

With the aim of broadening the industrial applications of PLA without compromising the biobased nature, new alternative plasticizers are continuously being proposed. Llanes *et al.* [15] reported the potential of malonate and fumarate isomers as environmentally friendly plasticizers for PLA with a noticeable decrease in glass transition temperature (T_g) from 58 °C (neat PLA) down to 22 °C for the plasticized formulation containing 12 wt.% dimethyl fumarate (DMF). Recently, Barandarian *et al.* [16] have reported the exceptional plasticization efficiency of different cinnamate esters with a noticeable increase in elongation at break from 3.9% (neat PLA) up to values comprised between 250–339% with 20 wt.% cinnamate esters, which was also reflected by a decrease in T_g from 61.7 °C (neat PLA) to values below 40 °C. Ivorra-Martinez *et al.* [17, 18] have shown the extraordinary plasticization efficiency of dibutyl itaconate (DBI) as environmentally friendly plasticizer for PLA. They reported an increase in elongation at break from 4.6% (neat PLA) up to 322% with just 10 wt.% DBI. Brüster *et al.* [19] explored the effect of conventional and reactive extrusion (REX) on the plasticization efficiency of terpene-based plasticizers. Other natural terpenes, such as geraniol or linalool have also been reported to possess excellent plasticizing properties, especially when they are reacted with carboxylic acids to form esters [20]. Geraniol esters have shown interesting plasticization properties on poly(3-hydroxybutyrate) as reported in a previous work [21] Nevertheless, despite the solubility parameters of P3HB and geraniol esters suggest good miscibility and hence, good plasticization, the overall plasticization effects of geranyl esters are not exceptional, due to the intrinsic difficulty to plasticize crystalline P3HB.

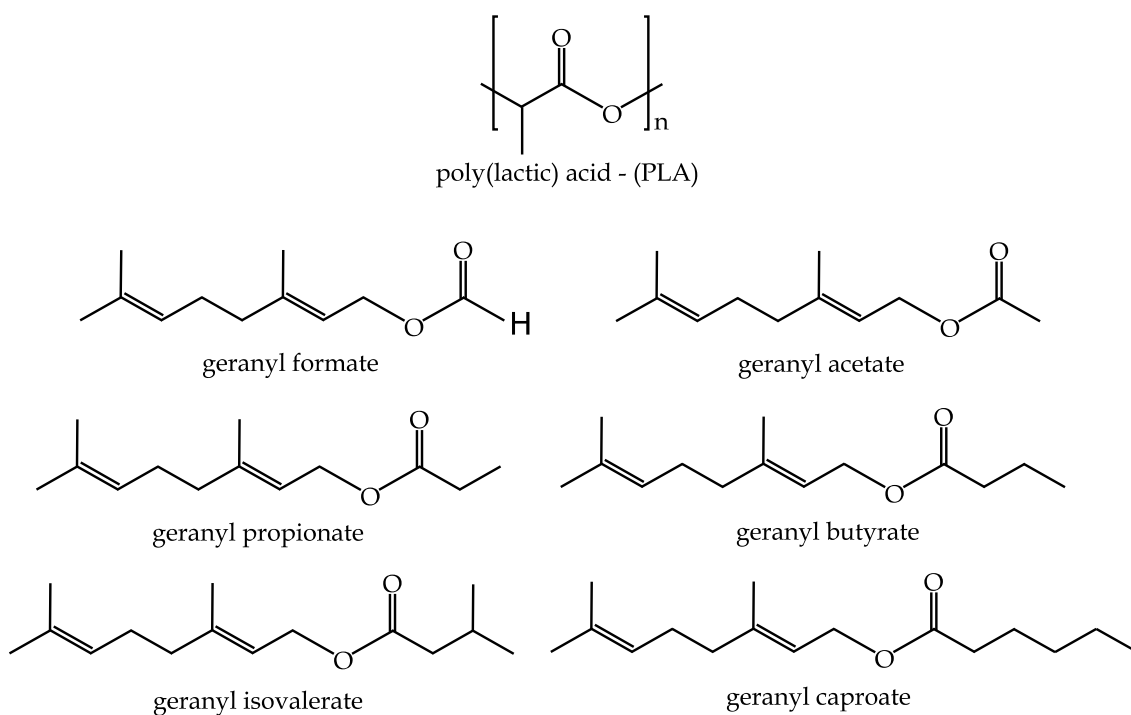
In this work, PLA is plasticized with a series of biobased plasticizers from geraniol. Specifically, geranyl formate, geranyl acetate, geranyl propionate, geranyl butyrate, geranyl isovalerate and geranyl caproate are tested as plasticizers for PLA in different formulations. Essentially, all those plasticizers possess a similar chemical structure but with different side chain lengths. All these esters are natural-based and thus, they also give an additional environmentally friendly value to PLA. In order to assess the plasticization effect that these esters exert over PLA, as well as other additional properties, mechanical, morphological, thermal, dynamical-thermal-mechanical, colorimetric, chemical and water properties are characterized and evaluated.

MATERIALS AND METHODS

Materials

PLA grade PURAPOL L130 was purchased from Total Corbion PLA (Gorinchem, The Netherlands) with a minimum L-isomer content of 99% and a melt flow index of 16 g/10 min (ISO 1133-A 210 °C/2.16 kg).

Geranyl acetate (>97% purity), geranyl propionate (>95%), geranyl butyrate (>95%), geranyl isovalerate (>95%), geranyl formate (>95%) and geranyl caproate (>95%) were supplied by Sigma Aldrich (Madrid, Spain). **Scheme III.2.4.1** shows the chemical structure of PLA and all the geranyl esters used in this work as plasticizers, while **Table III.2.4.1** gathers some properties of the selected geraniol esters.



Scheme III.2.4.1. Chemical structure of poly(lactic) acid and different geranyl-based plasticizers.

Table III.2.4.1. Physical and chemical properties of esters of geraniol used as plasticizers for PLA.

Geranyl ester	Density (g cm ⁻³)	Molecular weight (g mol ⁻¹)	Boiling point (°C) at 760 mmHg
Geranyl formate	0.921	182.263	216
Geranyl acetate	0.907	196.290	240 – 245
Geranyl propionate	0.905	210.317	252 – 254
Geranyl butyrate	0.894	224.34	242 – 243
Geranyl isovalerate	0.889	238.371	276 – 278
Geranyl caproate	0.892	252.398	240

Theoretical solubility study

When mixing a polymer and a plasticizer, their miscibility is essential to be taken into account. Van Krevelen and Hoftyzer [22], developed a methodology that is very useful to calculate the solubility parameter (δ) of both components by the group contribution method. **Equation III.2.4.1** shows the contribution of the dispersion (δ_d), polar (δ_p) and hydrogen bonding forces (δ_h), to the total solubility parameter (δ), and their relation.

$$\delta^2 = \delta_d^2 + \delta_p^2 + \delta_h^2 \quad (\text{III.2.4.1})$$

Each contribution is calculated according to **Equations III.2.4.2 to III.2.4.4**:

$$\delta_d = \frac{\sum F_{di}}{V} \quad (\text{III.2.4.2})$$

$$\delta_p = \frac{\sqrt{\sum F_{pi}^2}}{V} \quad (\text{III.2.4.3})$$

$$\delta_h = \frac{\sqrt{\sum E_{hi}}}{V} \quad (\text{III.2.4.4})$$

where V [cm³ mol⁻¹] stands for the molar volume, F_{di} [(M)/m³)^{1/2} mol⁻¹] corresponds to the group contributions of the molar attraction constant with regard to the dispersion component, F_{pi} [(M)/m³)^{1/2} mol⁻¹] stands for the characteristic molar

attraction constants related to the polar component, while E_{hi} [J mol⁻¹] values are representative for the hydrogen bonding energy which are almost constant per structural group.

Table III.2.4.2 presents all the solubility contributions and the general solubility parameter. The R_a parameter has also been calculated, which is representative for the distance between the solubility coordinates of the studied polymer and the coordinates of the studied plasticizer. If the R_a value is low, it implies a high miscibility between PLA and the plasticizer. If R_a is zero, it means a complete miscibility by both components. There exists a R_a threshold from which the solubility between polymer and plasticizer becomes poor. This value is R_0 , which is characteristic for each polymer and defines a spherical solubility region for the studied polymer. The center of this sphere is determined by the three solubility parameter contributions of PLA aforementioned. R_a is calculated according to **Equation III.2.4.5**:

$$R_a = \sqrt{4 \cdot (\delta_{d_{plast}} - \delta_{d_{PLA}})^2 + (\delta_{p_{plast}} - \delta_{p_{PLA}})^2 + (\delta_{h_{plast}} - \delta_{h_{PLA}})^2} \quad (\text{III.2.4.5})$$

Another important parameter to give a theoretical idea of the miscibility of a base polymer and a plasticizer, is the relative energy difference (RED). This parameter defines as the ratio between R_a and R_0 . In the case of PLA, R_0 is 10.7 MPa^{1/2} (**Equation III.2.4.6**) [23]. As the RED value becomes lower, the solubility between the polymer and the plasticizer becomes higher. If RED is equal to one, this means that both elements fall within the threshold of good miscibility, while values superior to 1 suggest poor solubility.

$$RED = \frac{R_a}{R_0} \quad (\text{III.2.4.6})$$

As it is observed in **Table III.2.4.2**, all the proposed plasticizers show RED values rather inferior to 1. This implies that all the plasticizers should show good solubility with PLA. Nevertheless, these values are theoretical, thus, they will be corroborated through experimental results.

Table III.2.4.2. Theoretical solubility parameters of PLA and geraniol esters used as plasticizers.

Material	δ_d (MPa ^{1/2})	δ_p (MPa ^{1/2})	δ_h (MPa ^{1/2})	δ (MPa ^{1/2})	Ra (MPa ^{1/2})	RED
PLA	15.33	8.44	10.98	20.66	-	-
Geranyl formate	15.16	2.48	5.95	16.47	7.81	0.73
Geranyl acetate	15.98	2.29	5.71	17.12	8.20	0.77
Geranyl propionate	15.88	2.11	5.49	16.93	8.51	0.80
Geranyl butyrate	15.83	1.96	5.29	16.80	8.68	0.81
Geranyl isovalerate	15.63	1.83	5.12	16.55	8.85	0.83
Geranyl caproate	15.90	1.73	4.97	16.75	9.08	0.85

Processing of plasticized PLA formulations with geraniol esters

PLA was first dried in a hot air drier at 100 °C for 5 h to remove any residual moisture, in order to avoid the hydrolysis of the polymer during processing. Then, PLA was mixed with each plasticizer at a constant proportion of 10 wt.%. Neat PLA was also processed without any plasticizer as control material. In order to produce all the formulations, a hot melt manufacturing process was performed in a 15 cc twin-screw micro compounder from Xplore instruments BV (Sittard, The Netherlands). All formulations were prepared using an analytical balance and then they were subjected to a thermal cycle at 100 rpm with a temperature profile of 190 °C for 2 minutes. Standard samples were obtained in a micro injection moulding unit from Xplore instruments BV (Sittard, The Netherlands) at 190 °C and an injection pressure of 8 bar.

Mechanical properties

The tensile behavior of the plasticized PLA formulations containing different geraniol esters, was measured using a universal test machine Ibertest ELIB 30 from SAE Ibertest (Madrid, Spain). A 5 kN load cell was used and the measurements followed the ISO 527. Samples were tested at room temperature and the crosshead speed was set at 20 mm min⁻¹. Five different specimens were tested and average values of the main tensile parameters were calculated.

Impact strength of the formulations of PLA with geraniol esters was obtained using notched samples with a Charpy impact pendulum (1-J) from Metrotec S.A. (San Sebastian, Spain), following ISO 179.

Shore D hardness was measured in a 676-D durometer from J. Bot Instruments (Barcelona, Spain) on rectangular samples with dimensions 80×10×4 mm³, according to

ISO 868:2003.

Morphological analysis

The morphology of the plasticized PLA blends with geraniol esters was studied by the observation of the fractured surface of broken samples from Charpy test through field emission scanning electron microscopy (FESEM). The samples were first sputtered with a gold-palladium alloy in an EMITECH sputter coating SC7620 model from Quorum Technologies, Ltd. (East Sussex, UK) and then a ZEISS ULTRA 55 microscope from Oxford Instruments (Abingdon, United Kingdom) operated at 2 kV was used to collect FESEM images.

Thermal properties

In order to study the thermal properties of the plasticized PLA materials, differential scanning calorimetry (DSC) tests were carried out in triplicate using a DSC Mettler-Toledo 821 calorimeter from Mettler-Toledo Inc. (Schwerzenbach, Switzerland) in nitrogen atmosphere using a flow rate of 66 mL min⁻¹. Samples with a weight between 7 and 9 mg were subjected to a dynamic program with three thermal steps: a first heating cycle from 30 °C to 180 °C, a cooling cycle down to 0 °C, and a final second heating cycle from 0 °C to 220 °C. The heating/cooling rate for all the stages was 10 °C min⁻¹. The percentage degree of crystallinity (χ_c %), was calculated from **Equation III.2.4.7**, using the data collected from the second heating step.

$$\chi_c(\%) = \frac{\Delta H_m - \Delta H_{cc}}{\Delta H_m^0 \cdot (1 - w)} \cdot 100 \quad (\text{III.2.4.7})$$

where $1-w$ is the weight fraction of PLA in each formulation, ΔH_m is the melting enthalpy of PLA, ΔH_{cc} is the cold crystallization enthalpy and ΔH_m^0 is the melt enthalpy of a 100% crystalline PLA, which is considered as 93 J/g [24].

Regarding the thermal degradation, it was assessed through thermogravimetric analysis (TGA). TGA characterization was carried out in a TG-DSC2 thermobalance from Mettler-Toledo (Columbus, OH, USA). Specimens with an average weight of 10 mg were subjected to a dynamic heating program from 30 °C to 700 °C at 10 °C/min under air atmosphere was used. All tests were performed in triplicate to obtain reliable results.

Thermo-mechanical properties

Dynamic mechanical thermal analysis (DMTA) was performed in a Mettler-Toledo DMA1 (Columbus, OH, USA). It worked in single cantilever mode. Samples with dimensions $20 \times 6 \times 3 \text{ mm}^3$ were used for DMTA characterization. The maximum dynamic deflection at the cantilever was set to $10 \text{ }\mu\text{m}$ and the frequency for the sinusoidal deformation was set to 1 Hz. Regarding the heating cycle, tests started at $-150 \text{ }^\circ\text{C}$ and samples were heated up to $100 \text{ }^\circ\text{C}$ with a heating rate of $2 \text{ }^\circ\text{C}/\text{min}$.

Attenuated total reflection-Fourier transform infrared (ATR-FTIR) spectroscopy

The chemical interactions in the PLA plasticized blends were analysed by means of attenuated total reflection-Fourier transform infrared spectroscopy (ATR-FTIR) spectroscopy. Spectra were recorded using a Bruker S.A Vector 22 (Madrid, Spain) coupled to a PIKE MIRacle™ single reflection diamond ATR accessory (Madison, Wisconsin, USA). Data were collected as the average of 20 scans between 4000 and 500 cm^{-1} with a spectral resolution of 2 cm^{-1} .

Colour characterization

Colour measurements were carried out using a Konica CM-3600d Colorflex-DIFF2 spectrophotometer from Hunter Associates Laboratory, Inc. (Reston, VA, USA.). $L^*a^*b^*$ colour coordinates were measured with L^* representing the luminance, a^* the colour coordinate from green ($a^* < 0$) to red ($a^* > 0$) and b^* standing for the colour coordinate from blue ($b^* < 0$) to yellow ($b^* > 0$). The yellowing index was calculated as recommended by ASTM E313. 10 measurements were done and the results averaged.

Water uptake and wetting properties

The water absorption of the samples was assessed by means of the water uptake test following ISO 62:2008. Samples ($80 \times 10 \times 4 \text{ mm}^3$) were immersed in distilled water at room temperature for a period of 11 weeks. Samples were extracted from the water each week and were then dried with paper to measure the mass on an analytical balance AG245 from Mettler-Toledo (Schwerzenbach, Switzerland). Samples were then again immersed in water after the measurement. The weight change was calculated by **Equation III.2.4.8**:

$$\text{Water absorption (\%)} = \frac{W_t - W_0}{W_0} \cdot 100 \quad (\text{III.2.4.8})$$

where W_t is the weight of the sample after the extraction and W_0 is the initial weight of the sample.

Additionally, surface wetting properties were obtained using an optical goniometer EasyDrop Standard model FM140 from KRÜSS GmbH (Hamburg, Germany) equipped with a video capture accessory kit. Double distilled water was used for contact angle measurements using the Drop Shape Analysis SW21; DSA1 software. Flat specimens with dimensions $80 \times 10 \times 4 \text{ mm}^3$ were used to obtain the water contact angle (θ_w) at room temperature. At least 10 different measurements were done and the obtained θ_w were averaged.

RESULTS AND DISCUSSION

Mechanical properties

Table III.2.4.3 gathers all the mechanical parameters relative to the tensile test carried out for all the formulations. Regarding the tensile modulus (E), all plasticizers provoke a clear decrease in this parameter. Neat PLA presents a tensile modulus of 3763 MPa, which is indicative of a brittle and resistant behavior, while all the plasticized PLA formulations show a decrease in tensile modulus down to 1755-2698 MPa. This indicates certain plasticization exerted by the terpenoids, which promote a decrease in the intensity of the Van der Waals forces between polymeric chains, making their interactions weaker [15], leading to a decrease in both tensile modulus and tensile strength. Interestingly, the plasticizers with higher molecular weight (*i.e.* geranyl isovalerate and caproate) provoke a smaller decrease in tensile modulus. This is probably ascribed due to the fact that low molecular weight plasticizers exert a higher lubricant effect over polymeric chains, as they can immerse more easily between them. In a similar manner, tensile strength was also reduced, from a value of 65.8 MPa for neat PLA down to 27-43 MPa for the plasticized PLA formulations. The most remarkable result observed in this analysis is the drastic increase in elongation at break undergone by the plasticized samples. Neat PLA presents an elongation at break of 8.1%, which is a characteristic behavior of a very brittle polymer with low ductility [25]. On the other hand, the decrease in the intensity of the attraction forces between polymeric chains gives rise to elongation at break values of 300% for the plasticized PLA with geranyl

acetate. The rest of the plasticizers allowed to obtain elongation at break values in the range 235-264%, which are also impressive numbers, considering the extreme brittleness of neat PLA. This feat again proves the effective plasticization of PLA with geraniol esters and also remarks the good miscibility assessed from the theoretical solubility parameter section.

The Shore D hardness values were also analyzed in **Table III.2.4.3**. This parameter follows a similar trend to that observed in the elastic modulus. The addition of the plasticizers reduces the hardness of PLA from 76.6 down to values in the range 37-70, where the highest values correspond to the plasticizers with the highest molecular weight. This fact is also ascribed to an increased chain mobility in the polymer as a result of the lubricant effect of the plasticizer.

On the contrary to hardness, impact strength (which is indicative of toughness) was increased thanks to the incorporation of the geraniol ester-based plasticizers into PLA. PLA showed a value of 1.1 kJ m⁻², while the rest of the samples exhibited values between 2.2 and 6.1 kJ m⁻², thus indicating a clear improvement in toughness. Again, geranyl acetate together with geranyl formate leads to obtain the highest impact strength, similar to the elongation at break trend, which could be a consequence of a better miscibility with PLA, as it was observed in the theoretical solubility study, where the RED value was the lowest for geranyl acetate and geranyl formate.

Table III.2.4.3. Main mechanical parameters obtained for each one of the plasticized PLA formulations.

Code	E (MPa)	σ_{\max} (MPa)	ϵ_b (%)	Shore D Hardness	Impact Strength (kJ/m ²)
PLA	3763 ± 38	65.6 ± 2.0	8.1 ± 0.2	76.6 ± 1.3	1.1 ± 0.2
PLA/10FORMATE	1755 ± 45	26.8 ± 3.4	262.4 ± 5.3	43.5 ± 1.5	5.2 ± 0.2
PLA/10ACETATE	1509 ± 29	30.4 ± 3.8	301.9 ± 3.5	63.3 ± 2.1	6.1 ± 0.4
PLA/10PROPIONATE	1865 ± 46	37.2 ± 2.3	264.3 ± 4.0	45.5 ± 1.9	2.2 ± 0.1
PLA/10BUTIRATE	2239 ± 41	32.3 ± 1.8	250.0 ± 5.7	37.8 ± 2.1	2.3 ± 0.2
PLA/10ISOVALERATE	2698 ± 32	43.2 ± 3.1	237.6 ± 2.2	68.9 ± 1.4	3.0 ± 0.2
PLA/10CAPROATE	2341 ± 37	41.6 ± 3.4	235.3 ± 6.3	70.0 ± 1.9	2.4 ± 0.4

Morphological analysis

In order to provide support to the mechanical results presented in the previous section, FESEM morphological analysis was carried out over the fractured surface of

Charpy impact test specimens. **Figure III.2.4.1** shows the FESEM images of all the formulations at 1500× magnification. **Figure III.2.4.1a** corresponds to neat PLA, and clearly shows the typical flat surface with very little roughness, which is representative for quite a brittle behavior with absence of plastic deformation [26]. Totally in contrast with this behavior, all the rest of plasticized PLA samples exhibit clear signs of plasticization. This is denoted by a rough and cavernous surface with even some filament-like formations [27]. This effect seems to be especially visible in **Figure III.2.4.1b** and **Figure III.2.4.1c**, which corresponds to plasticized PLA with geranyl formate and geranyl acetate respectively, which are the plasticized formulations with the highest elongation at break and impact strength as mentioned above. These results perfectly match the findings observed in the previous section, with all the plasticized samples presenting an effective visible plasticization and without signs of phase separation. This latter fact is also in total accordance with the theoretical miscibility results, which shown that all the plasticizers offered good compatibility with PLA.

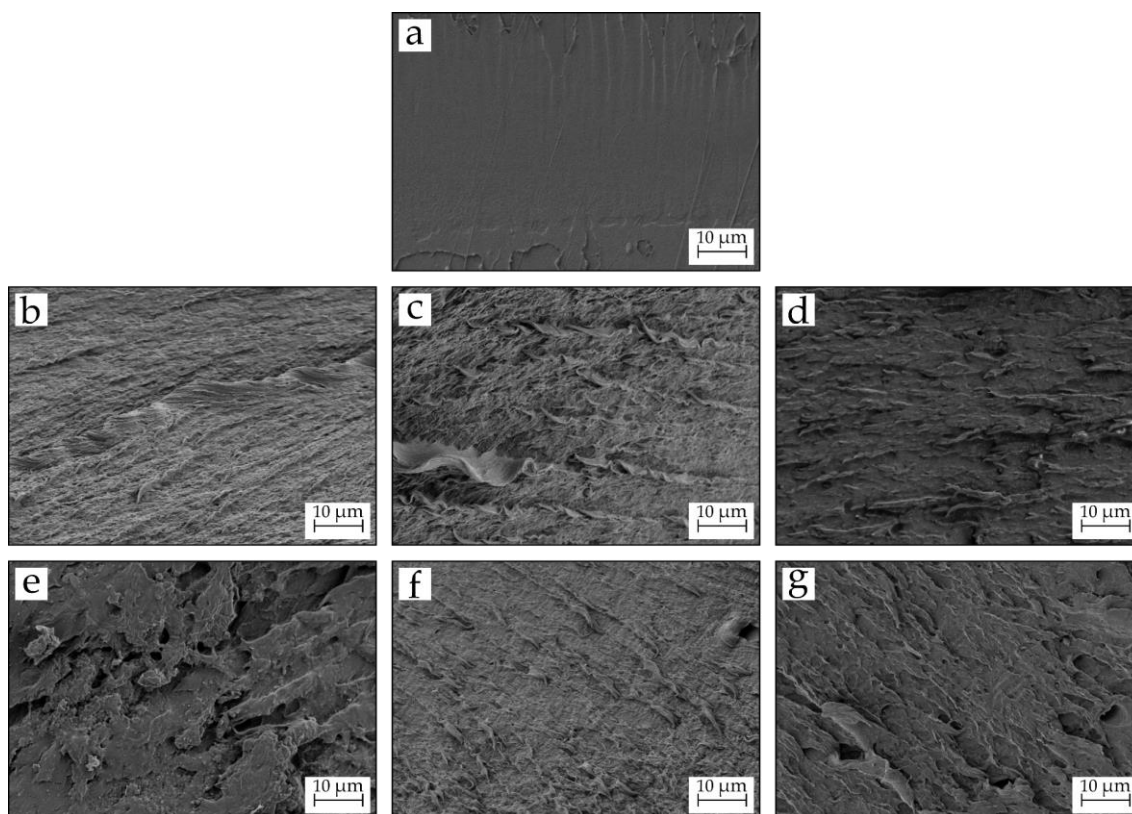


Figure III.2.4.1. FESEM images at 1500× magnification for each one of the plasticized PLA formulations: a) PLA, b) PLA/10FORMATE, c) PLA/10ACETATE, d) PLA/10PROPIONATE, e) PLA/10BUTYRATE, f) PLA/10ISOVALERATE and g) PLA/10CAPROATE.

Thermal properties

Figure III.2.4.2 shows all the thermograms that correspond to the second heating cycle obtained by differential scanning calorimetry (DSC), for neat PLA and all the plasticized formulations with geraniol esters. **Table III.2.4.4** gathers the main thermal parameters that have been extracted from those thermograms. Neat PLA exhibits a typical glass transition temperature (T_g) of 61.6 °C [28]. All the used plasticizers clearly decrease T_g down to values in the range 46-56 °C, which is indicative of an effective plasticization, especially in the case of PLA with geranyl caproate, which achieves a T_g value of 45 °C. This is ascribed to an increase in the mobility of the polymeric chains in the amorphous region of PLA. Very similar values were reported by Maiza *et al.* [29], in formulations of plasticized PLA with citrate esters. This fact demonstrates the effectiveness of these new natural plasticizers in comparison with most conventional PLA plasticizers such as TEC and ATBC. A similar trend is observed for the cold crystallization temperature peak (T_{cc}), which is shifted from a value of 102 °C (neat PLA) down to values of 91-100 °C in plasticized PLA formulations. This is also related to an increased chain mobility of the polymer as a result of the plasticizing effect, which makes these chains easier to rearrange into a crystalline formation and makes them more readily to pack [15]. The melting peak temperature does not suffer a noticeable change, as it fluctuates in the 171-173 °C range, although it seems that the plasticizers slightly decrease it. Regarding crystallinity, only geranyl butyrate increases it up to 39%, in comparison with 29% of neat PLA. This is due to the plasticizer increasing the concentration of crystal growth nuclei and thus catalyzing the crystallization of the polymer [30]. However, this effect was not observed for the rest of the plasticizers. All in all, these results prove a clear plasticization effect exerted by the geranyl esters.

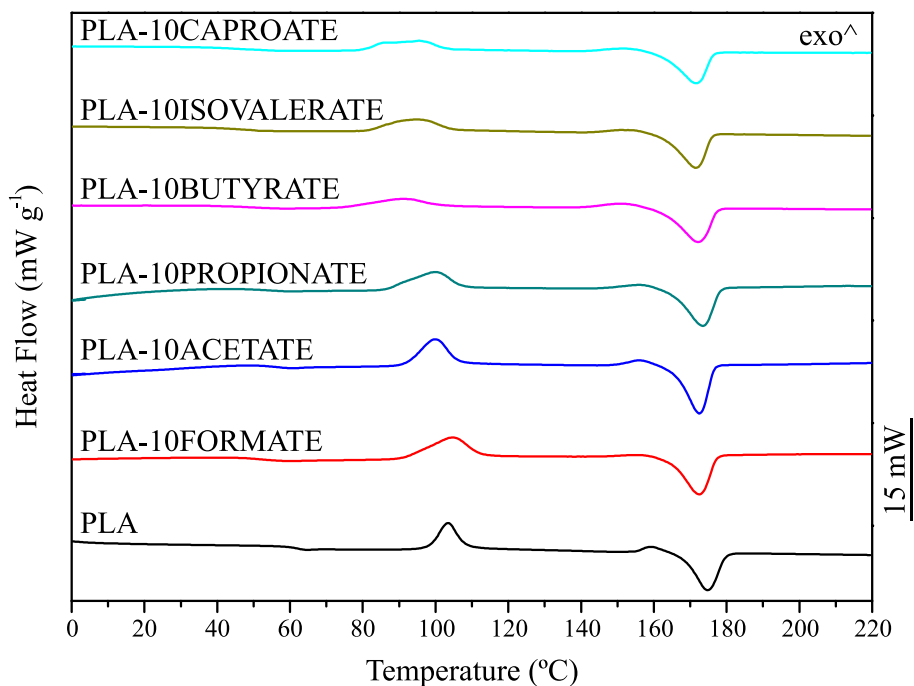


Figure III.2.4.2. Second heating cycle thermograms obtained by DSC of all the plasticized PLA formulations.

Table III.2.4.4. Main thermal parameters extracted from the DSC thermograms.

Code	T_g (°C)	T_{cc} (°C)	T_m (°C)	ΔH_{cc} (J g ⁻¹)	ΔH_m (J g ⁻¹)	χ_c (%)
PLA	61.6 ± 2.2	102.8 ± 1.1	173.3 ± 1.2	24.3 ± 0.8	51.7 ± 0.2	29.4 ± 0.3
PLA-10FORMATE	51.3 ± 3.1	104.6 ± 1.4	172.4 ± 1.4	27.2 ± 1.1	39.3 ± 0.7	14.5 ± 1.2
PLA-10ACETATE	55.9 ± 1.3	99.8 ± 1.1	172.6 ± 1.5	25.3 ± 1.2	43.5 ± 0.8	21.7 ± 1.1
PLA-10PROPIONATE	54.3 ± 2.0	99.8 ± 1.5	173.4 ± 2.0	26.9 ± 0.9	46.0 ± 1.2	22.8 ± 1.9
PLA-10BUTYRATE	47.6 ± 2.1	91.2 ± 1.4	172.2 ± 2.1	15.5 ± 0.7	48.3 ± 1.1	39.2 ± 1.5
PLA-10ISOVALERATE	50.4 ± 3.4	95.1 ± 1.3	171.6 ± 1.4	22.2 ± 0.7	46.5 ± 1.2	29.0 ± 1.9
PLA-10CAPROATE	45.9 ± 1.8	95.3 ± 1.4	171.5 ± 1.8	21.7 ± 0.9	43.9 ± 0.8	26.5 ± 1.3

Additionally to DSC analysis, the thermal degradation of all the plasticized PLA formulations with geraniol esters was studied by means of thermogravimetric analysis (TGA), and its first derivative (DTG). **Figure III.2.4.3** shows the TGA thermograms for each one of the developed formulations as well as the first derivative (DTG), which allows to better determine the maximum degradation rate. At first glance, it can be seen that neat PLA presents a typical one-step thermal degradation profile due to chain scission, with an onset degradation temperature (temperature at which the mass loss is 5%) of 357 °C and a maximum degradation rate temperature of 380 °C [31]. It can be seen

that when plasticizers are added to PLA, the thermodegradation profile becomes a two-step process. The first process, occurring between 200-300 °C is ascribed to plasticizer volatilization, leading to a decrease in the onset temperature down to values in the 233-279 °C range [32]. As it can be seen, the mass loss for all geraniol ester-based plasticizers is close to 10 wt.% in this first mass loss step, which is indicating very low plasticizer volatilization during processing. Interestingly, the onset degradation temperature becomes higher as the molecular weight of the plasticizer also increases. Thus, while geranyl formate (the plasticizer with the lowest molecular weight and chain length) presents an onset degradation temperature of 233 °C, geranyl caproate (the plasticizer with the highest molecular weight and largest chain length) presents a value of 279 °C for this parameter. This is obviously ascribed to the boiling point of the plasticizers, which becomes greater the higher their molecular weight is. Regarding the maximum degradation rate temperature, it does not vary in great measure in spite of introducing the plasticizers, although it is slightly lower than the value presented by neat PLA. This is the expected behaviour since the second degradation steps is ascribed to PLA degradation, once the plasticizer has been removed at lower temperature. Similar results were observed by Gálvez *et al.* [33], in blends of PLA plasticized with acetyl tributyl citrate (ATBC), where the maximum degradation rate temperature maintained in the range 364-370 °C. Finally, the residual mass is almost 0 in all the developed blends, which was an expected result as theoretically, at 700 °C all the components present in this study should be completely decomposed. The effect of the different geraniol ester-based plasticizers on thermal degradation can also be seen in **Table III.2.4.5** which gathers the main thermal degradation parameters.

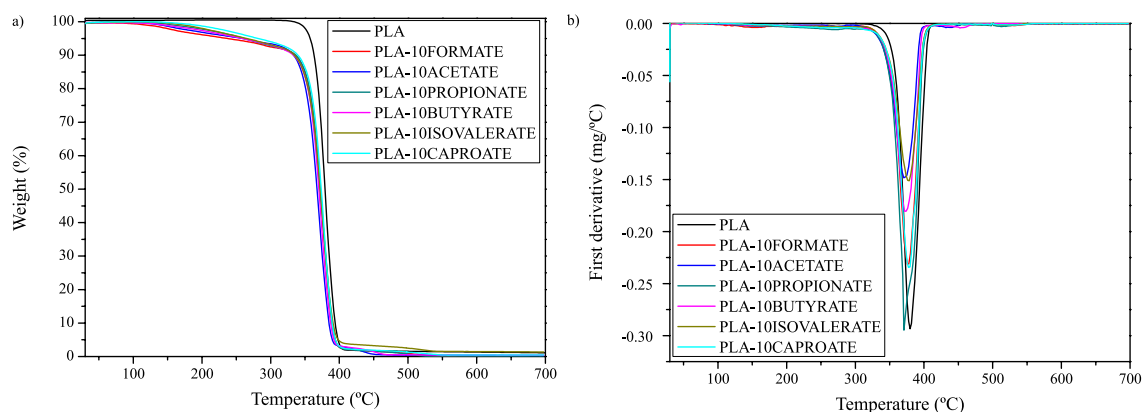


Figure III.2.4.3. a) Thermogravimetric analysis (TGA) thermograms of the plasticized PLA formulations with geraniol esters, b) first derivative of the TGA of all the developed formulations.

Table III.2.4.5. Main thermal parameters extracted from the TGA and DTG analyses.

Code	$T_{5\%}$ (°C)	T_{max} (°C)	Residue (%)
PLA	357.9 ± 2.0	380.0 ± 1.1	0.1 ± 0.1
PLA-10FORMATE	233.3 ± 3.2	375.9 ± 1.4	0.2 ± 0.1
PLA-10ACETATE	260.6 ± 3.3	370.8 ± 1.1	0.3 ± 0.1
PLA-10PROPIONATE	260.7 ± 3.0	378.5 ± 1.5	0.2 ± 0.1
PLA-10BUTYRATE	261.1 ± 3.1	373.3 ± 1.4	0.4 ± 0.1
PLA-10ISOVALERATE	266.5 ± 3.4	377.5 ± 1.3	0.3 ± 0.1
PLA-10CAPROATE	279.8 ± 3.8	378.1 ± 1.4	0.5 ± 0.1

Thermo-mechanical properties

Dynamic mechanical thermal analysis (DMTA) allowed to obtain the thermomechanical properties of the developed PLA-based formulations. **Figure III.2.4.4** shows the evolution of the storage modulus (E') and the dynamic damping factor ($\tan \delta$) in function of temperature for all the plasticized PLA formulations. Regarding the storage modulus, neat PLA presents an almost constant modulus (2361 at -20 °C) until it reaches 60 °C, when it suffers a drastic decrease (almost three fold) in the temperature range comprised between 60–70 °C. This is ascribed to the glass transition of the polymer occurring in this temperature range. After the glass transition, at approximately 80 °C, the storage modulus increases up to values close to 50 MPa. This last increase is related to the cold crystallization process of the polymer, as an increase in crystallinity is associated with an increase in stiffness, and hence, the storage modulus is increased. It is clearly observable that the plasticized samples see their sudden decrease related to the glass transition moved to lower temperatures, as it was expected from DSC results. The same effect occurs with the increase in storage modulus related to the cold crystallization temperature, which is also shifted towards lower temperatures in comparison with neat PLA. This is ascribed to an enhancement of chain mobility in the amorphous regions of PLA exerted by the plasticizers. The glass transition temperature (T_g) was calculated according to the peaks observed in the $\tan \delta$ graphs. Neat PLA presents a T_g of 65 °C, while the rest of the samples oscillate between 41 and 45 °C, which is a considerable decrease in this parameter (see **Table III.2.4.6**). These results perfectly match the ones reported in DSC analysis.

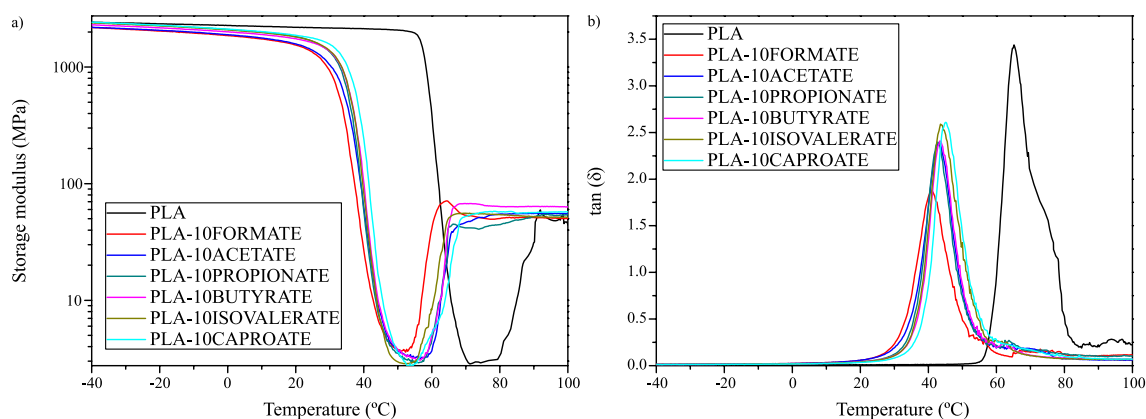


Figure III.2.4.4. a) Storage modulus (E') evolution *versus* temperature of all the plasticized PLA formulations, b) dynamic damping factor ($\tan \delta$) evolution *versus* temperature of all the plasticized PLA formulations.

Table III.2.4.6. Main thermal parameters obtained from dynamic-mechanical thermal analysis (DMTA).

Code	T_g (°C)	$\tan \delta$ peak height	E' at -20 °C (MPa)	E' at 100 °C (MPa)
PLA	65.0 ± 0.8	3.42 ± 0.3	2361 ± 25	45 ± 13
PLA-10FORMATE	41.1 ± 0.6	1.85 ± 0.2	2038 ± 33	47 ± 22
PLA-10ACETATE	43.1 ± 0.7	2.38 ± 0.4	2074 ± 14	50 ± 25
PLA-10PROPIONATE	42.7 ± 0.4	2.39 ± 0.3	2278 ± 41	49 ± 31
PLA-10BUTYRATE	43.5 ± 0.7	2.41 ± 0.2	2176 ± 37	68 ± 17
PLA-10ISOVALERATE	43.6 ± 0.5	2.59 ± 0.3	2268 ± 49	48 ± 28
PLA-10CAPROATE	45.1 ± 0.4	2.61 ± 0.3	2291 ± 52	52 ± 25

Attenuated total reflection-Fourier transform infrared (ATR-FTIR) spectroscopy

In order to assess possible chemical interactions between PLA and the geraniol ester-based plasticizers, Fourier transformed infrared spectroscopy (FTIR) was carried out. FTIR spectra are shown in **Figure III.2.4.5**. Neat PLA presents a strong band located at around 1750 cm^{-1} , which is ascribed to C-O stretching vibration of the carbonyl group [34]. Three bands can be observed between 1500 and 1300 cm^{-1} , which are related to symmetric and antisymmetric deformation vibrations of the C-H bond in methyl groups ($-\text{CH}_3$) [35]. Additionally, C-O-C symmetric and asymmetric vibrations can be attributed to the bands in the range 1260 - 1180 cm^{-1} . It can be observed that the addition of the different plasticizers does not change the FTIR spectra of PLA in a noticeable way. Nonetheless, it does provoke very slight changes. One of them is a very little decrease in the intensity of the peak at 1750 cm^{-1} , which could be ascribed to certain interaction

between the carbonyl groups of PLA and the oxygen based groups of the plasticizers, given that all plasticizers possess similar functionalization (ester groups). These groups can form hydrogen bonds with hydrogen in C-H bonds, thus varying the intensity that the C-O interaction provokes [36]. This could also be the reason for a change in the intensity of the peak located at 1180 cm^{-1} . The hydrogen bonding originated from the interaction between C-O-C bonds and C-H bonds in PLA and the plasticizers can directly affect the response that C-O-C gives in the infrared region [37]. All in all, the spectra of the plasticized PLA samples are very similar with each other, as the chemical structure of all the plasticizers is very similar, being the main difference their chain length.

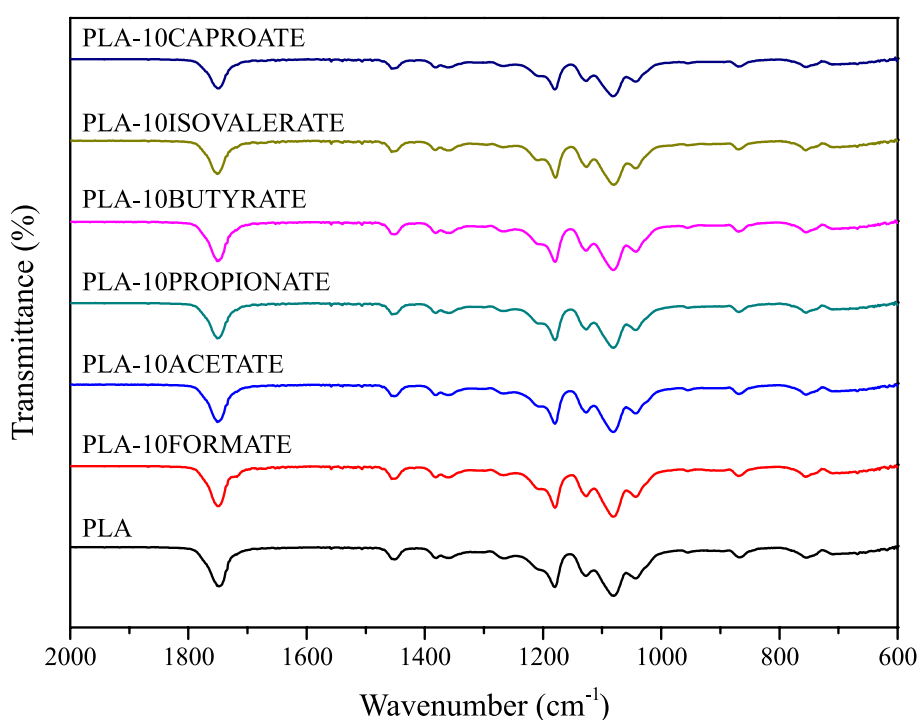


Figure III.2.4.5. FTIR spectra of neat PLA and plasticized PLA formulations with geraniol ester-based plasticizers.

Colour characterization

The visual appearance of the blends was assessed by colorimetric analysis, as this aspect is essential for the impression a product produced with those materials makes in the customer. **Table III.2.4.7** gathers the main $\text{CieL}^*a^*b^*$ colorimetric parameters of neat PLA and the plasticized PLA samples while **Figure III.2.4.6** shows the visual appearance of all the studied formulations. L^* stands for luminance, and it indicates the brightness of the colour of the samples, the higher this parameter is, the closer the colour is to pure white. It can be observed that all samples present a very similar luminance, with a range

between 36 and 38. This is ascribed to the typical white transparent colour of PLA, which is not greatly affected by the introduction of plasticizers in the blends, as it can be corroborated by **Figure III.2.4.6**. The colour coordinate a^* indicates green (negative) or red (positive) tonalities. In this case all samples present very similar negative values (between -0.3 and -0.8). These values are close to 0 as the colours presented by the samples are very close to white. The colour coordinate b^* indicates blue (negative) or yellow (positive) shades. As expected, all samples present positive values due to a certain approach to yellow. The plasticizers seem to increase this value, as they turn the colour of PLA towards a higher yellow degree, as it will be discussed with the following parameter. Finally, the yellowness index (YI), which indicates how the colour is changed from white to yellow, seems to increase as a result of the incorporation of the plasticizers into PLA. This can be slightly appreciated in **Figure III.2.4.6**, especially in sample g, which is plasticized with geranyl caproate and seems to present an opaquer colour. Nonetheless, all the samples are clearly transparent. Similar results and visual appearance were observed for PLA samples plasticized with ATBC and PEG [38], although the samples presented here preserve even better the natural colour of PLA.

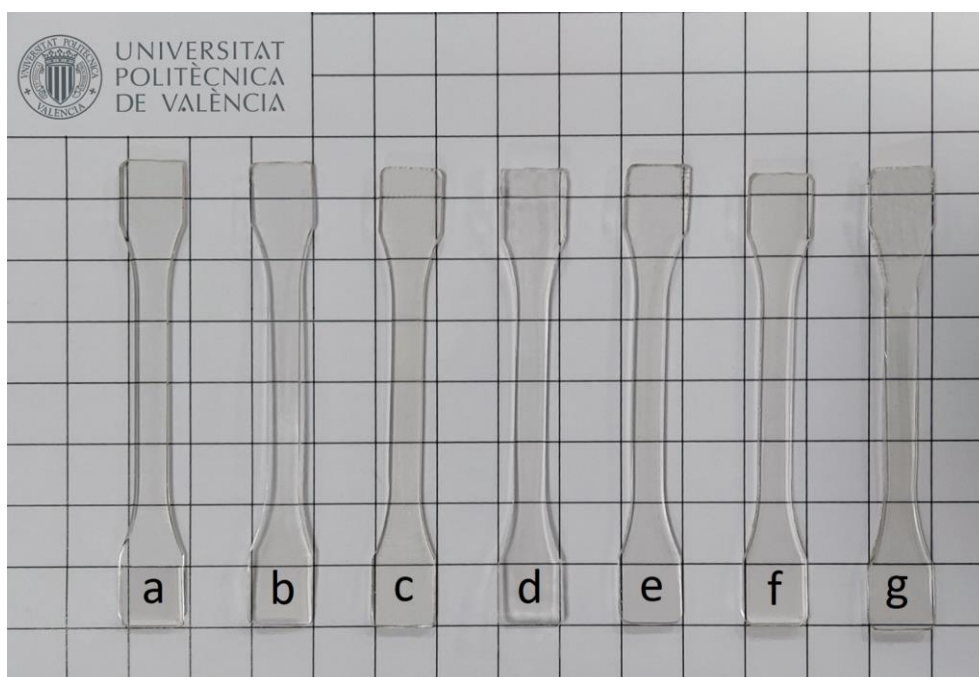


Figure III.2.4.6. Visual aspect of the developed samples: a) PLA, b) PLA/10FORMATE, c) PLA/10ACETATE, d) PLA/10PROPIONATE, e) PLA/10BUTYRATE, f) PLA/10ISOVALERATE and g) PLA/10CAPROATE.

Table III.2.4.7. Ciel^{*}a^{*}b^{*} colour coordinates and yellow index of the plasticized PLA samples with different geraniol esters.

Code	L [*]	a [*]	b [*]	YI
PLA	38.1 ± 0.1	-0.3 ± 0.1	1.2 ± 0.2	4.6 ± 0.3
PLA-10FORMATE	37.8 ± 0.1	-0.6 ± 0.1	2.2 ± 0.1	8.0 ± 0.3
PLA-10ACETATE	36.6 ± 0.1	-0.4 ± 0.1	2.1 ± 0.1	8.1 ± 0.5
PLA-10PROPIONATE	37.8 ± 0.1	-0.7 ± 0.1	2.8 ± 0.1	10.2 ± 0.3
PLA-10BUTIRATE	37.1 ± 0.1	-0.6 ± 0.1	2.9 ± 0.1	11.0 ± 0.3
PLA-10ISOVALERATE	38.5 ± 0.1	-0.4 ± 0.2	1.9 ± 0.1	7.0 ± 0.4
PLA-10CAPROATE	38.2 ± 0.1	-0.8 ± 0.1	2.8 ± 0.1	10.4 ± 0.1

Water uptake properties

Figure III.2.4.7 shows the evolution of water absorption over time for neat PLA and all the plasticized samples after being immersed in distilled water for 11 weeks. As it can be seen, neat PLA presents the lowest water absorption profile of all the presented materials, with a maximum water absorption of approximately 0.38 wt.% of water with relation to the initial weight of the sample. This fact indicates certain hydrophobic behavior in PLA. A similar behavior was observed by Dominguez-Candela *et al.* [34]. When the different plasticizers are added into PLA, its water absorption slightly increases, especially in the case of geranyl formate. All the plasticizers achieve maximum water uptake values at 11 weeks of approximately 0.45 wt.%, which could be ascribed to the plasticization effect that increases the free volume between the polymeric chains. After all, the plasticizers weaken the intermolecular attraction forces between PLA chains, thus increasing water diffusion within the polymer [39]. All those plasticizers provide a similar water absorption capacity to PLA, without much variability from the neat polymer. This could be ascribed to the fact that all of them possess a similar chemical structure, which does not possess great polarity, as there is only one oxygen-based functionalization (ester group), while the rest of the chemical structure is formed by C-H bonds, which are essentially non-polar. Interestingly, geranyl formate allows PLA to absorb a higher degree of water (up to 0.8 wt.%) in comparison to the rest of the samples. This could be due to the fact that it is the plasticizer with the lowest molecular weight among the studied ones, which accounts for a smaller molecule which could better insert between PLA chains, thus increasing in a slightly higher degree the free volume between them. This would translate in a higher capability to accept water in the internal structure of the polymer. Nonetheless, the general water absorption of the herein studied blends is quite low in comparison with other materials that are more

compromised by this property, as wood plastic composites, which can achieve water uptakes of more than 10 wt.% [40].

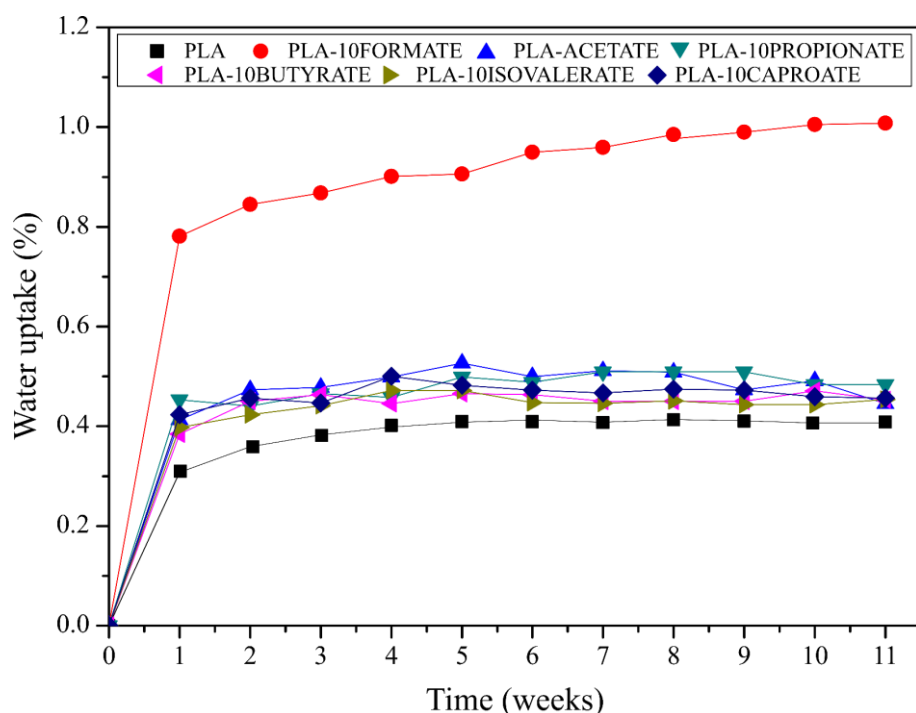


Figure III.2.4.7. Evolution of the water absorption of neat PLA and plasticized PLA formulations with geraniol ester-based plasticizers.

Wetting properties

Water contact angle measurements were taken in order to complement the water uptake results. In this case, the behavior of the materials after short-time exposition to water is studied. **Figure III.2.4.8** shows the visual appearance of distilled water drops over the surface of samples from each one of the materials as well as the contact angle they form with the flat surface. It can be observed in **Figure III.2.4.8a** that neat PLA presents a contact angle of 76.4° , which is indicative of a rather hydrophobic behavior, as this value is relatively close to 90° , which is the “highly hydrophobic” threshold [41]. A similar result was obtained by Jordá-Vilaplana *et al.* [41] for neat PLA. The plasticized samples present a slightly superior hydrophilic behavior, especially the sample with geranyl formate, which presents a contact angle of approximately 70° . As it was aforementioned, the inclusion of plasticizers in the polymer matrix increases the free volume between the PLA polymeric chains, thus making it easier for water to enter its structure, increasing hydrophilicity. Moreover, the used plasticizers possess oxygen-based functionality, which increase the polarity of the PLA/plasticizer blends. These

plasticizers present a non-polar fraction (C-H bonds) and a polar fraction (ester groups), therefore, the plasticizers with longer chain length, such as geranyl caproate, provide less polarity to PLA due to it having a higher non-polar fraction (longer C-H chains) and thus, the contact angle observed is superior to the angle observed for geranyl formate or geranyl acetate [42]. The contact angles of the samples with geranyl acetate, propionate, butyrate, isovalerate and caproate range from 72° to 74° , which are still lower than that of neat PLA. These results are in accordance with the results obtained in the water uptake section previously described.

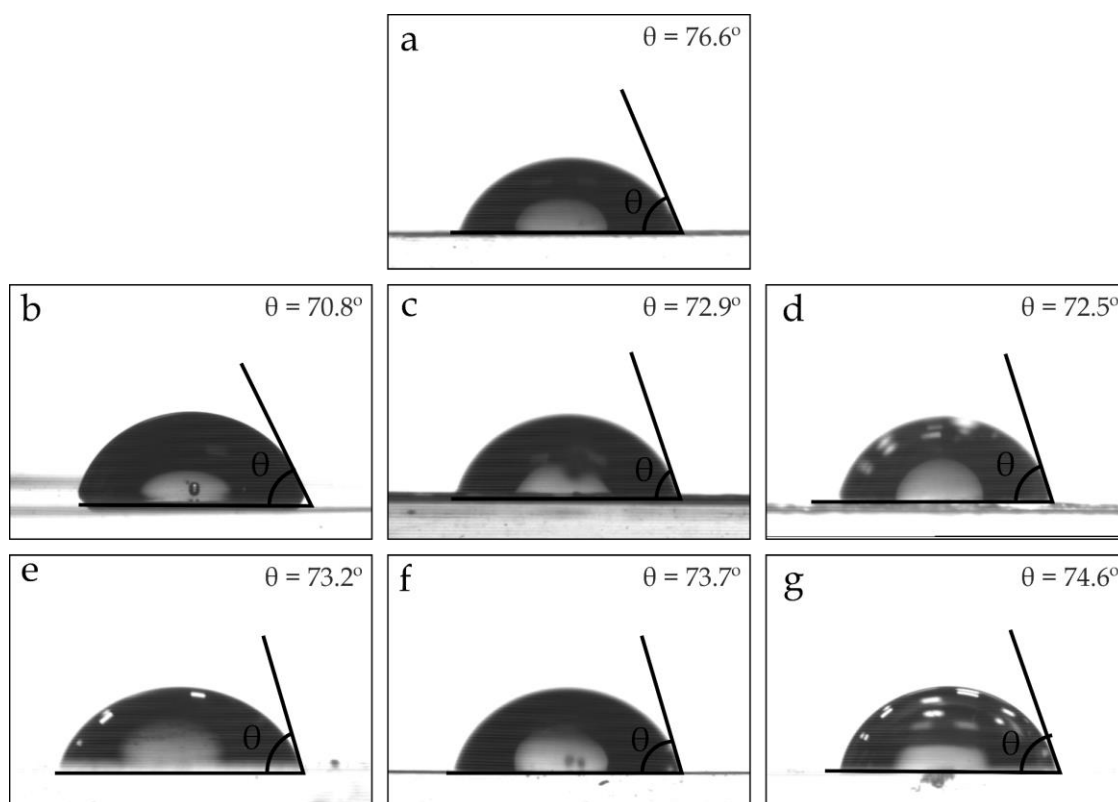


Figure III.2.4.8. Contact angle measurements of: a) PLA, b) PLA/10FORMATE, c) PLA/10ACETATE, d) PLA/10PROPIONATE, e) PLA/10BUTYRATE, f) PLA/10ISOVALERATE and g) PLA/10CAPROATE.

CONCLUSIONS

This work has shown that several geraniol esters with different chain lengths (geranyl formate, acetate, propionate, butyrate, isovalerate and caproate) can effectively plasticize poly(lactic acid) (PLA), providing excellent results in terms of ductility. The mechanical properties results showed that all the plasticizers drastically increased elongation at break from 8% up to values in the range 230-300%, which are quite

impressive results considering the poor ductility of neat PLA. Geranyl formate showed the highest elongation at break. Those results were confirmed by FESEM images, which exhibited clear signs of plasticization in the fractured surface of all the plasticized samples. Regarding their thermal behavior, DSC analysis showed a decrease of approximately 10 °C in the glass transition temperature, attributed to an increase in the chain mobility of the amorphous phase of PLA, thus, demonstrating an excellent plasticization effect. Thermogravimetric analysis (TGA) clearly indicated a slight reduction in the thermal stability of the blends due to the high volatility of the plasticizer in the temperature range 200-300 °C and DMTA results again pointed out a decrease in the glass transition temperature. Water properties revealed a slight increase in the water absorption of PLA, especially in the case of geranyl formate, which increased the free volume between the polymeric chains. All in all, this work presents a new alternative to traditional plasticizers such as poly(ethylene glycol) (PEG) or triethyl citrate (TEC), which are additionally environmentally friendly.

ACKNOWLEDGEMENTS

This research is a part of the grant PID2020-116496RB-C22, funded by MCIN/AEI/10.13039/501100011033 and the grant TED2021-131762A-I00, funded by MCIN/AEI/10.13039/501100011033 and by the European Union “NextGenerationEU”/PRTR. Authors also thank Generalitat Valenciana-GVA for funding this research through the grant numbers AICO/2021/025 and CIGE/2021/094. Funded with Aid for First Research Projects (PAID-06-22), Vice-rectorate for Research of the Universitat Politècnica de València (UPV). R.T.-O. wishes to thank UPV for the grant received through the PAID-01-20 program. J. I.-M. wants to thank FPU19/01759 grant funded by MCIN/AEI/10.13039/501100011033 and by ESF Investing in your future. J. G.-C. wants to thank FPU20/01732 grant funded by MCIN/AEI/10.13039/501100011033 and by ESF Investing in your future. V. M. thanks Generalitat Valenciana - GVA for funding a postdoc position through the APOSTD program co-funded by ESF Investing in your future, grant number CIAPOS/2021/67. Microscopy Services at UPV are also acknowledged by their help in collecting and analyzing images.

DATA AVAILABILITY STATEMENT

The raw/processed data required to reproduce these findings cannot be shared at this time due to technical or time limitations.

REFERENCES

- [1] Aversa, C., et al., *Compatibilization strategies and analysis of morphological features of poly (butylene adipate-co-terephthalate)(PBAT)/poly (lactic acid) PLA blends: A state-of-art review*. European Polymer Journal, 2022. 173: 111304.
- [2] Saniei, H. and S. Mousavi, *Surface modification of PLA 3D-printed implants by electrospinning with enhanced bioactivity and cell affinity*. Polymer, 2020. 196: 122467.
- [3] Singh, S., et al., *3D printed biodegradable composites: An insight into mechanical properties of PLA/chitosan scaffold*. Polymer Testing, 2020. 89: 106722.
- [4] Bhagia, S., et al., *Critical review of FDM 3D printing of PLA biocomposites filled with biomass resources, characterization, biodegradability, upcycling and opportunities for biorefineries*. Applied Materials Today, 2021. 24: 101078.
- [5] Moradi, S. and J.K. Yeganeh, *Highly toughened poly (lactic acid)(PLA) prepared through melt blending with ethylene-co-vinyl acetate (EVA) copolymer and simultaneous addition of hydrophilic silica nanoparticles and block copolymer compatibilizer*. Polymer Testing, 2020. 91: 106735.
- [6] Bhasney, S.M., A. Kumar, and V. Katiyar, *Microcrystalline cellulose, polylactic acid and polypropylene biocomposites and its morphological, mechanical, thermal and rheological properties*. Composites Part B: Engineering, 2020. 184: 107717.
- [7] Mulchandani, N., et al., *Toughened PLA-b-PCL-b-PLA triblock copolymer based biomaterials: effect of self-assembled nanostructure and stereocomplexation on the mechanical properties*. Polymer Chemistry, 2021. 12(26): 3806-3824.
- [8] Stefaniak, K. and A. Masek, *Green Copolymers Based on Poly (Lactic Acid) – Short Review*. Materials, 2021. 14(18): 5254.
- [9] Coudane, J., et al., *Poly (lactic acid)-based graft copolymers: Syntheses strategies and improvement of properties for biomedical and environmentally friendly applications: A review*. Molecules, 2022. 27(13): 4135.
- [10] Wang, G., et al., *Glass fiber reinforced PLA composite with enhanced mechanical properties, thermal behavior, and foaming ability*. Polymer, 2019. 181: 121803.
- [11] Belarbi, Y.E., et al., *Effect of printing parameters on mechanical behaviour of PLA-flax printed structures by fused deposition modelling*. Materials, 2021. 14(19): 5883.
- [12] Cesur, S., et al., *Production and characterization of elastomeric cardiac tissue-like patches for Myocardial Tissue Engineering*. Polymer Testing, 2020. 90: 106613.

- [13] Palai, B., S. Mohanty, and S.K. Nayak, *Synergistic effect of polylactic acid (PLA) and Poly (butylene succinate-co-adipate)(PBSA) based sustainable, reactive, super toughened eco-composite blown films for flexible packaging applications*. *Polymer Testing*, 2020. 83: 106130.
- [14] Hernández-López, M., et al., *Bio-based composite fibers from pine essential oil and PLA/PBAT polymer blend. Morphological, physicochemical, thermal and mechanical characterization*. *Materials Chemistry and Physics*, 2019. 234: 345-353.
- [15] Llanes, L.C., et al., *Mechanical and thermal properties of poly (lactic acid) plasticized with dibutyl maleate and fumarate isomers: Promising alternatives as biodegradable plasticizers*. *European Polymer Journal*, 2021. 142: 110112.
- [16] Barandiaran, A., et al., *Esters of Cinnamic Acid as Green Plasticizers for Polylactide Formulations with Improved Ductility*. *Macromolecular Materials and Engineering*, 2023. 308(8): 2300022.
- [17] Ivorra-Martinez, J., et al., *The Potential of an Itaconic Acid Diester as Environmentally Friendly Plasticizer for Injection-Molded Polylactide Parts*. *Macromolecular Materials and Engineering*, 2022. 307(12): 2200360.
- [18] Ivorra-Martinez, J., et al., *Effect of dibutyl itaconate on plasticization efficiency of a REX processed polylactide with peroxides*. *Polymer Testing*, 2023. 124: 108059.
- [19] Brüster, B., et al., *Plasticization of polylactide with myrcene and limonene as bio-based plasticizers: Conventional vs. reactive extrusion*. *Polymers*, 2019. 11(8): 1363.
- [20] da Silva Corrêa, L., et al., *Lipase-catalyzed esterification of geraniol and citronellol for the synthesis of terpenic esters*. *Applied biochemistry and biotechnology*, 2020. 190: 574-583.
- [21] Mangeon, C., et al., *Natural terpenes used as plasticizers for poly (3-hydroxybutyrate)*. *ACS Sustainable Chemistry & Engineering*, 2018. 6(12): 16160-16168.
- [22] Van Krevelen, D.W. and K. Te Nijenhuis, *Properties of polymers: their correlation with chemical structure; their numerical estimation and prediction from additive group contributions*. 2009: Elsevier.
- [23] Auras, R.A., et al., *Poly (lactic acid): synthesis, structures, properties, processing, and applications*. 2011: John Wiley & Sons.

- [24] Shankar, S., L.-F. Wang, and J.-W. Rhim, *Incorporation of zinc oxide nanoparticles improved the mechanical, water vapor barrier, UV-light barrier, and antibacterial properties of PLA-based nanocomposite films*. *Materials Science and Engineering: C*, 2018. 93: 289-298.
- [25] Murariu, M., et al., *Poly(lactide) (PLA)-CaSO₄ composites toughened with low molecular weight and polymeric ester-like plasticizers and related performances*. *European Polymer Journal*, 2008. 44(11): 3842-3852.
- [26] Bagheri, A., et al., *Fatigue testing on rotary friction-welded joints between solid ABS and 3D-printed PLA and ABS*. *European Journal of Mechanics-A/Solids*, 2022. 96: 104713.
- [27] Gomez-Caturla, J., et al., *Improvement of Poly (lactide) Ductile Properties by Plasticization with Biobased Tartaric Acid Ester*. *Macromolecular Materials and Engineering*, 2023. 308(7): 2200694.
- [28] Carbonell-Verdu, A., et al., *PLA films with improved flexibility properties by using maleinized cottonseed oil*. *European Polymer Journal*, 2017. 91: 248-259.
- [29] Maiza, M., M.T. Benaniba, and V. Massardier-Nageotte, *Plasticizing effects of citrate esters on properties of poly (lactic acid)*. *Journal of Polymer Engineering*, 2016. 36(4): 371-380.
- [30] Clarkson, C.M., et al., *Crystallization kinetics and morphology of small concentrations of cellulose nanofibrils (CNFs) and cellulose nanocrystals (CNCs) melt-compounded into poly (lactic acid)(PLA) with plasticizer*. *Polymer*, 2020. 187: 122101.
- [31] Oliveira, M., et al., *The role of shear and stabilizer on PLA degradation*. *Polymer Testing*, 2016. 51: 109-116.
- [32] Brdlík, P., et al., *Biodegradation of poly (lactic acid) biocomposites under controlled composting conditions and freshwater biotope*. *Polymers*, 2021. 13(4): 594.
- [33] Gálvez, J., et al., *Effect of extrusion screw speed and plasticizer proportions on the rheological, thermal, mechanical, morphological and superficial properties of PLA*. *Polymers*, 2020. 12(9): 2111.
- [34] Dominguez-Candela, I., et al., *Novel compatibilizers and plasticizers developed from epoxidized and maleinized chia oil in composites based on PLA and chia seed flour*. *European Polymer Journal*, 2022. 173: 111289.

- [35] Viamonte-Aristizábal, S., et al., *Synthesis of high molecular weight L-Polylactic acid (PLA) by reactive extrusion at a pilot plant scale: Influence of 1, 12-dodecanediol and di(trimethylol propane) as initiators*. European Polymer Journal, 2021. 161: 110818.
- [36] Masek, A., S. Cichosz, and M. Piotrowska, *Biocomposites of epoxidized natural rubber/poly (lactic acid) modified with natural fillers (Part I)*. International Journal of Molecular Sciences, 2021. 22(6): 3150.
- [37] Wang, J., et al., *Thermoplastic starch plasticized by polymeric ionic liquid*. European Polymer Journal, 2021. 148: 110367.
- [38] Arrieta, M.P., et al., *Disintegrability under composting conditions of plasticized PLA-PHB blends*. Polymer Degradation and Stability, 2014. 108: 307-318.
- [39] Ferri, J., et al., *The effect of maleinized linseed oil (MLO) on mechanical performance of poly (lactic acid)-thermoplastic starch (PLA-TPS) blends*. Carbohydrate polymers, 2016. 147: 60-68.
- [40] Liu, R., et al., *Comparison on properties of lignocellulosic flour/polymer composites by using wood, cellulose, and lignin flours as fillers*. Composites Science and Technology, 2014. 103: 1-7.
- [41] Jordá-Vilaplana, A., et al., *Surface modification of polylactic acid (PLA) by air atmospheric plasma treatment*. European polymer journal, 2014. 58: 23-33.
- [42] Zou, Y., et al., *Study on the influence of polar groups in pour point depressant on flow properties of Karamay crude oil*. Journal of Dispersion Science and Technology, 2023: 1-8.

IV. CONCLUSIONS

IV.1. Partial conclusions

Considering the objectives specified at the beginning of the thesis, partial conclusions related to each section are presented. These conclusions have been developed after analyzing the results of each of the studies conducted to complete this thesis.

IV.1.1. Regarding the development of environmentally friendly polymers through the reuse of mango waste

The extraction process of starch from mango kernel was successfully carried out with an approximate yield of 8%. This starch was then used to develop nanofibers by adding polyvinylpyrrolidone (PVP) and polyvinyl alcohol (PVA) through electrospinning. The obtained fibers had average diameters ranging from 80 to 339 nm, measured using scanning electron microscopy (FESEM) and atomic force microscopy (AFM), with the PVP fibers having the smallest diameter. These fibers are completely natural, biocompatible, and possess a large interfacial area, making them suitable for applications in the pharmaceutical and medical sectors.

The compatibility between the BioPP polymeric matrix and mango peel flour was significantly improved by using a compatibilizer based on itaconic acid and polypropylene (PP-g-IA) along with dicumyl peroxide (DCP). Mechanical properties (tensile, impact, and hardness) showed a clear improvement in formulations containing the compatibilizer, demonstrating enhanced adhesion of mango peel particles to the BioPP matrix. This was verified by FESEM morphology, resulting in a completely bio-based material.

Regarding the combination of PLA with mango kernel flour and tributyrin and triacetin as plasticizers, composite materials capable of mimicking wood with characteristic brown colors and completely biodegradable content were obtained. Mechanical, thermal, thermomechanical properties, and biodegradability were analyzed, showing an increase in the elongation at break from samples without plasticizers (4.4%) to those with tributyrin and triacetin (9.5% and 8.3%, respectively). Additionally, the glass transition temperature decreased due to the presence of both plasticizers, and biodegradability improved due to increased mobility of the polymeric chains.

The development of mango kernel flour films with glycerol yielded very positive

results. Mechanical, solubility, barrier properties, and biodegradability characterization indicated that the overall properties of the films improved as the particle size of mango kernel flour decreased, resulting in more homogeneous films. This allowed the production of biodegradable edible films with potential applications in the packaging sector.

Finally, the last study related to the development of starch-rich thermoplastic materials using mango kernel flour and plasticizers such as glycerol, sorbitol, and urea provided favorable results. Sorbitol-plasticized samples allowed for the production of the mechanically strongest materials, thanks to a higher concentration of hydrogen bonds between the starch present in mango kernel flour and sorbitol. Meanwhile, urea-containing samples showed higher elongations due to the prevention of starch retrogradation reactions, achieving elongation values of up to 42%.

IV.1.2. Regarding materials based on polylactic acid (PLA) with additives of natural origin

The addition of a natural plasticizer derived from tartaric acid, namely diethyl-L-tartrate, to PLA yielded very promising results, particularly in terms of mechanical and thermal response. The addition of up to 50% of the plasticizer in PLA resulted in elongation at break values of up to 600% for the sample with a 20% plasticizer content. Additionally, the glass transition temperature decreased from a characteristic value of 63 °C to values close to room temperature. Furthermore, the presence of the plasticizer improved the biodegradation rate of PLA in compost conditions, further enhancing one of the most interesting aspects of this polymer.

The results obtained from the combination of PLA with mandarin peel flour and α -terpinyl acetate demonstrated that the used plasticizer could dramatically improve the ductile properties of PLA, even in PLA blends with lignocellulosic fillers such as mandarin peel. Elongation at break values exceeding 300% were recorded for samples without mandarin particles and elongations of 200% in formulations with a 10% mandarin peel content. This indicates the feasibility of obtaining bio-based materials that promote circular economies with more than competitive properties compared to other polymers on the market.

The incorporation of geranyl acetate and linalyl acetate also significantly improved the ductile properties of PLA, with elongation values exceeding 210%. The solubility of these plasticizers was theoretically studied, estimating good miscibility between them

and PLA, a fact that was corroborated by mechanical and morphological results. Additionally, samples with dicumyl peroxide (DCP) were produced, showing a slight increase in stiffness compared to formulations with only plasticizer. This was due to a cross-linking effect catalyzed by the action of DCP.

Finally, the impact of the chain length of different geranyl esters as plasticizers for PLA was studied, incorporating 20% of each plasticizer. After analyzing mechanical, thermal, morphological, and thermomechanical results, it was concluded that all used esters effectively plasticized PLA and eliminated its brittleness. However, geranyl formate exhibited superior ductile properties compared to other plasticizers, with an elongation at break of 300% and a 10 °C reduction in the glass transition temperature compared to pure PLA.

IV.2. General conclusions

As general conclusions of this thesis, it is worth noting that numerous formulations with significant environmental potential have been successfully developed. Both in terms of materials obtained entirely from renewable sources, as well as materials that are additionally biodegradable. One of the most notable achievement has been enhancing biodegradability, particularly in the case of combining PLA with natural plasticizers. These materials represent a significant advancement and hold great promise across various sectors, especially in packaging, the food industry, and, in the case of mango starch nanofibers, the medical and pharmaceutical sectors.

Furthermore, the thesis has demonstrated the substantial potential of mango waste in terms of biorefinery, extracting starch and combining these residues with various polymers applicable in circular economies. Another sector that could benefit from some of these materials is furniture, as certain developed materials show significant potential as wood plastic composites, ideal for producing floors, frames, doors, and various products traditionally made from wood.

The possibility of using natural and innovative plasticizers to address the brittleness issues of PLA and improve its biodegradability in compost conditions has also been emphasized. This opens up applications across various sectors without compromising the environmental potential of PLA.

V. APÉNDICES

V.1. Índice de tablas

Tabla I.1. Fuentes de almidón de residuos de frutas, contenido en almidón, contenido en amilosa del almidón y tamaño medio de los gránulos de almidón. Adaptado de [69].	55
Tabla I.2. Compuestos a extraer de varios residuos de frutos cítricos y las técnicas de extracción empleadas para ello. Adaptado de [225].	89
Table III.1.1.1. Summary of compositions, experiment conditions and evaluation of the electrospun nanofibers preliminary studies according to the composition of the fibers, voltage (V), distance between the injector and the collector (D) and flux (F).	138
Table III.1.1.2. Summary of compositions and experiment conditions of the electrospun nanofibers according to the weight content (wt.%) of mango kernel starch (MKS) and PVA (distilled water as solvent), voltage (V), distance between the injector and the collector (D) and flux (F).	139
Table III.1.1.3. Summary of compositions and experiment conditions of the electrospun nanofibers according to the weight content (wt.%) of mango kernel starch (MKS) and PVP (using metoxyethanol as solvent), voltage (V), distance between the injector and the collector (D) and flux (F).	139
Table III.1.1.4. Diameter of the electrospun nanofibers made of MKS/PVA solution and their evaluation according to their morphology.	142
Table III.1.1.5. Diameter of the electrospun nanofibers made of MKS/PVP solutions.	145
Table III.1.1.6. Roughness measurements of the MKS/PVA and MKS/PVP electrospun nanofibers.	149
Table III.1.2.1. Summary of compositions according to the weight content (wt.%) of bioPP/MPF and different compatibilizers and additives.	165
Table III.1.2.2. Summary of mechanical properties of the injection-moulded samples of bioPP/MPF composites. Tensile modulus (E), maximum tensile strength (σ_{max}), elongation at break (ϵ_b), Shore D hardness, and impact (Charpy) strength.	170

Table III.1.2.3. Melting temperature (T_m), melting enthalpy (ΔH_m) and degree of crystallinity (X_c) of bioPP/MPF composites with different compatibilization strategies, obtained by differential scanning calorimetry (DSC). Main thermal degradation parameters of bioPP/MPF composites with different compatibilization strategies in terms of the onset degradation temperature at a mass loss of 5 wt.% ($T_{5\%}$), maximum degradation rate (peak) temperature (T_{deg}), and residual mass at 700 °C..... 176

Table III.1.2.4. Dynamic-mechanical properties of bioPP/MPF composites with different compatibilization strategies, at different temperatures..... 179

Table III.1.2.5. Contact angle (θ_w) of different bioPP/MPF composites with different compatibilization strategies at several times of exposure to distilled water: 0, 5, 10, 15, 20 and 30 minutes..... 180

Table III.1.3.1. Code for the developed films with different MKF particle size. 202

Table III.1.3.2. Average thickness and mechanical properties of the MKF/glycerol films from tensile test: tensile modulus (E), tensile strength (σ_{max}) and elongation at break (ϵ_b). 208

Table III.1.3.3. Moisture content and water solubility for MKF/glycerol films..... 209

Table III.1.3.4. Water contact angle at different times (0, 5, 10, 20 and 30 seconds) for MKF/glycerol films. 209

Table III.1.3.5. Luminance (L^*), colour coordinates (a^*b^*) and total colour difference (ΔE) of MKF/glycerol films with different MKF particle size..... 215

Table III.1.3.6. Arithmetic Roughness (R_a) of the MKF/glycerol films with different MKF particle size..... 219

Table III.1.4.1. Theoretical solubility parameters of PLA with tributyrin and triacetin plasticizers..... 235

Table III.1.4.2. Mechanical properties of PLA, PLA-MKSF composites obtained from tensile tests (elastic modulus - E_t , tensile strength - σ_t , elongation at break - % ϵ_b), shore D, impact strength..... 240

Table III.1.4.3. Glass transition temperature (T_g), cold crystallization peak temperature (T_{cc}), cold crystallization enthalpy (ΔH_{cc}), melting temperature (T_m), melting enthalpy (ΔH_m) and crystallinity X_c of the PLA-MKSF composites, obtained by differential scanning calorimetry (DSC)..... 244

Table III.1.4.4. Main thermal degradation parameters of the PLA-MKSF composites: onset degradation temperature at a mass loss of 5 wt.% ($T_{5\%}$), maximum degradation rate temperature (T_{deg}) and the residual mass at 700 °C.....	245
Table III.1.4.5. Main dynamic-mechanical parameters of the PLA MKSF composites.	247
Table III.1.4.6. Main colour parameters of the PLA-MKSF composites in terms of the Ciel*a*b* colour space ($L^*a^*b^*$) and the colour difference ΔE^*_{ab}	249
Table III.1.5.1. Composition of the different TPS developed formulations based on MKF.	268
Table III.1.5.2. Mechanical properties of the MKF TPS samples stored at 53% RH.....	274
Table III.1.5.3. Mechanical properties of the MKF TPS samples stored at 11% RH.....	274
Table III.1.5.4. Main thermal degradation parameters of the MKF TPS formulations with different plasticizers in terms of the onset degradation temperature at a mass loss of 5 wt.% ($T_{5\%}$), maximum degradation rate (peak) temperature (T_{deg}), and residual mass at 700 °C.	278
Table III.1.5.5. Colorimetric parameters related to the starch rich thermoplastic samples: L* (lightness), colour coordinates a* and b* and the difference in colour ΔE^*_{ab} taking the MKF-GLY sample as the reference.	280
Table III.2.1.1. Composition of the developed formulations of plasticized poly(lactide) (PLA) with diethyl L-tartrate (DET).	294
Table III.2.1.2. Theoretical solubility parameters of PLA with diethyl L-tartrate.....	296
Table III.2.1.3. Mechanical properties of the plasticized poly(lactide) (PLA) blends with diethyl L-tartrate (DET).	300
Table III.2.1.4. Main thermal parameters extracted from the DSC thermograms of the first heating cycle and the cooling cycle of the poly(lactide) (PLA) - diethyl L-tartrate (DET) blends.	304
Table III.2.1.5. Main thermal parameters extracted from the DSC thermograms of the poly(lactide) (PLA) - diethyl L-tartrate (DET) blends.	305
Table III.2.1.6. Thermal parameters related to the thermal degradation of poly(lactide) (PLA)-diethyl L-tartrate (DET) blends extracted from the TGA analysis.	307
Table III.2.1.7. Thermal parameters related to the thermal degradation of the PLA/DET blends extracted from the DMTA analysis.	308

Table III.2.2.1. Compositions of the developed formulations of PLA/TPF with TA plasticizer.....	323
Table III.2.2.2. Theoretical approach for the solubility of polylactide (PLA) formulations with α -terpinyl acetate.....	325
Table III.2.2.3. Summary of the mechanical parameters of the PLA/TPF composites regarding tensile test: tensile modulus (E), tensile strength (σ_{max}) and elongation at break (ϵ_b); Shore D hardness and impact strength.....	329
Table III.2.2.4. Glass transition temperature (T_g), Cold crystallization temperature (T_{cc}), Cold crystallization enthalpy (ΔH_{cc}) Melting temperature T_m , melting enthalpy (ΔH_m) and degree of crystallinity (χ_c) of PLA/TPF plasticized and unplasticized composites obtained by differential scanning calorimetry (DSC).	333
Table III.2.2.5. Main thermal degradation parameters of PLA/TPF composites plasticized with TA in terms of the onset degradation temperature at a mass loss of 5 wt.% ($T_{5\%}$), maximum degradation rate (peak) temperature (T_{deg}), and residual mass at 700 °C.	335
Table III.2.2.6. Dynamic-mechanical-thermal properties of PLA/TPF plasticized with α -terpinyl acetate (TA), at different temperatures.	337
Table III.2.2.7. Luminance and colour coordinates ($L^*a^*b^*$) of the PLA/TPF composites plasticized with α -terpinyl acetate.....	339
Table III.2.3.1. Composition of plasticized poly(lactide) formulations with terpenoid-based plasticizers processed by conventional and reactive (REX) extrusion.	355
Table III.2.3.2. Main parameters related to the theoretical approach for the solubility between poly(lactide) and terpenoid-based plasticizers.	357
Table III.2.3.3. Mechanical properties of PLA and plasticized PLA formulations with terpenoids in terms of tensile modulus (E), maximum tensile strength (σ_{max}), elongation at break (ϵ_b), Shore D hardness.	363
Table III.2.3.4. Summary of the DSC results for the PLA/terpene formulations: glass transition temperature (T_g), cold crystallization temperature (T_{cc}), melting temperature (T_m), cold crystallization enthalpy (ΔH_{cc}), melting enthalpy (ΔH_m) and degree of crystallinity (χ_c).....	367

Table III.2.3.5. Summary of the TGA results for the PLA/terpene formulations: initial temperature degradation at 5 wt.% loss ($T_{5\%}$), maximum rate degradation temperature (T_{deg}) and residual weight.....	368
Table III.2.3.6. Summary of the DMTA properties for the PLA/terpene formulations in terms of: storage modulus (E') and glass transition temperature (T_g).....	370
Table III.2.3.7. Summary of X-ray diffraction patterns (XRD) of neat PLA and plasticized PLA formulations with terpenes by conventional and reactive extrusion, in terms of the diffraction angle peak and d -spacing.	371
Table III.2.4.1. Physical and chemical properties of esters of geraniol used as plasticizers for PLA.....	385
Table III.2.4.2. Theoretical solubility parameters of PLA and geraniol esters used as plasticizers.....	387
Table III.2.4.3. Main mechanical parameters obtained for each one of the plasticized PLA formulations.....	391
Table III.2.4.4. Main thermal parameters extracted from the DSC thermograms.....	394
Table III.2.4.5. Main thermal parameters extracted from the TGA and DTG analyses.	396
Table III.2.4.6. Main thermal parameters obtained from dynamic-mechanical thermal analysis (DMTA).	397
Table III.2.4.7. Ciel* a^* * b^* colour coordinates and yellow index of the plasticized PLA samples with different geraniol esters.	400

V.2. Índice de figuras

Figura I.1. Clasificación de los polímeros según su origen y su biodegradabilidad.....	40
Figura I.2. Proceso de obtención del biopolietileno (bioPE).	42
Figura I.3. Proceso de obtención del biopolipropileno (bioPP) a partir del bioetileno..	43
Figura I.4. Proceso de descomposición de un poliéster en condiciones de compost (biodegradación).....	44
Figura I.5. Estructura química de la polivinilpirrolidona (PVP) y del polivinil alcohol (PVA).....	46
Figura I.6. Estructura química de algunos de los PHAs más utilizados: poli(3-hidroxi- <i>butirato</i>) (PHB), poli(3-hidroxi- <i>valerato</i>) (PHV) y poli(3-hidroxi- <i>butirato-co-3-hidroxi-<i>valerato</i></i>) (PHBV).	47
Figura I.7. Estructura química del ácido poliláctico (PLA).....	48
Figura I.8. Esquema de la estructura química de la amilosa y la amilopectina.	50
Figura I.9. Imagen FESEM de la estructura granular de almidón extraído del kernel del mango.	51
Figura I.10. Esquema de la disposición de la amilosa y la amilopectina dentro de los gránulos de almidón puro, donde se aprecia la diferenciación de la zona amorfa y la zona semicristalina. Reproducido de [58].	51
Figura I.11. Esquema del proceso de extracción de almidón de la patata utilizando metabisulfito de sodio.	53
Figura I.12. Esquema del proceso de gelatinización del almidón en medio acuoso.	57
Figura I.13. Representación esquemática del proceso de retrogradación del almidón..	58
Figura I.14. Representación esquemática de la interacción por puentes de hidrógeno entre el almidón y: a) glicerol; b) sorbitol.	60
Figura I.15. Esquema del proceso de <i>electrospinning</i>	64
Figura I.16. Aplicaciones del almidón en farmacia y medicina.....	65
Figura I.17. Esquema de las diferentes vías de síntesis del PLA.....	69
Figura I.18. Estructura química de los isómeros del PLA, los polímeros que produce cada isómero y el polímero que se obtiene como combinación de ambos isómeros.	70

Figura I.19. Proceso de hidrólisis y desintegración bacteriana del PLA bajo condiciones controladas de compost.....	72
Figura I.20. Estructura química de dos copolímeros del PLA.	76
Figura I.21. Representación esquemática de las principales teorías de plastificación. ..	78
Figura I.22. Estructura química de algunos de los plastificantes más utilizados para el PLA.....	79
Figura I.23. Esquema químico del geraniol, del linalool, del acetato de geranilo y del acetato de linalilo.....	80
Figura I.24. Reacción de esterificación que da lugar a la obtención del dietil-L-tartrato (DET).	81
Figura I.25. Esquema de la estructura del mango.	85
Figura I.26. Representación esquemática de los productos que pueden obtenerse de los diferentes residuos del mango.	87
Figura I.27. Esquema de terpenos presentes en frutos cítricos.....	93
Figura II.1. Representación esquemática de los objetivos de la presente tesis.....	119
Figure III.1.1.1. Morphology of the mango kernel starch (MKS): a) FESEM image at 1000× magnification of the mango kernel starch particles; b) Histogram of the length of the MKS particles; c) Histogram of the diameter of the MKS particles.	134
Figure III.1.1.2. FESEM images at 1000× magnification of all the fibers developed during preliminary studies specified in Table III.1.1.3.	137
Figure III.1.1.3. FESEM images at 2500× magnification of all the MKS/PVA fibers specified in Table III.1.1.3.....	143
Figure III.1.1.4. FESEM images at 2500× magnification of all the MKS/PVP fibers specified in Table III.1.1.5.....	146
Figure III.1.1.5. FESEM images at 5000× magnification and AFM images at a scan size of 4 μm of the optimal electrospun MKS/PVA and MKS/PVP obtained fibers (samples 7, 9, 20, 21 and 27).....	148
Figure III.1.1.6. Fiber diameter distributions of the optimal electrospun MKS/PVA and MKS/PVP fibers (samples 7, 9, 20, 21 and 27).	149
Figure III.1.2.1. Variation of the optical density of the carbonyl groups absorption bands (1720 cm ⁻¹) with extraction time in ethanol.	170

Figure III.1.2.2. Field emission scanning electron microscopy (FESEM) images at 1000× of the fractured surfaces of: (a) bioPP; (b) bioPP/MPF; (c) bioPP/MPF/PP-g-IA; (d) bioPP/MPF/DCP; (e) bioPP/MPF/PP-g-IA/DCP.	174
Figure III.1.2.3. Water uptake of uncompatibilized and compatibilized bioPP/MPF composites.	182
Figure III.1.2.4. Fourier Transformed Infrared Spectroscopy (FTIR) spectra of MPF, PP-g-IA, DCP and uncompatibilized and compatibilized bioPP/MPF composites in the wavenumber range 4000–500 cm ⁻¹	184
Figure III.1.2.5. Melt flow index (MFI) of the bioPP/MPF blends at 190 °C/2.16 kg. .	185
Figure III.1.3.1. Particle size distribution of milled mango kernel flour (MKF) after sieving at different size ranges.	201
Figure III.1.3.2. Evolution of the water contact angle of a distilled water drop onto the surface of MKF-500/400 film over time.	210
Figure III.1.3.3. FESEM images at 1000×magnification of the MKF/glycerol films: a) MKF-600/500; b) MKF-500/400; c) MKF-400/300; d) MKF-300/200 and e) MKF-200/100.	211
Figure III.1.3.4. Histograms of the MKF particles in the films after processing: a) MKF-600/500; b) MKF-500/400; c) MKF-400/300; d) MKF-300/200; e) MKF-200/100.	212
Figure III.1.3.5. Water vapour transmission rate (WVTR) of MKF/glycerol films with different particle size.	213
Figure III.1.3.6. Visual aspect of MKF/glycerol films: a) MKF-600/500; b) MKF-500/400; c) MKF-400/300; d) MKF-300/200 and e) MKF-200/100.	215
Figure III.1.3.7. Percentage of 2,2-diphenyl-1-picrylhydrazyl radical (DPPH) inhibition of MKF/glycerol films with different particle sizes of MKF.	216
Figure III.1.3.8. Biodegradation profile under controlled compost soil in terms of the incubation time of all the MKF/glycerol films with different MKF particle size.	218
Figure III.1.3.9. Visual appearance of the disintegration process of MKF/glycerol films over time with different MKF particle size.	218
Figure III.1.4.1. FESEM image of mango kernel seed flour (MKSF) particles at 150× with a marker scale of 20 μm.	232

Figure III.1.4.2. FESEM image of mango kernel seed flour (MKSF) particles at 1000× with a marker scale of 10 μm. a) PLA, b) PLA-MKSF, c) PLA-MKSF/TBN, d) PLA-MKSF/TCN.....	242
Figure III.1.4.3. Differential scanning calorimetry (DSC) thermograms of neat PLA and plasticized and unplasticized PLA-MKSF composites.	243
Figure III.1.4.4. Thermal degradation of PLA-MKSF composites, a) thermogravimetric (TGA), and b) first derivative (DTG) of neat PLA, plasticized and unplasticized PLA-MKSF composites.	245
Figure III.1.4.5. Plot evolution of (a) the storage modulus (E') and (b) the dynamic damping factor ($\tan \delta$) of the PLA-MKSF composites.	246
Figure III.1.4.6. Melt flow index (MFI) of neat PLA and PLA-MKSF composites.....	247
Figure III.1.4.7. The visual appearance of the PLA-MKSF composites.....	248
Figure III.1.4.8. Water contact angle measurements of plasticized and unplasticized PLA-MKSF composites.....	250
Figure III.1.4.9. Water uptake evolution of the PLA-MKSF composites over 11 weeks.	251
Figure III.1.4.10. Disintegration profile of the PLA-MKSF specimens over 12 weeks.	252
Figure III.1.4.11. Evolution of the visual appearance of the samples during the disintegration test. Size (25×2×1 mm ³).....	253
Figure III.1.5.1. FESEM morphology of mango kernel flour particles and their size distribution.....	264
Figure III.1.5.2. FESEM morphology of the extracted starch from mango kernel and the diameter and length distributions of the starch granules.	266
Figure III.1.5.3. Stress-strain curves of the MKF-based TPS developed in the preliminary study to assess the optimum plasticizer content.	267
Figure III.1.5.4. Evolution of the force during processing for all the MKF TPS samples.	271
Figure III.1.5.5. Schematic representation of the hydrogen bonding interaction between starch and: a) glycerol; b) sorbitol; c) urea.	272
Figure III.1.5.6. FESEM morphological images at 500× of each one of the developed TPS stored at 53% RH: a) MKF-GLY; b) MKF-SORB; c) MKF-UREA.....	275

Figure III.1.5.7. DSC thermograms of all the MKF TPS samples.	276
Figure III.1.5.8. Thermogravimetric analysis (TGA) and the first derivative (DTG) of the plasticized MKF TPS samples.....	277
Figure III.1.5.9. Storage modulus (G') evolution with temperature of the plasticized MKF TPS samples.	279
Figure III.1.5.10. Visual aspect of the MKF TPS samples: a) MKF-GLY; b) MKF-SORB; c) MKF-UREA.	280
Figure III.2.1.1. Stress - Strain curves of PLA and the plasticized PLA/DET samples.	299
Figure III.2.1.2. Field emission scanning electron microscopy (FESEM) images at 500× of the fractured surfaces of: a) neat PLA; b) PLA/10DET; c) PLA/20DET; d) PLA/30DET; e) PLA/40DET; f) PLA/50DET.	301
Figure III.2.1.3. Differential scanning calorimetry (DSC) thermograms of the first heating cycle of the plasticized PLA/DET blends.....	303
Figure III.2.1.4. Differential scanning calorimetry (DSC) thermograms of the cooling cycle of the plasticized PLA/DET blends.....	303
Figure III.2.1.5. Differential scanning calorimetry (DSC) thermograms of the second heating cycle of the plasticized PLA/DET blends.....	305
Figure III.2.1.6. Thermal decomposition of poly(lactide) (PLA)-diethyl L-tartrate (DET) blends a) Thermogravimetric (TG); b) First derivative (DTG).....	306
Figure III.2.1.7. Dynamic mechanical thermal analysis of poly(lactide) (PLA)-diethyl L-tartrate (DET) blends: a) storage modulus <i>vs</i> temperature; b) dynamic damping factor <i>vs</i> temperature.....	307
Figure III.2.1.8. FTIR spectra of the poly(lactide) (PLA)-diethyl L-tartrate (DET) blends.	309
Figure III.2.1.9. Disintegration process of poly(lactide) (PLA)-diethyl L-tartrate (DET) blends under controlled compost soil conditions.....	310
Figure III.2.1.10. Visual evolution of the biodegradation process of poly(lactide) (PLA)-diethyl L-tartrate (DET) blends.	311
Figure III.2.2.1. Tangerine peel flour morphology (TPF) (a) FESEM image at 250× magnification of TPF (b) Histogram of the particle size of TPF.	322

Figure III.2.2.2. FESEM images at 500× magnification of the PLA/TPF composites: a) PLA; b) PLA+10TPF; c) PLA+10TPF+22.5TA; d) PLA+20TPF+20TA; e) PLA+30TPF+17.5TA and f) PLA+20TA.	331
Figure III.2.2.3. DSC thermograms of all the PLA/TPF samples.	333
Figure III.2.2.4. Thermogravimetric analysis (TGA) and its first derivative of the plasticized and unplasticized PLA/TPF composites.	334
Figure III.2.2.5. Thermomechanical diagrams of the plasticized and unplasticized PLA/TPF composites: a) Storage Modulus (E'); b) Dynamic damping factor ($\tan \delta$). ..	337
Figure III.2.2.6. Visual appeal of the samples: a) PLA; b) PLA+20TA; c) PLA+10TPF d) PLA+10TPF+22.5TA; e) PLA+20TPF+20TA and f) PLA+30TPF+17.5TA.	338
Figure III.2.2.7. Contact angle measurements of the PLA/TPF composites: a) PLA; b) PLA+10TPF; c) PLA+10TPF+22.5TA; d) PLA+20TPF+20TA; e) PLA+30TPF+17.5TA and f) PLA+20TA.	340
Figure III.2.2.8. FTIR diagrams of neat PLA and the plasticized and unplasticized PLA/TPF composites.	341
Figure III.2.2.9. Disintegration profile of the plasticized and unplasticized PLA/TPF composites over time.	342
Figure III.2.2.10. Visual appearance of the disintegration process of PLA/TPF composites over time.	343
Figure III.2.3.1. Scheme of the chemical structures of polylactide (PLA), terpenoid-based plasticizers, <i>i.e.</i> linalyl acetate (LAc) and geranyl acetate (GAc), and free radical initiator, dicumyl peroxide (DCP) for reactive extrusion (REX).	354
Figure III.2.3.2. Schematic representation of the plausible reactions occurring during REX of PLA and terpenoids in presence of dicumyl peroxide (DCP).	362
Figure III.2.3.3. Field-emission scanning electron microscopy (FESEM) images of the fractured samples from the tensile tests at 1000×. a) PLA; b) PLA-10LAc; c) PLA-20LAc; d) PLA-20LAc-DCP; e) PLA-10GAc; f) PLA-20GAc and g) PLA-20GAc-DCP. Scale bar 10 μm	364
Figure III.2.3.4. Differential scanning calorimetry (DSC) thermograms of neat PLA and plasticized PLA formulations with terpenes by conventional and reactive extrusion, corresponding to the second heating cycle after removing thermal history.	366

Figure III.2.3.5. Thermogravimetric (TGA) behaviour for the PLA/terpene formulations in terms of a) mass loss and b) first derivative of neat PLA and plasticized PLA formulations with terpenes by conventional and reactive extrusion.	368
Figure III.2.3.6. Dynamic-mechanical thermal analysis (DMTA) behaviour of neat PLA and plasticized PLA formulations with terpenes by conventional and reactive extrusion. a) storage modulus <i>vs</i> temperature and b) dynamic damping factor ($\tan \delta$) <i>vs</i> temperature.....	370
Figure III.2.3.7. X-ray patterns of neat PLA and plasticized PLA formulations with terpenes by conventional and reactive extrusion.	371
Scheme III.2.4.1. Chemical structure of poly(lactic) acid and different geranyl-based plasticizers.....	384
Figure III.2.4.1. FESEM images at 1500 \times magnification for each one of the plasticized PLA formulations: a) PLA, b) PLA/10FORMATE, c) PLA/10ACETATE, d) PLA/10PROPIONATE, e) PLA/10BUTYRATE, f) PLA/10ISOVALERATE and g) PLA/10CAPROATE.	392
Figure III.2.4.2. Second heating cycle thermograms obtained by DSC of all the plasticized PLA formulations.....	394
Figure III.2.4.3. a) Thermogravimetric analysis (TGA) thermograms of the plasticized PLA formulations with geraniol esters, b) first derivative of the TGA of all the developed formulations.....	395
Figure III.2.4.4. a) Storage modulus (E') evolution <i>versus</i> temperature of all the plasticized PLA formulations, b) dynamic damping factor ($\tan \delta$) evolution <i>versus</i> temperature of all the plasticized PLA formulations.....	397
Figure III.2.4.5. FTIR spectra of neat PLA and plasticized PLA formulations with geraniol ester-based plasticizers.	398
Figure III.2.4.6. Visual aspect of the developed samples: a) PLA, b) PLA/10FORMATE, c) PLA/10ACETATE, d) PLA/10PROPIONATE, e) PLA/10BUTYRATE, f) PLA/10ISOVALERATE and g) PLA/10CAPROATE.....	399
Figure III.2.4.7. Evolution of the water absorption of neat PLA and plasticized PLA formulations with geraniol ester-based plasticizers.....	401
Figure III.2.4.8. Contact angle measurements of: a) PLA, b) PLA/10FORMATE, c) PLA/10ACETATE, d) PLA/10PROPIONATE, e) PLA/10BUTYRATE, f) PLA/10ISOVALERATE and g) PLA/10CAPROATE.....	402

